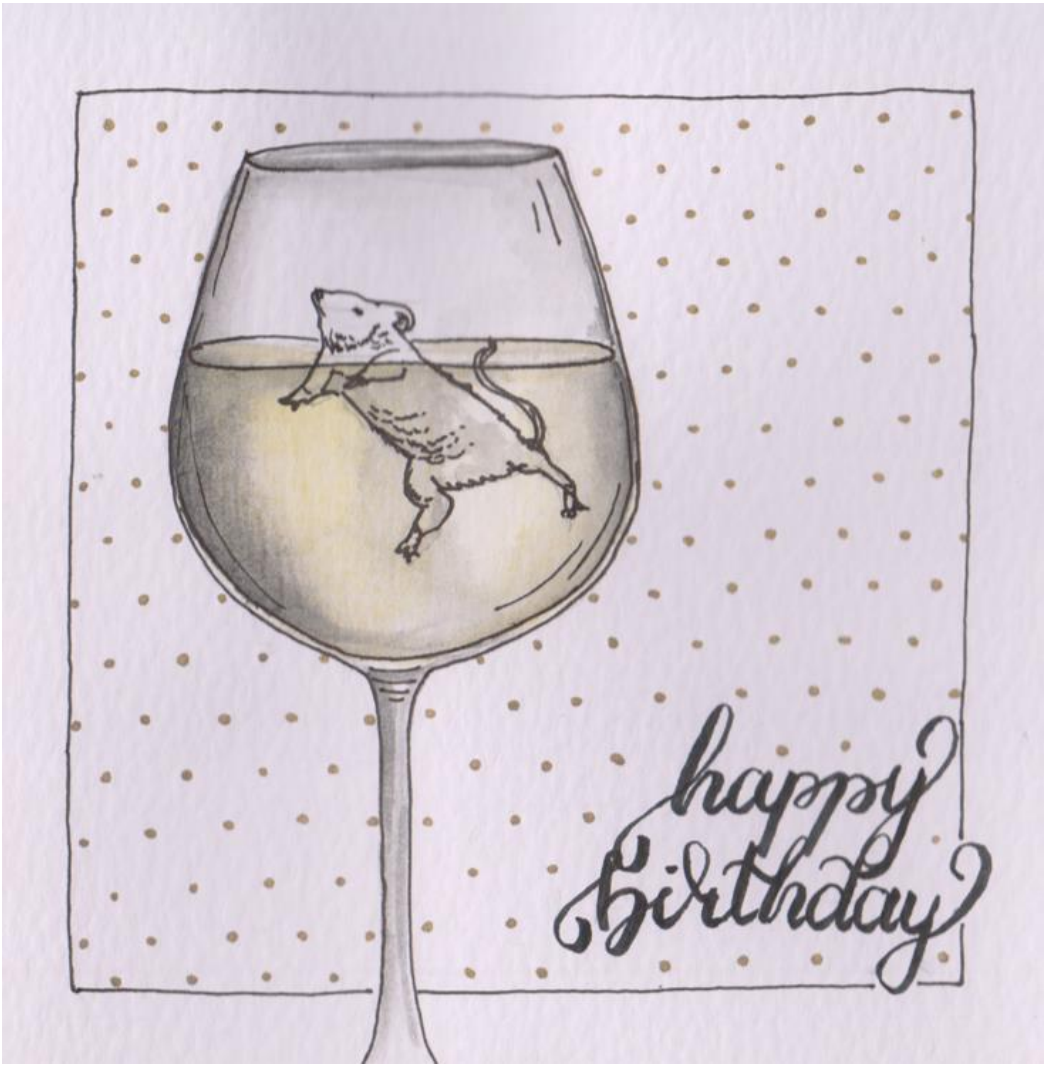
The contribution of the systemic inflammatory response to the outcome of spinal cord injury

Abi George Yates, MSci (Hons)

Oriel College, University of Oxford, Oxford UK



A thesis submitted for the degree of Doctor of Philosophy, Department of Pharmacology, University of Oxford



This beautiful birthday card, by my dear friend, Marta Bielinska, perfectly summarises my DPhil experience – mice and wine.

Abstract

Non-resolving inflammation in the spinal cord following traumatic injury causes the progressive destruction of neuronal tissue, which exacerbates functional deficits. However, therapy targeting inflammation within the spinal cord has, to date, generated equivocal results, and there remains no clinically approved pharmacological intervention for spinal cord injury (SCI). Therefore, there is an immediate need to identify novel therapeutic targets. Traumatic central nervous system injuries, including SCI, induce near-immediate peripheral inflammation, which is described as the acute phase response (APR). Previous studies have shown that suppression of the APR can attenuate leukocyte infiltration and associated secondary damage in models of brain injury. In light of these results, it was my hypothesis that there would be a direct relationship between the magnitude of the APR and the spinal cord injury pathology, and also that therapeutic manipulation of this response would lead to improved outcomes. This was tested in a mouse contusion model of SCI, which allowed for controlled variation of both the severity and level of injury. Following injury, the systemic response was characterised throughout the first 24 hours. The studies described herein indicate that SCI induces a robust APR, as evidenced by the increased hepatic expression of pro-inflammatory mediators, leukocyte mobilisation into the blood, and also recruitment to the liver and spleen. The magnitude of this response was dependent on the severity and level of injury, but the relationship was more complex than anticipated. Importantly, the APR preceded leukocyte infiltration to the spinal cord and, for this reason, a not previously recognised "therapeutic window" appears to exist. Here, a rapid increase in IL-1β expression within the liver was found to be a prominent feature of SCI that preceded the expression of the endogenous antagonist IL-1RA. IL-1RA was administered to rectify the early mismatch in expression, and, as a consequence, inflammation in the spinal cord was reduced. Further exploration of the systemic response to SCI revealed metabolite changes in peripheral tissues that were predictive of patient outcome. In mice, the acute metabolite changes were similar in sham and spinal cord injured mice but, at later time points, the SCI had an impact on the peripheral metabolome that was distinct from the changes induced by a sham operation. Normalisation of these changes might be expected to prevent some of the downstream peripheral sequelae associated with SCI. The role of extracellular vesicles (EVs)

as possible mediators of the APR was also explored. Plasma EVs were significantly increased two hours post-SCI, and EVs, isolated from donor SCI animals, were able to alter the hepatic expression profile of inflammatory genes *in vivo* in recipient animals. These results suggest that circulating EVs after SCI may serve to regulate the APR. Collectively, the data presented in this thesis show that SCI induces significant systemic changes that are dependent on the nature of the lesion and appear to influence the penultimate outcome. Manipulation of the APR in the first 24 hours after an SCI is a very accessible and mostly overlooked target for therapeutic intervention. IL-1RA treatment was already shown to be an effective therapy here, but my studies also highlight the abnormal expression of other cytokines by the liver, which could also be additionally targeted. It is shown that manipulation of circulating EV populations or the peripheral metabolome might otherwise also prove beneficial after SCI.

Acknowledgements

I am privileged to have undertaken this DPhil, to have worked in two, world-class institutions and to have met so many incredible people, who have made this experience so rewarding and memorable.

Firstly, to my supervisors. Daniel, the knowledge, skill, and alcohol tolerance that I have gained from you over the past 4 years has been invaluable. Thank you for your ongoing support and guidance, and I look forward to continuing our work together. Marc, thank you for making me feel so welcome in Brisbane, despite being thousands of miles from home. To have learnt from your impressive experience in SCI research has been amazing, I have thoroughly enjoyed working with you and hope to again soon. Yvonne, I am forever grateful for your expertise, insight and above all, patience. Thank you for putting up with my endless bullet points and numerous drafts – I do not doubt that this thesis is complete because of you. Your dog pictures and science memes have provided me with great entertainment, and I hope I have done you proud as the "first pancake".

Thank you to various collaborators, Suzie Anthony, Dave Carter, Naveed Akbar, Jana Vukovic and Emily Willis, for the opportunities to work on a variety of different projects during my DPhil. To my colleagues in the Welfare team at Oriel College; being a Junior Dean has been a rewarding experience, one which I have thoroughly enjoyed alongside my academic work – *Floreat Oriel*. I'd like to make a special thanks to Helen Stolp, my Master's supervisor at King's College London, who recommended me for the position, and to ISRT for their generous financial support, I would not be here without you.

A special thank you to members and visitors of the Anthony and Ruitenberg laboratories. Thank you to Fay Probert, who kindly taught me ^{1}H NMR metabolomics and multivariate analysis – Chapter 5 would not exist without your guidance. Thank you to Daniel Radford-Smith, Pippa Gleave and Karolina Weglinska for the entertainment and help throughout my time in Oxford, including midnight experiments and the weekly "PI And Researchers Training Initiative". And to Steven Dierksmeier, my first FHS student, for your assistance with the injury severity experiments – you've set the bar high for all future students.

To my Aussie friends, thank you to Trisha Jogia, Ellen Gillespie, Thomas Lao, Del Jung and Lydia Beaton. Our trips to Canberra for Spilt Milk festival, East Street food market and numerous bottomless brunches made for an incredible “study abroad” experience, and I look forward to when I can see you all again.

Thank you to my friends at both Somerville College and Oriel College for an unforgettable 4 years. Finally, I would like to thank my family. Mum and Dad, you have forever supported me and provided me with anything I could need for me to succeed, whether that be words of encouragement or food care packages. I love you both, dearly.

Publications during candidature

Hazelton, I.*, **Yates, A.G.***, Dale, A., Roodselaar, J., Akbar, N., Ruitenberg, M.J., Anthony, D.C. & Couch, Y. (2018) Exacerbation of acute traumatic brain injury by circulating extracellular vesicles. *Journal of Neurotrauma. 35*(4):639-651.

*Authors contributed equally to this work

Stolp, H.B., Fleiss, B., Aria, Y., Supramaniam, V., Vontell, R., Birtles, S., **Yates, A.G.**, Baburamani, A.A., Thornton, C., Rutherford, M., Edwards, A.D. & Gressens, P. (2019) Interneuron development is disrupted in preterm brains with diffuse white matter injury: observations in mouse and human. *Frontiers Physiology. 10*:955.

Yates, A.G., Anthony, D.C., Ruitenberg, M.J. & Couch, Y. (2019) Systemic immune response to traumatic CNS injuries – are extracellular vesicles the missing link? *Frontiers Immunology. 10*:2723.

Willis, E.F., MacDonald, K.P.A., Nguyen, Q.H., Labrador Garrido, A., Gillespie, E.R., Harley, S.B.R., Bartlett, P.F., Schroder, W., **Yates, A.G.**, Anthony, D.C., Rose-John, S., Ruitenberg, M.J. & Vukovic, J. (2020) Repopulating microglia promote brain repair in an IL-6-dependent manner. *Cell. 180*(5):833-846.

Yates, A.G., Jogia, T., Gillespie, E.R., Couch, Y., Ruitenberg, M.J. & Anthony, D.C. (2021) Acute IL-1RA treatment suppresses the peripheral and central inflammatory response to spinal cord injury. *Journal of Neuroinflammation. 18*(1):15.

Conference presentations during candidature

International Spinal Research Trust (ISRT) Network Meeting, London UK, 1st-2nd September 2017. Extracellular vesicles and acute spinal cord injury. *Poster presentation.*

Oxosome Annual Meeting, Oxford UK, 26th October 2017. Exacerbation of acute traumatic brain injury by circulating extracellular vesicles. *Oral presentation.*

UK-EV Forum, Birmingham UK, 12th December 2017. Exacerbation of acute traumatic brain injury by pro-inflammatory macrophage-derived extracellular vesicles. *Oral presentation.*

International Society of Neuroimmunology (ISNI) Congress, Brisbane Australia, 27th-31st August 2018. Exacerbation of acute traumatic brain injury by pro-inflammatory macrophage-derived extracellular vesicles. *Oral presentation.*

School of Biomedical Sciences Postgraduate Symposium, Brisbane Australia, 19th November 2018. The role of extracellular vesicles in the pathology of traumatic CNS injuries. *Oral presentation.*

International Spinal Research Trust (ISRT) Network Meeting, London UK, 6th-7th September 2019. The systemic response to SCI: the role of extracellular vesicles. *Poster presentation.*

International Spinal Research Trust (ISRT) SCI Research Seminars, International online, 29th September 2020. The systemic response to spinal cord injury – a novel therapeutic target. *Oral presentation.*

Table of contents

Abstract *ii*

Acknowledgements *iv*

Publications during candidature *vi*

Conference presentations during candidature *vii*

Table of contents *viii*

Table of figures *xiv*

Table of tables *xvii*

List of abbreviations *xviii*

Chapter 1: Introduction **1**

1.1 Introduction to spinal cord injury (SCI) **3**

1.1.1 Epidemiology of SCI *3*

1.1.2 Classification of SCI *3*

1.1.3 Current treatments *8*

1.2 Pathophysiology of SCI **10**

1.2.1 Primary phase *10*

1.2.2 Secondary phase *10*

1.2.3 The central response to SCI *13*

1.2.3.1 The blood-spinal cord barrier *13*

1.2.3.2 Soluble mediators *14*

1.2.3.3 Microglia *16*

1.2.3.4 Astrocytes *19*

1.2.4 The systemic response to SCI *22*

1.2.4.1 Neutrophils *27*

1.2.4.2 Monocytes and macrophages *29*

1.2.4.3 T- and B-lymphocytes *32*

1.2.5 Extracellular Vesicles *34*

1.3 Experimental SCI **39**

1.3.1 Rodent models of SCI 39
1.3.2 Treatments under investigation 44
1.3.2.1 Neuroprotective 44
1.3.2.2 Regenerative 45
1.3.2.3 Immunomodulatory 48
1.4 Aims of this thesis **52**
Chapter 2: Materials and methods **54**
2.1 Human plasma sample collection **55**
2.2 Animals **57**
2.3 Animal CNS injury models **57**
2.3.1 Spinal cord injury (SCI) model 57
2.3.2 Experimental design 58
2.4 Behaviour **59**
2.4.1 Basso mouse scale (BMS) 59
2.5 Tissue collection **60**
2.6 Peripheral leukocyte analysis **60**
2.6.1 Flow cytometry 60
2.7 Histology **64**
2.7.1 Immunohistochemistry with DAB 64
2.7.2 Immunofluorescence 64
2.7.3 Quantification and analysis of histology 65
2.8 Molecular biology **67**
2.8.1 mRNA extraction 67
2.8.2 cDNA conversion and qPCR 67
2.8.3 miRNA analysis 67
2.9 High pressure liquid chromatography (HPLC) **68**
2.10 Metabolomics **69**
2.10.1 Sample preparation 69

2.10.2 NMR experiments 69

2.10.3 NMR data pre-processing 70

2.11 EV analysis 70

2.11.1 EV isolation 70

2.11.2 EM imaging 70

2.11.3 Western blot 71

2.11.4 EV measurements 71

2.11.5 EV labelling 72

2.12 Cell culture 72

2.12.1 Human peripheral blood mononuclear cell (PBMC) isolation 72

2.13 Statistical analysis 73

Chapter 3: Acute IL-1RA treatment suppresses the peripheral and central inflammatory response to spinal cord injury 75

3.1 Introduction and aims 76

3.2 Methods specific to this chapter 80

3.2.1 Animals 80

3.2.2 SCI model 80

3.2.2.1 Treatment with IL-1RA 80

3.3 Results 81

3.3.1 SCI induces IgG infiltration, microglial cell death and neutrophil infiltration 81

3.3.2 SCI induces expression of inflammation-associated genes in the liver 83

3.3.3 SCI induces leukocyte mobilisation in the periphery 85

3.3.4 Peripheral IL-1RA treatment suppresses the SCI-induced APR 88

3.3.5 Peripheral IL-1RA reduces markers of secondary injury in the spinal cord 88

3.4 Discussion 91

3.4.1 SCI induces a robust APR which precedes spinal cord lesion progression 91

3.4.2 IL-1β and IL-1RA in secondary damage after SCI 93

3.5 Conclusions from this chapter 97

Chapter 4: The systemic response to spinal cord injury is both lesion level and injury severity dependent 99

4.1 Introduction 100

4.2 Methods specific to this chapter 103

4.2.1 Animals 103

4.2.2 SCI model 103

4.2.3 Spinal cord qPCR 103

4.3 Results 104

4.3.1 The magnitude of lesion pathology is injury severity dependent at T9 104

4.3.2 The magnitude of lesion pathology is injury severity dependent at T2 107

4.3.3 Expression of inflammation-associated genes in the spinal cord is SCI severity dependent 110

4.3.4 APR induced by SCI at T9 is injury severity dependent 113

4.3.5 APR induced by SCI at T2 is differentially injury severity dependent 116

4.3.6 SCI-induced APR is injury level dependent 118

4.3.7 HPLC results 120

4.4 Discussion 122

4.4.1 Spinal cord pathology is injury severity and lesion level dependent 122

4.4.2 SCI-induced APR is injury severity dependent 124

4.4.3 SCI-induced APR is lesion level dependent 126

4.5 Conclusions from this chapter 128

Chapter 5: SCI induces a metabolite signature in the periphery 129

5.1 Introduction and aims 130

5.2 Methods specific to this chapter 133

5.2.1 Human plasma 133

5.2.2 Animals and spinal cord injury model 133

5.2.3 Spinal cord tissue processing 133

5.3 Results 134

5.3.1 Acute SCI induces a metabolite signature in the periphery 134

5.3.2 SCI-induced changes in metabolite profiles are injury severity and lesion level dependent 142

5.3.2.1 Plasma 142

5.3.2.2 Liver 147

5.3.2.3 Spinal cord 152

5.3.3 Plasma metabolite profile as a predictor of patient outcome after SCI 157

5.4 Discussion 159

5.4.1 SCI induces a metabolite signature in the periphery 159

5.4.2 Central and peripheral metabolome are injury severity dependent 162

5.4.3 Plasma metabolites as prognostic markers after SCI 164

5.5 Conclusions from this chapter 166

5.6 Supplementary Figures for this chapter 168

Chapter 6: The contribution of extracellular vesicles to SCI 169

6.1 Introduction and aims 170

6.2 Methods specific to this chapter 173

6.2.1 Human plasma samples 173

6.2.2 Animals and spinal cord injury model 173

6.2.3 EV isolation and measurement 173

6.2.4 EV biodistribution 173

6.2.5 EV adoptive transfer – in vitro 174

6.2.6 EV adoptive transfer – in vivo 174

6.3 Results 175

6.3.1 SCI had no effect on circulating EVs in human plasma 175

6.3.2 SCI induced a hyperacute increase in circulating EVs, in a rodent contusion model 179

6.3.3 Circulating EVs following SCI are injury severity and lesion level dependent 181

6.3.4 SCI plasma EVs localise to APR-associated organs 184

6.3.5 SCI plasma EVs do not induce inflammation, in vitro 186

6.3.6 SCI plasma EVs alter the hepatic gene expression profile, in vivo 187

6.4 Discussion 189

6.4.1 SCI induced an increase in plasma EVs, 2 hours post-injury 189

6.4.2 SCI plasma EVs and the APR 193

6.5 Conclusions from this chapter 195

Chapter 7: General discussion 196

7.1.1 The role of the APR in SCI 199

7.1.2 Hepatic IL-1β as a therapeutic target for acute SCI 202

7.1.3 Brain vs. spinal cord 204

7.1.4 Future directions 206

7.1.5 Limitations 208

7.2 Concluding remarks 209

7.3 References 210

Appendix 243

Table of figures

Figure 1.1 Anatomy of the spinal cord. 5

Figure 1.2 Time course of spinal cord pathology and inflammation in the human after traumatic injury. 12

Figure 1.3 Pathophysiology of spinal cord injury. 15

Figure 1.4 Time course of the systemic response to SCI. 22

Figure 1.5 SCI-IDS is caused by a dysfunctional sympathetic-neuroendocrine adrenal reflex. 25

Figure 1.6 Visual representation of proposed hypothesis of EV-mediated activation of the APR following SCI. 38

Figure 1.7 Spinal cord leukocyte recruitment across species. 43

Figure 1.8 Pathophysiology of SCI: therapeutic targets. 51

Figure 2.1 Gating strategy for blood myeloid cells. 62

Figure 2.2 Gating strategy for spleen myeloid cells. 63

Figure 2.3 Schematic of OPLS-DA statistical analysis. 74

Figure 3.1 IL-1β signalling and opportunities for therapeutic intervention. 79

Figure 3.2 IL-1RA treatment strategy. 80

Figure 3.3 IgG infiltration, microglial and neutrophil density in the injured spinal cord. 82

Figure 3.4 Expression of inflammation-associated genes in the liver following SCI. 84

Figure 3.5 Leukocyte mobilisation in the periphery following SCI. 87

Figure 3.6 SCI-induced peripheral inflammation with IL-1RA treatment. 89

Figure 3.7 Spinal cord lesion pathology with IL-1RA treatment 90

Figure 3.8 Proposed mechanism of action of IL-1RA treatment. 98

Figure 4.1 The magnitude of functional loss and spinal cord lesion pathology following SCI of different injury severities at level T9. 105

Figure 4.2 Spinal cord lesion pathology following SCI of different injury severities at level T9. . 106

Figure 4.3 The magnitude of functional loss and spinal cord lesion pathology following SCI of different injury severities at level T2. 108

Figure 4.4 Spinal cord lesion pathology following SCI of different injury severities at level T2. . 109

Figure 4.5 Expression of inflammation-associated genes in the spinal cord following SCI. 112
Figure 4.6 The magnitude of the hepatic APR following SCI of different injury severities at level T9. 114
Figure 4.7 Leukocyte density in the liver following SCI of different injury severities at level T9.. 115
Figure 4.8 The magnitude of the APR following SCI of different injury severities at level T2. 117
Figure 4.9 Expression of inflammation-associated genes in the liver following T2 and T9 SCI. .. 119
Figure 4.10 Concentrations of corticosterone and noradrenaline in the plasma following SCI. ... 121
Figure 5.1 Human plasma metabolites following SCI. 135
Figure 5.2 Mouse plasma metabolites following SCI. 138
Figure 5.3 Mouse liver metabolites following SCI. 141
Figure 5.4 PCA scores plot of plasma metabolite profiles following SCI. 143
Figure 5.5 Perturbed plasma metabolites following SCI. 145
Figure 5.6 Key plasma metabolites disturbed following SCI. 146
Figure 5.7 PCA scores plot of liver metabolite profiles following SCI. 148
Figure 5.8 Liver metabolites disturbed following SCI. 150
Figure 5.9 Key liver metabolites disturbed following graded SCI. 151
Figure 5.10 PCA scores plot of spinal cord metabolite profiles following SCI. 153
Figure 5.11 Metabolites in the spinal cord perturbed after traumatic injury. 155
Figure 5.12 Metabolites in the spinal cord perturbed after traumatic injury. 156
Figure 5.13 Prediction of patient outcome with plasma metabolites. 158
Figure 5.14 Summary of SCI-induced metabolite changes in the rodent model. 167
Figure 6.1 Characterisation of plasma EVs following SCI in human patients. 177
Figure 6.2 Correlations of plasma EV concentration and human SCI parameters 178
Figure 6.3 Plasma EV concentration and size during the acute phase of SCI. 180
Figure 6.4 Plasma EV concentration and size following SCI at T9, 6 hours post-injury. 182
Figure 6.5 Plasma EV concentration and size following SCI at T2, 6 hours post-injury. 183
Figure 6.6 *In vivo* biodistribution of SCI plasma EVs. 185

Figure 6.7 Expression of inflammation-associated genes in PBMCs incubated with human SCI plasma EVs. 186
Figure 6.8 Hepatic expression of pro-inflammatory genes in response to naïve and SCI plasma EVs, 30 minute time point. 187
Figure 6.9 Hepatic expression of pro-inflammatory genes in response to naïve and SCI plasma EVs, 6 hour time point. 188
Figure 7.1 Visualisation of SCI-induced systemic response 198
Figure 7.2 Relationship between the APR and spinal cord neutrophil recruitment. 201

Supplementary Figure 5.1 OPLS-DA scores plot of rodent plasma metabolite profiles following SCI. 168
Supplementary Figure 5.2 Time between first and last ASIA score for SCI patients 168

Table of tables

Table 2.1 SCI patients demographics. 56

Table 2.2 Flow cytometry Antibodies. 62

Table 2.3 Antibodies for immunohistochemistry 66

Table 2.4 qPCR primers. 68

Table 2.5 Antibodies used for western blotting. 71

Table 5.1 Models generated with plasma metabolites following SCI. 136

Table 5.2 Models generated with liver metabolites following SCI. 139

List of abbreviations

ABC	Avidin-biotin complex
AD	Alzheimer's disease
APP	Acute phase protein
APR	Acute phase response
ASIA	American spinal cord injury association
BBB	Blood brain barrier
BSCB	Blood spinal cord barrier
C	Cervical
ChABC	Chondroitinase ABC
CNS	Central nervous system
CRP	C-reactive protein
CSF	Cerebrospinal fluid
CSPGs	Chondroitin sulphate proteoglycans
DAB	3,3'-Diaminobenzidine
DAMPs	Damage-associated molecular patterns
EAE	Experimental allergic encephalomyelitis
EVs	Extracellular vesicles
GFAP	Glial fibrillary acidic protein
HPLC	High performance liquid chromatography
Iba-1	Ionised calcium binding adaptor molecule 1
ICAM-1	Intracellular adhesion molecule 1
IFN(-γ)	Interferon (-γ)
IL-	Interleukin-
IL-1β	Interleukin-1β
IL-1RA	Interleukin-1 receptor antagonist
IL-1RAcP	Interleukin-1 receptor accessory protein
i.p.	Intraperitoneal
iPSC	Induced pluripotent stem cell
i.v.	Intravenous
IVIg	Intravenous immunoglobulin
kD	kilodyne
LPS	Lipopolysaccharide
MS	Multiple sclerosis
MSC	Mesenchymal stem cell
MODS	Multi-organ dysfunction syndrome
NF-κB	Nuclear factor-κB

NMR	Nuclear magnetic resonance
NOGO	Neurite outgrowth inhibitory protein
NSCs	Neural stem cells
OECs	Olfactory ensheathing cells
PAMPs	Pathogen-associated molecular patterns
PRR	Pattern recognition receptor
qPCR	Quantitative polymerase chain reaction
ROS	Reactive oxygen species
RT	Room temperature
SAA(-2)	Serum amyloid A(-2)
SCI	Spinal cord injury
SCI-IDS	Spinal cord injury-associated immunodeficiency syndrome
SIRS	Systemic inflammatory response syndrome
T	Thoracic
TBI	Traumatic brain injury
TGF-β	Transforming growth factor β
TLR	Toll-like receptor
TNF	Tumour necrosis factor
VCAM-1	Vascular cell adhesion molecule 1

Chapter 1: Introduction

Spinal cord injury (SCI) is defined as damage to the spinal cord, which causes temporary or permanent deficits in motor, sensory and/or autonomic function (Alizadeh et al. 2019). Recent advancements in medical management has led to a dramatic decrease in patient mortality, yet there has been no corresponding improvement in morbidity. As a result, SCI remains a leading cause of disability, affecting over 27 million people, globally (Injury and Spinal Cord Injury 2019), at a substantial financial and emotional cost. The primary, physical damage caused by SCI is unavoidable, however, the ongoing, non-resolving inflammation in the spinal cord causes additional injury and may be amenable to therapeutic intervention. Sadly, whilst acute treatments are available for stroke (Phipps and Cronin 2020) and traumatic brain injury (TBI) (Vella et al. 2017) to minimise this secondary damage, there is currently no clinically approved, therapeutic interventions for SCI that are recommended for routine use (Ahuja et al. 2017a). Therefore, there is a need to develop alternative strategies to target the inflammatory response in the spinal cord and improve functional outcomes after SCI.

Previous work from our laboratory has demonstrated that the magnitude of inflammation in the central nervous system (CNS) is dependent on a peripheral inflammatory response, termed the acute phase response (APR) (Campbell et al. 2008a; Campbell et al. 2005). Critically, it has been shown that inhibition of the APR in models of brain injury reduces central inflammation (Campbell et al. 2003; Campbell et al. 2007; Clausen et al. 2014), which suggests that the APR could be a therapeutic target for the acute treatment of SCI. However, many key questions remain, for example, the extent to which the APR contributes to lesion pathology is not clear. Moreover, it is unknown the mechanism by which the spinal cord communicates with the peripheral immune system. As such, it was the aim of this thesis to comprehensively characterise the systemic inflammatory response induced by SCI, and investigate the underlying signalling mechanism, to evaluate whether the APR can be manipulated to improve SCI outcomes.

This introduction aims to provide an overview of the pathophysiology of SCI, and the status of treatment strategies under investigation.

1.1 Introduction to spinal cord injury (SCI)

1.1.1 Epidemiology of SCI

The spinal cord acts as a conduit between the CNS and peripheral tissues and plays a critical role in motor, sensory and autonomic function. Therefore, damage to this structure can result in devastating physiological consequences. Globally, there are approximately 27 million people living with spinal cord injuries, which equates to 9.5 million years of life lived with disability (Injury and Spinal Cord Injury 2019). In the UK, there are over 16,000 new cases each year, which disproportionally affect men, at a ratio of 4:1 (Ahuja et al. 2017a; Chen et al. 2016). The age distribution of SCI patients is bimodal with an initial peak of incidence in young adults, and a second peak of adults over the age of 60 (Ahuja et al. 2017a). Whilst intraspinal infections, ischemia and tumours can all result in non-traumatic SCI, the majority of SCI cases occur due to physical trauma (Alizadeh et al. 2019; Anwar et al. 2016). Falls are the most prevalent cause, accounting for more than 50% of age-standardised incidents across nine different geographical regions (Injury and Spinal Cord Injury 2019). Additional leading causes of SCI include motor vehicle accidents, sports injuries and violence. In the past few decades, vast improvements in mortality have been achieved, however morbidity has continued at a great, and additive, financial cost (Middleton et al. 2012). Lifetime costs of SCI in the UK have been estimated at £1.43 billion, at an average of £1.12 million per case (McDaid et al. 2019).

1.1.2 Classification of SCI

SCI presents largely heterogeneously and outcome is dependent on the lesion level and severity of the injury. Lower thoracic injuries result in paraplegia, where sensory and motor function of the arms and trunk are largely spared, whereas high thoracic and cervical injuries cause tetraplegia, which affects all four limbs (Figure 1.1). Cervical injuries are most prevalent (50%), potentially due to the increased rotational ability of the cervical vertebrae compared to the rest of the spinal column, making them more vulnerable to damage (Torretti and Sengupta 2007), followed by thoracic (35%) and lumbar injuries (11%) (Hachem et al. 2017). SCI can also be defined as complete,

or incomplete (Alizadeh et al. 2019). A complete injury is described as total loss of function below the injury level, and both sides of the body are affected equally. Incomplete injury is evident when some function and feeling remains below the lesion site, and typically one side retains more motor and sensory function than the other. Incomplete injuries can be further classified according to the region of spinal cord affected; central cord syndrome and anterior cord syndrome affect the central grey matter and ventral portion, respectively, whereas Brown-Séquard syndrome affects one hemisphere, resulting in different ipsilateral and contralateral, motor and sensory consequences.

The degree of SCI is determined using the American spinal injury association (ASIA) impairment scale, which involves testing myotomes and dermatomes corresponding to defined muscle groups and areas of skin (van Middendorp et al. 2011; Maynard et al. 1997; Burns and Ditunno 2001). The scale ranges from complete loss of motor and sensory function (ASIA A) to normal neurological function (ASIA E) and is determined by collating information about preserved sensory and motor function, neurological level of injury, and the completeness and severity of the injury (Alizadeh et al. 2019). In this way, ASIA score can be used to predict the functional outcome of patients. For example, 91.7% of patients diagnosed as ASIA A will remain incapable of independent ambulation, compared to 60.6% and 38.2% of those diagnosed as ASIA B and C, respectively (van Middendorp et al. 2011). However, SCI classification can be impeded by spinal shock. Spinal shock is defined as a loss of sensation accompanied by motor paralysis with initial loss but gradual recovery of reflexes (Ditunno et al. 2004). Immediately following SCI, reflexes below the level of injury are depressed (hypoflexia) or absent (areflexia), due to loss of descending innervation. As days and weeks follow, reflexes return in predictable phases as novel synapses are established, but more receptors can be expressed acutely causing hypersensitivity to stimulation. Therefore, ASIA scoring is typically completed 72 hours after injury in order to provide accurate prognosis (Alizadeh et al. 2019).

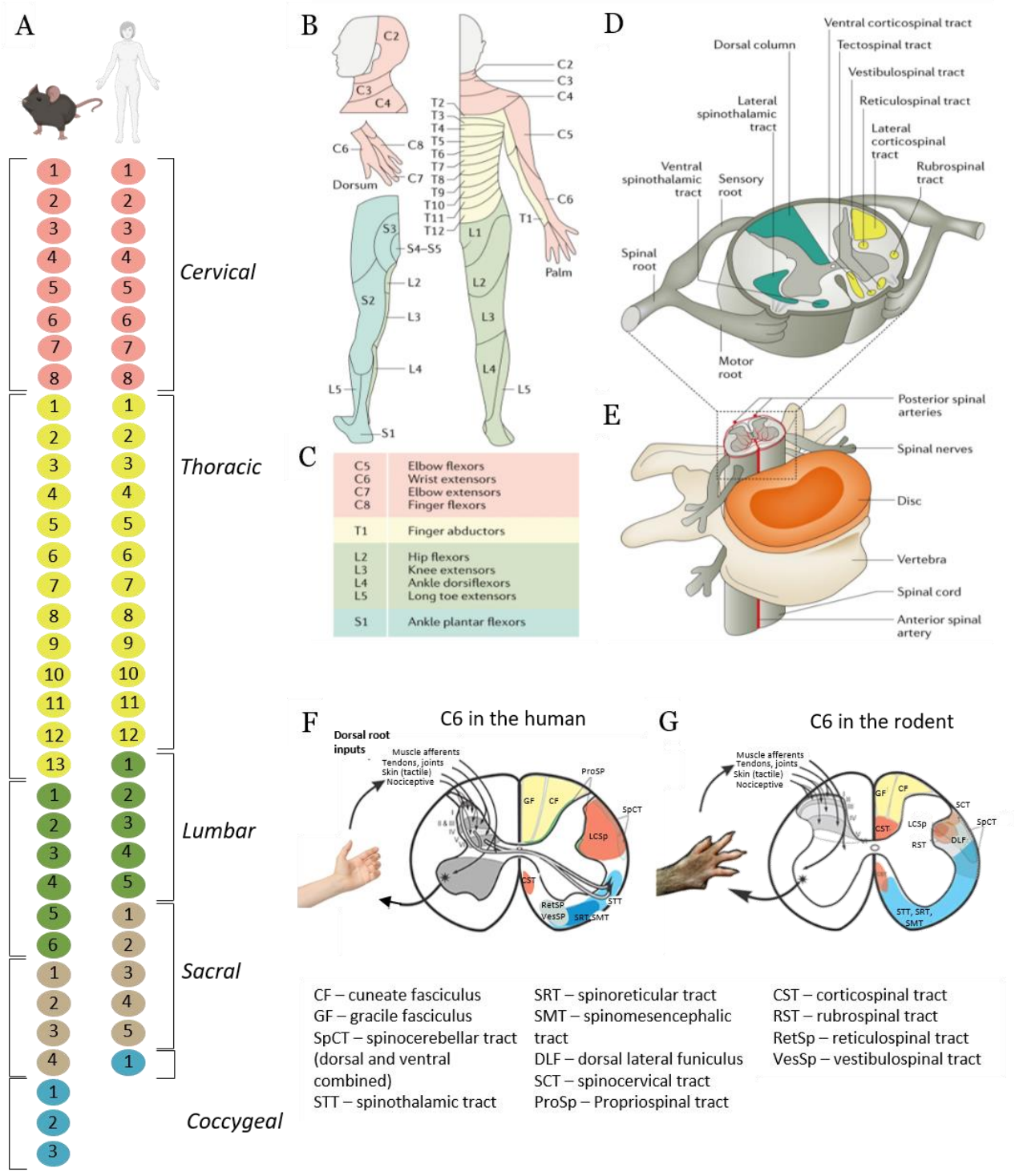


Figure 1.1 Anatomy of the spinal cord. The spinal cord connects the brain to the rest of the body and is encased in a bony vertebral column. It is organised into segments, which corresponds to 8 cervical, 12 thoracic, 5 lumbar, 5 sacral and 1 coccygeal segment in the human, and 8 cervical, 13 thoracic, 6 lumbar, 4 sacral and 3 coccygeal segments in the rodent (A). Each segment innervates a specific region of the body (B, C). Key white matter tracts in the human spinal cord (D). Blood is supplied to the spinal cord via the anterior and the left and right posterior arteries (E). Comparison of key ascending and descending tracts in the human (F) and the rodent (G); most notably, the corticospinal tract descends ventral and lateral in the human spinal cord, but dorsal in the rodent spinal cord. Figure adapted from (Ahuja et al. 2017b) and (Darian-Smith and Fisher 2019).

From the moment of trauma, SCI causes profound physiological changes. The spinal cord governs the autonomic nervous system; the parasympathetic branch is predominantly controlled by the vagus nerve, which originates from the medulla oblongata in the brain stem, whilst pre-ganglionic neurons of the sympathetic branch extend from the thoracolumbar region (T1-L2/3). Therefore, with lesions above T6, parasympathetic innervation of peripheral organs remains intact, whereas innervation of the sympathetic nervous system is interrupted, which often results in autonomic dysreflexia. Constitutive stimulation of the vasculature to maintain sympathetic tone is lost, which causes blood vessels to relax and dilate, resulting in dangerously low blood pressure, low heart rate and bradyarrhythmia. This is known as neurogenic shock and can be life-threatening (Ruiz et al. 2018). High thoracic (T1-6) and cervical injuries (C1-8) can also cause respiratory dysfunction, as denervation of muscles required for breathing (diaphragm, intercostal muscles) results in reduced vital capacity, which may, in turn, require mechanical ventilation. Certainly, this becomes a necessity with injuries above the level of phrenic motorneurons (C3-5) where complete paralysis of muscles of both inhalation and exhalation occurs. As a result, the ability to cough, which is required to clear bacteria and secretions from the lungs, can be weakened, leaving the patient at increased risk of infections such as pneumonia. Additional autonomic changes include an increase in circulating cortisol owing to denervation of the adrenal glands, and patients often require catecholamine treatment (Pruss et al. 2017). Identification, and treatment, of these changes are critical for appropriate acute patient care.

In the long term, consequences of SCI are not limited to motor and sensory loss. Neuropathic pain and spasticity are common because of structural compromise, as well as muscle atrophy and pressure sores due to immobility (Anwar et al. 2016). Disturbances in body composition such as hormonal imbalance, metabolic dysfunction and increased fat deposition are also often observed (Gorgey et al. 2014), which contribute to impaired glucose tolerance and insulin resistance (Goodus and McTigue 2020; Lee et al. 2005). Indeed, SCI patients are at greater risk of developing a range of metabolic disorders including cardiovascular disease, dyslipidaemia and diabetes (Banerjea et al. 2008; Cragg et al. 2013a; Cragg et al. 2013b). Whilst this can be partially attributed to decreased physical activity and muscle loss, immobility alone cannot fully explain the increased disease risk

(Smith and Yarar-Fisher 2016). Chronic autonomic dysregulation has been implicated as a contributing factor; patients with higher level injuries (high thoracic and cervical SCI) exhibit greater deficits in glucose and lipid metabolism (Raymond et al. 2010; Storch et al. 2005) than in patients with lower level injuries and non-injured individuals. However, mechanistic studies are yet to be completed.

SCI patients are also more susceptible to neurodegenerative disorders including multiple sclerosis (Lin et al. 2015), dementia (Huang et al. 2017), Alzheimer's disease (Yeh et al. 2018; Mahmoudi et al. 2021) and Parkinson's disease (Yeh et al. 2016). Although the underlying mechanisms are unknown, evidence suggests immune dysfunction plays a critical role; the trauma of SCI releases CNS-associated antigens, which may be responsible for provoking immune recognition (Yeh et al. 2016; Ankeny et al. 2009). As a result, these activated leukocytes may recognise and attack CNS proteins and cells. Certainly, SCI has been shown to activate B-cells (Ankeny et al. 2006; Ankeny and Popovich 2010) and autoantibodies have been detected in patients (Hayes et al. 2002), which may cause neurodegeneration in otherwise healthy CNS tissue (Ankeny et al. 2009). Systemic inflammation, as evidenced by increased circulating pro-inflammatory molecules, has also been shown to accelerate neurodegeneration (Cunningham et al. 2009) and is known to be triggered following SCI (Campbell et al. 2005; Hassanshahi et al. 2013; Kesani et al. 2014; Sun et al. 2016). Alternatively, SCI may induce abnormal protein deposition, which, combined with the injury-associated neuroinflammation, may initiate and/or exacerbate neurodegenerative disease mechanisms. Further studies are needed to better understand the pathophysiology of SCI-induced neurodegenerative disease if we are to increase patient survival (Yeh et al. 2016) and decrease disability in SCI.

SCI is also associated with increased prevalence of emotional disorders including anxiety and depression (Le and Dorstyn 2016; Williams and Murray 2015; Peterson et al. 2020); tetraplegics are at greater risk than paraplegics of developing depression (Khazaeipour et al. 2015). As a consequence, there is a higher incidence of suicide amongst those with SCI, compared to the general population (Savic et al. 2018). Sadly, the increased suicide rate is often considered unsurprising

owing to the effect of SCI on everyday life, but the dysfunctional immunological response to SCI has also been shown to contribute (do Espirito Santo et al. 2019; Wu et al. 2014), and a causal link between SCI-induced inflammation and the development of mood disorders has been shown. Experimental SCI has revealed an association between peripheral and spinal cord inflammation, and depressive- and anxiety-like behaviours after injury (Maldonado-Bouchard et al. 2016; do Espirito Santo et al. 2019). Moreover, the severity of SCI correlated with the extent of depressive behaviour and brain inflammation (Wu et al. 2016a). A study into the underlying mechanisms found that depressive-behaviour after SCI was associated with activated microglia in the hippocampus (Wu et al. 2014). Indeed, suppressing the inflammatory response has been shown to improve mood in SCI patients (Allison and Ditor 2015; Allison et al. 2017). However, it is unclear whether mood has an impact on functional recovery. Luedtke et al. (2014) alleviated depressive-like behaviour in a rat SCI model with selective serotonin reuptake inhibitor fluoxetine, which had no effect on motor scores. Conversely, Lee et al. (2012) reported functional improvement with the same anti-depressant drug regime, in conjunction with reduced blood spinal cord barrier (BSCB) breakdown, leukocyte infiltration and pro-inflammatory cytokine expression in the spinal cord, though these are likely to be a consequence of off-target effects (Altamura et al. 1994; Singh et al. 2001). Cumulatively, it is clear that SCI places immense burden on the physical and mental health of those affected.

1.1.3 Current treatments

Following SCI, patients typically undergo surgery in order to stabilise the spinal column and any vertebral fractures, to remove debris and decompress the cord. Ongoing pressure applied to the spinal cord, such as by bone fragments, restricts blood flow, which can cause ischemia and subsequent neuronal damage. Therefore, surgery to relieve this compression can improve blood flow and reduce the associated ischemic damage. Indeed, Dvorak et al. (2015) reported that surgery performed within 24 hours of injury, as opposed to later time points (range 24-168 hours), improved motor neurological recovery, suggesting that earlier surgical intervention best improves outcome. Although, the optimal therapeutic window for this approach remains unclear (Fehlings

and Perrin 2006). This may be combined with drainage of cerebrospinal fluid (CSF) to relieve intraspinal pressure caused by oedema (Kitchen et al. 2020) and constriction. In this way, secondary damage to the spared tissue surrounding the lesion can be limited. Early surgical intervention has also been associated with reduced incidence of acute complication, including pneumonia, and reduced length of hospital stay (Fehlings and Perrin 2006; McKinley et al. 2004). As a result, the concept of "Time is spine" has emerged, which highlights the importance of early intervention to improve prognosis (Ahuja et al. 2020).

Beyond surgery, the synthetic glucocorticoid methylprednisolone was considered standard treatment for acute SCI. Beneficial effects of methylprednisolone were first reported in human SCI patients by Bracken et al. (1990), who reported significant improvements in motor and sensory function with treatment compared to placebo. As a potent anti-inflammatory, its mechanistic efficacy was thought to be through protection from lipid peroxidation and oxidative stress caused by the host inflammatory response (Christie et al. 2008). However, subsequent randomised controlled trials found that any neurological improvements were modest and often exaggerated (Coleman et al. 2000; Ito et al. 2009; Evaniew et al. 2015). In fact, methylprednisolone has been shown to impede neurogenesis (Ye et al. 2018). It can also exacerbate oedema (Cabrera-Aldana et al. 2017), which authors attributed to suppressing the SCI-induced elevation in Aquarporin-4 expression. Moreover, treatment is associated with a number of side-effects including, but not limited to, gastrointestinal bleeding, respiratory and urinary tract infections, and sepsis (Evaniew et al. 2015; Liu et al. 2019). Therefore, it is no longer recommended for routine use.

There are acute therapies for stroke (Phipps and Cronin 2020) and TBI (Vella et al. 2017). However, as it stands, there are currently no clinically approved treatments available for acute SCI, and so there remains a great need to develop novel therapeutic interventions. One potential route for novel therapy in SCI is by targeting pathological mechanisms such as secondary injury progression.

1.2 Pathophysiology of SCI

1.2.1 Primary phase

Damage to the spinal cord following a neurotraumatic event occurs in two distinct phases (Alizadeh et al. 2019; Anwar et al. 2016). The initial, mechanical injury is defined as the primary phase, in which direct, structural damage to the spinal cord occurs. This can be classified as contusion with persistent or transient compression, distraction, laceration/transection, or a combination thereof (Alizadeh et al. 2019; Dumont et al. 2001). In humans, the most common presentation of mechanical insult is contusion with persistent compression, whereby bone fragments from vertebral burst fractures put pressure on the spinal cord, or fracture-dislocation injuries (Dumont et al. 2001). This physical insult causes disturbance to cell membranes, axon shearing and immediate cell death. Damage to blood vessels and disruption to the blood spinal cord barrier (BSCB) results in reduced blood supply and oxygen deprivation. Moreover, hypoxia, ionic imbalances and fluid accumulation drive cellular and vasogenic oedema (Kitchen et al. 2020). The primary phase occurs within a very short window of time, and is largely considered irreparable.

1.2.2 Secondary phase

Although not damaged after the initial injury, spared spinal cord tissue surrounding the lesion epicentre is highly susceptible to secondary damage, known as "bystander tissue damage" (Alizadeh et al. 2019). This is because the primary phase of SCI triggers a series of cellular, molecular and biochemical events in the spinal cord, collectively known as the secondary phase of injury (Figure 1.2). Shown to persist for days, weeks, even months after the initial insult, mechanisms of the secondary phase causes the progressive destruction of tissue initially spared after injury, which worsen functional recovery (Anwar et al. 2016; Fleming et al. 2006). This phenomenon was first described by Allen (1911), who reported that draining the intraspinal blood with a median longitudinal incision through the lesion improved motor function recovery in dogs. Allen proposed that there were two factors that contributed to injury: the direct physical impact and the subsequent influx of blood in the spinal cord (Losey and Anthony 2014). Whilst blood in the cord can cause

pressure and oedema leading to associated cell death, it was proposed that blood-borne factors could also be driving tissue damage. This finding paved the way for future studies, which have shown that the effects of secondary injury-associated damage ultimately dictate final lesion size and spared white matter, and therefore functional outcomes (Alizadeh et al. 2019; Dumont et al. 2001).

The secondary phase of injury can be further temporally divided into acute, sub-acute and chronic phases, each of which has distinct pathophysiology mechanisms (Figure 1.2). The acute phase immediately succeeds the primary, physical insult and features glutamate-mediated excitotoxicity (Park et al. 2004; Xu et al. 2004), glial cell activation, innate immune cell infiltration (neutrophils) (Fleming et al. 2006), free radical formation and oxidative stress, increased BSCB permeability, cellular damage, complement activation (Brennan et al. 2012) and release of pro-inflammatory mediators. As the lesion develops into the sub-acute phase, additional innate immune cells infiltrate the spinal cord (monocytes), as well as adaptive immune cells (T- and B-cells), which contribute to additional cell death and axonal demyelination (Ankeny et al. 2009; Fleming et al. 2006). Finally, in the chronic phase, the glial scar matures, and Wallerian degeneration, demyelination and apoptosis occurs leading to cavitation. In contrast to the primary phase, the secondary phase of injury may be amenable to therapeutic intervention by inhibiting any one or a combination of the above factors, and therefore is the subject of continued scientific research.

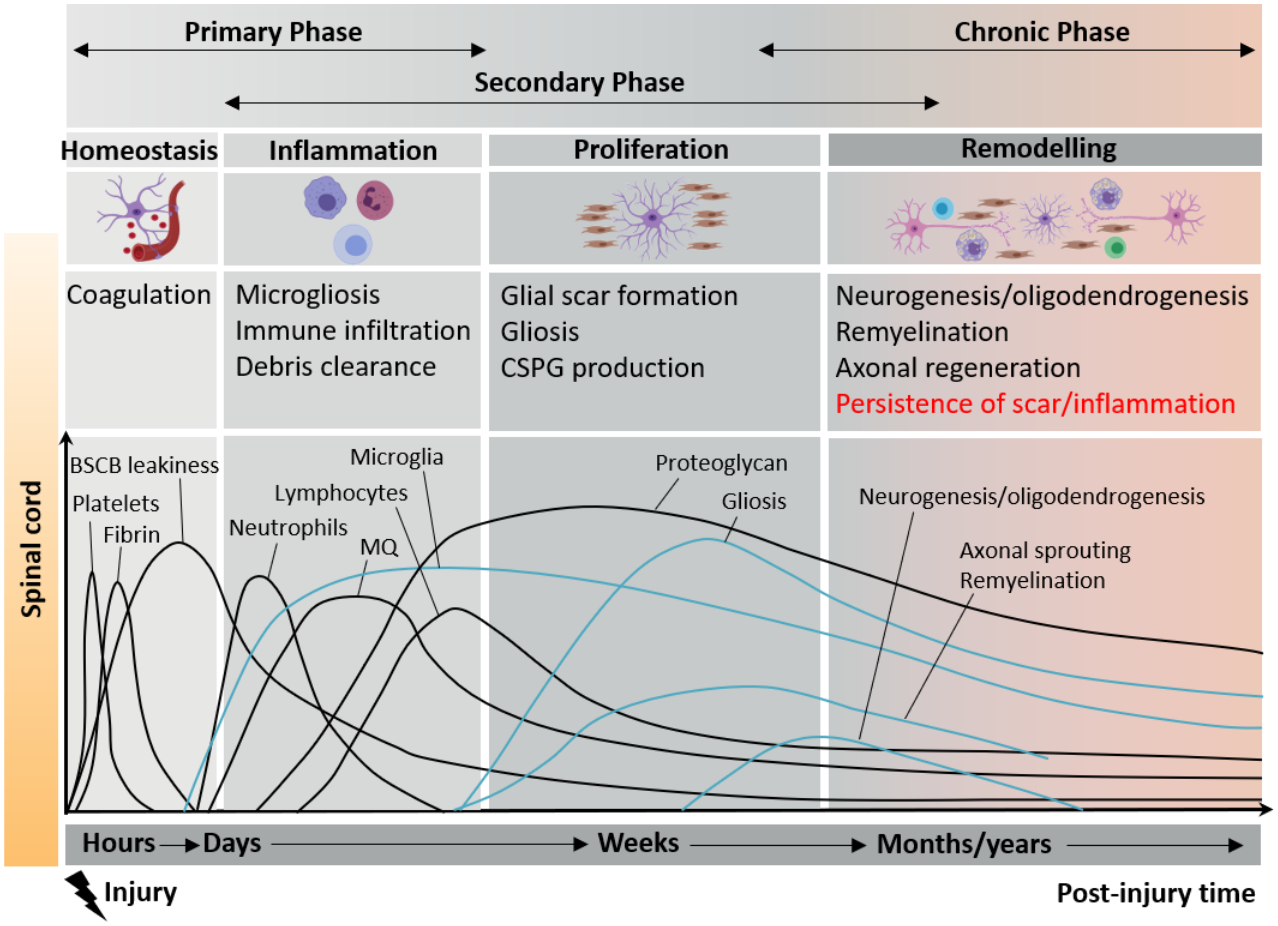


Figure 1.2 Time course of spinal cord pathology and inflammation in the human after traumatic injury. In response to trauma to the spinal cord, a sequence of neuroinflammatory events occur in distinct phases, which can persist for years after the initial injury. These phases are organised into the primary, secondary and chronic phase within which homeostasis, inflammation, proliferation and remodelling of the CNS occurs. The X axis indicates time after injury, and the Y axis indicates magnitude of response. BSCB – blood spinal cord barrier, CSPG – chondroitin sulphate proteoglycan, MQ – macrophages. Figure adapted from Shechter and Schwartz (2013).

1.2.3 The central response to SCI

1.2.3.1 The blood-spinal cord barrier

The main blood supply to the spinal cord is through three longitudinal arteries: the anterior spinal artery, and the right and left posterior arteries, with smaller intramedullary vessels and capillaries, which branch off and supply the spinal cord directly (Martirosyan et al. 2011). The blood-spinal cord barrier (BSCB) is the interface between the spinal cord parenchyma and the circulation, formed from endothelial cells, a basal membrane, pericytes and astrocytic end feet, which regulates the movement of molecules in and out of the CNS (Bartanusz et al. 2011). Physical damage to this structure is a hallmark of primary injury; whilst the larger vessels are typically spared, it is the smaller vessels that are more vulnerable to traumatic damage, and rupture (Alizadeh et al. 2019). In addition, the grey matter is more vulnerable to this haemorrhage-associated damage because it is more vascular, and, containing the cell bodies, is more energy demanding (Alizadeh et al. 2019). Initially, disruption of blood vessels allows blood components otherwise excluded from the CNS to enter the spinal cord parenchyma, which may cause direct cell death (Losey and Anthony 2014). For example, extravasated red blood cells undergo lysis and release iron (Blomster et al. 2013b), which reacts with hydrogen peroxide to generate hydroxyl radicals. This depletes endogenous anti-oxidants and causes oxidative damage by peroxidation of lipids and proteins, as well as injury to DNA (Bao and Liu 2004). Thus, haemorrhage can generate further neuronal and axonal damage, leading to exacerbated locomotor deficits (Losey et al. 2014). Indeed, functional outcome of SCI patients can be predicted from the extent of haemorrhage in the spinal cord (Boldin et al. 2006).

Dysfunction of the BSCB after SCI has been detected weeks and months after the initial damage (Popovich et al. 1996a; Whetstone et al. 2003) and contributes to the initiation of an inflammatory cascade. Expression of the adhesion molecules VCAM-1 and ICAM-1 on endothelial cells is increased (Hansen et al. 2016; Isaksson et al. 1999), whilst expression of tight junctions is decreased (He et al. 2017), which facilitate the transmigration of leukocytes into the spinal cord. Once there, these leukocytes release pro-inflammatory mediators including cytokines and reactive oxygen species (ROS), which, in turn, exacerbate primary injury. Certainly, blocking the interaction

between BSCB adhesion molecules and peripheral leukocytes inhibited their infiltration (Mabon et al. 2000) and reduced markers of oxidative damage (Geremia et al. 2012). As such, improvement in BSCB integrity has been associated with increased functional recovery (Chio et al. 2019).

1.2.3.2 Soluble mediators

Following traumatic injury, acute inflammation in the spinal cord is initiated and propagated by a series of soluble mediators, which include eicosanoids, cytokines and complement. Eicosanoids are a family of signalling molecules, derived from arachidonic acid, including prostaglandins and leukotrienes. Both mediators are increased in the spinal cord after SCI and contribute to pathophysiology (Hanada et al. 2012); prostaglandins increase oedema and vascular permeability (Sharma et al. 1993), whereas leukotrienes are potent chemoattractants and contribute to neutrophil recruitment to the spinal cord (Saiwai et al. 2010). Cytokines including IL-1β, IL-6 and TNF (Pineau and Lacroix 2007; Pineau et al. 2010), and chemokines such as CXCL1 (Campbell et al. 2002) (IL-8 in humans (Campbell et al. 2010)) are elevated in the spinal cord immediately after SCI (<5 minutes). They are produced by all the major classes of resident CNS cells (microglia, astrocytes, oligodendrocytes and neurons), although infiltrating leukocytes also contribute once they have invaded the parenchyma (Pineau and Lacroix 2007). Cytokines induce expression of adhesion molecules and act as chemoattractants, which facilitates leukocyte recruitment (Pineau et al. 2010). Moreover, they activate CNS resident and infiltrating immune cells (Figure 1.3). Interestingly, the endogenous IL-1 receptor antagonist (IL-1RA) is also upregulated in the spinal cord after injury. However, IL-1RA production is delayed in comparison to IL-1β production (Liu et al. 2008), which highlights how the lesion milieu is dominated by pro-inflammatory factors.

The complement cascade is also activated after SCI, as evidenced by increased C3a and C5a protein in the spinal cord (Brennan et al. 2015; Brennan et al. 2019). With peripheral insults, activation of this cascade mediates direct cell lysis, opsonisation of infected cells and pathogens for phagocytosis, and leukocyte chemotaxis, which aims to restore homeostasis (Brennan et al. 2012). However, in the spinal cord, complement has been shown to contribute to secondary demyelination and apoptosis, and, thus, is associated with worsened outcomes (Qiao et al. 2006). Certainly,

complement knock-out mice exhibit improved sensory and motor function following SCI (Galvan et al. 2008; Guo et al. 2010). It is important to note that whilst these soluble, pro-inflammatory mediators have a critical role in central inflammation, they are also released in the periphery and contribute to the systemic inflammatory response, which is introduced below.

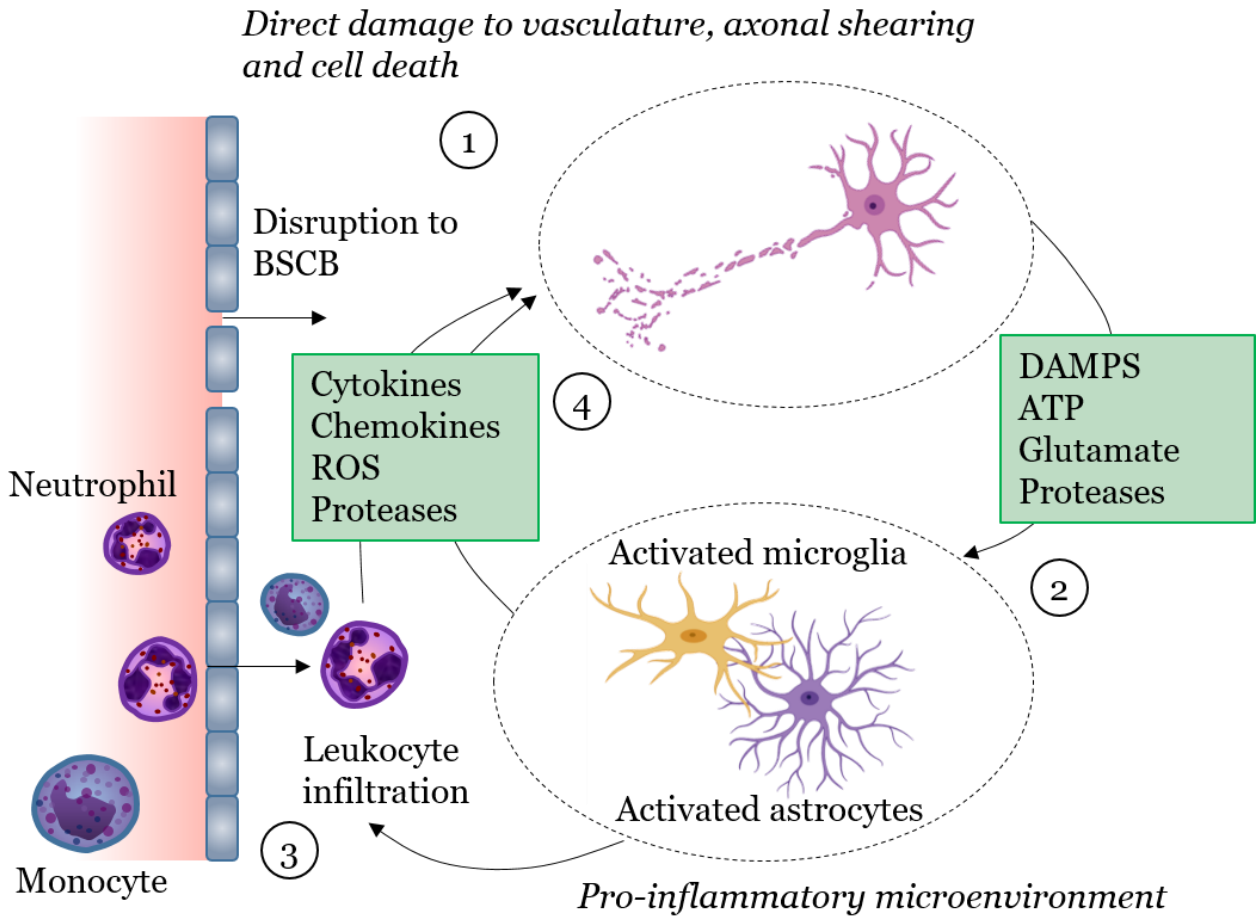


Figure 1.3 Pathophysiology of spinal cord injury. 1. The primary, mechanical injury to the spinal cord causes direct damage to the vasculature and disruption to the BSCB, axonal shearing, and immediate cell death. 2. DAMPs, including ATP, as well as glutamate and proteases are released from dead and dying cells, which activate the resident microglia and astrocytes. 3. Microglia and astrocytes release chemoattractants and induce expression of adhesion molecules, which facilitates the recruitment of peripheral leukocytes and generates a pro-inflammatory microenvironment in the spinal cord. 4. Infiltrated leukocytes, together with the glial cells, release cytokines, chemokines, ROS and proteases, which exacerbate the damage to neuronal tissue. BSCB – blood spinal cord barrier, DAMPS – damage associated molecular patterns, ROS – reactive oxygen species. This is an original figure.

1.2.3.3 Microglia

Microglia are the resident macrophages located in the brain and spinal cord which, together with astrocytes, constitute approximately 50% of cells in the CNS (Azevedo et al. 2009). In contrast to other myeloid cells, microglia are derived from the primitive yolk sac, rather than the bone marrow (Ginhoux et al. 2013). In addition, the CNS population of microglia is maintained by self-renewal, instead of from infiltrating circulating monocytes (Ajami et al. 2007), and so are fundamentally distinct from peripheral macrophages. It should be remembered that when monocytes do infiltrate the CNS parenchyma, they are indistinguishable from the resident cells in terms of morphology and most molecular markers, although there may be functional differences (London et al. 2013; Werner et al. 2020). Under normal physiological conditions, microglia display a ramified morphology, composed of a small cellular body and long, branched processes. Commonly referred to as "resting", microglia in this state (MΦ) have been found to be more active than previously appreciated. Microglial processes are dynamic, extending and retracting to survey and monitor CNS activity, including by direct contact with other cells (London et al. 2013). In this way, they perform immunosurveillance and maintenance of neuronal plasticity by elimination of dysfunctional synapses, phagocytosis of debris and intercellular signalling (London et al. 2013; Paolicelli et al. 2011). Microglia are extremely sensitive to changes in the homeostasis of the CNS and in response to damage and/or infection, cells undergo a physiological change. They assume an amoeboid morphology with fewer, denser processes and a larger cell body, and they proliferate and migrate to the site of injury. Depending on the microenvironment, microglia are often described as adopting an M1 or M2 activated phenotype, which are crudely designated pro- and anti-inflammatory, respectively. However, it is widely accepted that they exist on a spectrum and that the M1/M2 classification is complex and needs further investigation (David et al. 2015; Cherry et al. 2014). Despite this, multiple phenotypes have been described in the pathogenesis of SCI.

After injury, microglia are the first immune cells to respond and are activated by damage-associated molecular patterns (DAMPs) including myelin components, cellular debris and ATP, through toll-like receptors (TLRs) and pattern recognition receptors (PRRs) (Dibaj et al. 2010; Hawthorne and

Popovich 2011; Olson and Miller 2004). In this acute phase, the M1 phenotype is predominant, which has been shown to be neurotoxic via a number of mechanisms (Kigerl et al. 2009); microglial expression of the pro-inflammatory molecules IL-1β and TNF-α is evident within 5-15 minutes after injury (Pineau and Lacroix 2007), which, in turn, activate astrocytes (Liddelow et al. 2017). Microglia also release ROS, including superoxide, hydroxyl radicals and nitric oxide, and reactive nitrogen species (RNS), which cause oxidative damage by lipid peroxidation, damage to DNA and inhibition of mitochondria (Barger et al. 2007; Merrill et al. 1993). Microglia also increase expression of MHC-II complexes on their cell surface (Popovich et al. 1997), which present antigens to infiltrating leukocytes, thus contributing to immune cell activation and SCI-induced autoimmunity. Collectively, these responses induce cellular damage to endothelia, oligodendrocytes and neurons, which may result in downstream cell death.

Despite their clear neurotoxic effects, microglia are similarly important for wound healing (Li et al. 2020b). In the days following SCI, microglia proliferate and accumulate around the lesion border (Bellver-Landete et al. 2019). Their ability to phagocytose debris allows microglia to scavenge damaged cells and remove inhibitory factors such as myelin. Moreover, a population of M2-polarised microglia are evident in the spinal cord for up to 1 week post-injury, which is then supressed by the pro-inflammatory microenvironment (Kigerl et al. 2009). These M2-microglia have been shown not to be neurotoxic and may promote axonal growth, which suggests that they have a role in regeneration. Microglia are driven towards the M2 phenotype in response to IL-4 and IL-13 signalling, and are identified by increased production of anti-inflammatory cytokines such as IL-10 and TGF-β (Ma et al. 2015), and reduced expression of genes that are regulated by NF-κB. They have been shown to support axonal sprouting, oligodendrocyte maturation and remyelination (Miron et al. 2013; Stirling et al. 2014). As a result, some studies have explored the utility of driving an M2-microglial response *in vivo* to improve outcomes after SCI, with some reported success (Ma et al. 2015; Song et al. 2017; Guerrero et al. 2012). Although, it remains unknown whether microglia can interchange between M1 and M2 directly, or via the MΦ phenotype.

Multiple studies have exploited the development of oral CSFR1 antagonists (GW2580, PLX3397 & PLX5622), which can selectively target the microglial population, to identify their specific contribution to SCI. Gerber et al. (2018) reported that pre-treatment with GW2580 improved fine motor recovery in a mouse model of SCI, which authors attributed to reduced gliosis, indicating that microglia play a detrimental role. However, sustained microglial depletion with PLX3397 or PLX5622 has also been shown to worsen functional recovery (Bellver-Landete et al. 2019; Fu et al. 2020; Brennan et al. 2018; Li et al. 2020b). These studies reported disorganisation of the astrocytic scar and increased lesion size, as well as increased infiltration of blood-derived leukocytes, suggesting microglia are necessary to restrict secondary inflammatory damage from extending beyond the lesion site. It must be noted that GW2580 inhibited the microglial proliferative response to SCI, but did not deplete them, whilst PLX5622 did ablate microglial cells. This would, therefore, suggest that their presence is required for recovery, but that trauma-induced proliferation can have negative effects. Timing and the resulting phenotype are most likely to be important factors here. Certainly, unpublished work from Brennan et al. (2018) shows that limited microglial depletion at the time of injury is neuroprotective (treatment administered -14 to +7 dpi), but not in the weeks (+8 to +28 dpi) or months (+29 to +56 dpi) following injury. This must be considered if targeting microglia therapeutically.

Studies have highlighted that there are discrepancies in the microglial response to comparable injuries to the brain and spinal cord. Indeed, Schnell et al. (1999a) showed that microglial density was greater and more widespread following SCI compared to traumatic brain injury (TBI). Anatomically, the quantity, distribution and phenotype of microglia differs in the two CNS structures (Anthony and Couch 2014); the spinal cord has higher microglial cell density than the brain, with even numbers in the grey and white matter whilst the brain has more microglia in the grey matter specifically. In addition, the spinal cord microglia are homogenously distributed and feature higher levels of CD45 and CD11b, whereas microglia in the brain show regional differences and lower levels of these cell surface molecules. Thus, the microglial response to trauma differs in the brain and spinal cord.

1.2.3.4 Astrocytes

Astrocytes are defined as a subtype of glial cell, classically identified by expression of glial fibrillary acidic protein (GFAP) and S100β, which modulate the homeostasis of the CNS (Cabezas et al. 2014; Sofroniew and Vinters 2010). They are responsible for maintaining ionic balance and the uptake and metabolism of neurotransmitters such as glutamate and dopamine, which is important for neuronal excitability and synaptic transmission. Astrocytic end feet are also involved in maintaining the BBB/BSCB, with specialised channels and transporters to regulate the movement of ions and other molecules between the CNS and blood. Upon activation, astrocytes can assume an A1 or A2 phenotype (Liddelow et al. 2017; Zamanian et al. 2012); the A1 phenotype is associated with the upregulation of the complement cascade and considered neurotoxic. By contrast, the A2 phenotype is associated with the upregulation of neurotrophic factors and considered protective, however, this is a reductionist viewpoint (Li et al. 2020a).

Although not an immune cell *per se*, evidence clearly shows that A1-activated astrocytes have a pivotal role in neuroinflammation and pathology in response to SCI (Augusto-Oliveira et al. 2020; Gu et al. 2019; Pineau et al. 2010). For example, it has been proposed that astrocytes contribute to the initiation of intraspinal inflammation. Astrocytes are activated and produce pro-inflammatory molecules within minutes of injury (Pineau and Lacroix 2007). They have been shown to produce chemoattractants CXCL1, CXCL2 and CCL2, as well as IL-1β, which upregulates expression of adhesion molecules and therefore mediates neutrophil and pro-inflammatory monocyte recruitment to the spinal cord (Pineau et al. 2010; Pineau and Lacroix 2007). Release of these factors also modulate the microglial phenotype, with astrocytic TNF-α and IL-6 shown to promote the M1, neurotoxic phenotype (Pineau and Lacroix 2007). As such, inhibition of NF-κB-regulated genes in astrocytes specifically has been shown to reduce chemokine expression in the spinal cord and improve motor recovery in a rodent model of SCI (Brambilla et al. 2005). Moreover, SCI-induced dysfunctional astrocytes contribute to glutamate excitotoxicity due to deficits in uptake and anti-oxidant exhaustion (Bal-Price et al. 2002), along with increased BSCB disruption and oedema due to increased translocation of Aquaporin-4 to the plasma membrane (Kitchen et al.

2020). As with microglia, the astrocytic response to SCI is greater than that to TBI, as evidenced by greater upregulation of GFAP, which is indicative of increased astrocytic activation (Schnell et al. 1999a).

Beyond the acute phase of injury, astrocytes are primarily responsible for the formation of the glial scar. The glial scar is a heterogeneous structure surrounding the lesion epicentre which includes NG2+ oligodendrocyte precursor cells, fibroblasts, pericytes and extracellular matrix, although activated astrocytes are the major constituent (Yang et al. 2020; Bradbury and Burnside 2019). Beginning at 1-2 days and ceasing approximately 14 days after injury, activated astrocytes rapidly proliferate and mobilise to regions around the lesion core (Wanner et al. 2013) in a STAT-3 dependent manner (Okada et al. 2006; Herrmann et al. 2008). Astrocytes also undergo a phenotypic change; inflammatory signals in the lesion increase expression of GFAP and intermediate filaments nestin and vimentin (Baldwin et al. 1998; Herrmann et al. 2008). Moreover, cells become elongated with a bipolar or radial shape and reorient in the spinal cord. Thus, they transform into scar-forming astrocytes with overlapping processes, which are distinct from astrocytes in surrounding neuronal tissue (Wanner et al. 2013). It is interesting to note that while the processes of rodent astrocytes can be resolved, human astrocytes are larger and have more processes, so much as that they cannot be easily distinguished from each other (Augusto-Oliveira et al. 2020). Collectively, this forms a dense, mesh-like structure, which reaches maturation several weeks post-SCI and creates a physical barrier around the cavitation.

The glial scar is traditionally thought to prevent neuroregeneration as it obstructs neurite regrowth across the lesion (Bradbury and Burnside 2019). Early studies have shown that regenerating axons were unable to extend past the glial scar (Brown and Mc 1947; Clemente and Windle 1954), and this is one explanation for the poor recovery in humans that persists even today (Bradbury and Burnside 2019). In addition, astrocytes have been shown to release inhibitory molecules such as chondroitin sulphate proteoglycans (CSPGs) and neurite outgrowth inhibitor (NOGO) (Andrews et al. 2012; Schwab and Strittmatter 2014), which further impede neuronal sprouting (Cafferty et al. 2010; Niederost et al. 2002). Therefore, astrocytes have become a target for intervention for chronic SCI.

However, prevention of glial scar formation has been shown to worsen histological and functional outcomes. Inhibition of astrogliosis or formation of the glial scar has been shown to exacerbate lesion size, myelin damage, BSCB dysfunction and motor deficits (Faulkner et al. 2004; Gu et al. 2019; Wanner et al. 2013). Critically, these studies attributed this to an increase in infiltrating leukocytes into spinal cord tissue rostral and caudal of the lesion, which can exacerbate inflammation and cell death in spared spinal cord tissue. Therefore, the glial scar is simultaneously thought to be protective, restricting immune cells within the lesion to prevent the spread of inflammatory damage. Moreover, Anderson et al. (2016) showed that stimulated axon regrowth was attenuated when astrocytes were ablated, suggesting that astrocytes facilitate regeneration. As a result, it is becoming increasingly accepted that the glial scar plays a dual role in the pathophysiology of SCI, and the complexities are still poorly understood.

1.2.4 The systemic response to SCI

SCI is not exclusively a local event as it similarly has a profound effect on peripheral organs and the immune system (Figure 1.4). In response to injury or infection, a systemic inflammatory response is triggered termed the acute phase response (APR). The APR is largely co-ordinated by the liver and is characterised by changes in soluble factors including complement, cytokines and chemokines, followed by elevated circulating leukocytes and associated fever (Anthony and Couch 2014; Anthony et al. 2012). The primary role of the APR is to restore homeostasis by limiting infection, removing inflammatory stimuli and promoting repair, and it is highly effective in response to peripheral injury (Anthony and Couch 2014). However, when injury is to the brain or spinal cord, the resultant APR contributes to immune cell influx and non-resolving neuroinflammation in the otherwise "immune-specialised" CNS, causing additional damage and cell death (Anthony et al. 2012; Campbell et al. 2005; Campbell et al. 2008b). Therefore, it has been proposed that the APR exacerbates tissue injury after SCI.

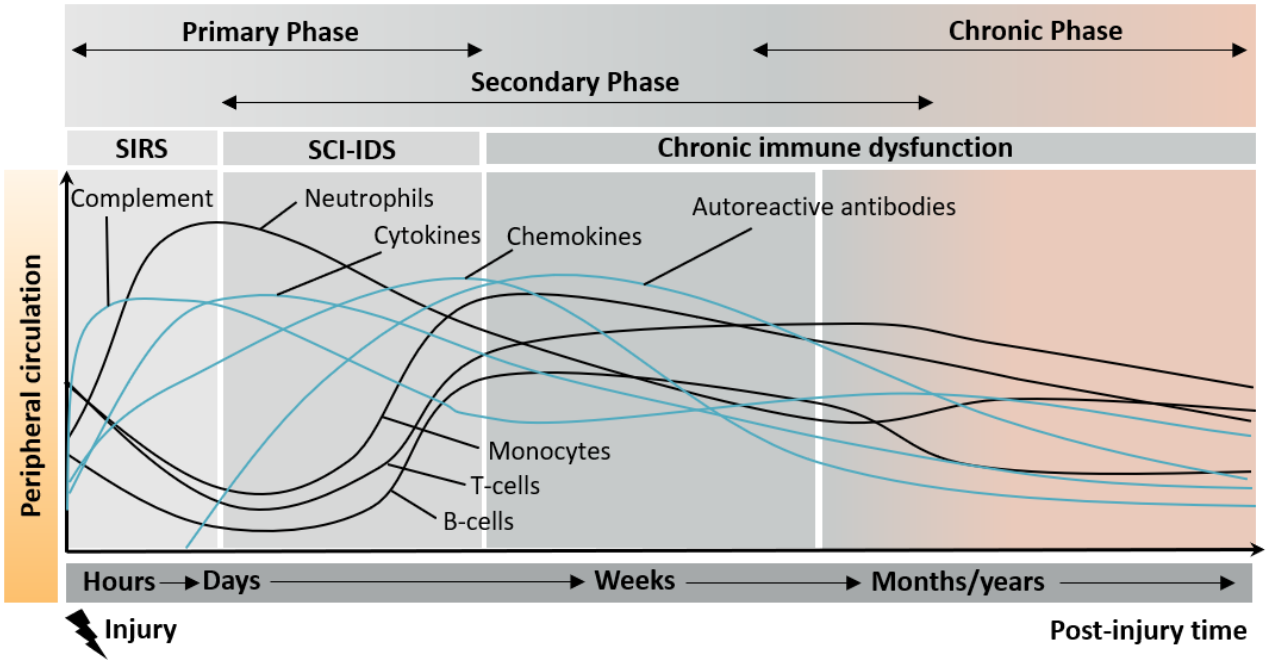


Figure 1.4 Time course of the systemic response to SCI. Immunological response to SCI is not restricted to the spinal cord. In the primary phase of SCI, a peripheral inflammatory response occurs, characterised by increasing circulating cytokines, chemokines, complement and neutrophils. This can cause systemic inflammatory response syndrome (SIRS). Injury also induces a decrease in circulating lymphocytes which results in immunodeficiency syndrome (SCI-IDS). Activated B-cells release autoantibodies which mediate SCI-induced autoimmunity. This is an original figure, generated from Biglari et al., (2015), Hassanshahi et al. (2013), Riegger et al. (2009) and Brennan et al. (2015).

Following CNS challenge, whether that be trauma, infection or inflammation, hepatic expression of pro-inflammatory molecules is significantly elevated within 2 hours (Campbell et al. 2005; Campbell et al. 2008b). Cytokines IL-1β, TNF and IL-6, chemokines CXCL1, CXCL10 and CCL2, as well as the acute phase proteins (APPs) such as SAA-2, the pentraxins such as CRP, all contribute to the APR and initiate a robust immune response (Campbell et al. 2007; Campbell et al. 2005; Wicker et al. 2019; Wilcockson et al. 2002). In addition, the complement system is activated (Brennan et al. 2012); circulating complement proteins are elevated following SCI (Brennan et al. 2019), which have been associated with worsened outcomes (Galvan et al. 2008; Brennan et al. 2015; Ankeny et al. 2009). Neutrophils and monocytes are mobilised from the bone marrow (Brennan et al. 2019) and spleen respectively (Blomster et al. 2013a), into the circulation, which then infiltrate the CNS as well as peripheral organs (Campbell et al. 2005; Campbell et al. 2008b). Leukocytes are also phenotypically altered in response to SCI (Bao et al. 2011a; Bao et al. 2009) with increased integrins and oxidative activity that exacerbate infiltration and cause tissue damage. As a result, development of systemic inflammatory response syndrome (SIRS) is not uncommon and can progress to multi-organ dysfunction syndrome (MODS), both of which significantly increase patient morbidity and mortality (Kesani et al. 2014; Sun et al. 2016). Although, it remains unknown whether the APR induced by SCI is dependent on the nature of the lesion, which will be explored in Chapter 4.

Interestingly, previous work from our laboratory has identified that the magnitude of CNS inflammation can be attenuated indirectly by targeting the APR. Inhibiting the production of acute phase proteins (Campbell et al. 2007) or Kupffer cell depletion (Campbell et al. 2008b), both reduce neutrophil recruitment to the CNS in models of TBI and SCI. Similarly, splenectomy at the time of SCI dramatically decreased infiltration of blood monocyte-derived macrophages into the spinal cord and improved motor function recovery (Blomster et al. 2013a). However, it must be acknowledged that the consequences of manipulating the APR is also more complex than initially thought; paradoxically, exacerbation of the APR with LPS after SCI has also been shown to reduce leukocyte infiltration and BSCB breakdown (Davis et al. 2005). By contrast, viral pre-challenge has been shown to worsen both systemic and brain inflammation after striatal IL-1β injection (Couch

et al. 2014). As such, it is clear that the timing and the nature of the inflammatory insult is influential.

Differences in the APR following comparable damage to the brain and spinal cord have also been reported (Campbell et al. 2005; Campbell et al. 2008b; Anthony and Couch 2014). Certainly, the brain and spinal cord respond very differently to injury. The loss of integrity of the BSCB is often more widespread than for the BBB in the brain, following trauma, as well as greater increases in local chemokine production and neutrophil recruitment to the spinal cord than the brain (Campbell et al. 2002; Schnell et al. 1999a). It remains unclear to this day why this should be the case, but it is of interest that the spinal cord appears to be more susceptible to the development of inflammatory lesions in the autoimmune encephalitis model of MS (Sun et al. 2004). This must be considered when developing novel therapies for SCI. For example, peripheral administration of the PPARα agonist fenofibrate attenuated the APR and neutrophil recruitment to the brain after intrastriatal injection of IL-1β (Dickens et al. 2017), yet was shown to be ineffective in experimental SCI (Almad et al. 2011). This demonstrates that the CNS should not necessarily be considered as a single entity and making assumptions about SCI based on data from brain injury is inappropriate.

Another systemic response to SCI is SCI-associated immunodeficiency syndrome (SCI-IDS; Figure 1.5). Circulating monocytes, T- and B-cells are significantly depleted within 24 hours of SCI, which persists for the first week after injury (Riegger et al. 2007; Riegger et al. 2009). As a result, patients are highly susceptible to infections, which has been shown to be an independent risk factor for significantly poorer neurological outcome (Failli et al. 2012). It is thought that SCI-IDS is, at least in part, mediated by dysfunction of a sympathetic-neuroendocrine adrenal reflex. Pruss et al. (2017) demonstrated that SCI at T1, but not T9, induced significant changes in circulating corticosterone (rodent cortisol) and noradrenaline, which were associated with leukocyte depletion and spontaneous pneumonia. The authors showed that these changes could be rescued when the adrenal glands were removed; adrenalectomy prevented the increase in plasma corticosterone, induced by high level SCI, and the leukocyte depletion of lymphoid organs. This led to the conclusion that dysfunctional innervation of the adrenal glands after SCI drives

immunosuppression. Brommer et al. (2016) similarly showed that malfunction of the sympathetic nervous system drives SCI-IDS, as spleen denervation following SCI at T3, but not SCI at T9, reduced bacterial load in the lungs and prevented splenic atrophy.

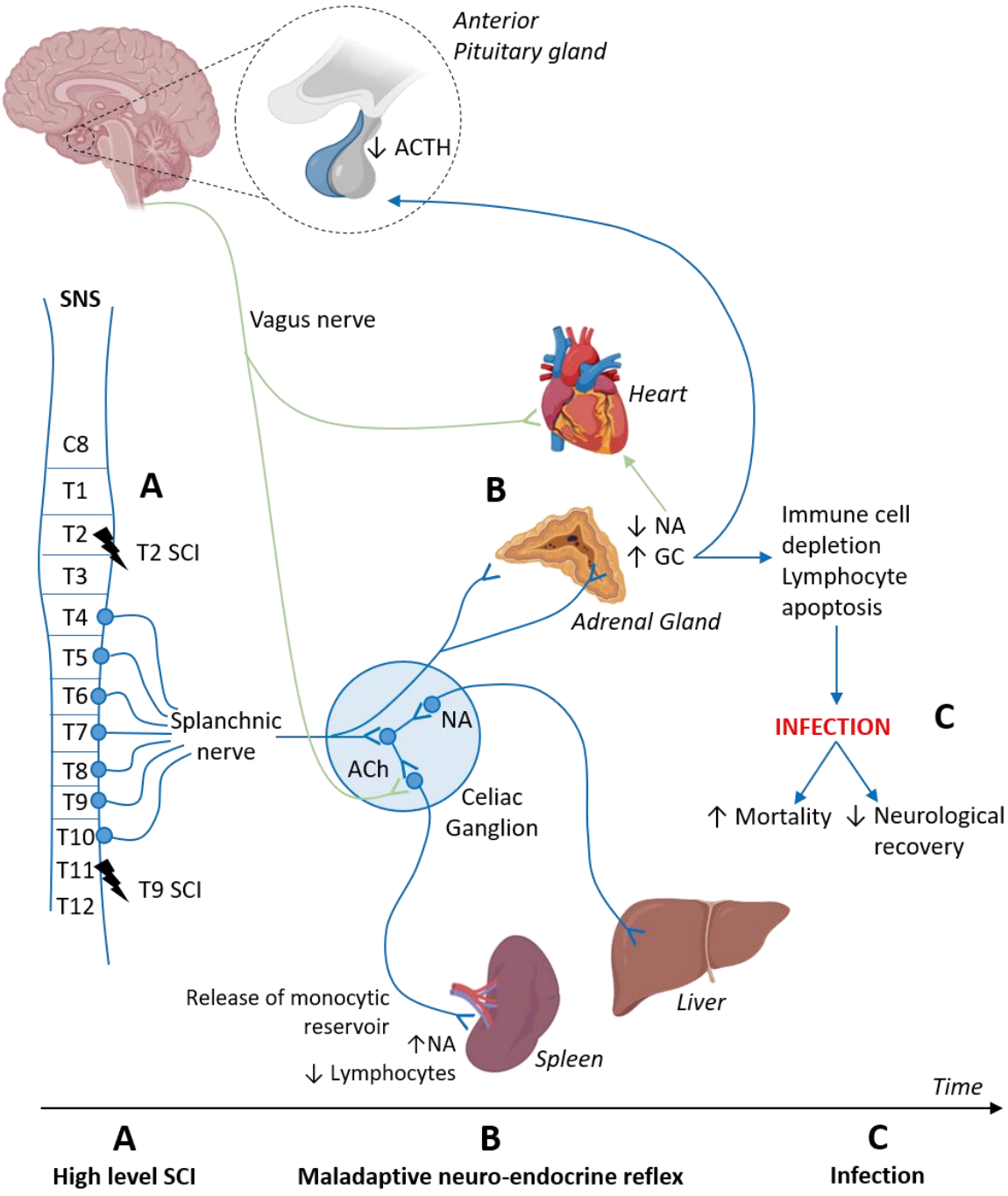


Figure 1.5 SCI-IDS is caused by a dysfunctional sympathetic-neuroendocrine adrenal reflex. Spinal cord injury (SCI) interrupts sympathetic innervation of peripheral immune organs, including the adrenal gland, spleen and liver (A). Dysregulation of the balance between parasympathetic and sympathetic signalling causes increased glucocorticoid (GC) and decreased noradrenaline (NA) release (B), resulting in immunosuppression and, in turn, increased risk of infection (C). This response is lesion level dependent. ACh – Acetyl choline, ACTH – Adrenocorticotropic hormone. Figure adapted from Pruss et al. (2017).

In addition to inflammation, SCI induces significant changes in hepatic metabolism (Goodus and McTigue 2020). Lipid deposition in the liver occurs rapidly in the subacute phase of injury (Sauerbeck et al. 2015), which is associated with insulin resistance and inflammation (Pagadala et al. 2012). In addition, plasma glucose is increased and associated with poor patient outcome (Kobayakawa et al. 2014). Taken together, these changes can constitute a distinct form of metabolic syndrome (Lee et al. 2005; Maruyama et al. 2008), which increases SCI patient risk of developing liver disease (Barbonetti et al. 2016; Kao et al. 2016), cardiovascular disease (Myers et al. 2007), diabetes (Lai et al. 2014; Lavela et al. 2006) and stroke (Wu et al. 2012b). The development of novel analytical techniques has enabled a more comprehensive understanding of the effect of neurotrauma on systemic metabolism. For example, ^{1}H NMR combined with multivariate analysis (PCA/OPLS-DA) enables the analysis of numerous aqueous and/or lipid metabolites, simultaneously, and has been used previously to identify severity and prognostic biomarkers after TBI (Oresic et al. 2016) and stroke (Jung et al. 2011). This strategy, termed metabolomics, will be explored in Chapter 5, to improve our understanding of SCI-induced metabolic dysfunction.

The gut also exhibits dysfunction after SCI, which is thought to have "disease-modifying" effects (Jogia and Ruitenberg 2020; Kigerl et al. 2018). It has previously been shown that the gut microbiota undergoes significant changes following traumatic CNS injury (Houlden et al. 2016). Certainly, Kigerl et al. (2016) demonstrated that experimental SCI induced gut dysbiosis and bacterial translocation, as evidenced by increased gut permeability, significant changes in the microbiome and the presence of bacteria in the lung. This was corroborated by O'Connor et al. (2018) who also showed SCI-induced differences in microbiota, which has then been verified in human SCI patients (Zhang et al. 2018; Gungor et al. 2016; Zhang et al. 2019a). In conjunction with SCI-IDS, this puts patients at increased risk of contracting infections, such as pneumonia and wound infections, which, in turn, increase morbidity and mortality (Cotton et al. 2005; Failli et al. 2012). These changes in the gut have been linked to cellular and molecular changes in gut-associated lymphatic tissue (Kigerl et al. 2016), as well as increased expression of pro-inflammatory cytokines in the intestine (O'Connor et al. 2018), suggesting a role for the immune response in gut dysfunction. Critically, exacerbation of gut dysbiosis after SCI impaired motor recovery, increased

lesion size and reduced spared white matter (Kigerl et al. 2016). By contrast, treatment with probiotics improved motor function score and increased spared white matter, indicating that modulating the gut response to SCI can also offer neuroprotection and improve outcomes (Kigerl et al. 2016).

1.2.4.1 Neutrophils

Neutrophils are the predominant granulocyte, a subtype of leukocyte, which are characterised by their multi-lobed nucleus and cytoplasmic granules, and are derived from granulo-monocytic progenitors in the bone marrow (Neirinckx et al. 2014). They constitute the most abundant blood-derived leukocyte and, with a small life-span of <24 hours, have a high turnover rate, which is tightly regulated. Circulating neutrophils perform an immunosurveillance role, until they encounter signals of injury and/or infection. In response to DAMPs/PAMPs, neutrophils are recruited from the blood across endothelial barriers, which is dependent on E-/P-selectins and the adhesion molecules VCAM-1 and ICAM-1, rearrangement of the junction proteins, and chemokines secreted by endothelial cells. In this way, they are among the first immune cell to reach a site of inflammation where they release their granular content, which include ROS such as myeloperoxidase (MPO), pro-inflammatory cytokines and proteases, phagocytose cell debris and form neutrophil traps (Neirinckx et al. 2014). In peripheral insults, these events occur quickly, and collectively neutralise any pathogens, resolve the wound, and restore tissue homeostasis (Shechter and Schwartz 2013). However, in the CNS, their recruitment is delayed and the magnitude of the response is reduced (Neirinckx et al. 2014). They cause additional cell death, axonal injury and demyelination, which exacerbates the injury. Therefore, neutrophils are, seemingly, always discouraged from entering the CNS.

Following injury to the spinal cord, unlike the brain, neutrophils are more rapidly recruited (Campbell et al. 2008a). They are mobilised from the bone marrow in a CXCL1/CXCLR2 dependent mechanism (Brennan et al. 2019) and reach peak density 24 hours post-SCI in rodents (Yates et al. 2021; Brennan et al. 2019), and 1-3 days in humans (Fleming et al. 2006). To facilitate their transmigration into the CNS, neutrophils release proteolytic enzymes including matrix

metalloproteinases (MMPs) (Kumar et al. 2018b) and neutrophil elastase (Kumar et al. 2018a). This mediates the degradation of the basement membrane and extracellular matrix (Bolton et al. 1998), which further compromises the vasculature and increases BSCB permeability, facilitating additional leukocyte infiltration (Lee et al. 2014; Losey and Anthony 2014). Once in the spinal cord parenchyma, neutrophils release an arsenal of pro-inflammatory molecules, ROS, cytokines and proteases, which can give rise to bystander cell death. These factors also activate the resident glial cells, thus indirectly contributing to the downstream neuroinflammation. Conversely, microglia appear to moderate the influx of neutrophils into the CNS (Otxoa-de-Amezaga et al. 2019), indicating there is cross-talk between immune cells in the CNS and the periphery to mediate the magnitude of neuroinflammation after traumatic injury.

Although considered part of the acute response, neutrophils have been shown to persist in the spinal cord (Fleming et al. 2006). Neutrophils typically have a very short life-span (40 hours in a tissue); it is thought they undergo apoptosis in the days following injury (Fleming et al. 2006) and are subsequently cleared by resident and infiltrating macrophages (Milich et al. 2019). Yet extravascular neutrophils are evident weeks after SCI (Fleming et al. 2006; Kigerl et al. 2006), suggesting ongoing recruitment albeit at a lesser extent than during the acute phase. BSCB permeability (Popovich et al. 1996a) and expression of chemoattractant molecules such as IL-1β and CCL2 (Pineau et al. 2010), are increased during this time frame, which may facilitate this prolonged influx. Alternatively, apoptosis may be suppressed and/or impaired and therefore cells identified in the aforementioned studies are residual from the acute phase. Certainly, neutrophil survival has been shown to be prolonged in response to inflammatory stimuli (Kim et al. 2011). However, the contribution of neutrophil infiltration to lesion pathology at later time points is unclear.

Neutrophils are largely considered detrimental to lesion progression and deficits after CNS injury. As such, reduced neutrophil infiltration has consistently been associated with improved histological and functional outcomes after stroke (Otxoa-de-Amezaga et al. 2019), TBI (Kenne et al. 2012) and SCI specifically (Lee et al. 2011; Nguyen et al. 2012; Brennan et al. 2019). Indeed, the magnitude of

circulating neutrophils is predictive of patient outcome (Brennan et al. 2019; Jogia et al. 2021). However, this viewpoint has been challenged; depletion of neutrophils by targeting mouse granulocyte markers $Ly6G^{+}GR\text{-}1^{+}$ during the acute phase of SCI reduced white matter sparing and subsequent motor recovery (Stirling et al. 2009). This suggests that at least a subtype of neutrophils may be beneficial. Heterogeneity in the neutrophil population has become more widely accepted (Rosales 2018); neutrophils exhibit multiple phenotypes in response to inflammation, which differ in expression of cytokines, TLRs and surface molecules, and have contrasting effects on macrophage activation (Tsuda et al. 2004). Although, the ratio of these phenotypes after SCI, and the downstream effects on lesion pathology remains unknown. Recently, a novel subtype, characteristic of immature neutrophils, has been identified, which has been shown to promote cell survival and axonal regrowth in a model of optic nerve crush through secretion of growth factors (Sas et al. 2020). Therefore, it has been proposed that neutrophils are required in the spinal cord to modulate the inflammatory response and initiate wound healing. However, it must be acknowledged that, despite these studies, there is more evidence that indicates that neutrophils contribute to CNS damage (Campbell et al. 2003).

1.2.4.2 Monocytes and macrophages

Monocytes are blood-derived mononuclear leukocytes of myeloid lineage. They are produced in the bone marrow, although mature monocytes can also reside in the subcapsular red pulp of the spleen, primed for deployment upon inflammatory stimulation. Once released into the circulation, monocytes have a half-life of approximately 1-3 days in humans or 17 hours in mice (Patel et al. 2017), after which they undergo apoptosis or infiltrate tissues where they differentiate into tissue-resident dendritic cells or macrophages (Coillard and Segura 2019). The fate of the monocyte-derived macrophages is dependent on their anatomical location (Coillard and Segura 2019); populations across different tissues and organs have been shown to have distinct RNA profiles, receptor expression and even functions (Bajpai et al. 2018; MacParland et al. 2018). Physiologically, monocytes and their macrophage progeny constitute a critical branch of the innate immune response, principally through their phagocytic abilities.

The concept of a spectrum between classically activated (M1) and alternatively activated (M2) phenotypes was first established with monocyte-derived macrophages (Gensel and Zhang 2015; Mills et al. 2000). In response to damage in the periphery, this enables a co-ordinated sequence of events that results in successful wound healing. First, monocyte-derived macrophages infiltrate the site of injury and exhibit an M1 phenotype, releasing ROS and pro-inflammatory molecules. They interact with pathogens and/or debris directly via PRRs or indirectly through interactions with antibodies and complement, which collectively enables them to engulf and digest harmful factors. In addition, they present antigens to T-cells to activate a specific immune response. At later stages, macrophages adopt an M2 phenotype, characterised by increased anti-inflammatory cytokine production (IL-10, TGF-β) and release of growth factors. This enables resolution of inflammation and the promotion of tissue remodelling and repair, after which macrophage numbers return to baseline. However, in response to damage in the spinal cord, M1/M2 resolution does not occur, and, instead, activated macrophages persist in the lesion chronically (Fleming et al. 2006; Beck et al. 2010; Popovich et al. 1997), contributing to non-resolving inflammation and associated damage.

In the days following SCI, pro-inflammatory monocytes infiltrate the spinal cord, recruited by intraspinal chemoattractant expression (IL-6, CXCL10, CCL2), with a maximum density 7 days post-injury (Fleming et al. 2006). These cells predominantly derive from the spleen and splenectomy at the time of injury reduced monocyte recruitment to the spinal cord and improved functional recovery (Blomster et al. 2013a), indicating that they have a deleterious effect on pathology. Indeed, through the use of chimeras, studies have demonstrated that peripheral monocyte-derived macrophages cause cell death, axonal dieback (Evans et al. 2014; Horn et al. 2008) and demyelination through a range of mechanisms. They produce ROS and nitric oxide which, in the combined compound peroxynitrite, causes lipid peroxidation and disrupted membrane integrity, and the irreversible oxidation of proteins and nucleic acids, which, in turn, triggers apoptosis. In addition, macrophages release cytokines, proteases and eicosanoids, which induce neuronal and glial toxicity, as well as attract additional leukocytes that amplify the inflammatory response. This is indicative of an M1 phenotype, which is driven by the inflammatory microenvironment (Kigerl et al. 2009). As a result, depletion of monocytes/macrophages in the

peripheral, but not central compartment, has been shown to improve functional and histopathological outcomes (Popovich et al. 1999; Lee et al. 2011).

In the chronic phase of injury, monocyte-derived macrophages remain in the lesion epicentre having transformed into lipid-rich, foamy macrophages (Fleming et al. 2006; Beck et al. 2010; Popovich et al. 1997), which have been detected in the spinal cord months after injury (Wang et al. 2015). Owing to ongoing bystander demyelination, myelin debris is often present in the spinal cord lesion. This debris is phagocytosed by recruited macrophages in a complement receptor 3-dependent mechanism (Sun et al. 2010), and can act as an inflammatory stimulus, driving an M1-like inflammatory phenotype. Phagocytosis of myelin causes macrophages to release pro-inflammatory cytokines (Kong et al. 2020; Wang et al. 2015; Sun et al. 2010) and promote neuronal apoptosis (Kong et al. 2020). In turn, the lipid-laden cells have reduced mobility, which is necessary for wound healing (Wang et al. 2015). As such, inhibition of myelin debris phagocytosis by genetic ablation of macrophage scavenger receptor 1, reduced the formation of foamy macrophages, which was associated with improved motor recovery (Kong et al. 2020).

It has been proposed that macrophages may also have beneficial roles in wound healing (Milich et al. 2019). In addition to the M1 inflammatory subtype, immunoregulatory monocyte-derived macrophages, indicative of an M2 phenotype, are actively recruited to the spinal cord after injury (Kigerl et al. 2009; Shechter et al. 2013), which have been shown to promote recovery in an IL-10-dependent manner (Shechter et al. 2009). They also produce TGF-β (McTigue et al. 2000) which is neuroprotective, as well as neurotrophic factors such as BDNF, which may promote repair. Moreover, their phagocytic activity clears the lesion site of debris and molecules inhibitory of axonal regrowth, which is necessary for optimal regeneration. Indeed, Shechter et al. (2009) showed that adoptive transfer of anti-inflammatory $CD115^{+}$ monocytes increased functional recovery and decreased lesion size. Many studies fixate on the M1/M2 polarisation, despite acknowledgement that activation of microglia/macrophages exists on a spectrum, which is likely hindering progress with this approach.

1.2.4.3 T- and B-lymphocytes

Unlike the innate immune response that elicits a non-specific immune response to DAMPs/PAMPs, the adaptive immune response requires complex antigen-dependent activation. Whilst many endogenous regulatory mechanisms exist to prevent recognition of self-antigens and production of autoreactive lymphocytes, evidence suggests that SCI can activate a lymphocyte-mediated autoimmune response, which cause progressive damage to the CNS (Jones 2014). Adaptive lymphocytes (T- and B-cells) are the last subsets of leukocytes to infiltrate the spinal cord after injury; cells are recruited within the first week and peak 2-weeks post-injury (Fleming et al. 2006; Kigerl et al. 2006; Wu et al. 2017). Fewer lymphocytes are observed in the spinal cord, compared to other leukocytes, and remain in the CNS chronically (Fleming et al. 2006; Kigerl et al. 2006). Their presence in the spinal cord has been shown to be multi-phasic and progressive (Sroga et al. 2003), suggesting ongoing recruitment, although the signalling mechanisms driving this are yet to be investigated. Transgenic strains of mice lacking functional T- and B-cells report improvements in motor recovery after SCI, which suggests that the adaptive immune response to injury contributes to functional deficits (Luchetti et al. 2010; Wu et al. 2012a). Although the exact mechanism of this SCI-induced autoimmunity is unknown, it is likely that the release of CNS-associated antigens, combined with activation of the immune response, drives inappropriate lymphocyte activation (Yeh et al. 2016).

T-cells have been shown to exert autoimmune responses after SCI, which may contribute to neuronal damage. Kil et al. (1999) demonstrated that T-cells isolated from SCI patients were autoreactive to myelin basic protein (MBP), which was replicated more recently by Zajarias-Fainsod et al. (2012). Patients included in these studies had been living with SCI for years, highlighting that SCI-induced autoimmunity is a chronic, rather than a transient sequela. Mechanistically, autoreactive T-cells can directly attack neurons and glial cells; they have been shown to induce cell death and demyelination. Alternatively, autoreactive T-cells can release pro-inflammatory cytokines and chemokines such as IFN-γ, IL-1β and CXCL10 (Jones et al. 2005), as well as activate resident microglia, thereby inducing inflammatory damage indirectly. Indeed, SCI

induced in athymic rats resulted in reduced T-cell infiltration of the spinal cord and improved locomotor recovery (Potas et al. 2006; Satzer et al. 2015). Moreover, adoptive transfer of T-cells isolated from spinal injured animals into naïve animals caused motor deficits characteristic of MS (Popovich et al. 1996b), supporting the premise that T-lymphocytes contribute to tissue damage after SCI. Jones et al. (2002) showed that transgenic mice with T-cells autoreactive to MBP exhibited exacerbated demyelination and reduced white matter sparing, associated with reduced functional recovery. Interestingly, authors identified increased numbers of IL-2- and IFN-γ producing MBP-reactive T-cells in the spleens of the transgenic mice alone, which suggests that autoreactive lymphocytes specific for CNS antigens are activated in the periphery. Autoreactive T-cells can also promote the activation of antigen-specific B-cells which in turn, have been shown to induce autoimmune-associated damage after SCI.

In response to SCI, B-cells become chronically activated (Ankeny et al. 2006) and their depletion has been shown to improve functional recovery, and reduce lesion size and inflammatory markers after SCI (Ankeny et al. 2009; Casili et al. 2016), indicating they have detrimental effects on histopathology and outcome. It is proposed that B-cells exert their effect through the production of autoantibodies against CNS antigens, in a complement- and Fc receptor-dependent mechanism. Ankeny et al. (2009) showed that antibodies from SCI-injured animals, but not uninjured animals, caused histological damage and motor deficits when injected into the spinal cord of naïve animals, which was attenuated in C3-/- and FcRγ-/- mice. Certainly, antibody titre in SCI patient sera is significantly increased and has been shown to be autoreactive (Hayes et al. 2002; Zajarias-Fainsod et al. 2012; Arevalo-Martin et al. 2018). Moreover, factors associated with B cell activation including B cell maturation antigen and proliferation-inducing ligand are upregulated in the blood of SCI patients (Saltzman et al. 2013), further implicating the adaptive immune response in SCI pathogenesis. Lucin et al. (2007) proposed that this dysfunctional humoral response to SCI was lesion level dependent as they found that high thoracic injuries (T3) suppressed antibody production, whilst low thoracic injuries (T9) did not. Authors reported that T3 injury specifically was associated with increased noradrenaline release and lymphocyte cell death in the spleen, suggesting the spleen is the source of autoantibody-producing B-cells after SCI. Despite this result,

lesion level differences in antibody production could not be corroborated with human clinical data (Arevalo-Martin et al. 2018).

SCI-induced autoimmunity can have additional injurious consequences that are not restricted to the spinal cord. For example, SCI induces production of antibodies against the high-affinity prostacyclin receptors on platelets which has been associated with the accelerated cardiovascular disease often reported in patients (Kahn et al. 2005). Autoreactive lymphocytes may also be responsible for the increased risk of MS (Lin et al. 2015) as myelin reactive T- and B-cells have clear pathogenic roles in this autoimmune, demyelinating disease (Anthony et al. 2014). In addition, SCI patients are at increased risk of developing type 2 diabetes, independently of known risk factors such as immobility and body mass index (Cragg et al. 2013a), which may also be driven by post-injury autoimmunity. Therefore, the adaptive immune response to SCI can contribute to both the central and systemic sequelae of SCI.

Despite the wealth of data showing the impact of the immune system on patient outcome after SCI, the mechanisms by which both the adaptive and innate immune responses are activated are still unclear.

1.2.5 Extracellular Vesicles

Studies investigating the impact of SCI on the periphery demonstrate that the systemic response to injury has a significant effect on lesion progression and overall patient outcome, and as such may be a viable therapeutic target. However, many critical questions remain that must be answered for effective translation to the clinic. Perhaps most importantly, it is not clear the mechanism by which the systemic response is triggered following SCI. Both neuronal and humoral mechanisms have been investigated, however vagotomised animals still exhibit peripheral inflammation (Konsman et al. 2000; Kox et al. 2012), and no molecular candidate can fully explain the response (Konsman et al. 2002). Instead, it has been proposed that extracellular vesicles (EVs) may mediate communication between the CNS and the peripheral immune system (Figure 1.6).

EVs are membrane-bound nanoparticles, enriched for proteins, lipids and nucleic acids, which are typically characterised according to their biogenesis (Colombo et al. 2014; Raposo and Stoorvogel 2013). Apoptotic bodies are the largest (1000-5000nm) and are derived from the plasma membrane as part of programmed cell death. Microvesicles (150-1000nm) also derive from the plasma membrane, but in a blebbing mechanism, whilst exosomes (40-150nm) are generated via the endolysomal pathway and stored in multi-vesicular bodies before being released by exocytosis. EVs have been shown to be released from almost all cell types, including neurons (Chivet et al. 2014; Lachenal et al. 2011), microglia (Kumar et al. 2017; Drago et al. 2017), astrocytes (Dickens et al. 2017), CNS endothelial cells (Couch et al. 2017b) and immune cells (Ridder et al. 2014; Verderio et al. 2012). In addition, EVs have been isolated from almost all bodily fluids, such as the CSF (Kuharic et al. 2019) and plasma (Hazleton et al. 2017), and they have a unique capacity to cross the BBB (Dickens et al. 2017), to exert their effects both locally and systemically in distant organs. As such, EVs have been identified as having a pivotal role in intercellular communication, including CNS-to-immune communication.

There is growing evidence to suggest that EVs initiate the APR following CNS injury. Indeed, it has consistently been shown that circulating EVs are significantly increased in both animal models and human patients of TBI (Hazleton et al. 2017; Kumar et al. 2017; Nekludov et al. 2014), stroke (Couch et al. 2017a) and inflammatory brain lesions (Couch et al. 2017b; Dickens et al. 2017). These plasma-derived populations have a pro-inflammatory phenotype (Li et al. 2018a), and have been shown to stimulate macrophages *in vitro* (Couch et al. 2017a), and a hepatic APR *in vivo* (Couch et al. 2017b; Dickens et al. 2017). Critically, inhibition of EV release from the CNS has been shown to attenuate the systemic response to brain inflammation, and subsequently inhibit leukocyte infiltration (Dickens et al. 2017), which is associated with increased tissue sparing and more favourable outcomes. In addition, exogenous administration of inflammatory EVs exacerbated the APR and lesion pathology after TBI (Hazleton et al. 2017). Collectively, these studies indicate that, not only do EVs mediate the communicatory pathway between the CNS and the periphery following trauma, but that manipulation of this pathway can protect the CNS from secondary damage.

The mechanism by which EVs exert their effect after traumatic CNS injury is unknown. To begin with, the cellular origin of the plasma-derived EVs responsible for initiating the APR is unclear, although it is evidently important as EVs from different activated cells have been shown to exacerbate inflammation at different magnitudes (Hazleton et al. 2017). Nekludov et al. (2014) showed a transcranial gradient in EV concentration after TBI; more EVs were detected in the cerebrovenous compared to arterial blood, indicating that the increase in circulating EVs originated from the brain. In line with this, EVs shed from brain endothelial cells (Andrews et al. 2016; Couch et al. 2017b) and microglia (Kumar et al. 2019; Kumar et al. 2017) have both shown increases following brain trauma. In addition, Dickens et al. (2017) showed that a proportion of plasma EVs released in response to brain inflammation are derived from astrocytes which translocate to the liver, spleen and lung, further linking EV-mediated signalling with the APR following CNS injury. From this, it is easy to assume that EV population changes are due to increased release from cells of the CNS. However, EVs derived from haematopoietic cells can also signal to the brain, and their uptake can be exacerbated by peripheral inflammation (Ridder et al. 2014). Leukocyte- and platelet-derived EVs are also increased after TBI (Nekludov et al. 2014). Delineating the origin of EVs could identify the critical players in CNS-periphery communication, and may identify a specific cellular target for EV-based therapeutics.

Functional analysis has identified features of EV composition which could contribute to the initiation and exacerbation of the APR (Kerr et al. 2018; Moyron et al. 2017). CNS trauma has been shown to alter the protein profile of circulating EVs; they are enriched for pro-inflammatory molecules, such as IL-1β (Drago et al. 2017; Kumar et al. 2017) and CCL2 (Hosseinkhani et al. 2018), indicating a direct inflammatory mechanism. EVs derived from different stimulated cells have also been shown to have different miRNA profiles (Hazleton et al. 2017), suggesting they may exert their effect indirectly through the transfer of specific genetic transcripts. Certainly, miRNA has been identified in astrocyte-shed EVs which target the PPAR-α pathway, leading to an increase in NFκB activity and hepatic cytokine expression (Dickens et al. 2017). Alternatively, EVs may also interact with leukocytes, as they have been shown to carry MHC class I and II, and co-stimulatory receptors, and therefore contribute to antigen presentation (Admyre et al. 2007; Admyre et al.

2006; Giri and Schorey 2008; Raposo et al. 1996). Kumar et al. (2017) showed that EVs depleted of their content with the surfactant PEG-TB lost their ability to activate microglia *in vitro*, making it clear that the composition of EVs is vital for their efficacy.

In comparison to brain injuries, the role of EVs following SCI specifically has been somewhat overlooked and the little data available are often contradictory. EVs isolated from the CSF of deceased SCI patients have been found to be enriched with inflammasome-associated proteins NLRP1, caspase-1 and ASC, indicating a pro-inflammatory phenotype (de Rivero Vaccari et al. 2016). Authors suggested that these EVs may induce an innate immune response, however no such experiments were performed to confirm this. Conversely, Brewster et al. (2020) incubated endothelial cells *in vitro* with EVs isolated from the plasma of SCI patients, yet reported that there was no induction of pro-inflammatory gene expression, although markers of oxidative stress were reduced. In fact, Kong et al. (2018) reported that EVs from the CSF of spinal injured rats promote neuronal proliferation. Therefore, there is no clear consensus on the role of EVs released after SCI, and their effect on SCI pathophysiology remains unknown (Osier et al. 2018; Yates et al. 2019). This will be investigated in Chapter 6.

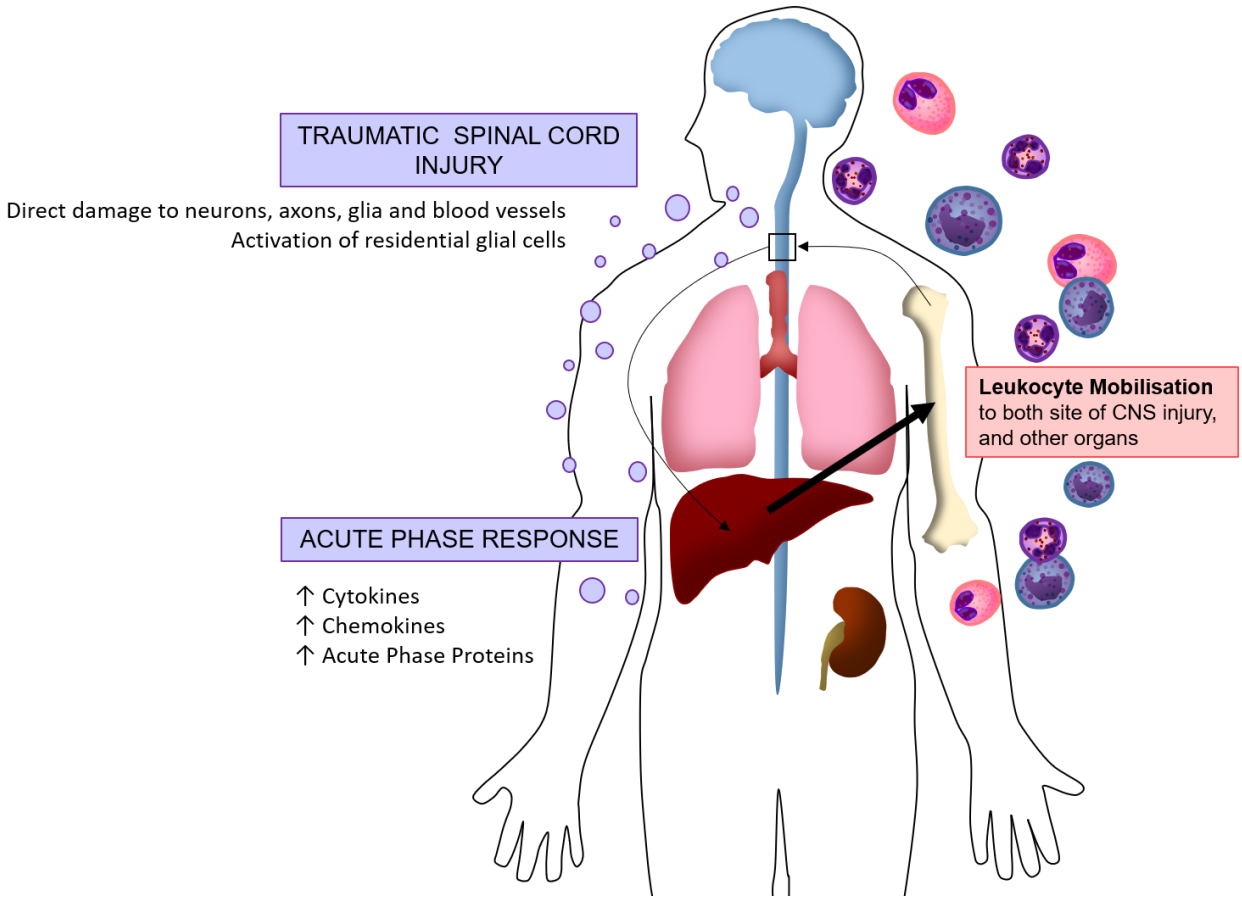


Figure 1.6 Visual representation of proposed hypothesis of EV-mediated activation of the APR following SCI. Traumatic injury to the spinal cord induces the release of EVs in the circulation, which localise to peripheral organs such as the liver and spleen and stimulate the acute phase response (APR). The increase in cytokines, chemokines and other acute phase proteins induces mobilisation of leukocytes from the bone marrow, which infiltrate the lesion site, contributing to the secondary phase of injury. This is an original figure.

1.3 Experimental SCI

1.3.1 Rodent models of SCI

The use of animal models in SCI research has become a commonly used tool to investigate underlying pathophysiology and trial new treatments. Rodents (mice and rats) share many characteristics with humans, which makes them good models for SCI. The human and rodent spinal cord share comparable structural, vascular and electrophysiological features. Whilst the rodent spinal cord has 34 spinal roots compared to the human 31, the segmental organisation is analogous across the species; for example, the cervical (C5-T1) and lumbar enlargements (T11-L2), which correspond to the nerves that innervate the upper and lower limbs respectively, extend from the same spinal cord segments in both rodents and humans (Harrison et al. 2013). Critically, rodents exhibit comparable functional, histological and immunological response to CNS trauma. Metz et al. (2000) demonstrated correlations between locomotor capacity and both lesion area and spared white matter, which was evident in rat and human SCI, thus validating the model. Rodents and humans also show similar leukocyte mobilisation and CNS infiltration in a predictable series of events (Figure 1.7): neutrophils, followed by monocytes, and then lymphocytes (Fleming et al. 2006; Kigerl et al. 2006), as well as the release of pro-inflammatory mediators (Lambertsen et al. 2012). However, despite all of the positive similarities, it is rather disappointing that so little work has translated from the pre-clinical models to man.

It must be acknowledged that the rat SCI model is more comparable to the human condition than the mouse model (Kjell and Olson 2016; Sroga et al. 2003). Histologically, during the chronic phase of SCI, a fluid-filled cystic cavity forms in the human and rat spinal cord, surrounded by spared white matter (Metz et al. 2000). Whereas in the mouse, the spinal cord lesion is instead filled with a connective-like tissue (Ma et al. 2001), due to the presence of fibroblast-like cells, which are absent in rat spinal cord lesions (Sroga et al. 2003). In addition, the timing of inflammatory cell infiltration of the spinal cord differs between species (Sroga et al. 2003); neutrophil density in the rat (Taoka et al. 1997) and human spinal cord (Fleming et al. 2006) returns to baseline within 2 weeks, yet remain elevated in the mouse (Kigerl et al. 2006). However, the generation and

availability of transgenic strains to study specific mechanisms and pathways, has resulted in mouse studies becoming more common. Importantly, comparable functional outcomes are observed following similar lesions in both species. Most rodent studies induce SCI at the thoracic level, which typically results in lower limb motor deficits, without affecting the forelimbs. This avoids autonomic consequences such as cardiac and respiratory dysfunction that require extensive post-operative care (Lilley et al. 2020). However, cervical-level injuries are more frequently observed in humans, and therefore are more clinically relevant, which is increasingly being targeted in animal models (Forgione et al. 2017; Lilley et al. 2020). In such cases, unilateral injuries are encouraged so that some innervation of the heart and respiratory muscles remain patent (Lilley et al. 2020).

Rodent models of SCI are characterised according to the manner in which injury is induced, of which contusion, compression and transection models are most prevalently used (Cheriyan et al. 2014; Ahmed et al. 2019). Contusion models induce injury with a transient, physical impact to the spinal cord, and represent the most common presentation of human SCI. By contrast, the compression model involves sustained pressure to the spinal cord, which mimics fracture dislocations and burst fractures. Alternatively, transection models simulate the severing of the spinal cord; whilst this type of injury is rarer in the clinic, this model represents penetrating injuries such as knife wounds.

The first contusion models involved dropping a weight onto the exposed spinal cord; variations of the height from which it is dropped allows for graded injury severity (Basso et al. 1996; Metz et al. 2000). However, this model is vulnerable to “weight bounce”, where the weight can bounce off the spinal cord and cause additional impacts, and therefore is highly variable. As a result, force-controlled impactors have been developed, which induce contusive injuries with greater control and consistency. These devices also monitor injury velocity, force and displacement from computer-generated impact graphs which allows for the identification, and therefore exclusion, of outliers. Contusion injuries necessitate good sham animals as controls, because of the amount of surgery required to successfully carry them out. Animals must first undergo a dorsal laminectomy to expose the spinal cord and the column is stabilised by clamping the caudal and rostral vertebrae.

Clamp slippage or crushing of the vertebrae are rare complications, which may result in unintentional damage to the cord, requiring the animal to be excluded from the study (Choo et al. 2009).

In the compression model, following laminectomy, a modified aneurysm clip is applied to the spinal cord at a specific force, for a defined amount of time, both of which can be adjusted to vary injury severity (Poon et al. 2007). Whilst this model is less expensive and easier to perform than the contusion model, inconsistent force and velocity at which the clip is applied can result in high variability (Cheriyan et al. 2014). Alternatively, calibrated forceps can be used to induce the compression bilaterally, however this technique lacks the initial contusion injury, which is associated with most human traumatic SCI. Some studies have explored a combined contusion-compression model (Forgione et al. 2017), although there is high mortality due to the severity of this model (Batchelor et al. 2010).

Transection models are less common than compression and contusion models, as this type of injury is rarely seen in SCI patients. However, this model of SCI is valuable to investigate neuronal regeneration, rather than pathophysiology (Cheriyan et al. 2014; Lukovic et al. 2015). Variants of this model include a full transection, where the spinal cord is severed completely, or a partial transection, also known as a hemi-section, where the spinal cord is selectively lesioned. The latter allows for direct comparison of injured and healthy fibres within the same animal and is more clinically relevant because it is more commonly observed in humans.

In addition to mechanical models, chemical models of SCI have also been developed. Injection of glutamate directly into the spinal cord causes excitotoxicity, increased central inflammation and associated motor deficit (Liu et al. 2008). Alternatively, various models of vascular dysfunction have been developed. Spinal cord ischemia can be photochemically induced (Piao et al. 2009a); the animal is injected with Rose Bengal and the blood vessels of the spinal cord are exposed to light for a select duration of time. This causes the formation of a clot in the blood vessel, and subsequent ischemic damage. Intraspinal injection of the vasoconstrictor endothelin-1 can cause similar ischemic damage and associated motor deficits (Carvalho et al. 2017). Alternatively, collagenase

can be injected into the spinal cord, allowing for a highly controlled, reproducible model of haemorrhage, which results in the infiltration of immune cells as well as neuronal damage (Losey et al. 2014). Although they do not take into account the interacting factors and overall physical insult, reductionist models such as these allow for the study of a specific feature of SCI pathophysiology.

Rodent models cannot recapitulate all clinical aspects of SCI. However, given the extensive anatomical and physiological similarities to human SCI, in addition to their reproducibility, high reproductive rate, condensed life span, moderate cost and ability to mimic different mechanisms of injury, mouse models are critical to develop novel therapies.

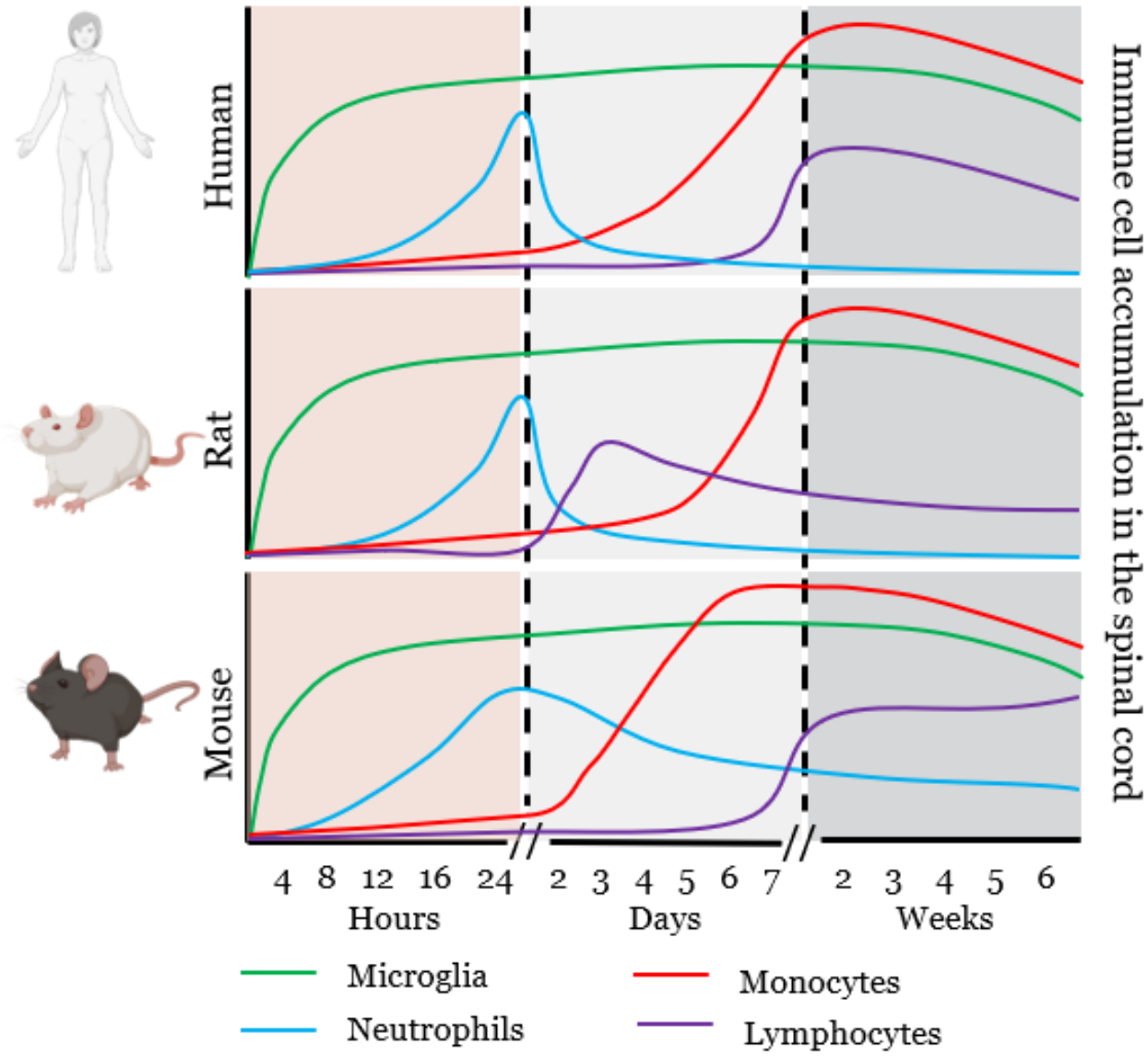


Figure 1.7 Spinal cord leukocyte recruitment across species. Comparison of the temporal accumulation of innate and adaptive immune cells in the spinal cord in the mouse, rat and human, following SCI. This is an original figure, generated using Fleming et al. (2006) and Sroga et al. (2003).

1.3.2 Treatments under investigation

1.3.2.1 Neuroprotective

Several therapeutic strategies are currently under investigation in the clinic to protect remaining neuronal tissue, spared after the initial injury (Figure 1.8). In humans, a number of drug combinations and strategies have made it to clinical trials. Riluzole and magnesium, a sodium channel blocker and NMDA receptor antagonist respectively, have both been shown to improve neuronal survival and white matter sparing by restricting glutamate-mediated excitotoxicity (Chow et al. 2012; Wu et al. 2013; Wiseman et al. 2009; Lee et al. 2010). Treatment of acute SCI with various growth factors have also yielded positive results; granulocyte colony stimulating factor, which promotes survival, proliferation and differentiation of haematopoietic cells, enhanced angiogenesis and improved functional recovery, in a rat SCI model (Kawabe et al. 2011). Additionally, the haemopoietic glycoprotein erythropoietin (EPO) has been shown to reduce SCI lesion size and improve motor function through anti-inflammatory and anti-apoptotic mechanisms (Gorio et al. 2002; King et al. 2007). Each of these pharmacological strategies exhibit neuroprotective potential, have been proven effective in animal models and have entered into human clinical trials (Badhiwala et al. 2018).

Non-pharmacological neuroprotective strategies include therapeutic hypothermia. By cooling the body to 32-34°C, the metabolic rate of the CNS is decreased, and has been shown to reduce inflammatory mediators and cell death (Sun et al. 2019; Yenari and Han 2012). Currently used to minimise preterm brain injury in infants born <37 weeks gestation (Rao et al. 2017), therapeutic hypothermia has been shown to preserve tissue and neurological function after stroke (Hong et al. 2014) and TBI (Adelson et al. 2013). In human SCI, both local and systemic hypothermia have been investigated. Local spinal cord hypothermia can be induced by irrigation of the subdural space with cold saline, and has been shown to reduce the incidence of neurological deficits (Cambria et al. 1997). Systemic hypothermia has been trialled in the clinic and improvements in neurological outcomes have also been reported, as evident by ASIA score conversion (Cappuccino et al. 2010;

Dididze et al. 2013; Levi et al. 2009; Madhavan et al. 2012). Although duration of treatment, maintenance temperature and rate of warming, all require optimisation (Wang and Pearse 2015).

1.3.2.2 Regenerative

Alongside the development of neuroprotective strategies, there is ongoing research focusing on neuroregeneration (Hutson and Di Giovanni 2019). It was first considered that CNS tissue was incapable of regeneration. However, this concept was challenged by David and Aguayo (1981), who demonstrated that transplantation of peripheral nerve into the injured spinal cord resulted in axonal growth within the graft (David and Aguayo 1981; Fawcett 2018). This landmark discovery indicated that there are factors in the damaged spinal cord that inhibit axonal regeneration, which seem to be absent in peripheral nervous system tissue. This changed the field of regenerative research, leading to the discovery of numerous inhibitory molecules, which may be therapeutically targeted to encourage axon regrowth.

In the chronic phase of SCI, components that contribute to the fibrous glial scar, such as CSPGs, form a physical barrier and impede axonal regeneration (Bradbury and Burnside 2019). Moreover, myelin-associated factors, oligodendrocyte myelin glycoprotein (OMgp), NOGO, further inhibit neurite growth (Cafferty et al. 2010). As a result, there has been development of treatments to overcome these barriers and encourage endogenous regeneration. The enzyme chondroitinase ABC (ChABC) can digest CSPGs, thereby making the lesion environment more permissible for neurite growth. Indeed, it has been shown to promote axonal regeneration and functional connections, which translates to improved motor recovery (Bradbury et al. 2002). This result is dependent on length of treatment, as sustained, long term ChABC treatment improved motor function to a greater extent than short term treatment (Burnside et al. 2018). Further research indicates that ChABC also has an anti-inflammatory effect; macrophages are polarised into the alternatively activated state (Bartus et al. 2014), which is thought to promote regeneration (Kigerl et al. 2009), and an IL-10-mediated response is induced (Didangelos et al. 2014). Greater improvements were observed when ChABC was combined with physiotherapy, demonstrating that a multifaceted approach is

required to not only remove barriers, but then to also encourage neuron regrowth (Wang et al. 2011).

Inhibitors of neurite growth can also be targeted directly. NOGO can be inhibited with a monoclonal anti-NOGO antibody (Chen et al. 2000b), which results in fibre sprouting and improved locomotion (Maier et al. 2009). Whereas, Rho/ROCK, regulators of the cytoskeleton, can be inhibited by antagonists Cethrin, Fasudil and Y-27632, which prevents collapse of the axonal growth cone, thus encouraging regeneration (Lehmann et al. 1999; Hara et al. 2000; Forgione and Fehlings 2014). Interestingly, Y-27632 also inhibits EV release (Catalano and O'Driscoll 2020), further associating EV signalling with SCI pathogenesis. Although additional work is required, many of these regenerative strategies are showing promising results in the clinic, particularly in conjunction with other therapies.

Cell-based therapies aim to generate new neuronal tissue to replace that which has been lost to injury and cell death (Assinck et al. 2017). Typically, these cells are derived from pluripotent stem cells, which have the capacity to proliferate and differentiate into several different cell types. Initial studies isolated cells from embryonic stem cells (Deshpande et al. 2006; McDonald et al. 1999), however due to ethical considerations, research has moved towards using induced pluripotent stem cells (iPSCs) or endogenous stem cell sources instead. These cells can be partially differentiated into neural, or oligodendrocyte progenitor cells, both of which have been studied in the context of SCI (Parr et al. 2007), however mesenchymal stem cells (MSCs) have been most frequently investigated (Cofano et al. 2019). Derived from iPSCs, bone marrow, adipose tissue or umbilical cord tissue, MSCs are multipotent stem cells with the ability to differentiate into cells of bone, cartilage and CNS, amongst others (Sanchez-Ramos et al. 2000; Nandoe Tewarie et al. 2009). When transplanted, cells can integrate into the remaining spinal cord tissue to form structural and functional connections. In addition, they secrete neurotrophic factors such as brain-derived growth factor and nerve growth factor, as well as anti-inflammatory cytokines IL-10 and IL-13, which facilitate neuroprotection and axonal regeneration (Cofano et al. 2019). Certainly, MSC transplantation has restored motor function in animal models of SCI (Oliveri et al. 2014; Osaka et

al. 2010). However, despite these positive outcomes, due to the proliferative nature of stem cells, there is a risk of tumour development (Lee et al. 2013), and the development of neuropathic pain has been reported (Kishk et al. 2010), therefore additional studies are required before being implemented in the clinic.

Transplantation of Schwann cells has also been shown to have therapeutic potential (Oudega and Xu 2006). Schwann cells are a type of glial cell, which form the myelin sheath that insulates peripheral neurons and contribute to axon regeneration after injury. After SCI, they have been shown to support tissue preservation, axonal growth, remyelination and functional recovery (Mousavi et al. 2019). Olfactory ensheathing cells (OECs) have similarly shown promise (Gomez et al. 2018). Along with their natural ability to undergo active, lifelong neurogenesis (Treloar et al. 2001), OECs are of interest as they have been shown to create a favourable environment for regeneration by modulating inflammation (Xie et al. 2019) and expressing neurotrophic factors (Woodhall et al. 2001). Indeed, several studies have demonstrated improved histological and functional outcomes with transplantation after SCI (Li et al. 1997; Wang et al. 2021), although contradictory results have been reported (Gomez et al. 2003). Neural stem cells (NSCs) have also been investigated; NSCs are multipotent stem cells, which can differentiate into neurons and glia in the CNS. Lu et al. (2012) demonstrated that NSCs implanted into an adult rat, lesioned spinal cord were able to integrate, extend axons and form functional connections. However, many issues remain with cell-based therapies. The regenerative distances do not scale; the growth cone can collapse upon reaching the other side of the lesion. Moreover, it must be acknowledged that the injection of a handful of cells in a complex structure is unlikely to make a direct difference. As such, it is perhaps unsurprising that minimal progress has been made with this strategy.

To improve stem cell integration and survival, as well as support axonal growth, biomaterials and scaffolds have been developed. In this way, they can replicate the extracellular matrix and fill the post-injury cystic cavity to allow new connections across the lesion. Several biomaterials have been engineered that have been shown to facilitate regeneration. For example, a fibrin matrix has been used with neural stem cells, resulting in dense axon growth which integrated into the spinal cord

and improved functional recovery (Lu et al. 2012). Similarly, hyaluronic acid-based hydrogels and the self-assembling peptide QL6 have been shown to be effective scaffolds to promote recovery (Thompson et al. 2018; Zweckberger et al. 2016). These biomaterials can then be specialised for example to contain growth factors or to biodegrade (Ahuja et al. 2017a). As novel, niche materials and therapies are developed, this regenerative strategy can be further optimised.

Despite the significant advances in neuroprotective and regenerative strategies, many difficulties remain, which hinder translation to the clinic. Critically, the spinal cord is highly complex and consists of billions of cells (Bahney and von Bartheld 2018). Restoring neuronal connections, not just structurally but functionally, is no small feat. As a result, it may be some time before a successful treatment for chronic SCI is available, although some promising neuroplasticity-promoting treatments are currently in clinical trials. By contrast, protecting spared spinal cord tissue, vulnerable to secondary damage, will maintain the already established functional connections. To do this, we must more fully understand the mechanisms which contribute to secondary damage. Once we have established these, we are more likely to see success using acute, neuroprotective strategies.

1.3.2.3 Immunomodulatory

It is clear from this introduction that the activation of the immune system contributes to secondary damage in the spinal cord after traumatic injury. However, whilst intraspinal inflammation is considered largely detrimental, it does have some positive attributes, including clearance of debris and stimulation of regeneration and remyelination (Chio et al. 2021b). As such, broad immunosuppression is not necessarily useful. Moreover, this approach can be potentially dangerous, as severe side effects include increased risk of infection. SCI patients are already immunocompromised, owing to SCI-IDS, and post-injury infections are associated with worsened patient outcomes (Failli et al. 2012). Therefore, there is a need to selectively modulate aspects of the SCI-induced immune response in order to minimise damage. A number of interventions have yielded promising results, which will be discussed here.

Minocycline, a broad spectrum antibiotic, has been shown to have neuroprotective effects in a range of CNS disorders, including both neurodegenerative (Chen et al. 2000a; Garcez et al. 2019) and traumatic injuries (Sheng et al. 2018; Sanchez Mejia et al. 2001). These previous studies have consistently reported improvements in neurological function and tissue loss in animal models and humans. Minocycline is principally considered an MMP inhibitor, which maintains BSCB integrity and reduces leukocyte recruitment (Brundula et al. 2002; Ryan et al. 2001). However, with the ability to cross the blood-CNS barrier (Brogden et al. 1975), it is also thought that minocycline can directly act upon central inflammation, exerting an anti-inflammatory effect by inhibiting microglial activation, in conjunction with reducing oxidative stress, caspase-1/3-dependent apoptosis and pro-inflammatory cytokine release (Garrido-Mesa et al. 2013; Nikodemova et al. 2006; Plane et al. 2010). In SCI specifically, minocycline treatment has been shown to improve motor function, as well as reduce apoptosis, cavitation and microglial density (Festoff et al. 2006; Stirling et al. 2004), and has therefore entered human clinical trials (Casha et al. 2012).

Treatment with intravenous immunoglobulin (IVIg) has shown similar therapeutic potential (Gillespie and Ruitenberg 2020). Consisting of IgG pooled from the plasma of healthy donors, IVIg administered in the acute phase of injury reduced spinal cord cavitation and improved functional recovery in mouse (Brennan et al. 2016) and rat models of SCI (Nguyen et al. 2012; Chio et al. 2019; Chio et al. 2021a). It has also been shown to be effective in the treatment of TBI (Jeong et al. 2014; Thom et al. 2017), highlighting it is a robust modulator of neuroinflammation. Although its mechanism of action is not fully understood, it has been proposed that it interacts with Fcγ receptors on innate immune cells, thereby modulating their response to inflammatory stimuli. Certainly, preclinical SCI studies demonstrated attenuated neutrophil and macrophage recruitment to the spinal cord, and reduced central expression of pro-inflammatory molecules. Alternatively, the beneficial effect of IVIg may be through the scavenging and neutralisation of components of the complement cascade (Brennan et al. 2016), which have been implicated in contributing to secondary injury after SCI (Brennan et al. 2015; Galvan et al. 2008). As a result, a human clinical trial investigating the neuroprotective effect of IVIg is underway (Australian Clinical Trials, ACTRN12616001385437).

Targeting soluble inflammatory mediators is a promising therapeutic strategy currently being explored (Ren et al. 2018; Azodi and Jacobson 2016). Master cytokines such as IL-1β, TNF and CXCL1 are upregulated in the CNS within minutes of traumatic injury (Pineau and Lacroix 2007; Campbell et al. 2002) and are associated with the mechanisms which drive secondary damage (McColl et al. 2007; Sato et al. 2012; Zhu et al. 2019). Therefore, they could be ideal therapeutic targets for the acute treatment of SCI. Indeed, anti-cytokine therapy has been trialled in a number of models of CNS injury. For example, etanercept, which blocks both transmembrane and soluble TNF, has been shown to reduce neutrophil infiltration of the brain and improve functional outcomes in models of stroke (Clausen et al. 2014), inflammatory brain lesion (Campbell et al. 2007) and SCI (Genovese et al. 2006). Similarly, antibody-mediated neutralisation of CXCL1 reduced the number of neutrophils in the blood, liver and brain after inflammatory insult (Campbell et al. 2003).

Inhibition of IL-1 signalling is of particular interest as IL-1β has its own endogenous antagonist, IL-1RA, which may be easily exploited for therapeutic gain. Certainly, treatment with IL-1RA has shown to reduce central inflammation, tissue loss and functional deficits in both rodents and human patients after TBI (Clausen et al. 2011; Hasturk et al. 2015b; Helmy et al. 2014) and stroke (Emsley et al. 2005; Greenhalgh et al. 2010; Maysami et al. 2016; Pradillo et al. 2017; Smith et al. 2018). In animal models of SCI, IL-1RA treatment has been shown to improve lesion size and motor function (Akuzawa et al. 2008; Hasturk et al. 2015a; Zong et al. 2012). However, these studies did not explore the underlying mechanisms, which will be addressed in chapter 3. IL-1β may also be neutralised with the monoclonal antibody canakinumab or the soluble decoy receptor rilonacept (Murray et al. 2015), however their efficacy to treat traumatic CNS injuries has not been evaluated.

Interestingly, many of the immunomodulatory therapeutics discussed here are unable to cross the BBB/BSCB, yet, in the preclinical studies, they were administered systemically. This suggests that these therapies may exert their beneficial effects, at least in part, by attenuating the peripheral inflammatory response.

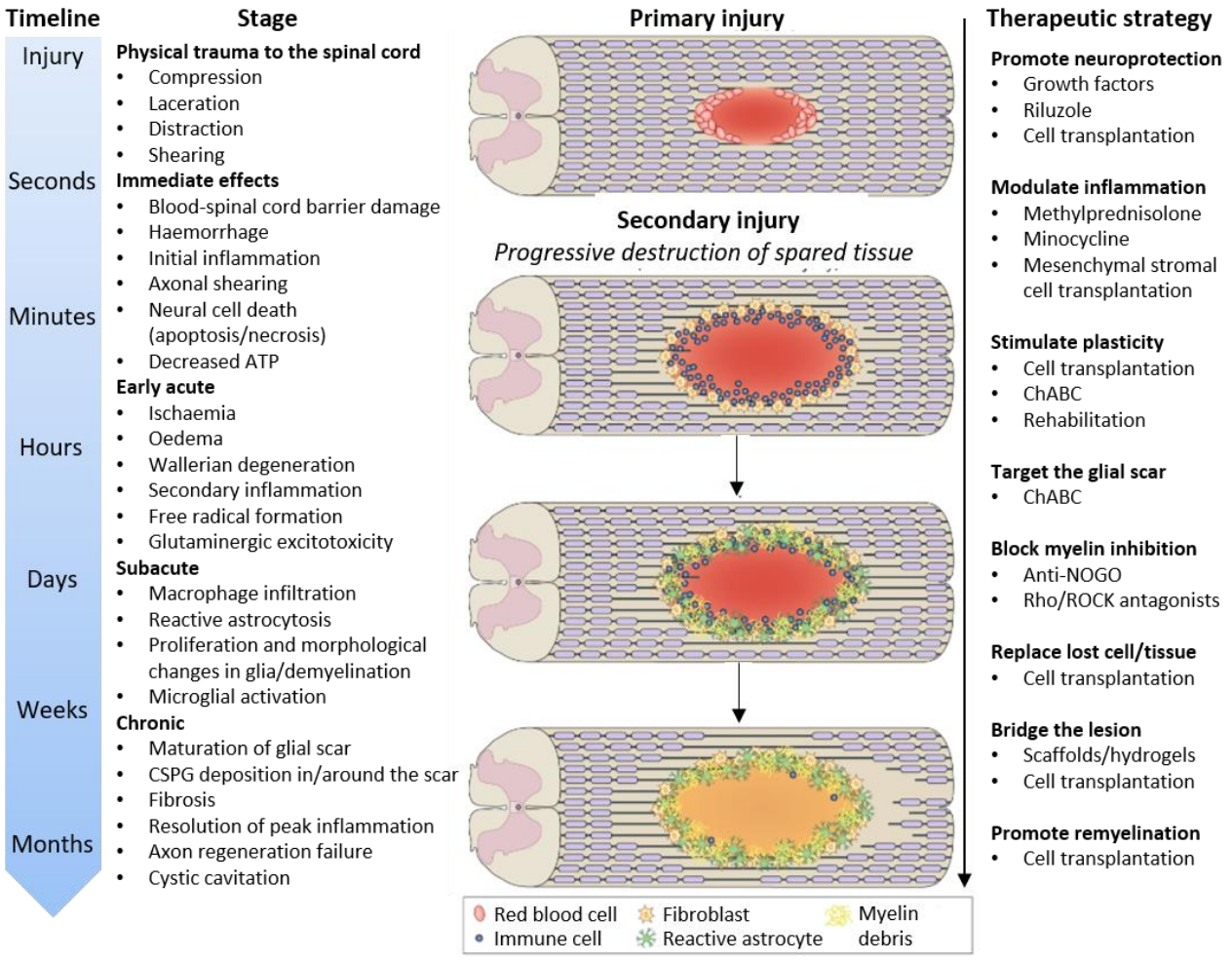


Figure 1.8 Pathophysiology of SCI: therapeutic targets. Traumatic injury to the spinal cord initiates a series of events, which results in the progressive destruction of neuronal tissue and functional deficits. Numerous therapeutic strategies have been investigated targeting the underlying mechanisms of SCI pathophysiology, however none are yet to be approved for use in the clinic. CSPG – chondroitin sulphate proteoglycan, ChABC – chondroitinase ABC, NOGO - neurite outgrowth inhibitory protein. Figure adapted from (Lindsay et al. 2020).

In this introduction, I have provided an overview of the pathophysiology of SCI, including the histological presentation and the contribution of the immune response, and the rodent models available. In turn, I have discussed the neuroprotective, regenerative and immunomodulatory strategies currently being investigated to improve functional outcomes. However, to date, none have been approved for routine use in the clinic. The consequences of SCI are not confined to the CNS; I have described how SCI induces a peripheral inflammatory response, termed the APR, which can exacerbate inflammation in the spinal cord and cause damage to peripheral organs. Previous work has suggested that inflammation in the CNS can be indirectly targeted by modulating this peripheral response, which presents an alternative strategy to treat acute SCI. However, the initiation signal, which triggers the APR, and the extent to which it contributes to lesion progression and functional recovery remains unclear. As such, there is a need to improve our understanding of the mechanisms underlying the systemic inflammatory response in order to critically evaluate its potential as a therapeutic target.

1.4 Aims of this thesis

The principal aim of this thesis was to comprehensively characterise the systemic response to SCI, to determine its influence on spinal cord inflammation and pathology, and to develop effective treatments. It is hypothesised that the SCI-induced APR contributes to lesion progression in the spinal cord, and, thus, would serve as a useful therapeutic target.

Specifically, this thesis aims:

1. *To examine the effect of inhibiting the peripheral immune response to SCI.*

To meet this aim, the peripheral inflammatory response to a lower thoracic spinal cord injury during the acute phase will be characterised. In turn, the effect of suppressing the APR with exogenous IL-1RA on peripheral and central inflammation will be examined. I hypothesise that SCI will induce a robust APR, suppression of which will improve spinal cord pathology. This will be explored in Chapter 3.

2. *To characterise the peripheral immune response to acute SCI at different severities and anatomical locations.*

To meet this aim, SCI will be induced within a range of forces (30kilodyne [kD], 70kD, 100kD), at 2 different lesion levels (T9 and T2), and the impact on the peripheral immune response will be evaluated. I hypothesise that there will be a positive correlation between the severity of the injury and the magnitude of the APR. In addition, I hypothesise that there will be a lesion level effect, with injury at T2 will inducing a greater response than injury at T9. This will be explored in Chapter 4.

3. *To investigate metabolic changes in the spinal cord and peripheral tissues after SCI.*

To meet this aim, ^{1}H NMR with multivariate analysis will be used to evaluate metabolite changes in the plasma and liver during the acute phase of SCI. In addition, the effect of injury severity or lesion level on the plasma, liver and spinal cord metabolome will be determined. I hypothesise that SCI will induce profound metabolic changes in central and peripheral tissues, which are dependent on the nature of the lesion. This will be explored in Chapter 5.

4. *To determine the contribution of EVs to the peripheral immune response after SCI.*

To meet this aim, the impact of SCI on the circulating EV population will be determined. Subsequently, the ability of SCI plasma EVs to modulate inflammation will be assessed both *in vitro* and *in vivo* through adoptive transfer experiments. I hypothesise that SCI will cause an increase in plasma EV concentration, and that these EVs can induce an inflammatory response. This will be explored in Chapter 6.

Chapter 2: Materials and methods

2.1 Human plasma sample collection

Plasma samples were collected from 29 SCI patients (male = 27, female = 2) upon admission to the Princess Alexandra Hospital, Brisbane Australia (Table 2.1), prior to the initiation of any treatment (HRECs: 15/QPAH/211, 16/QPAH/197). New injury severity score (NISS) (Osler et al. 1997; Jogia et al. 2021) and ASIA classification (Burns and Ditunno 2001; van Middendorp et al. 2011) were completed by a physiotherapist, to evaluate degree of general trauma, independent of the body region affected, and SCI, respectively. Plasma samples from healthy controls (male =9, female =5) were obtained from volunteers at the University of Queensland, and as part of the ongoing study of inflammatory diseases at the Department of Pharmacology, University of Oxford UK (CUREC Approval Reference: R55592/RE001). There was no significant difference in age between healthy controls (31±5) and SCI patients (36±3; unpaired student's t-test, p=0.478). All participants gave informed written consent for samples to be used in scientific research (Appendix).

Peripheral venous blood was collected into lithium-heparin-coated tubes. Samples were kept at room temperature (RT) and processed; blood was centrifuged at 1,000*g* for 10 minutes at RT, plasma was then transferred to a clean tube and spun for a further 15 minutes at 2,000*g*. Platelet-free plasma was isolated, snap-frozen in liquid nitrogen and stored at -80°C.

Samples were transported from Brisbane, Australia, to Oxford, UK under DEFRA import licence IMP/GEN/2018/04.

Table 2.1 SCI patients demographics. Description of SCI patients from whom blood samples were collected, and the nature of their injury. Where data was unavailable, cells were left blank. NISS – new injury severity score, ASIA – American spinal cord injury association score.

Patient number	Sex	Age	Level of injury	NISS	First ASIA	Last ASIA	Time between ASIA scores (days)	Time from injury to sample collection (hours)
#1	F	47	C5	24	B	C	269	10.75
#2	M	73	C4	18	C	C	220	10
#3	M	45	T9	50	A	B	96	6.5
#4	M	27	C4	24	C	D	42	14
#5	M	28	T4	43	A	A	165	7.5
#6	M	33	C5	38	A	A	261	4.5
#7	F	24	C5	33	A	A	180	4.5
#8	M	45	T4	43	A	A	130	7.25
#9	M	18	C6	32	B	D	41	12
#10	M	18	C4	17	B	D	165	7
#11	M	59	T5	43	A	A	339	9.5
#12	M	39	C3	30	B	B	250	4.75
#13	M	18	C4	20	C	D	22	6.5
#14	M	54	C6		A	A	303	6
#15	M	16	C5		C	D	21	8.5
#16	M	31	C4		A	A	179	10.3
#17	M	27	T4	43	A	A	173	28.75
#18	M	22	C6	29	A	A	244	
#19	M	63	C3	17	D	D	100	
#20	M	55	C5		B	A	159	26.75
#21	M	25	T12	34	C	D	45	22.5
#22	M	22	T10	43	A	A	85	36.75
#23	M	33	T12	29	B	C	85	22.5
#24	M	18	C4	30	A	A	295	
#25	M	24	C7	30	A	A	32	16.5
#26	M	21	C6	26				20.3
#27	M	73	C1	24	C	C	305	23.5
#28	M	60	T11	38	A	A	120	7.3
#29	M	30	T4	43	A	A	210	23.3

2.2 Animals

Adult C57BL/6 were used throughout this thesis. In Australia, WT animals were obtained from the Animal Resource Centre (Canningvale, Western Australia). All procedures were approved by The University of Queensland's Animal Ethics Committee (Anatomical Biosciences) and conducted in accordance with the Australian Code for the Care and Use of Animals for Scientific purposes.

In the UK, animals were obtained from Biomedical Services at the University of Oxford (UK) and all experiments were approved by the University of Oxford local committees (LERP, ACER) in accordance with the UK Animals (Scientific Procedures) Act, 1986, under project licence P996B4A4E.

All animals were housed in a pathogen-free facility, under standard diurnal lighting conditions (12 hours) with *ad libitum* access to food and water.

2.3 Animal CNS injury models

2.3.1 Spinal cord injury (SCI) model

A well-characterised contusion model was utilised to simulate spinal cord injury in this thesis (Scheff et al. 2003). Mice were anaesthetised by intraperitoneal injection, using a combination of tiletamine/57olazepam (50mg/kg; Virbac) and xylazine (10mg/kg; Troy Laboratories). Following excision of the lower thoracic region of the back, the paravertebral muscles were separated and anatomical landmarks were utilised to identify the appropriate vertebrae (Harrison et al. 2013). A dorsal laminectomy was then performed when applicable, as previously described (Blomster et al. 2013a; Blomster et al. 2013b; Scheff et al. 2003) to expose the cord. The column was clamped for stabilisation and a contusive SCI was inflicted using the Infinite Horizon Impactor (Precision Systems and Instrumentation). Post-SCI, the muscle and skin were closed with 6-90 polygalactin dissolvable sutures (Ethicon) and Michel wound clips (Kent Scientific), respectively. Age- and weight-matched sham-operated mice underwent the laminectomy surgery, but did not receive injury to the spinal cord. Following surgery, all mice received a single dose of buprenorphine in Hartmann's sodium lactate (1mg/kg, sub cutaneous; Sigma Aldrich) for analgesia. During the

course of the experiment, bladders were manually voided twice a day. As anaesthesia is known to have anti-inflammatory effects (Cruz et al. 2017), naïve mice received anaesthesia, but did not undergo any surgery, and were used to establish baseline results.

2.3.2 Experimental design

Power analysis was completed for sample size estimation (G*Power). Power analysis enables the identification of the number of animals required to achieve statistical significance between groups, whilst adhering to the 3 R's of animal research. In a previous study, a 4.3-fold increase in peripheral inflammatory markers in the SCI group compared to the control group was reported (Brennan et al. 2019), with a standard deviation of approximately 25%, which gives an effect size of 3.8. With an alpha of 0.05 (probability of a type I error – false positive rate) and power of 0.8 (1-β, where β is the probability of a type II error – false negative rate), the projected sample size needed to achieve this effect size is approximately n=3. Therefore, experiments in this thesis included groups with a minimum of n=5, in order to meet the aims and account for any variation, as well as to allow for subgroup comparisons.

For time course experiments, animals received either a bilateral 70kD SCI at level T9, or sham surgery as control, and were allowed to survive for 2, 6, 12 or 24 hours post-injury (n=5/group/time point). Naïve animal group (n=5) was used to establish baseline. At their respective time points, blood, fresh spleen and liver, and fixed liver and spinal cord were collected for flow cytometry, qPCR, immunohistochemical, metabolomic and plasma EV analysis.

To investigate the effect of suppressing the APR on spinal cord pathology, animals received a bilateral 70kD SCI at level T9, and 2 intraperitoneal injections of either human IL-1RA (100mg/kg, n=8) or vehicle (n=9), immediately following and 5 hours after injury. Fresh and fixed liver, and fixed spinal cords were collected 6 hours post-SCI. Randomisation of animals into treatment groups was achieved by blinding the doses, which were then handed to the surgeon by an independent assistant, who was unaware of the contents.

For injury severity and lesion level experiments, animals received a bilateral SCI at level T9 with a force of either 30kD, 70kD or 100kD (n=10/severity). At level T2, animals received a bilateral, single-impact SCI with a force of 30kD, or a double-impact SCI with a force of 70kD (n=12/severity), due to the increased width of the segment and the aim to replicate the paralysis achieved at T9. No 100kD SCI at T2 injury group was included as preliminary analysis of T9 study revealed no difference between 70kD and 100kD injury groups. All animals were allowed to survive for 6 hours. Blood and fresh liver were collected from all animals for plasma EV, HPLC, qPCR and metabolomic analysis. Fresh spinal cord was collected from half of the animals in each group (n=5/severity at T9, n=6/severity at T2) for qPCR and metabolomic analysis. Fresh spleen was collected from the T9 cohort for flow cytometry analysis. Remaining animals underwent fixation for collection of fixed liver and spinal cord for immunohistochemical analysis.

For EV adoptive transfer experiments, EVs were isolated from the plasma collected from naïve animals, or animals that received a 70kD SCI at level T9, 2 or 6 hours after injury. Plasma EVs from 3 donor animals were pooled for injection into 1 recipient animal. Naïve or SCI plasma EVs were intravenously injected into recipient animals and fresh liver was collected 30 minutes (n=3/group) or 6 hours (n=3-4/group) afterwards. For biodistribution studies, fresh liver, spleen, lung, spinal cord, brain, kidney, gut and heart were collected from recipient animals (n=5), 30 minutes after injection.

2.4 Behaviour

2.4.1 Basso mouse scale (BMS)

To assess general locomotor function, the Basso mouse scale (BMS) was utilised as per published guidelines (Basso et al. 2006). Mice were placed in an open field paradigm for 4 minutes and hind-limb movement, stepping ability, limb co-ordination and trunk/tail stability were evaluated by at least 2 single-blinded investigators. Animals were assigned corresponding scores on a scale of 0-9, where 9 indicates normal function.

2.5 Tissue collection

At their respective time points, mice were anaesthetised with 4% isoflurane and blood was collected by cardiac puncture with a heparinised 21G needle. Blood was immediately transferred into a tube lined with anti-coagulant and was centrifuged at 1,000*g* for 10 minutes at 4°C, and the cell pellet was immediately processed for flow cytometry. The supernatant was further centrifuged at either 2,000*g* or 13,000*g* for 10 minutes at 4°C to generate platelet-free plasma, which was snap-frozen in liquid nitrogen and stored at -80°C. Animals were then transcardially perfused with 20mL of heparinised saline (0.9% NaCl 10IU/mL heparin [Pfizer], 2%$NaNO_3$) and fresh peripheral tissue were collected for flow cytometry, qPCR and metabolomic analysis. Tissue was flash frozen in liquid nitrogen and stored at -80°C; fresh spleen was processed immediately for flow cytometry.

Tissue was then fixed by transcardiac perfusion with 30mL of Zamboni's fixative (2% picric acid, 2% paraformaldehyde [PFA], pH 7.2-7.4), or 4% PFA in 0.1M phosphate buffer (pH 7.4). Peripheral organs and the spinal column were dissected out and stored in fixative overnight at 4°C. Spinal cords were extracted the following day, and were stored in fixative at 4°C for an additional 24 hours. Tissue was cryoprotected with subsequent overnight incubations in 10% and 30% sucrose solutions, and embedded in optimal cutting temperature compound (OCT, ProSciTech). Fixed peripheral tissue (10µm) and spinal cord (transverse, 20µm) were sectioned using the Leica Cryostat and stored at -20°C or -80°C until staining.

2.6 Peripheral leukocyte analysis

2.6.1 Flow cytometry

Blood and spleen samples were analysed for granulocyte content by flow cytometry. For splenocyte preparations, fresh spleen was dissociated through a 70µm cell strainer (Life Technologies) and centrifuged for 5 minutes at 300*g*. Cells were then resuspended in 5mL of red blood cell (RBC) lysis buffer for 5 minutes at RT, before being centrifuged again for 5 minutes at 300*g* and resuspended in Dulbecco's PBS (DPBS). For yield quantification, samples were diluted 1:1 with Trypan blue and the concentration of live cells was determined with a haemocytometer. 5 million splenocytes per

sample were used for analysis. For blood preparation, the cell pellet isolated by centrifuging whole blood at 1000*g* for 10 minutes at 4°C, was resuspended in 4mM Ethylenediaminetetraacetic acid (EDTA; Sigma Aldrich) in DPBS. Samples were then diluted 1:5 in RBC lysis buffer for 5 minutes at RT, after which they were centrifuged for 10 minutes at 200*g* at 4°C. Cells were resuspended in 100µL of DPBS and used for analysis.

To exclude dead cells, splenocyte and blood samples were incubated with Zombie Green and Zombie Near Infrared (NIR; 1:100 in DPBS), respectively, for 20 minutes at RT in the dark. Cells were pelleted and resuspended in CD16/32 F_C block (BD Biosciences), diluted 1:200 in blocking buffer (0.5% Bovine serum albumin [BSA], 2mM EDTA in DPBS) to prevent non-specific binding, for 10 minutes on ice in the dark. For the identification of neutrophils and monocytes, samples were immunolabelled with appropriate fluorophore-conjugated antibodies (Table 2.2) for 20 minutes in the dark. Next, 1mL of blocking buffer was added to dilute any unbound antibody and cells were isolated by centrifugation at 300*g* for 10 minutes at 4°C. The cell pellet was resuspended in blocking buffer for analysis on the LSR II flow cytometer (BD Biosciences) with BD FACS Diva software.

For accurate interpretation, results were gated to exclude cell doublets and triplets, debris and dead cells. Neutrophils were defined as the $CD11b^{+}SSC^{hi}Ly6G^{+}$ population (Figure 2.1; Figure 2.2). Monocytes were defined as the $CD11b^{+}Ly6G^{-}$ population in the blood (Figure 2.1), and the $CD11b^{+}SSC^{lo}F4/80^{lo}Ly6C^{lo}$ population in the spleen (Figure 2.2). Propidium iodide-fluorescing counting beads were added to each sample and controls (10µL; Beckman Coulter) according to manufacturer's instructions, as an internal control to enable the absolute quantification of cell number.

Table 2.2 Flow cytometry Antibodies. The antigen specificity, clone, dilution and manufacturer for each antibody utilised to determine the number of granulocytes in the blood and spleen.

Antigen	Antibody (Clone)	Specificity	Dilution	Company
CD11b	BV 785™ Rat α-mouse/human CD11b (M1/70) (Spleen)	Myeloid immune cells	1:100	BioLegend
	PE Rat α-mouse/human CD11b (M1/70) (Blood)	Myeloid immune cells	1:200	BioLegend
Ly6G	Alexa Fluor® 647 Rat α-mouse Ly6G (1A8)	Granulocytes	1:100	BioLegend
Ly6C	V450 Rat α-mouse Ly6C (AL-21)	Monocytes/macrophages, granulocytes	1:100	BD Horizon
F4/80	PE Rat α-mouse F4/80	Macrophage subsets	1:50	BD Biosciences

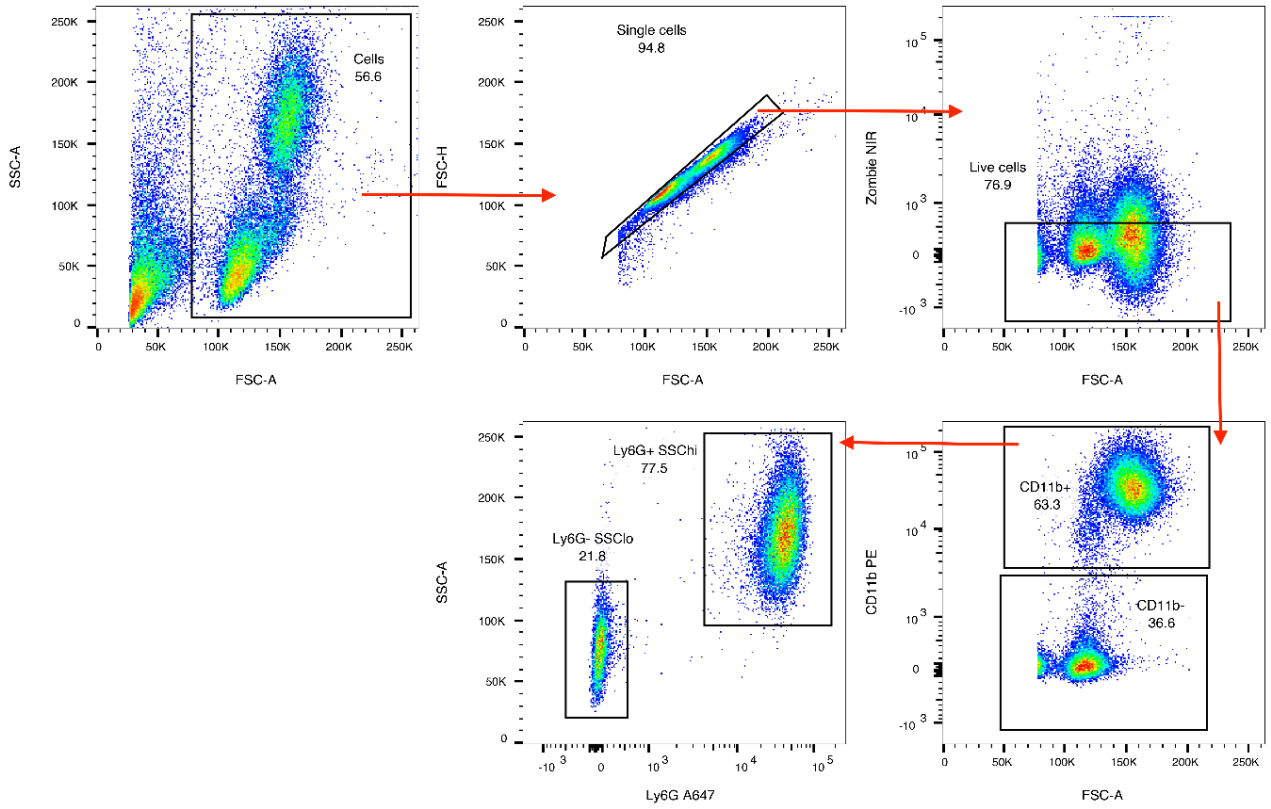


Figure 2.1 Gating strategy for blood myeloid cells. Cells were first gated to exclude debris, doublets and dead cells. Granulocytes and monocytes were defined as the $CD11b^{+}SSC^{hi}Ly6G^{+}$ and $CD11b^{+}Ly6G^{-}$ populations respectively.

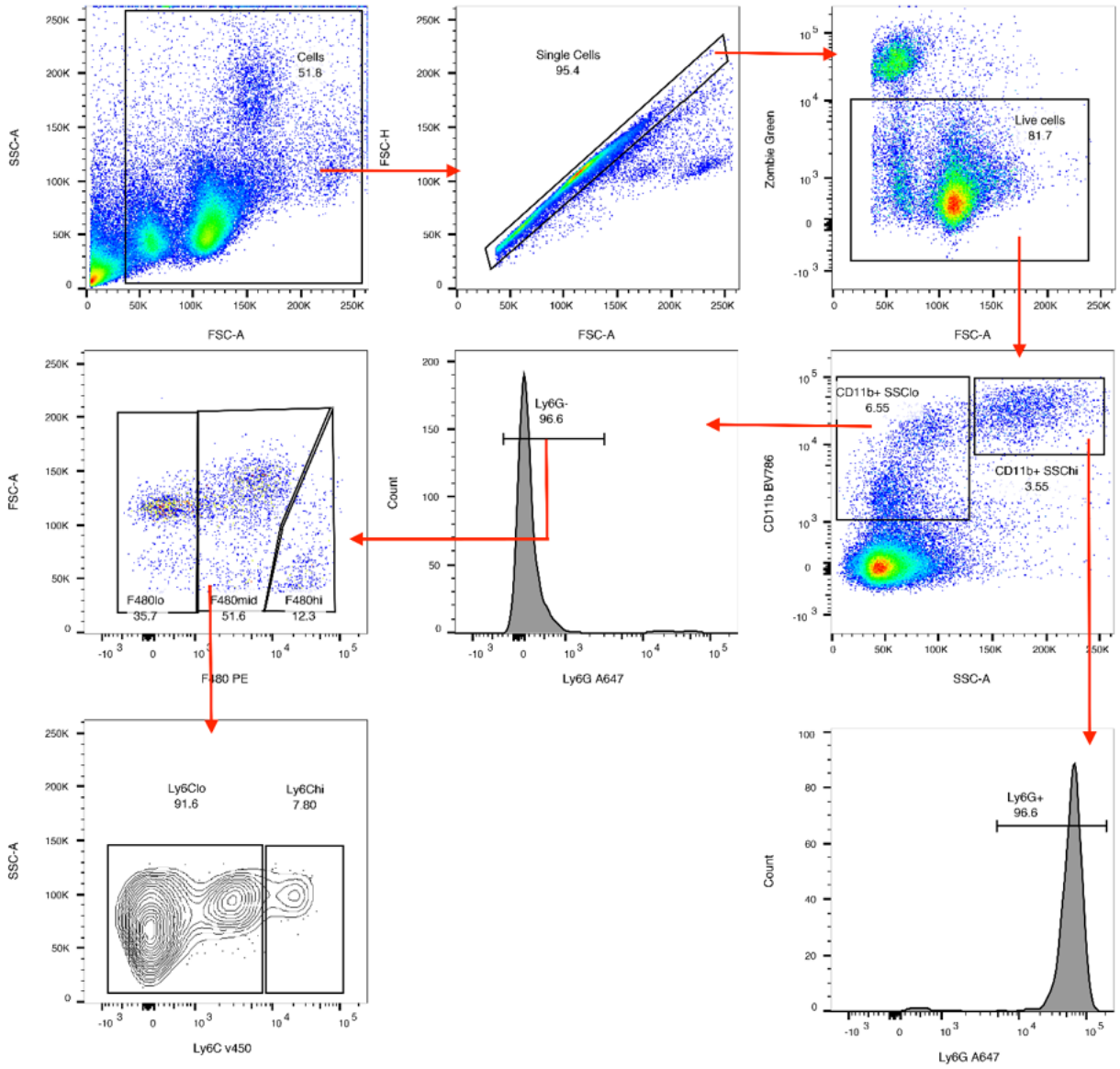


Figure 2.2 Gating strategy for spleen myeloid cells. Cells were first gated to exclude debris, doublets and dead cells. Granulocytes and monocytes were defined as the CD11b^{+}SSC^{hi}Ly6G^{+} and CD11b^{+}SSC^{lo}F4/80^{lo}Ly6C^{lo} populations, respectively.

2.7 Histology

2.7.1 Immunohistochemistry with DAB

For staining with the chromogenic reporter 3,3'-Diaminobenzidine (DAB), fixed tissue was dried in a 37°C oven for 15 minutes and briefly washed in PBS, before quenching endogenous peroxidase activity with 1% H_2O_2 in methanol for 10 minutes. Sections were then washed in PBS and blocked for endogenous avidin and biotin binding (1:20 in PBS for 15 minutes each, Vector Labs). Non-specific protein binding was blocked with 10% goat or horse serum in PBS for 1 hour at RT. Sections were incubated in primary antibody (Table 2.3), diluted in 1% serum in PBS, overnight at 4°C. Sections were washed in PBS (3 x 5 minutes) to remove any unbound antibody, and incubated in biotinylated secondary antibody (1:200; Vector Labs) diluted in 1% serum in PBS, for 2 hours at RT. Sections were washed in PBS (3 x 5 minutes) and incubated in ABC (1:100; ThermoFisher) for 1 hour at RT. For visualisation, sections were incubated in DAB until a satisfactory level of staining was achieved and 1% Harris Haematoxylin or cresyl violet was used as a counterstain for peripheral and CNS tissue respectively. Sections were then dehydrated through graded alcohols (80%, 90%, 2 x 100%; 5 minutes each), cleared with xylene (2 x 5 minutes) and mounted with DPX.

2.7.2 Immunofluorescence

Slides were dried at RT for 30 minutes and briefly washed in PBS. Non-specific binding was blocked with 10% BSA in PBS with 0.3% Triton X-100 for 1 hour at RT. Sections were then incubated overnight at 4°C in primary antibodies (Table 2.3), diluted in blocking buffer. Sections were washed in PBS (3 x 10 minutes) to remove any unbound antibody, and incubated in the appropriate fluorophore conjugated secondary antibodies, as well as Hoechst 33342 nuclear dye (1:1000; Sigma Aldrich), diluted in blocking buffer for 1 hour at RT. After a final wash in PBS (3 x 10 minutes), slides were mounted with DAKO fluorescent mounting medium (Sigma Aldrich).

2.7.3 Quantification and analysis of histology

For peripheral tissue, cells were quantified across three sections, in three representative fields per section, at 40x magnification. The average number of immunopositive cells was calculated and expressed as number of cells per mm^2. For the spinal cord, the number of immunofluorescent cells per section was determined using the Nikon Eclipse upright automated stereology and slide scanning microscope, with Stereo Investigator software. DAB-stained sections were imaged using Nikon light microscope with Basler camera and Manual WSIScanner software; area was calculated using ImageJ and cells were counted using the Leitz Dialux 20 light microscope. The number of cells per mm^2 was calculated at the lesion epicentre and sections either side, corresponding to ±1.0-1.5mm. All cell counting was performed blinded.

IgG staining was used as a surrogate marker for blood-spinal cord barrier breakdown following SCI. Stained sections were imaged using Nikon Eclipse upright automated stereology and slide scanning microscope and analysed using ImageJ. Appropriate thresholds were applied and the area of IgG staining per section was analysed across the lesion. The volume of extravascular IgG (proportional area) and staining intensity at lesion epicentre were calculated.

Table 2.3 Antibodies for immunohistochemistry. The antigen specificity, clone, dilution αand manufacturer for each antibody utilised for histological analysis.

	Antigen	Antibody (Clone)	Specificity	Dilution	Company
Primary Antibodies	Neutrophils	Rabbit α-mouse neutrophils	Neutrophils	1:10,000	Made in house; harvested from a rabbit immunised with whole mouse neutrophils and stimulant *Megathura crenulata* haemocyanin
	Iba-1	Rabbit α-mouse Iba-1	Microglia, macrophages	1:2,000	AbCam
		Rabbit α-mouse Iba-1		1:800	Wako Pure Chemical industries
	Ly6B.2	Rat α-mouse Ly6B.2	Neutrophils	1:200	Bio-Rad
Secondary Antibodies	α-rabbit	Goat α- rabbit biotinylated	N/A	1:200	Vector Labs
	α-mouse	Horse α-mouse biotinylated	Mouse IgG infiltrate	1:200	Vector Labs
	α-rat	Donkey α-rat 594	N/A	1:400	Jackson Immunoresearch
	α-rabbit	Donkey α-rabbit 647	N/A	1:400	Jackson Immunoresearch
	α-mouse	Goat α-mouse 488	Mouse IgG infiltrate	1:200	Jackson Immunoresearch

2.8 Molecular biology

2.8.1 mRNA extraction

RNA was extracted from approximately 30mg of snap-frozen fresh tissue, using the Qiagen© RNeasy Mini kit, according to manufacturer's instructions. Tissue was homogenised in 600µL of lysis buffer with a needle and syringe, and centrifuged at 13,000*g* for 3 minutes. RNA was precipitated by combining the supernatant 1:1 with 70% ethanol, and transferred to an RNeasy spin column. Samples were washed before RNA was eluted with 30 or 50µL of nuclease-free water, depending on the tissue type, and immediately placed on ice.

2.8.2 cDNA conversion and qPCR

RNA concentration was measured using a NanoDrop (ThermoFisher) and 1000ng of sample was converted to cDNA using the Applied Biosystems High Capacity cDNA conversion kit, following manufacturer's instructions. Real-time qPCR was performed with samples in duplicate (10-25ng/well) using SYBR green qPCR master mix (Applied Biosystems, PrimerDesign) with the Applied Biosystems QuantStudio Flex 7 or Roche LightCycler 480. All primers were purchased from PrimerDesign and Sigma Aldrich (Table 2.3) and relative expression was determined by the $2^{-\Delta\Delta Ct}$ method, normalised to a suitable housekeeping gene.

2.8.3 miRNA analysis

miRNA was extracted from fresh tissue using the miRNeasy Mini kit (Qiagen©) and detection was performed using the miRCURY LNA system (Qiagen©), following manufacturer's instructions. miRNA was converted to cDNA using the miRCURY LNA RT kit. And expression was measured with miRCURY LNA SYBR green PCR kit with appropriate assays.

Table 2.4 qPCR primers. Primer sequences used to assess relative expression of genes-of-interest

	Gene	Forward Primer	Reverse Primer
Mouse	GAPDH	5'-AACGACCCCTTCATTGAC-3'	5'-TCCACGACATACTCAGCAC-3'
	RPL13a	5'-GAGGTCGGGTGGAAGTACCA-3'	5'-TGCATCTTGGCCTTTTCCTT-3'
	IL-1β	5'-CAACCAACAAGTGATATTCTCCAT-3'	5'-GGGTGTGCCGTCTTTCATTA-3'
	TNF	5'-AGCCAGGAGGGAGAACAGA-3'	5'-CAGTGAGTGAAAGGGACAGAAC-3'
	CXCL1	5'-GCTGGGATTCACCTCAAGAAC-3'	5'-TGTGGCTATGACTTCGGTTTG-3'
	CXCL10	5'-CATCCCGAGCCAACCTTCC-3'	5'-CACTCAGACCCAGCAGGAT-3'
	SAA-2	5'-TGGCTGGAAAGATGGAGACAA-3'	5'-AAAGCTCTCTCTTGCATCACTG-3'
	IL-1Rn	5'-GACCTTTTACCTGAGAAACAAC-3'	5'-TAGGCACCATGTCTATCTTTTC-3'
Human	ACTB	Accession number, N_001101; Anchor nucleotide, 1195.	
	IL-1β	5'-TGGCAATGAGGATGACTTGTTC-3'	5'-CTGTAGTGGTGGTCGGAGATT-3'
	TNF	5'-AGGTTCTCTTCCTCTCACATAC-3'	5'-ATCATGCTTTCAGTGCTCATG-3'
	CXCL1	5'-CAGAGGAACCTCCAGTCTCAG-3'	5'-GGTACTCCTTGAATGCCACTTA-3'

2.9 High pressure liquid chromatography (HPLC)

HPLC analysis was carried out by Dr Lisa Folkes, Department of Oncology, University of Oxford.

For measurement of corticosterone, samples were separated using a Waters Acquity UPLC system and an ACE C18 column (3µm, 100 x 2.1mm) with an ACE C18 guard (3µm, 10 x 2.1mm) at 50°C. Samples were carried on an eluent (A: 0.1% formic acid, B: MeOH containing 0.1% formic acid with a gradient of 70-100%) with a flow rate of 0.2mL/minute. 5-pregnen-3β-ol-20-one-16α-carbonitrile was used as an internal standard. For measurement of noradrenaline, samples were separated using a Waters Acquity UPLC system and a Waters Atlantis T3 C18 column (3µm, 100 x 2.1mm) with a pre-column filter at 40°C. Samples were carried on eluent (A: 0.1% formic acid with 2mM HFBA, B: acetonitrile with a gradient of 15-45%), with a flow rate of 0.4mL/minute.

Analytes were detected with a Water Acquity TQ detector mass spectrometer, and plasma concentration was determined using calibrated standard solutions (corticosterone, noradrenaline bitartrate salt, both Sigma Aldrich). Chromatograms were displayed and analysed using Waters Empower 3 software.

2.10 Metabolomics

2.10.1 Sample preparation

Metabolites were extracted from liver and spinal cord samples as previously described (Waters et al. 2001). Fresh tissue was homogenised with a pestle and mortar on dry ice, and was combined with 50% acetonitrile (Sigma Aldrich), at a ratio of 1mg:80µL and vortexed. Samples were then centrifuged at 5070*g* for 5 minutes at 4°C. The supernatants were collected and lyophilised overnight, and stored at -80°C until NMR analysis. On the day of NMR analysis, lyophilised samples were defrosted at RT and resuspended in 600µL of NMR buffer (75mM sodium phosphate buffer prepared in D_2O, pH 7.4). Samples were briefly centrifuged at 2,500*g* for 5 minutes at 4°C to remove any particulate matter, before being transferred to a 5mm NMR tube.

For blood samples, 75µL of platelet-free plasma was combined with 475µL of NMR buffer, and then transferred to a 5mm NMR tube.

2.10.2 NMR experiments

All samples were measured using the 700-MHz Bruker AVII spectrometer operating at 16.4 T, equipped with a ^{1}H ($^{13}C/^{15}N$) TCI cryoprobe, as described previously (Jurynczyk et al. 2017; Yeo et al. 2019). Sample temperature was held at 310K. ^{1}H NMR spectra of liver samples were acquired using a spin-echo sequence (Carr-Purcell-Meiboom-Gill [CPMG]), a τ interval of 40µs, 96 loops, an echo time of 78ms, 96 data collections, an acquisition time of 1.5s, a relaxation delay of 3s, and a fixed receiver gain. Plasma spectra were acquired using a water suppression with a transverse relaxation filter that eliminates distortions (WASTED) sequence, as previously described (Aguilar et al. 2019). Spinal cord spectra were acquired with a Nuclear Overhauser Effect Spectroscopy (NOSEY) sequence, as previously described (Jurynczyk et al. 2017).

2.10.3 NMR data pre-processing

All spectra were phased, baseline corrected and chemical shifts referenced to the lactate-CH_3 doublet resonance at δ=1.33ppm in Topspin 4.0.7 (Bruker). Spectra were then uploaded to ACD/NMR processor academic edition 12.01 (Advanced Chemistry Development, Inc.) and regions were divided into 0.02ppm width 'buckets' and the absolute value of integral of each spectral bucked was unit variance scaled. Metabolite assignment was performed with reference to literature reviews (Lenz et al. 2003; Tang et al. 2004), the HMDB metabolite database, and 2D total correlation spectroscopy (TOCSY) experiments.

2.11 EV analysis

2.11.1 EV isolation

For each sample and/or condition, 100µL of platelet-free plasma was combined with 900µL EV-free PBS and ultracentrifuged at 120,000*g* for 120 minutes at 4°C. The supernatant was removed and the resulting EV pellet was then resuspended in 100µL PBS for downstream experiments and quantification. This was achieved by pipetting PBS onto the pellet several times, scraping the pellet off the side of the Eppendorf with the pipette tip, and pipetting up and down several times.

2.11.2 EM imaging

EM imaging was completed by Dr Errin Johnson, the Dunn School of Pathology, University of Oxford.

EVs were isolated from plasma as described in 2.11.1 and the EV pellet was resuspended in 4% PFA and diluted appropriately in PBS for optimal imaging; 10µL of EVs in solution was applied to freshly glow discharged carbon formvar 200 mesh copper grids for 2 minutes. The grids were blotted with filter paper, after which they were stained with 2% uranyl acetate for 10 seconds, blotted and air dried. Grids were then imaged in a FEI TEcnai 12 TEM at 12kV (GAtam OneView CMOS camera).

2.11.3 Western blot

EVs were isolated from plasma as described in 2.11.1 and the EV pellet was resuspended in 100µL of RIPA buffer with 1% protease and phosphatase inhibitors (ThermoFisher). Samples were sonicated for 5 minutes, and total protein was quantified by BCA assay (ThermoFisher). 40µg of exosomal protein was separated by electrophoresis, alongside protein extracted from approximately 5µg of mouse brain as control, and transferred onto a nitrocellulose membrane. The membrane was blocked for non-specific binding using 5% milk in PBST for 1 hour at RT, before overnight incubation with primary antibodies (Table 2.5), diluted in blocking buffer at 4°C. The membrane was then washed with PBST (3 x 5 minutes), and incubated with α-mouse (1:20) or α-rabbit (1:50) horseradish peroxidase conjugated secondary antibodies, as appropriate, for 1 hour at RT. After a final wash in PBST (3 x 5 minutes), the membrane was prepared for imaging using ECL (ThermoFisher), and visualised with a ChemiDoc (Bio-rad) by chemiluminescence.

Table 2.5 Antibodies used for western blotting. Clone, dilution and manufacturer of antibodies used in western blot of EVs.

Antibody [Clone]	**Dilution**	**Manufacturer**
Alix [3A9]	1:2,000	AbCam, Cambridge UK
TSG101 [4A10]	1:1,000	AbCam, Cambridge UK
CD9	1:1,000	System Biosciences, CA USA
HSP70	1:1,000	System Biosciences, CA USA
CD41	1:2,000	AbCam, Cambridge UK
Histone H3 [DH12]	1:2,000	New England Biolabs, MA USA

2.11.4 EV measurements

EV samples were measured using nanoparticle tracking analysis (NTA) to determine EV concentration and size. The system uses a laser which, when applied to a sample through a glass prism, illuminates particles within the sample. The laser light scattered by the particles is visualised by a microscope with 20x objective and recorded with a CMOS camera. Samples were appropriately

diluted with EV-free PBS to give a concentration of between 5 x 10^8 and 1 x 10^9 particles/mL for optimal measurements. 3-5 videos of 30-60 seconds, representative of different fields of view, were taken at camera level 12 with screen gain 2.0, temperature controlled at 25°C. All videos were analysed using NTA 3.3 software, with detection threshold, minimum particle size and blur set to automatic. Particle size is calculated by applying two-dimensional Stokes-Einstein equation: $< x, y >^2 = \frac{K_B T t_s}{3\pi\eta d_h}$ where $< x, y >^2$ is the mean squared displacement, K_B is Boltzmann's constant, T is the temperature of the solvent in Kelvin, t_s is the sampling time, η is the viscosity, and d_h is the hydrodynamic diameter.

2.11.5 EV labelling

EVs were isolated as described in 2.11.1 and transfected with non-mammalian (*C. Elegans*) transcript *cel*-miR-39-3p (Qiagen©) using the Exo-Fect kit (System Biosciences), following manufacturer's instructions. EVs were then combined 1:1 with fluorescent membrane dye PKH67 (2μM, Sigma Aldrich) for 5 minutes in the dark and the reaction was terminated with EV-free foetal bovine serum (FBS, generated in house by ultracentrifugation at 120,000*g* for 18 hours at 4°C). Labelled EVs were washed in PBS and isolated by ultracentrifugation (2.11.1), and the resulting pellet was resuspended in EV-free PBS.

2.12 Cell culture

2.12.1 Human peripheral blood mononuclear cell (PBMC) isolation

A total of 30mL of peripheral venous blood was collected from healthy adult male volunteers, into EDTA-spray coated tubes. Blood was gently layered onto Ficoll-Paque (GE Healthcare Sciences) and was centrifuged at 400*g* with no break for 25 minutes at RT. Plasma was removed and the PBMC fraction was collected by pasture pipette. Cells were combined with sterile PBS and centrifuged at 1,000*g* for 5 minutes at RT. The resulting cell pellet was resuspended in 1mL isolation buffer (1mM EDTA and 2% FBS in PBS); cells were counted and 4 million cells were seeded per well in a 6 well plate.

2.13 Statistical analysis

For analysis of metabolomics data, the integrals of the scaled spectral buckets were imported into R software (R foundation for statistical computing). Multivariate analysis was carried out using in house R scripts and the *ropls* package (Thevenot et al. 2015). To identify metabolic differences between injury groups, either principal component analysis (PCA) or orthogonal partial least square discriminant analysis (OPLS-DA) statistical methods were used (Jurynczyk et al. 2017). PCA is an unsupervised statistical approach that identifies metabolites driving the greatest separation in a dataset. Being unsupervised, the injury groups are not defined, and, therefore, results are unbiased. Loading plots were generated to identify any cluster separation and key loadings were evaluated. By contrast, OPLS-DA is a supervised multivariate analysis whereby the injury groups are defined as classes to identify variation and key metabolites (Figure 2.3). In this analysis, unequal class sizes were corrected and were separated into a training set (90%) and a test set (10%). The training set was used to build a model on which the test set was applied, and the predictive accuracy of the model was determined. Ten-fold cross-validation with 100 iterations was performed, resulting in 1,000 model outcomes. The mean accuracy, sensitivity and specificity of the model was compared to that of a separate model set created by permuting the class assignments (random chance). Sensitivity reflects the ability of the model to correctly identify true positives, whilst specificity reflects the ability of the model to correctly identify true negatives. The accuracy of the model, the degree to which it correctly classifies all samples, is then determined using the sensitivity and specificity outcomes.

All other analysis was completed with GraphPad Prism 7 software. Significant outliers were removed from datasets, as determined by the ROUT method, which is based on a 1% false discovery rate (Motulsky and Brown 2006). The D'Agostino-Pearson omnibus normality test was applied to all data, and the suitable parametric or non-parametric statistical analysis was used subsequently. Unpaired student's t-test, Mann-Whitney test, one- and two-way analysis of variance (ANOVA) and Kruskal-Wallis test were employed, with Sidak's or Dunn's post-hoc testing as appropriate. Results

were considered significant at $p<0.05$ with 95% confidence intervals. All quantitative data are expressed as mean ± standard error of the mean (SEM).

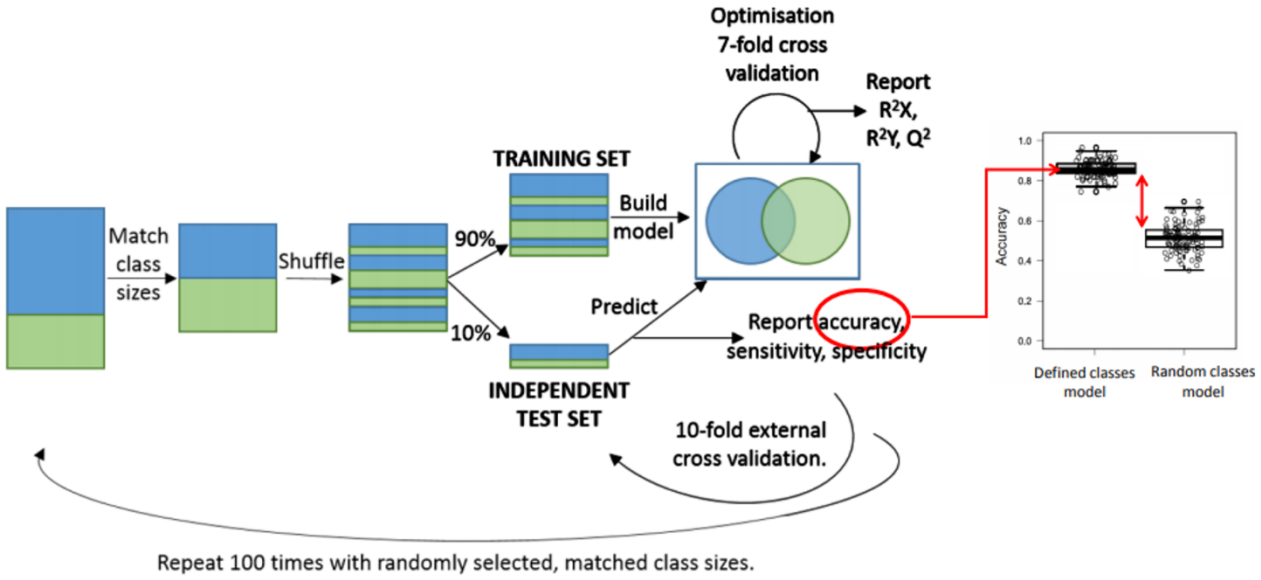


Figure 2.3 Schematic of OPLS-DA statistical analysis. OPLS-DA is a supervised multivariate analysis where variation between defined groups is investigated. First, class sizes are matched, shuffled and assigned into a training (90%) and test (10%) set. Models are built using the training set on which the test set is applied, and the predictive accuracy is calculated. Ten-fold cross-validation with 100 iterations are performed. The mean accuracy, sensitivity and specificity of the model is compared to one generated by random chance. Figure kindly provided by Dr Fay Probert.

Chapter 3: Acute IL-1RA treatment suppresses the peripheral and central inflammatory response to spinal cord injury

Data in this chapter has been published as:

Yates, A.G., Jogia, T., Gillespie, E.R., Couch, Y., Ruitenberg, M.J. & Anthony, D.C. (2021) Acute IL-1RA treatment suppresses the peripheral and central inflammatory response to spinal cord injury. *Journal of Neuroinflammation*. *18*(1):15.

3.1 Introduction and aims

After the initial injury, the pathophysiology of the secondary phase of SCI is characterised by ongoing inflammation in the spinal cord, which contributes to additional cell death and worsened functional loss (Anwar et al. 2016). It has long been accepted that targeting inflammation in the spinal cord is a promising therapeutic strategy to preserve neuronal tissue and improve patient outcomes. However, to date, there are no pharmaceutical agents that have reached the clinic. This has largely been attributed to poor bioavailability, due to the presence of the blood-CNS barrier. Therefore, there is a need for alternative approaches to limit inflammation in the spinal cord during the secondary phase of injury.

SCI exhibits two distinct phases of injury; the primary phase occurs immediately as a direct result of the insult, and is identified by disruption to the vasculature, axonal shearing and neuronal death (Anwar et al. 2016; Sun et al. 2016). By contrast, the secondary phase can persist for weeks, and even months, after the initial injury (Anwar et al. 2016; Wilson et al. 2013; Beck et al. 2010), and is mediated by activated resident glial cells and infiltrating leukocytes (Kumar and Loane 2012). Therefore, microglia and neutrophils are likely key initiators of secondary damage in the spinal cord after injury.

Microglia are specialised macrophages, which reside in the CNS and, in the absence of injury, perform immune surveillance and maintenance functions (David et al. 2018). Following SCI, microglia are the first myeloid cell type to respond, and are activated within minutes to hours post-injury by DAMPS released from dying cells, including ATP, NO and changes in extracellular ions such as sodium, potassium and calcium (Hawthorne and Popovich 2011; Dibaj et al. 2010). As mentioned in the general introduction, the role of microglia in SCI remains contested; microglial depletion has been shown to both improve (Gerber et al. 2018) and worsen histological and functional outcomes (Bellver-Landete et al. 2019) in SCI mice. It is likely that timing and activation state (Kigerl et al. 2009) of the microglia dictates their contribution to lesion progression, and it has been proposed that the peripheral immune response has an influence on their inflammatory response in the CNS.

Previous work utilising models of both SCI and TBI has consistently shown that the magnitude of inflammation in the CNS is dependent on a systemic inflammatory response, known as the APR, which is largely co-ordinated by the liver. In response to damage, hepatic expression of pro-inflammatory cytokines, including chemokines, as well as acute phase proteins, are significantly increased as early as 2 hours post-injury (Blond et al. 2002; Campbell et al. 2003; Campbell et al. 2007; Campbell et al. 2005; Wilcockson et al. 2002). These mediators trigger mobilisation and priming of leukocytes from the bone marrow (Brennan et al. 2019; Bao et al. 2009), which then translocate to the site of injury as well as peripheral organs (Gris et al. 2008).

Neutrophils are the first peripheral leukocytes to reach the spinal cord lesion following SCI (Fleming et al. 2006) and have consistently been shown to exacerbate CNS damage. They release proteases and generate oxidative species (Anwar et al. 2016; Neirinckx et al. 2014; Liu et al. 2020), which causes membrane damage, lipid peroxidation, DNA fragmentation and cellular injury (Donnelly and Popovich 2008). Moreover, neutrophils release pro-inflammatory mediators, such as CXCL1 (Schroder et al. 2006) and TNF (Nguyen et al. 2007), which propagate a chronic immune response. These events collectively result in apoptosis, necrosis and demyelination, which increases the size of the lesion and worsens motor deficits (Morganti-Kossmann et al. 2012). Indeed, inhibition of neutrophil recruitment to the spinal cord is associated with improved functional outcomes (Lee et al. 2011; Nguyen et al. 2012).

One potential way of inhibiting recruitment of immune cells to a spinal cord lesion, is by inhibiting the driving force, the APR. Suppression of the APR has proven to be neuroprotective in models of CNS injury. Depletion of liver Kupffer cells (Campbell et al. 2008b) and targeting acute phase proteins (Campbell et al. 2007; Campbell et al. 2008a; Clausen et al. 2014) have both reduced neutrophil infiltration of the brain and, as a consequence, lesion size. In SCI, splenectomy reduced infiltration of peripheral monocytes into the spinal cord, and was associated with improved outcomes (Blomster et al. 2013a). Moreover, denervation of the spleen reduced neutrophil recruitment to the spinal cord after traumatic injury (Monteiro et al. 2020). Therefore, targeting the APR presents an appealing alternative strategy to reducing the secondary phase of CNS injury.

However, the APR is a multifaceted process, and, therefore, selecting a specific target remains challenging.

IL-1β is an early component of the cytokine cascade and plays a detrimental role in the progression of CNS injury (Allan et al. 2005). It is a master cytokine in that it initiates a series of events, with a wide range of effects, including driving the expression of cytokines, chemokines and adhesion molecules. Upon the binding of IL-1β, IL-1 receptor 1 (IL-1R1) associates with the IL-1 receptor accessory protein (IL-1RAcP) (Korherr et al. 1997), which enables the approximation of the cytosolic Toll-IL-1-receptor domains and the binding of MyD88 (Figure 3.1). This triggers a cascade of kinases, which activates the transcription factor NF-κB and, in turn, induces the expression of inflammation-associated genes under its regulation (Dinarello 2018). IL-1β is highly potent (pM) and induces its own *de novo* synthesis, in a positive feedback loop, therefore its action is tightly regulated by the endogenous IL-1-receptor antagonist (IL-1RA). IL-1RA is a competitive antagonist; it binds to IL-1R1 to directly block IL-1β and thus prevents a downstream inflammatory response (Allan et al. 2005; Hannum et al. 1990). Although, IL-1 signalling is also regulated by numerous other mechanisms, including soluble decoy receptors and caspase-1 inhibitors (Allan et al. 2005; Fields et al. 2019), which highlights is biological importance.

In response to SCI, IL-1β is significantly increased, from undetectable levels (Allan et al. 2005; Vitkovic et al. 2000), <1 hour post-injury at both the mRNA and protein level, (de Rivero Vaccari et al. 2008; Pineau and Lacroix 2007; Sato et al. 2012; Wang et al. 1997). It is produced by resident and infiltrating immune cells (Zhu et al. 2019; Pineau and Lacroix 2007), which mediates leukocyte recruitment (Ching et al. 2005; Schnell et al. 1999b; Pineau et al. 2010) and microglial activation (Sato et al. 2012), and therefore it is associated with subsequent secondary damage. Indeed, IL-1β knock out (KO) mice exhibited improved locomotor activity and reduced lesion area after SCI (Sato et al. 2012). Similar results were found by Boato and colleagues (2013) who further showed that local application of IL-1β to the spinal cord lesion worsened neurological outcome. As such, IL-1β signalling plays a unique role in the pathophysiology of SCI, and so its inhibition may offer neuroprotection.

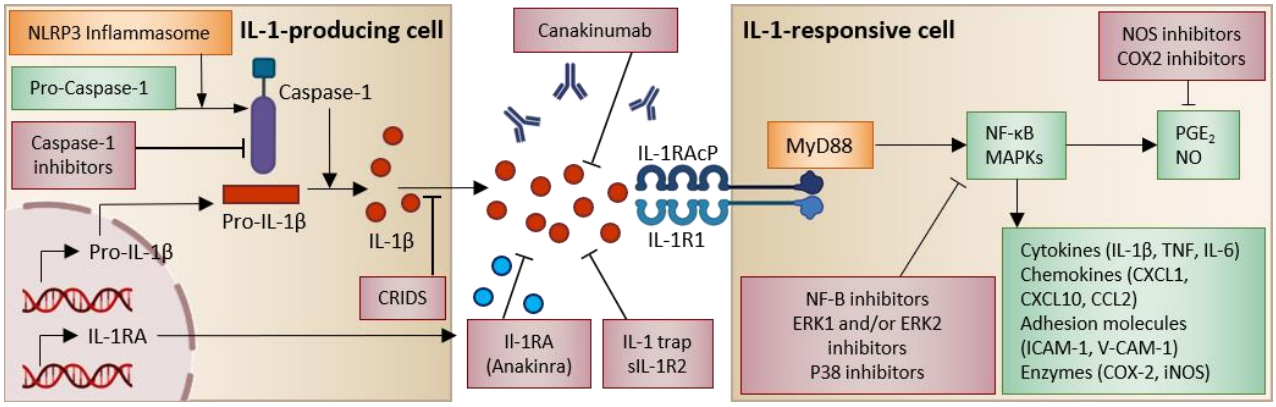


Figure 3.1 IL-1β signalling and opportunities for therapeutic intervention. The mature form of IL-1β is produced by cleavage of pro-IL-1β by caspase-1, which, itself, is activated from pro-caspase-1 by the NLRP3 inflammasome. Upon release, IL-1β binds to IL-1R1, which, associates with IL-1RAcP. This enables the binding of MyD88, and downstream activation of transcription factor NF-κB, and the expression of genes under its regulation. IL-1β signalling can be inhibited by the endogenous, competitive antagonist IL-1RA, the IL-1 trap decoy receptor (rilonacept), and neutralising antibodies (canakinumab). Figure adapted from Allan et al. (2005).

IL-1RA has been exploited as a therapeutic intervention in a range of inflammatory diseases, such as rheumatoid arthritis (Mertens and Singh 2009), systemic inflammatory diseases (Dinarello et al. 2012), as well as traumatic CNS injuries. Indeed, IL-1RA has been used in models of TBI and stroke where improvements in cognitive deficits (Newell et al. 2018; Clausen et al. 2011), tissue loss (Clausen et al. 2011) and leukocyte recruitment (Sun et al. 2017; Pradillo et al. 2012) have been reported. As a result, IL-1RA treatment has entered into human clinical trials (Emsley et al. 2005; Helmy et al. 2014; Helmy et al. 2016; Galea et al. 2018; Smith et al. 2018). In comparison to brain injuries, treatment of SCI with IL-1RA has been less investigated. Preliminary studies tended to apply IL-1RA locally to the lesion and reported histological and motor function improvements (Akuzawa et al. 2008; Nesic et al. 2001; Zong et al. 2012; Liu et al. 2008). Li et al. (2018b) and Hasturk et al. (2015a) both administered IL-1RA intraperitoneally into rat compression models of SCI. However, groups focused on the spinal cord only, using end point markers such as lesion size and cell necrosis and/or apoptosis. Therefore, the underlying mechanisms by which IL-1RA exerts its effects, as well as the effects on the systemic response, remain unknown.

The aims for this chapter were to (1) to characterise the peripheral inflammatory response to a lower thoracic spinal cord injury during the acute phase, and (2) to determine the effect of the exogenous IL-1RA on the peripheral inflammatory response and on lesion pathology.

3.2 Methods specific to this chapter

3.2.1 Animals

Female C57BL/6 mice, 8-12 weeks of age, were used in this chapter. Animals were obtained from the Animal Resource Centre (Canningvale, Australia), and allowed to acclimatise for 4 weeks prior to experimentation. All animals were housed in a pathogen-free facility, under standard diurnal lighting conditions (12 hours) with *ad libitum* access to food and water.

3.2.2 SCI model

To characterise the APR during the acute phase of injury, animals received a 70 kilodyne (kD) SCI at thoracic vertebral level 9 (T9), or sham surgery with no cord impact as control, as described in 2.3.1. Animals were allowed to survive for 2, 6, 12 or 24 hours (n=5/time point) and blood, fresh liver and spleen, and fixed liver and spinal cord were collected as described in 2.5.

3.2.2.1 Treatment with IL-1RA

Human IL-1RA was administered intraperitoneally at a dose of 100mg/kg in 200µL of sterile saline (vehicle), immediately following and 5 hours post-SCI (Figure 3.2). This treatment regime was designed using previous papers that had shown neuroprotective effects with IL-1RA (Akuzawa et al. 2008; Hasturk et al. 2015a; Sun et al. 2017), and because the biological half-life of IL-1RA is 4-6 hours (Akash et al. 2013). 200µL of sterile saline alone was injected as control. Fresh liver and fixed liver and spinal cord were collected 6 hours post-injury as described in 2.5.

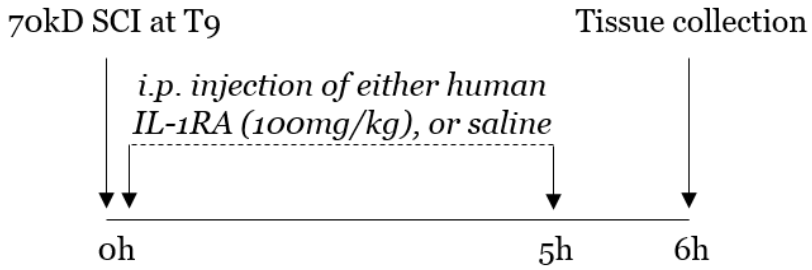


Figure 3.2 IL-1RA treatment strategy. Female C57BL/6 mice underwent a 70kD SCI at T9 and received an intraperitoneal injection of either human IL-1RA (100mg/kg; n=8) or saline (n=9). Animals received two doses of their respective treatment, the first immediately following SCI, and the second 5 hours post-injury. Tissue was collected 6 hours post-injury for analysis.

3.3 Results

3.3.1 SCI induces IgG infiltration, microglial cell death and neutrophil infiltration

To characterise the APR during the acute phase of SCI, the progression of lesion pathology, at the same time points, was evaluated, first. Infiltration of IgG was used as a surrogate marker for blood-spinal cord barrier breakdown, as proteins this large do not normally cross the intact barrier and are not normally found within the parenchyma (Hazleton et al. 2017). IgG volume as a percentage of total spinal cord volume (Figure 3.3Ai) and average epicentre IgG staining intensity (Figure 3.3Aii) were both calculated. No IgG staining was evident in any sham spinal cords at any time point, therefore only one sham column has been included for clarity. The percent volume of infiltrating IgG increased following SCI in a time dependent manner (one-way ANOVA, $p<0.0001$). Post-hoc analysis (Sidak's post-hoc test) revealed a significant difference between injured spinal cords collected 2 hours post-injury (15.1±2.0%) and those collected at 12 (28.4±3.1%; $p<0.01$) and 24 hours post-injury (45.0±0.6%; $p<0.0001$). Percent IgG volume at 24 hours after SCI was also increased compared to 6 (19.5±3.0%; $p<0.0001$) and 12 hour time points ($p<0.001$). As with volume, the average epicentre IgG staining density increased with time after SCI (one-way ANOVA, $p<0.0001$). Density was greatest 24 hours post-injury (52.4±1.8) which was significantly increased compared to density at 2 (30.5±1.4; $p<0.0001$), 6 (39.8±2.8; $p<0.01$) and 12 hours post-injury (42.5±1.8; $p<0.05$), with Sidak's post-hoc test.

Iba-1+ microglia were significantly decreased in the spinal cord lesion epicentre during the acute phase of injury, independent of time (Figure 3.3B; two-way ANOVA, injury $p<0.0001$, time $p=0.442$). By contrast, the density of Ly6B.2+ neutrophils in the spinal cord lesion epicentre increased with time following SCI (Figure 3.3C; two-way ANOVA, injury $p<0.0001$, time $p<0.0001$). Infiltration was evident at 2 hours (sham, 1.0±0.5/mm^2; SCI, 5.6±2.4; Sidak's post-hoc test, $p=0.367$) and 6 hours post-injury (sham, 1.0±0.5/mm^2; SCI, 10.0±1.8/mm^2; Sidak's post-hoc test, $p<0.001$). Although, notable increase in cell density was observed at 12 hours post-injury (sham, 1.6±0.6/mm^2; SCI, 205.6±5.3/mm^2; Sidak's post-hoc test, $p<0.0001$), and peaked 24 hours post-injury (sham, 1.4±0.5/mm^2; SCI, 414.7±5.6/mm^2; Sidak's post-hoc test, $p<0.0001$).

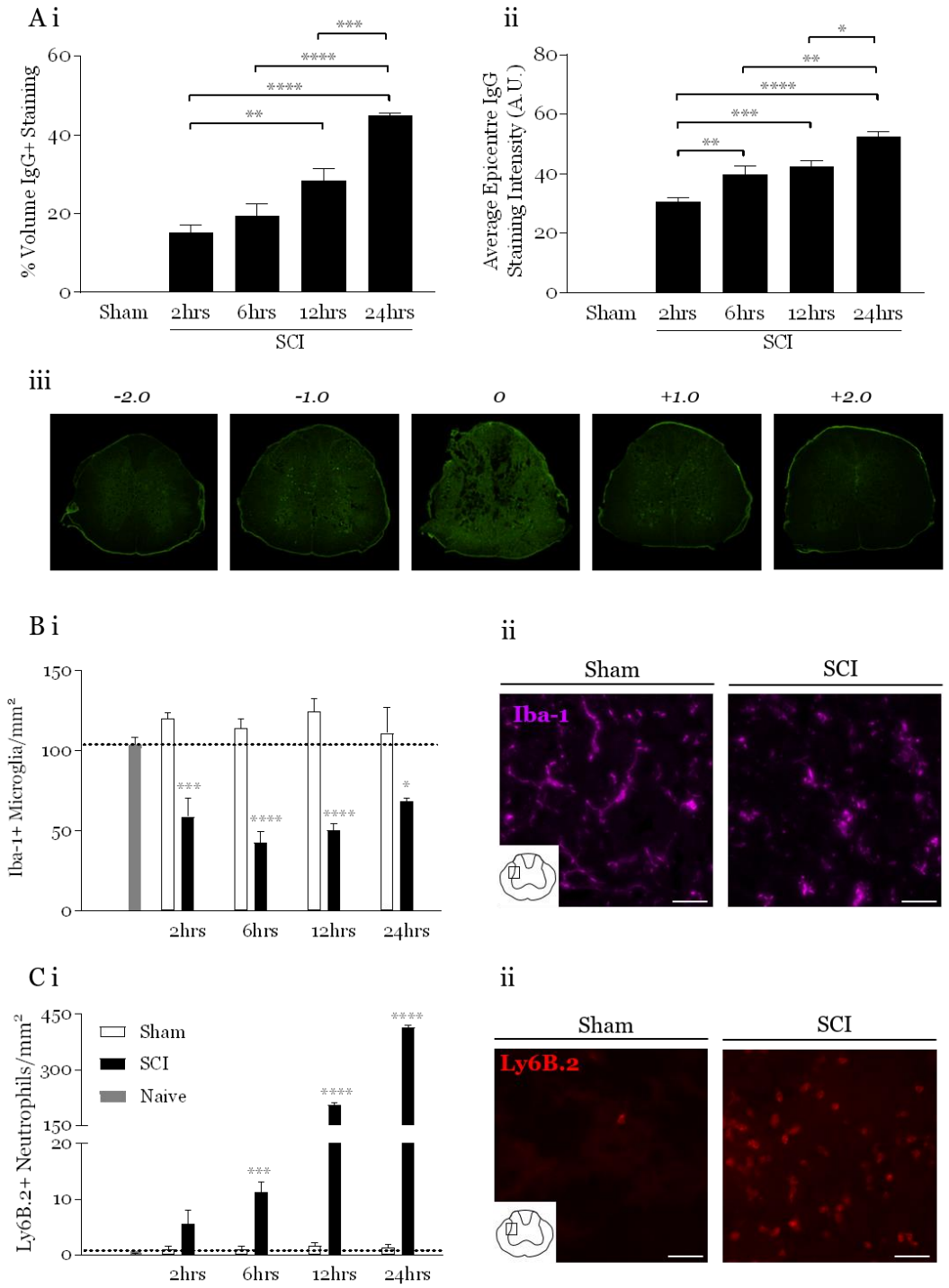


Figure 3.3 IgG infiltration, microglial and neutrophil density in the injured spinal cord. Female C57BL/6 mice underwent either a sham surgery (white bars, n=5/time point) or 70kD SCI (black bars, n=4-5/time point) at T9. Fixed spinal cords were collected at 2, 6, 12 and 24 hours post-injury for analysis of lesion pathology by immunohistochemistry, and results were compared to naïve baseline (grey bar, dotted line, n=5). Volume of IgG staining as a percentage of total spinal cord volume (Ai) and average IgG staining intensity at the epicentre (Aii) were used as surrogate markers of blood-spinal cord barrier break down. (Aiii) IgG staining through a spinal cord lesion. Cell density of Iba-1+ microglia at the lesion epicentre (B) and Ly6B.2+ neutrophils (C) at the lesion epicentre. Representative images of microglia and neutrophils in the spinal cord, 24 hours post-surgery, scale bar represents 100µm. Data are presented as mean ±SEM, and analysed by one- and two-way ANOVA, *p<0.05 **p<0.01 ***p<0.001 ****p<0.0001 with Sidak's post-hoc test, between sham and SCI groups.

3.3.2 SCI induces expression of inflammation-associated genes in the liver

Previous work from our group has demonstrated that quantifying RNA is an effective way of measuring the extent of the hepatic APR, and reflects subsequent protein levels (Campbell et al. 2003; Campbell et al. 2005). Therefore, relative expression of inflammation-associated genes in the liver was determined by qPCR. Hepatic expression of IL-1β (Figure 3.4A) and CXCL10 (Figure 3.4B) was increased in both sham and SCI animals compared to naïve animals at 2 hours post-injury. By 6 hours, expression in control animals had returned to baseline, but it remained elevated in SCI animals. However, this was not statistically significant when accounting for multiple comparisons. Expression of CXCL1 (Figure 3.4C) was significantly increased in injured and control animals over naïve baseline, yet expression was significantly decreased in SCI animals compared to sham at 6 hours (sham, 65.0±3.7; SCI, 45.7±8.0; Sidak's post-hoc test, $p<0.05$) and at 24 hours (sham, 29.7±5.5; SCI, 6.8±2.1; Sidak's post-hoc test, $p<0.01$). Similarly, expression of SAA-2 in SCI animals was increased compared to naïve animals, but it was decreased compared to sham animals at 6 hours post-injury, although this did not reach statistical significance (Figure 3.4D; sham, 765.1±90.0; SCI, 407.8±36.7; Sidak's post-hoc test, $p=0.182$). SCI also induced an increase in hepatic IL-1RA expression (Figure 3.4E), however the peak of its expression was delayed compared that of IL-1β, at 6 hours post-injury (sham, 7.7±0.8; SCI, 13.0±2.7; Sidak's post-hoc test, $p<0.05$). A trending increase in both sham and SCI groups, above naïve baseline, was observed as early as 2 hours post-operation, however this was not significant. By 12 hours, IL-1RA expression had returned to, and remained at, naïve baseline.

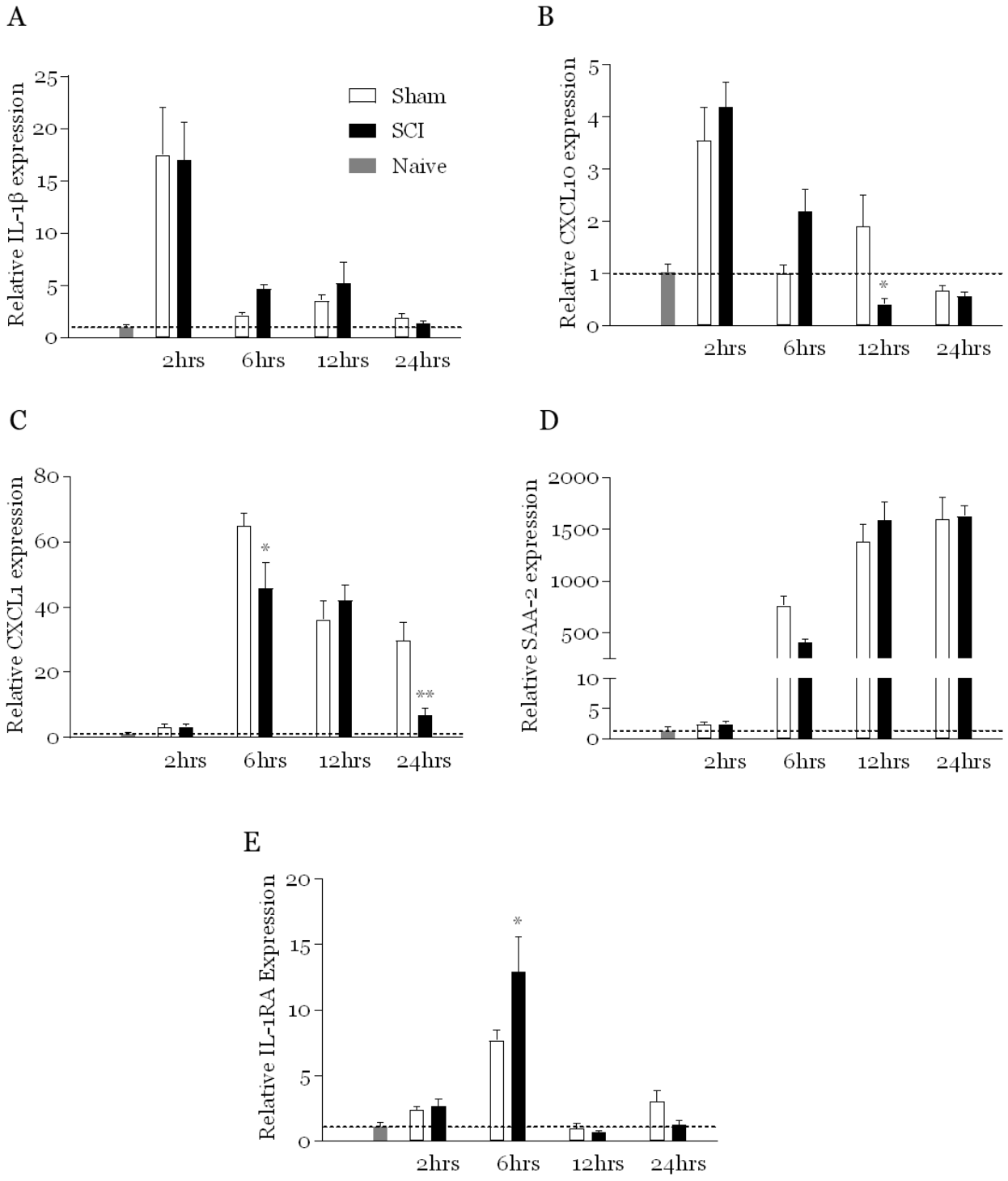


Figure 3.4 Expression of inflammation-associated genes in the liver following SCI. Female C57BL/6 mice underwent either a 70kD SCI (black bars, n=4-5/time point) or sham surgery (white bars, n=5/time point). Tissue was collected at 2, 6, 12 and 24 hours post-operation and was compared to naïve baseline (grey bar, dotted line, n=5). Relative hepatic expression of inflammatory genes IL-1β (A), CXCL10 (B), CXCL1 (C) and SAA-2 (D), and the IL-1 receptor antagonist IL-1RA (E) were determined by qPCR. Data are presented as mean ±SEM and were analysed by two-way ANOVA, *p<0.05 **p<0.01 with Sidak's post-hoc test, between sham and SCI groups.

3.3.3 SCI induces leukocyte mobilisation in the periphery

To evaluate the peripheral leukocyte response during the acute phase of SCI, leukocyte mobilisation in the blood and spleen was determined by flow cytometry, and infiltration of leukocytes to the liver was quantified by immunohistochemistry. The total number of $CD11b^{+}SSC^{hi}Ly6G^{+}$ cells/mL of blood was used as a marker of circulating granulocytes. Numbers were increased in both sham and SCI animals over naïve baseline at 2, 6 and 12 hours post-operation (Figure 3.5A); two-way ANOVA indicated there was no injury effect ($p=0.263$), but there was an effect of time ($p<0.001$). A trending increase in the number of granulocytes was observed in the blood of SCI animals, compared to sham animals 2 hours post-injury (sham, $7.0x10^{5}\pm1.3x10^{5}$/mL; SCI, $1.1x10^{6}\pm2.1x10^{5}$/mL), however this was not statistically significant (Sidak's post-hoc test, $p=0.255$). In the spleen, SCI induced an increase in the number of $CD11b^{+}SSC^{hi}Ly6G^{+}$ cells per spleen at 2, 6 and 12 hours post-injury, compared to naïve (Figure 3.5B), however there was no difference with sham controls (two-way ANOVA, injury $p=0.129$, time point $p<0.0001$). Again, a trending increase was evident at 2 hours (sham, $8.7x10^{5}\pm1.8x10^{5}$/spleen; SCI, $1.4x10^{6}\pm2.9x10^{5}$/spleen; Sidak's post-hoc test, $p=0.104$) and 6 hours post-SCI (sham, $7.3x10^{5}\pm9.9x10^{4}$/spleen; SCI, $1.3x10^{6}\pm1.3x10^{5}$/spleen; Sidak's post-hoc test, $p=0.072$). Retrospective power analysis revealed that statistical significance would have been achieved if $n=7$ and $n=6$ per group, at 2 and 6 hours post-injury respectively.

The total number of $CD11b^{+}Ly6G^{-}$ cells/mL of blood was used to specify circulating monocytes (Figure 3.5C); two-way ANOVA revealed no injury-associated ($p=0.167$) or time effects ($p=0.062$). At 2 hours, the number of blood monocytes was increased in both sham and SCI animals above naïve baseline. At 6 hours, circulating monocytes in sham animals returned to baseline ($1.2x10^{5}\pm2.0x10^{4}$/mL). In SCI animals, there seemed to be greater numbers of monocytes at this time point ($1.7x10^{5}\pm4.2x10^{4}$/mL), but it was not significant (Sidak's post-hoc test, $p=0.666$). Blood monocyte numbers were comparable in all groups at 12 and 24 hours. In the spleen, the number of $CD11b^{+}SSC^{lo}F4/80^{lo}Ly6C^{lo}$ monocytes was largely unaffected (Figure 3.5D; two-way ANOVA, injury $p=0.546$, time point $p<0.0001$). A non-significant increase in sham and SCI animals compared to naïve animals was observed at 2 hours. At 6, 12 and 24 hours, numbers were decreased

in all animals below naïve baseline; there were no significant differences between sham and SCI animals at any time point.

Immunostaining of fixed livers showed that SCI increases the density of neutrophils (Figure 3.5E; two-way ANOVA, injury $p<0.001$, time point $p<0.0001$). Post-hoc testing with Sidak's multiple comparisons revealed significant differences existed between sham and SCI groups at 2 hours (sham, 79.5±10.1/mm^2; SCI, 111.6±12.2/mm^2; $p<0.05$) and 6 hours post-injury (sham, 83.6±6.4/mm^2; SCI, 112.3±9.8/mm^2; $p<0.05$), and a trending increase at 12 hours post-injury (sham, 41.4±3.9/mm^2; SCI, 69.4±3.4/mm^2; $p=0.055$). In the blood, spleen and liver, the neutrophil response peaked 2 hours post-SCI, and decreased with time. By contrast, SCI increased the density of Iba-1+ macrophages present in the liver at the later time points (Figure 3.5F; two-way ANOVA, injury $p<0.0001$, time $p=0.733$); significant increases were observed 12 (sham, 290.8±16.5/mm^2; SCI, 353.9±13.3/mm^2; Sidak's post-hoc test, $p<0.05$) and 24 hours post-SCI (sham, 294.9±15.4/mm^2; SCI, 371.6±27.5/mm^2; Sidak's post-hoc test, $p<0.01$).

Taken together, these data indicate that SCI induces a peripheral inflammatory response, which largely subsides by 24 hours, whereas leukocyte recruitment and spinal cord damage continues to increase dramatically over the same time period.

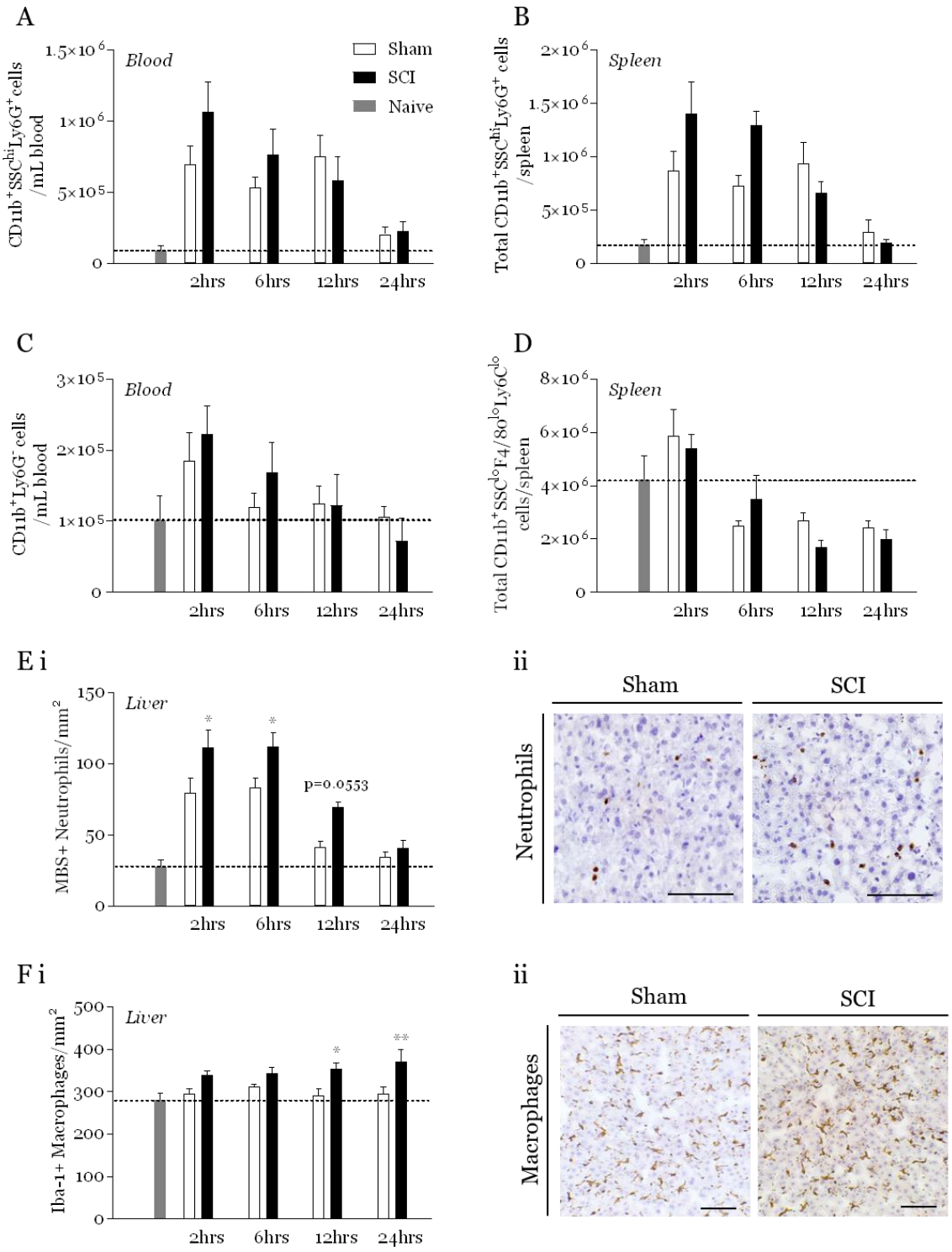


Figure 3.5 Leukocyte mobilisation in the periphery following SCI. Female C57BL/6 mice underwent either a 70kD SCI (black bars, n=4-5/time point) or sham surgery (white bars, n=5/time point). Tissue was collected at 2, 6, 12 and 24 hours post-operation and was compared to naïve baseline (grey bar, dotted line, n=5). Neutrophil mobilisation in the blood (A) and spleen (B) and monocyte mobilisation in the blood (C) and spleen (D) was determined by flow cytometry. Neutrophil (E) and macrophage (F) density in the liver was measured by immunohistochemistry. Representative images of neutrophil and macrophage density in each injury group at peak immune cell density; neutrophil and macrophage density were greatest at 2 and 24 hours post-SCI respectively. Scale bar represents 50µm. Data are presented as mean ±SEM and were analysed by two-way ANOVA, *p<0.05 **p<0.01 with Sidak's post-hoc test, between sham and SCI groups.

3.3.4 Peripheral IL-1RA treatment suppresses the SCI-induced APR

Given the delay between hepatic IL-1β and reciprocal IL-1RA expression, the effect of supplementing IL-1RA on inhibiting the IL-1β-mediated peripheral response was investigated.

qPCR analysis of the liver showed that treatment with IL-1RA induced a significant increase in IL-1β expression, upstream of IL-R1-mediated signalling (Figure 3.6A; SCI + saline, 4.7±0.4; SCI + IL-1RA, 7.8±1.0; student's unpaired t-test, $p<0.01$). CXCL10 expression remained unchanged (Figure 3.6B; SCI + saline, 1.9±0.2; SCI + IL-1RA, 3.1±0.8; student's unpaired t-test, $p=0.126$), however CXCL1 (Figure 3.6C; SCI + saline, 44.3±6.1; SCI + IL-1RA, 26.9±4.2; student's unpaired t-test, $p<0.05$) and SAA-2 (Figure 3.6D; SCI + saline, 572.1±43.6; SCI + IL-1RA, 357.5±35.7; student's unpaired t-test, $p<0.01$), downstream of IL-1β signalling, were significantly decreased. These data correlate with changes in the mobilisation of immune cells, as infiltration of neutrophils in the liver was also significantly decreased (Figure 3.6E; SCI + saline 98.9±7.5/mm^2; SCI + IL-1RA, 77.3±3.0/mm^2; student's unpaired t-test, $p<0.05$).

3.3.5 Peripheral IL-1RA reduces markers of secondary injury in the spinal cord

Next, the effect of IL-1RA treatment on spinal inflammation was evaluated. Fixed spinal cords were stained for IgG infiltration, microglia and neutrophils as markers of secondary damage and inflammation. The volume of infiltrating IgG, as a percentage of total spinal cord volume, was unaffected by IL-1RA treatment (Figure 3.7A; two-way ANOVA, treatment $p=0.223$). Similarly, the density of microglia through the spinal cord lesion was unchanged (Figure 3.7B; two-way ANOVA, treatment $p=0.312$). As expected, there was significant infiltration of neutrophils into the spinal cord in this model of SCI. Strikingly, this injury-dependent infiltration was significantly reduced by IL-1RA treatment (Figure 3.7C; two-way ANOVA, treatment, $p<0.001$); Sidak's post-hoc testing revealed a significant difference at the lesion epicentre (SCI + saline, 45.5±6.5/mm^2; SCI + IL-1RA, 26.4±5.6/mm^2; $p<0.01$). Therefore, systemic IL-1RA treatment suppresses the peripheral and central inflammatory response after SCI.

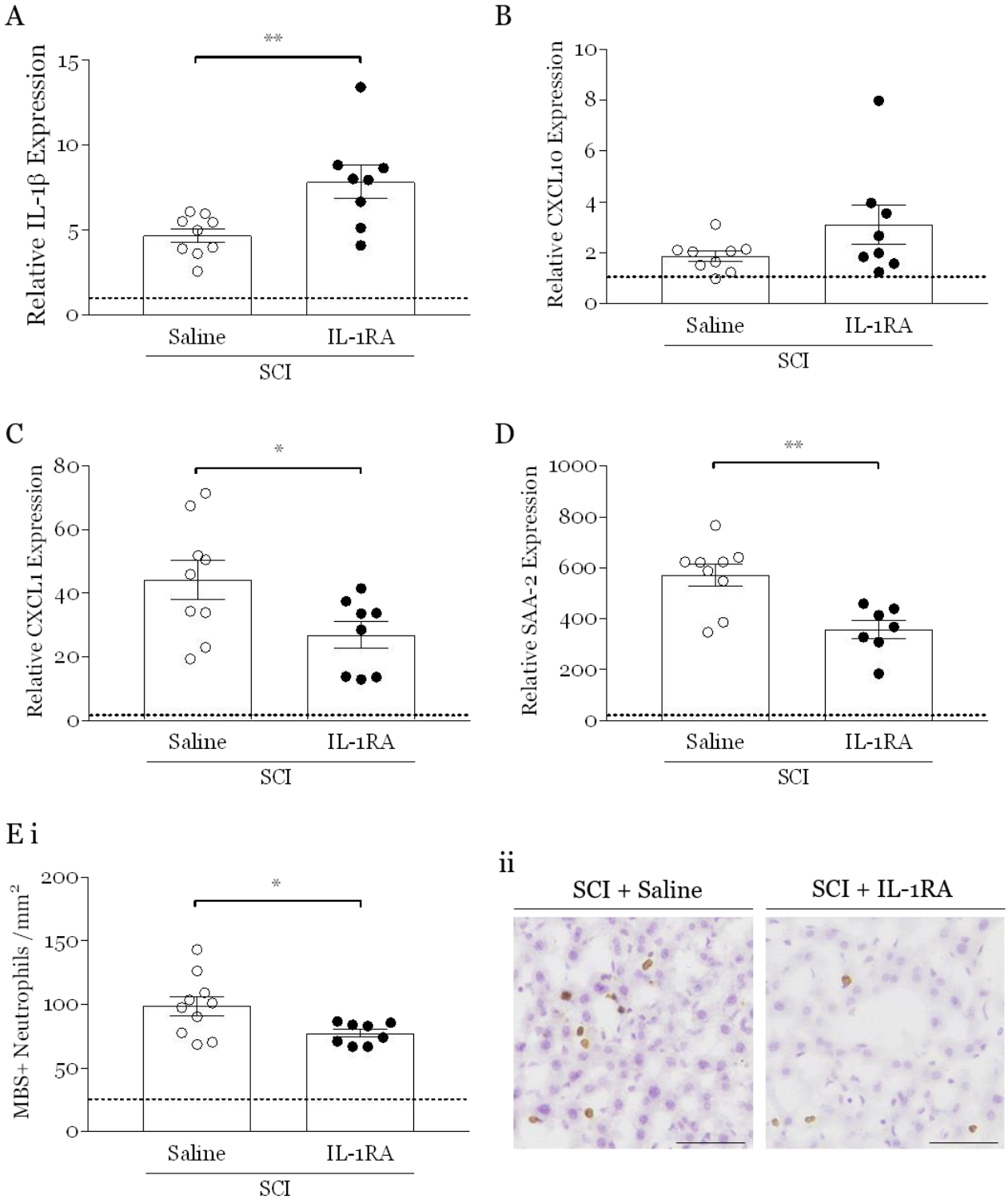


Figure 3.6 SCI-induced peripheral inflammation with IL-1RA treatment. Female C57BL/6 mice underwent a 70kD SCI at T9, and were treated with an intraperitoneal injection of either human IL-1RA (100mg/kg; black points, n=8) or saline as control (white points, n=9). Fresh and fixed liver was collected 6 hours later and compared with naïve baseline (dotted line, n=5). Relative expression of IL-1β (A), CXCL10 (B), CXCL1 (C) and SAA-2 (D) was measured by qPCR. Cell density of MBS+ neutrophils was calculated by immunohistochemistry (E i); representative images of neutrophils in the liver (ii), scale bar represents 100µm. Data are presented as mean ± SEM, and were analysed by student's unpaired t-test, *p<0.05 **p<0.01 compared to saline treated controls.

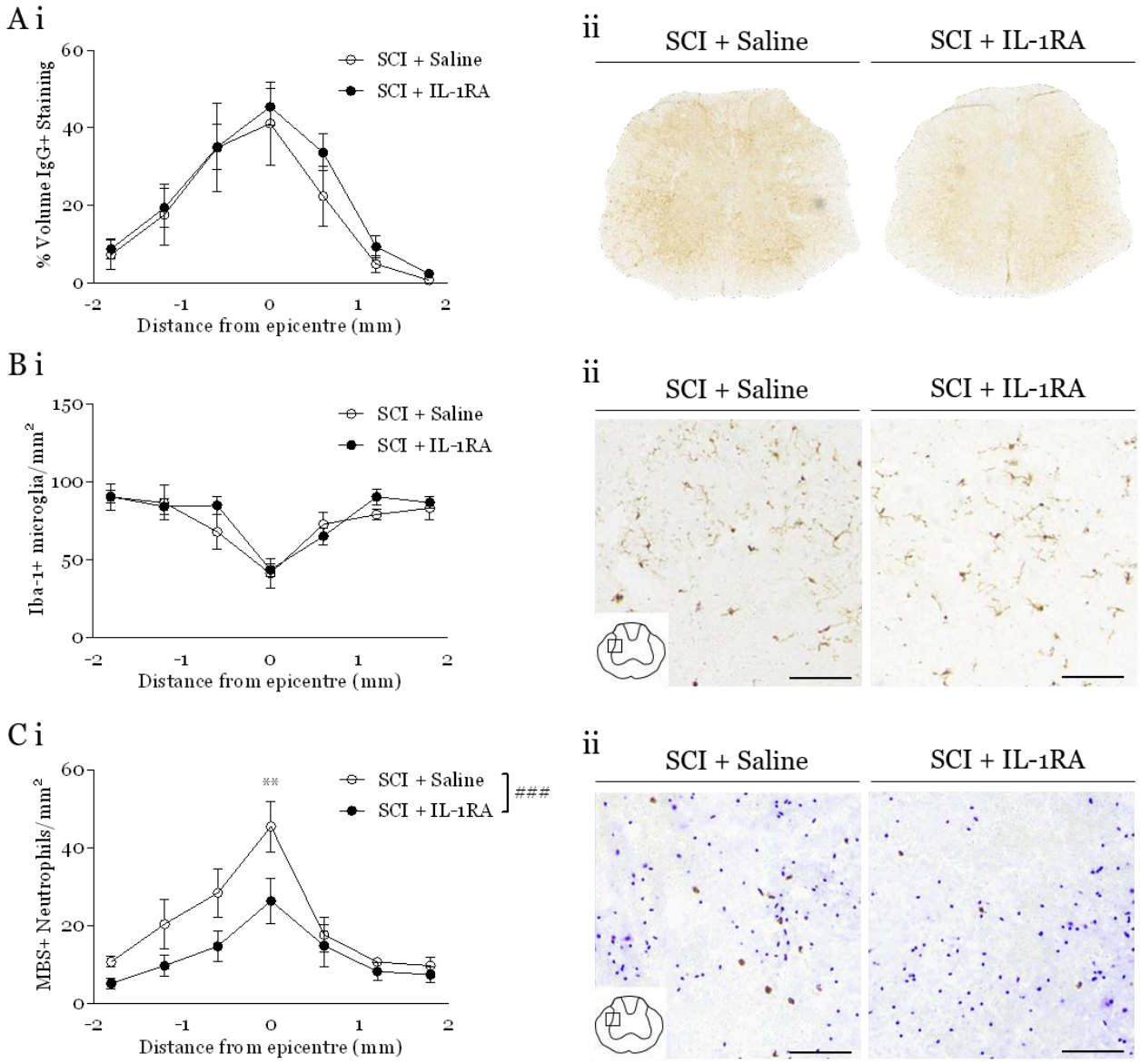


Figure 3.7 Spinal cord lesion pathology with IL-1RA treatment. Female C57BL/6 mice underwent a 70kD SCI and were treated with human IL-1RA (i.p. 100mg/kg; black points, n=8) immediately following, and 5 hours after impact, or saline as control (white points, n=5). Tissue was collected 6 hours post-injury and injury pathology was evaluated by immunohistochemistry analysis of fixed spinal cords. Breakdown of blood spinal cord barrier was determined by infiltration of IgG (A); representative image of a transverse section of spinal cord 0.6mm from the lesion epicentre. Microglia and neutrophil density was determined by Iba-1 and MBS staining, respectively. Representative images of immunopositive cells, taken at the lesion epicentre, scale bar represents 100µm. Data are presented as mean ±SEM, and analysed by two-way ANOVA, ###p<0.0001 treatment effect, **p<0.01 in Sidak's post-hoc test.

3.4 Discussion

Inflammation in the spinal cord following SCI contributes to further cell death after the initial injury (Alizadeh et al. 2019; Anwar et al. 2016) and is dependent upon a systemic inflammatory response, known as the APR (Anthony and Couch 2014). However, the relationship between the inflammatory responses in the CNS and the periphery, and the role it plays in lesion progression remains unclear. In this chapter, the SCI-induced APR during the acute phase of injury (≤24 hours) was characterised. In turn, it was determined whether lesion pathology could be manipulated by suppressing IL-1 signalling in the periphery with IL-1RA. Data presented here indicate that SCI induces a robust APR, as evidenced by increased neutrophils in the blood, liver and spleen, and hepatic expression of pro-inflammatory molecules, which precedes markers of spinal cord lesion progression. Moreover, peripheral IL-1RA treatment was shown to suppress this peripheral inflammation, and critically, neutrophil infiltration of the spinal cord, suggesting that IL-1RA could be used to reduce secondary damage after SCI.

3.4.1 SCI induces a robust APR which precedes spinal cord lesion progression

We have consistently shown that CNS trauma induces an APR, which modulates the secondary phase of injury (Campbell et al. 2008a; Campbell et al. 2003; Campbell et al. 2005). In our contusion model of SCI, it was confirmed that injury to the spinal cord induced a robust APR during the acute phase of injury; hepatic expression of a range of pro-inflammatory genes was significantly elevated above naïve baseline and, in turn, induced an increase in leukocyte mobilisation, and recruitment to the spinal cord and the liver. Peripheral analysis of sham animals indicates that the surgery itself induces a peripheral immune response. This is not unsurprising due to the invasiveness of the procedure, which initiates the wound healing cascade (MacLeod and Mansbridge 2016; Tidball and Villalta 2010). Despite this, additional trauma to the spinal cord specifically, which is relatively minor in comparison to the laminectomy alone, is sufficient to drive large changes in the peripheral inflammatory response, indicating that injury to the cord itself has a unique impact on the APR.

Activation of the APR results in mobilisation of immune cells. However, inappropriate infiltration of leukocytes into peripheral organs has been shown to cause cellular damage (Gris et al. 2008). This, in turn, leads to multi-organ dysfunction, which is not uncommon in SCI patients, where it significantly increases morbidity (Cotton et al. 2005; Stein et al. 2010; van Weert et al. 2014). Here, an increase in circulating neutrophils was detected in the blood at 2, 6 and 12 hours post-injury, consistent with both animal models (Brennan et al. 2019; Stirling and Yong 2008) and patient data (Bao et al. 2009), as well as in the spleen and liver. Given the blood filtering nature of the spleen, the increased number of neutrophils is likely due to the observed neutrophilia after SCI, although CNS trauma has also been shown to induce expression of pro-inflammatory molecules in this lymphatic organ (Offner et al. 2006), which could also be acting as chemoattractants. Data here also demonstrates an SCI-induced increase in neutrophil density in the liver, which is consistent with models of TBI and inflammatory brain lesions (Campbell et al. 2003; Campbell et al. 2008b; Hazleton et al. 2017), and is thought to be a consequence of general immune activation and, most importantly, the production of chemokines by the liver as part of the APR.

It is currently unclear how injury to any part of the CNS activates peripheral immune cells; whether the cells themselves become activated or whether the organs become activated and attract the cells. However, SCI has been shown to induce the upregulation of adhesion molecules on neutrophils (Bao et al. 2011a), whilst inflammation in the CNS has been shown to increase expression of adhesion molecules including ICAM-1 and VCAM-1 in the periphery (Campbell et al. 2007), which would enhance binding to endothelium and diapedesis in any number of organs. Indeed, SCI has been shown to induce immune cell infiltration in the lung and kidney (Gris et al. 2008). Here, we have demonstrated that SCI induces an increase in CXCL1 in the liver, which may contribute to neutrophil recruitment to this organ. CXCL1 is a potent chemoattractant for neutrophils and is often used as a surrogate marker for the leukocytes themselves, which also produce it. However, the expression of CXCL1 was delayed, peaking 6 hours post-SCI, which suggests that neutrophil infiltration to the liver may be initiated by an alternative mechanism, as suggested by Campbell et al. (2008b). By understanding more about the underlying mechanisms of the neutrophil response to SCI, we may be able to more effectively target it therapeutically.

Interestingly, during the acute phase of injury, the peripheral inflammatory response peaked early after SCI, whereas lesion pathology within the cord peaked at later time points. A similar delay in recruitment in the brain is observed after injury (Campbell et al. 2005). It is not clear why there should be a delay between the peripheral and central response; whether it is due to changes to the leukocytes or within the CNS, or a combination of these factors, remains unknown. Peripheral neutrophils may need to undergo priming, or remodelling, before they infiltrate the spinal cord. Bao et al. (2011a) showed that SCI induced an increase in surface integrins on circulating neutrophils, which would facilitate infiltration of the spinal cord. However, this was not observed until 12 hours post-injury. Alternatively, SCI has been shown to upregulate adhesion molecules in the spinal cord, yet an increase in ICAM-1 was only evident from 4 hours post-injury. Regardless of reason, it results in a 'therapeutic window', which may allow interventions to minimise bystander tissue damage during the secondary phase of injury.

3.4.2 IL-1β and IL-1RA in secondary damage after SCI

One of the peripheral components upregulated during this therapeutic window is IL-1 signalling. IL-1β is an important initiator of the inflammatory cascade (Allan et al. 2005) and its presence in the periphery has been shown to negatively impact CNS injury (Utagawa et al. 2008). Increased plasma IL-1β was associated with unfavourable patient outcomes following TBI (Di Battista et al. 2016) and systemic administration of IL-1β worsened BBB breakdown, oedema and neurological deficits in a model of stroke (McColl et al. 2007, 2008). McColl et al. (2007) further showed that peripheral IL-1β worsened neutrophilia and subsequent neutrophil infiltration of the brain. In our SCI model, hepatic expression of IL-1β was significantly elevated within 2 hours of injury, and its expression profile during the acute phase correlated with neutrophil load in the blood, spleen and liver. This occurs before the migration of neutrophils to the cord, suggesting IL-1β may mediate the neutrophil response to SCI, and therefore may be a viable therapeutic target.

Whilst IL-1β expression peaked 2 hours post-SCI, expression of IL-1RA was greatest 6 hours post-SCI. This apparent delay in reciprocal IL-1RA expression in the liver is consistent with expression in the spinal cord itself. Liu et al. (2008) showed that IL-1β protein in the cord is elevated 6 hours

after injury, whilst IL-1RA protein is initially decreased, and then significantly elevated compared to controls at 24 hours. Therefore, there is a clear temporal disconnect between the expression of IL-1β and its endogenous antagonist, where IL-1 signalling may go on unchecked, and thus might be amenable to therapeutic intervention.

To better understand IL-1 signalling during the acute phase, human IL-1RA was administered peripherally to SCI animals immediately following, and 5 hours after the impact. Previous studies investigating this treatment strategy in SCI have reported improvements in motor function, congruent with significant decreases in lesion size and cell death (Hasturk et al. 2015a; Li et al. 2018b; Liu et al. 2008; Zong et al. 2012). To investigate the mechanisms by which these improvements occur, the effect of IL-1RA on lesion pathology in the spinal cord was determined. Exogenous IL-1RA had no effect on SCI-induced decrease in microglia density or infiltrating IgG, confirming that injury severity was comparable in both groups. However, a significant decrease in neutrophil infiltration of the spinal cord during the acute phase of injury was observed with IL-1RA treatment, which may be neuroprotective. Indeed, it has consistently been shown that attenuation of neutrophil recruitment to the injured spinal cord is associated with improved sensory, autonomic and locomotor function (Lee et al. 2011; Nguyen et al. 2012). Therefore, IL-1RA treatment may also improve downstream functional outcomes after SCI, as evident with TBI (Newell et al. 2018) and stroke models (Maysami et al. 2016; Pradillo et al. 2017). Critically, neutrophil infiltration was not completely abolished. This may be fortuitous because complete depletion has been shown to worsen functional outcome (Stirling et al. 2009) and there is emerging evidence that neutrophils are required to initiate wound healing (Peiseler and Kubes 2019). The presence of both pro-injury and pro-repair neutrophils in the spinal cord suggests that investigation into the phenotype of the remaining neutrophils in the spinal cord lesion after IL-1RA treatment could be of interest.

In this chapter, the effect of peripheral IL-1RA treatment on the SCI-induced hepatic APR was evaluated for the first time. Paradoxically, IL-1β expression in the liver was increased with IL-1RA treatment, which is likely a compensatory response in the absence of feedback. Certainly, it has been shown that peripheral neutralisation of TNF after stroke, increases hepatic TNF expression,

yet granulocyte infiltration of the infarct was reduced (Clausen et al. 2014). Although the underlying mechanisms driving this increase in IL-1β expression are unknown, the critical aspect is that the downstream IL-1-mediated signalling itself is suppressed – CXCL1 and SAA-2 expression in the liver was decreased, as was neutrophil infiltration of the liver. This result suggests that the reduced neutrophil recruitment to the spinal cord is due to suppression of the peripheral inflammation. This validates the APR as therapeutic target after SCI, and is in keeping with previous studies in models of brain injury (Campbell et al. 2007; Campbell et al. 2008b), and negates the need to circumvent the problematic blood-CNS barrier. In the stroke paper by McColl et al. (2007), authors suggested that the increased neutrophil infiltration induced by systemic IL-1β expression was because of an increase in circulating CXCL1, which mobilised and directed neutrophil migration. Here, IL-1RA treatment suppressed hepatic CXCL1 expression, which is consistent with their hypothesis of the role of CXCL1 in neutrophil recruitment. As such, it can be proposed that IL-1RA inhibits downstream expression of CXCL1 in the liver, which in turn reduces neutrophil mobilisation and subsequent infiltration of the spinal cord (Figure 3.8). Moreover, when McColl et al. (2007) depleted neutrophils in their model, systemic IL-1β administration no longer had a detrimental effect on lesion pathology. This indicates that the neutrophil recruitment is the driving factor for CNS damage, and supports the conclusion that IL-1RA is neuroprotective by suppressing this mechanism.

It must be acknowledged that IL-1RA may also be exerting a direct effect on CNS inflammation. Previous studies investigating the pharmacokinetics of IL-1RA report its ability to cross the blood-CNS barrier (Galea et al. 2011; Greenhalgh et al. 2010) and blood-spinal cord barrier breakdown may allow passive accumulation. Pradillo et al. (2012) showed that delayed IL-1RA treatment (3 hours post-stroke) reduced infarct volume and neutrophil infiltration of the brain, which authors attributed to IL-1RA directly inhibiting pro-inflammatory microglia. Therefore, the reduction in infiltrating neutrophils observed here could be due to direct suppression of the IL-1 signalling in the spinal cord, without peripheral involvement. However, IL-1RA uptake to the CNS is extremely poor under both normal and pathological conditions (1-2% of plasma concentration; Greenhalgh et al. (2010)), therefore it is most likely having a peripheral, rather than a central effect.

Investigations into the use of peripheral anti-inflammatories as treatments for SCI are limited, yet data presented here indicate they could be a valid therapeutic strategy. Methylprednisolone, a synthetic glucocorticoid with greater potency than cortisol, was the only clinically approved drug for treatment during the acute phase after injury. However, recent studies have identified a lack of efficacy and increased risk of complications, including respiratory and urinary tract infections, and gastrointestinal haemorrhage (Evaniew et al. 2015; Liu et al. 2019). As a result, it is no longer recommended for routine use and an urgent need for alternatives remains (Ahuja et al. 2017a). Pharmacological studies have shown that immunomodulation with the antibiotic minocycline (Wells et al. 2003) or intravenous immunoglobulin (Brennan et al. 2016; Nguyen et al. 2012; Gillespie and Ruitenberg 2020) can improve histological and functional outcomes, and have both entered human clinical trials. However, both treatments have broad anti-inflammatory effects and so the underlying mechanisms are unknown. Here, it has been proposed that inhibition of IL-1 signalling specifically with IL-1RA has therapeutic potential. Anakinra, a recombinant version of human IL-1RA, is currently approved to treat a range of inflammatory diseases including rheumatoid arthritis (Mertens and Singh 2009). Given its excellent safety record and known pharmacokinetics (Dinarello et al. 2012), repurposing it for the treatment of SCI should be straightforward and rapid, and therefore should be explored.

For future work, it is also worth noting that the soluble decoy receptor rilonacept and the IL-1β neutralising monoclonal antibody canakinumab (Dubois et al. 2011; Baldwin et al. 2016) might also have similar actions. It would also be interesting to discover whether these agents would induce the rebound IL-1β production. Moreover, a limitation of this study was that only one dose of IL-1RA was investigated in this contusion model. As a result, more efficacious doses, as well as any significant off-target effects, may have been missed. Therefore, a dose-response study should be completed in order to identify the lowest effective dose, which will be important for toxicology, and will help validate the results.

3.5 Conclusions from this chapter

SCI induces a robust APR, characterised by hepatic expression of pro-inflammatory molecules and leukocyte mobilisation in the blood, which infiltrate the spleen and liver. This response precedes notable neutrophil infiltration of the spinal cord, indicating a therapeutic window may exist where intervention may limit secondary damage. Certainly, peripheral administration of human IL-1RA immediately following injury reduced neutrophil recruitment to the lesion site, thus indicating that IL-1RA could be used clinically following SCI to improve patient outcomes. Whether this effect is exerted directly, or indirectly by inhibiting the APR remains unclear, although, suppression of systemic inflammation can have its own independent benefits. From this data, long term studies of IL-1RA treatment on lesion pathology and functional outcomes are warranted.

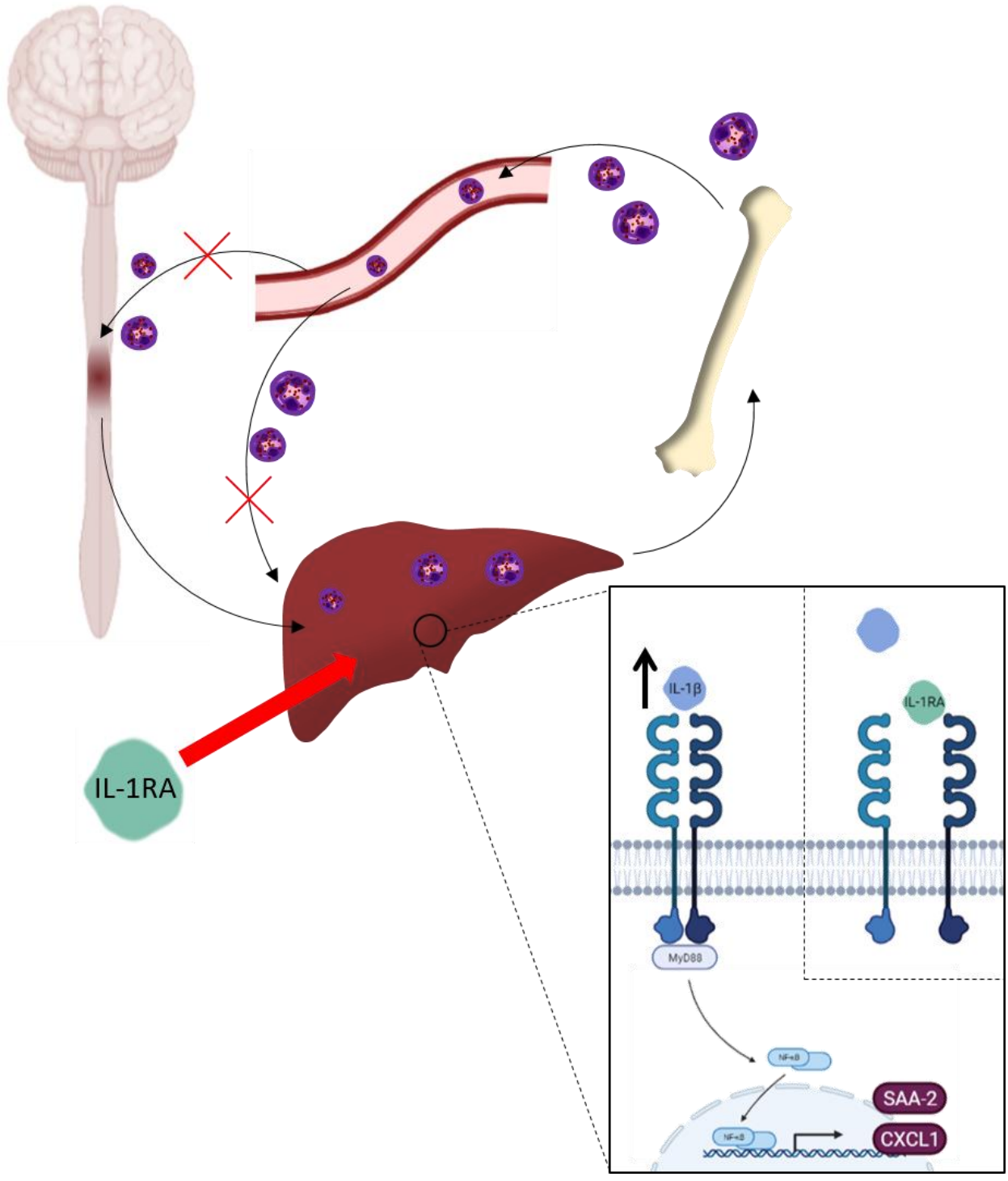


Figure 3.8 Proposed mechanism of action of IL-1RA treatment. SCI induces the upregulation of hepatic expression of IL-1β, and downstream pro-inflammatory molecules (CXCL1, SAA-2), which mobilises neutrophils from the bone marrow. Circulating neutrophils then infiltrate the spinal cord and peripheral organs and contribute to secondary damage. Treatment with IL-1RA inhibits IL-1β signalling in the liver, suppressing the expression of CXCL1 and SAA-2. This, in turn, suppresses neutrophil infiltration of the liver and the spinal cord, which may have neuroprotective effects.

Chapter 4: The systemic response to spinal cord injury is both lesion level and injury severity dependent

4.1 Introduction

In this chapter, I sought to discover whether the SCI-induced APR is dependent on the nature of the lesion. Systemic inflammation following SCI is well documented in patients and is associated with increased morbidity (Kesani et al. 2014; Sun et al. 2016). The systemic inflammatory response may therefore be an effective therapeutic target during the acute phase of injury. However, the APR is complex and its role in lesion progression remains incompletely understood in that both inhibition (Campbell et al. 2008b) and exacerbation (Davis et al. 2005) of peripheral inflammation reduces neutrophil recruitment to the spinal cord after traumatic injury. Thus, there is a need to improve our understanding of the mechanisms underlying the SCI-induced APR, and their contribution to pathology outcomes after SCI, in order to develop directed treatments.

It is not presently known whether the magnitude of the APR is dependent on the type of SCI lesion. In clinical studies, Stein et al. (2010) found that the development of organ dysfunction and failure strongly correlated with patient ASIA motor score and overall AIS grade. Moreover, Kesani et al. (2014) reported that SCI patients presenting with SIRS had higher injury severity scores, suggesting that the severity of the injury affects the systemic response. The increase in SIRS and organ dysfunction, as seen in patients with a more severe SCI, may be due to increased pathology within the cord itself. Indeed, lesion pathology typically shows a positive correlation with injury severity. It has been previously shown that with increased force and displacement of the spinal cord, length of lesion, cell death and the extent of scar tissue and functional deficits all increase (Ghasemlou et al. 2005; Ma et al. 2001), although this is not always the case (Fouad et al. 2021). Yang et al. (2005) further showed that expression of pro-inflammatory molecules (IL-1β, TNF, IL-6) is injury severity-dependent. These molecules are known to have a key role in the initiation of the secondary phase of injury (Pineau and Lacroix 2007), as they mediate activation of resident glia cells (Dibaj et al. 2010; Pineau et al. 2010). Consistent with this, it has been shown that there is increased GFAP reactivity with increasing SCI severity (Iwanami et al. 2005). Although the impact of injury severity on the microglia response has not been reported in a model of SCI, a severity-dependent increase in microglia density has been observed in a model of TBI (Wicker et al. 2019). Collectively, this

central inflammation worsens white matter sparing, and in turn spontaneous motor functional recovery (Noble and Wrathall 1989; Ghasemlou et al. 2005; Ma et al. 2001). However, these studies focused on the spinal cord only and there has been no investigation into the effect of SCI severity on the hepatic APR.

Mobilisation of leukocytes in the periphery is a hallmark of SCI, and precedes their infiltration into the spinal cord (Brennan et al. 2019). It has been shown that the magnitude of neutrophil (Yokota et al. 2016) and macrophage recruitment (Ghasemlou et al. 2005) to the spinal cord was dependent on the degree of injury. These immune cells are mobilised from the bone marrow (Brennan et al. 2019) and the splenic reservoir (Blomster et al. 2013a), respectively, in response to peripheral pro-inflammatory signals. Therefore, it stands to reason that SCI severity also has an influence on the APR, as it is the main driver of this systemic immune response. Certainly, in a model of CNS inflammation, intracranial injection of IL-1β induced neutrophil infiltration and expression of pro-inflammatory molecules in the liver in a dose dependent manner (Sa-Pereira et al. 2018). In addition, Wicker et al. (2019) demonstrated an injury severity-dependent increase in circulating acute phase proteins following TBI, suggesting there is a correlation between central and peripheral inflammation after CNS trauma. Elucidating the extent of this relationship is critical as it may influence the therapeutic approach to treat individual SCI patients.

In addition to the severity of the injury, the location of injury within the anatomy of the cord has proven to be pivotal for patient recovery. Higher level injuries (cervical to mid-thoracic) have been associated with increased incidence of respiratory complications, which persist for longer and increase the risk of intubation and death, compared to lower level injuries (Cotton et al. 2005; Jackson and Groomes 1994). Brouwers et al. (2020) reported improved recovery in SCI patients with lumbar injuries compared to those with thoracic injuries. Several studies have investigated the effect of SCI lesion level on the peripheral response, and whilst all have identified a level-dependent effect, it is unclear in which direction this occurs. For example, Fleming et al. (2012) and Bao et al. (2011b) observed increased hepatic cytokine expression and neutrophil mobilisation in a T4 clip compression SCI model when compared to T12 injuries. Moreover, Ogurcov et al. (2021) reported

increased circulating chemokines (CXCL1 and CXCL10) in patients following cervical SCI, compared to thoracic and lumbar SCI, 2-weeks post-injury. However, clinically, there is poor correlation between lesion level and the incidence of MODS (Stein et al. 2010). In addition, Hong et al. (2018) reported a decrease in circulating pro-inflammatory proteins in the plasma after cervical SCI, compared to thoracic, which authors attributed to sympathetic dysregulation. These data demonstrate that both severity and anatomical location have a profound influence on the peripheral inflammatory response to SCI, and these aspects of the injury warrant further investigation.

SCI-IDS, another systemic response to SCI, is characterised by a dramatic decrease in systemic lymphocytes (Riegger et al. 2009), which leaves patients more susceptible to infections, predominantly pneumonia (Jackson and Groomes 1994), and subsequently, worsened functional outcomes (Failli et al. 2012; Pruss et al. 2017). The underlying causes of SCI-IDS are not fully understood but it is likely that both severity and anatomical location of injury play important roles. It has been shown that SCI patients have increased plasma concentrations of cortisol and more frequently require catecholamine treatment, compared to patients with vertebrae fractures alone (Pruss et al. 2017). This autonomic dysfunction after SCI is lesion level-dependent (Brommer et al. 2016; Pruss et al. 2017). Whilst intact in lower level injuries, higher level injuries cause decentralisation of the adrenal glands. This causes a decrease in circulating catecholamines as well as an increase in glucocorticoids, such as cortisol, which can have endogenous anti-inflammatory effects (Schulze et al. 2014; Webster Marketon and Glaser 2008). However, the effect of injury severity on autonomic dysfunction has not yet been investigated in the acute phase of SCI.

The aims of this chapter were (1) to investigate the effects of SCI lesion level and injury severity on the APR, and (2) to determine how the sympathetic-neuroendocrine adrenal reflex is affected by these differential lesions.

4.2 Methods specific to this chapter

4.2.1 Animals

Female C57BL/6 mice, 8-12 weeks of age, were used in this chapter. Animals were obtained from the Animal Resource Centre (Canningvale, Australia), and allowed to acclimatise for 4 weeks prior to experimentation. All animals were housed in a pathogen-free facility, under standard diurnal lighting conditions (12 hours) with *ad libitum* access to food and water.

4.2.2 SCI model

To determine the effect of injury severity and lesion level on the APR, mice underwent a single-impact, bilateral SCI at level T9 with a force of 30kD, 70kD or 100kD (n=10/severity). Alternatively, at level T2, mice received either a single-impact, bilateral 30kD SCI, or a double-impact bilateral 70kD SCI (n=12/severity). The spinal cord at level T2 is wider than at T9 (Ahuja et al. 2017b), and so was struck twice in order to replicate the severe paralysis achieved with a T9 injury. 100kD injury group at T2 was not included as preliminary analysis of the APR following SCI at T9 revealed no difference between 70kD and 100kD groups. Control animals underwent a sham surgery at the corresponding lesion level without cord impact. For all experiments, surgeries were performed as described in 2.3.1, and animals were allowed to survive for 6 hours after which tissue was collected as described in 2.5. For each lesion level, 2 cohorts of mice were used: fresh liver was collected from both cohorts, 1 cohort was further perfused with fixative for collection of fixed liver and spinal cord. Blood, fresh spinal cord and spleen were collected from the second cohort.

4.2.3 Spinal cord qPCR

A 1cm segment of fresh spinal cord, encompassing the lesion and the immediate rostral and caudal regions, was homogenised with a pestle and mortar on dry ice, and 10-20mg of tissue was used for qPCR as outlined in 2.8.

4.3 Results

4.3.1 The magnitude of lesion pathology is injury severity dependent at T9

To determine the effect of SCI injury severity on central inflammation, animals were subjected to either a 30kD, 70kD or 100kD SCI at T9, which resulted in significantly greater displacement (Figure 4.1A; one-way ANOVA, $p<0.0001$). Control animals underwent sham surgery without spinal cord impact. Motor function was assessed 6 hours later and fixed spinal cord samples were collected immediately afterwards for immunohistochemical analysis.

BMS score indicated that the severe injuries caused complete hind limb paralysis at this time point (Figure 4.1B; one-way ANOVA, $p<0.0001$; 0.0±0.0 for both 70kD and 100kD SCI). Whereas the mild (30kD) injury induced a functional deficit (3.6±0.4; Sidak's post-hoc test, $p<0.0001$ compared to sham) but these paretic animals retained a significant level of hindlimb motor function (Sidak's post-hoc test, $p<0.0001$ compared to both 70kD and 100kD SCI). Lesion pathology also showed a positive correlation with injury severity (Figure 4.2). An increase in percent volume of IgG staining was observed in the 30kD (Figure 4.1C; 15.5±3.4%; $p=0.061$), 70kD (36.6±2.8; $p<0.0001$) and 100kD injured cords (43.8±4.1%; $p<0.0001$), compared to sham (3.5±1.3%). There was no significant difference between 70kD and 100kD injury groups (Sidak's post-hoc test, $p=0.523$), however both were significantly increased compared to the 30kD injury group (Sidak's post-hoc test, vs. 70kD $p<0.001$, vs. 100kD $p<0.0001$). The average IgG staining intensity at the lesion epicentre followed the same injury severity trend (Figure 4.1D; one-way ANOVA, $p<0.0001$). SCI injury severity also had an effect on Iba-1+ microglia density within the spinal cord lesion (Figure 4.1E-F). A decrease in microglia density at the lesion epicentre was evident following the more severe injuries (Sidak's post-hoc test, sham vs. 70kD $p<0.001$, sham vs. 100kD $p<0.0001$), but not following the mild 30kD injury (Sidak's post-hoc test, $p=0.982$ compared to sham). In addition, neutrophil recruitment to the spinal cord (Figure 4.1G-H) was greatest following 100kD SCI (Sidak's post-hoc test, $p<0.001$ compared to sham). Significant infiltration was also observed following 70kD SCI (Sidak's post-hoc test, $p<0.05$ compared to sham), whereas there was no difference between 30kD SCI and sham controls (Sidak's post-hoc test, $p=0.758$).

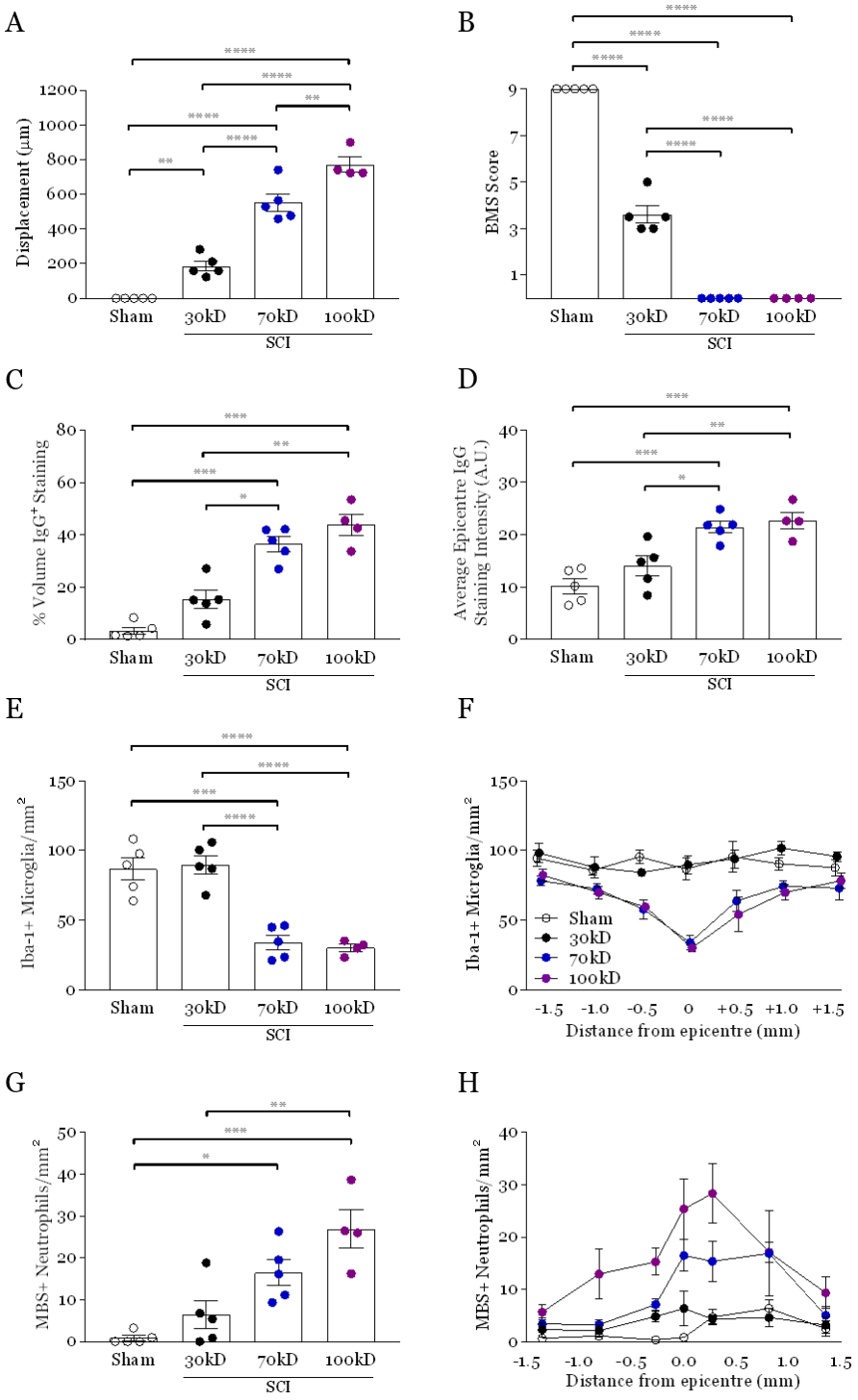


Figure 4.1 The magnitude of functional loss and spinal cord lesion pathology following SCI of different injury severities at level T9. Female C57BL/6 mice underwent either a 30kD (black points, n=5), 70kD (blue points, n=5) or 100kD (purple points, n=4) SCI, or sham surgery as control (white points, n=5) at level T9 (A). Motor function was assessed by BMS 6 hours post-injury (B) after which tissue was collected. The magnitude of lesion pathology was determined by immunohistochemistry analysis of fixed spinal cords. Volume of IgG as a percent of total spinal cord volume (C) and average epicentre IgG staining intensity (D) were used as markers of blood-spinal cord barrier breakdown. Iba-1+ microglia cell density calculated at the epicentre (E) and ±1.5mm (F). MBS+ neutrophil cell density calculated at the epicentre (G) and ±1.5mm (H). Data are presented as mean ±SEM, and analysed by one- or two-way ANOVA, *p<0.05 **p<0.01 ***p<0.001 ****p<0.0001 with Sidak's post-hoc test.

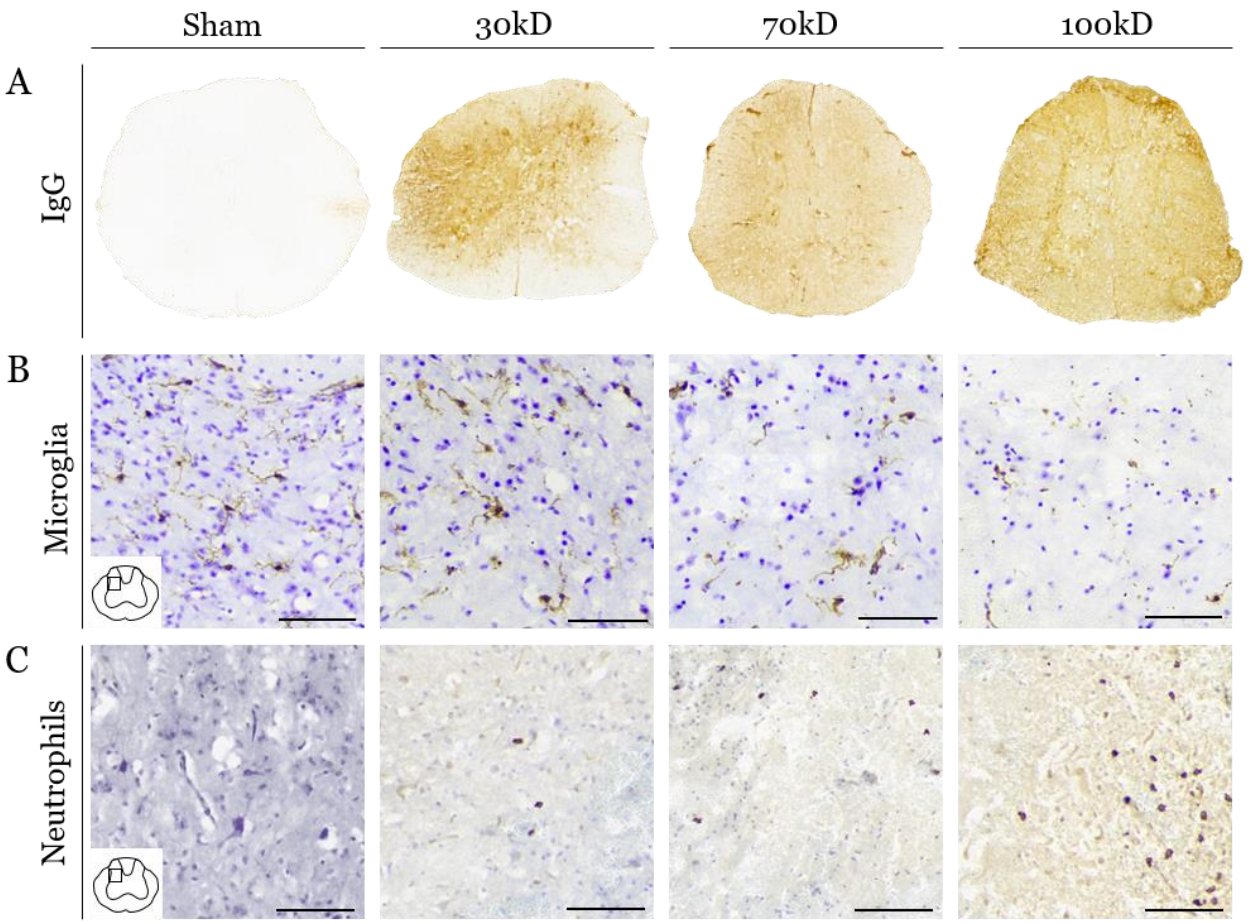


Figure 4.2 Spinal cord lesion pathology following SCI of different injury severities at level T9. Female C57BL/6 mice underwent either a 30kD, 70kD or 100kD SCI, or sham surgery as control at level T9. Fixed spinal cords were collected 6 hours later and stained with IgG (A), Iba-1 (B) and MBS (C), to evaluate blood-spinal cord barrier breakdown, microglia and neutrophil density, respectively. Scale bar represents 100µm.

4.3.2 The magnitude of lesion pathology is injury severity dependent at T2

To ascertain any lesion level effect, animals underwent either a single-impact, midline 30kD SCI, or double-impact 70kD SCI at T2 (Figure 4.3A; one-way ANOVA, $p<0.0001$). A 100kD T2 SCI group was not included here because preliminary analysis of the APR after SCI at T9 showed no difference between the 70kD and 100kD injury groups.

BMS analysis confirmed that 70kD SCI caused severe, near-complete hind limb paralysis (Figure 4.3B; 0.8±0.2; Sidak's post-hoc test, $p<0.0001$ compared to sham and 30kD groups). The mild 30kD injury induced a motor deficit, but limited function was preserved (Figure 4.3B; 4.1±0.3; Sidak's post-hoc test, $p<0.0001$ vs. sham, $p<0.0001$ vs. 70kD SCI groups). In the spinal cord, the percent volume of IgG staining (Figure 4.3C; Kruskal-Wallis test, $p<0.001$) and average epicentre IgG staining intensity (Figure 4.3D; Kruskal-Wallis test, $p<0.01$) were both significantly increased after a severe (70kD) SCI, compared to sham with Dunn's post-hoc test. A trending increase in both parameters was observed in the 30kD injury group, however results were not statistically significant from either sham or 70kD groups. Density of microglia in the lesion epicentre was significantly decreased after a 70kD SCI (Figure 4.3E; 16.1±2.2/mm^2; Sidak's post-hoc test, $p<0.0001$), but not a 30kD SCI (61.7±6.5/mm^2; Sidak's post-hoc test, $p=0.364$), compared to sham (73.1±5.9/mm^2). This result was unchanged when microglial density was evaluated spatially across the lesion (Figure 4.3F; two-way ANOVA, $p<0.0001$). The 70kD SCI group was significantly different from both the 30kD ($p<0.001$) and sham injury groups ($p<0.0001$); there was no difference between sham and 30kD groups ($p=0.101$). SCI was otherwise associated with neutrophil recruitment to the spinal cord (Figure 4.3G; one-way ANOVA, $p<0.001$), and this was greater following severe SCI (Sidak's post-hoc test, $p<0.05$). Further spatial analysis at the epicentre ±1.8mm also confirmed that neutrophil infiltration of the spinal cord was injury severity dependent (Figure 4.3H; two-way ANOVA, injury $p<0.0001$, distance from epicentre $p<0.0001$). Sidak's post-hoc analysis revealed again significant differences between sham and 30kD ($p<0.001$), sham and 70kD ($p<0.0001$), and 30kD and 70kD injury groups ($p<0.0001$). These data indicate that lesion pathology positively correlated with injury severity (Figure 4.4).

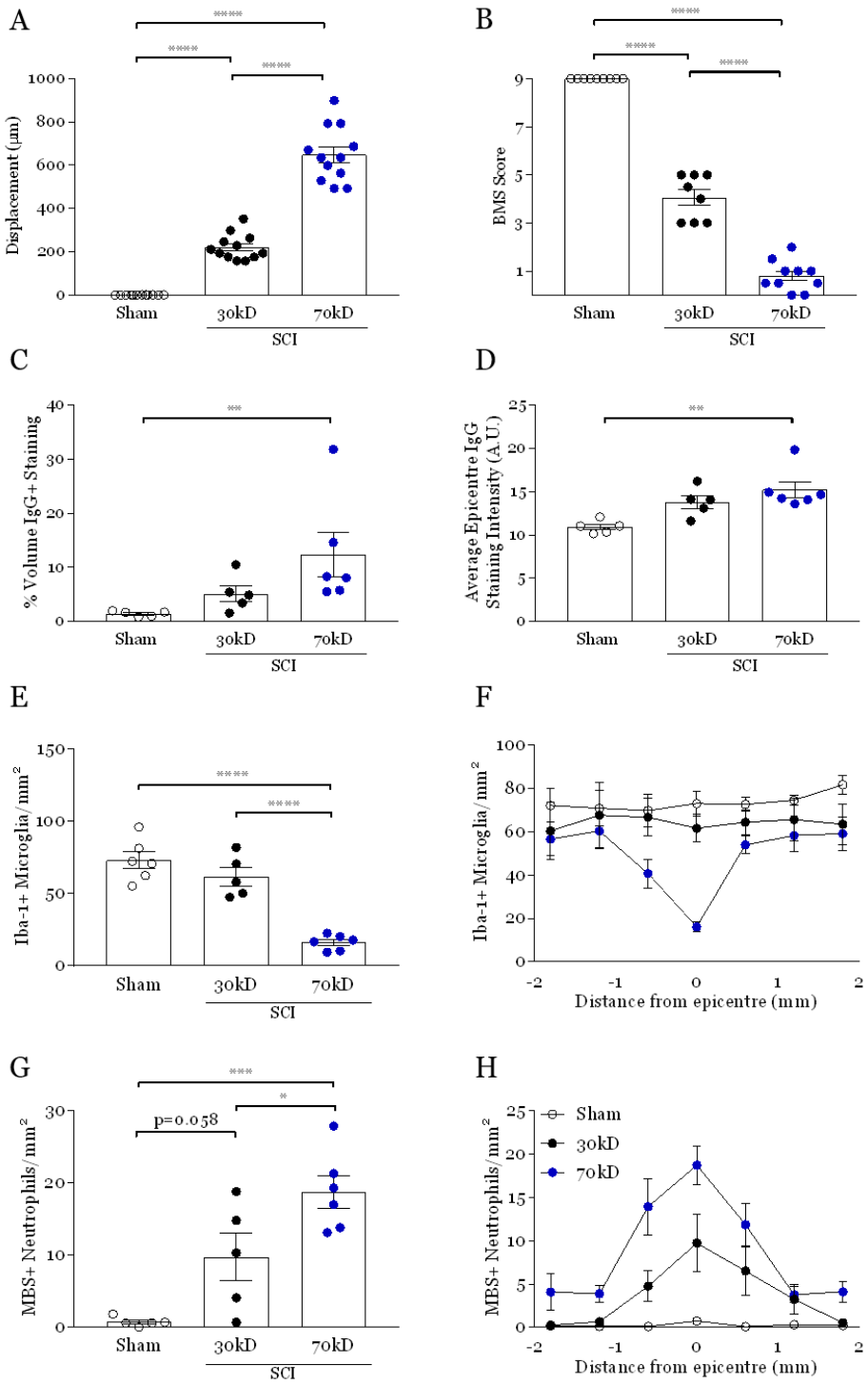


Figure 4.3 The magnitude of functional loss and spinal cord lesion pathology following SCI of different injury severities at level T2. Female C57BL/6 mice received either a single, midline 30kD (black points, n=12) or bilateral 70kD (blue points, n=12) SCI, or sham surgery (white points, n=12) at level T2. Motor function was assessed by BMS 6 hours post-injury (B) after which tissue was collected. The magnitude of lesion pathology was determined by immunohistochemistry analysis of fixed spinal cords. Volume of IgG as a percent of total spinal cord volume (C) and average epicentre IgG staining intensity (D) were used as markers of blood-spinal cord barrier breakdown. Iba-1+ microglia cell density calculated at the epicentre (E) and ±1.5mm (F). MBS+ neutrophil cell density calculated at the epicentre (G) and ±1.5mm (H). Data are presented as mean ±SEM, and analysed by one-, two-way ANOVA or Kruskal-Wallis test as appropriate, *p<0.05 **p<0.01 ***p<0.001 ****p<0.0001 with Sidak's or Dunn's post-hoc test.

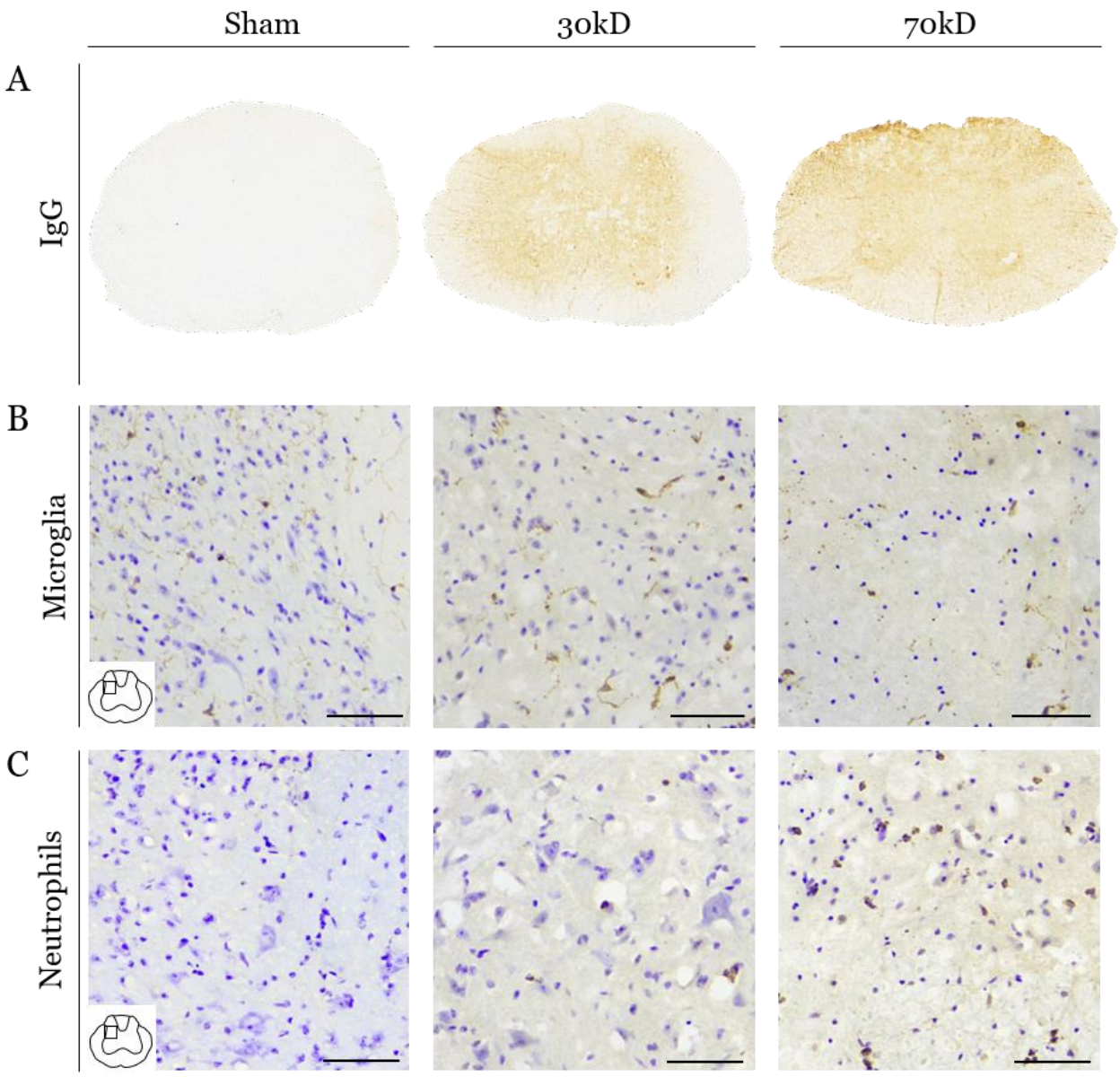


Figure 4.4 Spinal cord lesion pathology following SCI of different injury severities at level T2. Female C57BL/6 mice received either a single, midline 30kD or bilateral 70kD SCI, or sham surgery at level T2. Fixed spinal cords were collected 6 hours later and stained with IgG (A), Iba-1 (B) and MBS (C), to evaluate blood-spinal cord barrier breakdown, microglia and neutrophil density, respectively. Scale bar represents 100µm.

4.3.3 Expression of inflammation-associated genes in the spinal cord is SCI severity dependent

To further understand severity- and level-dependent changes in inflammation following SCI, qPCR of fresh spinal cord tissue samples was performed in a second cohort of mice.

Relative expression of IL-1β was increased in the spinal cord after a T9 SCI (Figure 4.5A; one-way ANOVA, $p=0.085$), which, surprisingly, was independent of injury severity as no significant differences were found between the 30kD, 70kD and 100kD groups. By contrast, SCI at T2 induced an increase in IL-1β expression in a severity dependent manner (Figure 4.5B; one-way ANOVA, $p<0.0001$); Sidak's post-hoc analysis revealed significant differences between sham and 30kD ($p<0.01$), sham and 70kD ($p<0.0001$), and the 30kD and 70kD groups ($p<0.05$). Compared to naïve baseline, greater expression of IL-1β was observed in the T9 SCI model than the T2 SCI model. However, compared to sham controls, SCI at T2 induced a greater SCI-specific response. SCI at T9 induced a 1.7-2.7-fold increase in IL-1β expression, whilst at T2, 30kD and 70kD SCI induced a 16.0 and 26.9-fold increase in expression, respectively. This was also evident for CXCL10 expression; SCI at T9 induced a 4.6-6.2-fold increase in CXCL10 expression (Figure 4.5C; one-way ANOVA, $p<0.01$), whereas SCI at T2 induced a 22.7-28.9-fold increase (Figure 4.5D; one-way ANOVA, $p<0.0001$), compared to sham. There was no SCI severity effect on CXCL10 expression in the spinal cord following either T9 or T2 injury.

SCI at T9 induced a considerably large increase in CXCL1 expression in the spinal cord, which was severity dependent (Figure 4.5E; one-way ANOVA, $p<0.0001$). There was no difference in expression levels in 30kD (229.6±36.7) and 70kD injury groups (236.8±33.8; Sidak's post-hoc test, $p>0.999$), yet expression was significantly increased in the 100kD injury group (458.6±48.4; Sidak's post-hoc test, vs. 30kD $p<0.01$, vs. 70kD $p<0.01$). Similarly, SCI at T2 induced a severity-dependent increase in CXCL1 expression in the cord (Figure 4.5F; one-way ANOVA, $p<0.0001$). At T9, 30kD, 70kD and 100kD SCI induced a 5.7, 5.9 and 11.5-fold increase in CXCL1 expression, respectively, whereas at T2, 30kD and 70kD SCI induced a 14.6 and 37.1-fold increase relative to sham, respectively.

SAA is predominantly produced in the liver and is undetectable in the CNS, however is produced by microglia and astrocytes in response to inflammation (Barbierato et al. 2017). Following a T9 injury, SAA-2 expression in the spinal cord was increased in all animals compared to naïve baseline, independent of spinal injury (Figure 4.5G; one-way ANOVA, $p=0.198$). By comparison, with injury induced at T2, spinal cord SAA-2 expression was significantly increased in SCI animals compared to sham animals (Figure 4.5H; one-way ANOVA, $p<0.001$), although there was no difference between 30kD (10.1±1.9) and 70kD injury groups (9.9±1.0; Sidak's post-hoc test, $p=0.999$).

Collectively, these data show that the magnitude of inflammation and histopathology in the spinal cord is proportional to the severity of the injury.

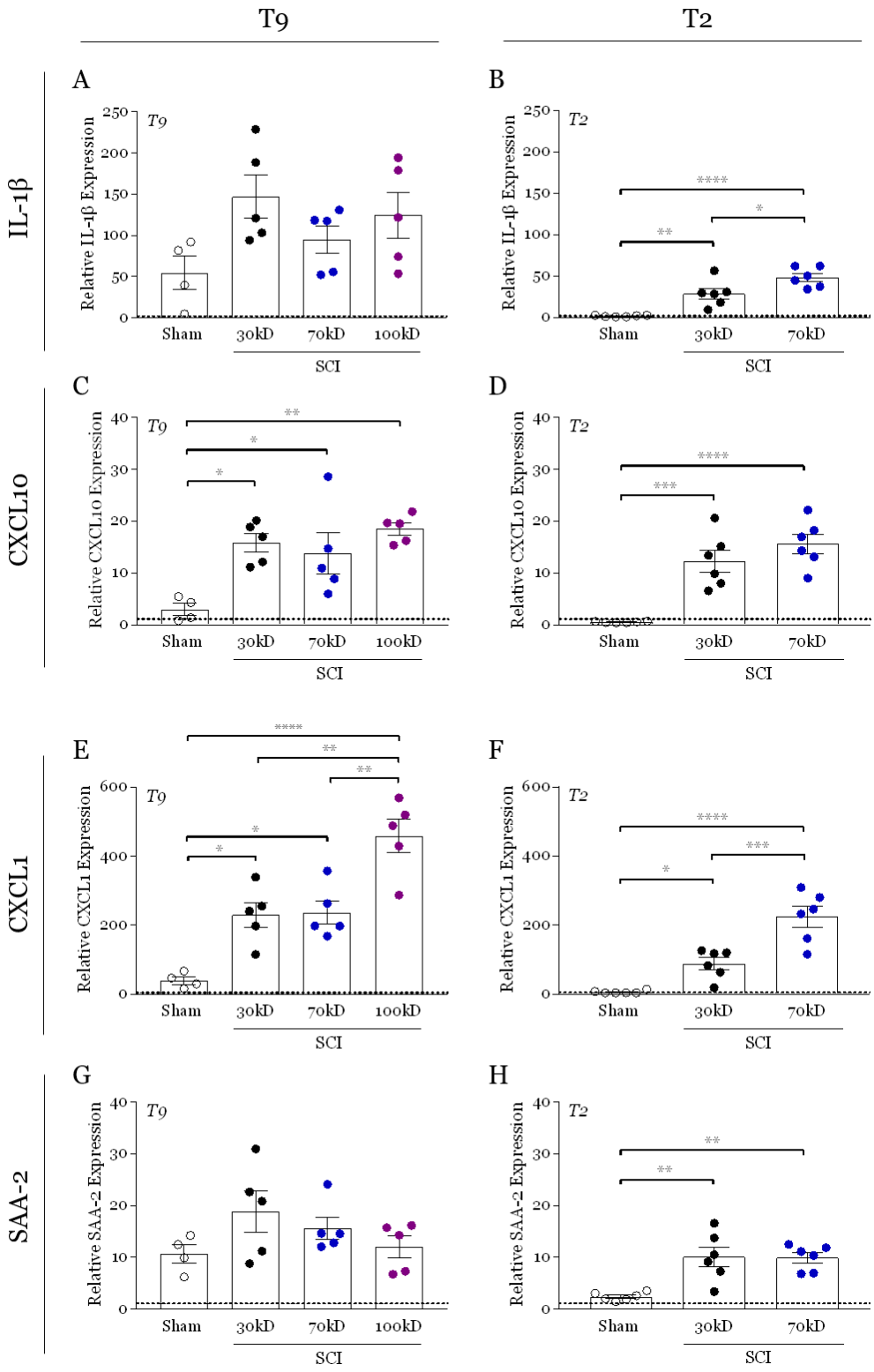


Figure 4.5 Expression of inflammation-associated genes in the spinal cord following SCI. Female C57BL/6 mice received either a 30kD (black points, n=6) or 70kD (blue points, n=6) SCI at T2, or 30kD (black points, n=5), 70kD (blue points, n=5) or 100kD (purple points, n=5) SCI at T9. Control animals underwent a sham surgery at the corresponding level (white points, n=4-6). Fresh spinal cords were collected 6 hours post-injury and relative expression of IL-1β (A, B), CXCL10 (C, D), CXCL1 (E, F) and SAA-2 (G, H) was determined by qPCR, normalised to naïve (n=4). Data are presented as mean ±SEM and was analysed by one-way ANOVA, *p<0.05 **p<0.01 ***p<0.001 ****p<0.0001 in Sidak's post-hoc test.

4.3.4 APR induced by SCI at T9 is injury severity dependent

Given that inflammatory markers in the spinal cord correlated with displacement, next, the effect of injury severity on the APR induced by SCI at T9 was examined. qPCR analysis of fresh liver showed a positive correlation between IL-1β expression and injury severity (Figure 4.6A; one-way ANOVA, $p<0.001$); there was no difference between 70kD (4.7±0.4) and 100kD injury groups (4.8±0.5; $p>0.99$), but both groups were significantly increased compared to 30kD injury group (2.9±0.3; vs. 70kD $p<0.05$, vs. 100kD $p<0.05$) and sham controls (2.2±0.2; vs. 70kD $p<0.001$, vs. 100kD $p<0.001$) with Sidak's post-hoc test. One-way ANOVA revealed that hepatic CXCL10 expression was also injury severity dependent (Figure 4.6B; $p<0.05$), although there were no significant differences between groups with post-hoc testing. By contrast, CXCL1 (Figure 4.6C; one-way ANOVA, $p<0.001$) and SAA-2 expression (Figure 4.6D; one-way ANOVA, $p<0.01$) inversely correlated with injury severity. Expression of these genes were elevated in the 30kD animals (CXCL1, 97.7±±2.8, $p<0.05$ and SAA-2, 1022.0±105.2, $p=0.505$ with Sidak's post-hoc test) compared to sham animals. However, compared to the mild injury group, expression was suppressed in the 70kD (CXCL1, 39.8±7.4, $p<0.0001$ and SAA-2, 485.1±53.9, $p<0.01$) and 100kD injury groups (CXCL1, 58.1±9.2, $p<0.01$ and SAA-2, 580.7±158.2, $p=0.054$) with Sidak's post-hoc testing. This was consistent with the cellular response in the periphery. Whilst blood neutrophils were largely unaffected at this time point (Figure 4.6E; one-way ANOVA, $p<0.05$), the proportion of neutrophils in the spleen was injury severity dependent (Figure 4.6F; one-way ANOVA, $p<0.0001$), with highest density after a 30kD SCI (3.9±0.3%), which was decreased in the 70kD (2.2±0.3%; Sidak's post-hoc test, $p<0.001$ compared to 30kD) and 100kD injury groups (3.1±0.2%; Sidak's post-hoc test, $p=0.195$ compared to 30kD). Liver neutrophil (Figure 4.6G; one-way ANOVA, $p=0.064$) and macrophage density (Figure 4.6H; one-way ANOVA, $p<0.05$) followed a similar pattern; over sham, 30kD SCI at T9 induced the most significant APR (Figure 4.7).

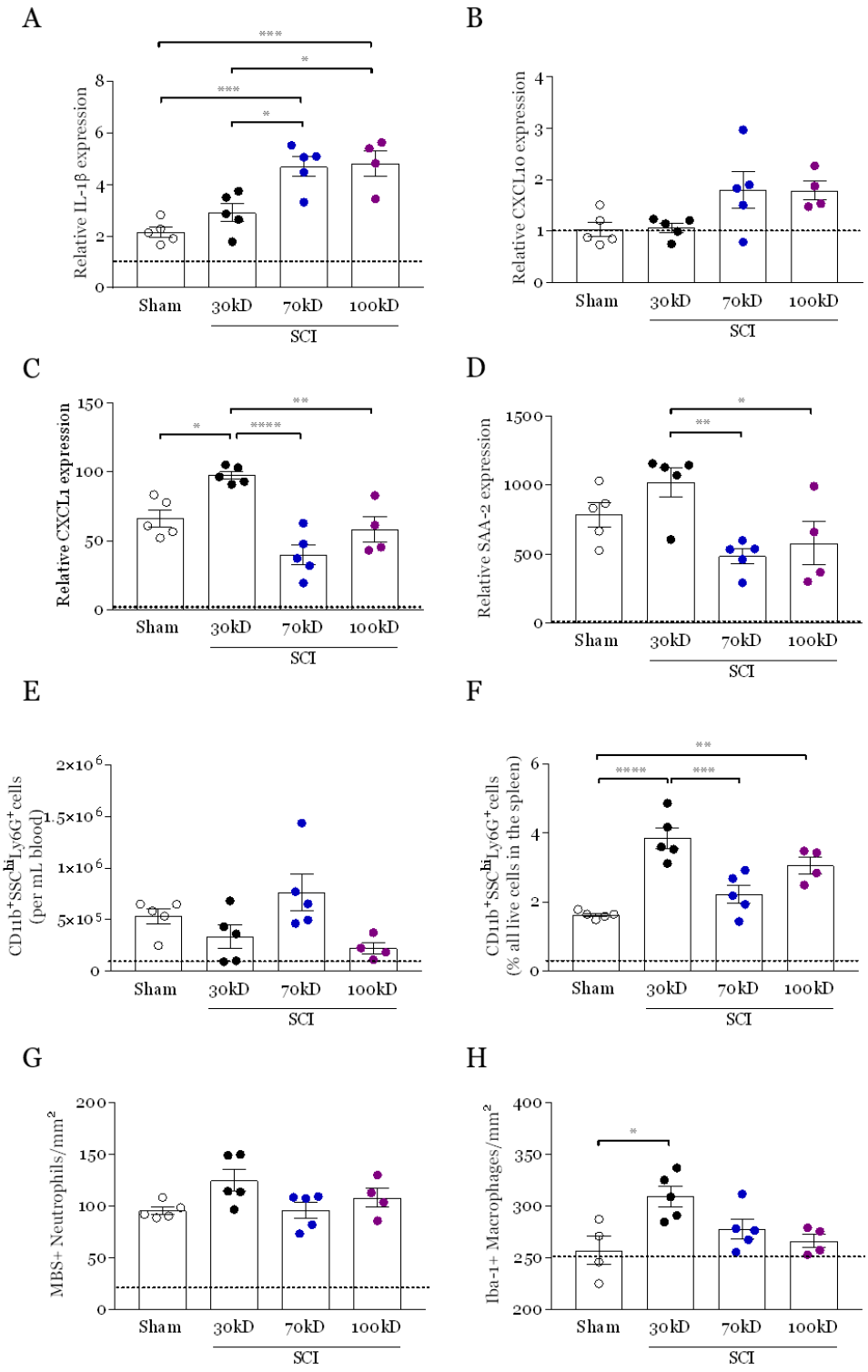


Figure 4.6 The magnitude of the hepatic APR following SCI of different injury severities at level T9. Female C57BL/6 mice received either a 30kD (black points, n=5), 70kD (blue points, n=5) or 100kD (purple points, n=4) SCI, or sham surgery (white points, n=5) at level T9. Peripheral tissue was collected 6 hours post-injury and analysis was compared to naïve baseline (dotted line, n=5). Hepatic expression of IL-1β (A), CXCL10 (B), CXCL1 (C) and SAA-2 (D) were determined by qPCR. Leukocyte mobilisation in the blood (E) and spleen (F) was measured by flow cytometry; granulocytes were defined as the $CD11b^{+}SSC^{hi}Ly6G^{+}$ population. Neutrophil (G) and macrophage (H) density in the liver was determined by immunohistochemistry. Data are presented as mean ±SEM and was analysed by one-way ANOVA, *p<0.05 **p<0.01 ***p<0.001 ****p<0.0001 in Sidak's post-hoc test.

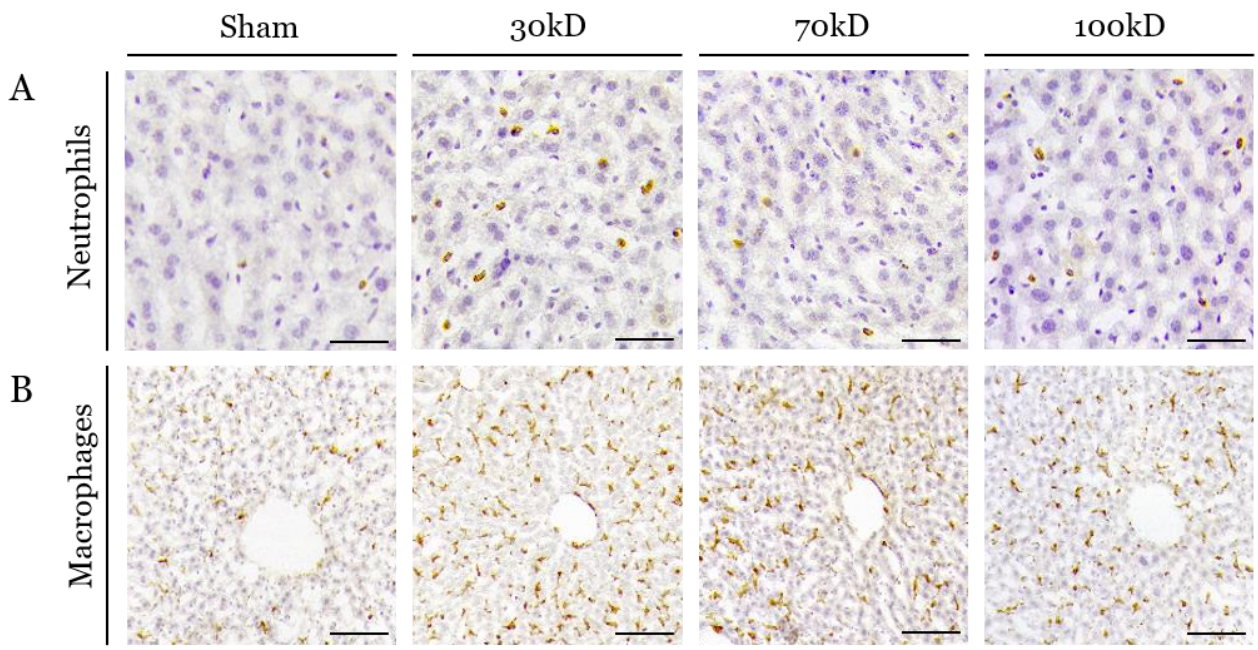


Figure 4.7 Leukocyte density in the liver following SCI of different injury severities at level T9. Female C57BL/6 mice underwent either a 30kD, 70kD or 100kD SCI, or sham surgery as control at level T9. Fixed livers were collected 6 hours later and stained with MBS (A) and Iba-1 (B) to visualise neutrophils and macrophages respectively. Scale bar represents 50µm in neutrophil pictograms and 100µm in macrophage pictograms.

4.3.5 APR induced by SCI at T2 is differentially injury severity dependent

It has previously been shown that peripheral inflammation is exacerbated in animals with higher level lesions (Fleming et al. 2012). Therefore, the effect of injury severity on the APR induced by SCI at T2 was then examined, to evaluate whether the severity-dependent response was still evident.

qPCR analysis of the liver revealed that expression of inflammation-associated genes was SCI severity dependent after a T2 injury. Although, in contrast to a T9 injury, SCI at T2 suppressed expression of IL-1β (Figure 4.8A; one-way ANOVA, $p<0.05$); there was no difference between sham (5.6±0.7) and 30kD injury groups (4.7±0.5; Sidak's post-hoc test, $p=0.67$), but expression was significantly decreased in the 70kD injury group compared to controls only (Sidak's post-hoc test, $p<0.05$). The remaining genes analysed showed the same patterns of expression following T2 and T9 SCI. Expression of CXCL10 (Figure 4.8B; one-way ANOVA, $p<0.0001$) was significantly increased in the 70kD injury group (2.8±0.2; Sidak's post-hoc test, $p<0.0001$), but not the 30kD injury group (1.1±0.1; Sidak's post-hoc test, $p>0.99$), compared to controls (1.1±0.1). Similarly, CXCL1 (Figure 4.8C; one-way ANOVA, $p<0.05$) and SAA-2 expression (Figure 4.8D; one-way ANOVA, $p<0.0001$) was decreased in the severe injury groups only. Neutrophil density in the liver showed a trending increase following SCI, which was not injury severity dependent (Figure 4.8E; one-way ANOVA, $p=0.063$). Analysis of macrophage density in the liver showed no significant differences between any groups (Figure 4.8F; one-way ANOVA, $p=0.917$).

Thus, whilst SCI induces a profound APR, some elements (CXCL1 and SAA-2 expression, leukocyte mobilisation) were suppressed after severe injury, but not mild injury.

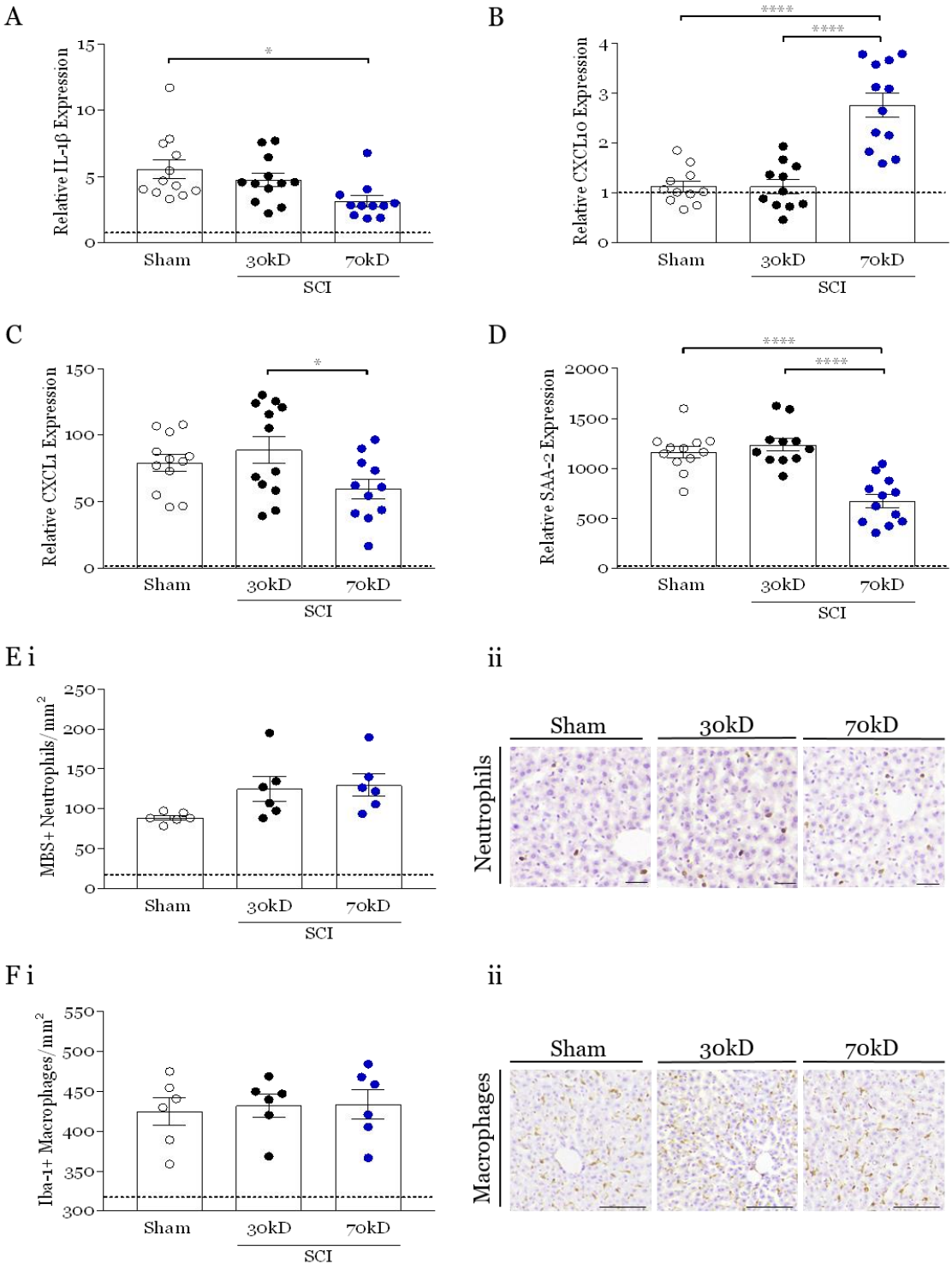


Figure 4.8 The magnitude of the APR following SCI of different injury severities at level T2. Female C57BL/6 mice received either a single, midline 30kD (black points, n=12) or bilateral 70kD (blue points, n=12) SCI, or sham surgery (white points, n=12) at level T2. Peripheral tissue was collected 6 hours post-injury and analysis was compared to naïve baseline (dotted line, n=5). Hepatic expression of IL-1β (A), CXCL10 (B), CXCL1 (C) and SAA-2 (D) were determined by qPCR. Neutrophil (E) and macrophage (F) density in the liver was determined by immunohistochemistry. Representative pictograms of leukocyte density in the liver, scale bar equals 50μm and 100μm for neutrophils and macrophages respectively. Data are presented as mean ±SEM and was analysed by one-way ANOVA, *p<0.05 **p<0.01 ***p<0.001 ****p<0.0001 in Sidak's post-hoc test.

4.3.6 SCI-induced APR is injury level dependent

To confirm that lesion level has a differential effect on the APR, hepatic expression of inflammation-associated genes following 70kD SCI at T2 and T9, and corresponding control animals was measured together for direct comparisons. Hepatic IL-1β was found to be lesion level dependent, 6 hours post-SCI (Figure 4.9A; two-way ANOVA, interaction $p<0.0001$); at T9, SCI induced a significant increase in IL-1β expression compared to sham (Sidak's post-hoc test, $p<0.01$), whereas, at T2, expression was suppressed compared to controls (Sidak's post-hoc test, $p<0.05$). CXCL10 expression was unaffected by lesion level at 6 hours (Figure 4.9B; two-way ANOVA, lesion level $p=0.131$, injury $p<0.0001$). Similarly, two-way ANOVA analysis of CXCL1 expression revealed no lesion level effect (Figure 4.9C; lesion level $p=0.072$, injury $p<0.001$). By contrast, hepatic SAA-2 expression was affected by lesion level when compared to their matching sham counterparts. Specifically, there was a significant difference between T2 and T9 animals (Figure 4.9D; two-way ANOVA, lesion level $p<0.001$, injury $p<0.0001$) and a significant interaction ($p<0.05$); the SCI-induced decrease in SAA-2 expression was greater at T2 (Sidak's post-hoc test, $p<0.0001$) than at T9 (sham, Sidak's post-hoc test, $p<0.05$). In conclusion, the acute peripheral inflammatory response is dependent on the level of spinal injury, particularly so for IL-1β expression.

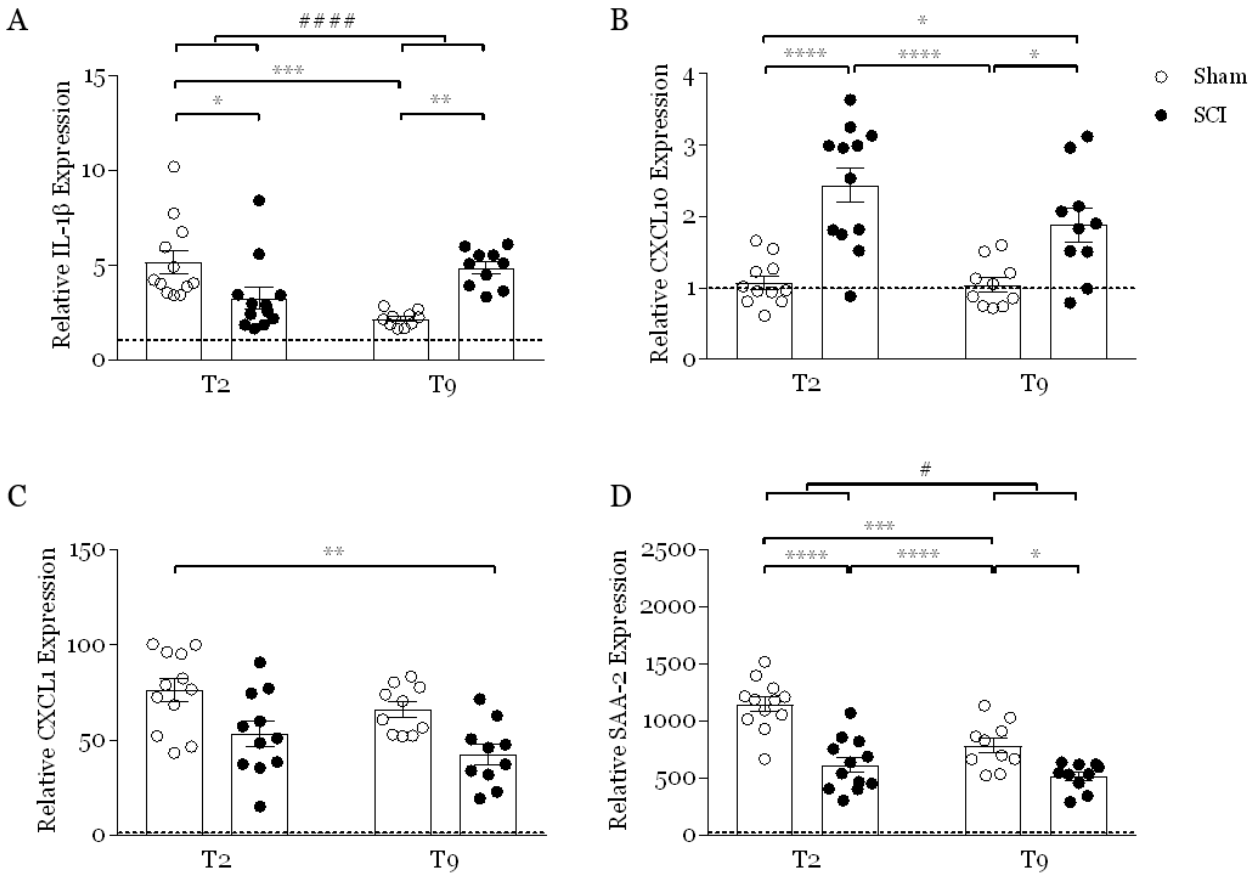


Figure 4.9 Expression of inflammation-associated genes in the liver following T2 and T9 SCI. cDNA generated from the livers of sham (white points, n=10-12) and 70kD SCI animals (black points, n=10-12), collected 6 hours post-injury, was measured together by qPCR for direct comparisons. Expression of IL-1β (A), CXCL10 (B), CXCL1 (C) and SAA-2 (D) was evaluated, normalised to naïve baseline (dotted line, n=5) to determine any lesion level effects. Data are presented as mean ±SEM, and analysed by two-way ANOVA, #p<0.05 ####p<0.0001 interaction, *p<0.05 **p<0.01 ***p<0.001 ****p<0.0001 in Sidak's post-hoc test.

4.3.7 HPLC results

To ascertain whether autonomic dysfunction was similarly affected by SCI lesion level and severity, HPLC analysis was performed on plasma samples, and the concentration of circulating corticosterone and noradrenaline were determined.

Plasma corticosterone concentration was significantly elevated above naïve baseline in all injury groups, at both injury levels. However, there were no significant differences between sham controls or SCI severity groups at T9 (Figure 4.10A; one-way ANOVA, $p=0.945$) or T2 (Figure 4.10B; one-way ANOVA, $p=0.229$). Plasma noradrenaline concentration was decreased in all groups compared to naïve. Following T9 SCI, there were no significant differences between sham controls and injury severity groups (Figure 4.10C; one-way ANOVA, $p=0.295$), however, following T2 SCI, one-way ANOVA analysis revealed a significant difference between injury groups (Figure 4.10D; $p<0.05$). A trending increase in plasma noradrenaline concentration was observed between sham and 70kD SCI, however this was not statistically significant (Sidak's post-hoc test, $p=0.061$).

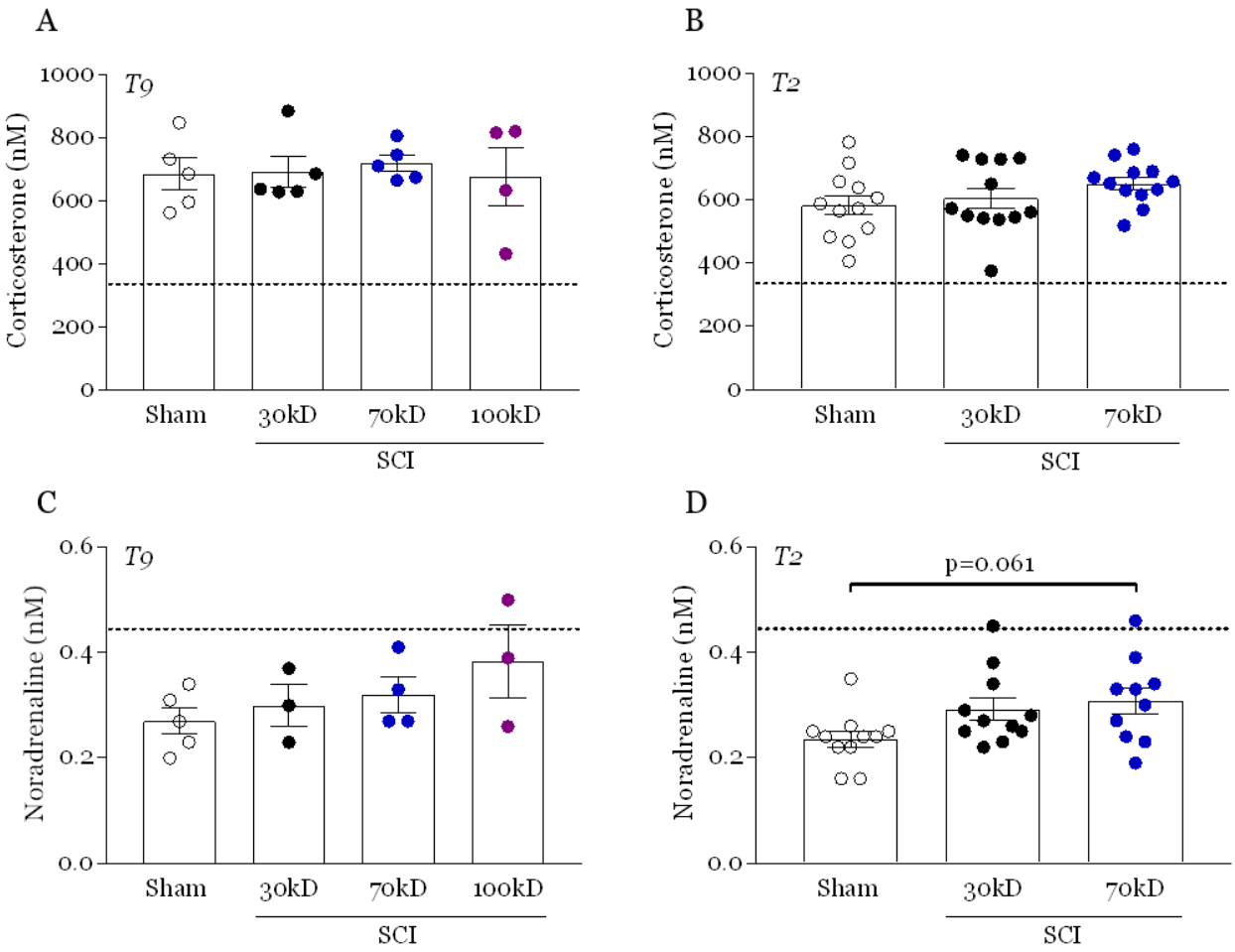


Figure 4.10 Concentrations of corticosterone and noradrenaline in the plasma following SCI. Female C57BL/6 received either a 30kD (midline) or 70kD SCI at T2 (bilateral), or a 30kD, 70kD or 100kD SCI at T9 (midline). Control animals underwent a sham surgery at the corresponding lesion level. Plasma was collected 6 hours later and circulating corticosterone (A, B) and noradrenaline (C, D) were determined by HPLC. Naïve plasma samples (n=3, dotted line) were used as baseline. Data are presented as mean ±SEM and were analysed by one-way ANOVA.

4.4 Discussion

Systemic inflammation after SCI correlates with injury severity scores and increases patient morbidity (Kesani et al. 2014; Stein et al. 2010; Sun et al. 2016). In turn, the concomitant SCI-IDS has similarly been associated with worsened patient outcomes, and is lesion level dependent (Brommer et al. 2016). However, the interaction between SCI severity and lesion level, and their effect on the resultant APR has not been investigated. In this chapter, the magnitude of central and peripheral inflammation was evaluated following SCI of different severities induced at either T9 or T2. Data presented here indicates that spinal cord histopathology after injury correlates with severity, as evidenced by increased BSCB breakdown and neutrophil infiltration, as well as decreased microglial density, with increasing force of impact. By contrast, many markers of peripheral inflammation exhibited an inverse correlation with the degree of injury, including neutrophil infiltration of peripheral organs and hepatic expression of CXCL1 and SAA-2. In addition, lesion level differences in pro-inflammatory cytokine expression were observed in both the spinal cord itself, and the liver. Collectively, these data indicate that the SCI-induced APR is dependent on injury severity and lesion level. It should be noted that sham surgery is, in all cases, a strong inducer of the APR and this should be considered in any analysis of SCI model and the role of the peripheral immune system.

4.4.1 Spinal cord pathology is injury severity and lesion level dependent

Functional outcome after SCI is directly associated with the magnitude of damage in the spinal cord (Hurd et al. 2013; Schucht et al. 2002), although there are discrepancies between lesion size and the magnitude of impairment (Fouad et al. 2021). Here, the histopathology of SCI of different severities during the acute phase was examined in a contusion model of SCI. Injuries induced at both T9 and T2 induced significant hind limb paralysis, and exhibited a severity-dependent increase in associated pathology. With increasing impact force, significantly greater IgG and neutrophil infiltration, and decreased microglial density were evident. The microglial response was consistent with previous studies (Ghasemlou et al. 2005; Ma et al. 2001; Schnell et al. 1999a; Bellver-Landete et al. 2019) and correlated with the extent of paralysis in these mice. Greater IgG

infiltration, as a % of total volume, was observed in the T9 injury model compared to T2, suggesting a lesion level effect on BSCB breakdown. Although, this can be attributed to differences in segmental size; T2 is immediately caudal to the cervical enlargement, therefore is much wider than the T9 segment (Ahuja et al. 2017b). By contrast, the magnitude of microglial cell death and neutrophil infiltration was comparable in the two models, which is likely to be due to inflammation in the spinal cord.

To explore the molecular mechanisms driving this histopathology, expression levels of pro-inflammatory cytokines in the spinal cord were measured. Consistent with previous reports (Yang et al. 2005; Stammers et al. 2012), a severity-dependent increase in pro-inflammatory cytokine expression was observed in the spinal cord. Specifically, at T2, IL-1β and CXCL1 expression exhibited a clear injury severity effect, where expression was significantly increased in the severe 70kD SCI group, compared to the mild 30kD SCI group. Both of these cytokines have been implicated in leukocyte recruitment to the CNS (Pineau and Lacroix 2007; Pineau et al. 2010). Indeed, a severity-dependent increase in neutrophil infiltration of the spinal cord was observed here. This was mirrored in the T9 injury model, although less pronounced as a result of the increased variability in the 30kD SCI group. Resident glial cells have been identified as the main contributors of intraspinal cytokine expression after SCI at this time point (Pineau and Lacroix 2007; Yang et al. 2004; Yang et al. 2005), however a significant decrease in microglial density was observed with more severe injury. Therefore, increased pro-inflammatory cytokine expression must derive from the remaining, activated glial cells, highlighting their significant contribution to spinal cord pathology.

Greater expression of pro-inflammatory cytokines was detected in the spinal cords injured at T9, compared to those injured at T2. This may be attributable to a surgery-associated inflammatory response, because T9 sham animals had significantly elevated cytokine expression above naïve baseline, which was not evident in T2 sham animals. Certainly, the T9 model requires a laminectomy where the dorsal spine of the T9 vertebra is removed to expose the spinal cord (Scheff et al. 2003). Even with excellent technique, this can result in unintentional spinal cord damage

(Choo et al. 2009), irritation of the dura and/or the underlying meninges, thus inducing cytokine expression. Whereas, a dorsal laminectomy is not required in the T2 model, where the large intervertebral space is exploited instead. By contrast, expression as fold-change compared to sham indicates that injury at T2 induces a greater SCI-specific inflammatory response in the spinal cord. This lesion level difference in cytokine expression may be due to anatomical variation between the spinal cord segments. The glia-to-neuron ratio decreases down the spinal cord, therefore there is a greater proportion of glial cells at T2 than at T9 (Bahney and von Bartheld 2018), which, as aforementioned, are the predominant producers of pro-inflammatory cytokines after injury (Pineau and Lacroix 2007). Interestingly, despite divergences in cytokine expression, this was not reflected in the cellular response. Greater IL-1β expression was detected in the spinal cord after T9 SCI compared to T2, which seems to correlate with leukocyte recruitment (Pineau et al. 2010), yet there was no difference in neutrophil infiltration between lesion levels. This may be because of the time at which spinal cords were analysed; tissue was collected 6 hours post-injury, but neutrophil recruitment continues 1-3 days after SCI (Fleming et al. 2006; Kigerl et al. 2006), therefore lesion level differences in histopathology may not become apparent until later time points. Taken together, these data indicate that the magnitude of neuroinflammation is influenced by both the severity and level of injury.

4.4.2 SCI-induced APR is injury severity dependent

In SCI patients, the severity of injury correlates with SIRS and multi-organ failure (Kesani et al. 2014; Stein et al. 2010). Certainly, the magnitude of neutrophil mobilisation after injury has been shown to be predictive of patient outcome (Brennan et al. 2019; Jogia et al. 2021). Our group has demonstrated that the APR is a valid therapeutic target after traumatic CNS injury (Campbell et al. 2007; Yates et al. 2021), and thus improving our understanding of the relationship between the central and peripheral inflammatory responses may assist in the development of neuroprotective treatments. To the best of our knowledge, the effect of SCI severity on the hepatic APR has not previously been investigated. In this chapter, CXCL1 and SAA-2 expression in the liver, and neutrophil infiltration of peripheral organs, were suppressed in the severe injury group compared

to the mild. This indicates that there seems to be an inverse correlation between SCI severity and the magnitude of the APR, which was unexpected. Neutralisation of CXCL1 reduced neutrophil recruitment to the CNS in a model of inflammatory brain lesion (Campbell et al. 2003); it would be of interest to investigate this intervention in our different severity models of SCI.

The suppressed APR after SCI is inconsistent with previous studies on brain injury. Wicker et al. (2019) and Sa-Pereira et al. (2018) reported an increase in peripheral pro-inflammatory molecules, proportional to severity, in models of TBI and brain inflammation, respectively. There is a plethora of anatomical and functional differences between the brain and spinal cord, which may explain the differences in the APR. Most notably in this context, injury to the spinal cord directly affects innervation of the sympathetic nervous system, whilst this does not necessarily happen after injury to the brain. SCI causes a dysfunctional sympathetic-neuroendocrine adrenal reflex (Brommer et al. 2016; Pruss et al. 2017). SCI-induced loss of sympathetic tone to the adrenal glands, with intact vagus nerve, causes the release of cortisol, which is a potent anti-inflammatory. Therefore, it was hypothesised that an injury severity-dependent release of circulating catecholamines may be responsible for suppression of the APR. Indeed, HPLC analysis revealed that SCI induced a decrease in plasma noradrenaline and increase in plasma corticosterone, consistent with loss of sympathetic tone. However, there was no SCI severity or level effect. Moreover, unexpectedly, sham animals, which had no damage to adrenal innervation, followed the same pattern. Given that naïve animals received anaesthetic, this indicates that the sympathetic response at this time point is trauma-associated and not necessarily reflective of CNS injury. Therefore, a different mechanism must be driving the suppression of the APR. An alternative hypothesis could be that the increasing breakdown of the vasculature and loss of microglia may result in a decrease in the release of injury signals from the CNS into the periphery.

Evidence of immune suppression after severe SCI was surprising at this time point. SCI-IDS has been well documented in patients during the subacute phase of injury (Riegger et al. 2007; Riegger et al. 2009). However, data in this chapter demonstrates an SCI-induced decrease in hepatic pro-inflammatory molecule expression and leukocyte mobilisation 6 hours post-injury, thus suggesting

that it may begin earlier than perhaps appreciated. SCI-IDS is principally associated with the adaptive immune response as circulating B- and T-cells are significantly depleted within 24 hours of SCI (Riegger et al. 2009), although decreases in blood innate immune cells have also been reported (Campagnolo et al. 2008; Riegger et al. 2009; Zhang et al. 2013). Here, an inverse correlation was observed between SCI severity at T9 and neutrophil numbers in the spleen, and neutrophil and macrophage density in the liver. It is unknown whether leukocytes are mobilised after SCI from a limited pool, or if they are continuously replenished. Therefore, it cannot be concluded whether the observed leukocyte depletion in severe injuries is due to SCI-IDS associated mechanisms (cell death, reduced release and/or production), or due to reallocation of immune cells from the periphery to the spinal cord. Given that SCI-IDS is associated with increased risk of developing infection, which, in turn, increase morbidity and worsen functional outcomes (Cotton et al. 2005; Failli et al. 2012), therapeutic interventions to target this response may need to be modified to take these factors into account. Once more, understanding the timing of inflammation within the cord, and the result of this and the initial injury on the systemic APR will be key to developing novel strategies to target these processes.

4.4.3 SCI-induced APR is lesion level dependent

Studies investigating the effect of SCI lesion level of the peripheral immune response have been contradictory. Fleming et al. (2012) previously reported that SCI-induced hepatic inflammation is exacerbated with higher level injuries; it was reported that there was increased influx of leukocytes and increased expression of IL-1β and CXCL1 following T4 SCI, compared to T12. Conversely, Sauerbeck et al. (2015) demonstrated that IL-1β and TNF-α expression in the liver was greater after thoracic SCI, compared to cervical. Here, no lesion level effect on neutrophil infiltration of the liver was observed, whilst hepatic IL-1β was suppressed following T2 SCI, yet increased following T9 SCI. These differences may be attributed to experimental design; each study used a different animal species, injury model and time point, all of which have been shown to affect the immunological response to neurotrauma (Cheriyan et al. 2014; Sroga et al. 2003; Yates et al. 2021). For example, Fleming et al. (2012) and Sauerbeck et al. (2015) both used rats, whilst mice were used in this

chapter and mobilisation of immune cells after SCI differs between the two rodent species (Kigerl et al. 2006; Sroga et al. 2003). Despite these contradictions, it remains clear that the location of the SCI lesion has a significant impact on the magnitude of the APR.

Hepatic IL-1β expression was found to be SCI lesion level dependent. As discussed in the previous chapter, IL-1β is a key pro-inflammatory molecule in the pathophysiology of SCI. Its peripheral administration has been shown to exacerbate CNS injury (McColl et al. 2007), whilst its inhibition has been shown to reduce neutrophil infiltration of the spinal cord (Yates et al. 2021). Taken together, these studies indicate that systemic IL-1β drives central inflammation after traumatic injury. Certainly, in this chapter, a correlation between IL-1β expression and neutrophil density in the spinal cord was observed following SCI at T9. However, in the T2 SCI model, injury suppressed hepatic IL-1β expression, yet neutrophil infiltration of the spinal cord remained comparable to the T9 SCI model. This would suggest that peripheral IL-1β signalling plays less of an important role after SCI than previously established, instead indicating that intraspinal IL-1β is the main driver of leukocyte recruitment (Pineau et al. 2010). A study to investigate the effect of exogenous IL-1RA on the APR and neutrophil infiltration of the spinal cord, in the T2 SCI model, would help clarify this mechanism.

It is unclear the mechanisms by which the observed SCI level differences in the APR occur, although sympathetic signalling may play a significant role (Lucin et al. 2007; Monteiro et al. 2020; Zhang et al. 2013). With low level injuries (T9), sympathetic innervation of peripheral organs, including the liver, spleen and adrenal glands, remains largely intact, whereas with high level injuries (T2), this innervation is disrupted (Hou and Rabchevsky 2014). Sympathetic fibres can induce expression of pro-inflammatory cytokines in liver Kupffer cells (Huan et al. 2017). In addition, loss of sympathetic stimulation, in conjunction with persistent vagal nerve stimulation can have an anti-inflammatory effect (Borovikova et al. 2000). Therefore, it can be proposed that direct sympathetic innervation of the liver induced IL-1β expression after SCI at T9, which is unable to occur after SCI at T2 because of sympathetic denervation. Indeed, Jung et al. (2000) showed that sympathetic activation directly induced hepatic IL-1β expression. Moreover, denervation of other peripheral

organs, such as the spleen and adrenal glands, by high level SCI has similarly had anti-inflammatory effects (Monteiro et al. 2020; Pruss et al. 2017). To explore this, post-ganglionic deafferentation (Brommer et al. 2016), to shield the liver from sympathetic innervation, in a T9 SCI model, could be investigated in future work.

4.5 Conclusions from this chapter

Following SCI, the magnitude of inflammation and histopathology in the spinal cord is dependent on the severity and level of injury, as evidenced by greater BSCB breakdown and neutrophil recruitment, reduced microglial cell density and increased expression of pro-inflammatory molecules. By contrast, many markers of the subsequent APR exhibited an inverse correlation. Hepatic CXCL1 and SAA-2 expression, as well as neutrophil mobilisation in the periphery, were suppressed. Given that SIRS and SCI-IDS are associated with higher patient morbidity (Bao et al. 2011b; Failli et al. 2012; Stein et al. 2010), data presented in this chapter may be valuable in improving treatment development and outcome prediction.

Chapter 5: SCI induces a metabolite signature in the periphery

5.1 Introduction and aims

Neuronal tissue has a high metabolic demand, and the spinal cord is no exception (Alizadeh et al. 2019). Following traumatic injury, the supply of energy metabolites is disrupted, which exacerbates neuronal damage. Compromised vasculature and oedema restrict perfusion, leading to oxygen deprivation and subsequent hypoxic damage (Fassbender et al. 2011; Hernandez-Gerez et al. 2019). The inflammatory response to SCI also increases demand, along with the generation of free radicals (Bao and Liu 2004) in conjunction with the release of glutamate (Xu et al. 2004), intracellular ions and ATP from dying cells (Park et al. 2004), all of which propagate cellular apoptosis and necrosis. However, the interaction between metabolic disruption in the central and peripheral compartments remains unclear. The liver plays a crucial role in metabolism and exhibits evidence of metabolic stress after SCI (Goodus and McTigue 2020). As SCI induces hepatic inflammation, which influences the magnitude of intraspinal inflammation, it stands to reason that metabolic changes in the spinal cord may result in metabolic changes in the periphery, or vice versa.

Metabolomics is a relatively new –omics approach, defined as the study of metabolite profiles in cells, tissues and biofluids (Posti et al. 2017; Patti et al. 2012). The strategy combines the use of analytical techniques, such as mass spectrometry or nuclear magnetic resonance (NMR), to measure the concentrations of many metabolites (either aqueous or lipid) simultaneously, which may be followed by multivariate statistical analysis. Principle component analysis (PCA) and orthogonal partial least square discriminant analysis (OPLS-DA) are strategies most commonly utilised; PCA is an unsupervised approach used to visualise variation and identify metabolically distinct subgroups in a dataset with no prior knowledge of experimental group. Whereas, OPLS-DA is a supervised approach (the experimental groups are defined and included in the analysis), which identifies metabolite differences between the groups of interest and combines these metabolites into a linear equation, allowing the classification of new, previously unseen, metabolomics data. This enables the comparison of a large number of metabolite concentrations, which facilitates a more comprehensive understanding of metabolism *in vivo*. Metabolomics has successfully been used to identify peripheral biomarkers in a range of neurological diseases,

including Alzheimer's disease (Varma et al. 2018; Lin et al. 2019), MS (Yeo et al. 2020; Sylvestre et al. 2020), and brain cancers (Baranovicova et al. 2019), as well as cerebrovascular accident (CVA) (Jung et al. 2011) and TBI (Posti et al. 2017; Oresic et al. 2016).

Previous studies have utilised metabolomics to confirm that SCI induces a specific metabolite profile in the peripheral biofluids. Changes in a number of metabolites have been reported in the CSF and plasma of human SCI patients (Wu et al. 2016b; Cyr et al. 2021; Singh et al. 2018) and rodent animal models (Peng et al. 2014; Figueroa et al. 2013a; Figueroa et al. 2013b; Jiang et al. 2010; Zhang et al. 2019b), with downstream pathway analysis revealing disturbances in amino acid and lipid metabolism. Interestingly, several of these studies have identified severity-dependent perturbations in peripheral metabolites, which may be used as prognostic markers. Certainly, acute hyperglycaemia has been shown to be a predictor of poor functional outcome of SCI patients (Kobayakawa et al. 2014), which may be linked to the controversial drug methylprednisolone. As such, the authors suggested that blood glucose be closely monitored during treatment. Wu et al. (2016b) detected six injury-severity-dependent metabolites, with mass spectrometry, in the CSF of SCI patients, and one in the serum, 5-hyroxylysine, which exhibited an inverse correlation with severity. In addition, Peng et al. (2014) used ^{1}H NMR and PCA/PLS-DA to identify significant changes in the plasma metabolome in a rodent model of SCI, which was able to distinguish between injury severity groups. Cyr et al. (2021) showed that patient enrichment for plasma sphingolipids was associated with reduced circulating inflammatory mediators (IL-6, CXCL10, CCL2) and improved outcome. However, to date no studies have investigated the hepatic metabolite profile following injury, and the point at which the SCI-specific metabolite signature becomes apparent has not been determined. A deeper understanding of these early metabolite changes could influence acute treatment.

The liver is responsible for lipid metabolism in the periphery, which is disrupted after SCI. From the first week of injury, fat accumulates in the liver (Sauerbeck et al. 2015; Goodus et al. 2018). Liver adiposity after SCI has been associated with increased circulating triglycerides and decreased insulin sensitivity, as well as elevated serum TNF-α, suggesting a relationship between injury-

mediated metabolism disruption and inflammation (Rankin et al. 2017). Indeed, an increase in liver ceramides has been reported after SCI (Sauerbeck et al. 2015), which are potent lipid signalling molecules and regulators of inflammation that have further been shown to induce insulin resistance, oxidative stress, and inflammation in the liver (Pagadala et al. 2012). These pathologies can lead to non-alcoholic fatty liver disease (NAFLD), which, in turn, can lead to non-alcoholic steatohepatitis (NASH) and cirrhosis, highlighting that SCI-induced metabolic consequences can persist into the chronic phase (Goodus and McTigue 2020). Due to rapid onset and progression, in the absence of a high fat/sugar diet, the high incidence of metabolic disorders after SCI is thought to be independent of immobility (Goodus and McTigue 2020). As such, SCI patients are at increased risk of liver-related death (Ekstedt et al. 2006; Barbonetti et al. 2016). The impact of lesion level and severity on the incidence of NAFLD/NASH has not yet been investigated in SCI patients. However, Sauerbeck et al. (2015) showed greater lipid deposition in the liver after cervical SCI, compared to thoracic SCI, in a rodent model, which indicates that the nature of the lesion affects hepatic lipid metabolism. It is not known whether this liver pathology is a cause or consequence of the metabolic syndrome induced by SCI. Identifying hepatic metabolite changes during the acute phase of injury could provide insight to the underlying mechanisms.

The aims for this chapter were (1) to determine the effect of SCI on the central and peripheral metabolite profile, and (2) to ascertain whether the peripheral metabolite changes are severity or lesion-level dependent.

5.2 Methods specific to this chapter

5.2.1 Human plasma

Blood samples were collected from 29 spinal cord injury patients (male=27, female=2) upon admission to hospital, and 10 healthy, age-matched controls (male=7, female=5), and platelet-free plasma was generated, as described in 2.1.

5.2.2 Animals and spinal cord injury model

In accordance with the 3 R's, plasma and fresh liver samples collected for time course (Chapter 3), and plasma, fresh liver and spinal cord from SCI level and severity experiments (Chapter 4) were used in this chapter for metabolite analysis.

5.2.3 Spinal cord tissue processing

A 1cm segment of fresh spinal cord, encompassing the lesion, and the immediate rostral and caudal regions, was homogenised with a pestle and mortar on dry ice, and 10-20mg of tissue was used for metabolomic analysis, as outlined in 2.10.

5.3 Results

5.3.1 Acute SCI induces a metabolite signature in the periphery

First, the effect of SCI on the plasma metabolite profile was investigated; plasma samples were collected from SCI patients (n=29) upon admission to the Princess Alexandra Hospital, Brisbane. Metabolites were measured by NMR and compared to healthy controls (n=12) by multivariate analysis.

The OPLS-DA model of plasma metabolite profiles was able to discriminate between SCI patients and healthy controls (Figure 5.1A), with significant accuracy (93±5%, $p<0.0001$), sensitivity (100±0%, $p<0.0001$) and specificity (86±11%, $p<0.0001$). Therefore, the model was able to correctly classify samples as SCI patients or healthy controls, with 93±5% of samples; the model identified true SCI patients 100±0% of the time (sensitivity) indicating it did not identify any false negatives. By contrast, the model identified true healthy controls 86±11% of the time (specificity), indicating that 14% of the healthy control samples were falsely classified as SCI patients by the model, and so were false positives.

The key metabolites driving the discrimination in the model were then investigated. Variable importance in projection (VIP) scores were generated which is a measure of a metabolite's importance to the model; the greater the VIP score, the greater the contribution to driving separation in the model. VIP analysis revealed that myo-inositol (Figure 5.1Bi; student's unpaired t-test, $p<0.0001$), glucose (Figure 5.1Bii; student's unpaired t-test, $p<0.0001$) and glutamine (Figure 5.1Biii; student's unpaired t-test, $p<0.0001$) were all increased in SCI patients, compared to healthy controls. By contrast, several resonances from mobile side chain lipoproteins (-CH_2)n were significantly decreased in SCI patients, compared to healthy controls (Figure 5.1Biv; student's t-test, $p<0.0001$).

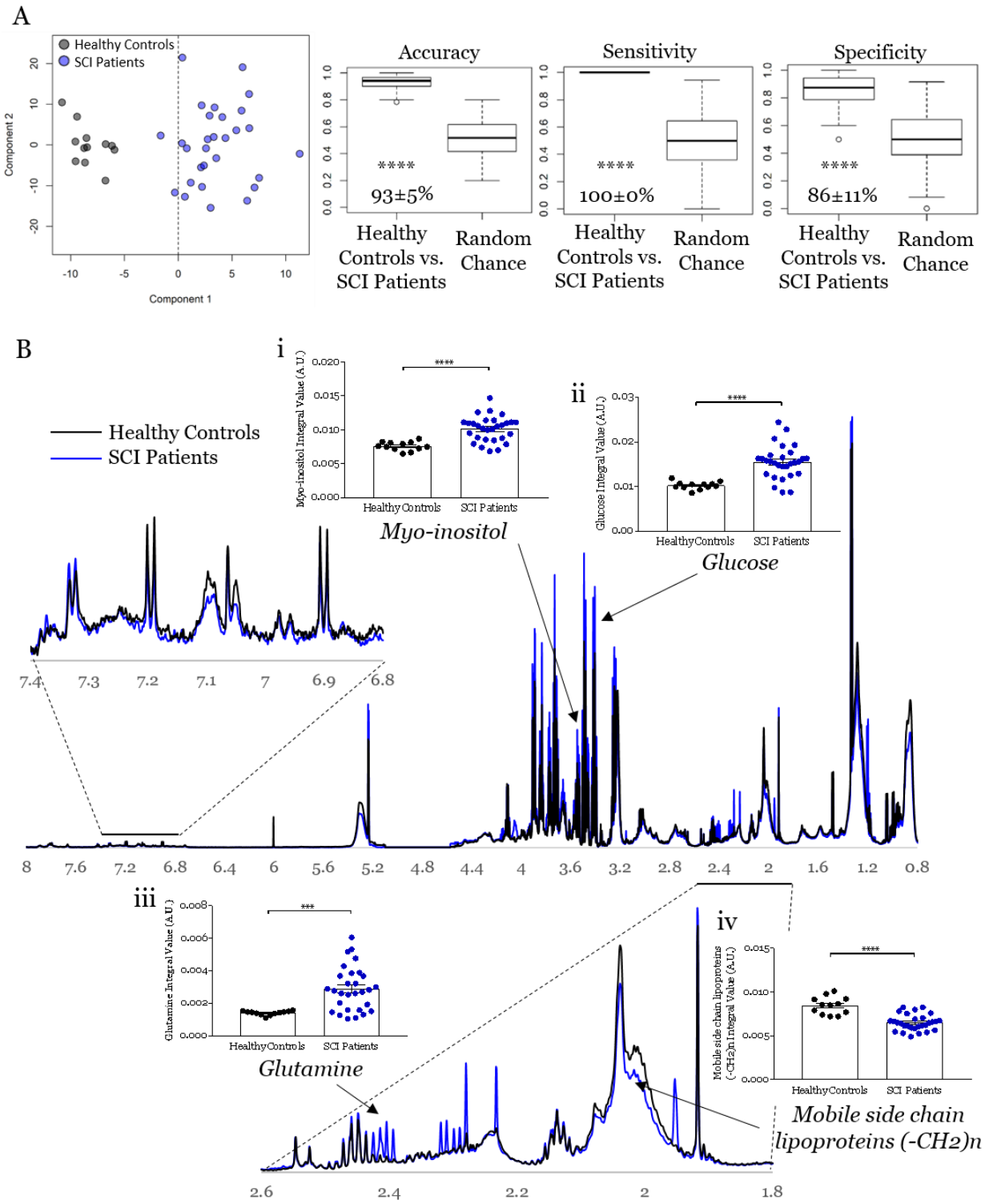


Figure 5.1 Human plasma metabolites following SCI. Platelet-free plasma was obtained from SCI patients (blue points, n=29) upon admission to the Princess Alexandra Hospital, Brisbane, and from healthy controls at the University of Queensland and the University at Oxford (black points, n=12). Plasma metabolites were measured by NMR; resulting spectra were processed and analysed by supervised multivariate analysis (OPLS-DA). A model was built separating the 2 groups, and the accuracy, sensitivity and specificity of this model was determined (A). Key metabolites identified as significant discriminants were further investigated with univariate analysis (B); myo-inositol (i), glucose (ii), glutamine (iii) and mobile side-chain lipoproteins (-CH2)n (iv). Data are presented as mean ±SEM, and were analysed by student's unpaired t-test, ***p<0.001, ****p<0.0001.

This result was confirmed in a mouse model of SCI, utilising samples collected for the time course experiment in Chapter 3. Animals received a 70kD SCI at level T9, or sham surgery as control, and tissue was collected at 2, 6, 12 and 24 hours post-injury.

An OPLS-DA model was built using rodent plasma from all time points (Table 5.1), which revealed that the model was able to discriminate between the plasma metabolite profiles of SCI and sham animals with an accuracy of 56±6% (student's unpaired t-test, $p<0.0001$). Whilst statistically significant, the model was only modestly better than random chance. Visualisation of the OPLS-DA scores plot identified a separation between 2 and hours, and 12 and 24 hours in the second component (Supplementary Figure 5.1), indicating that time after injury was having a significant effect. Therefore, spectra were combined into early (2 & 6 hours) and late (12 & 24 hours), and were reanalysed. The early model was unable to discriminate between sham and SCI animals (50±6% accuracy, 49±9% sensitivity, 52±9% specificity). However, the late model was able to distinguish between injury groups (84±7% accuracy, 78±11% sensitivity, 91±7% specificity).

Table 5.1 Models generated with plasma metabolites following SCI. Female C57BL/6 mice received a 70kD SCI at level T9, or sham surgery as control, and blood was collected at 2, 6, 12 and 24 hours post-injury (n=4-5/time point). Plasma was prepared and measured by NMR. Resulting spectra were processed and analysed by OPLS-DA. The accuracy, sensitivity and specificity ± standard deviation of these models were determined, and compared to the random model by student's unpaired t-test, ****$p<0.0001$.

Model	Accuracy (%)	Sensitivity (%)	Specificity (%)
All time points	56±6****	52±10	62±8****
Early (2 & 6 hours)	50±6	49±9	52±9
Late (12 & 24 hours)	84±7****	78±11****	91±7****

To directly compare the animal model with human patients, metabolites identified as significantly perturbed in SCI patient plasma, were investigated in mouse plasma. First, circulating myo-inositol was found to be injury and time dependent (Figure 5.2Ai; two-way ANOVA, injury $p<0.05$, time $p<0.01$). At the early time points, there was a modest increase in sham and SCI animals above naïve baseline with no difference between the injury groups. However, at the late time points, relative

myo-inositol concentration had decreased in sham animals, yet remained elevated in SCI animals (Sidak's post-hoc test, $p<0.05$). Glucose was increased in sham and SCI animals relative to naïve animals, at both early and late time points, although there was no significant effect of SCI specifically (Figure 5.2Aii; two-way ANOVA, injury $p=0.129$, time $p=0.207$). At early time points, glutamine levels were comparable between sham, SCI and naïve animals (Figure 5.2Aiii; two-way ANOVA, injury $p=0.077$, time $p=0.422$); at late time points, levels were significantly increased in SCI animals compared to controls (Sidak's post-hoc test, $p<0.05$). By contrast, mobile side chain lipoproteins (-CH2)n were decreased in the plasma of all animals compared to naïve at the early time points, which returned to baseline at the late time points (Figure 5.2Aiv; two-way ANOVA, injury $p=0.837$, time $p<0.0001$). Collectively, these metabolite changes in rodent plasma mirror those observed in the human plasma.

Metabolites identified as discriminatory in the rodent plasma model alone, were then evaluated. Consistently, amino acids with aromatic side chains were identified as key metabolites driving differences between sham and SCI animals. SCI induced an increase in plasma phenylalanine (Figure 5.2Bi; two-way ANOVA, injury $p<0.001$, time $p<0.01$); at early time points, levels of circulating phenylalanine in sham and SCI animals was comparable to naïve baseline. However, at late time points, concentrations in SCI animals were significantly increased compared to both naïve animals and sham controls (Sidak's post-hoc test, $p<0.0001$). Relative histidine concentration was also affected (Figure 5.2Bii; two-way ANOVA, injury $p=0.0712$, time $p=0.127$); plasma concentrations were significantly elevated in sham and SCI animals compared to naïve at early time points. At late time points, a decrease in concentration was observed in the sham group, but not the SCI group, resulting in a significant difference (Sidak's post-hoc test, $p<0.05$). Finally, circulating tyrosine was significantly increased in all animals above naïve baseline (Figure 5.2Biii; two-way ANOVA, injury $p<0.001$). The levels in SCI animals were significantly increased above sham controls at both early (Sidak's post-hoc test, $p<0.05$) and late (Sidak's post-hoc test, $p<0.01$) time points, although there was no effect of time ($p=0.808$).

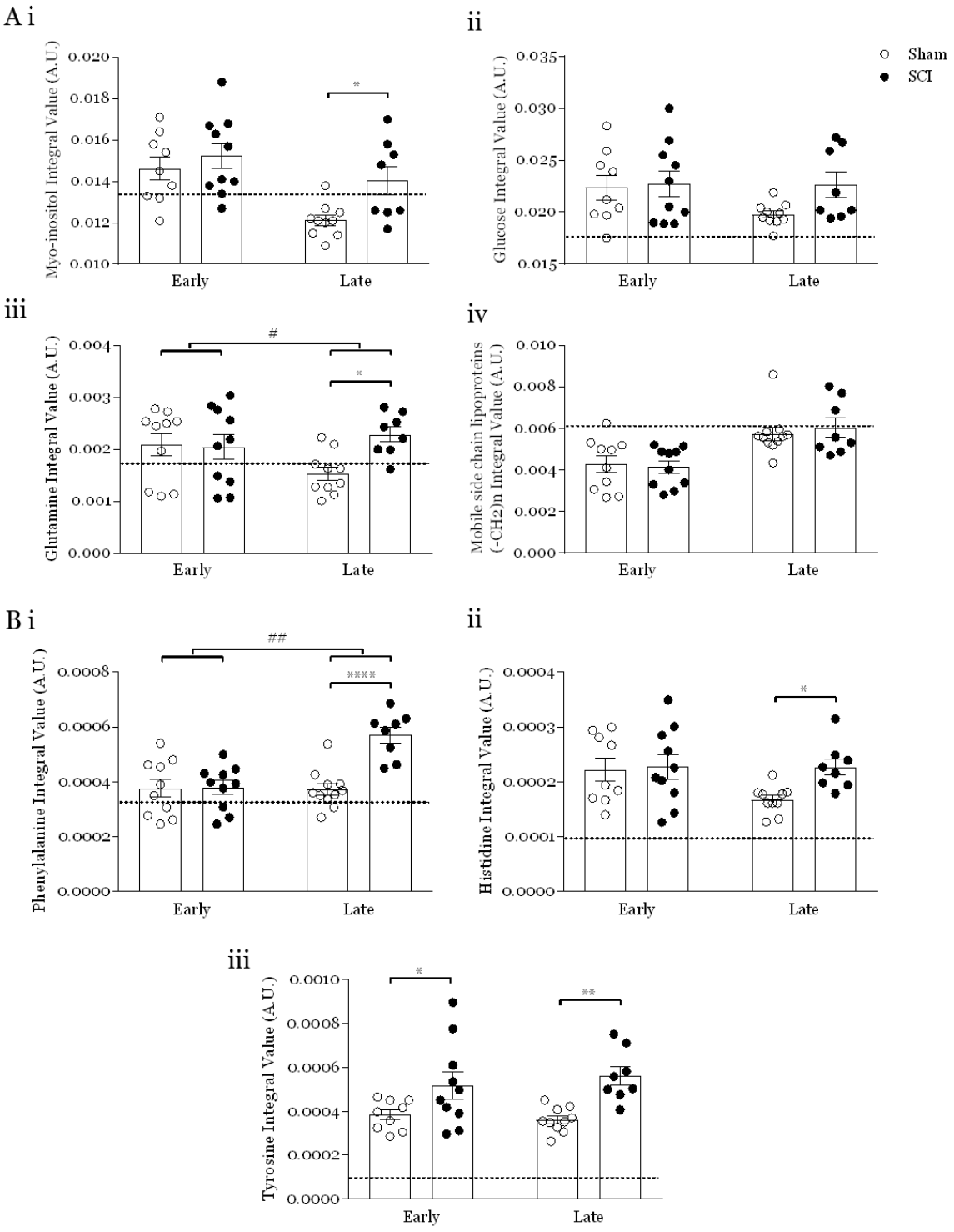


Figure 5.2 Mouse plasma metabolites following SCI. C57BL/6 underwent a 70kD SCI at T9 (black points) or sham surgery as control (white points) and plasma was collected at 2, 6, 12 and 24 hours post-injury (n=4-5/time point). Naïve animals were used to establish baseline (dotted line, n=3). Plasma metabolite profiles were analysed by OPLS-DA and key metabolites identified as significant in the late (12 & 24 hours) model were interrogated. Metabolites shown to change in human SCI plasma, were investigated in the mouse model (A); myo-inositol (i), glucose (ii), glutamine (iii) and mobile side-chain lipoproteins (-CH2)n (iv). Metabolites driving accuracy in the rodent model specifically were also examined (B); phenylalanine (i), histidine (ii), tyrosine (iii). Data are expressed as mean ±SEM, and analysed by two-way ANOA, #p<0.05 interaction, *p<0.05, **p<0.01, ****p<0.0001 in Sidak's post-hoc test.

Throughout this thesis, it has been evident that SCI causes profound inflammatory effects on the liver. Therefore, the effect of SCI on the hepatic metabolite profile was investigated (Table 5.2). Metabolites were extracted from fresh liver samples and analysed as above; surplus liver samples from additional experiments were included to increase n numbers. OPLS-DA of hepatic metabolite profiles was able to distinguish between sham and SCI animals when all time points were included (61±4% accuracy, 69±7% sensitivity, 56±6% specificity), and when separated into early (57±4% accuracy, 60±7% sensitivity, 56±8% specificity) and late (80±4% accuracy, 75±7% sensitivity, 86±6% specificity). Again, this discrimination between injury groups was time dependent, as the greater accuracy was achieved with the late model, compared to the early model.

Table 5.2 Models generated with liver metabolites following SCI. Female C57BL/6 mice received a 70kD SCI at level T9, or sham surgery as control, and fresh liver was collected at 2, 6, 12 and 24 hours post-injury (n=4-10/time point). Metabolites were extracted and measured by NMR. Resulting spectra were processed and analysed by OPLS-DA. The accuracy, sensitivity and specificity ± standard deviation of these models were determined, and compared to the random model by student's unpaired t-test, **p<0.01, ****p<0.0001.

Model	Accuracy (%)	Sensitivity (%)	Specificity (%)
All time points	61±4****	69±7****	56±6****
Early (2 & 6 hours)	57±4****	60±7****	56±8****
Late (12 & 24 hours)	80±4****	75±7****	86±6****

To compare metabolites across tissues, changes in plasma-associated discriminatory metabolites were investigated in the liver when present. The relative concentration of myo-inositol remained constant; there were no significant differences between naïve, sham or SCI animals, at either early or late time points (Figure 5.3Ai; two-way ANOVA, injury p=0.204, time p=0.064). Hepatic glucose, at early time points, also showed no difference between the three injury groups (Figure 5.3Aii; two-way ANOVA, injury p<0.01, time p<0.0001). However, at late time points, glucose was increased in sham animals compared to naïve animals, which was not observed in SCI animals; glucose was significantly decreased in the SCI group compared to sham (Sidak's post-hoc test, p<0.01). There was no injury effect on glutamine in the liver (Figure 5.3Aiii; two-way ANOVA,

injury p=0.449, time p<0.0001), although there was an effect of time, and a significant interaction (p<0.05). Glutamine was decreased in both sham and SCI animals below naïve baseline levels at early time points, and returned to baseline at the late time points. Similarly, for mobile side chain lipoproteins (-CH2)n, there was no significant difference between sham and SCI animals at either time point (Figure 5.3Aiv; two-way ANOVA, injury p=0.756, time p<0.05). However, an increase above naïve levels was observed for both sham and SCI groups at the early time points, which returned to baseline at the late time points.

Discriminatory metabolites in the liver OPLS-DA models were then investigated. Several metabolites were increased in both sham and SCI animals when compared to naïve animals at early time points. These metabolites then returned to baseline in sham controls at late time points, but remained significantly increased in animals with spinal injuries. Valine/proline (Figure 5.3Bi; two-way ANOVA, injury p<0.01, time p=0.777), acetoacetate (Figure 5.3Bii; two-way ANOVA, injury p<0.05, time p=0.763), arginine/lysine/leucine (Figure 5.3Biii, two-way ANOVA, injury p<0.05, time p=0.545), and lipid bCH2 (Figure 5.3Biv; two-way ANOVA, injury p<0.05, time p=0.570) all followed this pattern. Metabolites were significantly increased compared to sham animals at late time points only.

Thus, acute SCI induces metabolite changes in the liver, which are distinct from metabolite changes in the plasma.

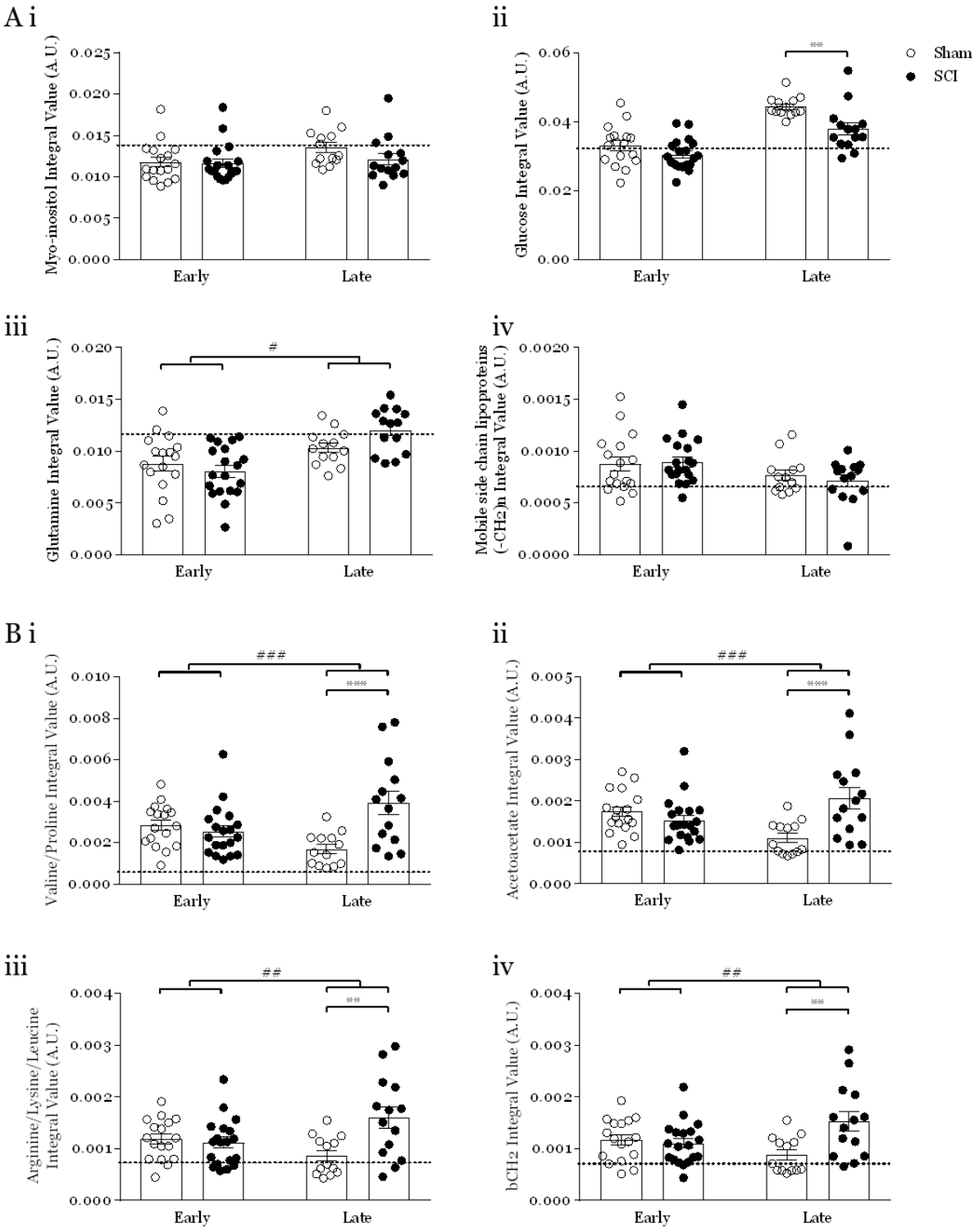


Figure 5.3 Mouse liver metabolites following SCI. C57BL/6 underwent a 70kD SCI at T9 (black points) or sham surgery as control (white points) and liver was collected at 2, 6, 12 and 24 hours post-injury (n=4-10/time point). Naïve animals were used to establish baseline (dotted line, n=3). Liver metabolite profiles were analysed by OPLS-DA and key metabolites identified as significant in the late (12 & 24 hours) model were interrogated. Metabolites shown to change in human SCI plasma, were investigated in the mouse model (A); myo-inositol (i), glucose (ii), glutamine (iii) and mobile side-chain lipoproteins (-CH2)n (iv). Metabolites driving accuracy in the rodent model specifically were also examined (B); valine/proline (i), acetoacetate (ii), arginine/lysine/leucine (iii) and bCH2 (iv). Data are expressed as mean ±SEM, and analysed by two-way ANOA, #p<0.05 interaction, *p<0.05, **p<0.01, ****p<0.0001 in Sidak's post-hoc test.

5.3.2 SCI-induced changes in metabolite profiles are injury severity and lesion level dependent

Next, the effect of injury severity and lesion level on the peripheral metabolome were determined. Previous studies have reported SCI severity-dependent changes in peripheral metabolites (Peng et al. 2014; Wu et al. 2016b). Tissue collected from SCI severity and level experiments in Chapter 4 was further examined here; mice underwent SCI of varying severities (30kD, 70kD, 100kD) at two different lesion levels (T9, T2). Plasma, fresh liver, and spinal cord were collected 6 hours post-injury for analysis of metabolite differences across the central and peripheral compartments.

5.3.2.1 Plasma

Owing to smaller n numbers, injury severity samples were analysed by unsupervised PCA to illustrate variation in the data whilst avoiding risk of overfitting associated with supervised methods such as OPLS-DA. The resulting PCA scores plot of T9 SCI samples revealed tight clustering of the naïve group whilst the metabolite profiles of the injury severity samples were more variable. Clear separation of naive animals from animals with spinal injuries was observed (Figure 5.4A). However, there appeared to be no cluster separation of the different injury severity groups. The PCA plot of T2 SCI samples also showed clear cluster separation between naïve animals and injured animals, however, again, there was no clear separation of mild and severe SCI groups (Figure 5.4B).

As there was no cluster separation between the 70kD and 100kD SCI groups at T9, they were combined to form a severe injury group for lesion level analysis. PCA scores plot of mild SCI groups showed no cluster separation of injury at T2 and at T9 (Figure 5.4C). For the severe injury groups, there was some separation of naïve group from SCI groups in the first component, and modest separation of T2 and T9 SCI groups in the second component, suggesting a small lesion level effect after severe injury (Figure 5.4D).

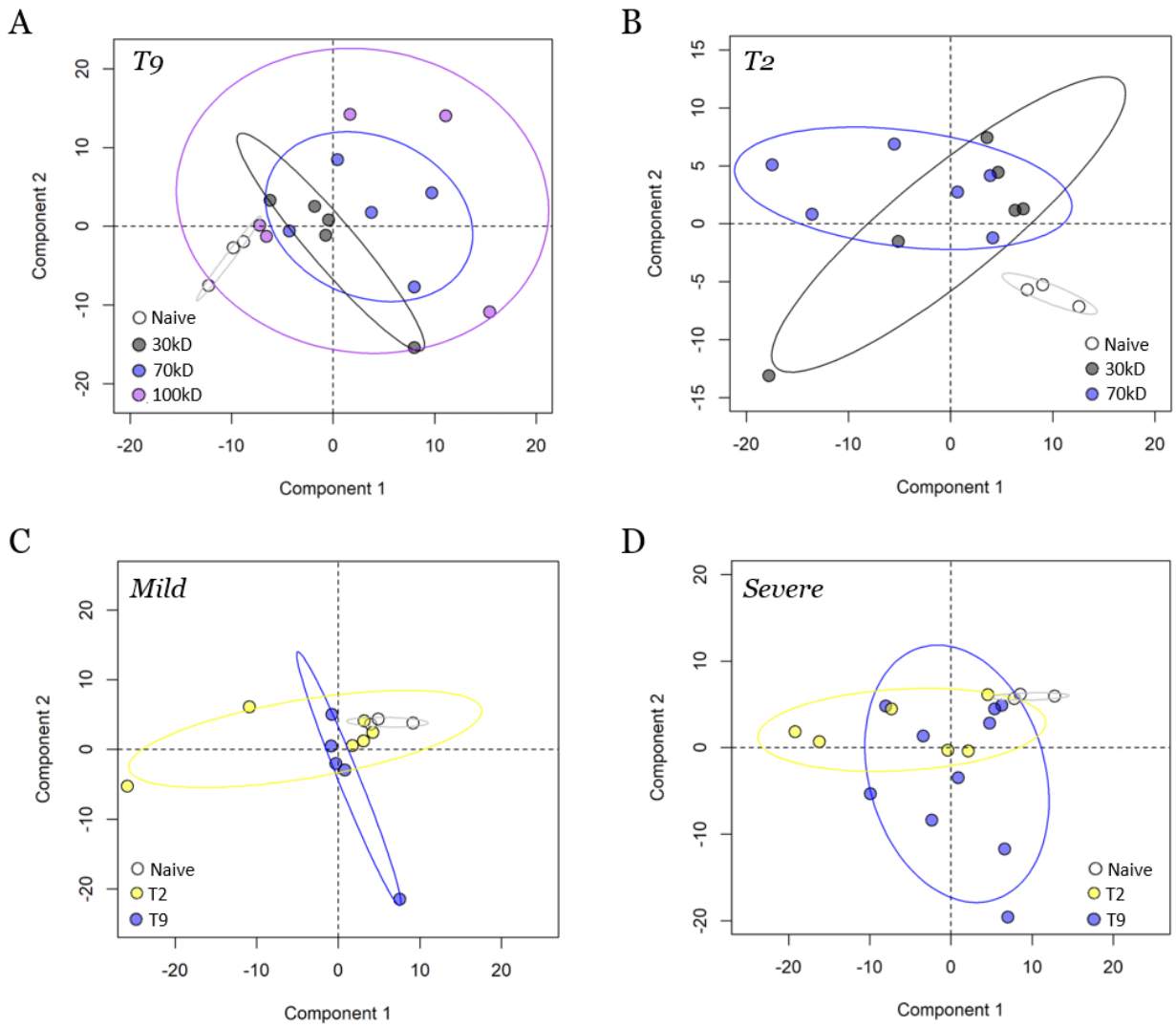


Figure 5.4 PCA scores plot of plasma metabolite profiles following SCI. Female C57BL/6 mice underwent a 30kD (n=5), 70kD (n=5) or 100kD SCI (n=5) at level T9, or a single-hit 30kD (n=6) or double-hit 70kD SCI (n=6) at level T2. Naïve animals (n=3) were included as baseline. Blood was collected 6 hours later and plasma metabolites were measured by NMR. Spectra were processed and analysed by PCA. PCA scores plots to compare the effect of injury severity at T9 (A) and T2 (B), and to compare the effect of lesion level following mild (C) and severe (D) injury.

SCI-dependent plasma metabolites were evaluated to identify any effect of injury severity. Consistent with the time course analysis, circulating myo-inositol (Figure 5.5A) and glucose (Figure 5.5B) were significantly increased in both sham and SCI animals, above naïve baseline. However, there was no effect of injury severity or lesion level. By contrast, glutamine exhibited an injury severity dependent decrease after T9 SCI (Figure 5.5Ci; one-way ANOVA, $p<0.001$). A trauma-induced increase was observed in the sham animals above naïve baseline. Plasma glutamine then decreased towards baseline with increasing force of SCI; 100kD SCI group was comparable to the

naïve group and was significantly decreased compared to sham ($p<0.001$) and 30kD ($p<0.05$). However, no differences between injury groups was observed after a T2 SCI (Figure 5.5Cii; one-way ANOVA, $p=0.863$), although a trauma-associated increase above naïve baseline is still evident. Lipid side-chains also showed differences between injury groups. Following T9 SCI, plasma mobile side chain lipoproteins (-CH2)n was increased in the more severe injury groups (70kD, 100kD), although this did not reach statistical significance (Figure 5.5Di; one-way ANOVA, $p=0.139$). However, a significant injury-severity dependent increase was observed with the injury at T2 (Figure 5.5Dii; one-way ANOVA, $p<0.05$); lipid side-chains were significantly increased in the 70kD injury group compared to sham controls (Sidak's post-hoc test, $p<0.05$).

A loadings plot was generated to identify key metabolites driving cluster separation in the first component of the PCA model. In agreement with the time course analysis, plasma phenylalanine was significantly increased in sham and SCI animals above naïve control, however there was no effect of injury severity following injury at either T9 (Figure 5.6Ai; one-way ANOVA, $p=0.587$) or T2 (Figure 5.6Aii; one-way ANOVA, $p=0.279$). Histidine and tyrosine were similarly unaffected by SCI severity (data not shown). It was found that many resonances corresponding to lipids were driving the separation between SCI animals and non-injured controls. Specifically, bCH2 was significantly increased after T9 (Figure 5.6Bi; one-way ANOVA, $p<0.05$) and T2 SCI (Figure 5.6Bii; one-way ANOVA, $p=0.054$), which was injury-severity dependent. Sidak's post-hoc analysis identified significant differences between sham and the most severe injuries only, at both levels (T9, $p<0.05$; T2, $p<0.05$). Lipid [=CH-CH2-CH=] exhibited the same increase with increasing SCI severity (Figure 5.6C). For all metabolites examined, there were no significant lesion level differences.

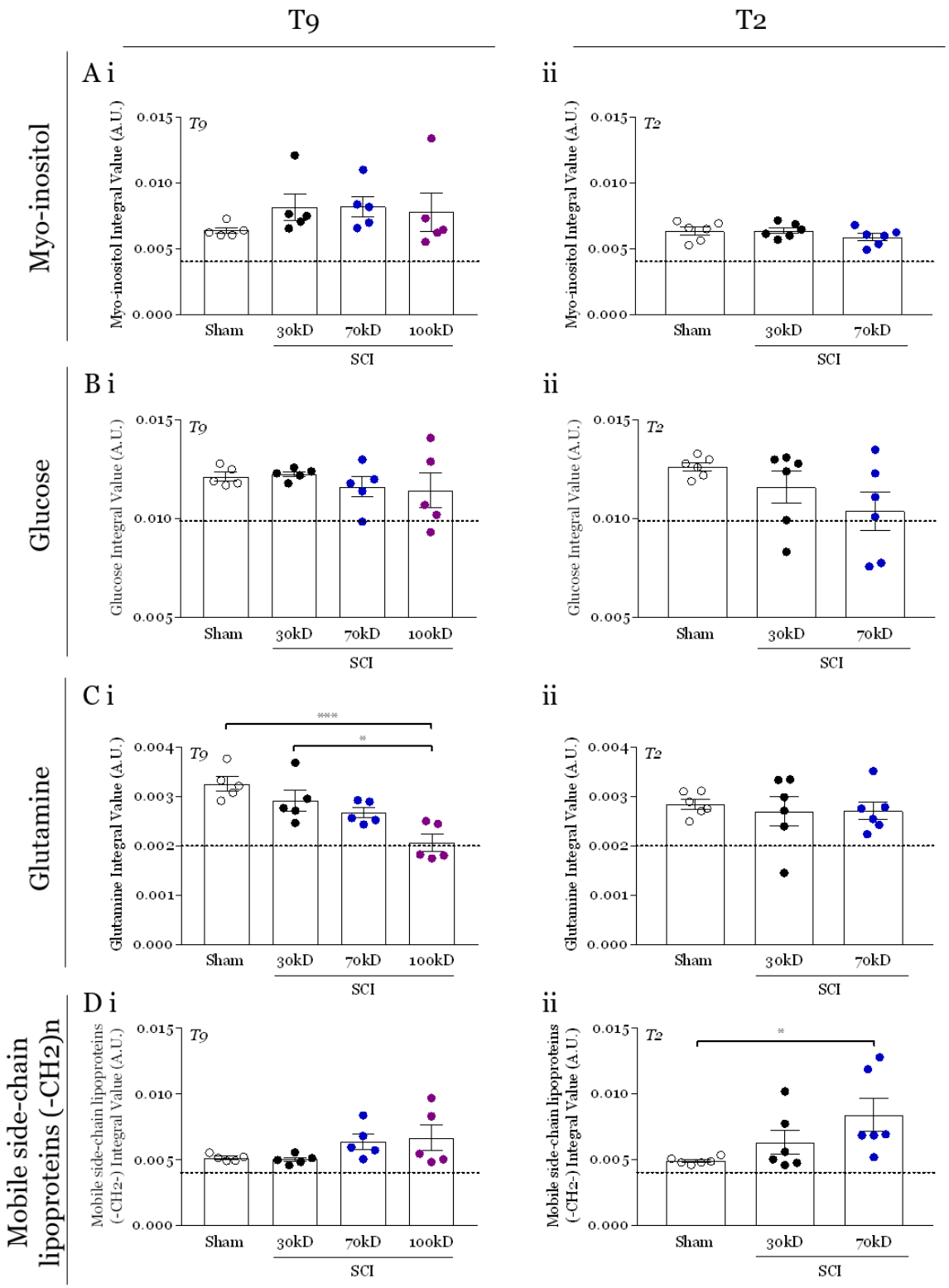


Figure 5.5 Perturbed plasma metabolites following SCI. Female C57BL/6 mice underwent a 30kD (black points), 70kD (blue points) or 100kD SCI (purple points) at T9, or a single-hit 30kD or double-hit 70kD SCI at level 2 (n=6/group). Sham animals underwent a laminectomy at their respective level but received no cord impact (white points). Plasma was collected 6 hours later and the metabolite profiles were compared between injury groups by PCA. Naïve plasma was used as baseline (dotted line, n=3). Key metabolites perturbed after SCI, myo-inositol (A), glucose (B), glutamine (C) and mobile side-chain lipoproteins (-CH2)n (D) were investigated. Data are expressed as mean ±SEM, and analysed by one-way ANOVA with Sidak's post-hoc test, *p<0.05, **p<0.01.

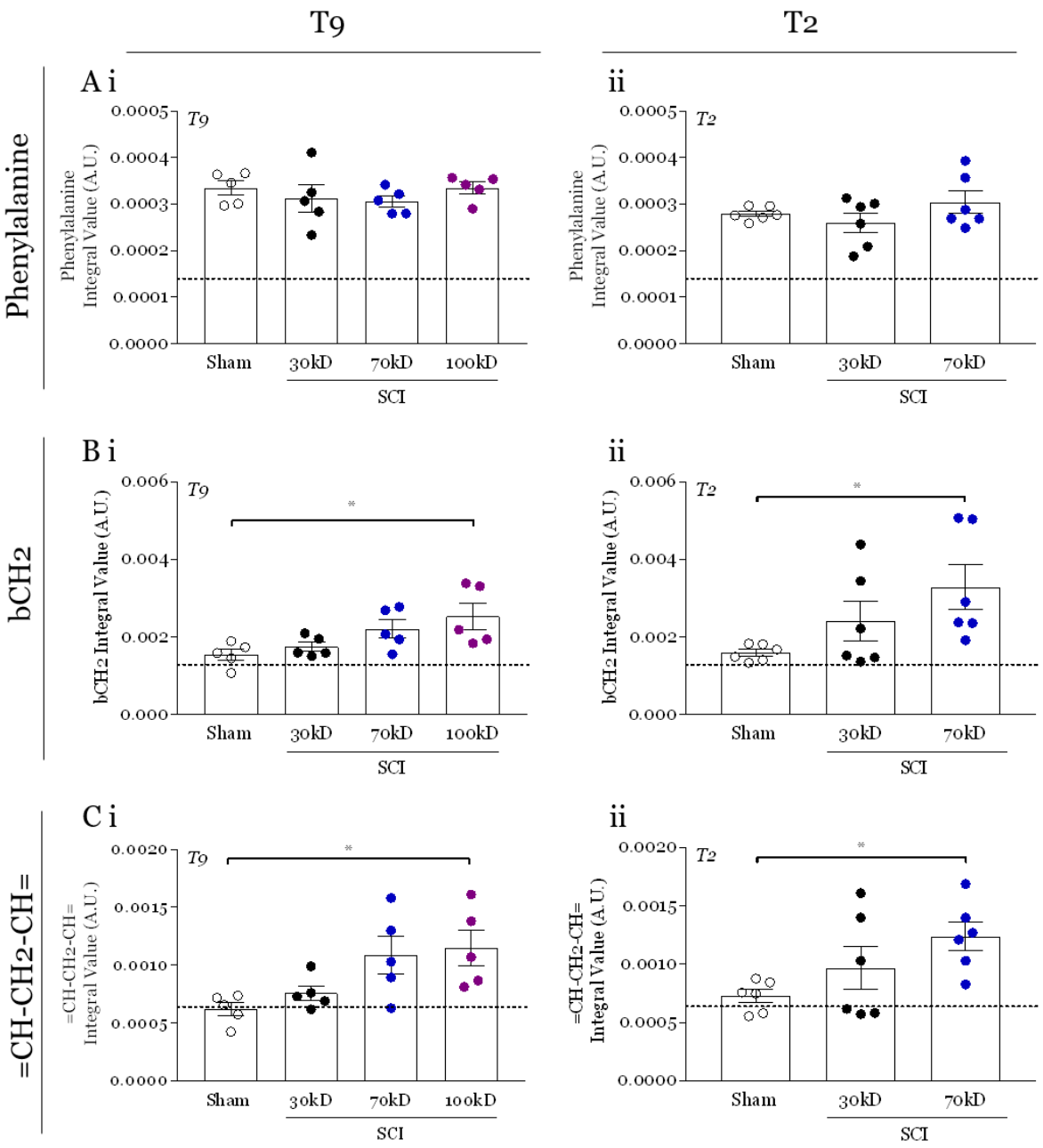


Figure 5.6 Key plasma metabolites disturbed following SCI. Female C57BL/6 mice underwent a 30kD (black points), 70kD (blue points) or 100kD SCI (purple points) at T9, or a single-hit 30kD midline or double-hit 70kD SCI at level 2 (n=6/group). Sham animals underwent a laminectomy at their respective level but received no cord impact (white points). Plasma was collected 6 hours later and the metabolite profiles were compared between injury groups by PCA. Naïve plasma used as baseline (dotted line, n=3). Key metabolites driving cluster separation were identified from the loadings plot for univariate analysis; phenylalanine (A), and lipid side-chains, bCH2 (B) and =CH-CH2-CH= (C). Data are presented as mean ±SEM, and analysed by one-way ANOVA, *p<0.05, in Sidak's post-hoc test.

5.3.2.2 Liver

In the liver, PCA scores plots showed significant cluster separation of naïve animals and SCI animals injured at T9 (Figure 5.7A) and T2 (Figure 5.7B), confirming that SCI induces a distinct hepatic metabolite profile. Although, at both levels, there was no cluster separation between injury groups. Similarly, when comparing T2 and T9 injuries, the naïve animal group clustered separately from the SCI groups in the first component. For mild injured animals, there was modest cluster separation in the second component (Figure 5.7C). This was not observed for the severe injury groups (Figure 5.7D).

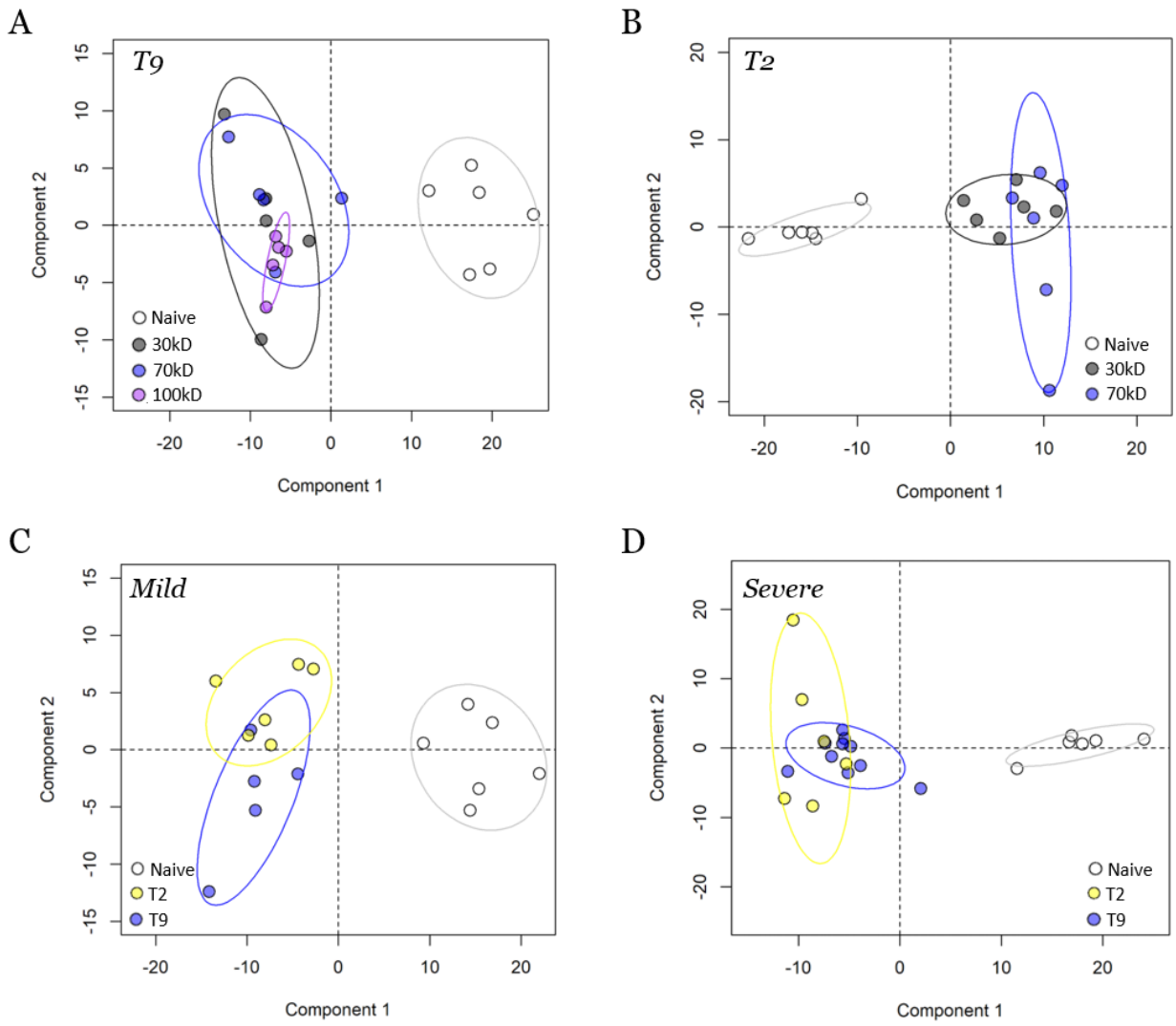


Figure 5.7 PCA scores plot of liver metabolite profiles following SCI. Female C57BL/6 mice underwent a 30kD, 70kD or 100kD SCI at level T9 (n=5/group), or a single-hit 30kD or double-hit 70kD SCI at level T2 (n=6/group). Fresh liver was collected 6 hours later and hepatic metabolites were measured by NMR. Naïve liver was used for baseline (n=6). Spectra were processed and analysed by PCA. PCA scores plots to compare the effect of injury severity at T9 (A) and T2 (B), and to compare the effect of lesion level on mild (C) and severe (D) injury.

Interrogation of key SCI metabolites revealed that the hepatic metabolite profile is both lesion-level and injury-severity dependent. Following injury at T9, there was a significant effect of SCI on hepatic myo-inositol (Figure 5.8Ai; one-way ANOVA $p<0.05$). However, there were no differences between injury groups with post-hoc testing. Whereas, following injury at T2, myo-inositol was significantly decreased after severe injury, but not mild (Figure 5.8Aii; Sidak's post-hoc test $p<0.01$). Similarly, in the T9 model, glucose in the liver was increased above naïve baseline, yet was unaffected by graded SCI (Figure 5.8Bi; one-way ANOVA, $p=0.640$). In the T2 model, hepatic

glucose was increased in sham and 30kD SCI animals compared to naïve animals, but not in the 70kD animals (Figure 5.8Bii; one-way ANOVA, $p<0.05$); there was a significant decrease in glucose with increasing severity (Sidak's post-hoc test, $p<0.05$). Glutamine was increased in the livers of all animals, above naïve baseline, however there was no effect of injury or lesion level (Figure 5.8C; one-way ANOVA, T9 $p=0.172$, T2 $p=0.560$). By contrast, mobile side-chain lipoproteins (-CH2)n increased with increasing SCI severity at T9 (Figure 5.8Di; one-way ANOVA, $p<0.05$), but there were no differences at T2 (Figure 5.8Dii; one-way ANOVA, $p=0.964$)

Examination of the loading plots identified additional (i.e. not identified in the human or rodent plasma samples) metabolites in the liver that were injury severity and lesion level dependent. At T9, valine/proline was increased in sham and SCI injury groups over naïve baseline, but there were no differences between groups (Figure 5.9Ai; one-way ANOVA, $p=0.289$). Whereas at T2, valine/proline was significantly increased in the 70kD injury group compared to sham controls, but the 30kD injury group was not (Figure 5.9Aii; one-way ANOVA, $p<0.05$). In addition, SCI at T9 had no effect on hepatic 2-hydroxybutyrate (Figure 5.9Bi; one-way ANOVA, $p=0.839$). However, SCI, at T2, caused an increase of this metabolite, which was severity dependent (Figure 5.9Bii; one-way ANOVA, $p<0.05$); 3-hydroxybutryate was significantly increased after severe injury, compared to both mild injury (Sidak's post-hoc test, $p<0.01$) and uninjured controls (Sidak's post-hoc test, $p<0.05$). Conversely, lysine increased in the liver with increasing SCI severity at T9 (Figure 5.9Ci; one-way ANOVA, $p<0.05$), which was not observed at T2 (Figure 5.9Cii; one-way ANOVA, $p=0.263$).

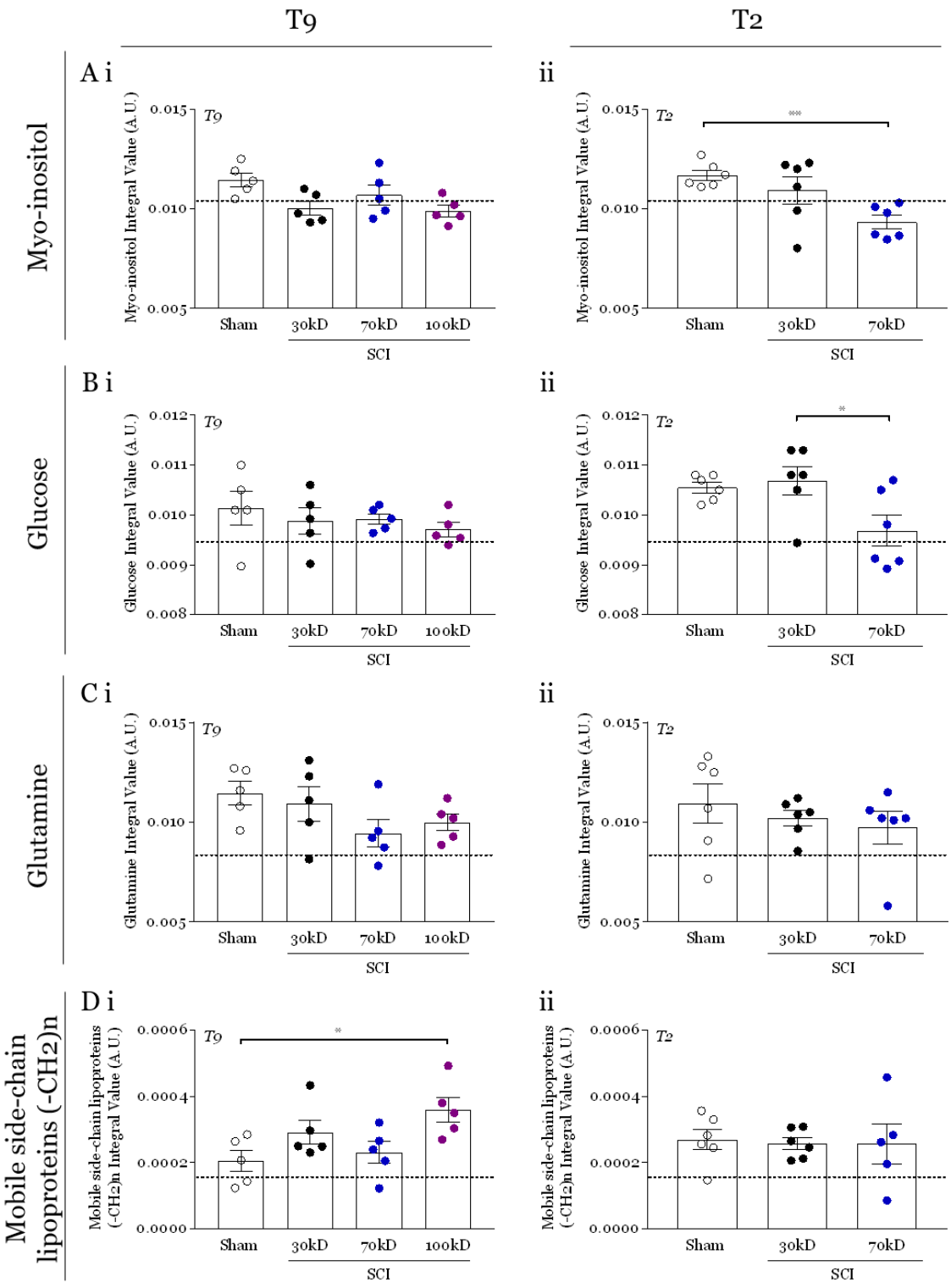


Figure 5.8 Liver metabolites disturbed following SCI. Female C57BL/6 mice underwent a 30kD (black points), 70kD (blue points) or 100kD SCI (purple points) at T9, or a single-hit 30kD or double-hit 70kD SCI at level 2 (n=6/group). Sham animals underwent a laminectomy at their respective level but received no cord impact (white points). Fresh liver was collected 6 hours later and the metabolite profiles were compared between injury groups by PCA. Naïve liver was used as baseline (dotted line, n=6). Key metabolites perturbed after SCI, myo-inositol (A), glucose (B), glutamine (C) and mobile side-chain lipoproteins (-CH2)n (D) were investigated. Naïve liver was used as baseline (dotted line, n=4). Data are expressed as mean ±SEM, and analysed by one-way ANOVA with Sidak's post-hoc test, *p<0.05, **p<0.01.

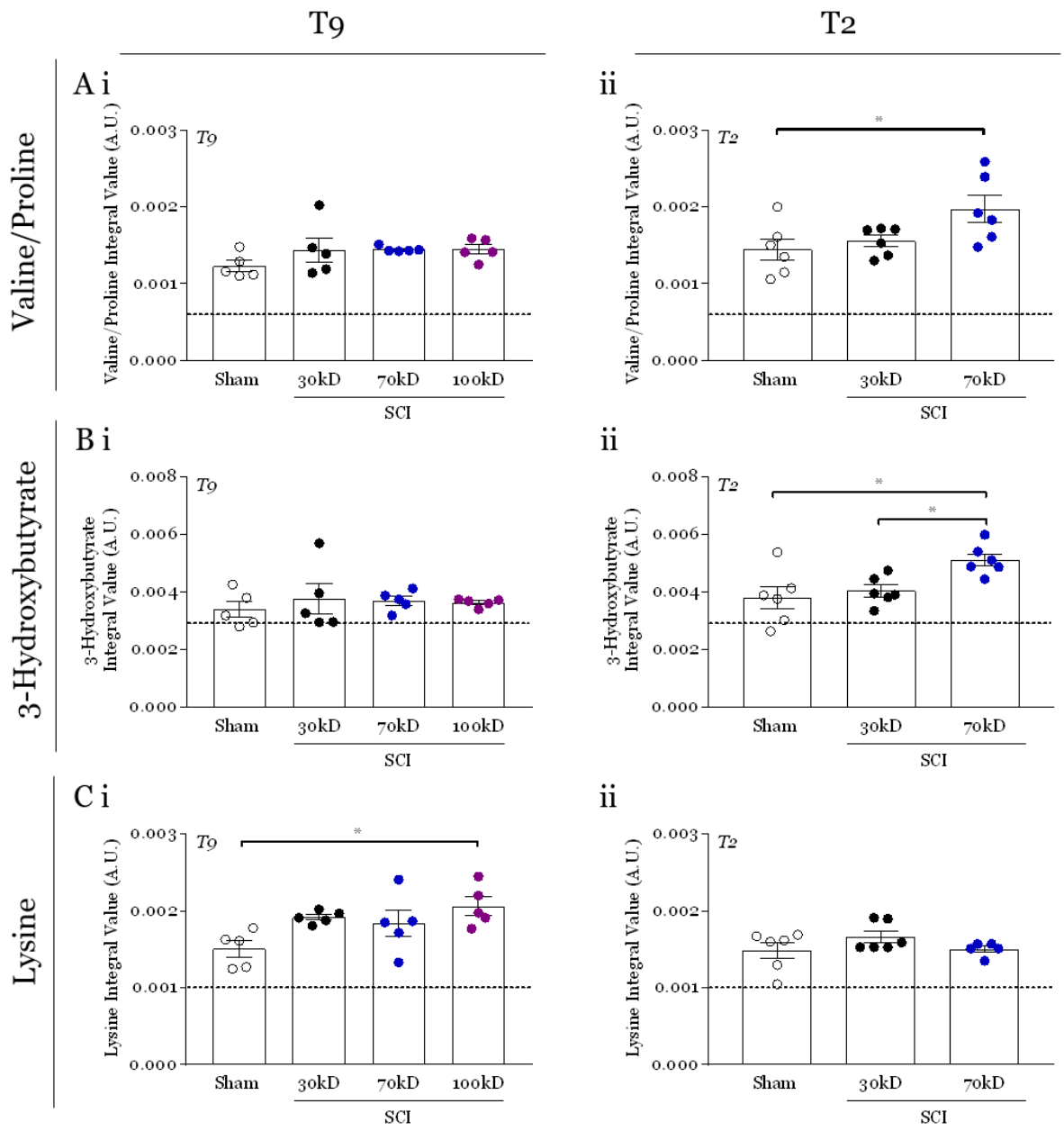


Figure 5.9 Key liver metabolites disturbed following graded SCI. Female C57BL/6 mice underwent a 30kD (black points), 70kD (blue points) or 100kD SCI (purple points) at T9, or a single-hit 30kD or double-hit 70kD SCI at level 2 (n=6/group). Sham animals underwent a laminectomy at their respective level but received no cord impact (white points). Fresh liver was collected 6 hours later and the metabolite profiles were compared between injury groups by PCA. Naïve liver was used as baseline (dotted line, n=6). Key metabolites driving cluster separation were identified from the loadings plot for univariate analysis; valine/proline (A), 3-hydroxybutyrate (B), lysine (C). Data are presented as mean ±SEM, and analysed by one-way ANOVA, *p<0.05, **p<0.01 in Sidak's post-hoc test.

5.3.2.3 Spinal cord

The effect of injury severity on metabolites in the spinal cord itself was then investigated, to enable comparison between the CNS with the periphery. A PCA scores plot of spinal cord metabolites following SCI at T9 (Figure 5.10A) revealed cluster separation between naïve and 100kD animals in the first component, indicating that very severe injury induces a significantly different central metabolite profile. 70kD SCI animals fell between the naïve and 100kD SCI animals in the first component. Interestingly, 30kD SCI animals showed some separation in the second component. PCA of spinal cord metabolites after T2 injury showed cluster separation of naïve animals from SCI animals (Figure 5.10B). Some separation of 70kD and 30kD clusters in the first component was also evident, however there were still many overlapping points.

The PCA plots of animals injured at T9 and T2 revealed no lesion level differences in spinal cord metabolite profiles. For both mild (Figure 5.10C) and severe injuries (Figure 5.10D), there was no cluster separation of T9 and T2.

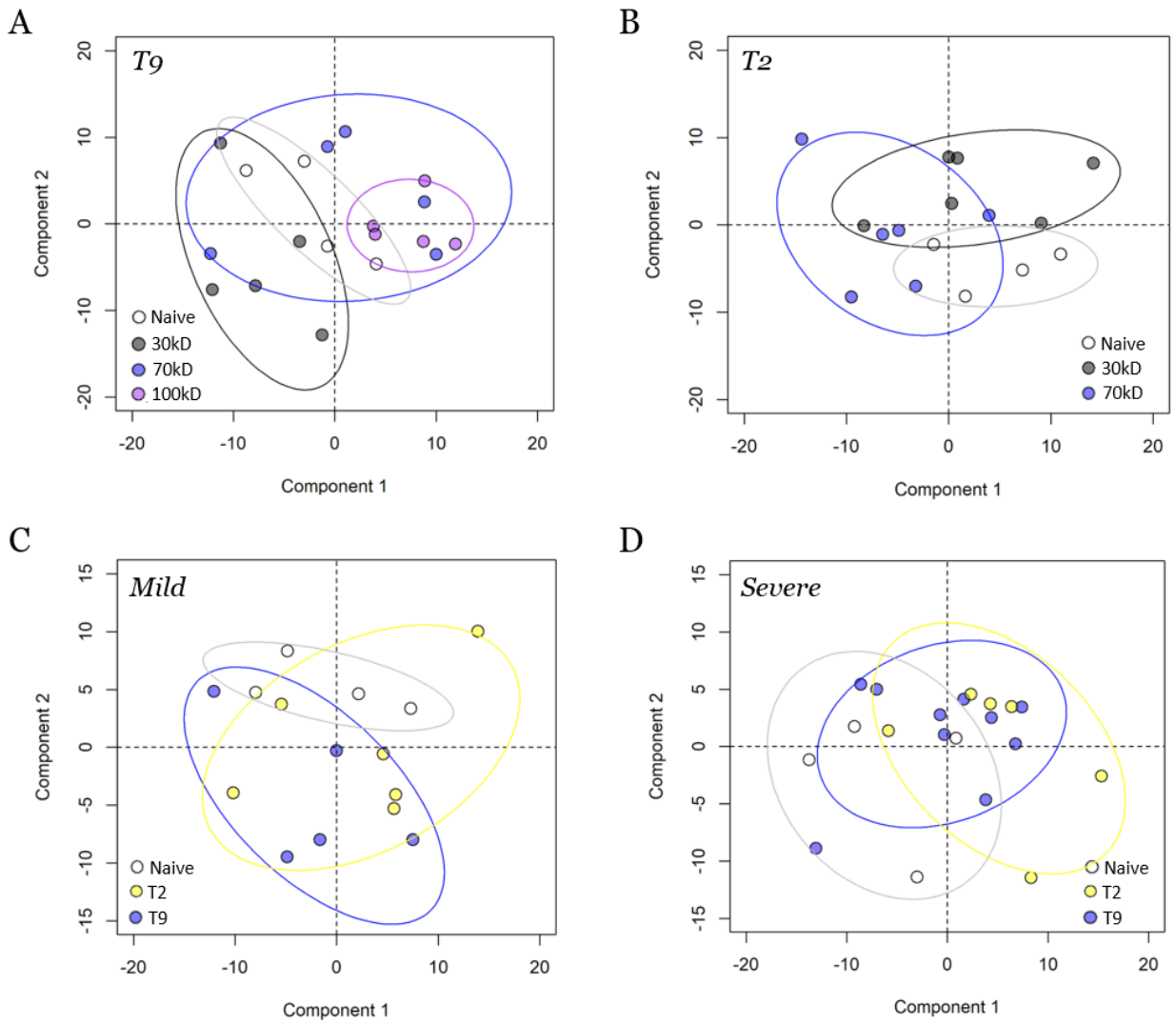


Figure 5.10 PCA scores plot of spinal cord metabolite profiles following SCI. Female C57BL/6 mice underwent a 30kD, 70kD or 100kD SCI at level T9 (n=5/group), or a single-hit 30kD or double-hit 70kD SCI at level T2 (n=6/group). Fresh spinal cord was collected 6 hours later and metabolites were measured by NMR. Naïve spinal cords were used as baseline (n=4). Spectra were processed and analysed by PCA. PCA scores plots to compare the effect of injury severity at T9 (A) and T2 (B), and to compare the effect of lesion level on mild (C) and severe (D) injury.

As with the plasma, there was no injury severity effect on myo-inositol in the spinal cord following T9 (Figure 5.11Ai; one-way ANOVA, $p=0.075$) or T2 injury (Figure 5.11Aii; one-way ANOVA, $p=0.528$). However, glucose was found to be SCI severity dependent. Animals with severe injuries (70kD, 100kD) at T9 had significantly decreased glucose in the spinal cord compared to animals with mild injuries, and uninjured controls (Figure 5.11Bi; one-way ANOVA, $p<0.01$). This injury dependent decrease was also observed with T2 injuries (Figure 5.11Bii; one-way ANOVA, $p=0.055$).

In addition, intraspinal glutamine was SCI severity dependent, although this was only evident with injuries at T9 (Figure 5.11Ci; one-way ANOVA, $p<0.05$) and not T2 (Figure 5.11Bii; one-way ANOVA, $p=0.776$). Interestingly, in the T9 SCI model, glutamine was increased in the mild injury group, and was significantly decreased with more severe injuries (Sidak's post-hoc test, 30kD vs. 100kD $p<0.05$). SCI had no effect on mobile side-chain lipoproteins (-CH2)n in the spinal cord following injury at T9 (Figure 5.11Di; one-way ANOVA, $p=0.055$) or T2 (Figure 5.11Dii; one-way ANOVA, $p=0.319$).

The loadings driving cluster separation of spinal cord metabolites specifically were then examined. Glutamate showed an injury severity increase at both lesion levels (Figure 5.12A; one-way ANOVA, T9 $p<0.01$, T2 $p<0.05$). At T9, the 70kD and 100kD SCI injury groups were significantly increased compared to both sham and 30kD SCI injury groups. Glutamate was also significantly increased in the 70kD animals at T2, compared to 30kD animals (Sidak's post-hoc test, $p<0.05$). Citrate exhibited the same injury severity dependent increase after injury (Figure 5.12B; one-way ANOVA, T9 $p<0.001$, T2 $p<0.01$); intraspinal citrate was significantly increased after severe injury at both levels, compared to mild injury or uninjured controls. Conversely, some metabolites were found to decrease with injury severity, in particular the branched chain amino acids. For example, at T9, valine in the spinal cord was increased in sham and 30kD animals compared to naïve baseline, which decreased with more severe injury (Figure 5.12Ci; one-way ANOVA, $p<0.01$). Post-hoc analysis showed that the 100kD injury group was significantly decreased compared to sham ($p<0.01$) and 30kD groups ($p<0.01$). At T2, severe SCI induced a significant decrease in valine, compared to mild SCI (Sidak's post-hoc test, $p<0.05$). Alanine levels were also decreased with increasing injury severity at both levels (Figure 5.12E; one-way ANOVA, T9 $p<0.01$, T2 $p<0.05$).

Taken together, SCI induces significant metabolite changes in the plasma, liver and spinal cord, which are dependent on the severity and level of the injury.

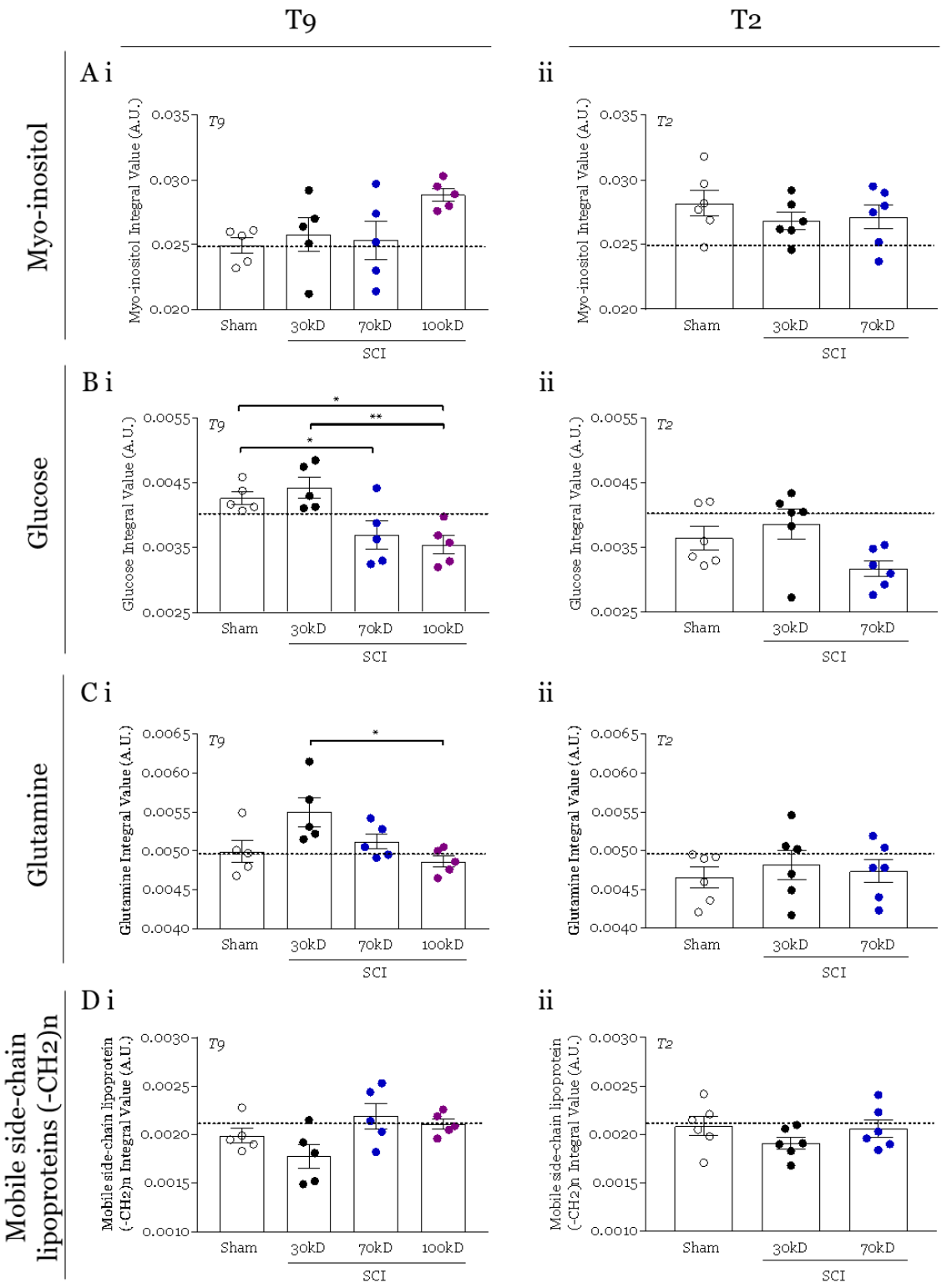


Figure 5.11 Metabolites in the spinal cord perturbed after traumatic injury. Female C57BL/6 mice underwent a 30kD (black points), 70kD (blue points) or 100kD SCI (purple points) at T9, or a single-hit 30kD or double-hit 70kD SCI at level 2 (n=6/group). Sham animals underwent a laminectomy at their respective level but received no cord impact (white points). Fresh spinal cord was collected 6 hours later and the metabolite profiles were compared between injury groups by PCA. Naïve spinal cord was used as baseline (dotted line, n=4). Key metabolites perturbed after SCI, myo-inositol (A), glucose (B), glutamine (C) and mobile side-chain lipoproteins (-CH2)n (D) were investigated. Data are expressed as mean ±SEM, and analysed by one-way ANOVA with Sidak's post-hoc test, *p<0.05, **p<0.01.

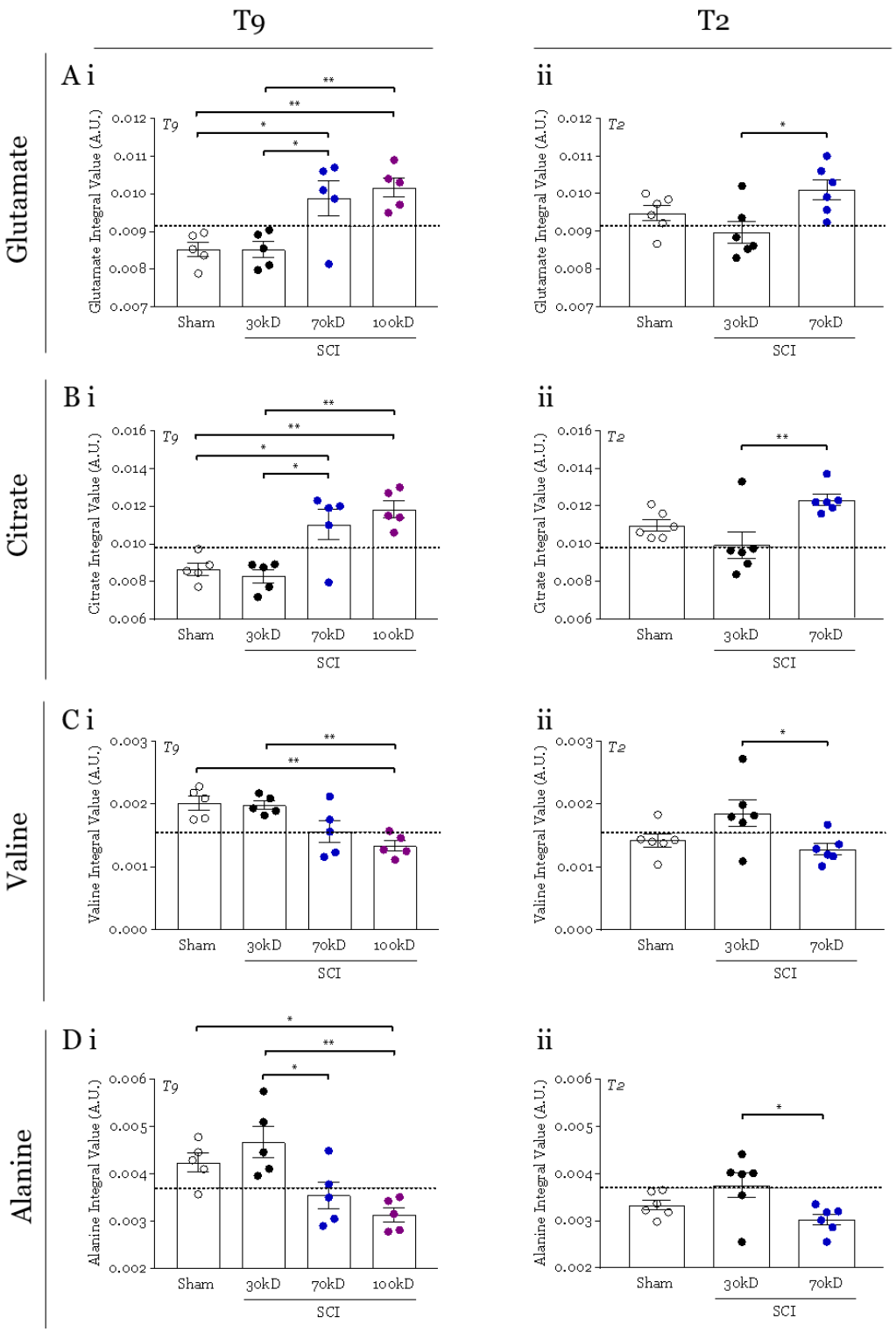


Figure 5.12 Metabolites in the spinal cord perturbed after traumatic injury. Female C57BL/6 mice underwent a 30kD (black points), 70kD (blue points) or 100kD SCI (purple points) at T9, or a single-hit 30kD or double-hit 70kD SCI at level 2 (n=6/group). Sham animals underwent a laminectomy at their respective level but received no cord impact (white points). Fresh spinal cord was collected 6 hours later and the metabolite profiles were compared between injury groups by PCA. Naïve spinal cord was used as baseline (dotted line, n=4). Key metabolites driving cluster separation were identified from the loadings plot for univariate analysis; glutamate (A), citrate (B), valine (C) and alanine (D). Data are presented as mean ±SEM, and analysed by one-way ANOVA, *p<0.05, **p<0.01 in Sidak's post-hoc test.

5.3.3 Plasma metabolite profile as a predictor of patient outcome after SCI

Given that the peripheral metabolome reflected the extent of spinal cord damage and functional deficit in our mouse model of SCI, it was determined whether the plasma metabolite profile could be predictive of patient outcome. As such, a new OPLS-DA model was generated using data from individuals who converted ASIA score between admission and discharge (converters, n=10) and those who did not (non-converters, n=18). The accuracy (59±12%, $p<0.0001$), sensitivity (62±15%, $p<0.0001$) and specificity (56±13%, $p<0.0001$) of the model were all significantly better than random chance (Figure 5.13A; student's t-tests). It must be noted that converters had significantly less time between the first ASIA score after injury, and the last ASIA score before discharge, when compared to non-converters (Supplementary Figure 5.2).

Univariate analysis of key SCI metabolites revealed no significant differences in plasma myo-inositol (Figure 5.13Bi; student's t-test, $p=0.493$), glucose (Figure 5.13Bii; student's unpaired t-test, $p=0.424$) or lipoprotein side-chains (Figure 5.13Biv; student's unpaired t-test, $p=0.396$). Circulating glutamine exhibited a trending decrease in the converters, with a 28.1% decrease compared to non-converters, however this was not statistically significant (Figure 5.13iii; student's t-test, $p=0.095$). Further interrogation of discriminatory metabolites in this model specifically, revealed that resonances corresponding to lipoprotein (Figure 5.13Ci; student's unpaired t-test, $p<0.05$) and histidine (Figure 5.13Cii; student's unpaired t-test, $p<0.05$) were significantly increased in converters, compared to non-converters. This indicates that the plasma metabolome is predictive of SCI patient outcome.

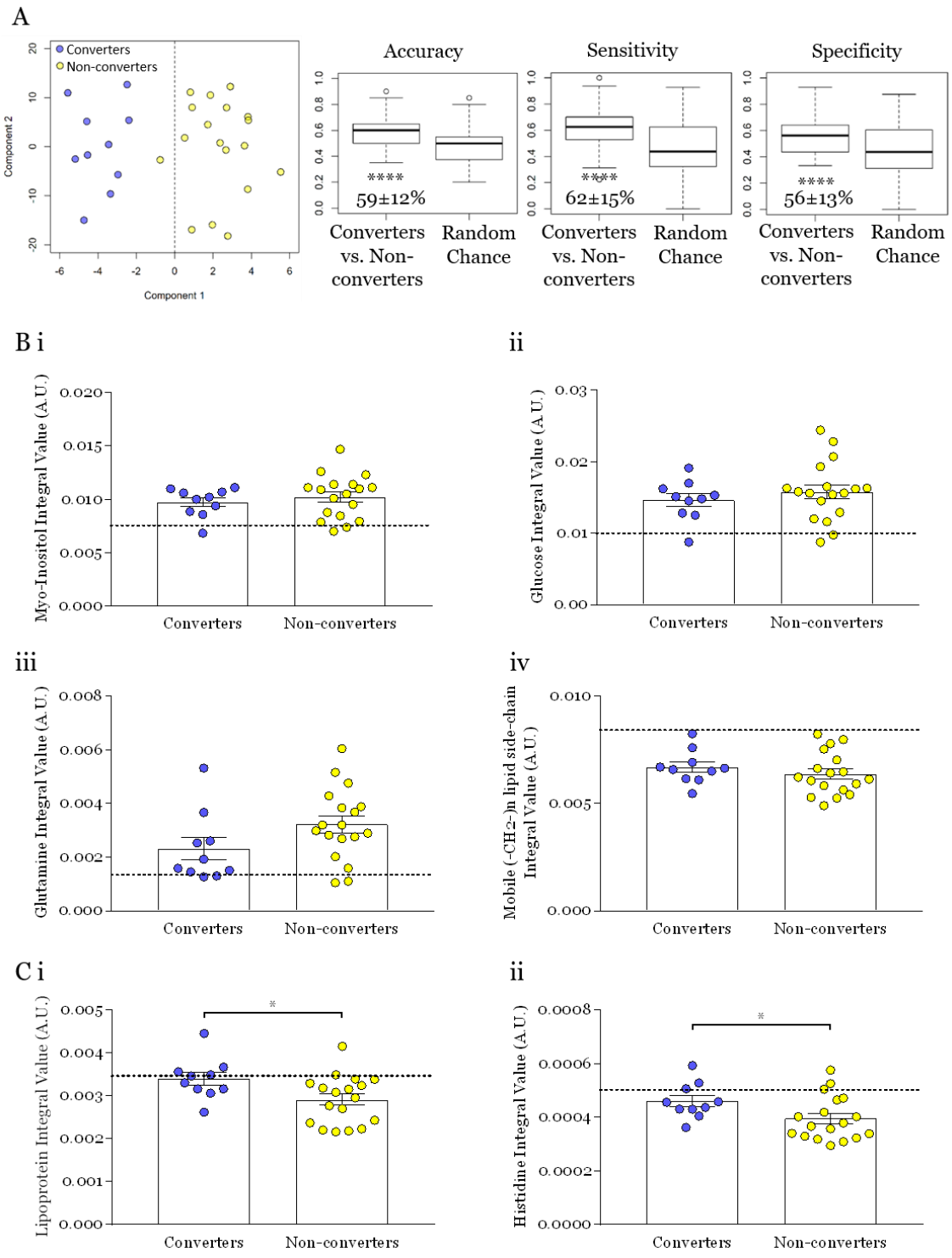


Figure 5.13 Prediction of patient outcome with plasma metabolites. Plasma metabolite profile of SCI patients who improved AIS score between admission and discharge (converters, blue points, n=10) was compared with those who did not (non-converters, yellow points, n=18), by multivariate analysis. OPLS-DA scores plot discriminating between converters and non-converters, with accuracy, sensitivity and specificity of the model (A). Key SCI-perturbed metabolites (B), myo-inositol (i), glucose (ii), glutamine (iii) and mobile side-chain lipoproteins (-CH2)n (iv), were further investigated in this cohort. Discriminatory metabolites in this model specifically, lipoprotein (Ci) and histidine (ii), were also investigated. Dotted line corresponds to healthy controls (n=12). Data are presented as mean ±SEM, and analysed by student's unpaired t-test. *p<0.05, ****p<0.0001.

5.4 Discussion

SCI patients are at increased risk of developing metabolic disorders, independent of immobility (Banerjea et al. 2008; Cragg et al. 2013a; Goodus and McTigue 2020). However, the underlying mechanisms driving these changes remain unknown. In this chapter, metabolomics was used to evaluate metabolite changes in peripheral tissues and the CNS during the acute phase of traumatic SCI. Data presented here indicate that SCI induces a metabolic signature in the plasma, liver and spinal cord, as evidenced by the perturbation of metabolites including myo-inositol, glucose and citrate, as well as a range of lipids and amino acids. The magnitude of these metabolite changes was found to be dynamic, dependent on time after injury, and the severity and the level of the lesion. In turn, metabolites were identified that were associated with improvement in ASIA score, suggesting that the plasma metabolite profile may provide insight into patient outcomes.

5.4.1 SCI induces a metabolite signature in the periphery

NMR metabolomics of biofluids is a relatively novel, non-invasive technique that allows the simultaneous comparison of approximately 90 aqueous metabolites. The measurement of metabolite changes in CSF and/or plasma has previously been used to effectively evaluate the physiological state of the CNS, which is otherwise inaccessible to interrogation. This technique has been utilised to determine stage and type of demyelinating disease in patients with MS (Jurynczyk et al. 2017; Yeo et al. 2020), and the presence and grade of brain tumours (Baranovicova et al. 2019), as well as the severity and prognosis of TBI (Oresic et al. 2016; Martha et al. 2021) and stroke (Jung et al. 2011; Kimberly et al. 2013). Wu et al. (2016b) demonstrated that SCI induced alterations in metabolites in patient CSF and serum samples collected during the subacute phase. Here, the plasma NMR metabolite profile is able to distinguish between SCI patients and healthy controls in the acute phase. Healthy volunteers were used as controls, therefore this outcome may be due to trauma, rather than injury to the spinal cord specifically. Indeed, acute trauma alone has been shown to induce peripheral metabolite changes (Peltz et al. 2015), most likely due to activation of the sympathetic nervous system; it may be interesting to compare TBI with SCI in future experiments. As such, the results of our human work were further explored in our contusion model

of SCI with appropriate sham controls. Consistent with the human cohort, analysis of plasma metabolite profiles was able to discriminate between sham and SCI animals. Interestingly, significant differences between the sham and SCI metabolomes were only detected in samples collected at later time points in the acute phase (12 & 24 hours) and not the early time points (2 & 6 hours), suggesting that there is a window when metabolic consequences of SCI may be amenable to therapy. Collectively, data presented in this chapter confirm that SCI induces a metabolite signature in the plasma which is time dependent.

It must be acknowledged that human plasma samples were obtained from 27 males and only 2 females. Therefore, there is a clear sex bias, which may be skewing the results. Indeed, it has previously been shown that the plasma metabolome is affected by sex (Vignoli et al. 2018; Krumsiek et al. 2015). For example, Vignoli et al. (2018) reported increased steroid derivatives and isoleucine, and decreased creatine in males, compared to females. However, given that SCI disproportionally affects more males than females (Chen et al. 2016), the cohort used in this chapter reflects what is observed in the clinic, and so the results obtained remain valuable.

The key metabolites driving the discrimination between SCI patients and healthy volunteers were found to be myo-inositol, glucose, glutamine and mobile lipid side-chains. When these metabolites were specifically examined in our rodent model, circulating myo-inositol, glucose and glutamine were increased in both sham and SCI animals above naïve baseline, indicating that the observed increase is trauma-associated. By comparison, by 12-24 hours, the levels of these metabolites remained elevated in the SCI animals only, indicating that there is an SCI-specific effect. Each of these metabolites have previously been associated with CNS injury. Myo-inositol is a component of myelin, and is associated with demyelination in the CNS (Jurynczyk et al. 2017; Fisher et al. 2002). Therefore, elevated plasma levels may be due to the release of myelin debris from the spinal cord after traumatic injury. Increased plasma glucose has been reported in SCI patients and hyperglycaemia worsens functional outcomes (Kobayakawa et al. 2014). Interestingly, plasma glutamine was increased in this patient cohort. Previous studies have described a decrease (Rogeri and Costa Rosa 2005). Tanhoffer et al. (2007) showed a decrease in plasma glutamine in a rat

model of SCI, which they suggest may contribute to the immune suppression after injury. However, the earliest time point analysed was 2 days post-SCI. As such, the results may reflect the early metabolic changes in a highly dynamic response. No difference in plasma mobile lipid side-chains between sham and SCI animals at either time point, indicating that this response is due to trauma alone.

Although there are clear similarities between the clinical and experimental data, several plasma-metabolites were identified to be discriminatory in the animal model, which were not in the human cohort. This may be because of increased variability that will always be a feature of clinical samples. Therefore, the animal model can provide unique insight into the pathophysiology of SCI, given the standardised injury and ability to control blood collection. The amino acids phenylalanine, histidine and tyrosine were all significantly increased in the plasma of both sham and SCI animals above naïve baseline at early time points, with an SCI-specific increase evident at the later time points. Alterations in the metabolism of these amino acids have been reported in patients with SCI and in animal models (Peng et al. 2014; Wu et al. 2016b), however the relevance of these changes to patient outcome remains unclear. Aromatic amino acids serve as precursors to many neurotransmitters and hormones, including dopamine, noradrenaline and adrenaline, whilst histidine is the precursor to histamine, suggesting that SCI affects these signalling pathways. Peng et al. (2014) found that disturbances in tyrosine metabolism contributed to SCI severity, and Nakashima et al. (2008) reported that inhibition of tyrosine phosphatase in the spinal cord improved histological and functional outcomes after injury. This would suggest that these amino acids have a pathological role after SCI, although additional studies are required to confirm this.

The liver plays a critical role in metabolism and SCI-associated hepatic pathology has been described in the days following injury (Goodus and McTigue 2020; Sauerbeck et al. 2015). Here, it is clear that SCI induces significant disturbance to hepatic metabolites within hours of injury, which may be driving the reported downstream pathologies. Interestingly, metabolites identified as discriminatory in the plasma, were largely unaffected in the liver. Instead, investigation of the key metabolites in the model revealed that hepatic amino acids and acetoacetate in the liver were

significantly increased after SCI, both of which have been associated with catabolism to generate energy substrates. Branched chain amino acids, isoleucine, leucine and valine, can be catabolised into acetyl-CoA and/or succinate-CoA and enter the TCA cycle (Zhang et al. 2017), and acetoacetate is a bi-product of ketosis (Demirel et al. 2020). Together, these metabolite changes may reflect the increased energy demands of the body after SCI and contribute to the metabolic disorders prevalent amongst patients (Rankin et al. 2017). It is interesting to note that branched chain amino acids have also been shown to support immune function, for example, by increasing phagocytic function of neutrophils (Nakamura et al. 2004).

Hepatic lipid side-chains [bCH2] were also increased in the acute phase; accumulation of lipid in the liver has previously been reported in the days following SCI (Sauerbeck et al. 2015). The data presented here suggests that changes in hepatic lipid metabolism occurs early, within the first 24 hours after injury. Increased lipid in the liver is known to develop into non-alcoholic fatty liver disease (Goodus and McTigue 2020), which increases the risk of patient death (Barbonetti et al. 2016). Therefore, therapeutic intervention targeting SCI-associated metabolic syndrome likely needs to be early to be effective.

5.4.2 Central and peripheral metabolome are injury severity dependent

It has previously been shown that metabolomics can identify biomarkers after SCI, with a particular focus on injury severity (Peng et al. 2014; Wu et al. 2016b). Here, severity-dependent metabolite changes were confirmed in rodent plasma and liver samples, most notably, many resonances corresponding to lipid side-chains. Circulating mobile (-CH2-)n, bCH2 and =CH-CH2-CH= were all increased with severe SCI, but not mild. Dyslipidaemia is a common consequence of SCI (Storch et al. 2005), as evidenced by increased serum cholesterol, triglycerides and low density lipoproteins (Vichiansiri et al. 2012). These disturbances in lipid metabolism may be due to severity-dependent increase in systemic inflammation, which this thesis has shown. Indeed, Rankin et al. (2017) previously correlated liver adiposity with TNF-α ($r=0.61$, $p=0.01$). Peng et al. (2014) used supervised multivariate analysis and metabolic pathway mapping to associate lipid metabolites in

the plasma with neurobehavioural recovery. Therefore, circulating lipid levels could be used to guide acute treatment and improve prognostic accuracy.

In addition to injury severity, some peripheral metabolites exhibited distinct changes following injury at the two levels (T9 and T2). It is known that the risk of developing metabolic disorders appears to be lesion level dependent (West et al. 2012). In our contusion model, hepatic glucose was significantly depleted following severe SCI at T2, but not T9. This cannot be attributed to the release of glucose into the circulation as, although there was an overall increase in plasma glucose induced by SCI, there was no lesion-level effect. As such, this may reflect altered glucose metabolism, which has been shown to be disturbed after SCI (Graham et al. 2019). This, in turn, may be due to dysfunction of the sympathetic nervous system. In response to injury, sympathetic signalling to the liver induces the production of glucose by gluconeogenesis and glycogenolysis, to generate energy substrate as part of the "fight-or-flight" response (Nonogaki 2000). Therefore, with high level injuries where sympathetic innervation is disrupted, induction of these metabolic pathways would not occur. In line with this, Banerjea et al. (2008) reported that the prevalence of diabetes is decreased in patients with higher level injuries (tetraplegia), compared with low level injuries (paraplegia). However, clinical studies investigating SCI lesion level differences in blood glucose levels are lacking and no level effect on circulating glucose was observed in our human cohort (data not shown). Hyperglycaemia has been shown to induce inflammation via NF-κB and produce ROS (Nishikawa et al. 2000), and impair the innate immune response (Perner et al. 2003; Turina et al. 2005), suggesting that it may contribute to the peripheral inflammatory response to SCI. Kobayakawa et al. (2014) showed that hyperglycaemia is predictive of patient outcome, and acute insulin treatment reversed hyperglycaemic damage in a rodent model. Therefore, the effect of the nature of the SCI lesion on plasma glucose is of interest and may influence acute patient treatment.

As with peripheral tissues, metabolite changes in the spinal cord itself are evident after SCI, which is consistent with a study by Fujieda et al. (2012), and are dependent on the severity of the injury. Of particular interest, a severity-dependent increase in intraspinal glutamate was detected. Excess

extracellular glutamate has previously been reported in the spinal cord after SCI, which can cause glutamate excitotoxicity, contributing to additional cell death (Barger et al. 2007; Xu et al. 2004). However, the metabolite extraction process used in this chapter does not discriminate between the intra- and extracellular components, suggesting this increase is due to impairment of glutamate metabolism. Indeed, under physiological conditions, glutamate is metabolised into glutamine by glutamine synthetase in astrocytes, which has been shown to be dysregulated following SCI (Liu et al. 2013), most likely owing to damage to the astrocytes. In line with this, a concurrent, severity-dependent decrease in glutamine was observed in these spinal cords. Given that spinal cord and peripheral tissues were collected from the same animals, the extent of damage within the spinal cord could be extrapolated from the plasma metabolome.

5.4.3 Plasma metabolites as prognostic markers after SCI

SCI presentation is highly heterogeneous and, with confounders such as spinal shock, accurate evaluation of patient prognosis are limited to ASIA scoring, 72 hours after injury (Alizadeh et al. 2019). Therefore, there is value in identifying biomarkers in the acute phase of injury, which are predictive of patient outcome, and it has been suggested that metabolomics is capable of achieving this (Probert et al. 2018). Certainly, metabolomic analysis of plasma collected from TBI patients upon admission (<12 hours after injury) was able to discriminate between those with favourable and unfavourable outcomes (Oresic et al. 2016; Martha et al. 2021). Here, plasma metabolite profiles of SCI patients who improved ASIA score between admission and discharge (converters), were compared to those who did not (non-converters). The resulting OPLS-DA model was able to predict patient improvement, with 59±12% accuracy, which is consistent with previous studies (Singh et al. 2018; Cyr et al. 2021). Although this was statistically significant, the model cannot be considered predictive of patient outcome, as it only slightly outperformed random chance (22% greater accuracy with the model). This somewhat disappointing result may be due to variability in the sample collection, which is likely to reduce model accuracy. In this chapter, it was shown that the time after injury impacts plasma metabolites and human plasma samples were collected from 4.5 to 36.75 hours after injury. Moreover, sample handling has been shown to reduce model

accuracy, where increased time between collection and processing significantly reduced predictive accuracy (Yeo et al. 2020). In line with this, the time between sample collection and processing for SCI patient blood was, once again, highly variable. As such, future work should include samples collected in a more consistent and systematic way to reduce variability. Given that model accuracy was increased with an optimised protocol (Yeo et al. 2020), it stands to reason that improving sample processing would improve the predictability of the outcome model and could provide prognostic value.

Despite the limitations of the outcome model, two metabolites were identified as discriminatory between converters and non-converters – lipoprotein and histidine. Disturbance of peripheral lipoproteins has consistently been associated with neurological disorders. For example, HDL/LDL are significantly lower in secondary progressive MS, compared to relapsing remitting (Yeo et al. 2020). Here, plasma-derived lipoprotein was significantly decreased in the non-converters compared to healthy controls, which was normalised in converters. Lipoproteins have been implicated in the APR and immune regulation. From previous chapters, it is known that SCI induces a robust APR, including substantial upregulation of APPs such as SAA-2, which contribute to leukocyte mobilisation and expression of pro-inflammatory molecules (Yates et al. 2021). SAA mediates a reduction in circulating lipoproteins (Jahangiri 2010), therefore the decrease observed here in the non-converter patients may be due to the SCI-induced APR. In which case, the increase in plasma lipoproteins in the converters may indirectly reflect an attenuated APR, which in turn is associated with improved outcomes (Campbell et al. 2008b; Jogia et al. 2021; Yates et al. 2021). Additional experiments would be required to confirm this hypothesis.

Similar to lipoprotein, histidine in the plasma was decreased in the non-converter group, which was increased in the converter group, to the level of healthy controls. Histidine is an amino acid with a range of functions including regulation of metals (zinc, iron, heavy metals) and enzymatic activity, as well as inflammatory responses via its derivative histamine. Decreases in circulating histidine have been shown in a range of acute and chronic inflammatory disorders. Consistent with results in this chapter, Kimberly et al. (2013) reported a reduction in plasma histidine in stroke

patients compared to controls. In SCI specifically, Peng et al. (2014) stated that histamine to histidine metabolism was related to neurobehavioural recovery, although authors did not explore how this might occur. Interestingly, histidine administration has been shown to be neuroprotective after traumatic CNS injuries. In a rodent model of stroke, intraperitoneal injection of histidine reduced leukocyte recruitment to the brain (Hiraga et al. 2007) and the size of the infarction (Adachi et al. 2005; Adachi et al. 2011), as well as improved cognitive outcomes (Liao et al. 2015). This was likely achieved through stimulation of histidine H2 receptors on peripheral leukocytes, which is known to inhibit expression of pro-inflammatory cytokines and adhesion molecules (Takahashi et al. 2002; Vannier et al. 1991). Therefore, treatment of SCI with the same strategy may improve patient outcomes.

It must be acknowledged that the number of days between the first and last (discharge) ASIA assessment for converters, was significantly less than that for non-converters, which may be confounding the results. The length of stay in hospital is associated with morbidity and worsens functional outcomes for patients (Sengupta et al. 2021), which may be attributed to post-injury complications, such as infections (Failli et al. 2012). As such, the metabolite differences observed between converters and non-converters may instead reflect the length of hospital stay and/or any complications. It would be of interest to evaluate any change in ASIA score between two fixed time points, for example between day 3 and day 42 post-injury, to determine whether the significant results remain.

5.5 Conclusions from this chapter

SCI induces distinct, tissue-specific metabolite changes in the plasma, liver and spinal cord itself, during the acute phase of injury, which are injury severity and lesion level dependent. Although additional samples must be collected with optimised processing, data presented in this chapter suggests that the plasma metabolite profile could be predictive of patient outcome after SCI.

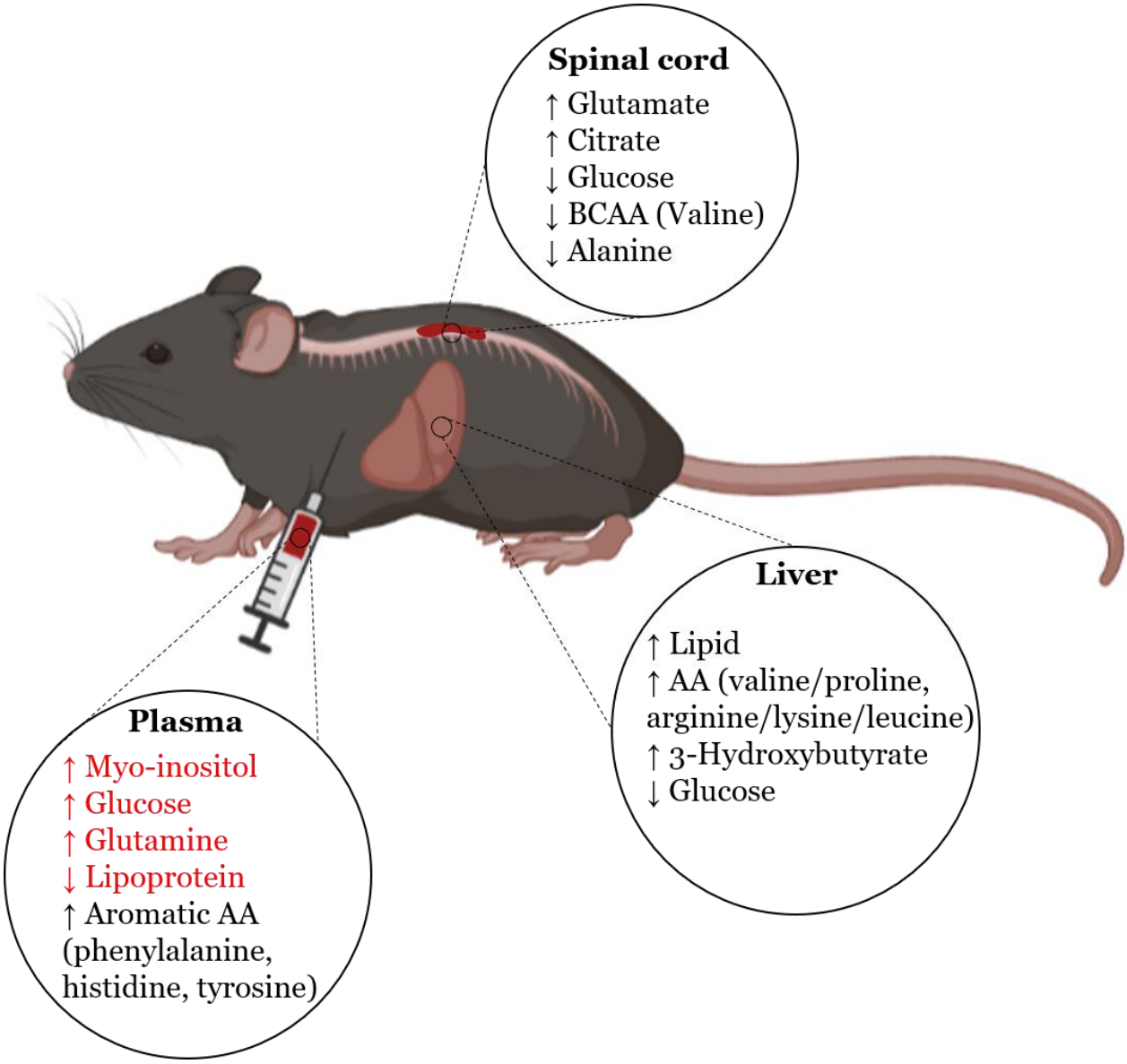
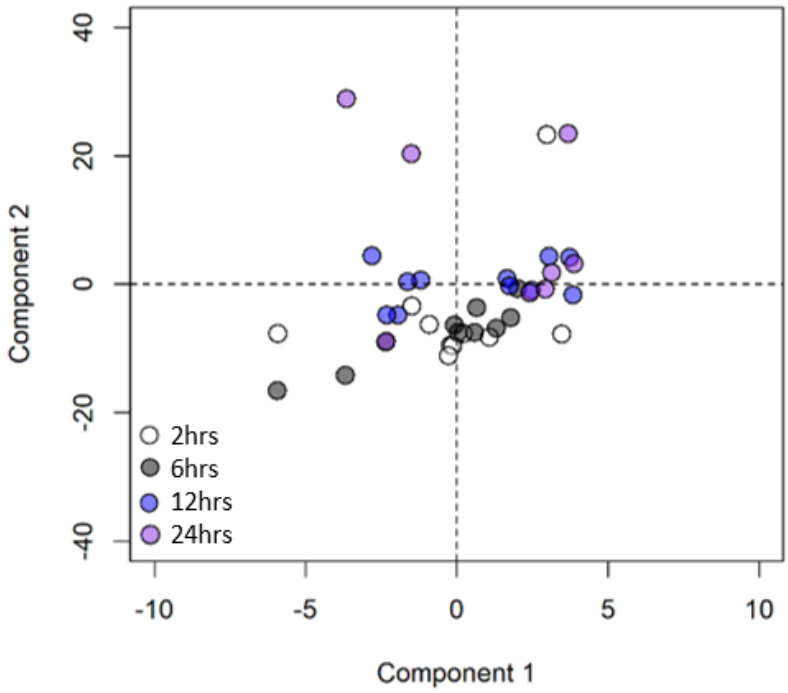
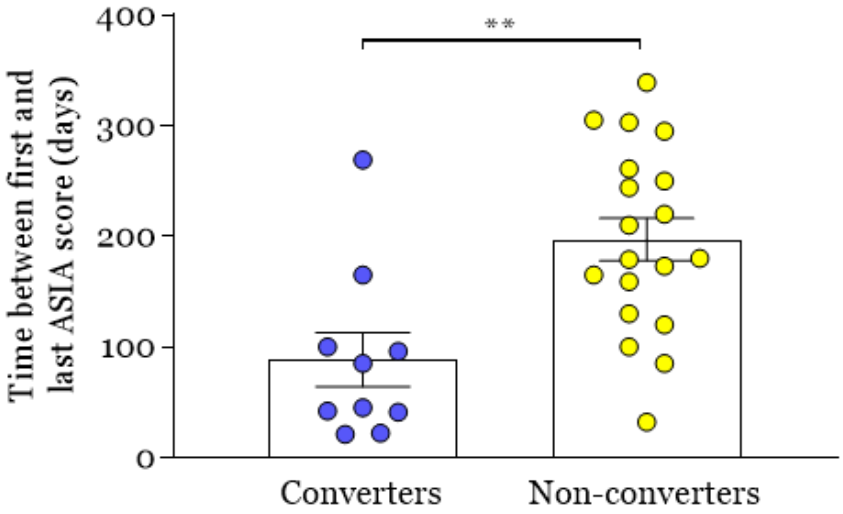


Figure 5.14 Summary of SCI-induced metabolite changes in the rodent model. Visualisation of the metabolites in the spinal cord, liver and plasma, which are altered in the acute phase of SCI, including the direction of change. Plasma metabolites highlighted in red correspond to those consistent with the human cohort. AA – amino acid, BCAA – branched chain amino acid.

5.6 Supplementary Figures for this chapter



Supplementary Figure 5.1 OPLS-DA scores plot of rodent plasma metabolite profiles following SCI. Female C57BL/6 mice underwent a 70kD SCI, or sham surgery as control, and blood was collected 2 (white points), 6 (black points), 12 (blue points) and 24 hours (purple points) post-injury (n=4-5/time point). Plasma was generated and measured by NMR. OPLS-DA multivariate analysis was performed with the spectra; visualisation of scores plot generated from plasma metabolite profiles following SCI.



Supplementary Figure 5.2 Time between first and last ASIA score for SCI patients. The time between the first ASIA score after injury, and the last ASIA score before discharge (days) in patients that converted (blue points, n=10) and those who did not (yellow points, n=18). Data are presented as mean ± SEM, and analysed by Mann-Whitney test, **p<0.01.

Chapter 6: The contribution of extracellular vesicles to SCI

6.1 Introduction and aims

Throughout this thesis, it has become evident that SCI induces profound changes in non-CNS tissue, including leukocyte mobilisation, gene expression changes in the liver, and metabolic disturbance. However, the initiation signal for the activation of this systemic response remains unknown. Both humoral and neuronal mechanisms have been investigated. Vagotomised animals still exhibit an APR (Konsman et al. 2000; Kox et al. 2012), and no molecular candidates have been identified that can fully explain the response (Konsman et al. 2002). In the absence of being able to elucidate a neural or humoral signal, there is growing evidence that extracellular vesicles (EVs) may be the missing link (Yates et al. 2019).

EVs are defined as all cell-derived particles encapsulated in a lipid bilayer, which are enriched for proteins, lipids and nucleic acids (Budnik et al. 2016; Colombo et al. 2014; Robbins et al. 2016). They have been shown to be released from almost all cell types, including neurons (Chivet et al. 2014; Lachenal et al. 2011), microglia (Drago et al. 2017; Kumar et al. 2017), astrocytes (Dickens et al. 2017) and CNS endothelial cells (Couch et al. 2017b), and they have been isolated from almost all bodily fluids, including CSF (Welton et al. 2017) and plasma (Hazleton et al. 2017). They have a unique capacity to disseminate information around the body, including across the blood-CNS barrier (Dickens et al. 2017), to exert their effects both locally and systemically to distant organs, making them obvious candidates for CNS-to-immune communication following SCI (Yates et al. 2019). Certainly, circulating EVs isolated from LPS-treated animals have been shown to cause gliosis and expression of pro-inflammatory molecules in the brains of naïve mice (Li et al. 2018a). EVs released from stimulated endothelial cells induced hepatic TNF and CXCL1 expression in naïve rats, inducing a sickness behaviour phenotype as a result (Couch et al. 2017b). Moreover, Balusu et al. (2016) showed that systemic inflammation induces EV release from the choroid plexus into the CSF, which then translocate to the brain. Together, these studies suggest the presence of a CNS-periphery communicatory axis that is mediated by EVs.

EV-mediated cell communication has been associated with a number of neurological diseases. They have been shown to be vectors of pathogenic protein transport in Alzheimer's and Parkinson's

disease (Jucker and Walker 2013; Saman et al. 2012; Shi et al. 2014). In addition, in brain cancers, tumour-derived EVs have been shown to facilitate growth and metastasis (Hoshino et al. 2015; Oushy et al. 2018; Skog et al. 2008). Given that EVs are capable of crossing the BBB (Dickens et al. 2017), plasma-derived EVs are likely to constantly report the physiological state of the CNS. As such, the circulating EV population may serve as useful biomarkers of insult. Indeed, neuron-derived EVs enriched for AD-associated proteins have been detected in human plasma in the preclinical phase of AD (Fiandaca et al. 2015). Moreover, increased CNS-derived EVs have been associated with relapse in MS patients (Minagar et al. 2001), and can used to discriminate between individuals with relapsing-remitting and progressive disease (Ebrahimkhani et al. 2017). Therefore, the study of peripheral EVs has shown that it can provide valuable information about the status of the CNS, which is, otherwise, largely inaccessible.

Previous work has shown that the circulating EV population is augmented in response to traumatic CNS injuries. Increases in plasma concentrations have consistently been reported in both animal models and human patients after stroke (Couch et al. 2017a; Yang et al. 2018), TBI (Andrews et al. 2016; Hazleton et al. 2017; Kumar et al. 2017; Nekludov et al. 2014; Zhao et al. 2017) and inflammatory brain lesions (Couch et al. 2017b; Dickens et al. 2017). Interestingly, Yang et al. (2019) reported that plasma-derived EVs were reduced in TNF KO mice after stroke, suggesting that the circulating EV population is associated with the magnitude of injury-associated neuroinflammation. In line with this, Clausen et al. (2014) demonstrated that the circulating EV concentration did correlate with the volume of infarct in experimental stroke. As such, plasma EVs may provide insight into the severity and progression of injury. Changes in the EV population may also be predictive of and/or contribute to long-term outcomes; TBI patients are at increased risk of developing neurodegenerative diseases and exhibit increased levels of exosomal tau and $A\beta_{42}$ (Gill et al. 2018). However, the effect of SCI on the circulating EV population remains unknown.

It has been proposed that EVs, released into the circulation after traumatic CNS injury, initiate the associated APR. In line with this, plasma-derived EVs isolated after stroke and inflammatory brain lesion have been shown to induce inflammation in macrophages *in vitro* (Couch et al. 2017a), and

a hepatic APR *in vivo* (Couch et al. 2017b; Dickens et al. 2017), respectively. In addition, plasma EV concentration correlated with CRP levels, indicative of systemic inflammation (Couch et al. 2017a). Critically, blocking EV release from the brain significantly attenuated the APR and neutrophil recruitment to the CNS after striatal IL-1β injection (Dickens et al. 2017). This not only indicates that EVs released after CNS trauma can trigger the APR, but that manipulation of this communication pathway could protect against secondary injury. Indeed, inhibition of EV release has been shown to reduce neuroinflammation and cell death, and improve behaviour deficits in rodent models of TBI (Kumar et al. 2019; Liu et al. 2017) and MS (Verderio et al. 2012). This mechanism of EV-mediated systemic inflammation after neurotrauma is yet to be demonstrated in the context of SCI. EVs enriched for inflammasome-associated proteins have been detected in the CSF of deceased patients, however their ability to induce an inflammatory response was not investigated (de Rivero Vaccari et al. 2016). Elucidating this may identify EVs as a viable therapeutic target after spinal injury.

The aims of this chapter were (1) to determine the effect of SCI on the circulating EV population, and (2) to evaluate the contribution of EVs to the APR and outcome after injury.

6.2 Methods specific to this chapter

6.2.1 Human plasma samples

Blood samples were collected from SCI patients (n=29) and healthy controls (n=8), and plasma was prepared, as described in 2.1. Samples were centrifuged at 2,000*g* for 5 minutes, prior to ultracentrifugation, to remove excess lipid.

6.2.2 Animals and spinal cord injury model

In accordance with the 3 R's, plasma samples collected for time course characterisation in Chapter 3, and for SCI level and severity experiments in Chapter 4, were utilised in this chapter to determine the effect of SCI on the circulating EV population.

6.2.3 EV isolation and measurement

For time course characterisation, EVs were isolated from 100µL of platelet-free plasma with the Hitachi CP100NX ultracentrifuge and P50A3 rotor. The EV pellet was resuspended and measured with the NanoSight LM10 (Malvern Panalytical). For biodistribution and *in vivo* experiments, EVs were isolated with the Optima XPN-100 ultracentrifuge (Beckman Coulter) and Type 70 Ti rotor (Beckman Coulter). All other EV isolations were performed with the Optima TLX Ultracentrifuge (Beckman Coulter) and TLA 110 rotor (Beckman Coulter). The EV pellet was resuspended and measured with the NanoSight NS500 (Malvern Panalytical).

6.2.4 EV biodistribution

EVs were isolated from either naïve plasma, or plasma from SCI animals collected 2 hours post-injury, and labelled as described in 2.11.5. Labelled EVs were injected intravenously into naïve mice and fresh tissues of interest (liver, spleen, lung, spinal cord, brain, kidney, gut and heart) were collected 30 minutes later. Unlabelled EVs and PKH67 dye only were injected into naïve mice as 2 separate controls.

miRNA was extracted from fresh tissue and analysed by qPCR as outlined in 2.8.3, using the *cel*-miR-39-3p PCR assay (Qiagen©). For imaging, fresh tissue was cut into 10µm sections with the

Leica cryostat and post-fixed in formalin for 20 minutes. Sections were incubated with Hoechst 33342 nuclear dye for 15 minutes, and mounted with DAKO fluorescent mounting medium.

6.2.5 EV adoptive transfer – in vitro

PBMCs isolated from the blood of healthy male volunteers were incubated with saline or LPS (100ng/mL, Sigma Aldrich) + IFN-γ (10ng/mL, R&D Systems) as baseline and positive control respectively, or plasma EVs derived from healthy controls or SCI patients, for 6 hours. EVs were isolated from 3.5mL of plasma. It has previously been shown that EVs can exacerbate inflammation (Hazleton et al. 2017), therefore a subset of PBMCs were pre-treated overnight with naïve or SCI plasma EVs and then challenged with LPS + IFN-γ for 6 hours.

6.2.6 EV adoptive transfer – in vivo

EVs were isolated from plasma collected from naïve animals, or animals with SCI, 2 or 6 hours after injury. Plasma from 3 donor mice were pooled and EVs were isolated for intravenous injection into 1 recipient mouse. Fresh liver was collected from recipient mice at 30 minutes or 6 hours after adoptive transfer.

6.3 Results

6.3.1 SCI had no effect on circulating EVs in human plasma

First, the isolation of EVs by ultracentrifugation was confirmed as per the ISEV recommended guidelines and previous studies (Couch et al. 2017b; Hazleton et al. 2017; Thery et al. 2018). EM imaging (Figure 6.1A) revealed the presence of both microvesicles and exosomes, as indicated by size analysis. Western blot of isolated plasma EVs showed enrichment of EV-associated proteins Alix and TSG101, expression of which was low in the brain lysate controls (Figure 6.1B). Histone H3, indicative of cellular contamination, was not detected in the EV samples, which further validates isolation of an EV-rich fraction.

The effect of SCI on the circulating EVs was then investigated; NTA measurements of plasma EVs revealed no significant difference between healthy controls and SCI patients (Figure 6.1C; healthy controls, $3.08x10^{10}$/mL; SCI Patients, $2.88x10^{10}$/mL; Mann-Whitney test, p=0.738). Size distribution analysis also showed no difference between SCI patients and healthy controls (Figure 6.1D; two-way ANOVA, p=0.449). To investigate whether any of these differences could be attributed to changes in any specific subclass of EV, the area under the curve for particles sized 5-135nm and 145-500nm, largely representing exosomes and microvesicles respectively, was calculated. There was no difference between groups for particles sized 5-135nm (Figure 6.1E; Mann-Whitney test, p=0.731), nor 145-500nm (Figure 6.1F; Mann-Whitney test, p=0.574) when analysed independently. No differences in mean (Figure 6.1G; student's unpaired t-test, p=0.191) or mode EV size (Figure 6.1H; Mann-Whitney test, p=0.497) were found between groups.

The characteristics of SCI patients and sample collection interaction was compared with EV concentrations to identify any parameters that may be influencing the results. There was no correlation between NISS score and plasma EV concentration (Figure 6.2A; linear regression, r^2=0.0007, p=0.900). Similarly, lesion level (Figure 6.2B; one-way ANOVA, p=0.737), ASIA score at admission (Figure 6.2C; one-way ANOVA; p=0.333), and the time between injury and sample collection (Figure 6.2D; linear regression, r^2=0.003, p=0.777) had no effect. To determine whether

circulating EVs correlated with systemic inflammation, plasma EV concentration was compared to patient CRP (Figure 6.2E; linear regression, r^2=0.144, p=0.082) and blood neutrophil levels (Figure 6.2F; linear regression, r^2=0.086, p=0.122). No significant correlations were observed.

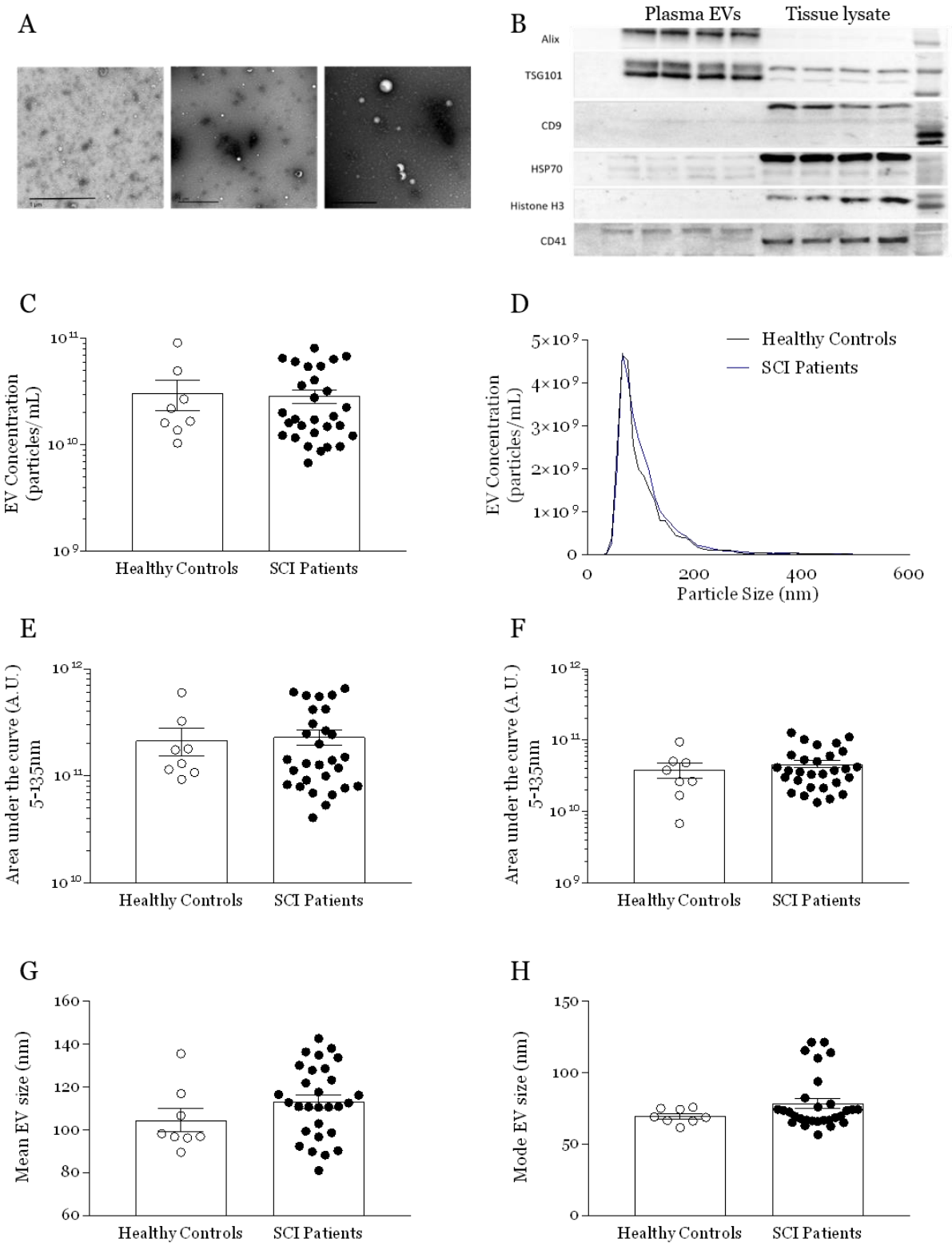


Figure 6.1 Characterisation of plasma EVs following SCI in human patients. EVs were isolated from the plasma of SCI patients upon admission (n=29, black points), or healthy controls (n=8, white points), by ultracentrifugation. Isolation of genuine EVs was confirmed by EM imaging (A) and western blot of EV markers (B). Plasma EV concentration (C) and size distribution (D) were measured by NTA with the NanoSight. Area under the curve was calculated to determine concentration of particles sized 5-135nm (E) and 145-500nm (F) independently. Mean (G) and mode (H) EV size were also evaluated. Data are presented as mean ±SEM, and analysed by two-way ANOVA, unpaired student's t-test or Mann-Whitney test, as dictated by normality distribution.

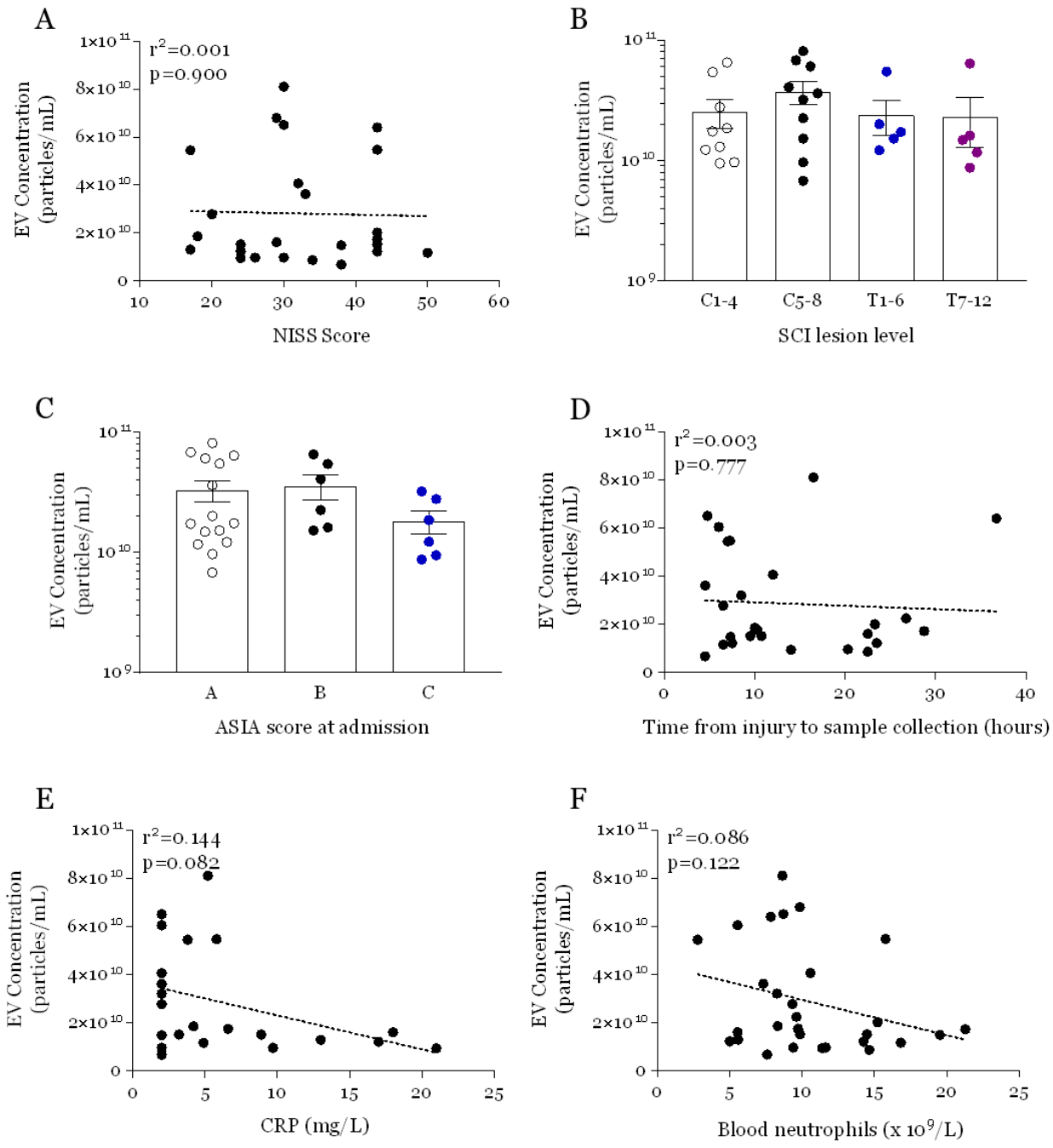


Figure 6.2 Correlations of plasma EV concentration and human SCI parameters. To identify any parameters that may be influencing the EV results, plasma EV concentration was compared to the characteristics of SCI and sample collection. The effect of NISS Score (A), lesion level (B) and ASIA score at admission (C) were all evaluated. The time between the injury and sample collection (D), the CRP (E) and blood neutrophil levels (F) were also correlated (E). Data are presented as mean ±SEM, and analysed by one-way ANOVA, Mann-Whitney test and linear regressions, as appropriate.

6.3.2 SCI induced a hyperacute increase in circulating EVs, in a rodent contusion model

The somewhat surprising clinical result was confirmed in a rodent contusion model of SCI. Plasma samples collected from the animals for the time course experiment in Chapter 3 were used for EV analysis. Two-way ANOVA indicated that there was no significant effect of SCI on plasma EV concentration, compared to sham. However, there were significant differences between time points (Figure 6.3A; two-way ANOVA, time point $p<0.0001$, injury $p=0.404$). At 2 hours post-injury, plasma EV concentration was significantly increased in SCI animals compared to naïve animals (naïve, $6.26x10^{10}$/mL; SCI, $2.37x10^{11}$/mL; Sidak's post-hoc test, $p<0.05$), but not sham animals ($1.6x10^{11}$/mL). Surprisingly, plasma EV concentrations for all subsequent time points were decreased in both sham and SCI animals, below naïve baseline. Naïve animals also received the anaesthetic regime given to all other mice but without any surgical intervention, so these results are specfic to injury. EV size was significantly affected by time but not by injury (Figure 6.3B; two-way ANOVA, time point $p<0.0001$, injury $p=0.094$). Sham and SCI plasma EV size was initially decreased below naïve baseline, 2 and 6 hours post-injury. By 24 hours post-injury, the size of SCI plasma EVs was significantly increased compared to naïve plasma EVs only (naïve, 169.7±6.5nm; SCI, 213.8±26.7nm; Sidak's post-hoc test, $p<0.05$).

As there were no differences in circulating EVs in total, the size distribution of EVs at each time point was then investigated. Statistical analysis revealed a significant difference between sham and SCI 2 hours (Figure 6.3C; two-way ANOVA, injury $p<0.0001$) and 12 hours post-injury (Figure 6.3D; two-analysis, injury $p<0.0001$). At 6 hours, the means suggested a trend, but it was not significant (Figure 6.3E; two-way ANOVA, injury $p=0.0822$). There was no difference 24 hours after SCI (Figure 6.3F; two-way ANOVA, injury $p=0.245$).

These data indicate that circulating EVs change in response to injury, but SCI *per se* does not have an effect.

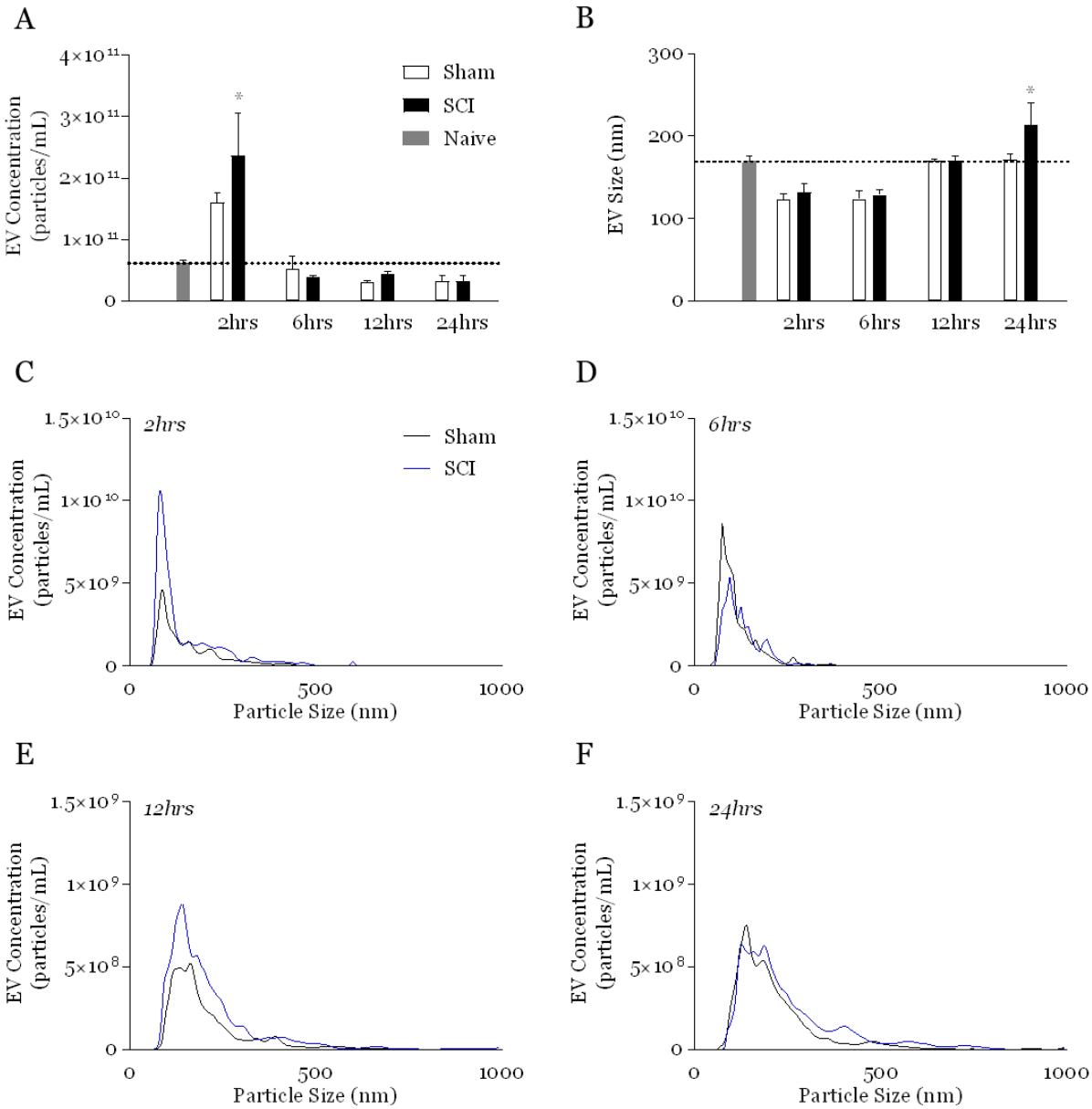


Figure 6.3 Plasma EV concentration and size during the acute phase of SCI. Female C57BL/6 mice underwent either a 70kD SCI (black bars, n=4-5/time point) or sham surgery (white bars, n=5/time point). Tissue was collected at 2, 6, 12 and 24 hours post-operation and was compared to naïve baseline (grey bar and dotted line, n=9). EV concentration (A) and size (B) was determined by NTA using the NanoSight. Size distribution of EVs collected 2 (C), 6 (D), 12 (E) and 24 hours (F) post-injury was evaluated. Data are presented as mean ±SEM, and were analysed by two-way ANOVA, *p<0.05 in Sidak's post-hoc test.

6.3.3 Circulating EVs following SCI are injury severity and lesion level dependent

Next, the effect of injury severity and lesion level on circulating EVs was explored, utilising plasma collected from the animals used in Chapter 4. EVs were isolated by ultracentrifugation and measured by NTA with the NanoSight.

SCI induced an increase in circulating EV concentration, which approached significance (Figure 6.4A; Kruskal-Wallis test, $p=0.089$). The average distribution of vesicle size and concentration, evaluated at 10nm intervals, revealed that SCI induced a significant increase in the plasma EV population, but this was independent of severity (Figure 6.4B; two-way ANOVA, injury severity $p<0.0001$, size intervals $p<0.0001$); sham was significantly different from each of the injury groups 30kD ($p<0.001$), 70kD ($p<0.0001$) and 100kD injury groups ($p<0.0001$) with Sidak's post-hoc testing. One-way ANOVA revealed no difference between groups for particles sized 5-135nm (Figure 6.4C; $p=0.208$). There was also no difference between groups for particles sized 145-500nm, although results approached significance (Figure 6.4D; Kruskal-Wallis test, $p=0.062$). Mean (Figure 6.4E; Kruskal-Wallis test, $p=0.607$) and mode particle size (Figure 6.4F; Kruskal-Wallis test, $p=0.198$) were unaffected by SCI injury severity.

At T2, SCI had no effect on total plasma EV concentration, although there were fewer EVs compared to injury at T9 (Figure 6.5A; Kruskal-Wallis test, $p=0.277$). Size distribution analysis revealed that 70kD SCI group was significantly different from both sham and 30kD SCI groups (Figure 6.5B; two-way ANOVA, injury severity $p<0.05$, size intervals $p<0.0001$; Sidak's post-hoc test, $p<0.05$). Further analysis revealed that there was no injury severity effect on particles sized 5-135nm (Figure 6.5C; one-way ANOVA, $p=0.606$). SCI severity also had no overall effect on particles sized 145-500nm (Figure 6.5D; one-way ANOVA, $p=0.083$), although a trending increase was observed following 70kD SCI, compared to 30kD SCI only (Sidak's post-hoc test, $p=0.082$). Mean (Figure 6.5E; one-way ANOVA, $p=0.350$) and mode particle size (Figure 6.5F; Kruskal-Wallis test, $p=0.608$) were similarly unaffected by SCI injury severity at T2. Taken together, SCI at both T9 and T2 can induce an increase in plasma EV concentration, which is severity-dependent, albeit variable.

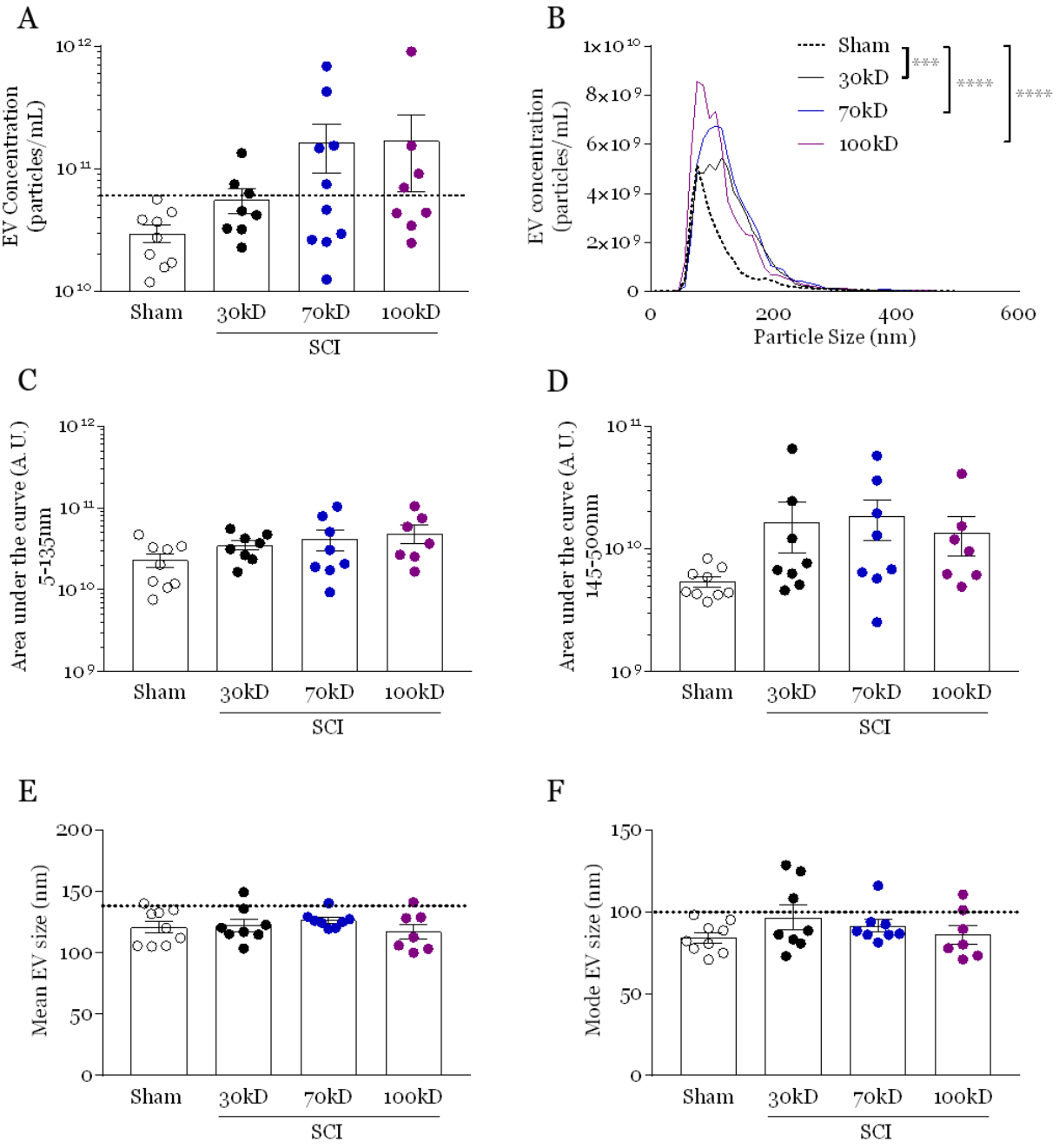


Figure 6.4 Plasma EV concentration and size following SCI at T9, 6 hours post-injury. Female C57BL/6 mice underwent either a 30kD (black points, n=8), 70kD (blue points, n=10) or 100kD SCI (purple points, n=8) at T9, or sham surgery as control (white points, n=9), and plasma was collected 6 hours later. EVs were isolated by ultracentrifugation and size and were measured with the NanoSight. Results were compared to naïve samples (dotted line, n=7). Total EV concentration (A) and size distribution (B) of SCI plasma EVs. Area under the curve, corresponding to relative concentration of EVs 5-135nm (exosomes, C) and 145-500nm (microvesicles, D). Mean (E) and mode (F) EV size. Data are presented as mean ±SEM, and analysed by one- or two-way ANOVA, or Kruskal-Wallis test, as appropriate, ***p<0.001 ****p<0.0001 in Sidak's post-hoc test.

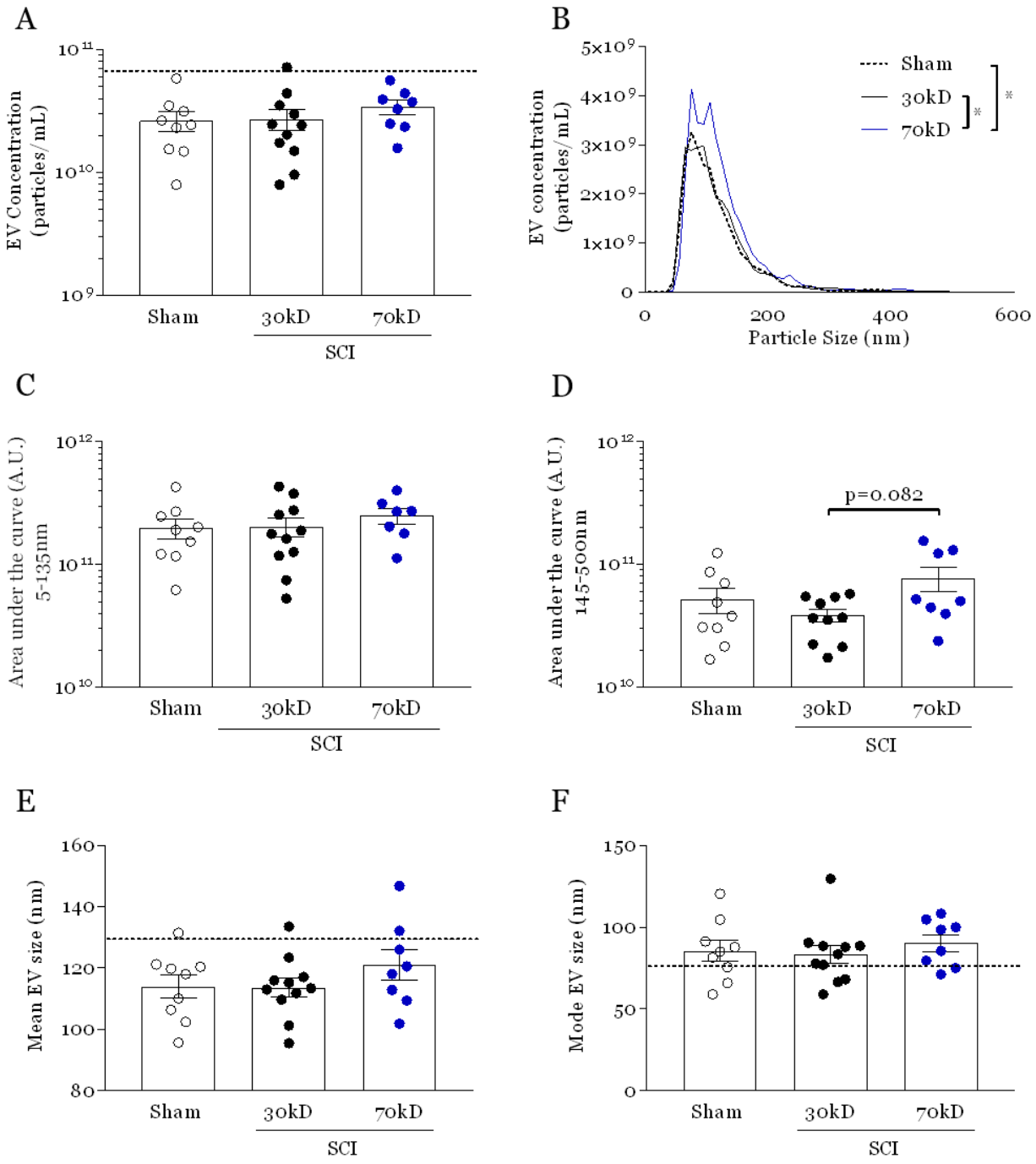


Figure 6.5 Plasma EV concentration and size following SCI at T2, 6 hours post-injury. Female C57BL/6 mice underwent either a single, midline 30kD (black points, n=11) or bilateral 70kD SCI (blue points, n=8), or sham surgery as control (white points, n=9), and plasma was collected 6 hours later. EVs were isolated by ultracentrifugation, and concentration and size were measured with the NanoSight. Results were compared to naïve samples (dotted line, n=7). Total EV concentration (A) and size distribution (B) of SCI plasma EVs. Area under the curve, corresponding to relative concentration of EVs 5-135nm (exosomes, C) and 145-500nm (microvesicles, D). Mean (E) and mode (F) EV size. Data are presented as mean ±SEM, and analysed by one- or two-way ANOVA, or Kruskal-Wallis test, as appropriate, *p<0.05 in Sidak's post-hoc test.

6.3.4 SCI plasma EVs localise to APR-associated organs

With the exception of the very early time point at 2 hours, plasma EV size and concentration appeared largely unaffected by injury. However, SCI may still have induced a change in their functionality. Therefore, the behaviour of the circulating EVs were then investigated. First, it was determined to which organs EVs localise *in vivo* after SCI. EVs were isolated from platelet-free plasma collected 2 hours post-injury and were dual labelled with fluorescent membrane dye PKH67 and by transfection with *cel*-miR-39-3p. Labelled EVs were injected into naïve mice and tissue was collected 30 minutes later for analysis.

Fluorescent microscopy revealed PKH67+EV puncta in the liver, spleen and lung, which were not observed in control animals that received an injection of dye alone (Figure 6.6A). This correlated with the qPCR analysis; the non-murine transcript *cel*-miR-39-3p was also detected in these organs (Figure 6.6B). No expression of the transcript was detected in any of the control tissues collected and so have not been included for clarity. A signal for *cel*-miR-39-3p was detected in the spinal cord itself, however subsequent experiments indicate that this is not SCI-specific and is most likely due to EVs in the blood trapped in the spinal cord (data not shown).

To evaluate whether the phenotype of the EVs affect their biodistribution, the relative load of SCI plasma EVs in peripheral organs was compared to the load of EVs isolated from naïve plasma. There was a significantly reduced signal from SCI plasma EVs compared to naïve EVs in the liver (Figure 6.6Ci; student's unpaired t-test, $p<0.01$), but not in the spleen (Figure 6.6Cii; student's unpaired t-test, $p=0.199$), nor in the lung (Figure 6.6Ciii; student's unpaired t-test, $p=0.907$). qPCR analysis of the EVs themselves revealed equal transfection efficiency of the transcript, confirming equal amounts of EV-associated transcript were administered in each group (Figure 6.6Civ; student's unpaired t-test, $p=0.724$).

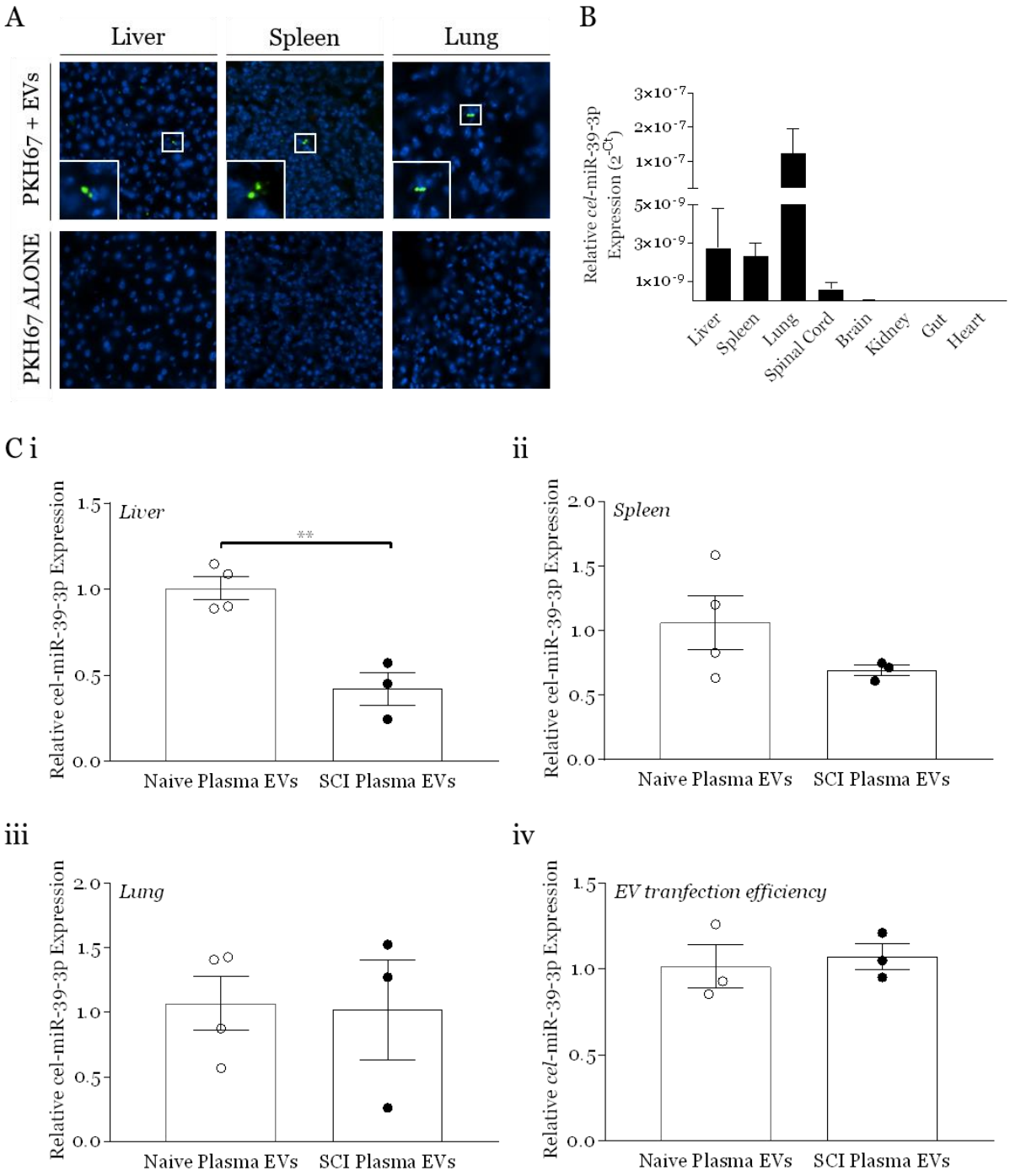


Figure 6.6 *In vivo* biodistribution of SCI plasma EVs. EVs were isolated by ultracentrifugation from platelet-free plasma, collected from SCI mice 2 hours post-injury. SCI plasma EVs were dual labelled with fluorescent membrane marker PKH67, and by transfection of *C. Elegans* specific nucleic acid *cel*-miR-39-3p. Dual labelled EVs were then intravenously injected into naïve mice (n=5) and tissue was collected 30 minutes later. The presence of PKH67+ EV puncta were detected in peripheral organs by fluorescent microscopy; naïve mice injected with free PKH67 dye were used as controls (A). Expression of *cel*-miR-39-3p was measured in organs by qPCR (B). EVs collected from naïve and SCI mice, 2 hours post-injury, were labelled with *cel*-miR-39-3p and intravenously injected into naïve mice (n=3-4). Fresh tissue was collected 30 minutes later and relative expression of the *cel*-miR-39-3p in the liver (i), spleen (ii) and lung (iii), and the EV transfection efficiency (n=3 technical repeats) was determined by qPCR. Data are presented as mean ±SEM and analysed by student's unpaired t-test, **p<0.01.

6.3.5 SCI plasma EVs do not induce inflammation, in vitro

To determine whether SCI plasma EVs had any pro-inflammatory effect, human plasma EVs were incubated with human PBMCs and expression of pro-inflammatory genes was evaluated. Expression of IL-1β (Figure 6.7A), TNF (Figure 6.7B), and CXCL1 (Figure 6.7C) was unchanged after incubation with naïve plasma EVs and SCI plasma EVs, compared to saline alone.

It has previously been shown that EVs can exacerbate existing inflammation (Hazleton et al. 2017). Therefore, PBMCs were pre-treated with naïve or SCI plasma EVs overnight and then incubated with LPS + IFN-γ for 6 hours. For all genes analysed, inflammatory challenge induced a significant increase in expression, however this was independent of EV incubation.

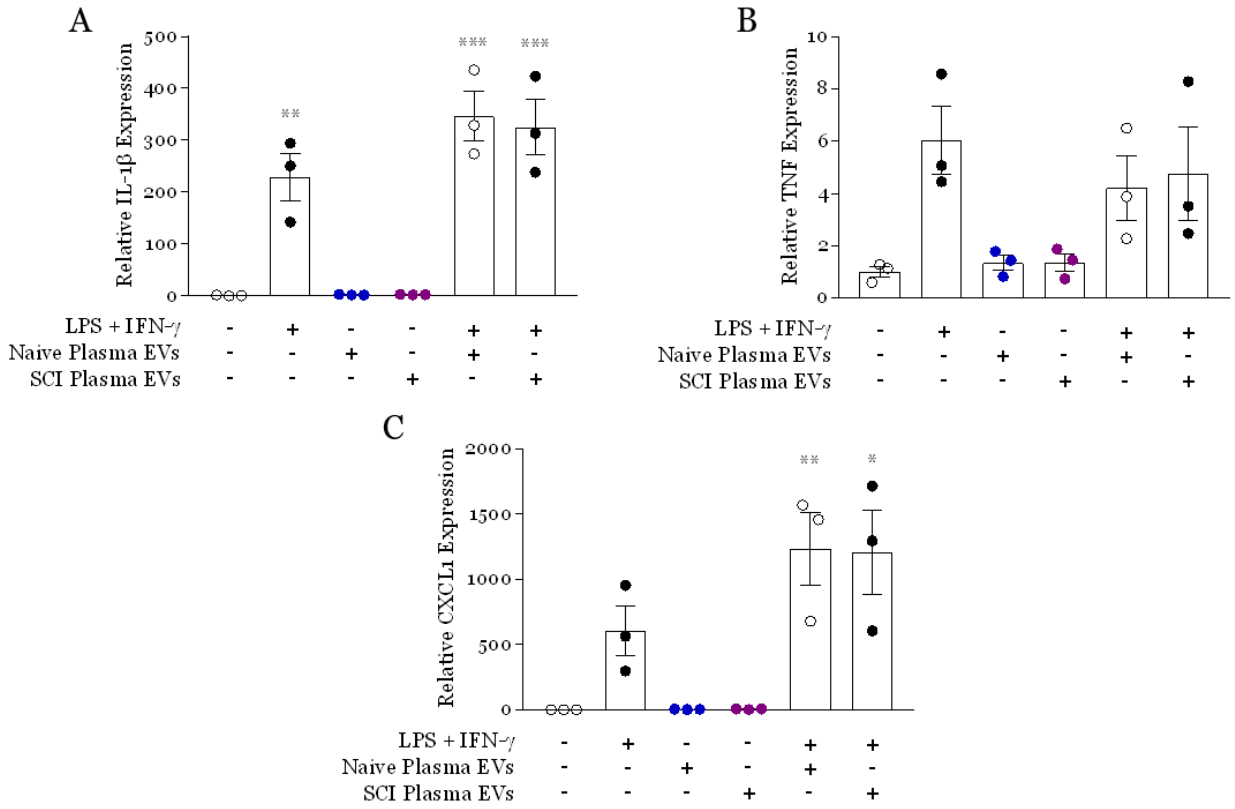


Figure 6.7 Expression of inflammation-associated genes in PBMCs incubated with human SCI plasma EVs. PBMCs were isolated from the blood of healthy male donors (n=3). Cells were incubated for 6 hours with saline, LPS + IFN-γ, naïve plasma EVs from healthy male donors or SCI plasma EVs from male SCI patients upon admission. A subset of cells was pre-treated with naïve or SCI plasma EVs overnight, before challenge with LPS + IFN-γ for 6 hours. RNA was then extracted from cells and relative expression of IL-1β (A), TNF (B) and CXCL1 (C) was determined by qPCR. Data are presented as mean ±SEM, and were analysed by one-way ANOVA. *p<0.05 **p<0.01 ***p<0.001 with Sidak's post-hoc test.

6.3.6 SCI plasma EVs alter the hepatic gene expression profile, in vivo

The inflammatory potential of SCI plasma EVs was then investigated *in vivo*. EVs were isolated from the plasma of animals with 70kD SCI and injected into naïve mice and tissue was collected for analysis of inflammatory markers. Naïve plasma EVs were injected into naïve mice as control.

Given the significant increase in plasma EV concentration 2 hours post-SCI, EVs were isolated from donor animals at this time point. In tissue collected from recipient animals 30 minutes after administration, hepatic IL-1β (Figure 6.8A; unpaired student's test, p=0.533), TNF (Figure 6.8B; unpaired student's t-test, p=0.789) or CXCL1 expression (Figure 6.8C; unpaired student's t-test, p=0.281) was unaffected. A trending increase was observed in CXCL10 expression with SCI plasma EVs, however this was not statistically significant (Figure 6.8Aiv; student's unpaired t-test, p=0.0627).

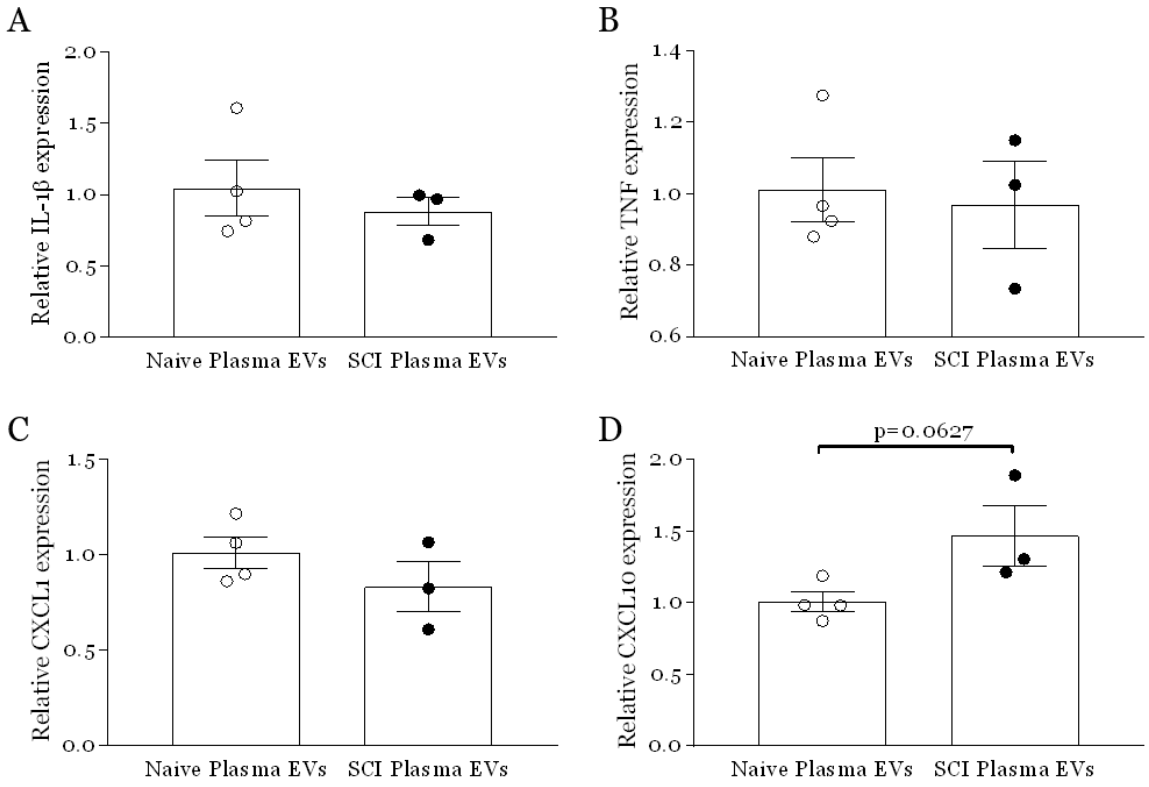


Figure 6.8 Hepatic expression of pro-inflammatory genes in response to naïve and SCI plasma EVs, 30 minute time point. Plasma EVs were isolated from donor animals with SCI 2 hours post-injury, and intravenously injected into naïve animals (n=3/group). Fresh liver of recipient animals was collected 30 minutes after administration. Relative, hepatic expression of IL-1β (A), TNF (B), CXCL1 (C) and CXCL10 (D) were determined by qPCR. Data are presented as mean ±SEM, and analysed by student's unpaired t-test.

EV and tissue collection were then altered; plasma EVs were collected from donor animals either 2 or 6 hours post-SCI, and tissue was collected from recipient naïve animals 6 hour after administration. Relative expression of hepatic IL-1β was significantly decreased with SCI plasma EVs (Figure 6.9A; two-way ANOVA, injury EVs $p<0.001$, tissue collection time $p=0.987$). By contrast, SCI plasma EVs induced a significant increase in TNF expression in the liver (Figure 6.9B; two-way ANOVA, injury EVs $p<0.05$, tissue collection time $p=0.482$). Hepatic CXCL1 (Figure 6.9C; two-way ANOVA, injury EVs $p=0.847$, tissue collection time $p=0.497$) and CXCL10 (Figure 6.9D; two-way ANOVA, injury EVs $p=0.358$, tissue collection time $p=0.276$) were unaffected by SCI plasma EVs. These data show that SCI plasma EVs are able to alter the hepatic expression profile of inflammation-associated genes, in otherwise uninjured animals.

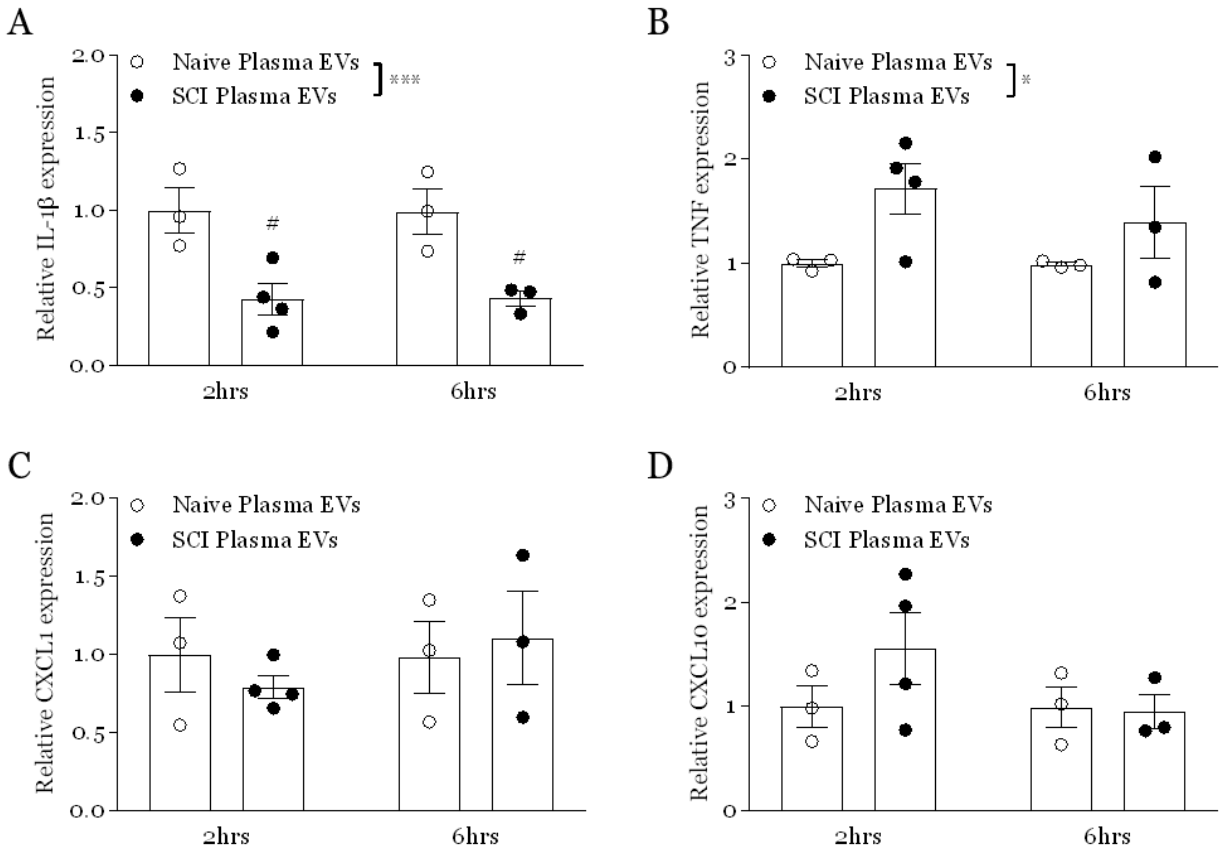


Figure 6.9 Hepatic expression of pro-inflammatory genes in response to naïve and SCI plasma EVs, 6 hour time point. Plasma EVs were isolated from donor animals with SCI at 2 or 6 hours post-injury, and intravenously injected into naïve animals (n=3-4/group). Fresh liver of recipient animals was collected at 6 hours after administration. Relative, hepatic expression of IL-1β (A), TNF (B), CXCL1 (C) and CXCL10 (D) were determined by qPCR. Data are presented as mean ±SEM, and analysed by two-way ANOVA. *p<0.01 ***p<0.001 main effect of injury EVs, #p<0.05 in Sidak's post-hoc test.

6.4 Discussion

In this thesis, it has been consistently shown that acute SCI induces an APR, which, in turn, influences the inflammatory response in the spinal cord (Campbell et al. 2005; Campbell et al. 2008b; Yates et al. 2021). Therefore, it has been proposed that the APR presents itself as a useful therapeutic target (Yates et al. 2021). However, the mechanism by which this response is triggered remains unclear. In this chapter, EVs were examined as potential mediators of the APR after SCI. The effect of injury on the circulating EV population was investigated in human SCI patients and a contusion rodent model of injury, during the acute phase of injury. In addition, the ability of these plasma-derived EVs to induce an inflammatory response was evaluated. Data presented here indicate that there is an EV response to injury; although no differences were observed in the human cohort, an increase in EVs was observed in the mouse model, 2 hours post-SCI compared to naïve baseline. Moreover, SCI plasma EVs localised to peripheral organs associated with the APR, and were able to alter inflammatory gene expression in the liver, *in vivo*, indicating a change in functionality. Although, these results appear to be due to injury, rather than SCI *per se*.

6.4.1 SCI induced an increase in plasma EVs, 2 hours post-injury

Previous work from our group with both animal models and clinical studies, has demonstrated that injury to the brain causes a significant increase in plasma EV concentration (Couch et al. 2017a; Dickens et al. 2017; Hazleton et al. 2017). However, data in this chapter suggests that this CNS injury-induced increase does not occur during the acute phase of SCI. In the clinical samples examined, there was no difference in plasma EV concentration, between SCI patients upon admission and healthy controls. This may be due to the heterogeneity of SCI patient presentation, although there were no correlations with NISS or ASIA score, or level of injury. Variations in blood processing and sample collection have also been shown to impact EV measurements, as red blood cells and platelets are easily activated and readily shed EVs (Coumans et al. 2017). No correlation was observed between plasma EV concentration and time from injury to sample collection, however the time taken for the blood to be processed after collection was highly variable and often not recorded, which may be confounding results.

That said, the results from clinical samples was mostly confirmed in our contusion model of SCI. In contrast to the patient data, a significant increase was observed in SCI animals compared to naïve baseline, 2 hours post-injury. This may be due to the time point evaluated; 2 hours is often too early to resolve in humans, for example, in this chapter, the earliest blood collection was 4.5 hours post-injury. At later time points in the acute phase, SCI induced a decrease in plasma-derived EVs. This is consistent with Khan et al. (2020) who reported a significant reduction in plasma EVs in SCI animals compared to naïve, 1 day post-injury. This result is in stark contrast to our previous work with acute brain injuries. The brain and spinal cord differ in anatomical structure and their responses to neurotrauma, which may impact EV release (Campbell et al. 2002; Schnell et al. 1999a). For example, greater vascular breakdown occurs after injury to the spinal cord compared to the brain (Schnell et al. 1999a). The disruption to the vasculature significantly reduced blood flow (Soubeyrand et al. 2013) may restrict release of factors from the spinal cord into the peripheral circulation. Certainly, reperfusion of the grey matter does not occur for the first 24 hours after injury (Fassbender et al. 2011). Therefore, EV signalling may play alternative roles after injury to different components of the CNS.

Clausen et al. (2014) reported a correlation between plasma microvesicle number and infarct size after stroke, and data in Chapter 4 showed that the SCI-induced APR is injury severity dependent. Here, an increase in circulating EVs with increasing severity seemed to be present after SCI at T9. However, this was not statistically significant; post-hoc power analysis revealed that an additional 1, 3 and 9 animals would be required for the 30kD, 70kD and 100kD groups respectively, to reach significance. Although, when analysed as a distribution of size (10nm intervals), SCI of each severity induced a significant increase, compared to sham. Further analysis of this result suggested that SCI induced an increase in microvesicles (145-500nm), specifically. This was also evident with SCI induced at T2; there was no effect of SCI on total plasma EV concentration, however when analysed at 10nm intervals, 70kD SCI was significantly different from both sham and 30kD SCI groups. Similarly, AUC revealed that this can be attributed to a trending increase in microvesicles. Microvesicles are EVs which are shed from the plasma membrane of cells in a budding mechanism, as opposed to apoptotic bodies and exosomes that are released through blebbing and the

endolysomal pathway, respectively (Budnik et al. 2016). It is not clear why there would be a shift towards microvesicle shedding specifically. Microvesicle release is mediated by influx of calcium, which can occur after shear stress (Pasquet et al. 1996). As such, this increase may reflect the axonal shearing and physical damage to the spinal cord during the primary phase of injury (Alizadeh et al. 2019). Although, it must be noted that calcium influx can also contribute to exosome release (Messenger et al. 2018). Given that EVs of different subpopulations exhibit distinct cargo (Arraud et al. 2014; Willms et al. 2018), it is likely that an increase in circulating microvesicles will have specific downstream functional effects, which may be relevant to SCI pathophysiology. Future work should include isolation and characterisation of the different subtypes in the SCI plasma EV population.

Whilst circulating EVs sized 145-500nm encompasses microvesicles, there is significant overlap in size between the different subpopulations of EVs (Willms et al. 2018). Therefore, particles of this size will also include small apoptotic bodies and large exosomes. As such, it cannot be concluded that SCI induces an increase in microvesicles based on the data presented in this chapter alone. Previous studies have reported changes in plasma microvesicles after neurotrauma based on size parameters, although this is often in conjunction with Annexin-V reactivity (Kumar et al. 2017; Tian et al. 2015). Annexin-V is a protein that binds to phosphatidylserine (PS) on the vesicular membrane (van Genderen et al. 2008). It is commonly conjugated to a fluorophore for use in flow cytometry and is proposed to identify microvesicles (Kumar et al. 2017; Rong et al. 2018; Tian et al. 2015). However, PS is also found on apoptotic bodies (Poon et al. 2019) and exosomes (Matsumura et al. 2019), which can skew results. In turn, Connor et al. (2010) reported that the majority of circulating microvesicles fail to bind to Annexin-V, further indicating it is not an accurate way of detecting microvesicles. Overall, specific markers for distinguishing between subtypes of EVs are currently lacking (Jeppesen et al. 2019), which makes these types of analysis difficult and would hamper studies of changes in plasma derived EVs after SCI.

Interestingly, SCI at T9 induced a greater increase in total plasma EV concentration, compared to SCI at T2, indicating that the level of injury has an effect on EV release into the circulation. This

may be due to the extent of inflammation in the spinal cord; as seen in Chapter 4, injury induced at T9 resulted in greater expression of pro-inflammatory cytokines in comparison to injury at T2, which are known to increase EV release (Balusu et al. 2016). In addition, greater BSCB breakdown was evident with T9 injury, therefore this increase in plasma EV concentration may reflect greater vascular damage in the spinal cord. Certainly, as highlighted here, the number of circulating EVs appears to increase with increasing injury severity. However, the origins of these EVs remain unknown. The circulating EV population is very heterogeneous; even within the classifications of apoptotic bodies, microvesicles and exosomes, subpopulations have been reported to exist (Willms et al. 2018). Given the large quantity of EVs in plasma, which are predominantly platelet-derived (Arraud et al. 2014), it is possible that SCI may induce an increase in CNS-derived EVs that is not evident in the total EV concentration. Therefore, enriching for CNS-specific EVs could be more informative (Mustapic et al. 2017). Previous studies have reported CNS surface markers on EVs, such as neuron-specific enolase and L1CAM, which have been utilised as biomarkers for traumatic injuries (Karnati et al. 2019). Indeed, Nekludov et al. (2014) and Kumar et al. (2017) utilised surface markers to report increases in CNS endothelial- and microglial-derived EVs after TBI. Therefore, SCI-induced differences may be detected in the number of CNS-derived EVs, specifically. However, there are concerns with regards to the specificity of these markers (Marangos et al. 1980; Tolan et al. 2013), which must be considered.

Several methodological challenges exist in the field of EV research. Indeed, whilst there are guidelines as to the minimum requirements for the study of EVs (Thery et al. 2018), there is currently no consensus on the best isolation and measurement techniques for accurate analysis. Here, ultracentrifugation at 120,000*g* was used to pellet EVs, which allows for the simultaneous isolation of exosomes and microvesicles (Thery et al. 2006). As it is unknown whether one population plays a more significant role in neurotrauma than the other, it was thought to be beneficial to include both of them in this study. This isolation method has been used by our group previously and yielded positive results (Hazleton et al. 2017). However, there are issues with purity. Contamination of samples with plasma-derived proteins and lipoproteins are unavoidable and known to interfere with quantification (Brennan et al. 2020). As a result, any SCI-mediated changes

in plasma EV concentration may be obscured. In turn, NTA was used to measure the size and concentration of EV samples. As a light scattering technique, inaccuracies can arise from other scattering sources such as aggregates of plasma proteins (McNicholas et al. 2017), although relative differences should still allow for conclusions. Alternative methods of EV isolation, such as size exclusion chromatography and affinity capture, as well as measurement techniques, such as tunable resistive pulse sensing and modified flow cytometry are available (Brennan et al. 2020; Coumans et al. 2017; Hartjes et al. 2019). However, each has its own pitfalls, which highlights that the technology may not have advanced enough yet, to accurately determine the effect of SCI on the circulating EV population.

6.4.2 SCI plasma EVs and the APR

It is currently unknown whether the changes in EV number, or the physicochemical properties of the EVs are responsible for inducing the APR after traumatic CNS injury. Therefore, it is possible that although changes in plasma EV concentration observed in the clinical or rodent samples were minimal, the biocomposition and functionality of the circulating EVs may be altered after SCI, which still contributes to the initiation of the peripheral response. Certainly, data in this chapter demonstrates that SCI plasma EVs localise to organs associated with the APR. Dual labelled EVs isolated from the plasma of SCI animals were detected in the liver, lung and spleen, as evident by expression of the synthetic *C. Elegans* miRNA. This result was confirmed with microscopy revealing fluorescent EV aggregates engulfed by cells in these organs. This is consistent with previous studies (Dickens et al. 2017; Akbar et al. 2017; Couch et al. 2017b) and is most likely due to their endogenous filtering nature. Significant accumulation was detected in the lung, which may be clinically relevant because a large proportion of SCI patients develop lung pathologies (Burns 2007; Jackson and Groomes 1994), however it seems more likely due to EV aggregation which is known to occur when particles are isolated by ultracentrifugation (Linares et al. 2015; Nordin et al. 2015). Interestingly, when the effect of SCI on EV biodistribution was investigated, it was revealed that fewer SCI plasma EVs accumulated in the liver, compared with plasma EVs from naïve animals. Analysis of expression in the EVs themselves confirmed that transfection efficiency was comparable

for both naïve and SCI plasma EVs, and therefore this result is not due to methodology. It is not clear whether this is because of increased EV clearance by the liver or decreased uptake. However, this does suggest that there is phenotypic change in the plasma EVs after SCI which causes them to behave differently *in vivo*.

It has been shown that circulating EVs adopt an inflammatory phenotype after CNS injury (Drago et al. 2017; Hazleton et al. 2017) and can initiate inflammation both *in vitro* (Couch et al. 2017a) and *in vivo* (Couch et al. 2017b). As such, adoptive transfers of SCI plasma EVs were performed, to determine any pro-inflammatory effect. Incubation of PBMCs with plasma EVs, whether from SCI patients or healthy controls, had no effect on the expression of pro-inflammatory genes. Although this is inconsistent with models of brain injury, the result is consistent with Brewster et al. (2020) who showed that SCI plasma EVs did not induce pro-inflammatory cytokine expression in endothelial cells. This suggests that EVs may not be potent enough on their own to induce an inflammatory response. However, pre-treatment with EVs similarly had no effect when cells were challenged with LPS + IFN-γ.

In contrast to the *in vitro* data, the *in vivo* data indicate that SCI plasma EVs can alter the hepatic expression of inflammation-associated genes. Surprisingly, adoptive transfer of SCI plasma EVs decreased hepatic IL-1β expression, which would suggest EVs may have an anti-inflammatory effect. It could be of interest to investigate the expression of anti-inflammatory cytokines, such as IL-10 and IL-4, in the recipient animals. Simultaneously, SCI plasma EVs induced an increase in TNF expression in the liver. Whilst this does not necessarily mimic the hepatic gene expression profile after SCI, it does show that injury-associated plasma EVs are physiologically different from naïve plasma EVs, and that they can influence peripheral inflammation, which warrants further investigation.

Some experimental limitations were identified in these adoptive transfer studies. Firstly, the method of EV isolation remains an issue. Ultracentrifugation has been shown to reduce the functionality of EVs (Mol et al. 2017), most likely due to the high speed causing structural damage. As such, the lack of positive response with SCI plasma EVs may be due to ultracentrifugation-

mediated damage. That being said, this technique has been used previously by our group and functionality was still evident (Hazleton et al. 2017). Alternatively, the number of EVs administered may have been too low, or the timing of EV collection may not be optimal. EV release continues days after SCI (Khan et al. 2020), in which case pooling EVs from across multiple time points for future adoptive transfer experiments may be more informative, although data presented here suggests the EV response is very acute (≤2 hours). Finally, no EV positive control was used; *in vivo* changes in gene expression were subtle and so a control group that is administered EVs from sources known to induce inflammation, such as from activated cells (Couch et al. 2017b) or brain injured patients (Couch et al. 2017a; Andrews et al. 2016) should be included. In this way, SCI plasma EV functionality can be more accurately assessed.

6.5 Conclusions from this chapter

SCI induces a hyperacute change in the circulating EV population, as evidenced by increased plasma EVs in our rodent model, 2 hours post-injury. Injury-associated plasma EVs localise to peripheral organs associated with the APR, and alter the hepatic inflammatory gene expression profile in otherwise uninjured animals. Thus, circulating EVs may contribute to the systemic response to SCI, which requires additional investigation.

Chapter 7: General discussion

In response to injury or infection, the APR mobilises leukocytes, such as neutrophils, which clear debris, eliminate pathogens and initiate wound healing (Anthony and Couch 2014). However, the APR induced by traumatic injury to the brain and spinal cord can contribute to the non-resolving inflammation in the CNS, which, in turn, contributes to secondary damage (Campbell et al. 2003; Campbell et al. 2005; Campbell et al. 2008b). Indeed, an excessive APR is associated with worsened patient outcomes after a number of different types of traumatic CNS injury (Kesani et al. 2014; Sun et al. 2016). Previous work from our laboratory has shown that the APR influences the histopathology of the spinal cord (Campbell et al. 2005; Campbell et al. 2008b; Davis et al. 2005), suggesting it may be a promising therapeutic target to limit damage and improve functional recovery. However, the relationship between the spinal cord and the peripheral inflammatory response, including the initiation signal, is poorly understood, and must be investigated for effective treatment development. As such, the purpose of this thesis was to explore the systemic response to spinal cord injury, and its contribution to outcome.

In this thesis, I have discovered that:

1. SCI induces a robust APR, which, when targeted with exogenous IL-1RA, suppresses the inflammatory response in the spinal cord and in the liver (Yates et al. 2021).
2. The character of the SCI-induced APR is influenced by the level and severity of the injury.
3. SCI induces a distinct metabolite profile in the spinal cord and peripheral tissues that is independent of the peripheral injury induced in the sham surgery at later time points.
4. There is an acute increase in EV number after sham or SCI, compared to naïve baseline, and the EVs from injured animals generate a distinct cytokine expression profile in the liver.

Taken together, the data presented in this thesis demonstrate that SCI induces significant systemic changes, as evidenced by increased hepatic expression of pro-inflammatory molecules, leukocyte mobilisation and metabolite disturbances (Figure 7.1). These changes are dependent on the severity and location of the spinal cord lesion, which highlights an important relationship between the CNS and the periphery, and may provide diagnostic and prognostic value. Importantly, suppression of the APR with IL-1RA, reduced neutrophil recruitment to the spinal cord, indicating that spinal cord

inflammation can be indirectly attenuated by targeting the peripheral inflammation. Moreover, SCI induces a hyperacute increase in circulating EVs, which precedes the hepatic inflammatory response, and, thus, may be the initiation signal for the APR. Indeed, the data presented here shows that injury-associated plasma EVs are physiologically different from naïve plasma EVs, and can modify inflammation in the liver. Collectively, the work from this thesis indicates that the SCI-induced APR does contribute to the outcome of the injury, and, thus, is a promising therapeutic target for acute SCI. Despite this, it is also clear that the pattern of the response is more complex than perhaps previously appreciated. Some general statements, however, can be made, which will be discussed here.

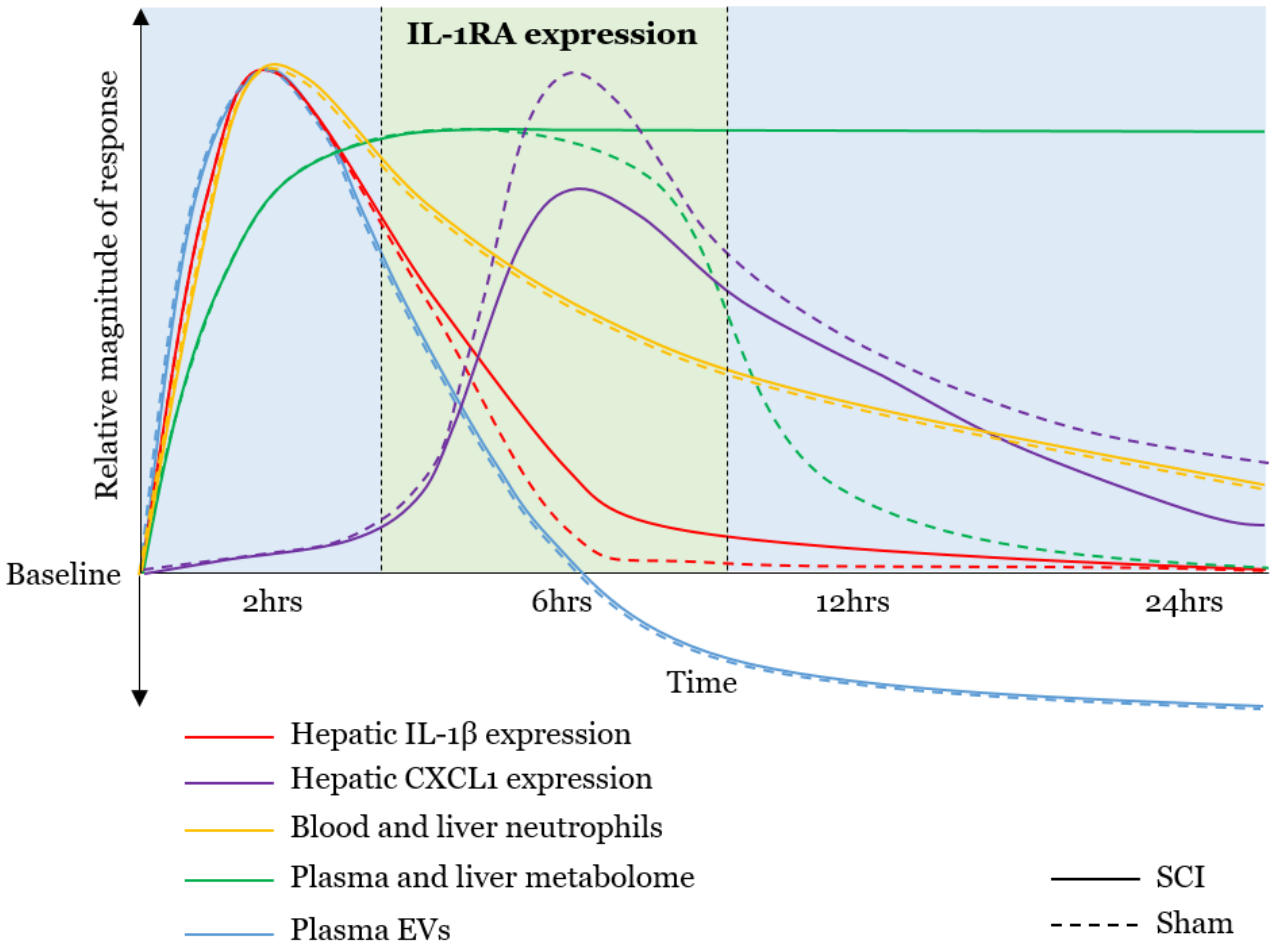


Figure 7.1 Visualisation of SCI-induced systemic response. Summary of the significant systemic changes induced by SCI, as demonstrated in this thesis: hepatic IL-1β (red) and CXCL1 (purple) expression, peripheral neutrophil mobilisation (yellow), peripheral metabolome (green) and plasma EVs (blue). Sham animals are designated dotted lines; SCI animals are designated solid lines. The period of significantly increased hepatic IL-1RA expression is highlighted in green.

7.1.1 The role of the APR in SCI

Peripheral inflammation after SCI is well documented, and is associated with poor patient outcomes (Jogia et al. 2021; Kesani et al. 2014; Sun et al. 2016). Numerous studies have demonstrated that inhibition of the APR reduces CNS inflammation, in animal models of stroke (Clausen et al. 2014), brain injury (Blomster et al. 2013a; Campbell et al. 2003; Campbell et al. 2007; Chio et al. 2010) and SCI (Campbell et al. 2008b; Genovese et al. 2006). In line with this, it is shown in this thesis that suppression of peripheral inflammation reduced leukocyte recruitment to the spinal cord (Yates et al. 2021), which is known to contribute to secondary damage (Neirinckx et al. 2014). Collectively, these studies would thus indicate that the APR after SCI is deleterious, and may be amenable to intervention. However, the role of the APR after traumatic CNS injuries is complex and some studies have generated contradictory results (Campbell et al. 2008b; Davis et al. 2005).

In contrast to the above conclusion, it has also been shown that post-conditioning with systemic LPS can reduce leukocyte infiltration of the CNS after traumatic injury (Bingham et al. 2013; Davis et al. 2005), suggesting that exacerbation of the APR is also neuroprotective. It is unknown the mechanism by which this would occur; it may an attempt by the APR to redistribute leukocytes away from the CNS lesion. Data from Brennan et al. (2019) suggest that neutrophils mobilised after SCI are from a fixed pool, and an inverse correlation between spinal cord and liver leukocyte density was observed here, which would support this concept. However, Davis et al. (2005) showed no corresponding increase in liver leukocyte density in injured animals with LPS treatment. Bingham et al. (2013) attributed their results to endotoxin tolerance. Endotoxin tolerance is a known phenomenon; TLR4 stimulation with LPS downregulates MyD88-mediated signalling, therefore inducing an anti-inflammatory effect (Piao et al. 2009b). Both TLR4 and IL-1 signalling are dependent on the MyD88 pathway (Cohen 2014). Therefore, LPS-mediated inhibition of MyD88, via TLR4, may be suppressing the peripheral IL-1β response, which is known to contribute to lesion pathology (Yates et al. 2021; McColl et al. 2007), and may explain the contradictory results. Naturally, this hypothesis is confounded by the fact that the animals in these previous studies had

no prior TLR4 stimulation. However, investigating the relationship between systemic TLR4 and IL-1 signalling after SCI may fortify our conclusion that the APR is a negative contributor to outcome.

The inverse relationship between SCI severity and some markers of peripheral inflammation was a surprising result. Given that suppression of the APR with IL-1RA reduced neutrophil recruitment to the spinal cord, it was hypothesised that the magnitude of the systemic inflammatory response would correlate positively with injury severity. However, unexpectedly, the opposite was observed (Figure 7.2). It is possible that there is a ceiling effect, and, above a certain magnitude, the APR is no longer the driver of the leukocyte recruitment to the CNS. Certainly, dose-response curves have shown a maximal effect of chemokine-mediated chemotaxis (Gomez-Cambronero et al. 2003). In addition, there may be another factor, which is influencing the extent of neutrophil infiltration. Intraspinal cytokines, including IL-1β and CXCL1, are known to mediate neutrophil infiltration (Campbell et al. 2003; Pineau et al. 2010). A severity-dependent increase in expression of these cytokines was observed in the spinal cord, which correlated with neutrophil density. Therefore, it can be proposed that it is a combination of the peripheral and central inflammation, which mediates leukocyte recruitment to the spinal cord after injury. In which case, the elevated neutrophil and macrophage density in the liver after mild injury, compared to severe, may instead be a consequence of APR activation combined with a weaker inflammatory signal from the spinal cord.

It is important to note that, whilst hepatic cytokine expression was decreased after severe injury compared to mild, the APR induced by all of the variations of SCI explored in this thesis was still significantly increased above naïve baseline. Therefore, the peripheral inflammation remains a therapeutic target for treatment development, independent of severity. For example, hepatic CXCL1 expression was reduced in severely injured animals compared to mild, yet expression was significantly increased compared to naïve, and so anti-CXCL1 treatment is still likely to have a beneficial effect in both severity models. In addition to its apparent influence of secondary damage in the spinal cord (Yates et al. 2021), the injury-induced systemic inflammatory response can also cause damage to peripheral organs (Bao et al. 2009; Gris et al. 2008). As such, attenuating SCI-induced peripheral inflammation can have multiple benefits.

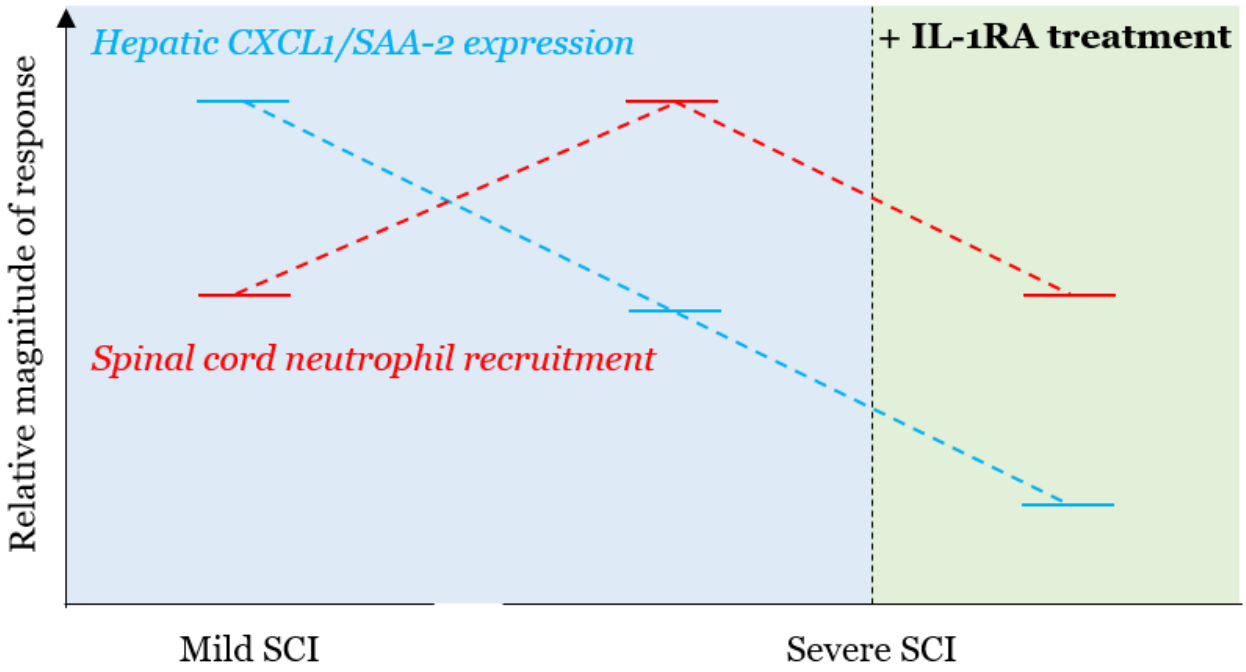


Figure 7.2 Relationship between the APR and spinal cord neutrophil recruitment. Summary of the pattern of hepatic CXCL1 and SAA-2 expression (blue) and concurrent neutrophil recruitment to the spinal cord (red) after mild SCI, severe SCI, and severe SCI + IL-1RA (highlighted in green.)

In addition to being a therapeutic target, the nature of the APR may also serve as a diagnostic and/or prognostic marker. SCI is currently diagnosed by neurological assessment (ASIA score) and MRI imaging (van Middendorp et al. 2011). However, the accuracy of ASIA scoring can be hindered by spinal shock and multi-trauma (Alizadeh et al. 2019), and, although MRI imaging can reveal structural damage (Miyanji et al. 2007), it is largely not predictive of functional outcomes (van Middendorp et al. 2011; Fouad et al. 2021). Here, the pattern of systemic inflammatory and metabolic changes was found to be dependent on the severity and location of the lesion. Therefore, interrogation of the peripheral response to SCI may provide useful information about the extent of damage to the spinal cord, which traditional diagnostic tests cannot provide (Bozzo et al. 2011). Certainly, Jogia et al. (2021) have previously shown that the extent of acute neutrophilia correlated with injury severity, and was predictive of poor neurological outcome. In this thesis, it is demonstrated that metabolite analysis of patient plasma, collected upon admission, is predictive of improvement in ASIA score before discharge. As such, metabolomic analysis of patient plasma

could provide an accurate, and rapid, prognosis. Indeed, data collected from the rodent model indicates that this may be achieved with samples collected as early as 12 hours after injury, although NMR-based platforms still need to be developed for routine clinical use.

The SCI-induced APR is multifaceted, and elucidating the timing of the different factors involved may assist in identifying novel therapeutic targets. Indeed, in this thesis, the mismatch between hepatic IL-1β and IL-1RA expression led to the investigation of IL-1RA as a treatment strategy. Here, by utilising samples collected for the characterisation of the APR, the systemic inflammatory response can be directly compared to the peripheral metabolome and circulating EV population. As such, it is apparent that the hyperacute increase in plasma EV concentration occurs early, prior to some markers of the APR, which suggests that EVs may be the initiation signal for the SCI-induced peripheral response. It would be of interest to inhibit EV release immediately following SCI, by injecting altenusin into the spinal cord (Dickens et al. 2017). By contrast, SCI-specific metabolite changes were not observed until later time points in the acute phase (12-24 hours). Given that metabolic disturbance in the liver is associated with inflammation (Pagadala et al. 2012; Rankin et al. 2017), these SCI-induced metabolite changes could be attributed to the APR. Critically, the aspects of the systemic response investigated in this thesis, preceded significant leukocyte recruitment to the spinal cord, which highlights a new "therapeutic window". As such, the inflammatory, metabolic and EV responses could all be exploited to improve outcomes.

7.1.2 Hepatic IL-1β as a therapeutic target for acute SCI

An interesting finding was the relationship between IL-1β and its endogenous antagonist IL-1RA, during the acute phase of SCI. IL-1β is a potent inflammatory molecule and so its physiological action is tightly regulated by IL-1RA (Allan et al. 2005). However, following trauma to the CNS, this balance becomes dysregulated. In the spinal cord, IL-1β expression is significantly elevated within minutes, yet corresponding IL-1RA expression is delayed (Liu et al. 2008). Evidently, this occurs in the periphery as well; hepatic IL-1β expression was greatest at 2 hours post-injury, whilst IL-1RA expression peaked 6 hours post-injury. This could be attributed to differences in synthesis, as mature IL-1β is rapidly produced from pro-IL-1β, which is already present in the cytosol, whereas

IL-1RA must be produced from the RNA level, which is slower by comparison (Figure 3.1 (Allan et al. 2005; Dinarello 2018)). Therefore, there are several hours when IL-1β signalling is occurring, unregulated. Moreover, IL-1β expression in the liver was found to be injury severity dependent. In a stroke model, McColl et al. (2007) showed that systemic administration of IL-1β exacerbated ischemic damage in a dose-dependent manner. As such, peripheral IL-1β after SCI must contribute to lesion progression. Taken together, data in this thesis adds to the body of evidence that IL-1 signalling plays a major pathogenic role in neuroinflammatory insults, and is a promising therapeutic target.

The work presented here indicates that inhibition of IL-1β-induced inflammation with IL-1RA can suppress the inflammatory response to the spinal cord and the liver after traumatic injury. Traditional broad-spectrum anti-inflammatories, such as glucocorticoids, are unsuitable to treat SCI as they often have severe side effects, such as immunosuppression. This is particularly problematic for patients, who often develop SCI-IDS and are already at risk of infections (Failli et al. 2012; Riegger et al. 2009). Therefore, specific targeting of IL-1β presents a novel therapeutic strategy. Here, our results show that the early systemic administration of IL-1RA during the acute phase of SCI significantly reduced neutrophil infiltration of the spinal cord. Given that neutrophils are largely considered detrimental to the CNS (Moxon-Emre and Schlichter 2011; Neirinckx et al. 2014), this discovery suggests that suppressing hepatic IL-1β-signalling may improve functional outcomes. As such, long-term effects on IL-1RA on SCI lesion pathology and function are warranted.

The rationale for exploring IL-1RA as a therapeutic strategy was the SCI-induced increase in hepatic IL-1β expression following injury at T9. However, following a comparable injury at T2, IL-1β expression in the liver was suppressed, which suggests that IL-1RA treatment may not be as effective in higher level injuries. Previous studies that investigated the efficacy of IL-1RA in animal models of SCI, including in this thesis, induced injury at low thoracic levels only (T5-9) (Hasturk et al. 2015a; Yates et al. 2021; Zong et al. 2012). However, it is known that the level of injury in SCI patients can influence acute care, for example whether or not catecholamine treatment is required

(Ahuja et al. 2017a; Hasturk et al. 2015a; Pruss et al. 2017; Yates et al. 2021; Zong et al. 2012). Therefore, the effect of injury level on the peripheral response should also be taken into account for treatment development. This can have implications for translatability and the design of human clinical trials; the inclusion of patients with a range of injury levels could result in variable results and inaccurate conclusions. From this, it is of interest to evaluate acute IL-1RA treatment in our T2 SCI model.

Despite the benefits of targeting IL-1β in acute SCI, there are some limitations that need to be addressed. It has been shown that anti-IL-1β treatment can increase the incidence of infections (Salliot et al. 2009), as the ability of the immune system to co-ordinate a response to pathogens is impaired. As discussed above, this may be concerning due to SCI-IDS, and will need to be investigated to critically evaluate the risk-benefit balance, as infections increase patient morbidity (Failli et al. 2012). In addition, IL-1 signalling has been shown to stimulate regeneration by inducing proliferation (McPherson et al. 2011). This highlights that the timing and magnitude of the intervention are critical for effective treatments, which need to be explored more fully in animal models before progression to the clinic. A dose-response study should be completed in order to address some of these issues.

7.1.3 Brain vs. spinal cord

Whilst both constitute the CNS, there are a number of differences, both anatomical and functional, between the brain and spinal cord. Most notably in the context of this thesis, the central response to traumatic injury is markedly different between the two structures; injury to the spinal cord causes greater vascular breakdown, and increased microglial and neutrophil recruitment, compared to an equivalent injury to the brain (Schnell et al. 1999a). This appears to hold true for the peripheral response as well. Exacerbation of the APR with LPS attenuated neutrophil recruitment to the spinal cord after SCI (Davis et al. 2005), but increased infiltration of the brain after stroke (McColl et al. 2007). Here, many changes in inflammatory markers in our SCI model were in contrast to previous publications with brain injury models. For example, hepatic expression of SAA-2 was suppressed after severe SCI, however Wicker et al. (2019) reported an increase in

circulating SAA after TBI. Moreover, Campbell et al. (2003) showed a positive correlation between CXCL1 expression in the liver and the amount of IL-1β injected into the brain. Whereas, here, CXCL1 expression was reduced in the severe SCI animals, compared to mild. Understanding the divergence between the SCI- and TBI-induced APR is critical for directed treatment development. Indeed, suppression of the APR with the PPARα agonist fenofibrate reduced neutrophil recruitment to the brain in a model of inflammatory brain lesion (Dickens et al. 2017), but it was shown to be ineffective in reducing intraspinal inflammation in a model of SCI (Almad et al. 2011). As a result, although studies of brain trauma may provide some insight, it must be acknowledged that comparable traumatic injury to the spinal cord will result in a different downstream APR and, as such, results from SCI studies should be considered independently.

To our knowledge, there is no study directly comparing the APR following injury to the brain and the spinal cord, which may be due to difficulties in defining a comparable injury. Injection of the same amount of IL-1β into the CNS caused a greater inflammatory response and associated pathology in the spinal cord than the brain (Campbell et al. 2002; Schnell et al. 1999b). Therefore, any differences in the APR could be misleading; differences in the magnitude of systemic inflammation may reflect the severity of the CNS injury, rather than a tissue-specific effect. Normalising to the magnitude of leukocyte infiltration, BBB/BSCB breakdown, or cell death, may be required for a more accurate comparison of the peripheral responses.

The different peripheral responses after comparable injury to the brain and spinal cord is most likely due to dysregulation of the autonomic nervous system. Even with low level injuries, such as at T9, segments of the spinal cord from which preganglionic neurons of the sympathetic nervous systemic extend will be compromised, owing to inflammation extending rostral (and caudal) from the lesion site (Knerlich-Lukoschus et al. 2008). Therefore, SCI can disrupt innervation of peripheral immune organs, including the liver, spleen and adrenal glands, which does not occur after TBI/stroke, and can contribute to an augmented immune response (Monteiro et al. 2020; Pruss et al. 2017). For example, plasma concentration of the potent anti-inflammatory cortisol decreases after TBI (Kusmenkov et al. 2019), but increased after SCI (Pruss et al. 2017). Although

we did not observe an effect of SCI level or severity on plasma corticosterone and noradrenaline at the time points explored in this thesis, direct sympathetic signalling (Huan et al. 2017; Jung et al. 2000), and the loss thereof, may still play a significant role in the APR.

Considering the differences in CNS and peripheral inflammation, it is likely that SCI plasma EVs also have a different effect on the APR and spinal cord pathology, compared to TBI and stroke plasma EVs. Previous functional studies from our laboratory, and others, have consistently demonstrated that brain injury-associated EVs are pro-inflammatory (Couch et al. 2017a; Couch et al. 2017b; Dickens et al. 2017; Kumar et al. 2017). However, here, SCI-associated EVs induced a decrease in hepatic IL-1β expression, suggesting they may instead have anti-inflammatory effects. Indeed, Murgoci et al. (2020) showed that microglial EVs derived from the spinal cord and brain had different protein content. Moreover, only microglial EVs from the spinal cord, not the brain, significantly attenuated glioma proliferation. This highlights how EVs derived from different components of the CNS can have differential effects, which must be considered in any subsequent diagnostics and treatment development.

7.1.4 Future directions

Data presented in this thesis show that the SCI-induced APR is amenable to therapeutic intervention. To date, there are no pharmacological treatments available in the clinic for acute SCI (Ahuja et al. 2017a; Wilson et al. 2013), which has often been attributed to the presence of the BSCB. Therefore, targeting the peripheral inflammatory response presents an alternative strategy to attenuate spinal cord inflammation. Indeed, our laboratory has previously demonstrated that this is an effective approach after brain injury (Campbell et al. 2003; Campbell et al. 2007; Campbell et al. 2008b). In particular, this thesis has shown that targeted suppression of peripheral IL-1β can modulate the spinal cord inflammatory response. Systemic anti-cytokine treatment has been employed successfully in various models of neurological disease. Neutralisation of peripheral TNF has been shown to ameliorate neutrophil recruitment to the CNS in models of brain injury (Campbell et al. 2007), stroke (Clausen et al. 2014) and SCI (Genovese et al. 2006), and anti-CXCL1 treatment had similar beneficial effects (Campbell et al. 2003). Therefore, there is evidence that

suppression of the APR by inhibiting a master cytokine is a viable therapeutic strategy, which justifies further investigation.

The additional benefit of therapeutically targeting IL-1β with IL-1RA is that there is a synthetic version available, Anakinra. Anakinra is currently clinically approved to treat rheumatoid arthritis (Mertens and Singh 2009), although it is also being explored as a treatment for a range of neuroinflammatory diseases. It has demonstrated efficacy in animal models and/or is in clinical trials for amyotrophic lateral sclerosis (Maier et al. (2015); NCT01277315), subarachnoid haemorrhage (Galea et al. 2018; Singh et al. 2014), multiple sclerosis (NCT04025554), TBI (Hasturk et al. 2015a) and stroke (Emsley et al. 2005; Smith et al. 2018). Moreover, Anakinra is being investigated as a therapy for metabolic disorders, such as diabetes (Moran et al. 2013; van Asseldonk et al. 2011), which are prevalent in SCI patients (Cragg et al. 2013a; Rankin et al. 2017). It would be of interest to perform metabolomic analysis of peripheral tissues from IL-1RA-treated animals to evaluate whether the intervention was able to ameliorate the SCI-induced metabolite changes. Combined with its excellent safety profile, Anakinra is an attractive therapeutic for acute SCI, which could be rapidly repurposed, without difficulties.

To enable the translation of IL-1RA treatment to the clinic, future experiments are required to optimise the treatment regime, including the dose, route of administration and duration of treatment. The timing of the initial dose will also need to be adjusted. Hepatic IL-1β expression was greatest 2 hours post-SCI, and, therefore, the first dose of IL-1RA was administered in our rodent model immediately following injury. However, this may prove logistically difficult for SCI patients, as it often takes hours for patients to be transported to hospital. That being said, the field of stroke medicine works with the concept of the “golden hour” for acute treatment (Phipps and Cronin 2020), which may be adapted for acute SCI. Anakinra can be stored at 4°C (Medicine 2021), and so may be able to be administered by paramedics for rapid and effective intervention, although this is dependent on accurate diagnosis at the scene.

7.1.5 Limitations

For effective understanding of the mechanisms driving SCI pathophysiology, as well as successful treatment development, a valid animal model, which accurately recapitulates the human condition is required. In this thesis, a mouse model of contusive SCI was utilised. Whilst the timing and magnitude of central and peripheral inflammation after SCI is a good reflection of the human condition (Biglari et al. 2015; Fleming et al. 2006; Hassanshahi et al. 2013; Jogia et al. 2021), there are some limitations with using this rodent model. Female mice were used due to the reduced risk of post-operative complications, known to occur in male mice. However, sex differences in the immune response are well established (Kosyreva et al. 2018). For example, the phagocytic capacity of macrophages and neutrophils are greater in women than men (Klein and Flanagan 2016), whereas expression of pro-inflammatory cytokines in macrophages is greater in men than women (Aomatsu et al. 2013). SCI affects more men than women at a ratio of 4:1 (Chen et al. 2016), therefore the results presented in this thesis may misrepresent the major proportion of the SCI population. This may have consequences for translation of novel therapeutic interventions, as immunomodulatory treatment may be effective in our mouse model, but may not have the same effect in patients. To effectively translate therapy from pre-clinical studies into the clinic, a mixed population of models should be used, including both mice and rats of both sexes, and using a variety of different ages of animals.

Sham animals were included in analysis in order to distinguish between trauma-associated and SCI-specific effects. However, it is clear that surgery itself can induce a robust APR, as evidenced by increased hepatic cytokine expression and leukocyte mobilisation. This cannot be attributed to the anaesthetic regime as naïve animals also received anaesthetic, and so this peripheral inflammatory response must be due to the trauma. This remains clinically relevant because many patients undergo surgery within days of the injury to remove bone fragments and decompress the spinal cord (Dvorak et al. 2015; McKinley et al. 2004). However, this may be obscuring any contribution of the spinal injury, specifically, in which case a less invasive model may be more suitable. Marinelli et al. (2019) recently developed a novel contusion model, which authors propose

is more reflective of the human condition: in this model, a laminectomy is not performed and impact is applied directly to the vertebra, thus minimising any surgery-associated peripheral inflammation. Although, it must be acknowledged that, despite the trauma response, evidence of an SCI-specific effect on the APR is still clear in our contusion model.

The use of a rodent *in vivo* model might also be limiting our progress in understanding the role of EV signalling in the pathophysiology of SCI. As well as mammals, SCI can be modelled in smaller vertebrates, such as zebrafish (Cigliola et al. 2020), which are also becoming increasingly popular in the study of EVs (Verweij et al. 2019a). Owing to their optical transparency, zebrafish are amenable to high-resolution EV tracking (Hyenne et al. 2019; Verweij et al. 2019b), and, therefore, fundamental EV mechanisms, including dissemination, adhesion and uptake, can be visualised. This allows whole system analysis to better understand EV biodistribution in real time. As such, by utilising these alternative injury models, it may be possible to understand more about how EVs are generated and migrate after SCI.

7.2 Concluding remarks

This thesis has demonstrated that SCI induces a profound, systemic inflammatory response, described as the APR, which is dependent on the nature of the injury, and may be activated by EVs. Work presented here shows that the peripheral response to SCI can provide useful information about the extent of damage in the spinal cord, and therefore can be predictive of patient outcome. Importantly, suppression of the APR with IL-1RA attenuated inflammation in the spinal cord, indicating that peripheral inflammation is a promising therapeutic target for acute SCI. As such, future work should explore the potential of IL-1RA, and other modulators of systemic inflammation, to limit spinal cord pathology and improve functional recovery. Taken together, this thesis has significantly improved our understanding of the contribution of the APR to the outcome of SCI.

7.3 References

Adachi, N., K. Liu, and T. Arai. 2005. 'Prevention of brain infarction by postischemic administration of histidine in rats', *Brain Res*, 1039: 220-3.

Adachi, N., K. Liu, K. Ninomiya, E. Matsuoka, A. Motoki, Y. Irisawa, and M. Nishibori. 2011. 'Reduction of the infarct size by simultaneous administration of L-histidine and diphenhydramine in ischaemic rat brains', *Resuscitation*, 82: 219-21.

Adelson, P. D., S. R. Wisniewski, J. Beca, S. D. Brown, M. Bell, J. P. Muizelaar, P. Okada, S. R. Beers, G. K. Balasubramani, D. Hirtz, and Consortium Paediatric Traumatic Brain Injury. 2013. 'Comparison of hypothermia and normothermia after severe traumatic brain injury in children (Cool Kids): a phase 3, randomised controlled trial', *Lancet Neurol*, 12: 546-53.

Admyre, C., B. Bohle, S. M. Johansson, M. Focke-Tejkl, R. Valenta, A. Scheynius, and S. Gabrielsson. 2007. 'B cell-derived exosomes can present allergen peptides and activate allergen-specific T cells to proliferate and produce TH2-like cytokines', *J Allergy Clin Immunol*, 120: 1418-24.

Admyre, C., S. M. Johansson, S. Paulie, and S. Gabrielsson. 2006. 'Direct exosome stimulation of peripheral human T cells detected by ELISPOT', *Eur J Immunol*, 36: 1772-81.

Aguilar, J. A., J. Cassani, F. Probert, J. Palace, T. D. W. Claridge, A. Botana, and A. M. Kenwright. 2019. 'Reliable, high-quality suppression of NMR signals arising from water and macromolecules: application to bio-fluid analysis', *Analyst*, 144: 7270-77.

Ahmed, R. U., M. Alam, and Y. P. Zheng. 2019. 'Experimental spinal cord injury and behavioral tests in laboratory rats', *Heliyon*, 5: e01324.

Ahuja, C. S., J. H. Badhiwala, and M. G. Fehlings. 2020. '"Time is spine": the importance of early intervention for traumatic spinal cord injury', *Spinal Cord*, 58: 1037-39.

Ahuja, C. S., S. Nori, L. Tetreault, J. Wilson, B. Kwon, J. Harrop, D. Choi, and M. G. Fehlings. 2017a. 'Traumatic Spinal Cord Injury-Repair and Regeneration', *Neurosurgery*, 80: S9-S22.

Ahuja, C. S., J. R. Wilson, S. Nori, M. R. N. Kotter, C. Druschel, A. Curt, and M. G. Fehlings. 2017b. 'Traumatic spinal cord injury', *Nat Rev Dis Primers*, 3: 17018.

Ajami, B., J. L. Bennett, C. Krieger, W. Tetzlaff, and F. M. Rossi. 2007. 'Local self-renewal can sustain CNS microglia maintenance and function throughout adult life', *Nat Neurosci*, 10: 1538-43.

Akash, M. S., K. Rehman, and S. Chen. 2013. 'IL-1Ra and its delivery strategies: inserting the association in perspective', *Pharm Res*, 30: 2951-66.

Akbar, N., J. E. Digby, T. J. Cahill, A. N. Tavare, A. L. Corbin, S. Saluja, S. Dawkins, et al. 2017. 'Endothelium-derived extracellular vesicles promote splenic monocyte mobilization in myocardial infarction', *JCI Insight*, 2.

Akuzawa, S., T. Kazui, E. Shi, K. Yamashita, A. H. Bashar, and H. Terada. 2008. 'Interleukin-1 receptor antagonist attenuates the severity of spinal cord ischemic injury in rabbits', *J Vasc Surg*, 48: 694-700.

Alizadeh, A., S. M. Dyck, and S. Karimi-Abdolrezaee. 2019. 'Traumatic Spinal Cord Injury: An Overview of Pathophysiology, Models and Acute Injury Mechanisms', *Front Neurol*, 10: 282.

Allan, S. M., P. J. Tyrrell, and N. J. Rothwell. 2005. 'Interleukin-1 and neuronal injury', *Nat Rev Immunol*, 5: 629-40.

Allen, A.R. 1911. 'Surgery of experimental lesion of spinal cord equivalent to crush injury of fracture dislocation of spinal column: a preliminary report.', *JAMA*, LVII: 878-80.

Allison, D. J., and D. S. Ditor. 2015. 'Targeting inflammation to influence mood following spinal cord injury: a randomized clinical trial', *J Neuroinflammation*, 12: 204.

Allison, D. J., A. R. Josse, D. A. Gabriel, P. Klentrou, and D. S. Ditor. 2017. 'Targeting inflammation to influence cognitive function following spinal cord injury: a randomized clinical trial', *Spinal Cord*, 55: 26-32.

Almad, A., A. T. Lash, P. Wei, A. E. Lovett-Racke, and D. M. McTigue. 2011. 'The PPAR alpha agonist gemfibrozil is an ineffective treatment for spinal cord injured mice', *Exp Neurol*, 232: 309-17.

Altamura, A. C., A. R. Moro, and M. Percudani. 1994. 'Clinical pharmacokinetics of fluoxetine', *Clin Pharmacokinet*, 26: 201-14.
Anderson, M. A., J. E. Burda, Y. Ren, Y. Ao, T. M. O'Shea, R. Kawaguchi, G. Coppola, B. S. Khakh, T. J. Deming, and M. V. Sofroniew. 2016. 'Astrocyte scar formation aids central nervous system axon regeneration', *Nature*, 532: 195-200.
Andrews, A. M., E. M. Lutton, S. F. Merkel, R. Razmpour, and S. H. Ramirez. 2016. 'Mechanical Injury Induces Brain Endothelial-Derived Microvesicle Release: Implications for Cerebral Vascular Injury during Traumatic Brain Injury', *Front Cell Neurosci*, 10: 43.
Andrews, E. M., R. J. Richards, F. Q. Yin, M. S. Viapiano, and L. B. Jakeman. 2012. 'Alterations in chondroitin sulfate proteoglycan expression occur both at and far from the site of spinal contusion injury', *Exp Neurol*, 235: 174-87.
Ankeny, D. P., Z. Guan, and P. G. Popovich. 2009. 'B cells produce pathogenic antibodies and impair recovery after spinal cord injury in mice', *J Clin Invest*, 119: 2990-9.
Ankeny, D. P., K. M. Lucin, V. M. Sanders, V. M. McGaughy, and P. G. Popovich. 2006. 'Spinal cord injury triggers systemic autoimmunity: evidence for chronic B lymphocyte activation and lupus-like autoantibody synthesis', *J Neurochem*, 99: 1073-87.
Ankeny, D. P., and P. G. Popovich. 2010. 'B cells and autoantibodies: complex roles in CNS injury', *Trends Immunol*, 31: 332-8.
Anthony, D. C., and Y. Couch. 2014. 'The systemic response to CNS injury', *Exp Neurol*, 258: 105-11.
Anthony, D. C., Y. Couch, P. Losey, and M. C. Evans. 2012. 'The systemic response to brain injury and disease', *Brain Behav Immun*, 26: 534-40.
Anthony, D. C., A. M. Dickens, N. Seneca, Y. Couch, S. Campbell, B. Checa, V. Kersemans, E. A. Warren, M. Tredwell, N. R. Sibson, V. Gouverneur, and D. Leppert. 2014. 'Anti-CD20 inhibits T cell-mediated pathology and microgliosis in the rat brain', *Ann Clin Transl Neurol*, 1: 659-69.
Anwar, M. A., T. S. Al Shehabi, and A. H. Eid. 2016. 'Inflammogenesis of Secondary Spinal Cord Injury', *Front Cell Neurosci*, 10: 98.
Aomatsu, M., T. Kato, E. Kasahara, and S. Kitagawa. 2013. 'Gender difference in tumor necrosis factor-alpha production in human neutrophils stimulated by lipopolysaccharide and interferon-gamma', *Biochem Biophys Res Commun*, 441: 220-5.
Arevalo-Martin, A., L. Grassner, D. Garcia-Ovejero, B. Paniagua-Torija, G. Barroso-Garcia, A. G. Arandilla, O. Mach, et al. 2018. 'Elevated Autoantibodies in Subacute Human Spinal Cord Injury Are Naturally Occurring Antibodies', *Front Immunol*, 9: 2365.
Arraud, N., R. Linares, S. Tan, C. Gounou, J. M. Pasquet, S. Mornet, and A. R. Brisson. 2014. 'Extracellular vesicles from blood plasma: determination of their morphology, size, phenotype and concentration', *J Thromb Haemost*, 12: 614-27.
Assinck, P., G. J. Duncan, B. J. Hilton, J. R. Plemel, and W. Tetzlaff. 2017. 'Cell transplantation therapy for spinal cord injury', *Nat Neurosci*, 20: 637-47.
Augusto-Oliveira, M., G. P. Arrifano, P. Y. Takeda, A. Lopes-Araujo, L. Santos-Sacramento, D. C. Anthony, A. Verkhratsky, and M. E. Crespo-Lopez. 2020. 'Astroglia-specific contributions to the regulation of synapses, cognition and behaviour', *Neurosci Biobehav Rev*, 118: 331-57.
Azevedo, F. A., L. R. Carvalho, L. T. Grinberg, J. M. Farfel, R. E. Ferretti, R. E. Leite, W. Jacob Filho, R. Lent, and S. Herculano-Houzel. 2009. 'Equal numbers of neuronal and nonneuronal cells make the human brain an isometrically scaled-up primate brain', *J Comp Neurol*, 513: 532-41.
Azodi, S., and S. Jacobson. 2016. 'Cytokine Therapies in Neurological Disease', *Neurotherapeutics*, 13: 555-61.
Badhiwala, J. H., C. S. Ahuja, and M. G. Fehlings. 2018. 'Time is spine: a review of translational advances in spinal cord injury', *J Neurosurg Spine*, 30: 1-18.
Bahney, J., and C. S. von Bartheld. 2018. 'The Cellular Composition and Glia-Neuron Ratio in the Spinal Cord of a Human and a Nonhuman Primate: Comparison With Other Species and Brain Regions', *Anat Rec (Hoboken)*, 301: 697-710.

Bajpai, G., C. Schneider, N. Wong, A. Bredemeyer, M. Hulsmans, M. Nahrendorf, S. Epelman, D. Kreisel, Y. Liu, A. Itoh, T. S. Shankar, C. H. Selzman, S. G. Drakos, and K. J. Lavine. 2018. 'The human heart contains distinct macrophage subsets with divergent origins and functions', *Nat Med*, 24: 1234-45.

Bal-Price, A., Z. Moneer, and G. C. Brown. 2002. 'Nitric oxide induces rapid, calcium-dependent release of vesicular glutamate and ATP from cultured rat astrocytes', *Glia*, 40: 312-23.

Baldwin, A. G., D. Brough, and S. Freeman. 2016. 'Inhibiting the Inflammasome: A Chemical Perspective', *J Med Chem*, 59: 1691-710.

Baldwin, S. A., R. Broderick, D. A. Blades, and S. W. Scheff. 1998. 'Alterations in temporal/spatial distribution of GFAP- and vimentin-positive astrocytes after spinal cord contusion with the New York University spinal cord injury device', *J Neurotrauma*, 15: 1015-26.

Balusu, S., E. Van Wonterghem, R. De Rycke, K. Raemdonck, S. Stremersch, K. Gevaert, M. Brkic, D. Demeestere, V. Vanhooren, A. Hendrix, C. Libert, and R. E. Vandenbroucke. 2016. 'Identification of a novel mechanism of blood-brain communication during peripheral inflammation via choroid plexus-derived extracellular vesicles', *EMBO Mol Med*, 8: 1162-83.

Banerjea, R., U. Sambamoorthi, F. Weaver, M. Maney, L. M. Pogach, and T. Findley. 2008. 'Risk of stroke, heart attack, and diabetes complications among veterans with spinal cord injury', *Arch Phys Med Rehabil*, 89: 1448-53.

Bao, F., C. S. Bailey, K. R. Gurr, S. I. Bailey, M. P. Rosas-Arellano, A. Brown, G. A. Dekaban, and L. C. Weaver. 2011a. 'Human spinal cord injury causes specific increases in surface expression of beta integrins on leukocytes', *J Neurotrauma*, 28: 269-80.

Bao, F., C. S. Bailey, K. R. Gurr, S. I. Bailey, M. P. Rosas-Arellano, G. A. Dekaban, and L. C. Weaver. 2009. 'Increased oxidative activity in human blood neutrophils and monocytes after spinal cord injury', *Exp Neurol*, 215: 308-16.

Bao, F., A. Brown, G. A. Dekaban, V. Omana, and L. C. Weaver. 2011b. 'CD11d integrin blockade reduces the systemic inflammatory response syndrome after spinal cord injury', *Exp Neurol*, 231: 272-83.

Bao, F., and D. Liu. 2004. 'Hydroxyl radicals generated in the rat spinal cord at the level produced by impact injury induce cell death by necrosis and apoptosis: protection by a metalloporphyrin', *Neuroscience*, 126: 285-95.

Baranovicova, E., T. Galanda, M. Galanda, J. Hatok, B. Kolarovszki, R. Richterova, and P. Racay. 2019. 'Metabolomic profiling of blood plasma in patients with primary brain tumours: Basal plasma metabolites correlated with tumour grade and plasma biomarker analysis predicts feasibility of the successful statistical discrimination from healthy subjects - a preliminary study', *IUBMB Life*, 71: 1994-2002.

Barbierato, M., M. Borri, L. Facci, M. Zusso, S. D. Skaper, and P. Giusti. 2017. 'Expression and Differential Responsiveness of Central Nervous System Glial Cell Populations to the Acute Phase Protein Serum Amyloid A', *Sci Rep*, 7: 12158.

Barbonetti, A., M. R. Caterina Vassallo, M. Cotugno, G. Felzani, S. Francavilla, and F. Francavilla. 2016. 'Low testosterone and non-alcoholic fatty liver disease: Evidence for their independent association in men with chronic spinal cord injury', *J Spinal Cord Med*, 39: 443-9.

Barger, S. W., M. E. Goodwin, M. M. Porter, and M. L. Beggs. 2007. 'Glutamate release from activated microglia requires the oxidative burst and lipid peroxidation', *J Neurochem*, 101: 1205-13.

Bartanusz, V., D. Jezova, B. Alajajian, and M. Digicaylioglu. 2011. 'The blood-spinal cord barrier: morphology and clinical implications', *Ann Neurol*, 70: 194-206.

Bartus, K., N. D. James, A. Didangelos, K. D. Bosch, J. Verhaagen, R. J. Yanez-Munoz, J. H. Rogers, B. L. Schneider, E. M. Muir, and E. J. Bradbury. 2014. 'Large-scale chondroitin sulfate proteoglycan digestion with chondroitinase gene therapy leads to reduced pathology and modulates macrophage phenotype following spinal cord contusion injury', *J Neurosci*, 34: 4822-36.

Basso, D. M., M. S. Beattie, and J. C. Bresnahan. 1996. 'Graded histological and locomotor outcomes after spinal cord contusion using the NYU weight-drop device versus transection', *Exp Neurol*, 139: 244-56.
Basso, D. M., L. C. Fisher, A. J. Anderson, L. B. Jakeman, D. M. McTigue, and P. G. Popovich. 2006. 'Basso Mouse Scale for locomotion detects differences in recovery after spinal cord injury in five common mouse strains', *J Neurotrauma*, 23: 635-59.
Batchelor, P. E., N. F. Kerr, A. M. Gatt, E. Aleksoska, S. F. Cox, A. Ghasem-Zadeh, T. E. Wills, and D. W. Howells. 2010. 'Hypothermia prior to decompression: buying time for treatment of acute spinal cord injury', *J Neurotrauma*, 27: 1357-68.
Beck, K. D., H. X. Nguyen, M. D. Galvan, D. L. Salazar, T. M. Woodruff, and A. J. Anderson. 2010. 'Quantitative analysis of cellular inflammation after traumatic spinal cord injury: evidence for a multiphasic inflammatory response in the acute to chronic environment', *Brain*, 133: 433-47.
Bellver-Landete, V., F. Bretheau, B. Mailhot, N. Vallieres, M. Lessard, M. E. Janelle, N. Vernoux, M. E. Tremblay, T. Fuehrmann, M. S. Shoichet, and S. Lacroix. 2019. 'Microglia are an essential component of the neuroprotective scar that forms after spinal cord injury', *Nat Commun*, 10: 518.
Biglari, B., T. Swing, C. Child, A. Buchler, F. Westhauser, T. Bruckner, T. Ferbert, H. Jurgen Gerner, and A. Moghaddam. 2015. 'A pilot study on temporal changes in IL-1beta and TNF-alpha serum levels after spinal cord injury: the serum level of TNF-alpha in acute SCI patients as a possible marker for neurological remission', *Spinal Cord*, 53: 510-4.
Bingham, D., C. M. John, J. Levin, S. S. Panter, and G. A. Jarvis. 2013. 'Post-injury conditioning with lipopolysaccharide or lipooligosaccharide reduces inflammation in the brain', *J Neuroimmunol*, 256: 28-37.
Blomster, L. V., F. H. Brennan, H. W. Lao, D. W. Harle, A. R. Harvey, and M. J. Ruitenberg. 2013a. 'Mobilisation of the splenic monocyte reservoir and peripheral CX(3)CR1 deficiency adversely affects recovery from spinal cord injury', *Exp Neurol*, 247: 226-40.
Blomster, L. V., G. J. Cowin, N. D. Kurniawan, and M. J. Ruitenberg. 2013b. 'Detection of endogenous iron deposits in the injured mouse spinal cord through high-resolution ex vivo and in vivo MRI', *NMR Biomed*, 26: 141-50.
Blond, D., S. J. Campbell, A. G. Butchart, V. H. Perry, and D. C. Anthony. 2002. 'Differential induction of interleukin-1beta and tumour necrosis factor-alpha may account for specific patterns of leukocyte recruitment in the brain', *Brain Res*, 958: 89-99.
Boato, F., K. Rosenberger, S. Nelissen, L. Geboes, E. M. Peters, R. Nitsch, and S. Hendrix. 2013. 'Absence of IL-1beta positively affects neurological outcome, lesion development and axonal plasticity after spinal cord injury', *J Neuroinflammation*, 10: 6.
Boldin, C., J. Raith, F. Fankhauser, C. Haunschmid, G. Schwantzer, and F. Schweighofer. 2006. 'Predicting neurologic recovery in cervical spinal cord injury with postoperative MR imaging', *Spine (Phila Pa 1976)*, 31: 554-9.
Bolton, S. J., D. C. Anthony, and V. H. Perry. 1998. 'Loss of the tight junction proteins occludin and zonula occludens-1 from cerebral vascular endothelium during neutrophil-induced blood-brain barrier breakdown in vivo', *Neuroscience*, 86: 1245-57.
Borovikova, L. V., S. Ivanova, M. Zhang, H. Yang, G. I. Botchkina, L. R. Watkins, H. Wang, N. Abumrad, J. W. Eaton, and K. J. Tracey. 2000. 'Vagus nerve stimulation attenuates the systemic inflammatory response to endotoxin', *Nature*, 405: 458-62.
Bozzo, A., J. Marcoux, M. Radhakrishna, J. Pelletier, and B. Goulet. 2011. 'The role of magnetic resonance imaging in the management of acute spinal cord injury', *J Neurotrauma*, 28: 1401-11.
Bracken, M. B., M. J. Shepard, W. F. Collins, T. R. Holford, W. Young, D. S. Baskin, H. M. Eisenberg, E. Flamm, L. Leo-Summers, J. Maroon, and et al. 1990. 'A randomized, controlled trial of methylprednisolone or naloxone in the treatment of acute spinal-cord injury. Results of the Second National Acute Spinal Cord Injury Study', *N Engl J Med*, 322: 1405-11.
Bradbury, E. J., and E. R. Burnside. 2019. 'Moving beyond the glial scar for spinal cord repair', *Nat Commun*, 10: 3879.

Bradbury, E. J., L. D. Moon, R. J. Popat, V. R. King, G. S. Bennett, P. N. Patel, J. W. Fawcett, and S. B. McMahon. 2002. 'Chondroitinase ABC promotes functional recovery after spinal cord injury', *Nature*, 416: 636-40.

Brambilla, R., V. Bracchi-Ricard, W. H. Hu, B. Frydel, A. Bramwell, S. Karmally, E. J. Green, and J. R. Bethea. 2005. 'Inhibition of astroglial nuclear factor kappaB reduces inflammation and improves functional recovery after spinal cord injury', *J Exp Med*, 202: 145-56.

Brennan, F. H., A. J. Anderson, S. M. Taylor, T. M. Woodruff, and M. J. Ruitenberg. 2012. 'Complement activation in the injured central nervous system: another dual-edged sword?', *J Neuroinflammation*, 9: 137.

Brennan, F. H., R. Gordon, H. W. Lao, P. J. Biggins, S. M. Taylor, R. J. Franklin, T. M. Woodruff, and M. J. Ruitenberg. 2015. 'The Complement Receptor C5aR Controls Acute Inflammation and Astrogliosis following Spinal Cord Injury', *J Neurosci*, 35: 6517-31.

Brennan, F. H., T. Jogia, E. R. Gillespie, L. V. Blomster, X. X. Li, B. Nowlan, G. M. Williams, et al. 2019. 'Complement receptor C3aR1 controls neutrophil mobilization following spinal cord injury through physiological antagonism of CXCR2', *JCI Insight*, 4.

Brennan, F. H., N. D. Kurniawan, J. Vukovic, P. F. Bartlett, F. Kasermann, T. V. Arumugam, M. Basta, and M. J. Ruitenberg. 2016. 'IVIg attenuates complement and improves spinal cord injury outcomes in mice', *Ann Clin Transl Neurol*, 3: 495-511.

Brennan, Faith H., Jodie C.E. Hall, Zhen Guan, and Phillip G. Popovich. 2018. 'Microglia limit lesion expansion and promote functional recovery after spinal cord injury in mice', *bioRxiv*: 410258.

Brennan, K., K. Martin, S. P. FitzGerald, J. O'Sullivan, Y. Wu, A. Blanco, C. Richardson, and M. M. Mc Gee. 2020. 'A comparison of methods for the isolation and separation of extracellular vesicles from protein and lipid particles in human serum', *Sci Rep*, 10: 1039.

Brewster, L. M., G. B. Coombs, V. P. Garcia, J. G. Hijmans, N. M. DeSouza, K. A. Stockelman, O. F. Barak, T. Mijacika, Z. Dujic, J. J. Greiner, A. A. Phillips, P. N. Ainslie, and C. A. DeSouza. 2020. 'Effects of circulating extracellular microvesicles from spinal cord-injured adults on endothelial cell function', *Clin Sci (Lond)*, 134: 777-89.

Brogden, R. N., T. M. Speight, and G. S. Avery. 1975. 'Minocycline: A review of its antibacterial and pharmacokinetic properties and therapeutic use', *Drugs*, 9: 251-91.

Brommer, B., O. Engel, M. A. Kopp, R. Watzlawick, S. Muller, H. Pruss, Y. Chen, M. J. DeVivo, F. W. Finkenstaedt, U. Dirnagl, T. Liebscher, A. Meisel, and J. M. Schwab. 2016. 'Spinal cord injury-induced immune deficiency syndrome enhances infection susceptibility dependent on lesion level', *Brain*, 139: 692-707.

Brouwers, Emjr, H. V. Meent, A. Curt, D. D. Maier, R. F. Abel, N. Weidner, R. Rupp, J. Kriz, A. F. J. de Haan, J. K. Kramer, A. J. F. Hosman, Rhma Bartels, Emsci participants, and investigators. 2020. 'Recovery after traumatic thoracic- and lumbar spinal cord injury: the neurological level of injury matters', *Spinal Cord*.

Brown, J. O., and Couch Gp Mc. 1947. 'Abortive regeneration of the transected spinal cord', *J Comp Neurol*, 87: 131-7.

Brundula, V., N. B. Rewcastle, L. M. Metz, C. C. Bernard, and V. W. Yong. 2002. 'Targeting leukocyte MMPs and transmigration: minocycline as a potential therapy for multiple sclerosis', *Brain*, 125: 1297-308.

Budnik, V., C. Ruiz-Canada, and F. Wendler. 2016. 'Extracellular vesicles round off communication in the nervous system', *Nat Rev Neurosci*, 17: 160-72.

Burns, A. S., and J. F. Ditunno. 2001. 'Establishing prognosis and maximizing functional outcomes after spinal cord injury: a review of current and future directions in rehabilitation management', *Spine (Phila Pa 1976)*, 26: S137-45.

Burns, S. P. 2007. 'Acute respiratory infections in persons with spinal cord injury', *Phys Med Rehabil Clin N Am*, 18: 203-16, v-vi.

Burnside, E. R., F. De Winter, A. Didangelos, N. D. James, E. C. Andreica, H. Layard-Horsfall, E. M. Muir, J. Verhaagen, and E. J. Bradbury. 2018. 'Immune-evasive gene switch enables regulated delivery of chondroitinase after spinal cord injury', *Brain*, 141: 2362-81.

Cabezas, R., M. Avila, J. Gonzalez, R. S. El-Bacha, E. Baez, L. M. Garcia-Segura, J. C. Jurado Coronel, F. Capani, G. P. Cardona-Gomez, and G. E. Barreto. 2014. 'Astrocytic modulation of blood brain barrier: perspectives on Parkinson's disease', *Front Cell Neurosci*, 8: 211.

Cabrera-Aldana, E. E., F. Ruelas, C. Aranda, R. Rincon-Heredia, A. Martinez-Cruz, A. Reyes-Sanchez, G. Guizar-Sahagun, and Y. Romo L. B. Tovar. 2017. 'Methylprednisolone Administration Following Spinal Cord Injury Reduces Aquaporin 4 Expression and Exacerbates Edema', *Mediators Inflamm*, 2017: 4792932.

Cafferty, W. B., P. Duffy, E. Huebner, and S. M. Strittmatter. 2010. 'MAG and OMgp synergize with Nogo-A to restrict axonal growth and neurological recovery after spinal cord trauma', *J Neurosci*, 30: 6825-37.

Cambria, R. P., J. K. Davison, S. Zannetti, G. L'Italien, D. C. Brewster, J. P. Gertler, A. C. Moncure, G. M. LaMuraglia, and W. M. Abbott. 1997. 'Clinical experience with epidural cooling for spinal cord protection during thoracic and thoracoabdominal aneurysm repair', *J Vasc Surg*, 25: 234-41; discussion 41-3.

Campagnolo, D. I., D. Dixon, J. Schwartz, J. A. Bartlett, and S. E. Keller. 2008. 'Altered innate immunity following spinal cord injury', *Spinal Cord*, 46: 477-81.

Campbell, S. J., D. C. Anthony, F. Oakley, H. Carlsen, A. M. Elsharkawy, R. Blomhoff, and D. A. Mann. 2008a. 'Hepatic nuclear factor kappa B regulates neutrophil recruitment to the injured brain', *J Neuropathol Exp Neurol*, 67: 223-30.

Campbell, S. J., P. M. Hughes, J. P. Iredale, D. C. Wilcockson, S. Waters, F. Docagne, V. H. Perry, and D. C. Anthony. 2003. 'CINC-1 is an acute-phase protein induced by focal brain injury causing leukocyte mobilization and liver injury', *FASEB J*, 17: 1168-70.

Campbell, S. J., Y. Jiang, A. E. Davis, R. Farrands, J. Holbrook, D. Leppert, and D. C. Anthony. 2007. 'Immunomodulatory effects of etanercept in a model of brain injury act through attenuation of the acute-phase response', *J Neurochem*, 103: 2245-55.

Campbell, S. J., U. Meier, S. Mardiguian, Y. Jiang, E. T. Littleton, A. Bristow, J. Relton, T. J. Connor, and D. C. Anthony. 2010. 'Sickness behaviour is induced by a peripheral CXC-chemokine also expressed in multiple sclerosis and EAE', *Brain Behav Immun*, 24: 738-46.

Campbell, S. J., V. H. Perry, F. J. Pitossi, A. G. Butchart, M. Chertoff, S. Waters, R. Dempster, and D. C. Anthony. 2005. 'Central nervous system injury triggers hepatic CC and CXC chemokine expression that is associated with leukocyte mobilization and recruitment to both the central nervous system and the liver', *Am J Pathol*, 166: 1487-97.

Campbell, S. J., D. C. Wilcockson, A. G. Butchart, V. H. Perry, and D. C. Anthony. 2002. 'Altered chemokine expression in the spinal cord and brain contributes to differential interleukin-1beta-induced neutrophil recruitment', *J Neurochem*, 83: 432-41.

Campbell, S. J., I. Zahid, P. Losey, S. Law, Y. Jiang, M. Bilgen, N. van Rooijen, D. Morsali, A. E. Davis, and D. C. Anthony. 2008b. 'Liver Kupffer cells control the magnitude of the inflammatory response in the injured brain and spinal cord', *Neuropharmacology*, 55: 780-7.

Cappuccino, A., L. J. Bisson, B. Carpenter, J. Marzo, W. D. Dietrich, 3rd, and H. Cappuccino. 2010. 'The use of systemic hypothermia for the treatment of an acute cervical spinal cord injury in a professional football player', *Spine (Phila Pa 1976)*, 35: E57-62.

Carvalho, W. A., C. P. Bahia, J. C. Teixeira, W. Gomes-Leal, and A. Pereira. 2017. 'Interlimb Dynamic after Unilateral Focal Lesion of the Cervical Dorsal Corticospinal Tract with Endothelin-1', *Front Neuroanat*, 11: 89.

Casha, S., D. Zygun, M. D. McGowan, I. Bains, V. W. Yong, and R. J. Hurlbert. 2012. 'Results of a phase II placebo-controlled randomized trial of minocycline in acute spinal cord injury', *Brain*, 135: 1224-36.

Casili, G., D. Impellizzeri, M. Cordaro, E. Esposito, and S. Cuzzocrea. 2016. 'B-Cell Depletion with CD20 Antibodies as New Approach in the Treatment of Inflammatory and Immunological Events Associated with Spinal Cord Injury', *Neurotherapeutics*, 13: 880-94.

Catalano, M., and L. O'Driscoll. 2020. 'Inhibiting extracellular vesicles formation and release: a review of EV inhibitors', *J Extracell Vesicles*, 9: 1703244.

Chen, M., V. O. Ona, M. Li, R. J. Ferrante, K. B. Fink, S. Zhu, J. Bian, L. Guo, L. A. Farrell, S. M. Hersch, W. Hobbs, J. P. Vonsattel, J. H. Cha, and R. M. Friedlander. 2000a. 'Minocycline

inhibits caspase-1 and caspase-3 expression and delays mortality in a transgenic mouse model of Huntington disease', *Nat Med*, 6: 797-801.
Chen, M. S., A. B. Huber, M. E. van der Haar, M. Frank, L. Schnell, A. A. Spillmann, F. Christ, and M. E. Schwab. 2000b. 'Nogo-A is a myelin-associated neurite outgrowth inhibitor and an antigen for monoclonal antibody IN-1', *Nature*, 403: 434-9.
Chen, Y., Y. He, and M. J. DeVivo. 2016. 'Changing Demographics and Injury Profile of New Traumatic Spinal Cord Injuries in the United States, 1972-2014', *Arch Phys Med Rehabil*, 97: 1610-9.
Cheriyan, T., D. J. Ryan, J. H. Weinreb, J. Cheriyan, J. C. Paul, V. Lafage, T. Kirsch, and T. J. Errico. 2014. 'Spinal cord injury models: a review', *Spinal Cord*, 52: 588-95.
Cherry, J. D., J. A. Olschowka, and M. K. O'Banion. 2014. 'Neuroinflammation and M2 microglia: the good, the bad, and the inflamed', *J Neuroinflammation*, 11: 98.
Ching, S., L. He, W. Lai, and N. Quan. 2005. 'IL-1 type I receptor plays a key role in mediating the recruitment of leukocytes into the central nervous system', *Brain Behav Immun*, 19: 127-37.
Chio, C. C., J. W. Lin, M. W. Chang, C. C. Wang, J. R. Kuo, C. Z. Yang, and C. P. Chang. 2010. 'Therapeutic evaluation of etanercept in a model of traumatic brain injury', *J Neurochem*, 115: 921-9.
Chio, J. C. T., J. Wang, A. Badner, J. Hong, V. Surendran, and M. G. Fehlings. 2019. 'The effects of human immunoglobulin G on enhancing tissue protection and neurobehavioral recovery after traumatic cervical spinal cord injury are mediated through the neurovascular unit', *J Neuroinflammation*, 16: 141.
Chio, J. C. T., J. Wang, V. Surendran, L. Li, M. M. Zavvarian, K. Pieczonka, and M. G. Fehlings. 2021a. 'Delayed administration of high dose human immunoglobulin G enhances recovery after traumatic cervical spinal cord injury by modulation of neuroinflammation and protection of the blood spinal cord barrier', *Neurobiol Dis*, 148: 105187.
Chio, J. C. T., K. J. Xu, P. Popovich, S. David, and M. G. Fehlings. 2021b. 'Neuroimmunological therapies for treating spinal cord injury: Evidence and future perspectives', *Exp Neurol*, 341: 113704.
Chivet, M., C. Javalet, K. Laulagnier, B. Blot, F. J. Hemming, and R. Sadoul. 2014. 'Exosomes secreted by cortical neurons upon glutamatergic synapse activation specifically interact with neurons', *J Extracell Vesicles*, 3: 24722.
Choo, A. M., J. Liu, Z. Liu, M. Dvorak, W. Tetzlaff, and T. R. Oxland. 2009. 'Modeling spinal cord contusion, dislocation, and distraction: characterization of vertebral clamps, injury severities, and node of Ranvier deformations', *J Neurosci Methods*, 181: 6-17.
Chow, D. S., Y. Teng, E. G. Toups, B. Aarabi, J. S. Harrop, C. I. Shaffrey, M. M. Johnson, M. Boakye, R. F. Frankowski, M. G. Fehlings, and R. G. Grossman. 2012. 'Pharmacology of riluzole in acute spinal cord injury', *J Neurosurg Spine*, 17: 129-40.
Christie, S. D., B. Comeau, T. Myers, D. Sadi, M. Purdy, and I. Mendez. 2008. 'Duration of lipid peroxidation after acute spinal cord injury in rats and the effect of methylprednisolone', *Neurosurg Focus*, 25: E5.
Cigliola, V., C. J. Becker, and K. D. Poss. 2020. 'Building bridges, not walls: spinal cord regeneration in zebrafish', *Dis Model Mech*, 13.
Clausen, B. H., M. Degn, N. A. Martin, Y. Couch, L. Karimi, M. Ormhoj, M. L. Mortensen, et al. 2014. 'Systemically administered anti-TNF therapy ameliorates functional outcomes after focal cerebral ischemia', *J Neuroinflammation*, 11: 203.
Clausen, F., A. Hanell, C. Israelsson, J. Hedin, T. Ebendal, A. K. Mir, H. Gram, and N. Marklund. 2011. 'Neutralization of interleukin-1beta reduces cerebral edema and tissue loss and improves late cognitive outcome following traumatic brain injury in mice', *Eur J Neurosci*, 34: 110-23.
Clemente, C. D., and W. F. Windle. 1954. 'Regeneration of severed nerve fibers in the spinal cord of the adult cat', *J Comp Neurol*, 101: 691-731.
Cofano, F., M. Boido, M. Monticelli, F. Zenga, A. Ducati, A. Vercelli, and D. Garbossa. 2019. 'Mesenchymal Stem Cells for Spinal Cord Injury: Current Options, Limitations, and Future of Cell Therapy', *Int J Mol Sci*, 20.

Cohen, P. 2014. 'The TLR and IL-1 signalling network at a glance', *J Cell Sci*, 127: 2383-90.
Coillard, A., and E. Segura. 2019. 'In vivo Differentiation of Human Monocytes', *Front Immunol*, 10: 1907.
Coleman, W. P., D. Benzel, D. W. Cahill, T. Ducker, F. Geisler, B. Green, M. R. Gropper, et al. 2000. 'A critical appraisal of the reporting of the National Acute Spinal Cord Injury Studies (II and III) of methylprednisolone in acute spinal cord injury', *J Spinal Disord*, 13: 185-99.
Colombo, M., G. Raposo, and C. Thery. 2014. 'Biogenesis, secretion, and intercellular interactions of exosomes and other extracellular vesicles', *Annu Rev Cell Dev Biol*, 30: 255-89.
Connor, D. E., T. Exner, D. D. Ma, and J. E. Joseph. 2010. 'The majority of circulating platelet-derived microparticles fail to bind annexin V, lack phospholipid-dependent procoagulant activity and demonstrate greater expression of glycoprotein Ib', *Thromb Haemost*, 103: 1044-52.
Cotton, B. A., J. P. Pryor, I. Chinwalla, D. J. Wiebe, P. M. Reilly, and C. W. Schwab. 2005. 'Respiratory complications and mortality risk associated with thoracic spine injury', *J Trauma*, 59: 1400-7; discussion 07-9.
Couch, Y., N. Akbar, S. Davis, R. Fischer, A. M. Dickens, A. A. Neuhaus, A. I. Burgess, P. M. Rothwell, and A. M. Buchan. 2017a. 'Inflammatory Stroke Extracellular Vesicles Induce Macrophage Activation', *Stroke*, 48: 2292-96.
Couch, Y., N. Akbar, J. Roodselaar, M. C. Evans, C. Gardiner, I. Sargent, I. A. Romero, A. Bristow, A. M. Buchan, N. Haughey, and D. C. Anthony. 2017b. 'Circulating endothelial cell-derived extracellular vesicles mediate the acute phase response and sickness behaviour associated with CNS inflammation', *Sci Rep*, 7: 9574.
Couch, Y., A. E. Davis, I. Sa-Pereira, S. J. Campbell, and D. C. Anthony. 2014. 'Viral pre-challenge increases central nervous system inflammation after intracranial interleukin-1beta injection', *J Neuroinflammation*, 11: 178.
Coumans, F. A. W., A. R. Brisson, E. I. Buzas, F. Dignat-George, E. E. E. Drees, S. El-Andaloussi, C. Emanueli, et al. 2017. 'Methodological Guidelines to Study Extracellular Vesicles', *Circ Res*, 120: 1632-48.
Cragg, J. J., V. K. Noonan, M. Dvorak, A. Krassioukov, G. B. Mancini, and J. F. Borisoff. 2013a. 'Spinal cord injury and type 2 diabetes: results from a population health survey', *Neurology*, 81: 1864-8.
Cragg, J. J., V. K. Noonan, A. Krassioukov, and J. Borisoff. 2013b. 'Cardiovascular disease and spinal cord injury: results from a national population health survey', *Neurology*, 81: 723-8.
Cruz, F. F., P. R. Rocco, and P. Pelosi. 2017. 'Anti-inflammatory properties of anesthetic agents', *Crit Care*, 21: 67.
Cunningham, C., S. Campion, K. Lunnon, C. L. Murray, J. F. Woods, R. M. Deacon, J. N. Rawlins, and V. H. Perry. 2009. 'Systemic inflammation induces acute behavioral and cognitive changes and accelerates neurodegenerative disease', *Biol Psychiatry*, 65: 304-12.
Cyr, A., Y. Zhong, S. E. Reis, R. A. Namas, A. Amoscato, B. Zuckerbraun, J. Sperry, R. Zamora, Y. Vodovotz, and T. R. Billiar. 2021. 'Analysis of the Plasma Metabolome after Trauma, Novel Circulating Sphingolipid Signatures, and In-Hospital Outcomes', *J Am Coll Surg*, 232: 276-87 e1.
Darian-Smith, C., and K. Fisher. 2019. 'Somatosensory system organisation in mammals and response to spinal injury', *Oxford Research Encylopedias*.
David, S., and A. J. Aguayo. 1981. 'Axonal elongation into peripheral nervous system "bridges" after central nervous system injury in adult rats', *Science*, 214: 931-3.
David, S., A. D. Greenhalgh, and A. Kroner. 2015. 'Macrophage and microglial plasticity in the injured spinal cord', *Neuroscience*, 307: 311-8.
David, S., A. Kroner, A. D. Greenhalgh, J. G. Zarruk, and R. Lopez-Vales. 2018. 'Myeloid cell responses after spinal cord injury', *J Neuroimmunol*, 321: 97-108.
Davis, A. E., S. J. Campbell, P. Wilainam, and D. C. Anthony. 2005. 'Post-conditioning with lipopolysaccharide reduces the inflammatory infiltrate to the injured brain and spinal cord: a potential neuroprotective treatment', *Eur J Neurosci*, 22: 2441-50.

de Rivero Vaccari, J. P., F. Brand, 3rd, S. Adamczak, S. W. Lee, J. Perez-Barcena, M. Y. Wang, M. R. Bullock, W. D. Dietrich, and R. W. Keane. 2016. 'Exosome-mediated inflammasome signaling after central nervous system injury', *J Neurochem*, 136 Suppl 1: 39-48.
de Rivero Vaccari, J. P., G. Lotocki, A. E. Marcillo, W. D. Dietrich, and R. W. Keane. 2008. 'A molecular platform in neurons regulates inflammation after spinal cord injury', *J Neurosci*, 28: 3404-14.
Demirel, A., J. Li, C. Morrow, S. Barnes, J. Jansen, B. Gower, K. Kirksey, D. Redden, and C. Yarar-Fisher. 2020. 'Evaluation of a ketogenic diet for improvement of neurological recovery in individuals with acute spinal cord injury: study protocol for a randomized controlled trial', *Trials*, 21: 372.
Deshpande, D. M., Y. S. Kim, T. Martinez, J. Carmen, S. Dike, I. Shats, L. L. Rubin, J. Drummond, C. Krishnan, A. Hoke, N. Maragakis, J. Shefner, J. D. Rothstein, and D. A. Kerr. 2006. 'Recovery from paralysis in adult rats using embryonic stem cells', *Ann Neurol*, 60: 32-44.
Di Battista, A. P., S. G. Rhind, M. G. Hutchison, S. Hassan, M. Y. Shiu, K. Inaba, J. Topolovec-Vranic, A. C. Neto, S. B. Rizoli, and A. J. Baker. 2016. 'Inflammatory cytokine and chemokine profiles are associated with patient outcome and the hyperadrenergic state following acute brain injury', *J Neuroinflammation*, 13: 40.
Dibaj, P., F. Nadrigny, H. Steffens, A. Scheller, J. Hirrlinger, E. D. Schomburg, C. Neusch, and F. Kirchhoff. 2010. 'NO mediates microglial response to acute spinal cord injury under ATP control in vivo', *Glia*, 58: 1133-44.
Dickens, A. M., Y. Romo L. B. Tovar, S. W. Yoo, A. L. Trout, M. Bae, M. Kanmogne, B. Megra, et al. 2017. 'Astrocyte-shed extracellular vesicles regulate the peripheral leukocyte response to inflammatory brain lesions', *Sci Signal*, 10.
Didangelos, A., M. Iberl, E. Vinsland, K. Bartus, and E. J. Bradbury. 2014. 'Regulation of IL-10 by chondroitinase ABC promotes a distinct immune response following spinal cord injury', *J Neurosci*, 34: 16424-32.
Dididze, M., B. A. Green, W. D. Dietrich, S. Vanni, M. Y. Wang, and A. D. Levi. 2013. 'Systemic hypothermia in acute cervical spinal cord injury: a case-controlled study', *Spinal Cord*, 51: 395-400.
Dinarello, C. A. 2018. 'Overview of the IL-1 family in innate inflammation and acquired immunity', *Immunol Rev*, 281: 8-27.
Dinarello, C. A., A. Simon, and J. W. van der Meer. 2012. 'Treating inflammation by blocking interleukin-1 in a broad spectrum of diseases', *Nat Rev Drug Discov*, 11: 633-52.
Ditunno, J. F., J. W. Little, A. Tessler, and A. S. Burns. 2004. 'Spinal shock revisited: a four-phase model', *Spinal Cord*, 42: 383-95.
do Espirito Santo, C. C., F. da Silva Fiorin, J. Ilha, Mmmf Duarte, T. Duarte, and A. R. S. Santos. 2019. 'Spinal cord injury by clip-compression induces anxiety and depression-like behaviours in female rats: The role of the inflammatory response', *Brain Behav Immun*, 78: 91-104.
Donnelly, D. J., and P. G. Popovich. 2008. 'Inflammation and its role in neuroprotection, axonal regeneration and functional recovery after spinal cord injury', *Exp Neurol*, 209: 378-88.
Drago, F., M. Lombardi, I. Prada, M. Gabrielli, P. Joshi, D. Cojoc, J. Franck, I. Fournier, J. Vizioli, and C. Verderio. 2017. 'ATP Modifies the Proteome of Extracellular Vesicles Released by Microglia and Influences Their Action on Astrocytes', *Front Pharmacol*, 8: 910.
Dubois, E. A., R. Rissmann, and A. F. Cohen. 2011. 'Rilonacept and canakinumab', *Br J Clin Pharmacol*, 71: 639-41.
Dumont, R. J., D. O. Okonkwo, S. Verma, R. J. Hurlbert, P. T. Boulos, D. B. Ellegala, and A. S. Dumont. 2001. 'Acute spinal cord injury, part I: pathophysiologic mechanisms', *Clin Neuropharmacol*, 24: 254-64.
Dvorak, M. F., V. K. Noonan, N. Fallah, C. G. Fisher, J. Finkelstein, B. K. Kwon, C. S. Rivers, et al. 2015. 'The influence of time from injury to surgery on motor recovery and length of hospital stay in acute traumatic spinal cord injury: an observational Canadian cohort study', *J Neurotrauma*, 32: 645-54.

Ebrahimkhani, S., F. Vafaee, P. E. Young, S. S. J. Hur, S. Hawke, E. Devenney, H. Beadnall, M. H. Barnett, C. M. Suter, and M. E. Buckland. 2017. 'Exosomal microRNA signatures in multiple sclerosis reflect disease status', *Sci Rep*, 7: 14293.

Ekstedt, M., L. E. Franzen, U. L. Mathiesen, L. Thorelius, M. Holmqvist, G. Bodemar, and S. Kechagias. 2006. 'Long-term follow-up of patients with NAFLD and elevated liver enzymes', *Hepatology*, 44: 865-73.

Emsley, H. C., C. J. Smith, R. F. Georgiou, A. Vail, S. J. Hopkins, N. J. Rothwell, P. J. Tyrrell, and Investigators Acute Stroke. 2005. 'A randomised phase II study of interleukin-1 receptor antagonist in acute stroke patients', *J Neurol Neurosurg Psychiatry*, 76: 1366-72.

Evaniew, N., V. K. Noonan, N. Fallah, B. K. Kwon, C. S. Rivers, H. Ahn, C. S. Bailey, S. D. Christie, D. R. Fourney, R. J. Hurlbert, A. G. Linassi, M. G. Fehlings, M. F. Dvorak, and Rhscir Network. 2015. 'Methylprednisolone for the Treatment of Patients with Acute Spinal Cord Injuries: A Propensity Score-Matched Cohort Study from a Canadian Multi-Center Spinal Cord Injury Registry', *J Neurotrauma*, 32: 1674-83.

Evans, T. A., D. S. Barkauskas, J. T. Myers, E. G. Hare, J. Q. You, R. M. Ransohoff, A. Y. Huang, and J. Silver. 2014. 'High-resolution intravital imaging reveals that blood-derived macrophages but not resident microglia facilitate secondary axonal dieback in traumatic spinal cord injury', *Exp Neurol*, 254: 109-20.

Failli, V., M. A. Kopp, C. Gericke, P. Martus, S. Klingbeil, B. Brommer, I. Laginha, Y. Chen, M. J. DeVivo, U. Dirnagl, and J. M. Schwab. 2012. 'Functional neurological recovery after spinal cord injury is impaired in patients with infections', *Brain*, 135: 3238-50.

Fassbender, J. M., S. R. Whittemore, and T. Hagg. 2011. 'Targeting microvasculature for neuroprotection after SCI', *Neurotherapeutics*, 8: 240-51.

Faulkner, J. R., J. E. Herrmann, M. J. Woo, K. E. Tansey, N. B. Doan, and M. V. Sofroniew. 2004. 'Reactive astrocytes protect tissue and preserve function after spinal cord injury', *J Neurosci*, 24: 2143-55.

Fawcett, J. W. 2018. 'The Paper that Restarted Modern Central Nervous System Axon Regeneration Research', *Trends Neurosci*, 41: 239-42.

Fehlings, M. G., and R. G. Perrin. 2006. 'The timing of surgical intervention in the treatment of spinal cord injury: a systematic review of recent clinical evidence', *Spine (Phila Pa 1976)*, 31: S28-35; discussion S36.

Festoff, B. W., S. Ameenuddin, P. M. Arnold, A. Wong, K. S. Santacruz, and B. A. Citron. 2006. 'Minocycline neuroprotects, reduces microgliosis, and inhibits caspase protease expression early after spinal cord injury', *J Neurochem*, 97: 1314-26.

Fiandaca, M. S., D. Kapogiannis, M. Mapstone, A. Boxer, E. Eitan, J. B. Schwartz, E. L. Abner, R. C. Petersen, H. J. Federoff, B. L. Miller, and E. J. Goetzl. 2015. 'Identification of preclinical Alzheimer's disease by a profile of pathogenic proteins in neurally derived blood exosomes: A case-control study', *Alzheimers Dement*, 11: 600-7 e1.

Fields, J. K., S. Gunther, and E. J. Sundberg. 2019. 'Structural Basis of IL-1 Family Cytokine Signaling', *Front Immunol*, 10: 1412.

Figueroa, J. D., K. Cordero, M. S. Llan, and M. De Leon. 2013a. 'Dietary omega-3 polyunsaturated fatty acids improve the neurolipidome and restore the DHA status while promoting functional recovery after experimental spinal cord injury', *J Neurotrauma*, 30: 853-68.

Figueroa, J. D., K. Cordero, M. Serrano-Illan, A. Almeyda, K. Baldeosingh, F. G. Almaguel, and M. De Leon. 2013b. 'Metabolomics uncovers dietary omega-3 fatty acid-derived metabolites implicated in anti-nociceptive responses after experimental spinal cord injury', *Neuroscience*, 255: 1-18.

Fisher, S. K., J. E. Novak, and B. W. Agranoff. 2002. 'Inositol and higher inositol phosphates in neural tissues: homeostasis, metabolism and functional significance', *J Neurochem*, 82: 736-54.

Fleming, J. C., C. S. Bailey, H. Hundt, K. R. Gurr, S. I. Bailey, G. Cepinskas, A. R. Lawendy, and A. Badhwar. 2012. 'Remote inflammatory response in liver is dependent on the segmental level of spinal cord injury', *J Trauma Acute Care Surg*, 72: 1194-201;discussion 202.

Fleming, J. C., M. D. Norenberg, D. A. Ramsay, G. A. Dekaban, A. E. Marcillo, A. D. Saenz, M. Pasquale-Styles, W. D. Dietrich, and L. C. Weaver. 2006. 'The cellular inflammatory response in human spinal cords after injury', *Brain*, 129: 3249-69.

Forgione, N., M. Chamankhah, and M. G. Fehlings. 2017. 'A Mouse Model of Bilateral Cervical Contusion-Compression Spinal Cord Injury', *J Neurotrauma*, 34: 1227-39.

Forgione, N., and M. G. Fehlings. 2014. 'Rho-ROCK inhibition in the treatment of spinal cord injury', *World Neurosurg*, 82: e535-9.

Fouad, K., P. G. Popovich, M. A. Kopp, and J. M. Schwab. 2021. 'The neuroanatomical-functional paradox in spinal cord injury', *Nat Rev Neurol*, 17: 53-62.

Fu, H., Y. Zhao, D. Hu, S. Wang, T. Yu, and L. Zhang. 2020. 'Depletion of microglia exacerbates injury and impairs function recovery after spinal cord injury in mice', *Cell Death Dis*, 11: 528.

Fujieda, Y., S. Ueno, R. Ogino, M. Kuroda, T. J. Jonsson, L. Guo, T. Bamba, and E. Fukusaki. 2012. 'Metabolite profiles correlate closely with neurobehavioral function in experimental spinal cord injury in rats', *PLoS One*, 7: e43152.

Galea, J., K. Ogungbenro, S. Hulme, A. Greenhalgh, L. Aarons, S. Scarth, P. Hutchinson, S. Grainger, A. King, S. J. Hopkins, N. Rothwell, and P. Tyrrell. 2011. 'Intravenous anakinra can achieve experimentally effective concentrations in the central nervous system within a therapeutic time window: results of a dose-ranging study', *J Cereb Blood Flow Metab*, 31: 439-47.

Galea, J., K. Ogungbenro, S. Hulme, H. Patel, S. Scarth, M. Hoadley, K. Illingworth, C. J. McMahon, N. Tzerakis, A. T. King, A. Vail, S. J. Hopkins, N. Rothwell, and P. Tyrrell. 2018. 'Reduction of inflammation after administration of interleukin-1 receptor antagonist following aneurysmal subarachnoid hemorrhage: results of the Subcutaneous Interleukin-1Ra in SAH (SCIL-SAH) study', *J Neurosurg*, 128: 515-23.

Galvan, M. D., S. Luchetti, A. M. Burgos, H. X. Nguyen, M. J. Hooshmand, F. P. Hamers, and A. J. Anderson. 2008. 'Deficiency in complement C1q improves histological and functional locomotor outcome after spinal cord injury', *J Neurosci*, 28: 13876-88.

Garcez, M. L., F. Mina, T. Bellettini-Santos, A. P. da Luz, G. L. Schiavo, J. M. C. Macieski, E. B. Medeiros, A. O. Marques, N. Q. Magnus, and J. Budni. 2019. 'The Involvement of NLRP3 on the Effects of Minocycline in an AD-Like Pathology Induced by beta-Amyloid Oligomers Administered to Mice', *Mol Neurobiol*, 56: 2606-17.

Garrido-Mesa, N., A. Zarzuelo, and J. Galvez. 2013. 'Minocycline: far beyond an antibiotic', *Br J Pharmacol*, 169: 337-52.

Genovese, T., E. Mazzon, C. Crisafulli, R. Di Paola, C. Muia, P. Bramanti, and S. Cuzzocrea. 2006. 'Immunomodulatory effects of etanercept in an experimental model of spinal cord injury', *J Pharmacol Exp Ther*, 316: 1006-16.

Gensel, J. C., and B. Zhang. 2015. 'Macrophage activation and its role in repair and pathology after spinal cord injury', *Brain Res*, 1619: 1-11.

Gerber, Y. N., G. P. Saint-Martin, C. M. Bringuier, S. Bartolami, C. Goze-Bac, H. N. Noristani, and F. E. Perrin. 2018. 'CSF1R Inhibition Reduces Microglia Proliferation, Promotes Tissue Preservation and Improves Motor Recovery After Spinal Cord Injury', *Front Cell Neurosci*, 12: 368.

Geremia, N. M., F. Bao, T. E. Rosenzweig, T. Hryciw, L. Weaver, G. A. Dekaban, and A. Brown. 2012. 'CD11d Antibody Treatment Improves Recovery in Spinal Cord-Injured Mice', *J Neurotrauma*, 29: 539-50.

Ghasemlou, N., B. J. Kerr, and S. David. 2005. 'Tissue displacement and impact force are important contributors to outcome after spinal cord contusion injury', *Exp Neurol*, 196: 9-17.

Gill, J., M. Mustapic, R. Diaz-Arrastia, R. Lange, S. Gulyani, T. Diehl, V. Motamedi, N. Osier, R. A. Stern, and D. Kapogiannis. 2018. 'Higher exosomal tau, amyloid-beta 42 and IL-10 are associated with mild TBIs and chronic symptoms in military personnel', *Brain Inj*, 32: 1277-84.

Gillespie, E. R., and M. Ruitenberg. 2020. 'Neuroinflammation after SCI: Current Insights and Therapeutic Potential of Intravenous Immunoglobulin', *J Neurotrauma*.

Ginhoux, F., S. Lim, G. Hoeffel, D. Low, and T. Huber. 2013. 'Origin and differentiation of microglia', *Front Cell Neurosci*, 7: 45.
Giri, P. K., and J. S. Schorey. 2008. 'Exosomes derived from M. Bovis BCG infected macrophages activate antigen-specific CD4+ and CD8+ T cells in vitro and in vivo', *PLoS One*, 3: e2461.
Gomez-Cambronero, J., J. Horn, C. C. Paul, and M. A. Baumann. 2003. 'Granulocyte-macrophage colony-stimulating factor is a chemoattractant cytokine for human neutrophils: involvement of the ribosomal p70 S6 kinase signaling pathway', *J Immunol*, 171: 6846-55.
Gomez, R. M., M. Y. Sanchez, M. Portela-Lomba, K. Ghotme, G. E. Barreto, J. Sierra, and M. T. Moreno-Flores. 2018. 'Cell therapy for spinal cord injury with olfactory ensheathing glia cells (OECs)', *Glia*, 66: 1267-301.
Gomez, V. M., S. Averill, V. King, Q. Yang, E. Doncel Perez, S. C. Chacon, R. Ward, M. Nieto-Sampedro, J. Priestley, and J. Taylor. 2003. 'Transplantation of olfactory ensheathing cells fails to promote significant axonal regeneration from dorsal roots into the rat cervical cord', *J Neurocytol*, 32: 53-70.
Goodus, M. T., and D. M. McTigue. 2020. 'Hepatic dysfunction after spinal cord injury: A vicious cycle of central and peripheral pathology?', *Exp Neurol*, 325: 113160.
Goodus, M. T., A. D. Sauerbeck, P. G. Popovich, R. S. Bruno, and D. M. McTigue. 2018. 'Dietary Green Tea Extract Prior to Spinal Cord Injury Prevents Hepatic Iron Overload but Does Not Improve Chronic Hepatic and Spinal Cord Pathology in Rats', *J Neurotrauma*, 35: 2872-82.
Gorgey, A. S., D. R. Dolbow, J. D. Dolbow, R. K. Khalil, C. Castillo, and D. R. Gater. 2014. 'Effects of spinal cord injury on body composition and metabolic profile - part I', *J Spinal Cord Med*, 37: 693-702.
Gorio, A., N. Gokmen, S. Erbayraktar, O. Yilmaz, L. Madaschi, C. Cichetti, A. M. Di Giulio, E. Vardar, A. Cerami, and M. Brines. 2002. 'Recombinant human erythropoietin counteracts secondary injury and markedly enhances neurological recovery from experimental spinal cord trauma', *Proc Natl Acad Sci U S A*, 99: 9450-5.
Graham, Z. A., J. A. Siedlik, L. Harlow, K. Sahbani, W. A. Bauman, H. A. Tawfeek, and C. P. Cardozo. 2019. 'Key Glycolytic Metabolites in Paralyzed Skeletal Muscle Are Altered Seven Days after Spinal Cord Injury in Mice', *J Neurotrauma*, 36: 2722-31.
Greenhalgh, A. D., J. Galea, A. Denes, P. J. Tyrrell, and N. J. Rothwell. 2010. 'Rapid brain penetration of interleukin-1 receptor antagonist in rat cerebral ischaemia: pharmacokinetics, distribution, protection', *Br J Pharmacol*, 160: 153-9.
Gris, D., E. F. Hamilton, and L. C. Weaver. 2008. 'The systemic inflammatory response after spinal cord injury damages lungs and kidneys', *Exp Neurol*, 211: 259-70.
Gu, Y., X. Cheng, X. Huang, Y. Yuan, S. Qin, Z. Tan, D. Wang, X. Hu, C. He, and Z. Su. 2019. 'Conditional ablation of reactive astrocytes to dissect their roles in spinal cord injury and repair', *Brain Behav Immun*, 80: 394-405.
Guerrero, A. R., K. Uchida, H. Nakajima, S. Watanabe, M. Nakamura, W. E. Johnson, and H. Baba. 2012. 'Blockade of interleukin-6 signaling inhibits the classic pathway and promotes an alternative pathway of macrophage activation after spinal cord injury in mice', *J Neuroinflammation*, 9: 40.
Gungor, B., E. Adiguzel, I. Gursel, B. Yilmaz, and M. Gursel. 2016. 'Intestinal Microbiota in Patients with Spinal Cord Injury', *PLoS One*, 11: e0145878.
Guo, Q., S. Li, Y. Liang, Y. Zhang, J. Zhang, C. Wen, S. Lin, H. Wang, and B. Su. 2010. 'Effects of C3 deficiency on inflammation and regeneration following spinal cord injury in mice', *Neurosci Lett*, 485: 32-6.
Hachem, L. D., C. S. Ahuja, and M. G. Fehlings. 2017. 'Assessment and management of acute spinal cord injury: From point of injury to rehabilitation', *J Spinal Cord Med*, 40: 665-75.
Hanada, M., Y. Sugiura, R. Shinjo, N. Masaki, S. Imagama, N. Ishiguro, Y. Matsuyama, and M. Setou. 2012. 'Spatiotemporal alteration of phospholipids and prostaglandins in a rat model of spinal cord injury', *Anal Bioanal Chem*, 403: 1873-84.
Hannum, C. H., C. J. Wilcox, W. P. Arend, F. G. Joslin, D. J. Dripps, P. L. Heimdal, L. G. Armes, A. Sommer, S. P. Eisenberg, and R. C. Thompson. 1990. 'Interleukin-1 receptor antagonist activity of a human interleukin-1 inhibitor', *Nature*, 343: 336-40.

Hansen, C. N., D. M. Norden, T. D. Faw, R. Deibert, E. S. Wohleb, J. F. Sheridan, J. P. Godbout, and D. M. Basso. 2016. 'Lumbar Myeloid Cell Trafficking into Locomotor Networks after Thoracic Spinal Cord Injury', *Exp Neurol*, 282: 86-98.

Hara, M., M. Takayasu, K. Watanabe, A. Noda, T. Takagi, Y. Suzuki, and J. Yoshida. 2000. 'Protein kinase inhibition by fasudil hydrochloride promotes neurological recovery after spinal cord injury in rats', *J Neurosurg*, 93: 94-101.

Harrison, M., A. O'Brien, L. Adams, G. Cowin, M. J. Ruitenberg, G. Sengul, and C. Watson. 2013. 'Vertebral landmarks for the identification of spinal cord segments in the mouse', *Neuroimage*, 68: 22-9.

Hartjes, T. A., S. Mytnyk, G. W. Jenster, V. van Steijn, and M. E. van Royen. 2019. 'Extracellular Vesicle Quantification and Characterization: Common Methods and Emerging Approaches', *Bioengineering (Basel)*, 6.

Hassanshahi, G., M. Amin, A. Shunmugavel, R. Vazirinejad, A. Vakilian, M. Sanji, A. Shamsizadeh, H. RafatPanah, N. M. Poor, S. R. Moosavi, and S. Taheri. 2013. 'Temporal expression profile of CXC chemokines in serum of patients with spinal cord injury', *Neurochem Int*, 63: 363-7.

Hasturk, A. E., E. R. Yilmaz, E. Turkoglu, M. Arikan, G. Togral, N. Hayirli, B. I. Erguder, and O. Evirgen. 2015a. 'Potential neuroprotective effect of Anakinra in spinal cord injury in an in vivo experimental animal model', *Neurosciences (Riyadh)*, 20: 124-30.

Hasturk, A. E., E. R. Yilmaz, E. Turkoglu, H. Kertmen, B. Horasanli, N. Hayirli, I. B. Erguder, and O. Evirgen. 2015b. 'Therapeutic evaluation of interleukin 1-beta antagonist Anakinra against traumatic brain injury in rats', *Ulus Travma Acil Cerrahi Derg*, 21: 1-8.

Hawthorne, A. L., and P. G. Popovich. 2011. 'Emerging concepts in myeloid cell biology after spinal cord injury', *Neurotherapeutics*, 8: 252-61.

Hayes, K. C., T. C. Hull, G. A. Delaney, P. J. Potter, K. A. Sequeira, K. Campbell, and P. G. Popovich. 2002. 'Elevated serum titers of proinflammatory cytokines and CNS autoantibodies in patients with chronic spinal cord injury', *J Neurotrauma*, 19: 753-61.

Hazleton, I., A. Yates, A. Dale, J. Roodselaar, N. Akbar, M. Ruitenberg, D. C. Anthony, and Y. Couch. 2017. 'Exacerbation of Acute Traumatic Brain Injury by Circulating Extracellular Vesicles', *J Neurotrauma*.

He, Z., Y. Zhou, Q. Wang, J. Li, Z. Zheng, J. Chen, H. Zhang, Z. Wang, H. Xu, and J. Xiao. 2017. 'Inhibiting endoplasmic reticulum stress by lithium chloride contributes to the integrity of blood-spinal cord barrier and functional recovery after spinal cord injury', *Am J Transl Res*, 9: 1012-24.

Helmy, A., M. R. Guilfoyle, K. L. H. Carpenter, J. D. Pickard, D. K. Menon, and P. J. Hutchinson. 2016. 'Recombinant human interleukin-1 receptor antagonist promotes M1 microglia biased cytokines and chemokines following human traumatic brain injury', *J Cereb Blood Flow Metab*, 36: 1434-48.

Helmy, A., M. R. Guilfoyle, K. L. Carpenter, J. D. Pickard, D. K. Menon, and P. J. Hutchinson. 2014. 'Recombinant human interleukin-1 receptor antagonist in severe traumatic brain injury: a phase II randomized control trial', *J Cereb Blood Flow Metab*, 34: 845-51.

Hernandez-Gerez, E., I. N. Fleming, and S. H. Parson. 2019. 'A role for spinal cord hypoxia in neurodegeneration', *Cell Death Dis*, 10: 861.

Herrmann, J. E., T. Imura, B. Song, J. Qi, Y. Ao, T. K. Nguyen, R. A. Korsak, K. Takeda, S. Akira, and M. V. Sofroniew. 2008. 'STAT3 is a critical regulator of astrogliosis and scar formation after spinal cord injury', *J Neurosci*, 28: 7231-43.

Hiraga, N., N. Adachi, K. Liu, T. Nagaro, and T. Arai. 2007. 'Suppression of inflammatory cell recruitment by histamine receptor stimulation in ischemic rat brains', *Eur J Pharmacol*, 557: 236-44.

Hong, J., A. Chang, M. M. Zavvarian, J. Wang, Y. Liu, and M. G. Fehlings. 2018. 'Level-Specific Differences in Systemic Expression of Pro- and Anti-Inflammatory Cytokines and Chemokines after Spinal Cord Injury', *Int J Mol Sci*, 19.

Hong, J. M., J. S. Lee, H. J. Song, H. S. Jeong, H. A. Choi, and K. Lee. 2014. 'Therapeutic hypothermia after recanalization in patients with acute ischemic stroke', *Stroke*, 45: 134-40.

Horn, K. P., S. A. Busch, A. L. Hawthorne, N. van Rooijen, and J. Silver. 2008. 'Another barrier to regeneration in the CNS: activated macrophages induce extensive retraction of dystrophic axons through direct physical interactions', *J Neurosci*, 28: 9330-41.
Hoshino, A., B. Costa-Silva, T. L. Shen, G. Rodrigues, A. Hashimoto, M. Tesic Mark, H. Molina, et al. 2015. 'Tumour exosome integrins determine organotropic metastasis', *Nature*, 527: 329-35.
Hosseinkhani, B., S. Kuypers, N. M. S. van den Akker, D. G. M. Molin, and L. Michiels. 2018. 'Extracellular Vesicles Work as a Functional Inflammatory Mediator Between Vascular Endothelial Cells and Immune Cells', *Front Immunol*, 9: 1789.
Hou, S., and A. G. Rabchevsky. 2014. 'Autonomic consequences of spinal cord injury', *Compr Physiol*, 4: 1419-53.
Houlden, A., M. Goldrick, D. Brough, E. S. Vizi, N. Lenart, B. Martinecz, I. S. Roberts, and A. Denes. 2016. 'Brain injury induces specific changes in the caecal microbiota of mice via altered autonomic activity and mucoprotein production', *Brain Behav Immun*, 57: 10-20.
Huan, H. B., X. D. Wen, X. J. Chen, L. Wu, L. L. Wu, L. Zhang, D. P. Yang, X. Zhang, P. Bie, C. Qian, and F. Xia. 2017. 'Sympathetic nervous system promotes hepatocarcinogenesis by modulating inflammation through activation of alpha1-adrenergic receptors of Kupffer cells', *Brain Behav Immun*, 59: 118-34.
Huang, S. W., W. T. Wang, L. C. Chou, T. H. Liou, and H. W. Lin. 2017. 'Risk of Dementia in Patients with Spinal Cord Injury: A Nationwide Population-Based Cohort Study', *J Neurotrauma*, 34: 615-22.
Hurd, C., N. Weishaupt, and K. Fouad. 2013. 'Anatomical correlates of recovery in single pellet reaching in spinal cord injured rats', *Exp Neurol*, 247: 605-14.
Hutson, T. H., and S. Di Giovanni. 2019. 'The translational landscape in spinal cord injury: focus on neuroplasticity and regeneration', *Nat Rev Neurol*, 15: 732-45.
Hyenne, V., S. Ghoroghi, M. Collot, J. Bons, G. Follain, S. Harlepp, B. Mary, et al. 2019. 'Studying the Fate of Tumor Extracellular Vesicles at High Spatiotemporal Resolution Using the Zebrafish Embryo', *Dev Cell*, 48: 554-72 e7.
Injury, G. B. D. Traumatic Brain, and Collaborators Spinal Cord Injury. 2019. 'Global, regional, and national burden of traumatic brain injury and spinal cord injury, 1990-2016: a systematic analysis for the Global Burden of Disease Study 2016', *Lancet Neurol*, 18: 56-87.
Isaksson, J., M. Farooque, A. Holtz, L. Hillered, and Y. Olsson. 1999. 'Expression of ICAM-1 and CD11b after experimental spinal cord injury in rats', *J Neurotrauma*, 16: 165-73.
Ito, Y., Y. Sugimoto, M. Tomioka, N. Kai, and M. Tanaka. 2009. 'Does high dose methylprednisolone sodium succinate really improve neurological status in patient with acute cervical cord injury?: a prospective study about neurological recovery and early complications', *Spine (Phila Pa 1976)*, 34: 2121-4.
Iwanami, A., J. Yamane, H. Katoh, M. Nakamura, S. Momoshima, H. Ishii, Y. Tanioka, N. Tamaoki, T. Nomura, Y. Toyama, and H. Okano. 2005. 'Establishment of graded spinal cord injury model in a nonhuman primate: the common marmoset', *J Neurosci Res*, 80: 172-81.
Jackson, A. B., and T. E. Groomes. 1994. 'Incidence of respiratory complications following spinal cord injury', *Arch Phys Med Rehabil*, 75: 270-5.
Jahangiri, A. 2010. 'High-density lipoprotein and the acute phase response', *Curr Opin Endocrinol Diabetes Obes*, 17: 156-60.
Jeong, S., B. Lei, H. Wang, H. N. Dawson, and M. L. James. 2014. 'Intravenous immunoglobulin G improves neurobehavioral and histological outcomes after traumatic brain injury in mice', *J Neuroimmunol*, 276: 112-8.
Jeppesen, D. K., A. M. Fenix, J. L. Franklin, J. N. Higginbotham, Q. Zhang, L. J. Zimmerman, D. C. Liebler, et al. 2019. 'Reassessment of Exosome Composition', *Cell*, 177: 428-45 e18.
Jiang, H., J. Peng, Z. Y. Zhou, Y. Duan, W. Chen, B. Cai, H. Yang, and W. Zhang. 2010. 'Establishing (1)H nuclear magnetic resonance based metabonomics fingerprinting profile for spinal cord injury: a pilot study', *Chin Med J (Engl)*, 123: 2315-9.
Jogia, T., T. Lubstorf, E. Jacobson, E. Scriven, S. Atresh, Q. H. Nguyen, T. Liebscher, J. M. Schwab, M. A. Kopp, J. Walsham, K. E. Campbell, and M. J. Ruitenberg. 2021. 'Prognostic value of

early leukocyte fluctuations for recovery from traumatic spinal cord injury', *Clin Transl Med*, 11: e272.
Jogia, T., and M. J. Ruitenberg. 2020. 'Traumatic Spinal Cord Injury and the Gut Microbiota: Current Insights and Future Challenges', *Front Immunol*, 11: 704.
Jones, T. B. 2014. 'Lymphocytes and autoimmunity after spinal cord injury', *Exp Neurol*, 258: 78-90.
Jones, T. B., D. M. Basso, A. Sodhi, J. Z. Pan, R. P. Hart, R. C. MacCallum, S. Lee, C. C. Whitacre, and P. G. Popovich. 2002. 'Pathological CNS autoimmune disease triggered by traumatic spinal cord injury: implications for autoimmune vaccine therapy', *J Neurosci*, 22: 2690-700.
Jones, T. B., R. P. Hart, and P. G. Popovich. 2005. 'Molecular control of physiological and pathological T-cell recruitment after mouse spinal cord injury', *J Neurosci*, 25: 6576-83.
Jucker, M., and L. C. Walker. 2013. 'Self-propagation of pathogenic protein aggregates in neurodegenerative diseases', *Nature*, 501: 45-51.
Jung, B. D., K. Kimura, H. Kitamura, K. Makondo, K. Kanehira, and M. Saito. 2000. 'Sympathetic activation of hepatic and splenic IL-1beta mRNA expression during oscillation stress in the rat', *J Vet Med Sci*, 62: 409-13.
Jung, J. Y., H. S. Lee, D. G. Kang, N. S. Kim, M. H. Cha, O. S. Bang, D. H. Ryu, and G. S. Hwang. 2011. '1H-NMR-based metabolomics study of cerebral infarction', *Stroke*, 42: 1282-8.
Jurynczyk, M., F. Probert, T. Yeo, G. Tackley, T. D. W. Claridge, A. Cavey, M. R. Woodhall, et al. 2017. 'Metabolomics reveals distinct, antibody-independent, molecular signatures of MS, AQP4-antibody and MOG-antibody disease', *Acta Neuropathol Commun*, 5: 95.
Kahn, N. N., W. A. Bauman, and A. K. Sinha. 2005. 'Appearance of a novel prostacyclin receptor antibody and duration of spinal cord injury', *J Spinal Cord Med*, 28: 97-102.
Kao, C. H., L. M. Sun, Y. S. Chen, C. L. Lin, J. A. Liang, C. H. Kao, and M. W. Weng. 2016. 'Risk of Nongenitourinary Cancers in Patients With Spinal Cord Injury: A Population-based Cohort Study', *Medicine (Baltimore)*, 95: e2462.
Karnati, H. K., J. H. Garcia, D. Tweedie, R. E. Becker, D. Kapogiannis, and N. H. Greig. 2019. 'Neuronal Enriched Extracellular Vesicle Proteins as Biomarkers for Traumatic Brain Injury', *J Neurotrauma*, 36: 975-87.
Kawabe, J., M. Koda, M. Hashimoto, T. Fujiyoshi, T. Furuya, T. Endo, A. Okawa, and M. Yamazaki. 2011. 'Neuroprotective effects of granulocyte colony-stimulating factor and relationship to promotion of angiogenesis after spinal cord injury in rats: laboratory investigation', *J Neurosurg Spine*, 15: 414-21.
Kenne, E., A. Erlandsson, L. Lindbom, L. Hillered, and F. Clausen. 2012. 'Neutrophil depletion reduces edema formation and tissue loss following traumatic brain injury in mice', *J Neuroinflammation*, 9: 17.
Kerr, N. A., J. P. de Rivero Vaccari, S. Abbassi, H. Kaur, R. Zambrano, S. Wu, W. D. Dietrich, and R. W. Keane. 2018. 'Traumatic Brain Injury-Induced Acute Lung Injury: Evidence for Activation and Inhibition of a Neural-Respiratory-Inflammasome Axis', *J Neurotrauma*.
Kesani, A. K., J. C. Urquhart, N. Bedard, P. Leelapattana, F. Siddiqi, K. R. Gurr, and C. S. Bailey. 2014. 'Systemic inflammatory response syndrome in patients with spinal cord injury: does its presence at admission affect patient outcomes? Clinical article', *J Neurosurg Spine*, 21: 296-302.
Khan, N. Z., T. Cao, J. He, R. M. Ritzel, Y. Li, R. J. Henry, C. Colson, B. A. Stoica, A. I. Faden, and J. Wu. 2020. 'Spinal cord injury alters microRNA and CD81+ exosome levels in plasma extracellular nanoparticles with neuroinflammatory potential', *Brain Behav Immun*.
Khazaeipour, Z., S. M. Taheri-Otaghsara, and M. Naghdi. 2015. 'Depression Following Spinal Cord Injury: Its Relationship to Demographic and Socioeconomic Indicators', *Top Spinal Cord Inj Rehabil*, 21: 149-55.
Kigerl, K. A., J. C. Gensel, D. P. Ankeny, J. K. Alexander, D. J. Donnelly, and P. G. Popovich. 2009. 'Identification of two distinct macrophage subsets with divergent effects causing either neurotoxicity or regeneration in the injured mouse spinal cord', *J Neurosci*, 29: 13435-44.
Kigerl, K. A., J. C. Hall, L. Wang, X. Mo, Z. Yu, and P. G. Popovich. 2016. 'Gut dysbiosis impairs recovery after spinal cord injury', *J Exp Med*, 213: 2603-20.

Kigerl, K. A., V. M. McGaughy, and P. G. Popovich. 2006. 'Comparative analysis of lesion development and intraspinal inflammation in four strains of mice following spinal contusion injury', *J Comp Neurol*, 494: 578-94.
Kigerl, K. A., K. Mostacada, and P. G. Popovich. 2018. 'Gut Microbiota Are Disease-Modifying Factors After Traumatic Spinal Cord Injury', *Neurotherapeutics*, 15: 60-67.
Kil, K., Y. C. Zang, D. Yang, J. Markowski, G. S. Fuoco, G. C. Vendetti, V. M. Rivera, and J. Z. Zhang. 1999. 'T cell responses to myelin basic protein in patients with spinal cord injury and multiple sclerosis', *J Neuroimmunol*, 98: 201-7.
Kim, M. H., J. L. Granick, C. Kwok, N. J. Walker, D. L. Borjesson, F. R. Curry, L. S. Miller, and S. I. Simon. 2011. 'Neutrophil survival and c-kit(+)-progenitor proliferation in Staphylococcus aureus-infected skin wounds promote resolution', *Blood*, 117: 3343-52.
Kimberly, W. T., Y. Wang, L. Pham, K. L. Furie, and R. E. Gerszten. 2013. 'Metabolite profiling identifies a branched chain amino acid signature in acute cardioembolic stroke', *Stroke*, 44: 1389-95.
King, V. R., S. A. Averill, D. Hewazy, J. V. Priestley, L. Torup, and A. T. Michael-Titus. 2007. 'Erythropoietin and carbamylated erythropoietin are neuroprotective following spinal cord hemisection in the rat', *Eur J Neurosci*, 26: 90-100.
Kishk, N. A., H. Gabr, S. Hamdy, L. Afifi, N. Abokresha, H. Mahmoud, A. Wafaie, and D. Bilal. 2010. 'Case control series of intrathecal autologous bone marrow mesenchymal stem cell therapy for chronic spinal cord injury', *Neurorehabil Neural Repair*, 24: 702-8.
Kitchen, P., M. M. Salman, A. M. Halsey, C. Clarke-Bland, J. A. MacDonald, H. Ishida, H. J. Vogel, et al. 2020. 'Targeting Aquaporin-4 Subcellular Localization to Treat Central Nervous System Edema', *Cell*, 181: 784-99 e19.
Kjell, J., and L. Olson. 2016. 'Rat models of spinal cord injury: from pathology to potential therapies', *Dis Model Mech*, 9: 1125-37.
Klein, S. L., and K. L. Flanagan. 2016. 'Sex differences in immune responses', *Nat Rev Immunol*, 16: 626-38.
Knerlich-Lukoschus, F., M. Juraschek, U. Blomer, R. Lucius, H. M. Mehdorn, and J. Held-Feindt. 2008. 'Force-dependent development of neuropathic central pain and time-related CCL2/CCR2 expression after graded spinal cord contusion injuries of the rat', *J Neurotrauma*, 25: 427-48.
Kobayakawa, K., H. Kumamaru, H. Saiwai, K. Kubota, Y. Ohkawa, J. Kishimoto, K. Yokota, R. Ideta, K. Shiba, H. Tozaki-Saitoh, K. Inoue, Y. Iwamoto, and S. Okada. 2014. 'Acute hyperglycemia impairs functional improvement after spinal cord injury in mice and humans', *Sci Transl Med*, 6: 256ra137.
Kong, F. L., X. P. Wang, Y. N. Li, and H. X. Wang. 2018. 'The role of exosomes derived from cerebrospinal fluid of spinal cord injury in neuron proliferation in vitro', *Artif Cells Nanomed Biotechnol*, 46: 200-05.
Kong, F. Q., S. J. Zhao, P. Sun, H. Liu, J. Jie, T. Xu, A. D. Xu, et al. 2020. 'Macrophage MSR1 promotes the formation of foamy macrophage and neuronal apoptosis after spinal cord injury', *J Neuroinflammation*, 17: 62.
Konsman, J. P., G. N. Luheshi, R. M. Bluthe, and R. Dantzer. 2000. 'The vagus nerve mediates behavioural depression, but not fever, in response to peripheral immune signals; a functional anatomical analysis', *Eur J Neurosci*, 12: 4434-46.
Konsman, J. P., P. Parnet, and R. Dantzer. 2002. 'Cytokine-induced sickness behaviour: mechanisms and implications', *Trends Neurosci*, 25: 154-9.
Korherr, C., R. Hofmeister, H. Wesche, and W. Falk. 1997. 'A critical role for interleukin-1 receptor accessory protein in interleukin-1 signaling', *Eur J Immunol*, 27: 262-7.
Kosyreva, A. M., O. V. Makarova, L. V. Kakturskiy, L. P. Mikhailova, M. N. Boltovskaya, and K. A. Rogov. 2018. 'Sex differences of inflammation in target organs, induced by intraperitoneal injection of lipopolysaccharide, depend on its dose', *J Inflamm Res*, 11: 431-45.
Kox, M., M. Vaneker, J. G. van der Hoeven, G. J. Scheffer, C. W. Hoedemaekers, and P. Pickkers. 2012. 'Effects of vagus nerve stimulation and vagotomy on systemic and pulmonary inflammation in a two-hit model in rats', *PLoS One*, 7: e34431.

Krumsiek, J., K. Mittelstrass, K. T. Do, F. Stuckler, J. Ried, J. Adamski, A. Peters, et al. 2015. 'Gender-specific pathway differences in the human serum metabolome', *Metabolomics*, 11: 1815-33.
Kuharic, J., K. Grabusic, V. S. Tokmadzic, S. Stifter, K. Tulic, O. Shevchuk, P. Lucin, and A. Sustic. 2019. 'Severe Traumatic Brain Injury Induces Early Changes in the Physical Properties and Protein Composition of Intracranial Extracellular Vesicles', *J Neurotrauma*, 36: 190-200.
Kumar, A., R. J. Henry, B. A. Stoica, D. J. Loane, G. Abulwerdi, S. A. Bhat, and A. I. Faden. 2019. 'Neutral Sphingomyelinase Inhibition Alleviates LPS-Induced Microglia Activation and Neuroinflammation after Experimental Traumatic Brain Injury', *J Pharmacol Exp Ther*, 368: 338-52.
Kumar, A., and D. J. Loane. 2012. 'Neuroinflammation after traumatic brain injury: opportunities for therapeutic intervention', *Brain Behav Immun*, 26: 1191-201.
Kumar, A., B. A. Stoica, D. J. Loane, M. Yang, G. Abulwerdi, N. Khan, A. Kumar, S. R. Thom, and A. I. Faden. 2017. 'Microglial-derived microparticles mediate neuroinflammation after traumatic brain injury', *J Neuroinflammation*, 14: 47.
Kumar, H., H. Choi, M. J. Jo, H. P. Joshi, M. Muttigi, D. Bonanomi, S. B. Kim, E. Ban, A. Kim, S. H. Lee, K. T. Kim, S. Sohn, X. Zeng, and I. Han. 2018a. 'Neutrophil elastase inhibition effectively rescued angiopoietin-1 decrease and inhibits glial scar after spinal cord injury', *Acta Neuropathol Commun*, 6: 73.
Kumar, H., M. J. Jo, H. Choi, M. S. Muttigi, S. Shon, B. J. Kim, S. H. Lee, and I. B. Han. 2018b. 'Matrix Metalloproteinase-8 Inhibition Prevents Disruption of Blood-Spinal Cord Barrier and Attenuates Inflammation in Rat Model of Spinal Cord Injury', *Mol Neurobiol*, 55: 2577-90.
Kusmenkov, T., M. Braunstein, H. J. Schneider, M. Bidlingmaier, W. C. Prall, W. Flatz, W. Boecker, and V. Bogner. 2019. 'Initial free cortisol dynamics following blunt multiple trauma and traumatic brain injury: A clinical study', *J Int Med Res*, 47: 1185-94.
Lachenal, G., K. Pernet-Gallay, M. Chivet, F. J. Hemming, A. Belly, G. Bodon, B. Blot, G. Haase, Y. Goldberg, and R. Sadoul. 2011. 'Release of exosomes from differentiated neurons and its regulation by synaptic glutamatergic activity', *Mol Cell Neurosci*, 46: 409-18.
Lai, Y. J., C. L. Lin, Y. J. Chang, M. C. Lin, S. T. Lee, F. C. Sung, W. Y. Lee, and C. H. Kao. 2014. 'Spinal cord injury increases the risk of type 2 diabetes: a population-based cohort study', *Spine J*, 14: 1957-64.
Lambertsen, K. L., K. Biber, and B. Finsen. 2012. 'Inflammatory cytokines in experimental and human stroke', *J Cereb Blood Flow Metab*, 32: 1677-98.
Lavela, S. L., F. M. Weaver, B. Goldstein, K. Chen, S. Miskevics, S. Rajan, and D. R. Gater, Jr. 2006. 'Diabetes mellitus in individuals with spinal cord injury or disorder', *J Spinal Cord Med*, 29: 387-95.
Le, J., and D. Dorstyn. 2016. 'Anxiety prevalence following spinal cord injury: a meta-analysis', *Spinal Cord*, 54: 626.
Lee, A. S., C. Tang, M. S. Rao, I. L. Weissman, and J. C. Wu. 2013. 'Tumorigenicity as a clinical hurdle for pluripotent stem cell therapies', *Nat Med*, 19: 998-1004.
Lee, J. H., J. Roy, H. M. Sohn, M. Cheong, J. Liu, A. T. Stammers, W. Tetzlaff, and B. K. Kwon. 2010. 'Magnesium in a polyethylene glycol formulation provides neuroprotection after unilateral cervical spinal cord injury', *Spine (Phila Pa 1976)*, 35: 2041-8.
Lee, J. Y., H. Y. Choi, H. J. Ahn, B. G. Ju, and T. Y. Yune. 2014. 'Matrix metalloproteinase-3 promotes early blood-spinal cord barrier disruption and hemorrhage and impairs long-term neurological recovery after spinal cord injury', *Am J Pathol*, 184: 2985-3000.
Lee, J. Y., H. S. Kim, H. Y. Choi, T. H. Oh, and T. Y. Yune. 2012. 'Fluoxetine inhibits matrix metalloprotease activation and prevents disruption of blood-spinal cord barrier after spinal cord injury', *Brain*, 135: 2375-89.
Lee, M. Y., J. Myers, A. Hayes, S. Madan, V. F. Froelicher, I. Perkash, and B. J. Kiratli. 2005. 'C-reactive protein, metabolic syndrome, and insulin resistance in individuals with spinal cord injury', *J Spinal Cord Med*, 28: 20-5.

Lee, S. M., S. Rosen, P. Weinstein, N. van Rooijen, and L. J. Noble-Haeusslein. 2011. 'Prevention of both neutrophil and monocyte recruitment promotes recovery after spinal cord injury', *J Neurotrauma*, 28: 1893-907.
Lehmann, M., A. Fournier, I. Selles-Navarro, P. Dergham, A. Sebok, N. Leclerc, G. Tigyi, and L. McKerracher. 1999. 'Inactivation of Rho signaling pathway promotes CNS axon regeneration', *J Neurosci*, 19: 7537-47.
Lenz, E. M., J. Bright, I. D. Wilson, S. R. Morgan, and A. F. Nash. 2003. 'A 1H NMR-based metabonomic study of urine and plasma samples obtained from healthy human subjects', *J Pharm Biomed Anal*, 33: 1103-15.
Levi, A. D., B. A. Green, M. Y. Wang, W. D. Dietrich, T. Brindle, S. Vanni, G. Casella, G. Elhammady, and J. Jagid. 2009. 'Clinical application of modest hypothermia after spinal cord injury', *J Neurotrauma*, 26: 407-15.
Li, J. J., B. Wang, M. C. Kodali, C. Chen, E. Kim, B. J. Patters, L. Lan, S. Kumar, X. Wang, J. Yue, and F. F. Liao. 2018a. 'In vivo evidence for the contribution of peripheral circulating inflammatory exosomes to neuroinflammation', *J Neuroinflammation*, 15: 8.
Li, T., Y. T. Li, and D. Y. Song. 2018b. 'The expression of IL-1beta can deteriorate the prognosis of nervous system after spinal cord injury', *Int J Neurosci*, 128: 778-82.
Li, X., M. Li, L. Tian, J. Chen, R. Liu, and B. Ning. 2020a. 'Reactive Astrogliosis: Implications in Spinal Cord Injury Progression and Therapy', *Oxid Med Cell Longev*, 2020: 9494352.
Li, Y., P. M. Field, and G. Raisman. 1997. 'Repair of adult rat corticospinal tract by transplants of olfactory ensheathing cells', *Science*, 277: 2000-2.
Li, Y., X. He, R. Kawaguchi, Y. Zhang, Q. Wang, A. Monavarfeshani, Z. Yang, et al. 2020b. 'Microglia-organized scar-free spinal cord repair in neonatal mice', *Nature*, 587: 613-18.
Liao, R. J., L. Jiang, R. R. Wang, H. W. Zhao, Y. Chen, Y. Li, L. Wang, L. Y. Jie, Y. D. Zhou, X. N. Zhang, Z. Chen, and W. W. Hu. 2015. 'Histidine provides long-term neuroprotection after cerebral ischemia through promoting astrocyte migration', *Sci Rep*, 5: 15356.
Liddelow, S. A., K. A. Guttenplan, L. E. Clarke, F. C. Bennett, C. J. Bohlen, L. Schirmer, M. L. Bennett, et al. 2017. 'Neurotoxic reactive astrocytes are induced by activated microglia', *Nature*, 541: 481-87.
Lilley, E., M. R. Andrews, E. J. Bradbury, H. Elliott, P. Hawkins, R. M. Ichiyama, J. Keeley, A. T. Michael-Titus, L. D. F. Moon, S. Pluchino, J. Riddell, K. Ryder, and P. K. Yip. 2020. 'Refining rodent models of spinal cord injury', *Exp Neurol*, 328: 113273.
Lin, C. N., C. C. Huang, K. L. Huang, K. J. Lin, T. C. Yen, and H. C. Kuo. 2019. 'A metabolomic approach to identifying biomarkers in blood of Alzheimer's disease', *Ann Clin Transl Neurol*, 6: 537-45.
Lin, C. W., Y. P. Huang, and S. L. Pan. 2015. 'Spinal cord injury is related to an increased risk of multiple sclerosis: a population-based, propensity score-matched, longitudinal follow-up study', *J Neurotrauma*, 32: 655-9.
Linares, R., S. Tan, C. Gounou, N. Arraud, and A. R. Brisson. 2015. 'High-speed centrifugation induces aggregation of extracellular vesicles', *J Extracell Vesicles*, 4: 29509.
Lindsay, S. L., G. A. McCanney, A. G. Willison, and S. C. Barnett. 2020. 'Multi-target approaches to CNS repair: olfactory mucosa-derived cells and heparan sulfates', *Nat Rev Neurol*, 16: 229-40.
Liu, C., W. Wu, B. Zhang, J. Xiang, and J. Zou. 2013. 'Temporospatial expression and cellular localization of glutamine synthetase following traumatic spinal cord injury in adult rats', *Mol Med Rep*, 7: 1431-6.
Liu, S., G. Y. Xu, K. M. Johnson, C. Echetebu, Z. S. Ye, C. E. Hulsebosch, and D. J. McAdoo. 2008. 'Regulation of interleukin-1beta by the interleukin-1 receptor antagonist in the glutamate-injured spinal cord: endogenous neuroprotection', *Brain Res*, 1231: 63-74.
Liu, X., Z. Zhao, R. Ji, J. Zhu, Q. Q. Sui, G. E. Knight, G. Burnstock, C. He, H. Yuan, and Z. Xiang. 2017. 'Inhibition of P2X7 receptors improves outcomes after traumatic brain injury in rats', *Purinergic Signal*, 13: 529-44.
Liu, Z., Y. Yang, L. He, M. Pang, C. Luo, B. Liu, and L. Rong. 2019. 'High-dose methylprednisolone for acute traumatic spinal cord injury: A meta-analysis', *Neurology*, 93: e841-e50.

Liu, Z., X. Yao, W. Jiang, W. Li, S. Zhu, C. Liao, L. Zou, R. Ding, and J. Chen. 2020. 'Advanced oxidation protein products induce microglia-mediated neuroinflammation via MAPKs-NF-kappaB signaling pathway and pyroptosis after secondary spinal cord injury', *J Neuroinflammation*, 17: 90.

London, A., M. Cohen, and M. Schwartz. 2013. 'Microglia and monocyte-derived macrophages: functionally distinct populations that act in concert in CNS plasticity and repair', *Front Cell Neurosci*, 7: 34.

Losey, P., and D. C. Anthony. 2014. 'Impact of vasculature damage on the outcome of spinal cord injury: a novel collagenase-induced model may give new insights into the mechanisms involved', *Neural Regen Res*, 9: 1783-6.

Losey, P., C. Young, E. Krimholtz, R. Bordet, and D. C. Anthony. 2014. 'The role of hemorrhage following spinal-cord injury', *Brain Res*, 1569: 9-18.

Lu, P., Y. Wang, L. Graham, K. McHale, M. Gao, D. Wu, J. Brock, A. Blesch, E. S. Rosenzweig, L. A. Havton, B. Zheng, J. M. Conner, M. Marsala, and M. H. Tuszynski. 2012. 'Long-distance growth and connectivity of neural stem cells after severe spinal cord injury', *Cell*, 150: 1264-73.

Luchetti, S., K. D. Beck, M. D. Galvan, R. Silva, B. J. Cummings, and A. J. Anderson. 2010. 'Comparison of immunopathology and locomotor recovery in C57BL/6, BUB/BnJ, and NOD-SCID mice after contusion spinal cord injury', *J Neurotrauma*, 27: 411-21.

Lucin, K. M., V. M. Sanders, T. B. Jones, W. B. Malarkey, and P. G. Popovich. 2007. 'Impaired antibody synthesis after spinal cord injury is level dependent and is due to sympathetic nervous system dysregulation', *Exp Neurol*, 207: 75-84.

Luedtke, K., S. M. Bouchard, S. A. Woller, M. K. Funk, M. Aceves, and M. A. Hook. 2014. 'Assessment of depression in a rodent model of spinal cord injury', *J Neurotrauma*, 31: 1107-21.

Lukovic, D., V. Moreno-Manzano, E. Lopez-Mocholi, F. J. Rodriguez-Jimenez, P. Jendelova, E. Sykova, M. Oria, M. Stojkovic, and S. Erceg. 2015. 'Complete rat spinal cord transection as a faithful model of spinal cord injury for translational cell transplantation', *Sci Rep*, 5: 9640.

Ma, M., D. M. Basso, P. Walters, B. T. Stokes, and L. B. Jakeman. 2001. 'Behavioral and histological outcomes following graded spinal cord contusion injury in the C57Bl/6 mouse', *Exp Neurol*, 169: 239-54.

Ma, S. F., Y. J. Chen, J. X. Zhang, L. Shen, R. Wang, J. S. Zhou, J. G. Hu, and H. Z. Lu. 2015. 'Adoptive transfer of M2 macrophages promotes locomotor recovery in adult rats after spinal cord injury', *Brain Behav Immun*, 45: 157-70.

Mabon, P. J., L. C. Weaver, and G. A. Dekaban. 2000. 'Inhibition of monocyte/macrophage migration to a spinal cord injury site by an antibody to the integrin alphaD: a potential new anti-inflammatory treatment', *Exp Neurol*, 166: 52-64.

MacLeod, A. S., and J. N. Mansbridge. 2016. 'The Innate Immune System in Acute and Chronic Wounds', *Adv Wound Care (New Rochelle)*, 5: 65-78.

MacParland, S. A., J. C. Liu, X. Z. Ma, B. T. Innes, A. M. Bartczak, B. K. Gage, J. Manuel, et al. 2018. 'Single cell RNA sequencing of human liver reveals distinct intrahepatic macrophage populations', *Nat Commun*, 9: 4383.

Madhavan, K., D. M. Benglis, M. Y. Wang, S. Vanni, N. Lebwohl, B. A. Green, and A. D. Levi. 2012. 'The use of modest systemic hypothermia after iatrogenic spinal cord injury during surgery', *Ther Hypothermia Temp Manag*, 2: 183-92.

Mahmoudi, E., P. Lin, M. D. Peterson, M. Meade, D. G. Tate, and N. Kamdar. 2021. 'Traumatic Spinal Cord Injury and Risk of Early and Late Onset Alzheimer's Disease and related Dementia: Large Longitudinal Study', *Arch Phys Med Rehabil*.

Maier, A., N. Deigendesch, K. Muller, J. H. Weishaupt, A. Krannich, R. Rohle, F. Meissner, K. Molawi, C. Munch, T. Holm, R. Meyer, T. Meyer, and A. Zychlinsky. 2015. 'Interleukin-1 Antagonist Anakinra in Amyotrophic Lateral Sclerosis--A Pilot Study', *PLoS One*, 10: e0139684.

Maier, I. C., R. M. Ichiyama, G. Courtine, L. Schnell, I. Lavrov, V. R. Edgerton, and M. E. Schwab. 2009. 'Differential effects of anti-Nogo-A antibody treatment and treadmill training in rats with incomplete spinal cord injury', *Brain*, 132: 1426-40.

Maldonado-Bouchard, S., K. Peters, S. A. Woller, B. Madahian, U. Faghihi, S. Patel, S. Bake, and M. A. Hook. 2016. 'Inflammation is increased with anxiety- and depression-like signs in a rat model of spinal cord injury', *Brain Behav Immun*, 51: 176-95.
Marangos, P. J., I. C. Campbell, D. E. Schmechel, D. L. Murphy, and F. K. Goodwin. 1980. 'Blood platelets contain a neuron-specific enolase subunit', *J Neurochem*, 34: 1254-8.
Marinelli, S., V. Vacca, F. De Angelis, L. Pieroni, T. Orsini, C. Parisi, M. Soligo, V. Protto, L. Manni, R. Guerrieri, and F. Pavone. 2019. 'Innovative mouse model mimicking human-like features of spinal cord injury: efficacy of Docosahexaenoic acid on acute and chronic phases', *Sci Rep*, 9: 8883.
Martha, S. R., K. F. Chen, Y. Lin, and H. J. Thompson. 2021. 'Plasma Phospholipid Metabolites Associate With Functional Outcomes Following Mild Traumatic Brain Injury in Older Adults', *Biol Res Nurs*, 23: 127-35.
Martirosyan, N. L., J. S. Feuerstein, N. Theodore, D. D. Cavalcanti, R. F. Spetzler, and M. C. Preul. 2011. 'Blood supply and vascular reactivity of the spinal cord under normal and pathological conditions', *J Neurosurg Spine*, 15: 238-51.
Maruyama, Y., M. Mizuguchi, T. Yaginuma, M. Kusaka, H. Yoshida, K. Yokoyama, Y. Kasahara, and T. Hosoya. 2008. 'Serum leptin, abdominal obesity and the metabolic syndrome in individuals with chronic spinal cord injury', *Spinal Cord*, 46: 494-9.
Matsumura, S., T. Minamisawa, K. Suga, H. Kishita, T. Akagi, T. Ichiki, Y. Ichikawa, and K. Shiba. 2019. 'Subtypes of tumour cell-derived small extracellular vesicles having differently externalized phosphatidylserine', *J Extracell Vesicles*, 8: 1579541.
Maynard, F. M., Jr., M. B. Bracken, G. Creasey, J. F. Ditunno, Jr., W. H. Donovan, T. B. Ducker, S. L. Garber, R. J. Marino, S. L. Stover, C. H. Tator, R. L. Waters, J. E. Wilberger, and W. Young. 1997. 'International Standards for Neurological and Functional Classification of Spinal Cord Injury. American Spinal Injury Association', *Spinal Cord*, 35: 266-74.
Maysami, S., R. Wong, J. M. Pradillo, A. Denes, H. Dhungana, T. Malm, J. Koistinaho, et al. 2016. 'A cross-laboratory preclinical study on the effectiveness of interleukin-1 receptor antagonist in stroke', *J Cereb Blood Flow Metab*, 36: 596-605.
McColl, B. W., N. J. Rothwell, and S. M. Allan. 2007. 'Systemic inflammatory stimulus potentiates the acute phase and CXC chemokine responses to experimental stroke and exacerbates brain damage via interleukin-1- and neutrophil-dependent mechanisms', *J Neurosci*, 27: 4403-12.
———. 2008. 'Systemic inflammation alters the kinetics of cerebrovascular tight junction disruption after experimental stroke in mice', *J Neurosci*, 28: 9451-62.
McDaid, D., A. L. Park, A. Gall, M. Purcell, and M. Bacon. 2019. 'Understanding and modelling the economic impact of spinal cord injuries in the United Kingdom', *Spinal Cord*, 57: 778-88.
McDonald, J. W., X. Z. Liu, Y. Qu, S. Liu, S. K. Mickey, D. Turetsky, D. I. Gottlieb, and D. W. Choi. 1999. 'Transplanted embryonic stem cells survive, differentiate and promote recovery in injured rat spinal cord', *Nat Med*, 5: 1410-2.
McKinley, W., M. A. Meade, S. Kirshblum, and B. Barnard. 2004. 'Outcomes of early surgical management versus late or no surgical intervention after acute spinal cord injury', *Arch Phys Med Rehabil*, 85: 1818-25.
McNicholas, K., J. Y. Li, M. Z. Michael, and J. M. Gleadle. 2017. 'Albuminuria is not associated with elevated urinary vesicle concentration but can confound nanoparticle tracking analysis', *Nephrology (Carlton)*, 22: 854-63.
McPherson, C. A., M. Aoyama, and G. J. Harry. 2011. 'Interleukin (IL)-1 and IL-6 regulation of neural progenitor cell proliferation with hippocampal injury: differential regulatory pathways in the subgranular zone (SGZ) of the adolescent and mature mouse brain', *Brain Behav Immun*, 25: 850-62.
McTigue, D. M., P. G. Popovich, T. E. Morgan, and B. T. Stokes. 2000. 'Localization of transforming growth factor-beta1 and receptor mRNA after experimental spinal cord injury', *Exp Neurol*, 163: 220-30.
Medicine, US National Library of. 2021. 'Anakinra', Accessed 28/03/21. https://medlineplus.gov/druginfo/meds/a602001.html#:~:text=Store%20anakinra%20syringes%20in%20the,for%20more%20than%2024%20hours.

Merrill, J. E., L. J. Ignarro, M. P. Sherman, J. Melinek, and T. E. Lane. 1993. 'Microglial cell cytotoxicity of oligodendrocytes is mediated through nitric oxide', *J Immunol*, 151: 2132-41.
Mertens, M., and J. A. Singh. 2009. 'Anakinra for rheumatoid arthritis: a systematic review', *J Rheumatol*, 36: 1118-25.
Messenger, S. W., S. S. Woo, Z. Sun, and T. F. J. Martin. 2018. 'A Ca(2+)-stimulated exosome release pathway in cancer cells is regulated by Munc13-4', *J Cell Biol*, 217: 2877-90.
Metz, G. A., A. Curt, H. van de Meent, I. Klusman, M. E. Schwab, and V. Dietz. 2000. 'Validation of the weight-drop contusion model in rats: a comparative study of human spinal cord injury', *J Neurotrauma*, 17: 1-17.
Middleton, J. W., A. Dayton, J. Walsh, S. B. Rutkowski, G. Leong, and S. Duong. 2012. 'Life expectancy after spinal cord injury: a 50-year study', *Spinal Cord*, 50: 803-11.
Milich, L. M., C. B. Ryan, and J. K. Lee. 2019. 'The origin, fate, and contribution of macrophages to spinal cord injury pathology', *Acta Neuropathol*, 137: 785-97.
Mills, C. D., K. Kincaid, J. M. Alt, M. J. Heilman, and A. M. Hill. 2000. 'M-1/M-2 macrophages and the Th1/Th2 paradigm', *J Immunol*, 164: 6166-73.
Minagar, A., W. Jy, J. J. Jimenez, W. A. Sheremata, L. M. Mauro, W. W. Mao, L. L. Horstman, and Y. S. Ahn. 2001. 'Elevated plasma endothelial microparticles in multiple sclerosis', *Neurology*, 56: 1319-24.
Miron, V. E., A. Boyd, J. W. Zhao, T. J. Yuen, J. M. Ruckh, J. L. Shadrach, P. van Wijngaarden, A. J. Wagers, A. Williams, R. J. M. Franklin, and C. Ffrench-Constant. 2013. 'M2 microglia and macrophages drive oligodendrocyte differentiation during CNS remyelination', *Nat Neurosci*, 16: 1211-18.
Miyanji, F., J. C. Furlan, B. Aarabi, P. M. Arnold, and M. G. Fehlings. 2007. 'Acute cervical traumatic spinal cord injury: MR imaging findings correlated with neurologic outcome--prospective study with 100 consecutive patients', *Radiology*, 243: 820-7.
Mol, E. A., M. J. Goumans, P. A. Doevendans, J. P. G. Sluijter, and P. Vader. 2017. 'Higher functionality of extracellular vesicles isolated using size-exclusion chromatography compared to ultracentrifugation', *Nanomedicine*, 13: 2061-65.
Monteiro, S., A. G. Pinho, M. Macieira, C. Serre-Miranda, J. R. Cibrao, R. Lima, C. Soares-Cunha, N. L. Vasconcelos, J. Lentilhas-Graca, S. Duarte-Silva, A. Miranda, M. Correia-Neves, A. J. Salgado, and N. A. Silva. 2020. 'Splenic sympathetic signaling contributes to acute neutrophil infiltration of the injured spinal cord', *J Neuroinflammation*, 17: 282.
Moran, A., B. Bundy, D. J. Becker, L. A. DiMeglio, S. E. Gitelman, R. Goland, C. J. Greenbaum, et al. 2013. 'Interleukin-1 antagonism in type 1 diabetes of recent onset: two multicentre, randomised, double-blind, placebo-controlled trials', *Lancet*, 381: 1905-15.
Morganti-Kossmann, Cristina, Ramesh Raghupathi, and Andrew I. R. Maas. 2012. *Traumatic brain and spinal cord injury : challenges and developments* (Cambridge University Press: Cambridge).
Motulsky, H. J., and R. E. Brown. 2006. 'Detecting outliers when fitting data with nonlinear regression - a new method based on robust nonlinear regression and the false discovery rate', *BMC Bioinformatics*, 7: 123.
Mousavi, M., A. Hedayatpour, K. Mortezaee, Y. Mohamadi, F. Abolhassani, and G. Hassanzadeh. 2019. 'Schwann cell transplantation exerts neuroprotective roles in rat model of spinal cord injury by combating inflammasome activation and improving motor recovery and remyelination', *Metab Brain Dis*, 34: 1117-30.
Moxon-Emre, I., and L. C. Schlichter. 2011. 'Neutrophil depletion reduces blood-brain barrier breakdown, axon injury, and inflammation after intracerebral hemorrhage', *J Neuropathol Exp Neurol*, 70: 218-35.
Moyron, R. B., A. Gonda, M. J. Selleck, X. Luo-Owen, R. D. Catalano, T. O'Callahan, C. Garberoglio, D. Turay, and N. R. Wall. 2017. 'Differential protein expression in exosomal samples taken from trauma patients', *Proteomics Clin Appl*, 11.
Murgoci, A. N., M. Duhamel, A. Raffo-Romero, K. Mallah, S. Aboulouard, C. Lefebvre, F. Kobeissy, I. Fournier, M. Zilkova, D. Maderova, M. Cizek, D. Cizkova, and M. Salzet. 2020. 'Location of neonatal microglia drives small extracellular vesicles content and biological functions in vitro', *J Extracell Vesicles*, 9: 1727637.

Murray, K. N., A. R. Parry-Jones, and S. M. Allan. 2015. 'Interleukin-1 and acute brain injury', *Front Cell Neurosci*, 9: 18.
Mustapic, M., E. Eitan, J. K. Werner, Jr., S. T. Berkowitz, M. P. Lazaropoulos, J. Tran, E. J. Goetzl, and D. Kapogiannis. 2017. 'Plasma Extracellular Vesicles Enriched for Neuronal Origin: A Potential Window into Brain Pathologic Processes', *Front Neurosci*, 11: 278.
Myers, J., M. Lee, and J. Kiratli. 2007. 'Cardiovascular disease in spinal cord injury: an overview of prevalence, risk, evaluation, and management', *Am J Phys Med Rehabil*, 86: 142-52.
Nakamura, I., K. Ochiai, and M. Imawari. 2004. 'Phagocytic function of neutrophils of patients with decompensated liver cirrhosis is restored by oral supplementation of branched-chain amino acids', *Hepatol Res*, 29: 207-11.
Nakashima, S., S. A. Arnold, E. T. Mahoney, S. D. Sithu, Y. P. Zhang, S. E. D'Souza, C. B. Shields, and T. Hagg. 2008. 'Small-molecule protein tyrosine phosphatase inhibition as a neuroprotective treatment after spinal cord injury in adult rats', *J Neurosci*, 28: 7293-303.
Nandoe Tewarie, R. S., A. Hurtado, R. H. Bartels, A. Grotenhuis, and M. Oudega. 2009. 'Stem cell-based therapies for spinal cord injury', *J Spinal Cord Med*, 32: 105-14.
Neirinckx, V., C. Coste, R. Franzen, A. Gothot, B. Rogister, and S. Wislet. 2014. 'Neutrophil contribution to spinal cord injury and repair', *J Neuroinflammation*, 11: 150.
Nekludov, M., F. Mobarrez, D. Gryth, B. M. Bellander, and H. Wallen. 2014. 'Formation of microparticles in the injured brain of patients with severe isolated traumatic brain injury', *J Neurotrauma*, 31: 1927-33.
Nesic, O., G. Y. Xu, D. McAdoo, K. W. High, C. Hulsebosch, and R. Perez-Pol. 2001. 'IL-1 receptor antagonist prevents apoptosis and caspase-3 activation after spinal cord injury', *J Neurotrauma*, 18: 947-56.
Newell, E. A., B. P. Todd, J. Mahoney, A. A. Pieper, P. J. Ferguson, and A. G. Bassuk. 2018. 'Combined Blockade of Interleukin-1alpha and -1beta Signaling Protects Mice from Cognitive Dysfunction after Traumatic Brain Injury', *eNeuro*, 5.
Nguyen, D. H., N. Cho, K. Satkunendrarajah, J. W. Austin, J. Wang, and M. G. Fehlings. 2012. 'Immunoglobulin G (IgG) attenuates neuroinflammation and improves neurobehavioral recovery after cervical spinal cord injury', *J Neuroinflammation*, 9: 224.
Nguyen, H. X., T. J. O'Barr, and A. J. Anderson. 2007. 'Polymorphonuclear leukocytes promote neurotoxicity through release of matrix metalloproteinases, reactive oxygen species, and TNF-alpha', *J Neurochem*, 102: 900-12.
Niederost, B., T. Oertle, J. Fritsche, R. A. McKinney, and C. E. Bandtlow. 2002. 'Nogo-A and myelin-associated glycoprotein mediate neurite growth inhibition by antagonistic regulation of RhoA and Rac1', *J Neurosci*, 22: 10368-76.
Nikodemova, M., I. D. Duncan, and J. J. Watters. 2006. 'Minocycline exerts inhibitory effects on multiple mitogen-activated protein kinases and IkappaBalpha degradation in a stimulus-specific manner in microglia', *J Neurochem*, 96: 314-23.
Nishikawa, T., D. Edelstein, X. L. Du, S. Yamagishi, T. Matsumura, Y. Kaneda, M. A. Yorek, D. Beebe, P. J. Oates, H. P. Hammes, I. Giardino, and M. Brownlee. 2000. 'Normalizing mitochondrial superoxide production blocks three pathways of hyperglycaemic damage', *Nature*, 404: 787-90.
Noble, L. J., and J. R. Wrathall. 1989. 'Correlative analyses of lesion development and functional status after graded spinal cord contusive injuries in the rat', *Exp Neurol*, 103: 34-40.
Nonogaki, K. 2000. 'New insights into sympathetic regulation of glucose and fat metabolism', *Diabetologia*, 43: 533-49.
Nordin, J. Z., Y. Lee, P. Vader, I. Mager, H. J. Johansson, W. Heusermann, O. P. Wiklander, et al. 2015. 'Ultrafiltration with size-exclusion liquid chromatography for high yield isolation of extracellular vesicles preserving intact biophysical and functional properties', *Nanomedicine*, 11: 879-83.
O'Connor, G., E. Jeffrey, D. Madorma, A. Marcillo, M. T. Abreu, S. K. Deo, W. D. Dietrich, and S. Daunert. 2018. 'Investigation of Microbiota Alterations and Intestinal Inflammation Post-Spinal Cord Injury in Rat Model', *J Neurotrauma*, 35: 2159-66.

Offner, H., S. Subramanian, S. M. Parker, M. E. Afentoulis, A. A. Vandenbark, and P. D. Hurn. 2006. 'Experimental stroke induces massive, rapid activation of the peripheral immune system', *J Cereb Blood Flow Metab*, 26: 654-65.

Ogurcov, S., I. Shulman, E. Garanina, D. Sabirov, I. Baichurina, M. Kuznetcov, G. Masgutova, A. Kostennikov, A. Rizvanov, V. James, and Y. Mukhamedshina. 2021. 'Blood Serum Cytokines in Patients with Subacute Spinal Cord Injury: A Pilot Study to Search for Biomarkers of Injury Severity', *Brain Sci*, 11.

Okada, S., M. Nakamura, H. Katoh, T. Miyao, T. Shimazaki, K. Ishii, J. Yamane, A. Yoshimura, Y. Iwamoto, Y. Toyama, and H. Okano. 2006. 'Conditional ablation of Stat3 or Socs3 discloses a dual role for reactive astrocytes after spinal cord injury', *Nat Med*, 12: 829-34.

Oliveri, R. S., S. Bello, and F. Biering-Sorensen. 2014. 'Mesenchymal stem cells improve locomotor recovery in traumatic spinal cord injury: systematic review with meta-analyses of rat models', *Neurobiol Dis*, 62: 338-53.

Olson, J. K., and S. D. Miller. 2004. 'Microglia initiate central nervous system innate and adaptive immune responses through multiple TLRs', *J Immunol*, 173: 3916-24.

Oresic, M., J. P. Posti, M. H. Kamstrup-Nielsen, R. S. K. Takala, H. F. Lingsma, I. Mattila, S. Jantti, et al. 2016. 'Human Serum Metabolites Associate With Severity and Patient Outcomes in Traumatic Brain Injury', *EBioMedicine*, 12: 118-26.

Osaka, M., O. Honmou, T. Murakami, T. Nonaka, K. Houkin, H. Hamada, and J. D. Kocsis. 2010. 'Intravenous administration of mesenchymal stem cells derived from bone marrow after contusive spinal cord injury improves functional outcome', *Brain Res*, 1343: 226-35.

Osier, N., V. Motamedi, K. Edwards, A. Puccio, R. Diaz-Arrastia, K. Kenney, and J. Gill. 2018. 'Exosomes in Acquired Neurological Disorders: New Insights into Pathophysiology and Treatment', *Mol Neurobiol*, 55: 9280-93.

Osler, T., S. P. Baker, and W. Long. 1997. 'A modification of the injury severity score that both improves accuracy and simplifies scoring', *J Trauma*, 43: 922-5; discussion 25-6.

Otxoa-de-Amezaga, A., F. Miro-Mur, J. Pedragosa, M. Gallizioli, C. Justicia, N. Gaja-Capdevila, F. Ruiz-Jaen, A. Salas-Perdomo, A. Bosch, M. Calvo, L. Marquez-Kisinousky, A. Denes, M. Gunzer, and A. M. Planas. 2019. 'Microglial cell loss after ischemic stroke favors brain neutrophil accumulation', *Acta Neuropathol*, 137: 321-41.

Oudega, M., and X. M. Xu. 2006. 'Schwann cell transplantation for repair of the adult spinal cord', *J Neurotrauma*, 23: 453-67.

Oushy, S., J. E. Hellwinkel, M. Wang, G. J. Nguyen, D. Gunaydin, T. A. Harland, T. J. Anchordoquy, and M. W. Graner. 2018. 'Glioblastoma multiforme-derived extracellular vesicles drive normal astrocytes towards a tumour-enhancing phenotype', *Philos Trans R Soc Lond B Biol Sci*, 373.

Pagadala, M., T. Kasumov, A. J. McCullough, N. N. Zein, and J. P. Kirwan. 2012. 'Role of ceramides in nonalcoholic fatty liver disease', *Trends Endocrinol Metab*, 23: 365-71.

Paolicelli, R. C., G. Bolasco, F. Pagani, L. Maggi, M. Scianni, P. Panzanelli, M. Giustetto, T. A. Ferreira, E. Guiducci, L. Dumas, D. Ragozzino, and C. T. Gross. 2011. 'Synaptic pruning by microglia is necessary for normal brain development', *Science*, 333: 1456-8.

Park, E., A. A. Velumian, and M. G. Fehlings. 2004. 'The role of excitotoxicity in secondary mechanisms of spinal cord injury: a review with an emphasis on the implications for white matter degeneration', *J Neurotrauma*, 21: 754-74.

Parr, A. M., I. Kulbatski, and C. H. Tator. 2007. 'Transplantation of adult rat spinal cord stem/progenitor cells for spinal cord injury', *J Neurotrauma*, 24: 835-45.

Pasquet, J. M., J. Dachary-Prigent, and A. T. Nurden. 1996. 'Calcium influx is a determining factor of calpain activation and microparticle formation in platelets', *Eur J Biochem*, 239: 647-54.

Patel, A. A., Y. Zhang, J. N. Fullerton, L. Boelen, A. Rongvaux, A. A. Maini, V. Bigley, R. A. Flavell, D. W. Gilroy, B. Asquith, D. Macallan, and S. Yona. 2017. 'The fate and lifespan of human monocyte subsets in steady state and systemic inflammation', *J Exp Med*, 214: 1913-23.

Patti, G. J., O. Yanes, and G. Siuzdak. 2012. 'Innovation: Metabolomics: the apogee of the omics trilogy', *Nat Rev Mol Cell Biol*, 13: 263-9.

Peiseler, M., and P. Kubes. 2019. 'More friend than foe: the emerging role of neutrophils in tissue repair', *J Clin Invest*, 129: 2629-39.

Peltz, E. D., A. D'Alessandro, E. E. Moore, T. Chin, C. C. Silliman, A. Sauaia, K. C. Hansen, and A. Banerjee. 2015. 'Pathologic metabolism: an exploratory study of the plasma metabolome of critical injury', *J Trauma Acute Care Surg*, 78: 742-51.
Peng, J., J. Zeng, B. Cai, H. Yang, M. J. Cohen, W. Chen, M. W. Sun, C. D. Lu, and H. Jiang. 2014. 'Establishment of quantitative severity evaluation model for spinal cord injury by metabolomic fingerprinting', *PLoS One*, 9: e93736.
Perner, A., S. E. Nielsen, and J. Rask-Madsen. 2003. 'High glucose impairs superoxide production from isolated blood neutrophils', *Intensive Care Med*, 29: 642-5.
Peterson, M. D., N. Kamdar, A. Chiodo, and D. G. Tate. 2020. 'Psychological Morbidity and Chronic Disease Among Adults With Traumatic Spinal Cord Injuries: A Longitudinal Cohort Study of Privately Insured Beneficiaries', *Mayo Clin Proc*, 95: 920-28.
Phipps, M. S., and C. A. Cronin. 2020. 'Management of acute ischemic stroke', *BMJ*, 368: l6983.
Piao, M. S., J. K. Lee, J. W. Jang, S. H. Kim, and H. S. Kim. 2009a. 'A mouse model of photochemically induced spinal cord injury', *J Korean Neurosurg Soc*, 46: 479-83.
Piao, W., C. Song, H. Chen, M. A. Diaz, L. M. Wahl, K. A. Fitzgerald, L. Li, and A. E. Medvedev. 2009b. 'Endotoxin tolerance dysregulates MyD88- and Toll/IL-1R domain-containing adapter inducing IFN-beta-dependent pathways and increases expression of negative regulators of TLR signaling', *J Leukoc Biol*, 86: 863-75.
Pineau, I., and S. Lacroix. 2007. 'Proinflammatory cytokine synthesis in the injured mouse spinal cord: multiphasic expression pattern and identification of the cell types involved', *J Comp Neurol*, 500: 267-85.
Pineau, I., L. Sun, D. Bastien, and S. Lacroix. 2010. 'Astrocytes initiate inflammation in the injured mouse spinal cord by promoting the entry of neutrophils and inflammatory monocytes in an IL-1 receptor/MyD88-dependent fashion', *Brain Behav Immun*, 24: 540-53.
Plane, J. M., Y. Shen, D. E. Pleasure, and W. Deng. 2010. 'Prospects for minocycline neuroprotection', *Arch Neurol*, 67: 1442-8.
Poon, I. K. H., M. A. F. Parkes, L. Jiang, G. K. Atkin-Smith, R. Tixeira, C. D. Gregory, D. C. Ozkocak, et al. 2019. 'Moving beyond size and phosphatidylserine exposure: evidence for a diversity of apoptotic cell-derived extracellular vesicles in vitro', *J Extracell Vesicles*, 8: 1608786.
Poon, P. C., D. Gupta, M. S. Shoichet, and C. H. Tator. 2007. 'Clip compression model is useful for thoracic spinal cord injuries: histologic and functional correlates', *Spine (Phila Pa 1976)*, 32: 2853-9.
Popovich, P. G., Z. Guan, P. Wei, I. Huitinga, N. van Rooijen, and B. T. Stokes. 1999. 'Depletion of hematogenous macrophages promotes partial hindlimb recovery and neuroanatomical repair after experimental spinal cord injury', *Exp Neurol*, 158: 351-65.
Popovich, P. G., P. J. Horner, B. B. Mullin, and B. T. Stokes. 1996a. 'A quantitative spatial analysis of the blood-spinal cord barrier. I. Permeability changes after experimental spinal contusion injury', *Exp Neurol*, 142: 258-75.
Popovich, P. G., B. T. Stokes, and C. C. Whitacre. 1996b. 'Concept of autoimmunity following spinal cord injury: possible roles for T lymphocytes in the traumatized central nervous system', *J Neurosci Res*, 45: 349-63.
Popovich, P. G., P. Wei, and B. T. Stokes. 1997. 'Cellular inflammatory response after spinal cord injury in Sprague-Dawley and Lewis rats', *J Comp Neurol*, 377: 443-64.
Posti, J. P., A. M. Dickens, M. Oresic, T. Hyotylainen, and O. Tenovuo. 2017. 'Metabolomics Profiling As a Diagnostic Tool in Severe Traumatic Brain Injury', *Front Neurol*, 8: 398.
Potas, J. R., Y. Zheng, C. Moussa, M. Venn, C. A. Gorrie, C. Deng, and P. M. Waite. 2006. 'Augmented locomotor recovery after spinal cord injury in the athymic nude rat', *J Neurotrauma*, 23: 660-73.
Pradillo, J. M., A. Denes, A. D. Greenhalgh, H. Boutin, C. Drake, B. W. McColl, E. Barton, S. D. Proctor, J. C. Russell, N. J. Rothwell, and S. M. Allan. 2012. 'Delayed administration of interleukin-1 receptor antagonist reduces ischemic brain damage and inflammation in comorbid rats', *J Cereb Blood Flow Metab*, 32: 1810-9.
Pradillo, J. M., K. N. Murray, G. A. Coutts, A. Moraga, F. Oroz-Gonjar, H. Boutin, M. A. Moro, I. Lizasoain, N. J. Rothwell, and S. M. Allan. 2017. 'Reparative effects of interleukin-1 receptor

antagonist in young and aged/co-morbid rodents after cerebral ischemia', *Brain Behav Immun*, 61: 117-26.
Probert, F., A. Walsh, M. Jagielowicz, T. Yeo, T. D. W. Claridge, A. Simmons, S. Travis, and D. C. Anthony. 2018. 'Plasma Nuclear Magnetic Resonance Metabolomics Discriminates Between High and Low Endoscopic Activity and Predicts Progression in a Prospective Cohort of Patients With Ulcerative Colitis', *J Crohns Colitis*, 12: 1326-37.
Pruss, H., A. Tedeschi, A. Thiriot, L. Lynch, S. M. Loughhead, S. Stutte, I. B. Mazo, et al. 2017. 'Spinal cord injury-induced immunodeficiency is mediated by a sympathetic-neuroendocrine adrenal reflex', *Nat Neurosci*, 20: 1549-59.
Qiao, F., C. Atkinson, H. Song, R. Pannu, I. Singh, and S. Tomlinson. 2006. 'Complement plays an important role in spinal cord injury and represents a therapeutic target for improving recovery following trauma', *Am J Pathol*, 169: 1039-47.
Rankin, K. C., L. C. O'Brien, L. Segal, M. R. Khan, and A. S. Gorgey. 2017. 'Liver Adiposity and Metabolic Profile in Individuals with Chronic Spinal Cord Injury', *Biomed Res Int*, 2017: 1364818.
Rao, R., S. Trivedi, Z. Vesoulis, S. M. Liao, C. D. Smyser, and A. M. Mathur. 2017. 'Safety and Short-Term Outcomes of Therapeutic Hypothermia in Preterm Neonates 34-35 Weeks Gestational Age with Hypoxic-Ischemic Encephalopathy', *J Pediatr*, 183: 37-42.
Raposo, G., H. W. Nijman, W. Stoorvogel, R. Liejendekker, C. V. Harding, C. J. Melief, and H. J. Geuze. 1996. 'B lymphocytes secrete antigen-presenting vesicles', *J Exp Med*, 183: 1161-72.
Raposo, G., and W. Stoorvogel. 2013. 'Extracellular vesicles: exosomes, microvesicles, and friends', *J Cell Biol*, 200: 373-83.
Raymond, J., A. R. Harmer, J. Temesi, and C. van Kemenade. 2010. 'Glucose tolerance and physical activity level in people with spinal cord injury', *Spinal Cord*, 48: 591-6.
Ren, H., X. Chen, M. Tian, J. Zhou, H. Ouyang, and Z. Zhang. 2018. 'Regulation of Inflammatory Cytokines for Spinal Cord Injury Repair Through Local Delivery of Therapeutic Agents', *Adv Sci (Weinh)*, 5: 1800529.
Ridder, K., S. Keller, M. Dams, A. K. Rupp, J. Schlaudraff, D. Del Turco, J. Starmann, et al. 2014. 'Extracellular vesicle-mediated transfer of genetic information between the hematopoietic system and the brain in response to inflammation', *PLoS Biol*, 12: e1001874.
Riegger, T., S. Conrad, K. Liu, H. J. Schluesener, M. Adibzahdeh, and J. M. Schwab. 2007. 'Spinal cord injury-induced immune depression syndrome (SCI-IDS)', *Eur J Neurosci*, 25: 1743-7.
Riegger, T., S. Conrad, H. J. Schluesener, H. P. Kaps, A. Badke, C. Baron, J. Gerstein, K. Dietz, M. Abdizahdeh, and J. M. Schwab. 2009. 'Immune depression syndrome following human spinal cord injury (SCI): a pilot study', *Neuroscience*, 158: 1194-9.
Robbins, P. D., A. Dorronsoro, and C. N. Booker. 2016. 'Regulation of chronic inflammatory and immune processes by extracellular vesicles', *J Clin Invest*, 126: 1173-80.
Rogeri, P. S., and L. F. Costa Rosa. 2005. 'Plasma glutamine concentration in spinal cord injured patients', *Life Sci*, 77: 2351-60.
Rong, H., Y. Fan, M. Yang, B. Zhang, D. Sun, Z. Zhao, D. Wang, et al. 2018. 'Brain-derived microparticles activate microglia/macrophages and induce neuroinflammation', *Brain Res*, 1694: 104-10.
Rosales, C. 2018. 'Neutrophil: A Cell with Many Roles in Inflammation or Several Cell Types?', *Front Physiol*, 9: 113.
Ruiz, I. A., J. W. Squair, A. A. Phillips, C. D. Lukac, D. Huang, P. Oxciano, D. Yan, and A. V. Krassioukov. 2018. 'Incidence and Natural Progression of Neurogenic Shock after Traumatic Spinal Cord Injury', *J Neurotrauma*, 35: 461-66.
Ryan, M. E., A. Usman, N. S. Ramamurthy, L. M. Golub, and R. A. Greenwald. 2001. 'Excessive matrix metalloproteinase activity in diabetes: inhibition by tetracycline analogues with zinc reactivity', *Curr Med Chem*, 8: 305-16.
Sa-Pereira, I., J. Roodselaar, Y. Couch, M. Consentino Kronka Sosthenes, M. C. Evans, D. C. Anthony, and H. B. Stolp. 2018. 'Hepatic acute phase response protects the brain from focal inflammation during postnatal window of susceptibility', *Brain Behav Immun*, 69: 486-98.

Saiwai, H., Y. Ohkawa, H. Yamada, H. Kumamaru, A. Harada, H. Okano, T. Yokomizo, Y. Iwamoto, and S. Okada. 2010. 'The LTB4-BLT1 axis mediates neutrophil infiltration and secondary injury in experimental spinal cord injury', *Am J Pathol*, 176: 2352-66.

Salliot, C., M. Dougados, and L. Gossec. 2009. 'Risk of serious infections during rituximab, abatacept and anakinra treatments for rheumatoid arthritis: meta-analyses of randomised placebo-controlled trials', *Ann Rheum Dis*, 68: 25-32.

Saltzman, J. W., R. A. Battaglino, L. Salles, P. Jha, S. Sudhakar, E. Garshick, H. L. Stott, R. Zafonte, and L. R. Morse. 2013. 'B-cell maturation antigen, a proliferation-inducing ligand, and B-cell activating factor are candidate mediators of spinal cord injury-induced autoimmunity', *J Neurotrauma*, 30: 434-40.

Saman, S., W. Kim, M. Raya, Y. Visnick, S. Miro, S. Saman, B. Jackson, A. C. McKee, V. E. Alvarez, N. C. Lee, and G. F. Hall. 2012. 'Exosome-associated tau is secreted in tauopathy models and is selectively phosphorylated in cerebrospinal fluid in early Alzheimer disease', *J Biol Chem*, 287: 3842-9.

Sanchez-Ramos, J., S. Song, F. Cardozo-Pelaez, C. Hazzi, T. Stedeford, A. Willing, T. B. Freeman, S. Saporta, W. Janssen, N. Patel, D. R. Cooper, and P. R. Sanberg. 2000. 'Adult bone marrow stromal cells differentiate into neural cells in vitro', *Exp Neurol*, 164: 247-56.

Sanchez Mejia, R. O., V. O. Ona, M. Li, and R. M. Friedlander. 2001. 'Minocycline reduces traumatic brain injury-mediated caspase-1 activation, tissue damage, and neurological dysfunction', *Neurosurgery*, 48: 1393-9; discussion 99-401.

Sas, A. R., K. S. Carbajal, A. D. Jerome, R. Menon, C. Yoon, A. L. Kalinski, R. J. Giger, and B. M. Segal. 2020. 'A new neutrophil subset promotes CNS neuron survival and axon regeneration', *Nat Immunol*.

Sato, A., H. Ohtaki, T. Tsumuraya, D. Song, K. Ohara, M. Asano, Y. Iwakura, T. Atsumi, and S. Shioda. 2012. 'Interleukin-1 participates in the classical and alternative activation of microglia/macrophages after spinal cord injury', *J Neuroinflammation*, 9: 65.

Satzer, D., C. Miller, J. Maxon, J. Voth, C. DiBartolomeo, R. Mahoney, J. R. Dutton, W. C. Low, and A. M. Parr. 2015. 'T cell deficiency in spinal cord injury: altered locomotor recovery and whole-genome transcriptional analysis', *BMC Neurosci*, 16: 74.

Sauerbeck, A. D., J. L. Laws, V. V. Bandaru, P. G. Popovich, N. J. Haughey, and D. M. McTigue. 2015. 'Spinal cord injury causes chronic liver pathology in rats', *J Neurotrauma*, 32: 159-69.

Savic, G., M. J. DeVivo, H. L. Frankel, M. A. Jamous, B. M. Soni, and S. Charlifue. 2018. 'Suicide and traumatic spinal cord injury-a cohort study', *Spinal Cord*, 56: 2-6.

Scheff, S. W., A. G. Rabchevsky, I. Fugaccia, J. A. Main, and J. E. Lumpp, Jr. 2003. 'Experimental modeling of spinal cord injury: characterization of a force-defined injury device', *J Neurotrauma*, 20: 179-93.

Schnell, L., S. Fearn, H. Klassen, M. E. Schwab, and V. H. Perry. 1999a. 'Acute inflammatory responses to mechanical lesions in the CNS: differences between brain and spinal cord', *Eur J Neurosci*, 11: 3648-58.

Schnell, L., S. Fearn, M. E. Schwab, V. H. Perry, and D. C. Anthony. 1999b. 'Cytokine-induced acute inflammation in the brain and spinal cord', *J Neuropathol Exp Neurol*, 58: 245-54.

Schroder, A. K., M. von der Ohe, U. Kolling, J. Altstaedt, P. Uciechowski, D. Fleischer, K. Dalhoff, X. Ju, M. Zenke, N. Heussen, and L. Rink. 2006. 'Polymorphonuclear leucocytes selectively produce anti-inflammatory interleukin-1 receptor antagonist and chemokines, but fail to produce pro-inflammatory mediators', *Immunology*, 119: 317-27.

Schucht, P., O. Raineteau, M. E. Schwab, and K. Fouad. 2002. 'Anatomical correlates of locomotor recovery following dorsal and ventral lesions of the rat spinal cord', *Exp Neurol*, 176: 143-53.

Schulze, J., A. Vogelgesang, and A. Dressel. 2014. 'Catecholamines, steroids and immune alterations in ischemic stroke and other acute diseases', *Aging Dis*, 5: 327-39.

Schwab, M. E., and S. M. Strittmatter. 2014. 'Nogo limits neural plasticity and recovery from injury', *Curr Opin Neurobiol*, 27: 53-60.

Sengupta, D., A. Bindra, N. Kumar, K. Goyal, P. K. Singh, A. Chaturvedi, R. Malhotra, and A. K. Mishra. 2021. 'Respiratory morbidity and mortality of traumatic cervical spinal cord injury at a level I trauma center in India', *Spinal Cord Ser Cases*, 7: 36.

Sharma, H. S., Y. Olsson, F. Nyberg, and P. K. Dey. 1993. 'Prostaglandins modulate alterations of microvascular permeability, blood flow, edema and serotonin levels following spinal cord injury: an experimental study in the rat', *Neuroscience*, 57: 443-9.

Shechter, R., A. London, C. Varol, C. Raposo, M. Cusimano, G. Yovel, A. Rolls, M. Mack, S. Pluchino, G. Martino, S. Jung, and M. Schwartz. 2009. 'Infiltrating blood-derived macrophages are vital cells playing an anti-inflammatory role in recovery from spinal cord injury in mice', *PLoS Med*, 6: e1000113.

Shechter, R., O. Miller, G. Yovel, N. Rosenzweig, A. London, J. Ruckh, K. W. Kim, E. Klein, V. Kalchenko, P. Bendel, S. A. Lira, S. Jung, and M. Schwartz. 2013. 'Recruitment of beneficial M2 macrophages to injured spinal cord is orchestrated by remote brain choroid plexus', *Immunity*, 38: 555-69.

Shechter, R., and M. Schwartz. 2013. 'CNS sterile injury: just another wound healing?', *Trends Mol Med*, 19: 135-43.

Sheng, Z., Y. Liu, H. Li, W. Zheng, B. Xia, X. Zhang, V. W. Yong, and M. Xue. 2018. 'Efficacy of Minocycline in Acute Ischemic Stroke: A Systematic Review and Meta-Analysis of Rodent and Clinical Studies', *Front Neurol*, 9: 1103.

Shi, M., C. Liu, T. J. Cook, K. M. Bullock, Y. Zhao, C. Ginghina, Y. Li, et al. 2014. 'Plasma exosomal alpha-synuclein is likely CNS-derived and increased in Parkinson's disease', *Acta Neuropathol*, 128: 639-50.

Singh, A., R. N. Srivastava, A. Agrahari, S. Singh, S. Raj, T. Chatterji, A. A. Mahdi, R. K. Garg, and R. Roy. 2018. 'Proton NMR based serum metabolic profile correlates with the neurological recovery in treated acute spinal cord injury (ASCI) subjects: A pilot study', *Clin Chim Acta*, 480: 150-60.

Singh, N., S. J. Hopkins, S. Hulme, J. P. Galea, M. Hoadley, A. Vail, P. J. Hutchinson, S. Grainger, N. J. Rothwell, A. T. King, and P. J. Tyrrell. 2014. 'The effect of intravenous interleukin-1 receptor antagonist on inflammatory mediators in cerebrospinal fluid after subarachnoid haemorrhage: a phase II randomised controlled trial', *J Neuroinflammation*, 11: 1.

Singh, V. P., N. K. Jain, and S. K. Kulkarni. 2001. 'On the antinociceptive effect of fluoxetine, a selective serotonin reuptake inhibitor', *Brain Res*, 915: 218-26.

Skog, J., T. Wurdinger, S. van Rijn, D. H. Meijer, L. Gainche, M. Sena-Esteves, W. T. Curry, Jr., B. S. Carter, A. M. Krichevsky, and X. O. Breakefield. 2008. 'Glioblastoma microvesicles transport RNA and proteins that promote tumour growth and provide diagnostic biomarkers', *Nat Cell Biol*, 10: 1470-6.

Smith, C. J., S. Hulme, A. Vail, C. Heal, A. R. Parry-Jones, S. Scarth, K. Hopkins, M. Hoadley, S. M. Allan, N. J. Rothwell, S. J. Hopkins, and P. J. Tyrrell. 2018. 'SCIL-STROKE (Subcutaneous Interleukin-1 Receptor Antagonist in Ischemic Stroke): A Randomized Controlled Phase 2 Trial', *Stroke*, 49: 1210-16.

Smith, D. L., Jr., and C. Yarar-Fisher. 2016. 'Contributors to Metabolic Disease Risk Following Spinal Cord Injury', *Curr Phys Med Rehabil Rep*, 4: 190-99.

Sofroniew, M. V., and H. V. Vinters. 2010. 'Astrocytes: biology and pathology', *Acta Neuropathol*, 119: 7-35.

Song, J. W., K. Li, Z. W. Liang, C. Dai, X. F. Shen, Y. Z. Gong, S. Wang, X. Y. Hu, and Z. Wang. 2017. 'Low-level laser facilitates alternatively activated macrophage/microglia polarization and promotes functional recovery after crush spinal cord injury in rats', *Sci Rep*, 7: 620.

Soubeyrand, M., E. Laemmel, C. Court, A. Dubory, E. Vicaut, and J. Duranteau. 2013. 'Rat model of spinal cord injury preserving dura mater integrity and allowing measurements of cerebrospinal fluid pressure and spinal cord blood flow', *Eur Spine J*, 22: 1810-9.

Sroga, J. M., T. B. Jones, K. A. Kigerl, V. M. McGaughy, and P. G. Popovich. 2003. 'Rats and mice exhibit distinct inflammatory reactions after spinal cord injury', *J Comp Neurol*, 462: 223-40.

Stammers, A. T., J. Liu, and B. K. Kwon. 2012. 'Expression of inflammatory cytokines following acute spinal cord injury in a rodent model', *J Neurosci Res*, 90: 782-90.

Stein, D. M., J. Menaker, K. McQuillan, C. Handley, B. Aarabi, and T. M. Scalea. 2010. 'Risk factors for organ dysfunction and failure in patients with acute traumatic cervical spinal cord injury', *Neurocrit Care*, 13: 29-39.

Stirling, D. P., K. Cummins, M. Mishra, W. Teo, V. W. Yong, and P. Stys. 2014. 'Toll-like receptor 2-mediated alternative activation of microglia is protective after spinal cord injury', *Brain*, 137: 707-23.

Stirling, D. P., K. Khodarahmi, J. Liu, L. T. McPhail, C. B. McBride, J. D. Steeves, M. S. Ramer, and W. Tetzlaff. 2004. 'Minocycline treatment reduces delayed oligodendrocyte death, attenuates axonal dieback, and improves functional outcome after spinal cord injury', *J Neurosci*, 24: 2182-90.

Stirling, D. P., S. Liu, P. Kubes, and V. W. Yong. 2009. 'Depletion of Ly6G/Gr-1 leukocytes after spinal cord injury in mice alters wound healing and worsens neurological outcome', *J Neurosci*, 29: 753-64.

Stirling, D. P., and V. W. Yong. 2008. 'Dynamics of the inflammatory response after murine spinal cord injury revealed by flow cytometry', *J Neurosci Res*, 86: 1944-58.

Storch, M. J., D. Konig, D. Bultermann, A. Blum, S. Vogt, M. Baumstark, A. Berg, and A. Schmid. 2005. 'Lipid profile in spinal cord-injured women with different injury levels', *Prev Med*, 40: 321-5.

Sun, D., T. A. Newman, V. H. Perry, and R. O. Weller. 2004. 'Cytokine-induced enhancement of autoimmune inflammation in the brain and spinal cord: implications for multiple sclerosis', *Neuropathol Appl Neurobiol*, 30: 374-84.

Sun, M., R. D. Brady, D. K. Wright, H. A. Kim, S. R. Zhang, C. G. Sobey, M. R. Johnstone, T. J. O'Brien, B. D. Semple, S. J. McDonald, and S. R. Shultz. 2017. 'Treatment with an interleukin-1 receptor antagonist mitigates neuroinflammation and brain damage after polytrauma', *Brain Behav Immun*, 66: 359-71.

Sun, X., Z. B. Jones, X. M. Chen, L. Zhou, K. F. So, and Y. Ren. 2016. 'Multiple organ dysfunction and systemic inflammation after spinal cord injury: a complex relationship', *J Neuroinflammation*, 13: 260.

Sun, X., X. Wang, T. Chen, T. Li, K. Cao, A. Lu, Y. Chen, D. Sun, J. Luo, J. Fan, W. Young, and Y. Ren. 2010. 'Myelin activates FAK/Akt/NF-kappaB pathways and provokes CR3-dependent inflammatory response in murine system', *PLoS One*, 5: e9380.

Sun, Y. J., Z. Y. Zhang, B. Fan, and G. Y. Li. 2019. 'Neuroprotection by Therapeutic Hypothermia', *Front Neurosci*, 13: 586.

Sylvestre, D. A., C. M. Slupsky, R. I. Aviv, W. Swardfager, and A. Y. Taha. 2020. 'Untargeted metabolomic analysis of plasma from relapsing-remitting multiple sclerosis patients reveals changes in metabolites associated with structural changes in brain', *Brain Res*, 1732: 146589.

Takahashi, H. K., A. Yoshida, H. Iwagaki, T. Yoshino, H. Itoh, T. Morichika, M. Yokoyama, T. Akagi, N. Tanaka, S. Mori, and M. Nishibori. 2002. 'Histamine regulation of interleukin-18-initiating cytokine cascade is associated with down-regulation of intercellular adhesion molecule-1 expression in human peripheral blood mononuclear cells', *J Pharmacol Exp Ther*, 300: 227-35.

Tang, H., Y. Wang, J. K. Nicholson, and J. C. Lindon. 2004. 'Use of relaxation-edited one-dimensional and two dimensional nuclear magnetic resonance spectroscopy to improve detection of small metabolites in blood plasma', *Anal Biochem*, 325: 260-72.

Tanhoffer, R. A., R. K. Yamazaki, E. A. Nunes, A. I. Pchevozniki, A. M. Pchevozniki, C. Nogata, J. Aikawa, S. J. Bonatto, G. Brito, M. D. Lissa, and L. C. Fernandes. 2007. 'Glutamine concentration and immune response of spinal cord-injured rats', *J Spinal Cord Med*, 30: 140-6.

Taoka, Y., K. Okajima, M. Uchiba, K. Murakami, S. Kushimoto, M. Johno, M. Naruo, H. Okabe, and K. Takatsuki. 1997. 'Role of neutrophils in spinal cord injury in the rat', *Neuroscience*, 79: 1177-82.

Thery, C., S. Amigorena, G. Raposo, and A. Clayton. 2006. 'Isolation and characterization of exosomes from cell culture supernatants and biological fluids', *Curr Protoc Cell Biol*, Chapter 3: Unit 3 22.

Thery, C., K. W. Witwer, E. Aikawa, M. J. Alcaraz, J. D. Anderson, R. Andriantsitohaina, A. Antoniou, et al. 2018. 'Minimal information for studies of extracellular vesicles 2018 (MISEV2018): a position statement of the International Society for Extracellular Vesicles and update of the MISEV2014 guidelines', *J Extracell Vesicles*, 7: 1535750.

Thevenot, E. A., A. Roux, Y. Xu, E. Ezan, and C. Junot. 2015. 'Analysis of the Human Adult Urinary Metabolome Variations with Age, Body Mass Index, and Gender by Implementing a Comprehensive Workflow for Univariate and OPLS Statistical Analyses', *J Proteome Res*, 14: 3322-35.

Thom, V., T. V. Arumugam, T. Magnus, and M. Gelderblom. 2017. 'Therapeutic Potential of Intravenous Immunoglobulin in Acute Brain Injury', *Front Immunol*, 8: 875.

Thompson, R. E., J. Pardieck, L. Smith, P. Kenny, L. Crawford, M. Shoichet, and S. Sakiyama-Elbert. 2018. 'Effect of hyaluronic acid hydrogels containing astrocyte-derived extracellular matrix and/or V2a interneurons on histologic outcomes following spinal cord injury', *Biomaterials*, 162: 208-23.

Tian, Y., B. Salsbery, M. Wang, H. Yuan, J. Yang, Z. Zhao, X. Wu, Y. Zhang, B. A. Konkle, P. Thiagarajan, M. Li, J. Zhang, and J. F. Dong. 2015. 'Brain-derived microparticles induce systemic coagulation in a murine model of traumatic brain injury', *Blood*, 125: 2151-9.

Tidball, J. G., and S. A. Villalta. 2010. 'Regulatory interactions between muscle and the immune system during muscle regeneration', *Am J Physiol Regul Integr Comp Physiol*, 298: R1173-87.

Tolan, N. V., N. Vidal-Folch, A. Algeciras-Schimnich, R. J. Singh, and S. K. Grebe. 2013. 'Individualized correction of neuron-specific enolase (NSE) measurement in hemolyzed serum samples', *Clin Chim Acta*, 424: 216-21.

Torretti, J. A., and D. K. Sengupta. 2007. 'Cervical spine trauma', *Indian J Orthop*, 41: 255-67.

Treloar, H. B., J. C. Bartolomei, B. W. Lipscomb, and C. A. Greer. 2001. 'Mechanisms of axonal plasticity: lessons from the olfactory pathway', *Neuroscientist*, 7: 55-63.

Tsuda, Y., H. Takahashi, M. Kobayashi, T. Hanafusa, D. N. Herndon, and F. Suzuki. 2004. 'Three different neutrophil subsets exhibited in mice with different susceptibilities to infection by methicillin-resistant Staphylococcus aureus', *Immunity*, 21: 215-26.

Turina, M., D. E. Fry, and H. C. Polk, Jr. 2005. 'Acute hyperglycemia and the innate immune system: clinical, cellular, and molecular aspects', *Crit Care Med*, 33: 1624-33.

Utagawa, A., J. S. Truettner, W. D. Dietrich, and H. M. Bramlett. 2008. 'Systemic inflammation exacerbates behavioral and histopathological consequences of isolated traumatic brain injury in rats', *Exp Neurol*, 211: 283-91.

van Asseldonk, E. J., R. Stienstra, T. B. Koenen, L. A. Joosten, M. G. Netea, and C. J. Tack. 2011. 'Treatment with Anakinra improves disposition index but not insulin sensitivity in nondiabetic subjects with the metabolic syndrome: a randomized, double-blind, placebo-controlled study', *J Clin Endocrinol Metab*, 96: 2119-26.

van Genderen, H. O., H. Kenis, L. Hofstra, J. Narula, and C. P. Reutelingsperger. 2008. 'Extracellular annexin A5: functions of phosphatidylserine-binding and two-dimensional crystallization', *Biochim Biophys Acta*, 1783: 953-63.

van Middendorp, J. J., B. Goss, S. Urquhart, S. Atresh, R. P. Williams, and M. Schuetz. 2011. 'Diagnosis and prognosis of traumatic spinal cord injury', *Global Spine J*, 1: 1-8.

van Weert, K. C., E. J. Schouten, J. Hofstede, H. van de Meent, H. R. Holtslag, and R. J. van den Berg-Emons. 2014. 'Acute phase complications following traumatic spinal cord injury in Dutch level 1 trauma centres', *J Rehabil Med*, 46: 882-5.

Vannier, E., L. C. Miller, and C. A. Dinarello. 1991. 'Histamine suppresses gene expression and synthesis of tumor necrosis factor alpha via histamine H2 receptors', *J Exp Med*, 174: 281-4.

Varma, V. R., A. M. Oommen, S. Varma, R. Casanova, Y. An, R. M. Andrews, R. O'Brien, et al. 2018. 'Brain and blood metabolite signatures of pathology and progression in Alzheimer disease: A targeted metabolomics study', *PLoS Med*, 15: e1002482.

Vella, M. A., M. L. Crandall, and M. B. Patel. 2017. 'Acute Management of Traumatic Brain Injury', *Surg Clin North Am*, 97: 1015-30.

Verderio, C., L. Muzio, E. Turola, A. Bergami, L. Novellino, F. Ruffini, L. Riganti, et al. 2012. 'Myeloid microvesicles are a marker and therapeutic target for neuroinflammation', *Ann Neurol*, 72: 610-24.
Verweij, F. J., V. Hyenne, G. Van Niel, and J. G. Goetz. 2019a. 'Extracellular Vesicles: Catching the Light in Zebrafish', *Trends Cell Biol*, 29: 770-76.
Verweij, F. J., C. Revenu, G. Arras, F. Dingli, D. Loew, D. M. Pegtel, G. Follain, G. Allio, J. G. Goetz, P. Zimmermann, P. Herbomel, F. Del Bene, G. Raposo, and G. van Niel. 2019b. 'Live Tracking of Inter-organ Communication by Endogenous Exosomes In Vivo', *Dev Cell*, 48: 573-89 e4.
Vichiansiri, R., J. Saengsuwan, N. Manimmanakorn, S. Patpiya, A. Preeda, K. Samerduen, and E. Poosiripinyo. 2012. 'The prevalence of dyslipidemia in patients with spinal cord lesion in Thailand', *Cholesterol*, 2012: 847462.
Vignoli, A., L. Tenori, C. Luchinat, and E. Saccenti. 2018. 'Age and Sex Effects on Plasma Metabolite Association Networks in Healthy Subjects', *J Proteome Res*, 17: 97-107.
Vitkovic, L., J. Bockaert, and C. Jacque. 2000. '"Inflammatory" cytokines: neuromodulators in normal brain?', *J Neurochem*, 74: 457-71.
Wang, C. X., J. A. Olschowka, and J. R. Wrathall. 1997. 'Increase of interleukin-1beta mRNA and protein in the spinal cord following experimental traumatic injury in the rat', *Brain Res*, 759: 190-6.
Wang, D., R. M. Ichiyama, R. Zhao, M. R. Andrews, and J. W. Fawcett. 2011. 'Chondroitinase combined with rehabilitation promotes recovery of forelimb function in rats with chronic spinal cord injury', *J Neurosci*, 31: 9332-44.
Wang, G. Y., Z. J. Cheng, P. W. Yuan, H. P. Li, and X. J. He. 2021. 'Olfactory ensheathing cell transplantation alters the expression of chondroitin sulfate proteoglycans and promotes axonal regeneration after spinal cord injury', *Neural Regen Res*, 16: 1638-44.
Wang, J., and D. D. Pearse. 2015. 'Therapeutic Hypothermia in Spinal Cord Injury: The Status of Its Use and Open Questions', *Int J Mol Sci*, 16: 16848-79.
Wang, X., K. Cao, X. Sun, Y. Chen, Z. Duan, L. Sun, L. Guo, P. Bai, D. Sun, J. Fan, X. He, W. Young, and Y. Ren. 2015. 'Macrophages in spinal cord injury: phenotypic and functional change from exposure to myelin debris', *Glia*, 63: 635-51.
Wanner, I. B., M. A. Anderson, B. Song, J. Levine, A. Fernandez, Z. Gray-Thompson, Y. Ao, and M. V. Sofroniew. 2013. 'Glial scar borders are formed by newly proliferated, elongated astrocytes that interact to corral inflammatory and fibrotic cells via STAT3-dependent mechanisms after spinal cord injury', *J Neurosci*, 33: 12870-86.
Waters, N. J., E. Holmes, A. Williams, C. J. Waterfield, R. D. Farrant, and J. K. Nicholson. 2001. 'NMR and pattern recognition studies on the time-related metabolic effects of alpha-naphthylisothiocyanate on liver, urine, and plasma in the rat: an integrative metabonomic approach', *Chem Res Toxicol*, 14: 1401-12.
Webster Marketon, J. I., and R. Glaser. 2008. 'Stress hormones and immune function', *Cell Immunol*, 252: 16-26.
Wells, J. E., R. J. Hurlbert, M. G. Fehlings, and V. W. Yong. 2003. 'Neuroprotection by minocycline facilitates significant recovery from spinal cord injury in mice', *Brain*, 126: 1628-37.
Welton, J. L., S. Loveless, T. Stone, C. von Ruhland, N. P. Robertson, and A. Clayton. 2017. 'Cerebrospinal fluid extracellular vesicle enrichment for protein biomarker discovery in neurological disease; multiple sclerosis', *J Extracell Vesicles*, 6: 1369805.
Werner, Y., E. Mass, P. Ashok Kumar, T. Ulas, K. Handler, A. Horne, K. Klee, A. Lupp, D. Schutz, F. Saaber, C. Redecker, J. L. Schultze, F. Geissmann, and R. Stumm. 2020. 'Cxcr4 distinguishes HSC-derived monocytes from microglia and reveals monocyte immune responses to experimental stroke', *Nat Neurosci*, 23: 351-62.
West, C. R., P. Mills, and A. V. Krassioukov. 2012. 'Influence of the neurological level of spinal cord injury on cardiovascular outcomes in humans: a meta-analysis', *Spinal Cord*, 50: 484-92.
Whetstone, W. D., J. Y. Hsu, M. Eisenberg, Z. Werb, and L. J. Noble-Haeusslein. 2003. 'Blood-spinal cord barrier after spinal cord injury: relation to revascularization and wound healing', *J Neurosci Res*, 74: 227-39.

Wicker, E., L. Benton, K. George, W. Furlow, and S. Villapol. 2019. 'Serum Amyloid A Protein as a Potential Biomarker for Severity and Acute Outcome in Traumatic Brain Injury', *Biomed Res Int*, 2019: 5967816.
Wilcockson, D. C., S. J. Campbell, D. C. Anthony, and V. H. Perry. 2002. 'The systemic and local acute phase response following acute brain injury', *J Cereb Blood Flow Metab*, 22: 318-26.
Williams, R., and A. Murray. 2015. 'Prevalence of depression after spinal cord injury: a meta-analysis', *Arch Phys Med Rehabil*, 96: 133-40.
Willms, E., C. Cabanas, I. Mager, M. J. A. Wood, and P. Vader. 2018. 'Extracellular Vesicle Heterogeneity: Subpopulations, Isolation Techniques, and Diverse Functions in Cancer Progression', *Front Immunol*, 9: 738.
Wilson, J. R., N. Forgione, and M. G. Fehlings. 2013. 'Emerging therapies for acute traumatic spinal cord injury', *CMAJ*, 185: 485-92.
Wiseman, D. B., A. T. Dailey, D. Lundin, J. Zhou, A. Lipson, A. Falicov, and C. I. Shaffrey. 2009. 'Magnesium efficacy in a rat spinal cord injury model', *J Neurosurg Spine*, 10: 308-14.
Woodhall, E., A. K. West, and M. I. Chuah. 2001. 'Cultured olfactory ensheathing cells express nerve growth factor, brain-derived neurotrophic factor, glia cell line-derived neurotrophic factor and their receptors', *Brain Res Mol Brain Res*, 88: 203-13.
Wu, B., D. Matic, N. Djogo, E. Szpotowicz, M. Schachner, and I. Jakovcevski. 2012a. 'Improved regeneration after spinal cord injury in mice lacking functional T- and B-lymphocytes', *Exp Neurol*, 237: 274-85.
Wu, J. C., Y. C. Chen, L. Liu, T. J. Chen, W. C. Huang, H. Cheng, and S. Tung-Ping. 2012b. 'Increased risk of stroke after spinal cord injury: a nationwide 4-year follow-up cohort study', *Neurology*, 78: 1051-7.
Wu, J., Z. Zhao, A. Kumar, M. M. Lipinski, D. J. Loane, B. A. Stoica, and A. I. Faden. 2016a. 'Endoplasmic Reticulum Stress and Disrupted Neurogenesis in the Brain Are Associated with Cognitive Impairment and Depressive-Like Behavior after Spinal Cord Injury', *J Neurotrauma*, 33: 1919-35.
Wu, J., Z. Zhao, B. Sabirzhanov, B. A. Stoica, A. Kumar, T. Luo, J. Skovira, and A. I. Faden. 2014. 'Spinal cord injury causes brain inflammation associated with cognitive and affective changes: role of cell cycle pathways', *J Neurosci*, 34: 10989-1006.
Wu, Y., Y. H. Lin, L. L. Shi, Z. F. Yao, X. M. Xie, Z. S. Jiang, J. Tang, J. G. Hu, and H. Z. Lu. 2017. 'Temporal kinetics of CD8(+) CD28(+) and CD8(+) CD28(-) T lymphocytes in the injured rat spinal cord', *J Neurosci Res*, 95: 1666-76.
Wu, Y., K. Satkunendrarajah, Y. Teng, D. S. Chow, J. Buttigieg, and M. G. Fehlings. 2013. 'Delayed post-injury administration of riluzole is neuroprotective in a preclinical rodent model of cervical spinal cord injury', *J Neurotrauma*, 30: 441-52.
Wu, Y., F. Streijger, Y. Wang, G. Lin, S. Christie, J. M. Mac-Thiong, S. Parent, et al. 2016b. 'Parallel Metabolomic Profiling of Cerebrospinal Fluid and Serum for Identifying Biomarkers of Injury Severity after Acute Human Spinal Cord Injury', *Sci Rep*, 6: 38718.
Xie, J., Y. Li, J. Dai, Y. He, D. Sun, C. Dai, H. Xu, and Z. Q. Yin. 2019. 'Olfactory Ensheathing Cells Grafted Into the Retina of RCS Rats Suppress Inflammation by Down-Regulating the JAK/STAT Pathway', *Front Cell Neurosci*, 13: 341.
Xu, G. Y., M. G. Hughes, Z. Ye, C. E. Hulsebosch, and D. J. McAdoo. 2004. 'Concentrations of glutamate released following spinal cord injury kill oligodendrocytes in the spinal cord', *Exp Neurol*, 187: 329-36.
Yang, L., P. C. Blumbergs, N. R. Jones, J. Manavis, G. T. Sarvestani, and M. N. Ghabriel. 2004. 'Early expression and cellular localization of proinflammatory cytokines interleukin-1beta, interleukin-6, and tumor necrosis factor-alpha in human traumatic spinal cord injury', *Spine (Phila Pa 1976)*, 29: 966-71.
Yang, L., N. R. Jones, P. C. Blumbergs, C. Van Den Heuvel, E. J. Moore, J. Manavis, G. T. Sarvestani, and M. N. Ghabriel. 2005. 'Severity-dependent expression of pro-inflammatory cytokines in traumatic spinal cord injury in the rat', *J Clin Neurosci*, 12: 276-84.
Yang, T., Y. Dai, G. Chen, and S. Cui. 2020. 'Dissecting the Dual Role of the Glial Scar and Scar-Forming Astrocytes in Spinal Cord Injury', *Front Cell Neurosci*, 14: 78.

Yang, Y., A. Boza-Serrano, C. J. R. Dunning, B. H. Clausen, K. L. Lambertsen, and T. Deierborg. 2018. 'Inflammation leads to distinct populations of extracellular vesicles from microglia', *J Neuroinflammation*, 15: 168.

Yang, Y., Y. Ye, C. Kong, X. Su, X. Zhang, W. Bai, and X. He. 2019. 'MiR-124 Enriched Exosomes Promoted the M2 Polarization of Microglia and Enhanced Hippocampus Neurogenesis After Traumatic Brain Injury by Inhibiting TLR4 Pathway', *Neurochem Res*, 44: 811-28.

Yates, A. G., D. C. Anthony, M. J. Ruitenberg, and Y. Couch. 2019. 'Systemic Immune Response to Traumatic CNS Injuries-Are Extracellular Vesicles the Missing Link?', *Front Immunol*, 10: 2723.

Yates, A. G., T. Jogia, E. R. Gillespie, Y. Couch, M. J. Ruitenberg, and D. C. Anthony. 2021. 'Acute IL-1RA treatment suppresses the peripheral and central inflammatory response to spinal cord injury', *J Neuroinflammation*, 18: 15.

Ye, J., Y. Qin, Y. Tang, M. Ma, P. Wang, L. Huang, R. Yang, K. Chen, C. Chai, Y. Wu, and H. Shen. 2018. 'Methylprednisolone inhibits the proliferation of endogenous neural stem cells in nonhuman primates with spinal cord injury', *J Neurosurg Spine*, 29: 199-207.

Yeh, T. S., Y. C. Ho, C. L. Hsu, and S. L. Pan. 2018. 'Spinal cord injury and Alzheimer's disease risk: a population-based, retrospective cohort study', *Spinal Cord*, 56: 151-57.

Yeh, T. S., Y. P. Huang, H. I. Wang, and S. L. Pan. 2016. 'Spinal cord injury and Parkinson's disease: a population-based, propensity score-matched, longitudinal follow-up study', *Spinal Cord*, 54: 1215-19.

Yenari, M. A., and H. S. Han. 2012. 'Neuroprotective mechanisms of hypothermia in brain ischaemia', *Nat Rev Neurosci*, 13: 267-78.

Yeo, T., F. Probert, M. Jurynczyk, M. Sealey, A. Cavey, T. D. W. Claridge, M. Woodhall, P. Waters, M. I. Leite, D. C. Anthony, and J. Palace. 2019. 'Classifying the antibody-negative NMO syndromes: Clinical, imaging, and metabolomic modeling', *Neurol Neuroimmunol Neuroinflamm*, 6: e626.

Yeo, T., M. Sealey, Y. Zhou, L. Saldana, S. Loveless, T. D. W. Claridge, N. Robertson, G. DeLuca, J. Palace, D. C. Anthony, and F. Probert. 2020. 'A blood-based metabolomics test to distinguish relapsing-remitting and secondary progressive multiple sclerosis: addressing practical considerations for clinical application', *Sci Rep*, 10: 12381.

Yokota, K., T. Saito, K. Kobayakawa, K. Kubota, M. Hara, M. Murata, Y. Ohkawa, Y. Iwamoto, and S. Okada. 2016. 'The feasibility of in vivo imaging of infiltrating blood cells for predicting the functional prognosis after spinal cord injury', *Sci Rep*, 6: 25673.

Zajarias-Fainsod, D., J. Carrillo-Ruiz, H. Mestre, I. Grijalva, I. Madrazo, and A. Ibarra. 2012. 'Autoreactivity against myelin basic protein in patients with chronic paraplegia', *Eur Spine J*, 21: 964-70.

Zamanian, J. L., L. Xu, L. C. Foo, N. Nouri, L. Zhou, R. G. Giffard, and B. A. Barres. 2012. 'Genomic analysis of reactive astrogliosis', *J Neurosci*, 32: 6391-410.

Zhang, C., Y. Jing, W. Zhang, J. Zhang, M. Yang, L. Du, Y. Jia, et al. 2019a. 'Dysbiosis of gut microbiota is associated with serum lipid profiles in male patients with chronic traumatic cervical spinal cord injury', *Am J Transl Res*, 11: 4817-34.

Zhang, C., W. Zhang, J. Zhang, Y. Jing, M. Yang, L. Du, F. Gao, et al. 2018. 'Gut microbiota dysbiosis in male patients with chronic traumatic complete spinal cord injury', *J Transl Med*, 16: 353.

Zhang, Q., X. Liu, L. Yan, R. Zhao, J. An, C. Liu, and H. Yang. 2019b. 'Danshen extract (Salvia miltiorrhiza Bunge) attenuate spinal cord injury in a rat model: A metabolomic approach for the mechanism study', *Phytomedicine*, 62: 152966.

Zhang, S., X. Zeng, M. Ren, X. Mao, and S. Qiao. 2017. 'Novel metabolic and physiological functions of branched chain amino acids: a review', *J Anim Sci Biotechnol*, 8: 10.

Zhang, Y., Z. Guan, B. Reader, T. Shawler, S. Mandrekar-Colucci, K. Huang, Z. Weil, et al. 2013. 'Autonomic dysreflexia causes chronic immune suppression after spinal cord injury', *J Neurosci*, 33: 12970-81.

Zhao, Z., Y. Zhou, Y. Tian, M. Li, J. F. Dong, and J. Zhang. 2017. 'Cellular microparticles and pathophysiology of traumatic brain injury', *Protein Cell*.

Zhu, L., X. Liu, D. P. Nemeth, D. J. DiSabato, K. G. Witcher, D. B. McKim, B. Oliver, et al. 2019. 'Interleukin-1 causes CNS inflammatory cytokine expression via endothelia-microglia bi-cellular signaling', *Brain Behav Immun*, 81: 292-304.
Zong, S., G. Zeng, B. Wei, C. Xiong, and Y. Zhao. 2012. 'Beneficial effect of interleukin-1 receptor antagonist protein on spinal cord injury recovery in the rat', *Inflammation*, 35: 520-6.
Zweckberger, K., C. S. Ahuja, Y. Liu, J. Wang, and M. G. Fehlings. 2016. 'Self-assembling peptides optimize the post-traumatic milieu and synergistically enhance the effects of neural stem cell therapy after cervical spinal cord injury', *Acta Biomater*, 42: 77-89.

Appendix

Queensland Government

Princess Alexandra Hospital
Metro South Health

THE UNIVERSITY OF QUEENSLAND
AUSTRALIA

Title	Blood and Stool Biomarker Analysis in Traumatic Spinal Injury
Short Title	BBTSI
HREC Number	HREC/15/QPAH/211
Project Sponsor	University of Queensland
Principal Investigators	Dr. Kate Campbell A/Prof. Marc Ruitenberg
Associate Investigator(s)	Dr Sridhar Atresh, Prof. Tim Geraghty, Prof. Jean-Pierre Levesque, Mrs Esther Jacobson
Location	Princess Alexandra Hospital, Brisbane

Part 1

What does my participation involve?

1. Introduction

You are invited to take part in this research project. This is because you have had a significant traumatic injury.

This Participant Information Sheet/Consent Form tells you about the research project. It explains the test involved. Knowing what is involved will help you decide if you want to take part in the research.

Please read this information carefully. Ask questions about anything that you don't understand or want to know more about. Before deciding whether or not to take part, you might want to talk about it with a relative or friend

Participation in this research is voluntary. If you don't wish to take part, you don't have to. You will receive the best possible care whether or not you take part.

If you decide you want to take part in the research project, you will be asked to sign the consent form. By signing it you are telling us that you:

- Understand what you have read, or what was read out to you
- Consent to take part in the research project
- Consent to have the tests that are described
- Consent to the use of your personal and health information as described

You will be given a copy of the signed Participant Information and Consent Form to keep.

2. What is the purpose of this research?

The purpose of this study is for us to better understand how your body is reacting to the injury that you have experienced, and how this response may influence your recovery.

The responsible investigators in Australia are A/Prof. Marc Ruitenberg at the University of Queensland, and Dr Kate Campbell, a Staff Specialist and Director of Research, Orthopaedic Department at the Princess Alexandra Hospital.

3. What does participation in this research involve?

You may be able to participate in this study if you are over 16 years and have had an acute traumatic injury.

You will be asked to provide 7 blood samples in total for the specific purposes of this research project. Wherever possible, the timing of these samples will coincide with the collection of blood samples for your standard routine care protocol whilst you are in hospital for this injury. Several tubes of blood will be collected for a variety of tests, but the total volume taken being is relatively small (up to 50ml of blood).

The research team will also organise collection of up to 7 samples of your stool at regular intervals. The purpose of collecting these stool samples is to analyse and further expand understanding of the how your gut microenvironment, in particular the type of bacteria that normally live there, may change following your injury, and how this may impact upon your recovery and wellbeing. These faecal samples will be taken from the stool that you produce naturally and thus will not involve any invasive procedure to you.

The timing for collection of blood and faecal samples is as follows*:

On the day of your injury
On the 1st day after your injury
On the 3rd day after your injury
On the 7th day (i.e. 1 week) after your injury
On the 21st day (i.e. 3 weeks) after your injury
On the 42nd day (i.e. 6 weeks) after your injury, and
During the week that you are discharged from hospital

* *Timing will be adhered to as strictly as possible but may vary somewhat because of logistics.*

Once your blood and stool samples have been collected, they will be processed locally in a research laboratory at The University of Queensland. Your blood and stool will be profiled for

inflammatory changes and/or changes in the microbiota (bacteria) that normally live there, with the aim to define how they are changed as a result of your injury. This analysis will include a detailed assessment of your white blood cells, including their activation state. This may also include the freezing down and storing some of these cells for future genetic analysis of genes associated with inflammation. The non-cellular part of your blood sample, i.e. the blood plasma, will also be frozen and stored as part of a Biobank (a collection of samples for research purposes), which will allow more detailed (molecular) analysis and characterisation; the latter will take place locally at The University of Queensland, and possibly also overseas at Oxford University (UK) or the Ohio State University Wexner Medical Centre (USA) as part of an international collaboration between these institutions.

The data that we will obtain from the blood and stool samples donated by you will be analysed to see how early inflammatory changes (blood) and/or alterations in your gut microbiota (stool) may be prognostic and/or correlate with your recovery, and more generally also to better understand how the body responds to a major traumatic accident. We may also part of the blood sample to screen for variations (polymorphisms) in genes that may affect way our bodies respond to a major challenge, i.e. the trauma that you have experienced. Any results from such experiments will always be used in de-identified format, i.e. they will not be directly relatable to you.

We may contact you in the future to ask you some questions about your recovery following your injury.

4. Duration of the project:

Your involvement in this study will be for up to 12 months. The duration of the whole research project will be approximately three (3) years.

5. Costs associated with participation:

There are no costs associated with participating in this research project, nor will you be paid for taking part.

6. What do I have to do?

You need to provide consent so that the study blood and stool samples can be taken, and also that you agree with these being used for biomedical research purposes. Taking part in this study will not restrict your diet, regular medication, or lifestyle in any way, nor would it stop you donating blood.

7. Other relevant information about the research project

If you have been diagnosed with some medical conditions you may not be eligible to take part in this trial. This situation will be assessed by your doctor. These conditions include, but are not limited to:

An existing neurological condition
A diagnosis of cancer within the last five (5) years
Human Immunodeficiency Virus (HIV)
An immunological disorder

A current known infection

This research project has been designed to make sure the researchers interpret the results in a fair and appropriate way.

8. Do I have to take part in this research project?

Participation in any research project is voluntary. If you do not wish to take part, you do not have to. If you decide to take part and later change your mind, you are free to withdraw from the project at any stage.
Your decision whether to take part or not to take part, or to take part and then withdraw, will not affect your routine treatment, your relationship with those treating you or your relationship with the Princess Alexandra Hospital.

9. What are the alternatives to participation?

You do not have to take part in this research project to receive treatment. If you do not consent to taking part in this study, your medical care will continue as directed by your doctor without the study blood samples being taken.

10. What are the possible benefits of taking part?

You will not receive any direct benefit from this research. We hope that the information learned from this study can be used in the future to benefit the medical care of people with similar injuries.

11. What are the possible risks and disadvantages of taking part?

You are unlikely to be at any additional risk or disadvantage by giving an extra 50ml blood sample. If any complications or injuries occur as a result of your participation in this project, you will receive appropriate medical treatment.

Taking faecal samples does not present any risk to you, as these samples will be taken from stools you will have naturally produced.

12. Can I have other treatments during this research project?

Yes, you can receive other medical treatments while you are on this research project.

13. What if I withdraw from this research project?

If you decide to withdraw from the project, please notify a member of the research team before you withdraw and you will be asked to sign a form confirming that you wish to withdraw from this study.
If you do withdraw your consent during the research project, the study doctor and relevant study staff will not collect additional personal information from you, although personal information already collected will be retained to ensure that the results of the research project can be measured properly and to comply with law.
You should be aware that data collected by the sponsor up to the time you withdraw will form part of the research project results.

14. Could this research project be stopped unexpectedly?

This research project may be stopped unexpectedly for a variety of reasons. These may include reasons such as decisions made by the sponsor or by local regulatory/health authorities.

15. What happens when the research project ends?

We expect the results of the study to be published in medical journals, which can be made available to you if you wish.

Part 2

How is the research project being conducted?

16. What will happen to information about me?

By signing the consent form you consent to the Princess Alexandra Hospital collecting, using and disclosing personal information for the research project as further detailed below.

You will be assigned a unique study number as a participant in this study which will be linked to your name. This unique study number will be used in any records that contain information about you which have been collected for the purposes of the research project, so that your identity (i.e. your name and any other information that could identify you) is kept confidential.

Records linking your name to the unique study number will only be used for the purposes of the research project and will be kept in a locked filing cabinet in a locked office and will only be made accessible to designated research project personnel, unless permitted otherwise by law.

However, information about your participation in the research project may also be recorded in the patient records that the hospital collects and holds about you during your treatment at the hospital (these patient records include your name, date of birth and other personal details).

While in most cases the information collected about you during the research project will only be used and disclosed in de-identified form, your health records and any information collected during the research project may be accessed by authorised representatives of:

- the Project Sponsors - being the University of Queensland
- the Princess Alexandra Hospital,

for the purposes of verifying and monitoring the research study procedures and data, ensuring compliance with regulatory requirements, and as otherwise required by law. By signing the Consent Form, you authorise the disclosure of your information to the regulatory authorities and entities as noted above.

It is anticipated that the results of this research project will be published and/or presented in a variety of forums. In any publication and/or presentation, information will be provided in such a way that you cannot be identified.

Unless specified otherwise in this section 14 or permitted by law, all information about you which is collected for the research project will only be used and disclosed using the unique study number or in another de-identified format.

Regulations in Australia require all research related data and hospital medical records to be kept for a minimum of fifteen years. Hence your records will be kept for that period of time and then will be disposed of in line with contemporary data disposal systems.

17. Complaints and compensation

If you suffer any injuries or complications as a result of this research project, you should contact the study team as soon as possible and you will be assisted with arranging appropriate medical treatment. If you are eligible for Medicare, you can receive any medical treatment required to treat the injury or complication, free of charge, as a public patient in any Australian public hospital.

18. Who is organising and funding the research?

This research project is being conducted and funded by the University of Queensland and the Princess Alexandra Hospital. No member of the research team will receive any personal financial benefit from your involvement in this research project, other than their ordinary wages.

19. Who has reviewed the research project?

All research in Australia involving humans is reviewed by an independent group of people called a Human Research Ethics Committee (HREC). The ethical aspects of this research project have been approved by the Metro South HREC and the University of Queensland.
This project will be carried out according to the *National Statement on Ethical Conduct in Human Research (2007)*. This statement has been developed to protect the interests of people who agree to participate in human research studies.

20. Further information and who to contact.

If you want any further information concerning this project, you can contact the Study Coordinator and Associate Investigator:

Esther Jacobson
Phone: 07 34437290
Email: e.jacobson@uq.edu.au

Depending in the nature of your query, you may then be referred to the person best placed to answer your question.

If you have any complaints about any aspect of the project, the way it is being conducted or any questions about being a research participant in general, then you may contact:

Metro South Human Research Ethics Committee
Phone: +61 (07) 3443 8049, or
Email: EthicsResearch.PAH@health.qld.gov.au.

Consent Form

Title	Blood and Stool Biomarker Analysis following Traumatic Spinal Injury
Short Title	BBTSI
HREC Number	HREC/15/QPAH/211
Project Sponsor	University of Queensland
Principal Investigators	Dr Kate Campbell and A/Prof Marc Ruitenberg
Associate Investigator(s)	Dr Sridhar Atresh, Prof Tim Geraghty, Prof Jean-Pierre Levesque, Mrs Esther Jacobson
Location	Princess Alexandra Hospital, Brisbane

Declaration by Participant

I have read the Participant Information Sheet, or it was read to me in a language I understand.
I understand the purposes, procedures and risks of the research described in the project.
I give permission for my relevant medical information to be released to The University of Queensland for the purposes of this project. I understand that such information will remain confidential and be stored in a secure non-identifiable form.
I consent to having my blood samples stored in a non-identifiable format, and understand that these will be analysed for studying inflammation as part of this study, and possibly also other future research projects for the purpose of studying spinal cord injury only.
I had an opportunity to ask questions and I am satisfied with the answers I have received.
I freely agree to participate in this research project as described and understand that I am free to withdraw at any time during the study without affecting my future health care.
I understand that I will be given a signed copy of this document to keep.

Name of Participant (please _____

Signature _____ Date _____

If the participant is physically unable to sign, their verbal consent **must** be witnessed.

Name of Witness* to Participant's Verbal Consent (please print) _____

Signature _____ Date _____

* Witness is not to be the investigator, a member of the study team or their delegate. In the event that an interpreter is used, she/he may not act as a witness to the consent process. Witness must be 18 years or older.

Declaration by Study Doctor/ Researcher†

I have given a verbal explanation of the research project, its procedures and risks and I believe that the participant has understood that explanation.

Name of Study Doctor/ Researcher† (please print) _____

Signature _____ Date _____

† A senior member of the research team must provide the explanation of, and information concerning, the research project.

Note: All parties signing the consent section must date their own signature.

Form for Withdrawal of Participation

Title	Blood Biomarker Analysis following Traumatic Spinal Injury
Short Title	BBTSI
HREC Number	HREC/15/QPAH/211
Project Sponsor	University of Queensland
Principal Investigators	Dr Kate Campbell and A/Prof Marc Ruitenberg
Associate Investigator(s)	Dr Sridhar Atresh, Prof Tim Geraghty, Prof Jean-Pierre Levesque, Mrs Esther Jacobson
Location	Princess Alexandra Hospital, Brisbane

Declaration by Participant

I wish to withdraw from participation in the above research project and understand that such withdrawal will not affect my routine treatment, my relationship with those treating me or my relationship with Princess Alexandra Hospital.

Name of Participant (please _____

Signature _____ Date _____

In the event that the participant's decision to withdraw is communicated verbally, the Study Doctor/ Researcher will need to provide a description of the circumstances below.

Declaration by Study Doctor/ Researcher†

I have given a verbal explanation of the implications of withdrawal from the research project and I believe that the participant has understood that explanation.

Name of Study Doctor/
Researcher† (please print) _____

Signature _____ Date _____

† A senior member of the research team must provide the explanation of and information concerning withdrawal from the research project.

Note: All parties signing the consent section must date their own signature.

DEPARTMENT OF PHARMACOLOGY

Mansfield Road, Oxford, OX1 3QT
Tel: +44(0)1865 271856

Dr Fay Probert/ Dr Helen Ashdown
01865 281135
fay.probert@pharm.ox.ac.uk/helen.ashdown@phc.ox.ac.uk

PARTICIPANT CONSENT FORM

CUREC Approval Reference: R55592/RE001

Obtaining plasma and serum samples from healthy volunteers for inflammatory disease study

Study Summary: Our lab undertakes a number of research projects aimed at understanding inflammatory diseases including those of the central nervous system (Multiple sclerosis and neuromyelitis optica) and bowel (ulcerative colitis and Crohn's disease). While REC approval is in place for these projects for the collection of patient plasma and serum samples, we frequently need corresponding samples from healthy volunteers to act as age and gender matched controls. This study will involve the collection of serum and plasma samples from healthy volunteers within the university to aid our understanding of inflammatory diseases.

		Please initial each box
1	I confirm that I have read and understand the information sheet version 1.2 dated 2nd Feb 2018 for the above study. I have had the opportunity to consider the information, ask questions and have had these answered satisfactorily.	☐
2	I understand that my participation is voluntary and that I am free to withdraw at any time, without giving any reason, and without penalty. . I understand that I will not be able to withdraw once my information has been combined with other participants' information for analysis.	☐
3	I understand that this project has been reviewed by, and received ethics clearance through, the University of Oxford Central University Research Ethics Committee.	☐
4	I understand that research data collected during the study may be looked at by designated individuals from the University of Oxford where it is relevant to my taking part in this study. I give permission for these individuals to access my data.	☐
5	I understand that a blood sample will be taken during the study and that this sample will be tested for comparison with inflammatory disease samples. I understand that the sample will be destroyed if I withdraw my consent for the test.	☐
6	I consider these samples a gift to the University of Oxford and I understand I will not gain any direct personal benefit from this.	☐
7	I understand who will have access to personal data provided, how the data will be stored and what will happen to the data at the end of the project.	☐
8	I understand how to raise a concern or make a complaint.	☐
9	I agree to take part in the above study.	☐

Optional: I agree for my personal data to be kept in a secure database for the purpose of contacting me about future studies. ☐

Optional: I agree for my anonymised samples to be used in future ethically approved projects of inflammatory diseases. ☐

Optional: I agree for my anonymised samples to be used in research studies of inflammatory diseases involving animals. ☐

Optional: I give the research team permission to approach me in the future to provide further samples. I understand that I am under no obligation to provide further samples. ☐

Name of Volunteer	Date	Signature

Name of person taking consent	Date	Signature

Blood taking record

SUBSEQUENT DONATIONS

Date	Volume	Ongoing consent obtained?	Participant Signature	Researcher taking consent

JOURNAL OF NEUROTRAUMA 35:639–651 (February 15, 2018)
© Mary Ann Liebert, Inc.
DOI: 10.1089/neu.2017.5049

Exacerbation of Acute Traumatic Brain Injury by Circulating Extracellular Vesicles

Isla Hazelton,[1,2,*] Abi Yates,[1,*] Ashley Dale,[1,2] Jay Roodselaar,[1] Naveed Akbar,[3] Marc J. Ruitenberg,[2] Daniel C. Anthony,[1] and Yvonne Couch[4]

Downloaded by OXFORD UNIVERSITY from www.liebertpub.com at 07/17/21. For personal use only.

Abstract

Inflammatory lesions in the brain activate a systemic acute-phase response (APR), which is dependent on the release of extracellular vesicles (EVs) into the circulation. The resulting APR is responsible for regulating leukocyte mobilization and subsequent recruitment to the brain. Factors that either exacerbate or inhibit the APR will also exacerbate or inhibit central nervous system (CNS) inflammation as a consequence and have the potential to influence ongoing secondary damage. Here, we were interested to discover how the circulating EV population changes after traumatic brain injury (TBI) and how manipulation of the circulating EV pool impacts on the outcome of TBI. We found the number of circulating EVs increased rapidly post-TBI, and this was accompanied by an increase in CNS and hepatic leukocyte recruitment. In an adoptive transfer study, we then evaluated the outcomes of TBI after administering EVs derived from either *in vitro* macrophage or endothelial cell lines stimulated with lipopolysaccharide (LPS), or from murine plasma from an LPS challenge using the air-pouch model. By manipulating the circulating EV population, we were able to demonstrate that each population of transferred EVs increased the APR. However, the characteristics of the response were dependent on the nature of the EVs; specifically, it was significantly increased when animals were challenged with macrophage-derived EVs, suggesting that the cellular origins of EVs may determine their function. Selectively targeting EVs from macrophage/monocyte populations is likely to be of value in reducing the impact of the systemic inflammatory response on the outcome of traumatic CNS injury.

Keywords: blood–brain barrier; extracellular vesicles; inflammation; microglia; traumatic brain injury

Introduction

Although the causes of traumatic brain injury (TBI) are largely unavoidable, the ensuing inflammatory response to the injury may be susceptible to therapeutic intervention.[1] However, targeting inflammation within the brain is problematic owing to the presence of the blood–brain barrier (BBB). It has become clear that the magnitude of the inflammatory response within the brain is dependent on the degree of activation of the acute-phase response (APR) in the periphery and in the liver in particular.[2,3] The anatomical and molecular pathways that carry injury signals from the brain to the liver to activate the APR are poorly understood.[4] However, inhibition of the APR using neutralizing agents directed against acute-phase proteins,[5] or by the inhibition of nuclear factor kappa B,[6] has shown that it is possible to ameliorate inflammation in the brain by suppressing the hepatic APR. Thus, targeting the afferent signaling pathways from the brain to the liver may provide some level of neuroprotection after acute TBI.

Simple humoral or neural pathways were considered to be responsible for initializing the APR post-TBI, but other studies have cast doubt on these claims; vagotomized animals still exhibit a peripheral response to central nervous system (CNS) injury,[7] and although the ratio of local and systemic cytokine/chemokine production after CNS injury has been found to be a critical factor dictating local leukocyte recruitment,[8] no cytokine/chemokine route between the CNS and the periphery has been established.[4] The emerging field of extracellular vesicles (EVs)[9] provides a potentially promising vehicle for brain-liver communication post-TBI.[10] EVs are divided into three main categories depending on their biogenesis[11]: 1) exosomes (40–150 nm) are small EVs that are released from endosomes; 2) microvesicles, also referred to as ectosomes and microparticles (150–1000 nm), bud directly from

[1]Department of Pharmacology, University of Oxford, Oxford, United Kingdom.
[2]School of Biomedical Sciences, The University of Queensland, Queensland, Australia.
[3]Department of Cardiovascular Medicine, RDM-Investigative Medicine, University of Oxford, Oxford, United Kingdom.
[4]Acute Stroke Programme, RDM-Investigative Medicine, University of Oxford, Oxford, United Kingdom.
*These authors contributed equally to this work.

the plasma membrane; and 3) apoptotic bodies (1000–5000 nm) are secreted after programmed cell death. EVs of types 1 and 2 are secreted by almost all cell types and are known to be released by neurons, astrocytes,[12] endothelial cells,[13,14] microglia,[15,16] and oligodendrocytes in the CNS.[17] Indeed, EVs derived from the circulation of an animal after a CNS inflammatory challenge have been shown to activate the hepatic APR and are likely to be largely, although not necessarily exclusively, of endothelial cell origin.[18] Thus, EVs present a novel form of paracrine communication after CNS injury and may induce the hepatic APR responsible for secondary damage post-TBI.

Here, we show that CNS trauma is directly correlated with an increase in circulating EV concentration. Further, we have demonstrated that, by manipulating the circulating EV pool by delivering EVs derived from an inflammatory background, it is possible to augment the APR, and exacerbate TBI, in a cell-line–dependent manner. These data introduce, for the first time, a new level of functionality for circulating EV populations after traumatic CNS injury.

Downloaded by OXFORD UNIVERSITY from www.liebertpub.com at 07/17/21. For personal use only.

Methods

Animals

Male C57BL/6 mice, 8–10 weeks of age, were housed under standard diurnal lighting conditions (12 h) with *ad libitum* access to food and water. All procedures were carried out in accord with the UK Animals (Scientific Procedures) Act (1986) and licensed protocols were approved by local committees (LERP and ACER, University of Oxford) and carried out under license number 30/3076. For surgery, animals were anesthetized in a 2% isoflurane/oxygen mix (2 L/min) and placed in a stereotactic frame (Stoetling Co., Wood Dale, IL) under maintenance anaesthesia (1.5%). All efforts were made to adhere to the ARRIVE guidelines at all times.

Traumatic brain injury model

A well characterized controlled cortical impact (CCI) model was utilized to simulate a TBI.[19] The instrument was composed of a linear unit, consisting of an interconnected motor and ram, as well as a microprocessor (Hatteras Instruments, Inc., Cary, NC). The size and shape of the impactor tip, velocity of the impact, contusion depth, and dwell time could be adjusted to vary injury severity. For this study, a 1.1-mm stainless steel flat tip with beveled edge was used with a speed of 1.5 m/s and dwell time of 85 ms to a depth of 0.5 mm.

Surgery

After excision of the scalp, a circular craniotomy of 2 mm in diameter was performed at bregma anteroposterior −2 mm, mediolateral −2 mm. An impactor tip was then centered at the craniotomy site, perpendicular to the exposed brain. The tip was then lowered until it made contact with the dural surface without tissue deformation. After an upward retraction of 20 mm, the tip advanced a total of 20.5 mm into the somatosensory cortex to induce the TBI. Post-TBI, bleeding was allowed to resolve before the skull section was replaced and the scalp was closed using glue. Animals were then allowed to survive for 2, 6, 12, and 24 h before culling and tissue collection. Sham-operated mice underwent craniotomy, but not cranial trauma. All animals received subcutaneous saline in the immediate post-operative period and wound sites were treated with Marcaine.

Tissue collection

Blood was collected by cardiac puncture into heparinized needles. Animals underwent intracardiac perfusion with heparinized saline, and fresh spleen and liver tissue were snap frozen at −80°C for polymerase chain reaction (PCR). Tissue was then fixed by intracardiac perfusion with 4% paraformaldehyde (PFA), and brain, liver, and spleen were collected and cryoprotected using 30% sucrose. Tissue was cut at 10–12 μm with Leica cryostat (Leica Biosystems, Wetzlar, Germany).

Immunohistochemistry

Immunostaining was performed as previously described using an avidin-biotin-peroxidase method using 3,3′-diaminobenzidine (Abcam, Cambridge, UK) to visualize the stain.[20] To assess cellular changes, brain sections were stained for neutrophils (MBS; made in-house [rabbit antibody harvested from a rabbit immunized with whole rat neutrophils and stimulant *Megathura crenulata* hemocyanin]; 1:1000 as previously described[21,22]) and ionized calcium binding adaptor molecule 1 $(Iba1)^+$ microglia (Iba-1; 1:500; ab178847; AbCam) with a cresyl violet counterstain. BBB breakdown was assessed by quantifying the presence of serum in the parenchyma (immunoglobulin G [IgG]; BA-9200; 1:200; Vector Laboratories, Peterborough, UK), and lesion volume was established using a cresyl violet stain. Liver and splenic tissues were stained with MBS and Iba-1 with hemotoxylin counter stain.

Quantification of macrophage and neutrophil number in liver and spleen

Quantification of splenic and hepatic macrophages and neutrophils, positive for Iba-1 and MBS respectively, was performed in five representative fields at 40× where the average number of positive cells was calculated and expressed as number of cells per mm^2. The five fields were selected from three 10-μm sections chosen at random from liver or spleen.

Quantification of blood–brain barrier breakdown

IgG staining density was used as a surrogate marker for BBB breakdown and was analyzed using imageJ (version 1.8.0_101; NIH, Bethesda, MD) software on images of whole coronal sections. The threshold of the images was adjusted after subtracting an appropriate background to ensure that only specific staining was quantified. Total area of IgG stain was measured, as well as stain intensity to quantify the amount of tissue IgG.

Quantification of central nervous system microglia and neutrophil numbers

Neutrophil and microglial numbers were quantified from sections −1.6 to −2.8 mm relative to Bregma in 10-μm sections at 100-μm intervals. The region of interest in each slice was specified by the area of neuronal loss (as defined by absence of cresyl violet staining) and area of infiltration of MBS^+ neutrophils or $Iba\text{-}1^+$ microglia using a Leica microscope (Leica Biosystems). Total number of cells across 12 sections was quantified and expressed as average number of cells per mm^2.

Quantification of lesion size

Lesion size was determined by measuring the area of dead or dying cells in the cortex post-TBI. Sections were stained with cresyl violet, and the lesion was traced with the camera lucida (Leitz Laborlux). Tissue was considered dead or dying when cresyl violet staining was reduced and cells were small and deformed with no visible nucleolus. The average area of cell death across three sections per animal was calculated with ImageJ (NIH).

Cell culture

Murine brain vascular endothelial cells (bEND.3; ATCC® CRL-2299™) and murine macrophages (RAW 264.7; ATCC®

Downloaded by OXFORD UNIVERSITY from www.liebertpub.com at 07/17/21. For personal use only.

TIB-71™) were cultured under standard cell-culture conditions (5% CO_2 in air, 37°C humidified) using readily available cell-culture medium (Dulbecco's modified Eagle's medium, 10% EV-free fetal calf serum [FCS] and 1% antibiotics). Cells were stimulated with 10 ng/mL of lipopolysaccharide (LPS) for 6 h before harvesting of EVs from supernatant as above. EV-free serum was generated in-house by ultracentrifuging standard heat-inactivated FCS for 18 h at 120,000*g*.

Air-pouch model

The air-pouch model of systemic inflammation was performed using C57BL/6 mice as previously described.[23] Mice were injected with 2.5 mL of sterile air twice under general anesthesia; 48 h apart. Twenty-four hours after the second sterile air injection, mice were injected with 1 mL of 1.5 mg/kg of LPS. Six hours post-injection, animals were culled and blood was collected by heparinized needle.

Extracellular vesicle isolation

Blood from animals was spun at 2700*g* for 10 min at 4°C to separate plasma and remove platelets. Platelet-free plasma was then ultracentrifuged at 120,000*g* for 120 min to pellet the EVs, which were then resuspended in phosphate-buffered saline (PBS; Thermo Fisher Scientific, Waltham, MA). For cell-culture supernatant, dead cells and debris were spun at 3,000*g* for 10 min at 4°C before ultracentrifugation at 120,000*g* for 120 min to pellet EVs, which were resuspended as above. All ultracentrifugation steps were performed using the Beckman Coulter (Brea, CA) Type 70 Ti rotor at 4°C.

Tuneable resistive pulse sensing

Tuneable resistive pulse sensing (TRPS) measurements were performed with the qNano (Izon Science, Cambridge, MA) on plasma-isolated EVs. A NP150 nanopore was used to accurately measure particles between 80 and 200 nm. CPC100B calibration particles at dilutions of 1:500, 1:1000, 1:3000, and 1:5000, at pressures 5, 7, or 10, were used to calibrate the pore. Calibration curves were run until 1000 particles had been counted. Samples were diluted 1:50, and the particle rate curve was run at corresponding calibration pressures until 500–1000 particles had been counted. Samples were calibrated and evaluated at 5-nm intervals.

Transmission electron microscopy

Transmission electron microscopy (TEM) imaging was used to validate the presence of EVs in our pellet. Plasma-derived EVs were fixed in 2% PFA and diluted 1:20 in PBS for optimum imaging. Then, 10 μL of isolated EVs were applied to freshly glow discharged carbon formvar 200 mesh copper grids for 2 min before being blotted with filter paper. The grids were then stained with 2% uranyl acetate for 10 secs, blotted, and air dried. Grids were imaged in a FEI TEcnai 12 TEM at 12 kV (GAtan OneView CMOS camera; Gatan Inc., Pleasanton, CA).

Western blotting

Total protein was extracted from plasma-derived vesicle fractions using radioimmunoprecipitation assay buffer and quantified using a micro bicinchoninic acid kit (Thermo Scientific, Loughborough, UK). Then, 25 μg of total protein extracted from EVs was loaded for electrophoresis, in parallel with protein extracted from whole-brain lysates as a control, and transferred onto a polyvinylidene difluoride membrane. Blotting was performed overnight using antibodies against vesicle markers Tsg101 (1:250 in 5% bovine serum albumin; 4A10 Ab83; Abcam), Alix (1:500 in 5% milk; 3A9 ab117600; Abcam), CD31 (1:2000 in 5% milk; Abcam), CD68 (1:2000 in 5% milk; Abcam), and histone-H3 (DIH2; 1:2000 in 5% milk; New England Biolabs Ltd, Hitchin, UK). Detection was performed using horseradish-peroxidase–conjugated secondary antibodies (1:10,000), and blots were visualized using chemiluminescence and a ChemiDoc (Bio-Rad Laboratories Ltd, Whatford, UK).

Extracellular vesicle adoptive transfer

C57BL/6 mice received an intravenous injection of 150 uL of either sterile saline, plasma-derived EVs isolated from the air-pouch model, EVs isolated from murine macrophages (RAW264.7), or EVs isolated from brain vascular endothelial cells (b.END3) immediately post-TBI. Animals were allowed to survive for 6 h before fresh and fixed liver and fixed brain were collected as previously described. Before injection of EVs derived from plasma, macrophages, or endothelial cells into TBI animals, their concentration and size were measured using TRPS. A $\sim$10× higher concentration of plasma-derived EVs was injected in comparison to RAW 264.7 macrophage-cell-line–derived EVs because of the lower specificity of plasma-derived EVs given that macrophage- and endothelial-cell–derived EVs will originate from one cell line only, whereas plasma-derived EVs are originating from a multitude of cell types and represent only a small proportion (c.10%) of the EVs in the circulation.[23] Macrophage- and endothelial-cell–derived EV injections were adjusted to the same concentration of 9.81×10^8 particles/mL before injection.

RNA extraction and complementary DNA conversion

RNA extraction was performed on snap-frozen liver tissue using the Qiagen® RNEasy Mini Kit (Qiagen Ltd, Manchester, UK) as per the manufacturer's instructions. Eluted RNA was quantified using a Nanodrop and considered acceptable for complementary (cDNA) conversion if 260/280 and 260/230 ratios were >2. Next, 1000 ng of whole RNA was converted to cDNA using the high-capacity cDNA kit (Applied Biosystems, Warrington, UK), as per the manufacturer's instructions.

Quantitative polymerase chain reaction

Real-time quantitative PCR was performed on 25 ng of cDNA using SYBR green and the relative standard curve method, as described previously.[24] Forward and reverse primers for *tnf* (F: GCCTCCCTCTCATCAGTTCTAT, R: TTTGCTACGACGTGG GCTA), *il1β* (F: CAACCAACAAGTGATATTCTCCAT, R: GGG TGTGCCGTCTTTCATTA), *il6* (F: TCCATCCAGTTGCCTTC TTG, R: GGTCTGTTGGGAGTGGTATC), *cxcl1* (F: GCTGGGA TTCACCTCAAGAAC, R: TGTGGCTATGACTTCGGTTTG), *cxcl10* (F: CATCCCGAGCCAACCTTCC, R: CACTCAGACCC AGCAGGAT), and *saa2* (F:, R:) were used.

Statistical analysis

All data were analyzed using Graphpad Prism software (version 6; GraphPad Prism Inc., La Jolla, CA). Analysis of data was performed using two-way analysis of variance (ANOVA) or one-way ANOVA, as appropriate. Data were considered significant at $p < 0.05$. Tukey's or Holm-Sidak's multiple comparisons post-hoc testing was applied as appropriate. All data sets are presented as mean ± standard error of the mean; *n* are included in figure legends.

Results

Cortical impact results in blood–brain barrier breakdown and localized inflammation

Here, we wished to perform a basic characterization of a model of cortical impact where the center of the lesion was positioned posterior to bregma, at the level of the posterior parietal association

area. This position was chosen to be clinically silent, with minimal behavioral effects, in order to focus study on the molecular pathology (Supplementary Fig. 1) (see online supplementary material at http://www.liebertpub.com). To assess BBB breakdown, infiltration of serum IgG was used, quantifying both the volume of tissue positive for IgG immunoreactivity (Fig. 1A) as well as the density of staining (Fig. 1B). Sham animals showed no BBB breakdown at any time post-surgery; as such, only one sham column has been included in the graph, but shams for each time point were included in the analysis; at no time point were shams any different from one another. The volume of IgG infiltration increased with time post-TBI (Fig. 1C) with significant differences found between the volume of tissue containing IgG after 2 and 6 h compared to 24 h (Fig. 1A; two-way ANOVA; injury, $p < 0.0001$; time, $p < 0.01$; injury:time, $p < 0.01$). The volumes after 2 h ($0.7725 \pm 0.4253\,mm^3$), 6 h ($1.37 \pm 0.4981\,mm^3$), but not 12 h ($4.332 \pm 1.575\,mm^3$) were found to be significantly smaller than 24 h post-TBI ($6.965 \pm 1.553\,mm^3$; Tukey's post-hoc vs. 2 h, $p < 0.01$; vs. 6 h, $p < 0.05$). IgG density is correlated with the amount of IgG that has ''leaked'' into the tissue. It is accepted that this is a semiquantitative measure. IgG density increased over time (Fig. 1B; two-way ANOVA; injury, $p < 0.0001$; time, $p < 0.01$; injury:time, $p < 0.01$). The most intense IgG stain was observed at 24 h post-TBI, which gave an intensity of 138.4 ± 5.918 (arbitrary units), which was significantly greater than the densities at 12 h (57.31 ± 18.10; Tukey's post-hoc, $p < 0.01$), 6 h (27.74 ± 19.24; $p < 0.01$), and 2 h (8.6 ± 4.397; $p < 0.0001$) post-TBI (Fig. 1B).

Lesion size was measured by quantifying the area of dead and dying neurons on a Nissl stain (Fig. 1D,E; two-way ANOVA; injury, $p < 0.0001$; time, $p < 0.01$; injury:time, not significant [ns]). TBI animals had significantly larger lesions at 6 h ($0.647 \pm 0.1310\,mm^3$; Tukey's post-hoc, $p < 0.05$), 12 h ($1.092 \pm 0.2588\,mm^3$; $p < 0.01$), and 24 h ($1.307 \pm 0.1875\,mm^3$; $p < 0.001$) post-TBI when compared to sham animals. Lesion size increased with time, with area of cell death significantly greater at 24 h compared to 2 h (Tukey's post-hoc test; $p < 0.05$) and 6 h ($p < 0.05$), but not 12 h.

Any traumatic CNS injury is associated with some degree of CNS inflammation. Here, we investigated infiltrating polymorphonuclear cells, as well as Iba-1^+ microglia. Total brain neutrophil infiltration into the lesion was found to be significantly higher at later time points (Fig. 1F,G; two-way ANOVA; injury, $p < 0.0001$; time, $p < 0.0001$; injury:time, $p < 0.0001$). Post-hoc testing (Tukey's) revealed significant differences between 2 and 6 h post-TBI (4.33 ± 2.333 and 4.5 ± 1.936, respectively) when compared to 12 h (59.25 ± 5.105; 2 h, $p < 0.01$; 6 h, $p < 0.05$). Animals surviving 24 h post-TBI (80.33 ± 13.91) also had significantly higher CNS neutrophils compared to the 2- or 6-h time points post-TBI (2 h, $p < 0.001$; 6 h, $p < 0.01$).

As well as an increase in neutrophil number, there was also a significant difference in the number of Iba-1^+ microglia found post-TBI ($43.96 \pm 3.11/mm^2$) when compared to sham surgery ($23.14 \pm 1.215/mm^2$; Fig. 1H,I; two-way ANOVA; injury, $p < 0.001$; time, ns; injury:time, ns). Although this general increase in Iba-1^+ cells and did not change over time, it is interesting to note that when Iba-1 positivity was assessed at regular intervals laterally from the core of the lesion (similar to analysis and digitization performed previously[21]), the spread of Iba-1^+ microglia increased with time, with Iba-1^+ cells being found as far as 1.2 mm away from the epicentre of the lesion by 24 h (Supplementary Fig. 2) (see online supplementary material at http://www.liebertpub.com).

It should be noted that this lesion generates a significant systemic inflammatory response. Peripheral macrophage and neutrophil recruitment were examined in the liver and spleen (Supplementary Fig. 3) (see online supplementary material at http://www.liebertpub.com). Hepatic macrophage numbers were not affected by TBI whereas splenic macrophages were (two-way ANOVA; injury, $p < 0.01$; time, ns; injury:time, ns), and neutrophil infiltration was increased at all times post-injury in both liver (two-way ANOVA; injury, $p < 0.0001$; time, $p < 0.05$; injury:time, ns) and spleen (two-way ANOVA; injury, $p < 0.0001$; time, $p < 0.5$; injury:time, ns).

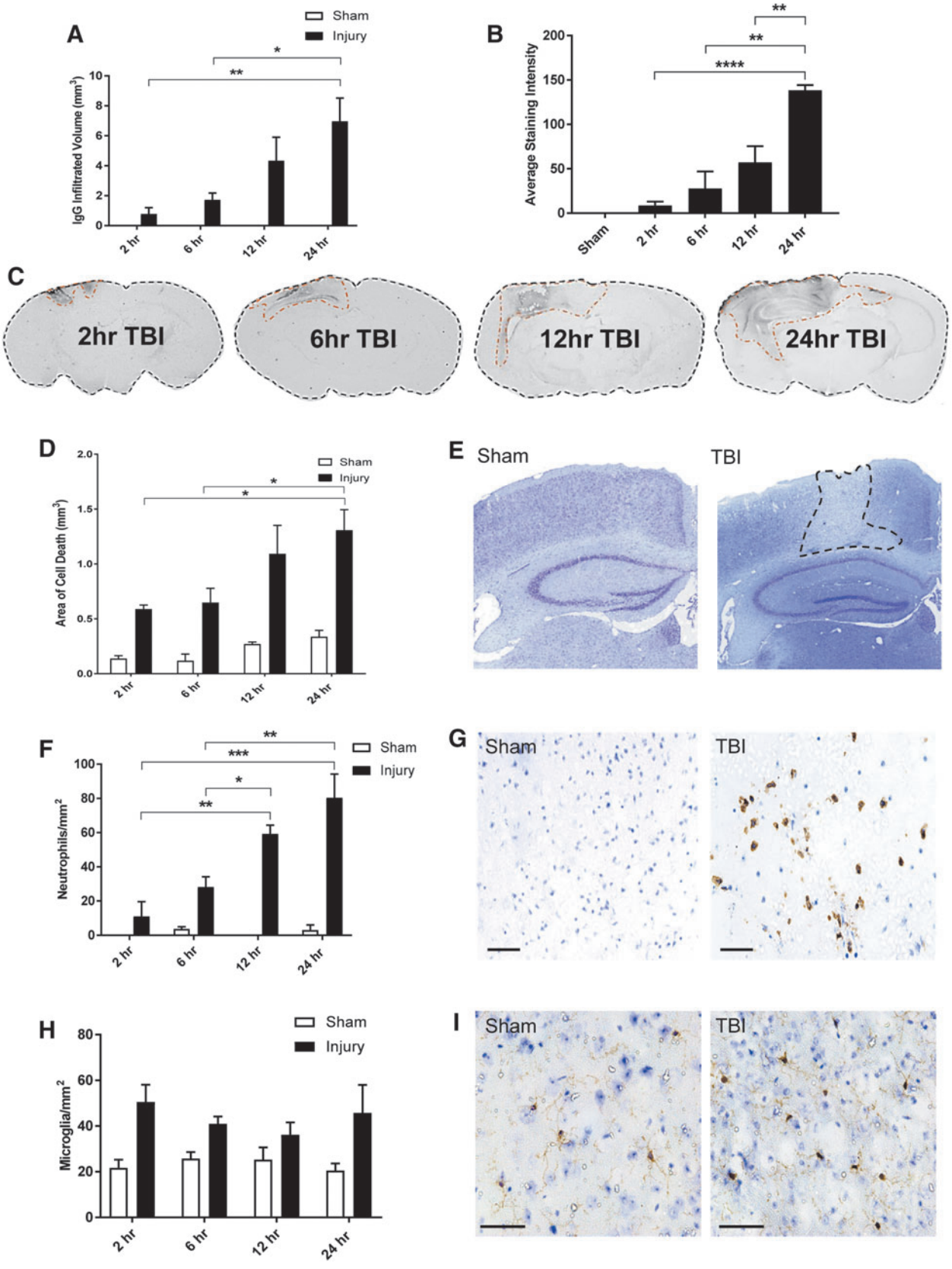
Traumatic brain injury causes an increase in circulating extracellular vesicle numbers

To assess the concentration of EVs circulating in plasma, pelleted EVs were analyzed using TRPS. Compared to sham, TBI caused a significant increase in EV number in the circulation independent of time (Fig. 2A; two-way ANOVA; injury, $p < 0.05$; time, ns; injury:time, ns). A trend was observed between sham and TBI animals where increasing survival time appeared to be associated with an increase in EV number. Twenty-four hours gave the highest concentration of circulating EVs (4.27×10^{11} particles/mL). However, this did not reach significance. When the mean diameters of the particles were compared, we observed that the vesicles decreased in size post-injury (Fig. 2B; two-way ANOVA; injury, $p < 0.01$; time, $p < 0.01$; injury:time, ns). Post-hoc testing (Tukey's) revealed that the mean diameter at 24 h (94.33 ± 2.404 nm) was significantly different from both 6 h (101.67 ± 7.12 nm; $p < 0.05$) and 12 h (102.66 ± 2.88 nm; $p < 0.01$), indicating that smaller EVs get released with longer survival times. All EV fractions isolated from

FIG. 1. Characterization of the molecular pathology of traumatic brain injury over the posterior parietal association area. C57BL/6 mice received a TBI at 70 kdyne and were allowed to survive for either 2, 6, 12, or 24 h. Brain tissue was collected and stained for markers of injury; IgG, indicative of blood–brain barrier breakdown, cresyl violet for neurons, MBS^+ for neutrophils, and Iba-1^+ for microglia. (**A**) IgG infiltrated volume (mm^3) increased with the duration of injury and was undetectable in sham-operated animals across all time points. (**B**) Cumulative density of IgG staining in the brain was analyzed using ImageJ (NIH, Bethesda, MD) to quantify the mean raw intensity of DAB-stained images. Mean raw intensity of IgG is increased 24 h post-TBI compared to 2 and 6 h and nondetectable in the sham across all time points. (**C**) IgG stained area at 2, 6, 12, and 24 h time points. (**D**) Area of cell death determined by quantifying the area of dead or dying neurons from cresyl violet stain across the brain sections. (**E**) Representative pictograms showing the area of cell death following a TBI and a sham surgery. Dotted line highlights lesioned area post-TBI. Scale bar represents 200 μm. (**F**) Neutrophil density increased after injury and over time. Neutrophil infiltration in the ipsilateral cortex is significantly increased after 12 and 24 h compared to 2 and 6 h. Neutrophils were undetectable in the sham animals at 2 and 12 h post-surgery. (**G**) Representative pictograms showing neutrophil infiltration to brain tissue after a TBI and a sham surgery. Scale bar represents 10 μm. (**H**) Iba-1^+ microglia number/mm^2 around the lesion site increases after impact of injury at 2- and 24-h survival time; duration of injury had no impact. (**I**) Representative pictograms showing activated and ramified microglia in the brains of TBI- and sham-operated animals. Scale bar represents 10 μm. Data are mean ± standard error of the mean, $n = 5$; *$p < 0.05$; **$p < 0.01$; ***$p < 0.01$; ****$p < 0.0001$. DAB, diaminobenzidene; Iba, ionized calcium binding adaptor molecule; IgG, immunoglobulin G; MBS, anti-neutrophil polygG; TBI, traumatic brain injury. Color image is available online at www.liebertpub.com/neu

Downloaded by OXFORD UNIVERSITY from www.liebertpub.com at 07/17/21. For personal use only.

Downloaded by OXFORD UNIVERSITY from www.liebertpub.com at 07/17/21. For personal use only.



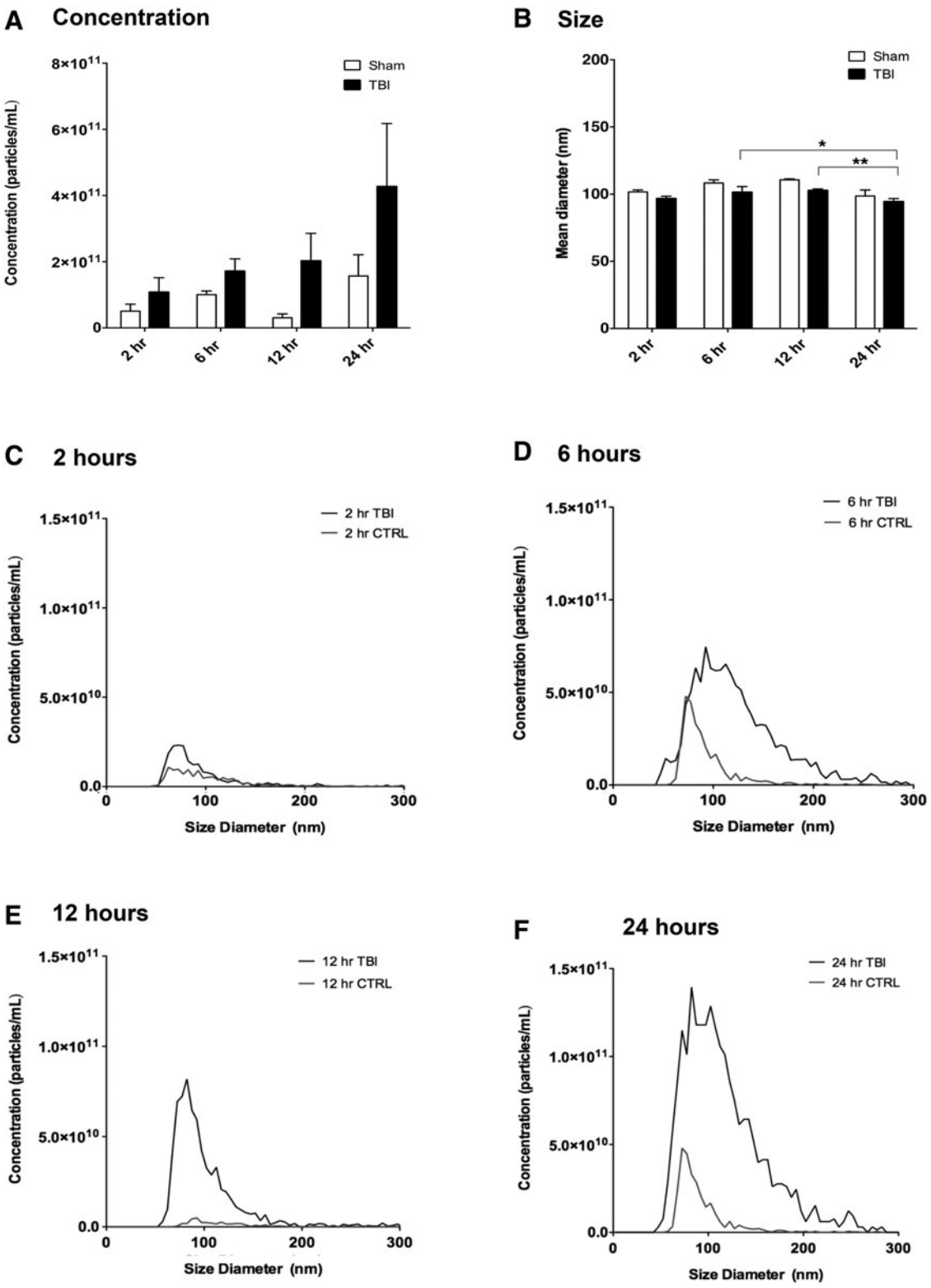


FIG. 2. TBI increases EV number and decreases size. C57BL/6 mice received a TBI at 70 kdyne and were allowed to survive for either 2, 6, 12, or 24 h. Plasma was collected, ultracentrifuged, and assessed using tuneable resistive pulse sensing (TRPS). The impact of the injury seemed to increase the production of EVs (**A**) and decreased EV size after 24 h compared to 6 and 12 h (**B**). Representative TRPS plots for 2 hours (**C**), 6 h (**D**), 12 h (**E**), and 24 h (**F**) show the raw changes in size and number in TBI versus sham. Mean ± standard error of the mean, $n = 3$; $^{*}p < 0.05$; $^{**}p < 0.01$ (time). CTRL, control; EVs, extracellular vesicles; TBI, traumatic brain injury.

Downloaded by OXFORD UNIVERSITY from www.liebertpub.com at 07/17/21. For personal use only.

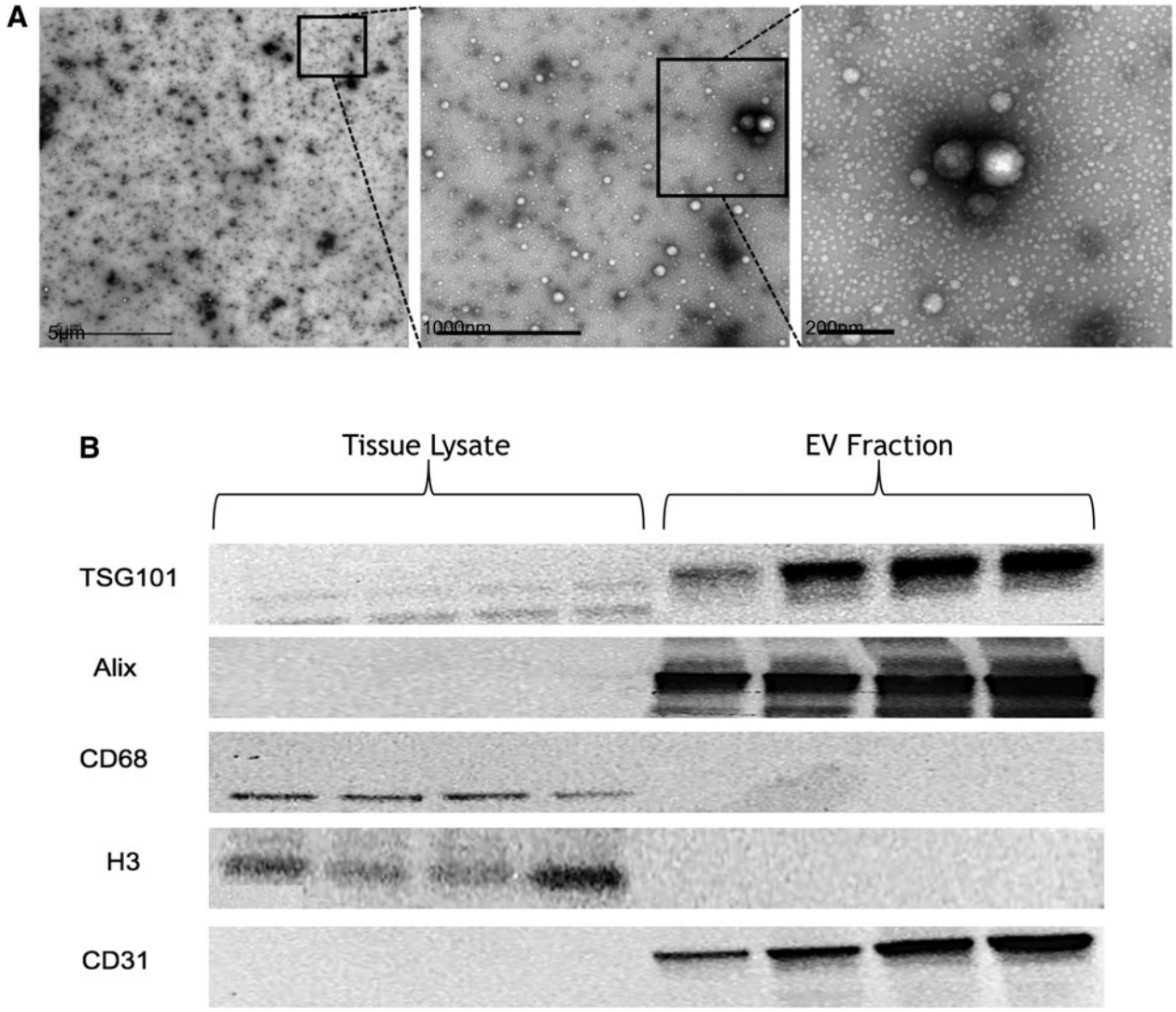


FIG. 3. Phenotypic analysis of a mixed EV population isolated by ultracentrifugation. Blood of animals was collected and 200 μL of plasma was isolated (2700*g* for 10 min). Plasma was then ultracentrifuged for 2 h at 120,000*g*. Presence of EVs in ultracentrifuged plasma was confirmed using EM imaging and western blotting. (**A**) EM of the 120,000*g* EV pellet derived from 200 μL of plasma shows a mixed population of vesicles. (**B**) Western blot analysis of EV pellet derived from 200 μL of plasma. Primary antibodies used were TSG101, Alix, CD68, H3, and CD31. As a control, cell lysate of whole-brain tissue was used. To rule out cellular contamination of the EV preparation, H3 primary antibody was used. Scale bars: 5 μm, 1000 nm, and 200 nm, as marked. EM, electron microscopy; EV, extracellular vesicle.

Downloaded by OXFORD UNIVERSITY from www.liebertpub.com at 07/17/21. For personal use only.

plasma showed a standard distribution when analyzed with TRPS (Fig. 2C–F). EVs were confirmed by TEM and western blotting as per International Society for Extracellular Vesicles (ISEV) guidelines and our previous work.[22,25,26] TEM revealed the presence of EVs of both microvesicle and exosome biogenesis, based on size (Fig. 3A). Western blotting showed that plasma-derived EV samples were positive for EV markers TSG101, Alix, and CD31 and negative for cell lysate controls CD68 and H3 (Fig. 3B). These results indicate the presence of a mixed population of EVs (exosomes and microvesicles) after isolation without cellular contamination.

Exogenous inflammatory extracellular vesicles exacerbate acute injury after traumatic brain injury

To determine the degree to which the composition of circulating inflammatory EVs contributes to the outcomes of TBI, we established a model of systemic inflammation using an LPS air-pouch model (a standard method for pyrogen testing; see Methods), as well as using *in vitro* models of inflammation using LPS-challenged mouse macrophages (RAW 264.7) or brain vascular endothelial cells (b.END3). EVs are released into the circulation post-injury in a rapid manner; thus, we aimed to look at an acute time point post-injury (6 h) in order to determine what effects early manipulation of the circulating EV pool had.

The volume of IgG extravasation increased when EVs were injected into the bloodstream (Fig. 4A,B,D; one-way ANOVA; $p < 0.01$). In the post-hoc testing (Holm-Sidak), significant differences were found between IgG volume after plasma-derived EV injection ($5.442 \pm 0.4987\,mm^3$; $p < 0.01$), macrophage-derived EV injection ($5.411 \pm 0.5882\,mm^3$; $p < 0.01$), and endothelial-cell–derived EV injection ($5.398 \pm 0.3043\,mm^3$; $p < 0.01$) when compared to a sterile saline injection ($2.636 \pm 0.5018\,mm^3$). The most

intense IgG stain was observed in the macrophage-derived EV-injected group (Fig. 4B; 56.11 ± 6.606). This was the only treatment found to be significantly different when compared to the sterile saline-injected group in post-hoc tests (36.84 ± 14.30; $p < 0.05$). The area of cell death in the brain was also exacerbated by exogenous EVs (Fig. 4C,E; one-way ANOVA; $p < 0.05$). Animals injected with endothelial-derived EVs ($2.689 \pm 0.3315\,mm^2$) had significantly larger lesions than saline-injected animals ($1.164 \pm 0.2445\,mm^2$) as determined by the Holm-Sidak post-hoc test ($p < 0.01$). Animals injected with plasma- and macrophage-derived EVs also exhibited greater cell death, with lesion sizes of 2.066 ± 0.2262 and $1.816 \pm 0.3138\,mm^2$, respectively; however these data did not reach significance. In addition to the investigation of structural changes in animals challenged with exogenous inflammatory EVs, we also investigated the degree to which CNS microglia and recruited neutrophil populations were affected by the manipulation of the circulating EV pool. Significant differences in microglial numbers/mm^2 were found in animals injected with EVs derived from plasma and cell culture (Fig. 4F; one-way ANOVA; $p < 0.01$). Post-hoc testing (Holm-Sidak) showed that significant increases in microglial number in plasma-derived EV-injected animals ($80.87 \pm 6.502/mm^2$; $p < 0.01$), macrophage-derived EV-injected animals ($79.49 \pm 2.95/mm^2$; $p < 0.01$), and endothelial-cell–derived EV-injected animals ($71.1 \pm 1.988/mm^2$; $p < 0.05$) when compared to controls ($52.65 \pm 5.511/mm^2$). In animals receiving a TBI with a saline challenge, there was an average of 49.8 ± 6.367 neutrophils in the brain, which increased upon challenge with exogenous inflammatory EVs (Fig. 4G; one-way ANOVA; $p < 0.05$). Animals receiving EVs from LPS-challenged macrophages displayed an average of 101.3 ± 12.7 neutrophils, which was significantly elevated when compared to animals receiving a saline injection ($p < 0.05$).

Extracellular vesicle origin determines the degree of hepatic inflammation

By manipulating the circulating pool of EVs through delivery of ''primed'' exogenous vesicles, we set out to find how this may affect both TBI and its associated APR. Here, we examined both the recruitment of immune cells to liver and spleen, as well as cytokine and chemokine messenger RNA (mRNA) expression in liver in animals whose circulating pool of EVs had been manipulated with exogenous EVs from inflammatory sources. Plasma-derived EVs from the LPS air-pouch model and macrophage-derived EVs from LPS-stimulated RAW cells had the most significant effects on neutrophil recruitment, but little effect on macrophage recruitment, to both liver and spleen (Supplementary Fig. 4) (see online supplementary material at http://www.liebertpub.com). In liver, the macrophage-derived EV injected group was found to be significantly different compared to the sterile saline group for all of the transcripts examined, with fold changes as high as 66.9 for the relative expression of *cxcl10* (Fig. 5E). In animals injected with endothelial-cell–derived EVs, the gene expression varied significantly for *cxcl10* ($p < 0.05$) and *il1β* ($p < 0.01$) when compared to the relative gene expression of saline-injected animals (Fig. 5; one-way ANOVA; Holm-Sidak post-hoc test). For the plasma-derived EV group, relative gene expression levels did not vary significantly from the saline-injected group across for all transcripts except *saa2* (Fig. 5F). Plasma-derived EV-injected animals displayed a significantly higher fold change for *saa2* (8.713 ± 1.237) compared to saline-injected animals (Fig. 5F; one-way ANOVA; 2.060 ± 1.097; Holm-Sidak post-hoc test; $p < 0.05$).

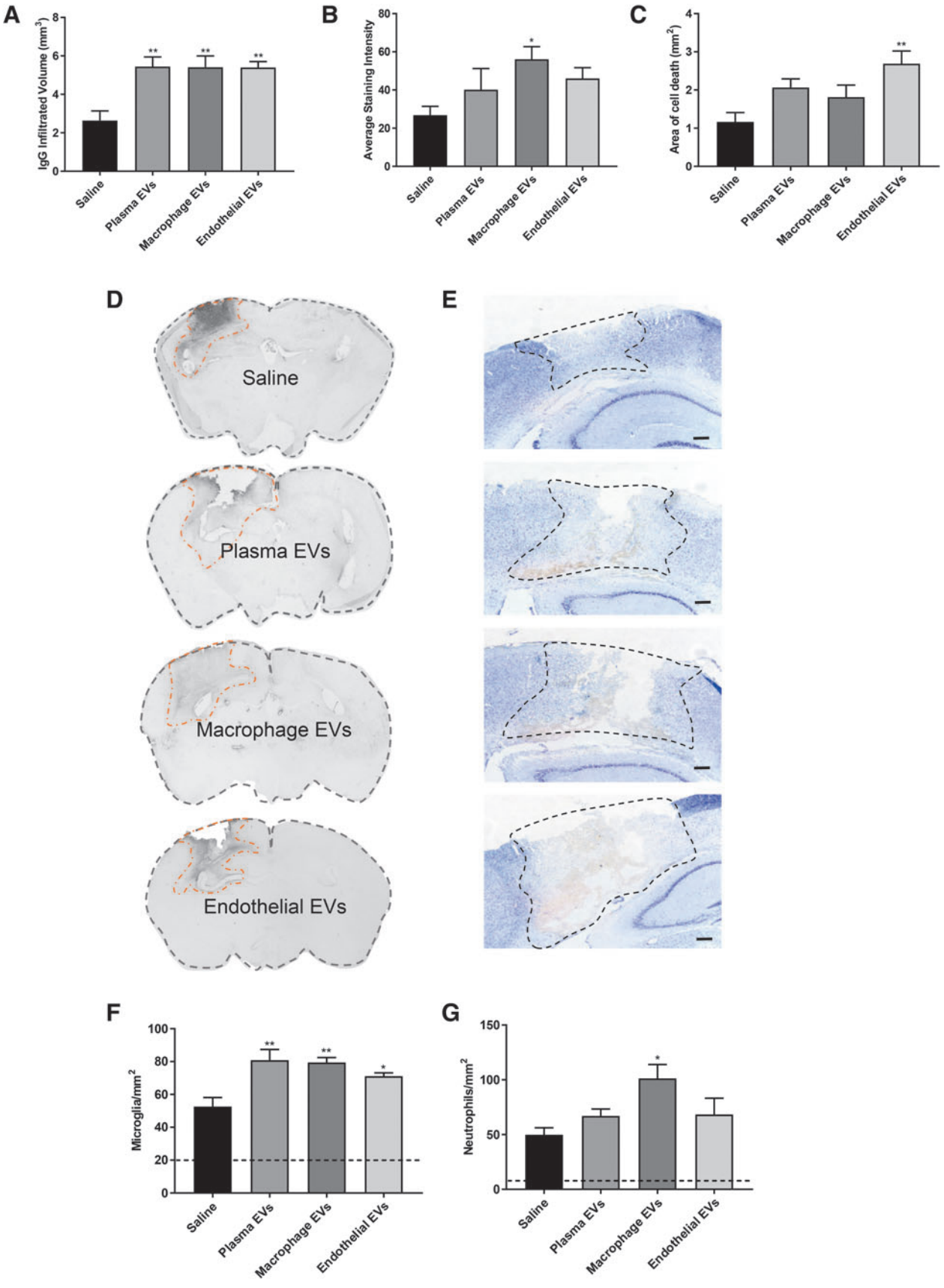
Discussion

In this study, we have shown, for the first time, that manipulating the circulating pool of EVs immediately after traumatic CNS injury significantly worsens lesion area, BBB breakdown, and systemic inflammation. We have shown that traumatic injury to the CNS in the mouse results in an elevation of circulating EVs, and that by enriching this population, particularly with LPS-stimulated macrophage-derived EVs, we can exacerbate the inflammatory response to TBI. To our knowledge, this is the first time that circulating EVs have been shown to influence the outcome of traumatic CNS injury and significantly opens the field of EV research in trauma.

The model of TBI used in this study was focused on the posterior parietal association area, rather than either the sensory or motor cortices. The lack of significant behavioral effects resulted in a clinically silent lesion where we were able to study the CNS pathology and its effects on the systemic immune system in relative isolation. The model used here generated a typical lesion which increased in size over time and showed classic signs of CNS inflammation, including microglial activation, IgG infiltration, and neutrophil recruitment. BBB breakdown was observed at all time points in this model. Given that increased barrier permeability and higher numbers of CNS neutrophils play key roles in the progression of CNS inflammation,[27] understanding more about the

FIG. 4. Exogenously administered EVs increase blood–brain barrier breakdown, lesion size, and microglia and neutrophil density in the brain post-TBI. C57BL/6 mice were either injected with saline ($n = 4$), plasma-derived EVs from the air-pouch LPS model ($n = 3$), or from cell cultures stimulated with LPS, specifically macrophage cell-line–derived EVs ($n = 4$) or endothelial-cell–derived EVs ($n = 4$), before receiving a TBI at 70 kdyne with 6-h recovery time. Brain tissue was collected and stained for IgG (representative of blood–brain barrier breakdown), cresyl violet to measure area of cell death, Iba-1^+ for microglia, and MBS^+ for neutrophils. (**A**) IgG volume was increased after injection of plasma-, macrophage-, and endothelial-derived EVs compared to sterile saline. (**B**) Cumulative density of IgG in the brain was analyzed using ImageJ (NIH, Bethesda, MD) to quantify the mean raw intensity of DAB-stained images. Mean raw intensity of IgG was only increased in the macrophage-derived EV-injected animals compared to sterile saline. (**C**) Area of cell death, as determined by lack of cresyl violet staining and small, abnormal cells, was increased in the endothelial-derived EV-injected animals compared to sterile saline only. (**D**) Representative images of IgG staining in animals in each group. (**E**) Representative images of lesions in animals in each group. Dotted lines indicate the boundary between healthy and damaged tissue. (**F**) Microglial number was increased after the injection of either plasma-, macrophage-, or endothelial-cell–derived EVs compared to saline injection. (**G**) Neutrophil number was significantly increased in the brain after injection of macrophage-derived EVs only. Data are mean ± standard error of the mean; $*p < 0.05$; $**p < 0.01$ when compared to saline-injected controls. Dashed line represents average of sham animals. EV, extracellular vesicle; Iba-1, ionized calcium binding adaptor molecule 1; IgG, immunoglobulin G; LPS, lipopolysaccharide; MBS, anti-neutrophil polylgG; TBI, traumatic brain injury. Color image is available online at www.liebertpub.com/neu

Downloaded by OXFORD UNIVERSITY from www.liebertpub.com at 07/17/21. For personal use only.



Downloaded by OXFORD UNIVERSITY from www.liebertpub.com at 07/17/21. For personal use only.

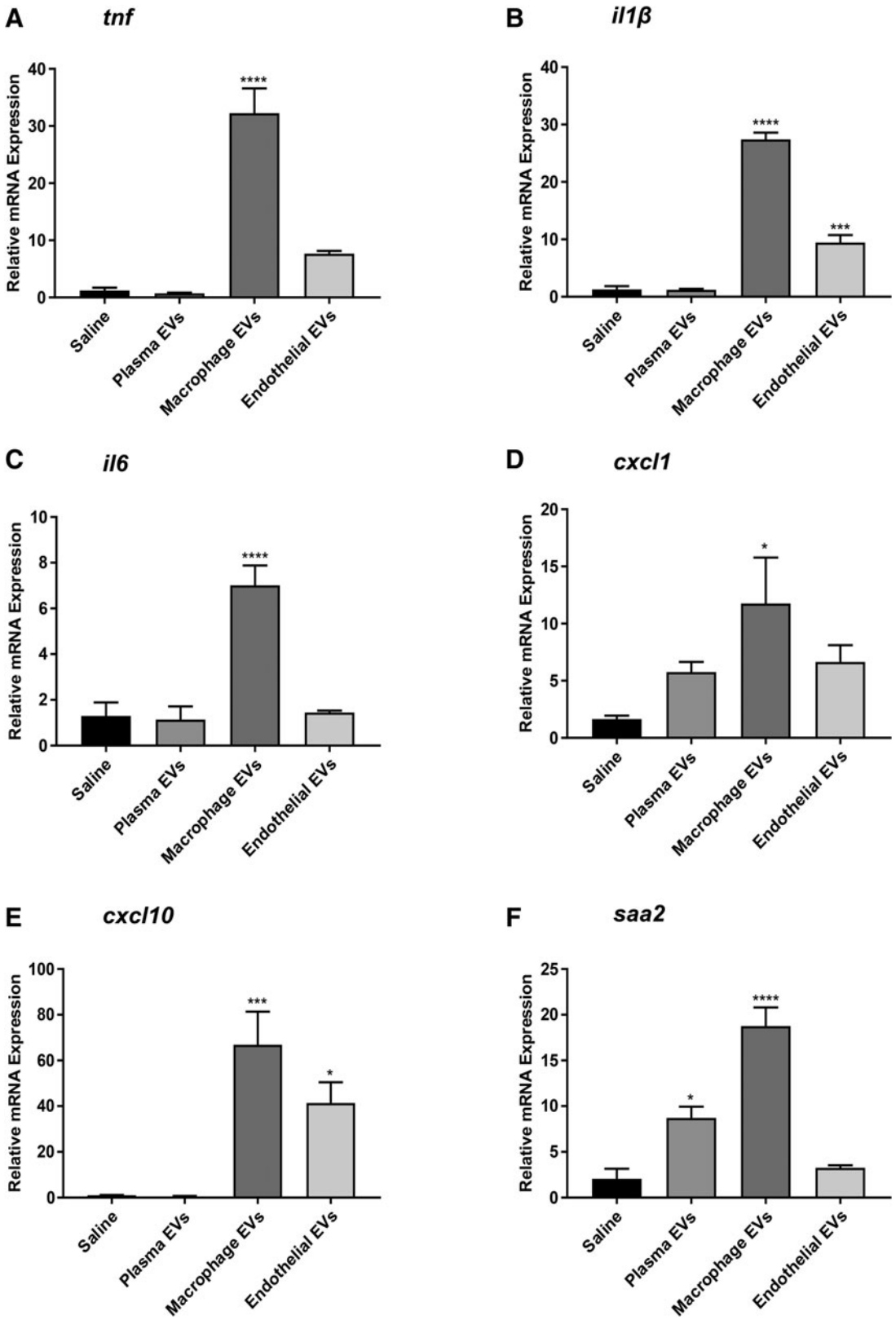


FIG. 5. Exogenously administered primed EVs increase expression of hepatic APR genes. C57BL/6 mice were either injected with saline ($n=4$), plasma-derived EVs ($n=3$), macrophage-cell-line–derived EVs ($n=4$) or endothelial-cell–derived EVs ($n=4$) before receiving a TBI with 6-h recovery time. RNA was extracted from snap frozen liver and converted into cDNA. cDNA was tested for different pro-inflammatory cytokines and chemokines using qPCR. GAPDH was used as the referencing house keeper. Primed EVs increased the relative expression of pro-inflammatory genes, especially EVs isolated from primed macrophages. qPCR analysis shows (A) *tnf*, (B) *il1β*, (C) *il6*, (D) *cxcl1*, (E) *cxcl10*, and (F) *saa2* mRNA expression after injection of primed EVs of different origin. Data are mean ± standard error of the mean, $n=3$; *$p<0.05$; ***$p<0.001$; ****$p<0.0001$ when compared to saline-injected controls. cDNA, complementary DNA; EV, extracellular vesicle; GAPDH, glyceraldehyde 3-phosphate dehydrogenase; mRNA, messenger RNA; qPCR, quantitative polymerase chain reaction; TBI, traumatic brain injury.

Downloaded by OXFORD UNIVERSITY from www.liebertpub.com at 07/17/21. For personal use only.

Downloaded by OXFORD UNIVERSITY from www.liebertpub.com at 07/17/21. For personal use only.

mechanisms which may lead to this recruitment is fundamental to the development of acute therapies for traumatic injury. Leukocyte infiltration has been shown to rely on systemic events that follow CNS injury.[28] For example, the hepatic APR brings about mobilization of leukocytes from reservoirs within the bone marrow and the cells then travel to the site of injury, as well as, surprisingly, to the liver itself.[29,30] These events occur very rapidly with reports of hepatic activation even preceding CNS immune activation in injury models.[31] As such, we chose to investigate the mechanisms of this communication at a very early time point, 6 h, where the CNS injury has yet to establish itself, but where systemic inflammation and CNS inflammation have begun to be observed. By studying and manipulating the pool of circulating EVs at this acute time point, we may begin to understand the means by which the populations of peripheral immune cells are mobilized after the initial injury.

The BBB is uniquely placed to signal CNS injury to the systemic immune system and, as a consequence, recruit immune cells to the parenchyma. There are two major routes which may mediate this communication: neural and humoral. Vagotomized animals still demonstrate a significant APR,[7] and the transport of centrally induced cytokines and chemokines is incredibly complex, with little egress of proinflammatory mediators from the inflamed brain.[32] Recent reports using choroid plexus explants and cells suggest that epithelial cells in this scenario are capable of secreting EVs as part of this communication system.[33] We were therefore interested to discover whether circulating EVs might be the means of communication between the CNS and the liver in TBI.

Previous reports, in line with the data herein, have shown that TBI, in both the mouse and humans, results in an increase in the number of circulating EVs.[34–36] In addition, in this study, we have shown that the size of the EVs was different after TBI; showing a slight trend toward decreased mean diameter. This suggests a shift from microvesicles to exosomes in the acute phase post-injury. It is possible that the level of barrier breakdown, or internal CNS inflammatory mechanisms, might play a role in this switch from larger EVs to smaller exosomes, but the reasons for, and the functional results of, this change remain speculative. Recent studies have suggested that exosomes retain the cargo necessary for functional transcription of microRNA (miRNA) species, whereas microvesicles do not.[37] Taken with reports showing that EVs carry specific miRNA transcripts post-TBI,[38] and data from this study showing EVs of different origins express different miRNAs (Supplementary Fig. 5) (see online supplementary material at http://www.liebertpub.com), these data could suggest a shift toward exosomes for the purposes of increasing miRNA regulation of gene transcription post-injury. However, experiments beyond the scope of this study are required to confirm this theory.

Given the increases in EVs post-injury, we were interested to discover what impact manipulating the circulating EV pool had on the outcomes of CNS trauma. The leading cause of mortality post-TBI is systemic infection and consequent multisystem organ failure.[39] However, the processes underlying this are very poorly understood. We aimed to shed some light on the issue by investigating whether EVs from primed sources were able to bring about inflammation in the periphery, and how that influences the outcomes of TBI. We chose to use EVs derived from cells from the CNS barrier system, because they are uniquely placed to respond to CNS trauma and have been shown to exert effects on the liver in inflammatory brain injury models,[22] EVs derived from cells of the systemic immune system, which are known to mobilize after CNS injury, and EVs derived from an *in vivo* inflammation model to demonstrate the effects of a more heterogenous EV population.

We were able to successfully activate the systemic inflammatory response by adoptive transfer of EVs from animals with systemic inflammation (LPS air-pouch model) and from cell lines activated with LPS. This fills in some of the gaps in the literature given that, to our knowledge, no existing studies have evaluated the effect of exogenous, activated EVs on CNS inflammation in an injury model. Our results demonstrate that EVs from different cell populations are capable of uniquely exacerbating TBI, when exogenously administered immediately post-injury. Strikingly, activated macrophages in particular induce a marked systemic APR and increase in neutrophil recruitment to the injured brain, suggesting some degree of cellular specificity when it comes to EV-related injury signals. Plasma-derived EVs from our LPS air-pouch model had less of a proinflammatory effect on our TBI model. This could be attributed to a number of reasons. The population of EVs present in the plasma will be extremely heterogenous, with large numbers yet to be identified with common cellular markers.[23] As such, it could be hypothesized that LPS *in vivo* results in the generation of proinflammatory and anti-inflammatory EVs from different cell populations. Unfortunately, as yet, there are few reliable techniques for identifying the origins of EVs in a mixed population, although specialized flow cytometry is beginning to advance the field.[40]

Previous work from our laboratory has demonstrated that the number of leukocytes recruited to the injured CNS could be increased by priming the animal with systemic injections of hepatic chemokines.[30] Based on the data presented here, it could be hypothesized that our EVs might contain similar chemokines, or that they were able to inherently activate the liver, which, in turn, secretes chemokines activating leukocyte mobilization. Our previous studies have demonstrated that EVs from an inflammatory brain model do not contain significant amounts of IL-1β[22]; however, primed EVs from cell culture have been reported to contain both IL-1β and TNF-α,[9] both of which are capable of initiating an APR.[41] As a consequence of our findings, efforts directed toward preventing the EV population from reaching the liver might be of therapeutic importance.

Conclusion

To our knowledge, this study is one of the first to investigate and differentiate inflammatory changes in both the periphery and CNS, as well as quantify EV populations in the bloodstream, during the first 24 h after traumatic injury to the CNS. Further, this is the first evidence showing that peripheral inflammation can be brought by manipulating the circulating EV population with ''primed'' EVs in order to exacerbate CNS injury. This study highlights the need for some important further work to understand the both the differences in the molecular profile of EVs produced in response to injury, and to determine the exact routes of their communication, from biogenesis to uptake. Such experiments will lead to an improved mechanistic understanding of the physiological events that are set in motion in the acute stages after a traumatic CNS injury, and place us in a better position to develop novel therapeutic strategies.

Acknowledgments

The authors acknowledge the assistance of Dr. Errin Johnson (Bioimaging Facility, Dunn School, University of Oxford) for taking the EM images of our EVs. This work was funded by the Medical Research Council (to Y.C.), the Lundbeck Foundation (to N.A.), and Spinal Research – Nathalie Rose Barr Award (to D.A. and A.Y.).

Author Disclosure Statement

No competing financial interests exist.

References

1. Rubartelli, A. (2014). DAMP-mediated activation of NLRP3-inflammasome in brain sterile inflammation: the fine line between healing and neurodegeneration. Front. immunol. 5, 99.
2. Campbell, S.J., Zahid, I., Losey, P., Law, S., Jiang, Y., Bilgen, M., van Rooijen, N., Morsali, D., Davis, A.E., and Anthony, D.C. (2008). Liver Kupffer cells control the magnitude of the inflammatory response in the injured brain and spinal cord. Neuropharmacology 55, 780–787.
3. Campbell, S.J., Hughes, P.M., Iredale, J.P., Wilcockson, D.C., Waters, S., Docagne, F., Perry, V.H., and Anthony, D.C. (2003). CINC-1 is identified as an acute-phase protein induced by focal brain injury causing leukocyte mobilization and liver injury. FASEB J. 17, 1168–1170.
4. Anthony, D.C., Couch, Y., Losey, P., Evans, M.C. (2012). The systemic response to brain injury and disease. Brain Behav. Immunol. 26, 534–540.
5. Campbell, S.J., Jiang, Y., Davis, A.E., Farrands, R., Holbrook, J., Leppert, D., and Anthony, D.C. (2007). Immunomodulatory effects of etanercept in a model of brain injury act through attenuation of the acute-phase response. J. Neurochem. 103, 2245–2255.
6. Campbell, S., Deacon, R., Jiang, Y., Ferrari, C., Pitossi, F., and Anthony, D. (2007). Overexpression of IL-1 beta by adenoviral-mediated gene transfer in the rat brain causes a prolonged hepatic chemokine response, axonal injury and the suppression of spontaneous behaviour. Neurobiol. Dis. 27, 151–163.
7. Kox, M., Vaneker, M., van der Hoeven, J.G., Scheffer, G.J., Hoedemaekers, C.W., and Pickkers, P. (2012). Effects of vagus nerve stimulation and vagotomy on systemic and pulmonary inflammation in a two-hit model in rats. PLoS One 7, e34431.
8. Anthony, D.C., and Couch Y. (2014). The systemic response to CNS injury. Exp. Neurol. 258, 105–111.
9. Yáñez-Mó, M., Siljander, P.R., Andreu, Z., Zavec, A.B., Borràs, F.E., Buzas, E.I., Buzas, K., Casal, E., Cappello, F., Carvalho, J., Colás, E., Cordeiro-da Silva, A., Fais, S., Falcon-Perez, J.M., Ghobrial, I.M., Giebel, B., Gimona, M., Graner, M., Gursel, I., Gursel, M., Heegaard, N.H., Hendrix, A., Kierulf, P., Kokubun, K., Kosanovic, M., Kralj-Iglic, V., Krämer-Albers, E.M., Laitinen, S., Lässer, C., Lener, T., Ligeti, E., Linē, A., Lipps, G., Llorente, A., Lötvall, J., Manček-Keber, M., Marcilla, A., Mittelbrunn, M., Nazarenko, I., Nolte-'t Hoen, E.N., Nyman, T.A., O'Driscoll, L., Olivan, M., Oliveira, C., Pállinger, É., Del Portillo, H.A., Reventós, J., Rigau, M., Rohde, E., Sammar, M., Sánchez-Madrid, F., Santarém, N., Schallmoser, K., Ostenfeld, M.S., Stoorvogel, W., Stukelj, R., Van der Grein, S.G., Vasconcelos, M.H., Wauben, M.H., and De Wever, O. (2015). Biological properties of extracellular vesicles and their physiological functions. J. Extracell. Vesicles 4, 27066.
10. Kumar, A., Stoica, B.A., Loane, D.J., Yang, M., Abulwerdi, G., Khan, N., Thom, S.R., and Faden, A.I. (2017). Microglial-derived microparticles mediate neuroinflammation after traumatic brain injury. J. Neuroinflammation 14, 47.
11. Raposo, G., and Stoorvogel, W. (2013). Extracellular vesicles: exosomes, microvesicles, and friends. J. Cell Biol. 200, 373–383.
12. Dickens, A.M., Tovar, Y.R., Yoo, S.W., Trout, A.L., Bae, M., Kanmogne, M., Megra, B., Williams, D.W., Witwer, K.W., Gacias, M., Tabatadze, N., Cole, R.N., Casaccia, P., Berman, J.W., Anthony, D.C., and Haughey, N.J. (2017). Astrocyte-shed extracellular vesicles regulate the peripheral leukocyte response to inflammatory brain lesions. Sci. Signal. 10, eaai7696.
13. Paul, D., Baena, V., Ge, S., Jiang, X., Jellison, E.R., Kiprono, T., Agalliu, D., and Pachter, J.S. (2016). Appearance of claudin-5+ leukocytes in the central nervous system during neuroinflammation: a novel role for endothelial-derived extracellular vesicles. J. Neuroinflammation 13, 292.
14. Yamamoto, S., Niida, S., Azuma, E., Yanagibashi, T., Muramatsu, M., Huang, T.T., Sagara, H., Higaki, S., Ikutani, M., Nagai, Y., Takatsu, K., Miyazaki, K., Hamashima, T., Mori, H., Matsuda, N., Ishii, Y., and Sasahara, M. (2015). Inflammation-induced endothelial cell-derived extracellular vesicles modulate the cellular status of pericytes. Sci. Rep. 5, 8505.
15. Antonucci, F., Turola, E., Riganti, L., Caleo, M., Gabrielli, M., Perrotta, C., Novellino, L., Clementi, E., Giussani, P., Viani, P., Matteoli, M., and Verderio, C. (2012). Microvesicles released from microglia stimulate synaptic activity via enhanced sphingolipid metabolism. EMBO J. 31, 1231–1240.
16. Joshi, P., Turola, E., Ruiz, A., Bergami, A., Libera, D.D., Benussi, L., Giussani, P., Magnani, G., Comi, G., Legname, G., Ghidoni, R., Furlan, R., Matteoli, M., and Verderio, C. (2014). Microglia convert aggregated amyloid-beta into neurotoxic forms through the shedding of microvesicles. Cell Death Differ. 21, 582–593.
17. Chivet, M., Hemming, F., Pernet-Gallay, K., Fraboulet, S., and Sadoul, R. (2012). Emerging role of neuronal exosomes in the central nervous system. Front. Physiol. 3, 145.
18. Couch, Y., Evans, M.C., Gardiner, C., Sargent, I., Losey, P., Lambertsen, K.L., and Anthony, D.C. (2014). Brain-derived microvesicles confer sickness behaviours by switching on the acute phase response in the liver. J. Neuroimmunology 275, 57–57.
19. Onyszchuk, G., Al-Hafez, B., He, Y.Y., Bilgen, M., Berman, N.E., and Brooks, W.M. (2007). A mouse model of sensorimotor controlled cortical impact: characterization using longitudinal magnetic resonance imaging, behavioral assessments and histology. J. Neurosci. Methods 160, 187–196.
20. Evans, M.C., Couch, Y., Sibson, N., and Turner, M.R. (2013). Inflammation and neurovascular changes in amyotrophic lateral sclerosis. Mol. Cell. Neurosci. 53, 34–41.
21. Couch, Y., Davis, A.E., Sá-Pereira, I., Campbell, S.J., and Anthony, D.C. (2014). Viral pre-challenge increases central nervous system inflammation after intracranial interleukin-1beta injection. J. Neuroinflammation 11, 178.
22. Couch, Y, Akbar, N., Roodselaar, J., Evans, M.C., Gardiner, C., Sargent, I., Romero, I.A., Bristow, A, Buchan, A.M., Haughey, N., and Anthony, D.C. (2017). Circulating endothelial cell-derived extracellular vesicles mediate the acute phase response and sickness behaviour associated with CNS inflammation. Sci. Rep. 7, 9574.
23. Dragovic, R.A., Southcombe, J.H., Tannetta, D.S., Redman, C.W., and Sargent, I.L. (2013). Multicolor flow cytometry and nanoparticle tracking analysis of extracellular vesicles in the plasma of normal pregnant and pre-eclamptic women. Biol. Reprod. 89, 151.
24. Couch, Y., Xie, Q., Lundberg, L., Sharp, T., and Anthony, D.C. (2015). A Model of Post-Infection Fatigue Is Associated with Increased TNF and 5-HT2A Receptor Expression in Mice. PLoS One 10, e0130643.
25. Lotvall, J., Hill, A.F., Hochberg, F., Buzas, E.I., Di Vizio, D., Gardiner, C., Gho, Y.S., Kurochkin, I.V., Mathivanan, S., Quesenberry, P., Sahoo, S., Tahara, H., Wauben, M.H., Witwer, K.W., and Thery, C. (2014). Minimal experimental requirements for definition of extracellular vesicles and their functions: a position statement from the International Society for Extracellular Vesicles. J. Extracell. Vesicles 3, 26913.
26. Couch, Y., Akbar, N., Davis, S., Fischer, R., Dickens, A.M., Neuhaus, A.A., Burgess, A.I., Rothwell, P.M., and Buchan, A.M. (2017). Inflammatory Stroke Extracellular Vesicles Induce Macrophage Activation. Stroke 48, 2292–2296.
27. Zhang, B., and Gensel, J.C. (2014). Is neuroinflammation in the injured spinal cord different than in the brain? Examining intrinsic differences between the brain and spinal cord. Exp. Neurol. 258, 112–120.
28. Gonzalez, R., Glaser, J., Liu, M.T., Lane, T.E., and Keirstead, H.S. (2003). Reducing inflammation decreases secondary degeneration and functional deficit after spinal cord injury. Exp. Neurol. 184, 456–463.
29. Campbell, S.J., Anthony, D.C., Oakley, F., Carlsen, H., Elsharkawy, A.M., Blomhoff, R., and Mann, D.A. (2008). Hepatic nuclear factor kappa B regulates neutrophil recruitment to the injured brain. J. Neuropathol. Exp. Neurol. 67, 223–230.
30. Campbell, S.J., Perry, V.H., Pitossi, F.J., Butchart, A.G., Chertoff, M., Waters, S., Dempster, R., and Anthony, D.C. (2005). Central nervous system injury triggers hepatic CC and CXC chemokine expression that is associated with leukocyte mobilization and recruitment to both the central nervous system and the liver. Am. J. Pathol. 166, 1487–1497.
31. Chapman, K.Z., Dale, V.Q., Denes, A., Bennett, G., Rothwell, N.J., Allan, S.M., and McColl, B.W. (2009). A rapid and transient peripheral inflammatory response precedes brain inflammation after experimental stroke. J. Cereb. Blood Flow Metab. 29, 1764–1768.
32. Banks, W.A. (2005). Blood-brain barrier transport of cytokines: a mechanism for neuropathology. Curr. Pharm. Des. 11, 973–984.

Downloaded by OXFORD UNIVERSITY from www.liebertpub.com at 07/17/21. For personal use only.

33. Balusu, S., Van Wonterghem, E., De Rycke, R., Raemdonck, K., Stremersch, S., Gevaert, K., Brkic, M., Demeestere, D., Vanhooren, V., Hendrix, A., Libert, C., and Vandenbroucke, R.E. (2016). Identification of a novel mechanism of blood-brain communication during peripheral inflammation via choroid plexus-derived extracellular vesicles. EMBO Mol. Med. 8, 1162–1183.
34. Nekludov, M., Mobarrez, F., Gryth, D., Bellander, B.M., and Wallen, H. (2014). Formation of microparticles in the injured brain of patients with severe isolated traumatic brain injury. J. Neurotrauma 31, 1927–1933.
35. Zhao, Z., Zhou, Y., Tian, Y., Li, M., Dong, J.F., and Zhang, J. (2017). Cellular microparticles and pathophysiology of traumatic brain injury. Protein Cell 8, 801–810.
36. Tian, Y., Salsbery, B., Wang, M., Yuan, H., Yang, J., Zhao, Z., Wu, X., Zhang, Y., Konkle, B.A., Thiagarajan, P., Li, M., Zhang, J., and Dong, J.F. (2015). Brain-derived microparticles induce systemic coagulation in a murine model of traumatic brain injury. Blood 125, 2151–2159.
37. Kanada, M., Bachmann, M.H., Hardy, J.W., Frimannson, D.O., Bronsart, L., Wang, A., Sylvester, M.D., Schmidt, T.L., Kaspar, R.L., Butte, M.J., Matin, A.C., and Contag, C.H. (2015). Differential fates of biomolecules delivered to target cells via extracellular vesicles. Proc. Natl. Acad. Sci. U. S. A. 112, E1433–E1442.
38. Harrison, E.B., Hochfelder, C.G., Lamberty, B.G., Meays, B.M., Morsey, B.M., Kelso, M.L., Fox, H.S., and Yelamanchili, S.V. (2016). Traumatic brain injury increases levels of miR-21 in extracellular vesicles: implications for neuroinflammation. FEBS open Bio.6, 835–846.
39. Corral, L., Javierre, C.F., Ventura, J.L., Marcos, P., Herrero, J.I., and Mañez, R. (2012). Impact of non-neurological complications in severe traumatic brain injury outcome. Crit. Care 16, R44.
40. Stoner, S.A., Duggan, E., Condello, D., Guerrero, A., Turk, J.R., Narayanan, P.K., and Nolan, J.P. (2016). High sensitivity flow cytometry of membrane vesicles. Cytometry A. 89, 196–206.
41. Baumann, H., and Gauldie, J. (1994). The acute-phase response. Immunol. Today 15, 74–80.

Address correspondence to:
Daniel C. Anthony, PhD
Department of Pharmacology
University of Oxford
Mansfield Road
London OX1 3QT
United Kingdom

E-mail: daniel.anthony@pharm.ox.ac.uk

Downloaded by OXFORD UNIVERSITY from www.liebertpub.com at 07/17/21. For personal use only.

frontiers in Immunology

MINI REVIEW
published: 20 November 2019
doi: 10.3389/fimmu.2019.02723

Systemic Immune Response to Traumatic CNS Injuries—Are Extracellular Vesicles the Missing Link?

Abi G. Yates[1,2], *Daniel C. Anthony*[1]*, *Marc J. Ruitenberg*[2] *and Yvonne Couch*[3]

[1] Department of Pharmacology, Medical Sciences Division, University of Oxford, Oxford, United Kingdom, [2] School of Biomedical Sciences, Faculty of Medicine, University of Queensland, Brisbane, QLD, Australia, [3] Acute Stroke Programme, RDM-Investigative Medicine, University of Oxford, Oxford, United Kingdom

Inflammation following traumatic injury to the central nervous system (CNS) persists long after the primary insult and is known to exacerbate cell death and worsen functional outcomes. Therapeutic interventions targeting this inflammation have been unsuccessful, which has been attributed to poor bioavailability owing to the presence of blood-CNS barrier. Recent studies have shown that the magnitude of the CNS inflammatory response is dependent on systemic inflammatory events. The acute phase response (APR) to CNS injury presents an alternative strategy to modulating the secondary phase of injury. However, the communication pathways between the CNS and the periphery remain poorly understood. Extracellular vesicles (EVs) are membrane bound nanoparticles that are regulators of intercellular communication. They are shed from cells of the CNS including microglia, astrocytes, neurons and endothelial cells, and are able to cross the blood-CNS barrier, thus providing an attractive candidate for initiating the APR after acute CNS injury. The purpose of this review is to summarize the current evidence that EVs play a critical role in the APR following CNS injuries.

Keywords: extracellular vesicles, traumatic brain injury, spinal cord injury, inflammation, acute phase response

OPEN ACCESS

Edited by:
Bert A. 'T Hart,
University Medical Center Groningen, Netherlands

Reviewed by:
Jorge Tolivia,
University of Oviedo, Spain
Yoshiro Ohara,
Kanazawa Medical University, Japan

***Correspondence:**
Daniel C. Anthony
daniel.anthony@pharm.ox.ac.uk

Specialty section:
This article was submitted to Multiple Sclerosis and Neuroimmunology, a section of the journal Frontiers in Immunology

Received: *04 September 2019*
Accepted: *06 November 2019*
Published: *20 November 2019*

Citation:
Yates AG, Anthony DC, Ruitenberg MJ and Couch Y (2019) Systemic Immune Response to Traumatic CNS Injuries—Are Extracellular Vesicles the Missing Link? Front. Immunol. 10:2723. doi: 10.3389/fimmu.2019.02723

INTRODUCTION

Acute CNS injuries, including traumatic brain and spinal cord injury (TBI; SCI), as well as stroke, are a major global burden (1, 2). These neurological disorders have a collective global incidence rate of 500–700 per 100,000 people (3), and have extremely high morbidity, requiring lifelong subsequent care at a substantial financial and emotional cost (4, 5). Whilst the primary causes of TBI and SCI, and even to some extent stroke, are largely unavoidable, the ensuing secondary injury and ongoing inflammatory response can significantly worsen outcome and could be amenable to therapeutic intervention (6–9). The mechanisms that promote the inflammatory response to injury, and the communication pathways that convey messages about CNS health status to the systemic immune system, are the subject of intense investigation, but it is becoming clear that extracellular vesicles (EVs) play a pivotal role.

Acute CNS Injury—Primary vs. Secondary Injury

Damage to the CNS following a neurotraumatic event occurs in two distinct phases (7, 10, 11). The primary phase is largely mechanical, whereby the physical insult causes direct structural damage to

neuronal tissue and the vasculature, resulting in immediate cell death, and hemorrhage, ischemia and/or oedema.

The primary phase occurs within a short window of time, whereas the secondary phase has been shown to persist for days, weeks, even months after the injury (12, 13). Although not damaged directly during the initial insult, CNS tissue surrounding the injury is highly vulnerable to secondary damage (10, 14). Hypoxia, excitotoxicity, free radical formation, breakdown of blood-CNS barriers and release of proteases, all contribute to further cell death (10, 15). Moreover, activated microglia and astrocytes, as well as infiltrating leukocytes from the periphery, release cytokines and chemokines that create a pro-inflammatory microenvironment (6, 7, 13). Collectively, this results in the progressive destruction of CNS tissue, known as "bystander tissue damage", which considerably impairs functional recovery (16).

Previous studies utilizing rodent models have shown that the secondary phase of traumatic CNS injury is dependent on the acute phase response (APR), a systemic inflammatory response occurring predominantly in the liver (17). In response to CNS damage, hepatic expression of pro-inflammatory mediators significantly increases as early as 2 h post-insult (17–21). In turn, these mediators trigger the mobilization and priming of leukocytes from the bone marrow, which then translocate to the site of injury, as well as seemingly uninvolved peripheral organs. The spleen releases its reservoir of pro-inflammatory monocytes and increases expression of IFN-γ, TNF, and IL-6 amongst others (22–24). Systemic inflammatory response syndrome (SIRS) which can lead to multi-organ dysfunction syndrome (MODS) is also not uncommon in patients (25–29). Concurrent immunosuppression of the adaptive immune components is often observed (30, 31), leaving patients also highly susceptible to infections. Peripheral immune responses thus significantly increase patient mortality and morbidity.

Interestingly, suppression of the peripheral inflammatory response has been shown to ameliorate CNS inflammation (20, 32–35). Modulation of the APR by targeting the production of acute phase proteins, or Kupffer cell depletion, both reduce neutrophil recruitment to the CNS in models of TBI and SCI (20, 33). Therefore, suppression of the APR may offer an alternative strategy of minimizing tissue loss and functional deficits after traumatic CNS injuries. However, it must be acknowledged that modulating systemic inflammation is complex; paradoxically, exacerbating periphery inflammation has similarly been shown to reduce lesion size and leukocyte infiltration of the CNS post-injury (36, 37). As such, it has been suggested that the systemic response can also serve as an immune "distraction", redistributing leukocyte populations from the injured CNS to other sites, although it remains unclear to where the leukocytes redistribute (17). It is likely that timing of the inflammatory insult is key, and improving our understanding of it will ease therapeutic targeting.

The initiation signal for the activation of the peripheral response is unclear. Both humoral and neuronal methods have been investigated, yet vagotomized animals still exhibit an APR (38, 39), and thus far no consistent molecular candidates have been identified that can fully explain this response (40). There is growing evidence that extracellular vesicles, novel mediators of communication between distant organs, provide the missing link.

Extracellular Vesicles

Extracellular vesicles (EVs) is a general term that defines all cell-derived particles encapsulated in a lipid bilayer, which are enriched for proteins, lipids, and nucleic acids (41–44). They are typically classified according to their biogenesis (**Figure 1**); apoptotic bodies (1,000–5,000 nm) are released from the plasma membrane as part of programmed cell death, microvesicles (150–1,000 nm) are blebbed from the cell membrane, whilst exosomes (40–150 nm) are generated via the endolysosomal pathway and stored in multivesicular bodies (MVB) prior to release by exocytosis.

Whilst EVs have been investigated as a phenomenon for more than 30 years, the significant role EVs play in intercellular communication is only just being recognized. Indeed, a plethora of studies have identified EVs as important mediators of not only normal physiology, but also of pathology. They have been shown to be released from almost all cell types, including neurons (45, 46), microglia (47, 48), astrocytes (35), and CNS endothelial cells (49). EVs have also been isolated from almost all bodily fluids, including cerebrospinal fluid (CSF) (50, 51) and plasma (52). They have shown a unique capacity to disseminate information around the body, including across the blood-CNS barrier (35), to exert their effects both locally and systemically to distant organs, making them attractive candidate mediators of CNS-to-immune communication following injury.

EV-mediated cell communication has been associated in a number of neurological diseases, where they have been shown to be vectors of pathogenic proteins, propagating both Alzheimer's and Parkinson's disease (53–56). In brain cancers, EVs derived from tumor cells have been shown to act locally in facilitating proliferation, growth and angiogenesis (57–60), as well as distally in other organs aiding metastasis (61). In turn, distal cancers are able to metastasize to the brain via EVs as well (61–63). In the periphery, circulating EVs isolated from LPS-treated animals have been shown to induce gliosis and expression of pro-inflammatory molecules in the brains of naïve mice (64). Moreover, EVs released from stimulated brain endothelial cells have been shown to induce hepatic TNF and CXCL1 expression in naïve rats, in turn inducing a sickness behavior phenotype (49). Together, these studies suggest the presence of a CNS-periphery communicatory axis that is mediated by EVs. As such, investigating EVs in the context of traumatic CNS injuries is of great interest. Here, we will evaluate the current evidence that EVs mediate the communicatory pathways between the CNS and the periphery following traumatic CNS injury.

TRAUMATIC BRAIN INJURY (TBI)

TBI is a devastating disorder, affecting over 55 million people globally (2). The current lack of available treatments is commonly attributed to gaps in our knowledge of the secondary phase

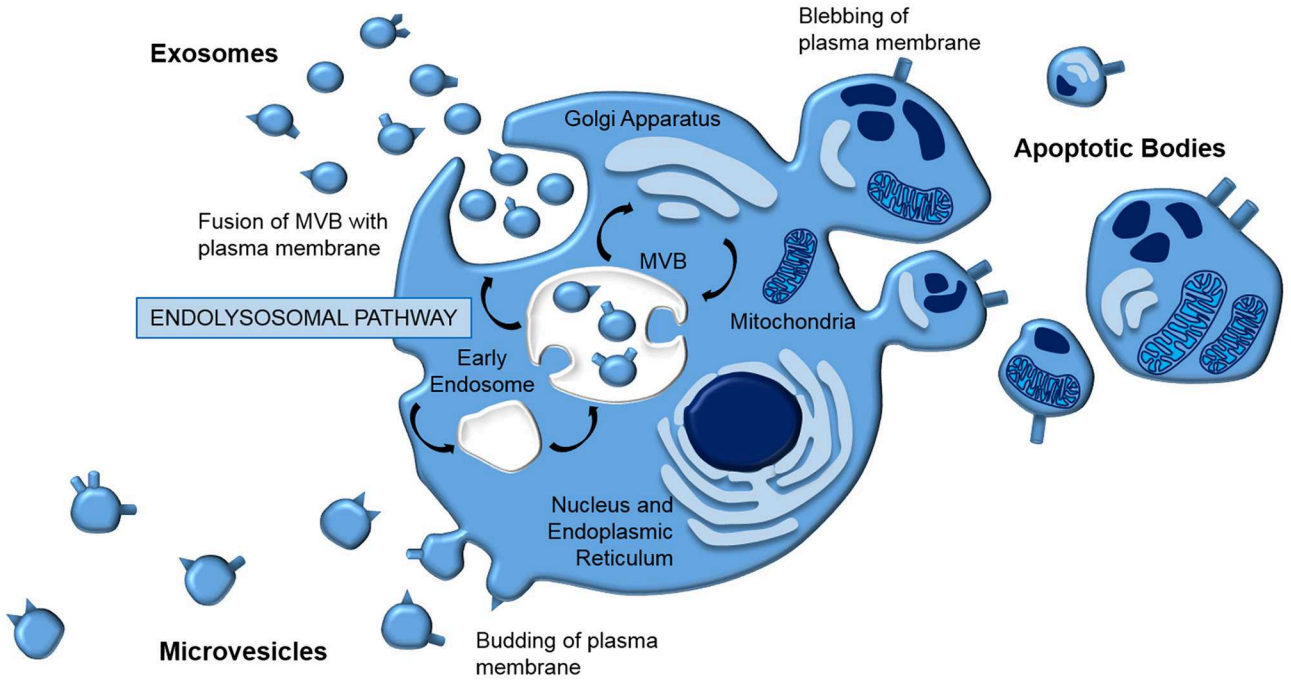


FIGURE 1 | EV biogenesis. EVs are typically classed according to their biogenesis. Apoptotic bodies and microvesicles are released from the plasma membrane in blebbing and budding mechanisms, respectively. In contrast, exosomes are generated by the endolysomal pathway; internal budding of an endosome results in a multivesicular body which fuses with the plasma membrane, releasing exosomes by exocytosis.

of injury (14). Human clinical data has confirmed that TBI induces a robust inflammatory response in the periphery which is predictive of poor outcome (65). In conjunction, numerous studies have consistently demonstrated that circulating EVs are significantly elevated in TBI patients during the acute phase of injury (66, 67). For example, Nekludov et al. (66) showed a transcranial gradient in EV concentration; more EVs were detected in the cerebrovenous compared to arterial blood, indicating that the increase in circulating EVs originated from the brain. Increases in EVs in the circulation of patients with TBI have been reflected in rodent studies (35, 48, 49, 52, 68, 69). Hazelton et al. (52) showed an increase in plasma EVs during the first 24 h after TBI, whilst Couch et al. (49) and Dickens et al. (35) both showed increases in an IL-1β model of inflammatory focal brain lesions. Critically, inhibition of EV release from the CNS has been shown to attenuate the systemic response to brain inflammation, and subsequently inhibit leukocyte infiltration (35). Nekludov et al. further demonstrated that whilst leukocyte- and platelet-derived EVs were increased after injury, the circulating EVs were predominantly of endothelial origin, the concentration of which was 7-fold greater than in healthy controls. Dickens et al. (35) showed however that a proportion of plasma EVs released after striatal IL-1β injection are derived from astrocytes, and that these translocate to the liver, spleen, and lung, further linking EV-mediated signaling with the APR following CNS injury. Microglia and astrocytes both release EVs in response to DAMP-mediated activation with ATP (47). In turn, microglia-derived EVs enriched for IL-1β have been reported in the plasma of TBI patients (48). From these studies, it is easy to assume that EV population changes are due to increased release from cells of the CNS. However, EVs derived from hematopoietic cells can also signal to the brain, and their uptake here was exacerbated by peripheral inflammation (70). Delineating the origin of EVs could identify the critical players in CNS-periphery communication, and may identify a specific cellular target for EV-based therapeutics.

Functional analysis of plasma EVs from models of brain injury determined that plasma EVs were pro-inflammatory and able to induce a systemic inflammatory response in naïve rats, in the absence of CNS injury (49). It has been established that EVs are capable of interacting with granulocytes and lymphocytes; they have been shown to carry MHC class I and II, and contribute to antigen presentation (71–75). Therefore, they may directly activate the peripheral immune system through receptor-ligand mechanisms. Moreover, microvesicles and apoptotic bodies are enriched for phosphatidylserine (PS) on the outer leaflet, which not only assists in promoting budding, but also encourages uptake by macrophages and dendritic cells (76, 77). This is highly relevant considering the ongoing apoptosis of CNS cells post-injury. Kumar et al. (48) showed that EVs depleted of their content with the surfactant PEG-TB had lost their ability to activate microglia *in vitro*, making it clear that the composition of EVs is vital for them to exert their effect.

As well as surface chemistry, EV cargo appears to be key to the function of the EVs after TBI. Plasma EVs isolated from TBI patients were found to have distinct and unique protein profiles in comparison to those isolated from healthy controls (68, 78). When exogenous pro-inflammatory EVs were administered intravenously to a model of TBI, the EVs were found to exacerbate both the APR, and the subsequent neuroinflammation and pathology (52). Importantly, this response was dependent on the cellular origin of the EVs. Particles derived from macrophages had the greatest effect on hepatic expression of pro-inflammatory molecules, as well as infiltrating neutrophils in the brain, compared to those from endothelial cells and plasma samples. Cargo analysis revealed differential miRNA content in the different EVs, suggesting the particles exert their effect through transfer of specific genetic transcripts. Indeed, Dickens et al. (35) identified that miRNA in astrocyte-derived EVs target the PPAR-α pathway, leading to increased NFκB activity and cytokine production in the liver. However, EVs have been found to be enriched for pro-inflammatory molecules themselves, including cytokines, chemokines, and inflammasome proteins. Inflammatory EVs have been reported to transport IL-1β (47, 48, 79, 80), IL-6 and CCL2 (81), as well as chemokine receptors, such as CCR5 (82). Collectively, these studies suggest a more direct mechanism of initiating and propagating inflammation.

In addition to the activation of a systemic inflammatory response, TBI-associated coagulopathy (TBI-AC) has been associated with EV signaling (83). Following injury, TBI patients often develop a hypercoagulable state, leading to an increased risk of thrombosis (84–86). This has been associated with increased mortality (84), and platelet dysfunction has been reported to play a causal role (83). It is thought that the circulating EV population is predominantly shed from platelets (87), and these platelet-derived particles have greater procoagulant activity than platelets themselves (88). TBI induces the release of EVs from platelets (66, 67, 69), and circulating microparticles following TBI were shown to have procoagulant properties *ex vivo* (89). Moreover, Tian et al. (69) were able to reproduce systemic coagulopathy in uninjured mice through adoptive transfer of TBI plasma EVs. Together, these data indicate that platelet-derived EVs may be responsible for TBI-AC, which could be attributed to the exposure of PS on the outer EV leaflet. It is also likely that brain-derived particles interact with platelets directly to promote systemic coagulation and thrombosis. Astrocyte- and neuronal-derived EVs have been isolated from the blood of TBI animals, and were found to be procoagulant in phenotype (69). Thus, EV-mediated changes in systemic function are not limited to alterations in inflammatory status after injury.

SPINAL CORD INJURY (SCI)

In comparison to brain pathologies, the role of EVs following SCI has been somewhat overlooked. Whilst systemic inflammation has been well-documented in SCI patients (26, 90–93), studies have focused on its contribution to functional outcome rather than the manner in which it is communicated. To our knowledge, there is currently no data that describes changes in the circulating EV population and their influence on pathophysiology of SCI. That being said, EVs have been isolated from the CSF of deceased SCI patients (94). These EVs were found to be enriched for the inflammasome-associated proteins NLRP1, caspase-1, and ASC, suggesting a pro-inflammatory phenotype. The authors speculated that these EVs may be able to trigger an innate immune response *in vivo,* which would correspond with TBI associated data, however, EV-mediated effects on systemic inflammation and immune activation were not investigated. These authors additionally demonstrated that neuronal exosomes loaded with siRNA could localize to the lesion epicenter following SCI when injected systemically, further supporting the hypothesis of an EV-mediated CNS-periphery communicatory axis.

Preliminary, unpublished data from our group suggest that SCI induces a significant increase in plasma-derived EVs during the acute phase of injury, which is consistent with human and animal models with brain injuries. However, it is necessary to determine the specific role of these SCI-induced changes in the circulating EV population in propagating peripheral inflammation and the subsequent effect on lesion development. Whilst TBI data may provide some insight, it must be acknowledged that the overall impact on the APR and lesion progression is likely to be different (17). Anatomically, the distribution of gray and white matter, as well as the distribution and phenotype of microglia are quite different in the spinal cord compared to the brain. Moreover, they both respond differently to traumatic injury in that the blood-spinal cord barrier (BSCB) shows greater breakdown after trauma compared to the blood-brain barrier (BBB), and also that there is increased local CXC chemokine expression and recruitment of neutrophils to the parenchyma of the spinal cord compared to the brain. Regarding the systemic response, peripheral administration of the PPARα agonist fenofibrate blocked the APR and neutrophil recruitment to the brain after an intrastriatal microinjection of IL-1β injection (35), however it was found to be an ineffective treatment in experimental SCI (95). These differences must be taken into consideration when assessing the impact of EV signaling following injury, as manipulation of the cascade after SCI may have differential effects on lesion progression and patient recovery compared to TBI.

EVS AS THERAPY

It is clear that interrupting EV signaling may be useful to treat inflammation, but some groups have also used the EVs themselves as a therapeutic agent, specifically EVs derived from stem cells. This strategy is certainly attractive, circumventing the ethical issues with embryonic and fetal stem cells, as well as being less invasive with low or no tumorigenicity. Moreover, the ability to use autografted stem cells will eliminate the risk of rejection. Most studies to date have almost exclusively utilized EVs released by mesenchymal stem cells (MSCs), and these have consistently been shown to improve functional recovery and behavior deficits in models of TBI (96, 97) and SCI (98–100). EVs derived from progenitor cells, such as endothelial colony-forming cells (101) and neural stem cells (102), appear to have similar neuroprotective effects in

animal models. Kobayashi et al. (103) demonstrated that EVs derived from induced pluripotent stem cells (iPSCs) were able to both increase angiogenesis and the rate of wound closure in a model of skin wound healing. Whether iPSC-EVs have therapeutic potential in the context of TBI/SCI remains to be investigated.

The mechanisms underlying the neuroprotective actions of stem cell-derived EVs are currently under investigation. To date, they have been shown to be internalized by endothelial cells (101), neurons (104), astrocytes (104), oligodendrocytes (105), and microglia (106) in the CNS, suggesting they may exert their effect directly. However, improvements after injury are not necessarily due to prevention of cell death, as no change in lesion volume has often been reported (97, 107). Rather, EVs may exert their effect by stimulating endogenous restorative mechanisms that promote recovery. Zhang et al. (97) have shown MSC-EVs enhanced vascular density and neurogenesis, with a concurrent reduction in brain inflammation in a TBI model. Increased angiogenesis has also been shown in a model of SCI (108), following treatment with MSC-EVs. One potential mechanism that has been proposed is the transfer of miRNAs (11). Xin et al. (104) demonstrated that EV-associated miR-133b transferred to astrocytes and neurons was responsible for stimulating neurite outgrowth in their stroke model, and that inhibition of miRNA machinery proteins attenuated this effect (109). Exosomal miR-17-92 (109, 110), miR-134 (105), and miR-124-3p (111) have additionally been implicated in neuroprotection. Bioengineering MSCs to produce EVs overexpressing these transcripts are currently under investigation (110, 112–114). In the majority of these studies, EVs are administered intravenously to the periphery which is important as MSC-EVs have been shown to additionally modulate the systemic immune response following traumatic CNS injuries. In a model of SCI, improvements in locomotor function have been attributed to suppression of the systemic immune response by stimulated MSC-EVs, as circulating neutrophils were reduced and monocytes were retained in the spleen (100). MSC-EVs have been shown to localize to this organ (106), and splenectomies improve neurological outcomes in models of SCI (22); it would be of interest to investigate the effect of MSC-EVs in injury models with splenectomy to determine if their beneficial effect remains.

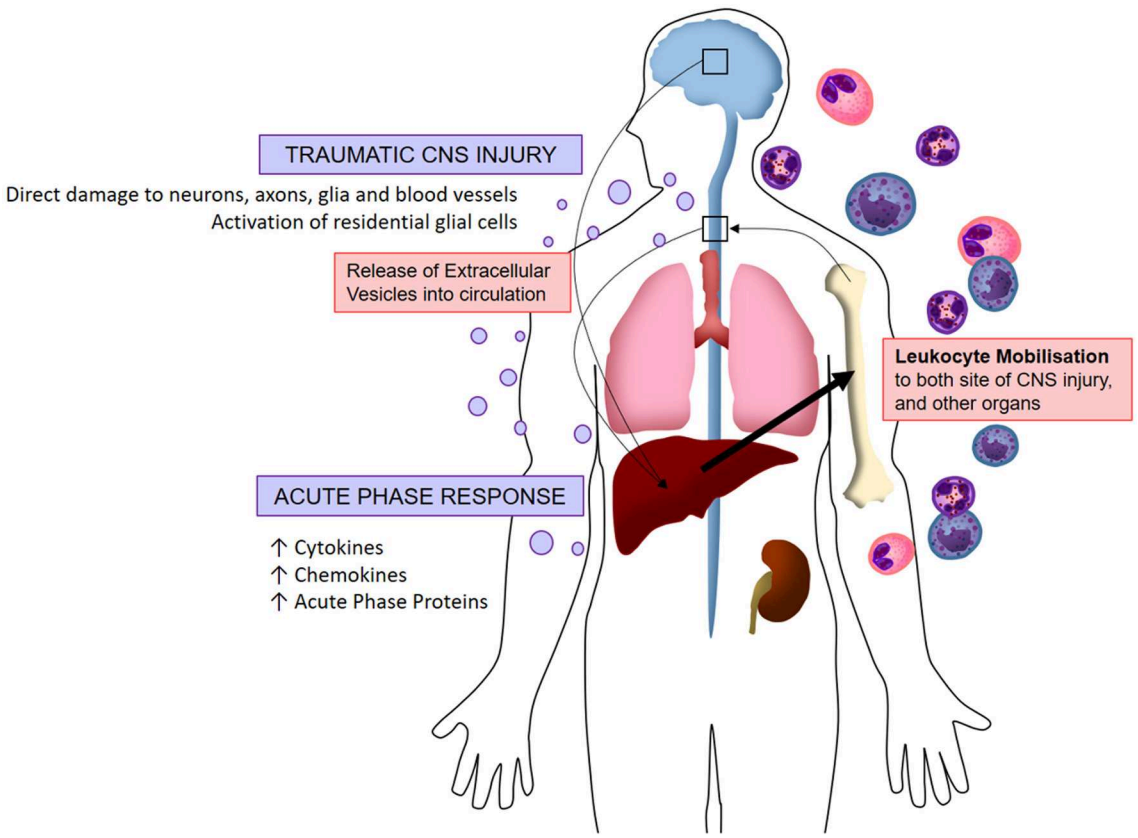


FIGURE 2 | Visualized hypothesis of EV-mediated systemic inflammation response to traumatic CNS injury. Acute traumatic injuries to the brain and spinal cord induce the release of extracellular vesicles into circulation. These EVs localize to peripheral organs whereby they induce the production of pro-inflammatory molecules (chemokines, cytokines, acute phase proteins), in turn stimulating the mobilization of leukocytes which infiltrate both the CNS and peripheral organs. This systemic immune response is referred to as the acute phase response.

CONCLUSIONS

In the last decade, interest in EVs has increased exponentially for both biomarker and therapeutic purposes, as more studies identify EV signaling as a key component of normal physiology and pathology. However, whilst fields such as gynecology have led the way, the investigation of the role that EVs play in the context of acquired neurological diseases is relatively new. Here, we have discussed how it has been consistently shown that the circulating EV population is altered by trauma to the CNS (**Figure 2**). The collected evidence presented here suggests that EVs mediate the systemic response following CNS injury, and that manipulation of this pathway can protect the CNS from secondary damage. However, our understanding of the underlying mechanisms and the consequences of manipulation of the EV population, is limited, and fundamental questions remain. For instance, it is unclear whether EV biogenesis after injury is different from the mechanisms that govern basal EV production. It also remains unclear whether the absolute number of EVs in the circulation is the most important factor, or whether the enrichment of circulating EVs from CNS-derived populations, that is barely detectable in the periphery without specific markers, is more important. Moving forward, it is clear that the role of EVs in the pathogenesis of systemic inflammation following CNS injury warrants further investigation to underpin development of successful therapeutic strategies and improve functional outcomes.

AUTHOR CONTRIBUTIONS

Manuscript was written by AY. Manuscript was edited by DA, MR, and YC.

FUNDING

AY was funded by the Nathalie Rose Barr Award from International Spinal Research Trust.

REFERENCES

1. Collaborators GBDS. Global, regional, and national burden of stroke, 1990–2016: a systematic analysis for the Global Burden of Disease Study 2016. *Lancet Neurol.* (2019) 18:439–58. doi: 10.1016/S1474-4422(19)30034-1
2. Injury GBDTB, Spinal Cord Injury C. Global, regional, and national burden of traumatic brain injury and spinal cord injury, 1990–2016: a systematic analysis for the Global Burden of Disease Study 2016. *Lancet Neurol.* (2019) 18:56–87. doi: 10.1016/S1474-4422(18)30415-0
3. Collaborators GBDN. Global, regional, and national burden of neurological disorders, 1990–2016: a systematic analysis for the Global Burden of Disease Study 2016. *Lancet Neurol.* (2019) 18:459–80. doi: 10.1016/S1474-4422(18)30499-X
4. Rajsic S, Gothe H, Borba HH, Sroczynski G, Vujicic J, Toell T, et al. Economic burden of stroke: a systematic review on post-stroke care. *Eur J Health Econ.* (2019) 20:107–34. doi: 10.1007/s10198-018-0984-0
5. Fountain DM, Kolias AG, Laing RJ, Hutchinson PJ. The financial outcome of traumatic brain injury: a single centre study. *Br J Neurosurg.* (2017) 31:350–5. doi: 10.1080/02688697.2016.1244254
6. Anwar MA, Al Shehabi TS, Eid AH. Inflammogenesis of secondary spinal cord injury. *Front Cell Neurosci.* (2016) 10:98. doi: 10.3389/fncel.2016.00098
7. Pearn ML, Niesman IR, Egawa J, Sawada A, Almenar-Queralt A, Shah SB, et al. Pathophysiology associated with traumatic brain injury: current treatments and potential novel therapeutics. *Cell Mol Neurobiol.* (2017) 37:571–85. doi: 10.1007/s10571-016-0400-1
8. Wimmer I, Zrzavy T, Lassmann H. Neuroinflammatory responses in experimental and human stroke lesions. *J Neuroimmunol.* (2018) 323:10–8. doi: 10.1016/j.jneuroim.2018.07.003
9. Maestrini I, Strbian D, Gautier S, Haapaniemi E, Moulin S, Sairanen T, et al. Higher neutrophil counts before thrombolysis for cerebral ischemia predict worse outcomes. *Neurology.* (2015) 85:1408–16. doi: 10.1212/WNL.0000000000002029
10. Alizadeh A, Dyck SM, Karimi-Abdolrezaee S. Traumatic spinal cord injury: an overview of pathophysiology, models and acute injury mechanisms. *Front Neurol.* (2019) 10:282. doi: 10.3389/fneur.2019.00282
11. Venkat P, Chen J, Chopp M. Exosome-mediated amplification of endogenous brain repair mechanisms and brain and systemic organ interaction in modulating neurological outcome after stroke. *J Cereb Blood Flow Metab.* (2018) 38:2165–78. doi: 10.1177/0271678X18782789
12. Hay JR, Johnson VE, Young AM, Smith DH, Stewart W. Blood-brain barrier disruption is an early event that may persist for many years after traumatic brain injury in humans. *J Neuropathol Exp Neurol.* (2015) 74:1147–57. doi: 10.1093/jnen/74.12.1147
13. Feng Y, Liao S, Wei C, Jia D, Wood K, Liu Q, et al. Infiltration and persistence of lymphocytes during late-stage cerebral ischemia in middle cerebral artery occlusion and photothrombotic stroke models. *J Neuroinflammation.* (2017) 14:248. doi: 10.1186/s12974-017-1017-0
14. Kumar A, Loane DJ. Neuroinflammation after traumatic brain injury: opportunities for therapeutic intervention. *Brain Behav Immun.* (2012) 26:1191–201. doi: 10.1016/j.bbi.2012.06.008
15. Werner C, Engelhard K. Pathophysiology of traumatic brain injury. *Br J Anaesth.* (2007) 99:4–9. doi: 10.1093/bja/aem131
16. Xiong Y, Mahmood A, Chopp M. Current understanding of neuroinflammation after traumatic brain injury and cell-based therapeutic opportunities. *Chin J Traumatol.* (2018) 21:137–51. doi: 10.1016/j.cjtee.2018.02.003
17. Anthony DC, Couch Y. The systemic response to CNS injury. *Exp Neurol.* (2014) 258:105–11. doi: 10.1016/j.expneurol.2014.03.013
18. Campbell SJ, Hughes PM, Iredale JP, Wilcockson DC, Waters S, Docagne F, et al. CINC-1 is an acute-phase protein induced by focal brain injury causing leukocyte mobilization and liver injury. *FASEB J.* (2003) 17:1168–70. doi: 10.1096/fj.02-0757fje
19. Campbell SJ, Perry VH, Pitossi FJ, Butchart AG, Chertoff M, Waters S, et al. Central nervous system injury triggers hepatic CC and CXC chemokine expression that is associated with leukocyte mobilization and recruitment to both the central nervous system and the liver. *Am J Pathol.* (2005) 166:1487–97. doi: 10.1016/S0002-9440(10)62365-6
20. Campbell SJ, Zahid I, Losey P, Law S, Jiang Y, Bilgen M, et al. Liver Kupffer cells control the magnitude of the inflammatory response in the injured brain and spinal cord. *Neuropharmacology.* (2008) 55:780–7. doi: 10.1016/j.neuropharm.2008.06.074
21. Wilcockson DC, Campbell SJ, Anthony DC, Perry VH. The systemic and local acute phase response following acute brain injury. *J Cereb Blood Flow Metab.* (2002) 22:318–26. doi: 10.1097/00004647-200203000-00009
22. Blomster LV, Brennan FH, Lao HW, Harle DW, Harvey AR, Ruitenberg MJ. Mobilisation of the splenic monocyte reservoir and peripheral CX(3)CR1 deficiency adversely affects recovery from spinal cord injury. *Exp Neurol.* (2013) 247:226–40. doi: 10.1016/j.expneurol.2013.05.002
23. Offner H, Subramanian S, Parker SM, Afentoulis ME, Vandenbark AA, Hurn PD. Experimental stroke induces massive, rapid activation of the peripheral immune system. *J Cereb Blood Flow Metab.* (2006) 26:654–65. doi: 10.1038/sj.jcbfm.9600217

24. Seifert HA, Offner H. The splenic response to stroke: from rodents to stroke subjects. *J Neuroinflammation.* (2018) 15:195. doi: 10.1186/s12974-018-1239-9
25. Liao Y, Liu P, Guo F, Zhang ZY, Zhang Z. Oxidative burst of circulating neutrophils following traumatic brain injury in human. *PLoS ONE.* (2013) 8:e68963. doi: 10.1371/journal.pone.0068963
26. Sun X, Jones ZB, Chen XM, Zhou L, So KF, Ren Y. Multiple organ dysfunction and systemic inflammation after spinal cord injury: a complex relationship. *J Neuroinflammation.* (2016) 13:260. doi: 10.1186/s12974-016-0736-y
27. Qin W, Zhang X, Yang S, Li Y, Yuan J, Yang L, et al. Risk factors for multiple organ dysfunction syndrome in severe stroke patients. *PLoS ONE.* (2016) 11:e0167189. doi: 10.1371/journal.pone.0167189
28. Weaver LC, Bao F, Dekaban GA, Hryciw T, Shultz SR, Cain DP, et al. CD11d integrin blockade reduces the systemic inflammatory response syndrome after traumatic brain injury in rats. *Exp Neurol.* (2015) 271:409–22. doi: 10.1016/j.expneurol.2015.07.003
29. Chaikittisilpa N, Krishnamoorthy V, Lele AV, Qiu Q, Vavilala MS. Characterizing the relationship between systemic inflammatory response syndrome and early cardiac dysfunction in traumatic brain injury. *J Neurosci Res.* (2018) 96:661–70. doi: 10.1002/jnr.24100
30. Ritzel RM, Doran SJ, Barrett JP, Henry RJ, Ma EL, Faden AI, et al. Chronic alterations in systemic immune function after traumatic brain injury. *J Neurotrauma.* (2018) 35:1419–36. doi: 10.1089/neu.2017.5399
31. Brommer B, Engel O, Kopp MA, Watzlawick R, Muller S, Pruss H, et al. Spinal cord injury-induced immune deficiency syndrome enhances infection susceptibility dependent on lesion level. *Brain.* (2016) 139(Pt 3):692–707. doi: 10.1093/brain/awv375
32. Campbell SJ, Deacon RM, Jiang Y, Ferrari C, Pitossi FJ, Anthony DC. Overexpression of IL-1beta by adenoviral-mediated gene transfer in the rat brain causes a prolonged hepatic chemokine response, axonal injury and the suppression of spontaneous behaviour. *Neurobiol Dis.* (2007) 27:151–63. doi: 10.1016/j.nbd.2007.04.013
33. Campbell SJ, Jiang Y, Davis AE, Farrands R, Holbrook J, Leppert D, et al. Immunomodulatory effects of etanercept in a model of brain injury act through attenuation of the acute-phase response. *J Neurochem.* (2007) 103:2245–55. doi: 10.1111/j.1471-4159.2007.04928.x
34. Clausen BH, Degn M, Martin NA, Couch Y, Karimi L, Ormhoj M, et al. Systemically administered anti-TNF therapy ameliorates functional outcomes after focal cerebral ischemia. *J Neuroinflammation.* (2014) 11:203. doi: 10.1186/PREACCEPT-2982253041347736
35. Dickens AM, Tovar YRLB, Yoo SW, Trout AL, Bae M, Kanmogne M, et al. Astrocyte-shed extracellular vesicles regulate the peripheral leukocyte response to inflammatory brain lesions. *Sci Signal.* (2017) 10:eaai7696. doi: 10.1126/scisignal.aai7696
36. Davis AE, Campbell SJ, Wilainam P, Anthony DC. Post-conditioning with lipopolysaccharide reduces the inflammatory infiltrate to the injured brain and spinal cord: a potential neuroprotective treatment. *Eur J Neurosci.* (2005) 22:2441–50. doi: 10.1111/j.1460-9568.2005.04447.x
37. Sa-Pereira I, Roodselaar J, Couch Y, Consentino Kronka Sosthenes M, Evans MC, Anthony DC, et al. Hepatic acute phase response protects the brain from focal inflammation during postnatal window of susceptibility. *Brain Behav Immun.* (2018) 69:486–98. doi: 10.1016/j.bbi.2018.01.008
38. Konsman JP, Luheshi GN, Bluthe RM, Dantzer R. The vagus nerve mediates behavioural depression, but not fever, in response to peripheral immune signals; a functional anatomical analysis. *Eur J Neurosci.* (2000) 12:4434–46. doi: 10.1046/j.0953-816X.2000.01319.x
39. Kox M, Vaneker M, van der Hoeven JG, Scheffer GJ, Hoedemaekers CW, Pickkers P. Effects of vagus nerve stimulation and vagotomy on systemic and pulmonary inflammation in a two-hit model in rats. *PLoS ONE.* (2012) 7:e34431. doi: 10.1371/journal.pone.0034431
40. Konsman JP, Parnet P, Dantzer R. Cytokine-induced sickness behaviour: mechanisms and implications. *Trends Neurosci.* (2002) 25:154–9. doi: 10.1016/S0166-2236(00)02088-9
41. Budnik V, Ruiz-Canada C, Wendler F. Extracellular vesicles round off communication in the nervous system. *Nat Rev Neurosci.* (2016) 17:160–72. doi: 10.1038/nrn.2015.29
42. Colombo M, Raposo G, Thery C. Biogenesis, secretion, and intercellular interactions of exosomes and other extracellular vesicles. *Annu Rev Cell Dev Biol.* (2014) 30:255–89. doi: 10.1146/annurev-cellbio-101512-122326
43. Raposo G, Stoorvogel W. Extracellular vesicles: exosomes, microvesicles, and friends. *J Cell Biol.* (2013) 200:373–83. doi: 10.1083/jcb.201211138
44. Robbins PD, Dorronsoro A, Booker CN. Regulation of chronic inflammatory and immune processes by extracellular vesicles. *J Clin Invest.* (2016) 126:1173–80. doi: 10.1172/JCI81131
45. Chivet M, Javalet C, Laulagnier K, Blot B, Hemming FJ, Sadoul R. Exosomes secreted by cortical neurons upon glutamatergic synapse activation specifically interact with neurons. *J Extracell Vesicles.* (2014) 3:24722. doi: 10.3402/jev.v3.24722
46. Lachenal G, Pernet-Gallay K, Chivet M, Hemming FJ, Belly A, Bodon G, et al. Release of exosomes from differentiated neurons and its regulation by synaptic glutamatergic activity. *Mol Cell Neurosci.* (2011) 46:409–18. doi: 10.1016/j.mcn.2010.11.004
47. Drago F, Lombardi M, Prada I, Gabrielli M, Joshi P, Cojoc D, et al. ATP modifies the proteome of extracellular vesicles released by microglia and influences their action on astrocytes. *Front Pharmacol.* (2017) 8:910. doi: 10.3389/fphar.2017.00910
48. Kumar A, Stoica BA, Loane DJ, Yang M, Abulwerdi G, Khan N, et al. Microglial-derived microparticles mediate neuroinflammation after traumatic brain injury. *J Neuroinflammation.* (2017) 14:47. doi: 10.1186/s12974-017-0819-4
49. Couch Y, Akbar N, Roodselaar J, Evans MC, Gardiner C, Sargent I, et al. Circulating endothelial cell-derived extracellular vesicles mediate the acute phase response and sickness behaviour associated with CNS inflammation. *Sci Rep.* (2017) 7:9574. doi: 10.1038/s41598-017-09710-3
50. Kuharic J, Grabusic K, Tokmadzic VS, Stifter S, Tulic K, Shevchuk O, et al. Severe traumatic brain injury induces early changes in the physical properties and protein composition of intracranial extracellular vesicles. *J Neurotrauma.* (2019) 36:190–200. doi: 10.1089/neu.2017.5515
51. Welton JL, Loveless S, Stone T, von Ruhland C, Robertson NP, Clayton A. Cerebrospinal fluid extracellular vesicle enrichment for protein biomarker discovery in neurological disease; multiple sclerosis. *J Extracell Vesicles.* (2017) 6:1369805. doi: 10.1080/20013078.2017.1369805
52. Hazleton I, Yates A, Dale A, Roodselaar J, Akbar N, Ruitenberg M, et al. Exacerbation of acute traumatic brain injury by circulating extracellular vesicles. *J Neurotrauma.* (2017) 35:639–51. doi: 10.1089/neu.2017.5049
53. Jucker M, Walker LC. Self-propagation of pathogenic protein aggregates in neurodegenerative diseases. *Nature.* (2013) 501:45–51. doi: 10.1038/nature12481
54. Vella LJ, Hill AF, Cheng L. Focus on extracellular vesicles: exosomes and their role in protein trafficking and biomarker potential in Alzheimer's and Parkinson's Disease. *Int J Mol Sci.* (2016) 17:173. doi: 10.3390/ijms17020173
55. Saman S, Kim W, Raya M, Visnick Y, Miro S, Saman S, et al. Exosome-associated tau is secreted in tauopathy models and is selectively phosphorylated in cerebrospinal fluid in early Alzheimer disease. *J Biol Chem.* (2012) 287:3842–9. doi: 10.1074/jbc.M111.277061
56. Shi M, Liu C, Cook TJ, Bullock KM, Zhao Y, Ginghina C, et al. Plasma exosomal alpha-synuclein is likely CNS-derived and increased in Parkinson's disease. *Acta Neuropathol.* (2014) 128:639–50. doi: 10.1007/s00401-014-1314-y
57. Quezada C, Torres A, Niechi I, Uribe D, Contreras-Duarte S, Toledo F, et al. Role of extracellular vesicles in glioma progression. *Mol Aspects Med.* (2018) 60:38–51. doi: 10.1016/j.mam.2017.12.003
58. Skog J, Wurdinger T, van Rijn S, Meijer DH, Gainche L, Sena-Esteves M, et al. Glioblastoma microvesicles transport RNA and proteins that promote tumour growth and provide diagnostic biomarkers. *Nat Cell Biol.* (2008) 10:1470–6. doi: 10.1038/ncb1800
59. Oushy S, Hellwinkel JE, Wang M, Nguyen GJ, Gunaydin D, Harland TA, et al. Glioblastoma multiforme-derived extracellular vesicles drive normal astrocytes towards a tumour-enhancing phenotype. *Philos Trans R Soc Lond B Biol Sci.* (2018) 373:1737. doi: 10.1098/rstb.2016.0477
60. Ciregia F, Urbani A, Palmisano G. Extracellular vesicles in brain tumors and neurodegenerative diseases. *Front Mol Neurosci.* (2017) 10:276. doi: 10.3389/fnmol.2017.00276

61. Hoshino A, Costa-Silva B, Shen TL, Rodrigues G, Hashimoto A, Tesic Mark M, et al. Tumour exosome integrins determine organotropic metastasis. *Nature*. (2015) 527:329–35. doi: 10.1038/nature15756
62. Gener Lahav T, Adler O, Zait Y, Shani O, Amer M, Doron H, et al. Melanoma-derived extracellular vesicles instigate proinflammatory signaling in the metastatic microenvironment. *Int J Cancer*. (2019) 145:2521–34. doi: 10.1002/ijc.32521
63. Fong MY, Zhou W, Liu L, Alontaga AY, Chandra M, Ashby J, et al. Breast-cancer-secreted miR-122 reprograms glucose metabolism in premetastatic niche to promote metastasis. *Nat Cell Biol*. (2015) 17:183–94. doi: 10.1038/ncb3094
64. Li JJ, Wang B, Kodali MC, Chen C, Kim E, Patters BJ, et al. *In vivo* evidence for the contribution of peripheral circulating inflammatory exosomes to neuroinflammation. *J Neuroinflammation*. (2018) 15:8. doi: 10.1186/s12974-017-1038-8
65. Jacome T, Tatum D. Systemic inflammatory response syndrome (SIRS) score independently predicts poor outcome in isolated traumatic brain injury. *Neurocrit Care*. (2018) 28:110–6. doi: 10.1007/s12028-017-0410-y
66. Nekludov M, Mobarrez F, Gryth D, Bellander BM, Wallen H. Formation of microparticles in the injured brain of patients with severe isolated traumatic brain injury. *J Neurotrauma*. (2014) 31:1927–33. doi: 10.1089/neu.2013.3168
67. Morel N, Morel O, Petit L, Hugel B, Cochard JF, Freyssinet JM, et al. Generation of procoagulant microparticles in cerebrospinal fluid and peripheral blood after traumatic brain injury. *J Trauma*. (2008) 64:698–704. doi: 10.1097/TA.0b013e31816493ad
68. Kerr NA, de Rivero Vaccari JP, Abbassi S, Kaur H, Zambrano R, Wu S, et al. Traumatic brain injury-induced acute lung injury: evidence for activation and inhibition of a neural-respiratory-inflammasome axis. *J Neurotrauma*. (2018) 35:2067–76. doi: 10.1089/neu.2017.5430
69. Tian Y, Salsbery B, Wang M, Yuan H, Yang J, Zhao Z, et al. Brain-derived microparticles induce systemic coagulation in a murine model of traumatic brain injury. *Blood*. (2015) 125:2151–9. doi: 10.1182/blood-2014-09-598805
70. Ridder K, Keller S, Dams M, Rupp AK, Schlaudraff J, Del Turco D, et al. Extracellular vesicle-mediated transfer of genetic information between the hematopoietic system and the brain in response to inflammation. *PLoS Biol*. (2014) 12:e1001874. doi: 10.1371/journal.pbio.1001874
71. Raposo G, Nijman HW, Stoorvogel W, Liejendekker R, Harding CV, Melief CJ, et al. B lymphocytes secrete antigen-presenting vesicles. *J Exp Med*. (1996) 183:1161–72. doi: 10.1084/jem.183.3.1161
72. Admyre C, Bohle B, Johansson SM, Focke-Tejkl M, Valenta R, Scheynius A, et al. B cell-derived exosomes can present allergen peptides and activate allergen-specific T cells to proliferate and produce TH2-like cytokines. *J Allergy Clin Immunol*. (2007) 120:1418–24. doi: 10.1016/j.jaci.2007.06.040
73. Admyre C, Johansson SM, Paulie S, Gabrielsson S. Direct exosome stimulation of peripheral human T cells detected by ELISPOT. *Eur J Immunol*. (2006) 36:1772–81. doi: 10.1002/eji.200535615
74. Giri PK, Schorey JS. Exosomes derived from M. Bovis BCG infected macrophages activate antigen-specific CD4+ and CD8+ T cells *in vitro* and *in vivo*. *PLoS ONE*. (2008) 3:e2461. doi: 10.1371/journal.pone.0002461
75. Utsugi-Kobukai S, Fujimaki H, Hotta C, Nakazawa M, Minami M. MHC class I-mediated exogenous antigen presentation by exosomes secreted from immature and mature bone marrow derived dendritic cells. *Immunol Lett*. (2003) 89:125–31. doi: 10.1016/S0165-2478(03)00128-7
76. Kobayashi N, Karisola P, Pena-Cruz V, Dorfman DM, Jinushi M, Umetsu SE, et al. TIM-1 and TIM-4 glycoproteins bind phosphatidylserine and mediate uptake of apoptotic cells. *Immunity*. (2007) 27:927–40. doi: 10.1016/j.immuni.2007.11.011
77. Fitzner D, Schnaars M, van Rossum D, Krishnamoorthy G, Dibaj P, Bakhti M, et al. Selective transfer of exosomes from oligodendrocytes to microglia by macropinocytosis. *J Cell Sci*. (2011) 124(Pt 3):447–58. doi: 10.1242/jcs.074088
78. Moyron RB, Gonda A, Selleck MJ, Luo-Owen X, Catalano RD, O'Callahan T, et al. Differential protein expression in exosomal samples taken from trauma patients. *Proteomics Clin Appl*. (2017) 11:1700061. doi: 10.1002/prca.201700061
79. Bianco F, Pravettoni E, Colombo A, Schenk U, Moller T, Matteoli M, et al. Astrocyte-derived ATP induces vesicle shedding and IL-1 beta release from microglia. *J Immunol*. (2005) 174:7268–77. doi: 10.4049/jimmunol.174.11.7268
80. Bianco F, Perrotta C, Novellino L, Francolini M, Riganti L, Menna E, et al. Acid sphingomyelinase activity triggers microparticle release from glial cells. *EMBO J*. (2009) 28:1043–54. doi: 10.1038/emboj.2009.45
81. Hosseinkhani B, Kuypers S, van den Akker NMS, Molin DGM, Michiels L. Extracellular vesicles work as a functional inflammatory mediator between vascular endothelial cells and immune cells. *Front Immunol*. (2018) 9:1789. doi: 10.3389/fimmu.2018.01789
82. Mack M, Kleinschmidt A, Bruhl H, Klier C, Nelson PJ, Cihak J, et al. Transfer of the chemokine receptor CCR5 between cells by membrane-derived microparticles: a mechanism for cellular human immunodeficiency virus 1 infection. *Nat Med*. (2000) 6:769–75. doi: 10.1038/77498
83. Zhao Z, Zhou Y, Tian Y, Li M, Dong JF, Zhang J. Cellular microparticles and pathophysiology of traumatic brain injury. *Protein Cell*. (2017) 8:801. doi: 10.1007/s13238-017-0414-6
84. de Oliveira Manoel AL, Neto AC, Veigas PV, Rizoli S. Traumatic brain injury associated coagulopathy. *Neurocrit Care*. (2015) 22:34–44. doi: 10.1007/s12028-014-0026-4
85. Samuels JM, Moore EE, Silliman CC, Banerjee A, Cohen MJ, Ghasabyan A, et al. Severe traumatic brain injury is associated with a unique coagulopathy phenotype. *J Trauma Acute Care Surg*. (2019) 86:686–93. doi: 10.1097/TA.0000000000002173
86. Laroche M, Kutcher ME, Huang MC, Cohen MJ, Manley GT. Coagulopathy after traumatic brain injury. *Neurosurgery*. (2012) 70:1334–45. doi: 10.1227/NEU.0b013e31824d179b
87. Arraud N, Linares R, Tan S, Gounou C, Pasquet JM, Mornet S, et al. Extracellular vesicles from blood plasma: determination of their morphology, size, phenotype and concentration. *J Thromb Haemost*. (2014) 12:614–27. doi: 10.1111/jth.12554
88. Sinauridze EI, Kireev DA, Popenko NY, Pichugin AV, Panteleev MA, Krymskaya OV, et al. Platelet microparticle membranes have 50- to 100-fold higher specific procoagulant activity than activated platelets. *Thromb Haemost*. (2007) 97:425–34. doi: 10.1160/TH06-06-0313
89. Midura EF, Jernigan PL, Kuethe JW, Friend LA, Veile R, Makley AT, et al. Microparticles impact coagulation after traumatic brain injury. *J Surg Res*. (2015) 197:25–31. doi: 10.1016/j.jss.2015.02.064
90. Bao F, Bailey CS, Gurr KR, Bailey SI, Rosas-Arellano MP, Dekaban GA, et al. Increased oxidative activity in human blood neutrophils and monocytes after spinal cord injury. *Exp Neurol*. (2009) 215:308–16. doi: 10.1016/j.expneurol.2008.10.022
91. Kesani AK, Urquhart JC, Bedard N, Leelapattana P, Siddiqi F, Gurr KR, et al. Systemic inflammatory response syndrome in patients with spinal cord injury: does its presence at admission affect patient outcomes? Clinical article. *J Neurosurg Spine*. (2014) 21:296–302. doi: 10.3171/2014.3.SPINE13784
92. Stein DM, Menaker J, McQuillan K, Handley C, Aarabi B, Scalea TM. Risk factors for organ dysfunction and failure in patients with acute traumatic cervical spinal cord injury. *Neurocrit Care*. (2010) 13:29–39. doi: 10.1007/s12028-010-9359-9
93. van Weert KC, Schouten EJ, Hofstede J, van de Meent H, Holtslag HR, van den Berg-Emons RJ. Acute phase complications following traumatic spinal cord injury in Dutch level 1 trauma centres. *J Rehabil Med*. (2014) 46:882–5. doi: 10.2340/16501977-1858
94. de Rivero Vaccari JP, Brand F III, Adamczak S, Lee SW, Perez-Barcena J, Wang MY, et al. Exosome-mediated inflammasome signaling after central nervous system injury. *J Neurochem*. (2016) 136 (Suppl. 1):39–48. doi: 10.1111/jnc.13036
95. Almad A, Lash AT, Wei P, Lovett-Racke AE, McTigue DM. The PPAR alpha agonist gemfibrozil is an ineffective treatment for spinal cord injured mice. *Exp Neurol*. (2011) 232:309–17. doi: 10.1016/j.expneurol.2011.09.023
96. Kim DK, Nishida H, An SY, Shetty AK, Bartosh TJ, Prockop DJ. Chromatographically isolated CD63+CD81+ extracellular vesicles from mesenchymal stromal cells rescue cognitive impairments after TBI. *Proc Natl Acad Sci USA*. (2016) 113:170–5. doi: 10.1073/pnas.1522297113

97. Zhang Y, Chopp M, Zhang ZG, Katakowski M, Xin H, Qu C, et al. Systemic administration of cell-free exosomes generated by human bone marrow derived mesenchymal stem cells cultured under 2D and 3D conditions improves functional recovery in rats after traumatic brain injury. *Neurochem Int.* (2017) 111:69–81. doi: 10.1016/j.neuint.2016.08.003
98. Lu Y, Zhou Y, Zhang R, Wen L, Wu K, Li Y, et al. Bone mesenchymal stem cell-derived extracellular vesicles promote recovery following spinal cord injury via improvement of the integrity of the blood-spinal cord barrier. *Front Neurosci.* (2019) 13:209. doi: 10.3389/fnins.2019.00209
99. Wang L, Pei S, Han L, Guo B, Li Y, Duan R, et al. Mesenchymal stem cell-derived exosomes reduce A1 astrocytes via downregulation of phosphorylated NFkappaB P65 subunit in spinal cord injury. *Cell Physiol Biochem.* (2018) 50:1535–59. doi: 10.1159/000494652
100. Ruppert KA, Nguyen TT, Prabhakara KS, Toledano Furman NE, Srivastava AK, Harting MT, et al. Human mesenchymal stromal cell-derived extracellular vesicles modify microglial response and improve clinical outcomes in experimental spinal cord injury. *Sci Rep.* (2018) 8:480. doi: 10.1038/s41598-017-18867-w
101. Gao W, Li F, Liu L, Xu X, Zhang B, Wu Y, et al. Endothelial colony-forming cell-derived exosomes restore blood-brain barrier continuity in mice subjected to traumatic brain injury. *Exp Neurol.* (2018) 307:99–108. doi: 10.1016/j.expneurol.2018.06.001
102. Vogel A, Upadhya R, Shetty AK. Neural stem cell derived extracellular vesicles: attributes and prospects for treating neurodegenerative disorders. *EBioMedicine.* (2018) 38:273–82. doi: 10.1016/j.ebiom.2018.11.026
103. Kobayashi H, Ebisawa K, Kambe M, Kasai T, Suga H, Nakamura K, et al. Editors' Choice Effects of exosomes derived from the induced pluripotent stem cells on skin wound healing. *Nagoya J Med Sci.* (2018) 80:141–53. doi: 10.18999/nagjms.80.2.141
104. Xin H, Li Y, Liu Z, Wang X, Shang X, Cui Y, et al. MiR-133b promotes neural plasticity and functional recovery after treatment of stroke with multipotent mesenchymal stromal cells in rats via transfer of exosome-enriched extracellular particles. *Stem Cells.* (2013) 31:2737–46. doi: 10.1002/stem.1409
105. Xiao Y, Geng F, Wang G, Li X, Zhu J, Zhu W. Bone marrow-derived mesenchymal stem cells-derived exosomes prevent oligodendrocyte apoptosis through exosomal miR-134 by targeting caspase-8. *J Cell Biochem.* (2018) 120:2109–18. doi: 10.1002/jcb.27519
106. Lankford KL, Arroyo EJ, Nazimek K, Bryniarski K, Askenase PW, Kocsis JD. Intravenously delivered mesenchymal stem cell-derived exosomes target M2-type macrophages in the injured spinal cord. *PLoS ONE.* (2018) 13:e0190358. doi: 10.1371/journal.pone.0190358
107. Otero-Ortega L, Laso-Garcia F, Gomez-de Frutos MD, Rodriguez-Frutos B, Pascual-Guerra J, Fuentes B, et al. White matter repair after extracellular vesicles administration in an experimental animal model of subcortical stroke. *Sci Rep.* (2017) 7:44433. doi: 10.1038/srep44433
108. Huang JH, Yin XM, Xu Y, Xu CC, Lin X, Ye FB, et al. Systemic administration of exosomes released from mesenchymal stromal cells attenuates apoptosis, inflammation, and promotes angiogenesis after spinal cord injury in rats. *J Neurotrauma.* (2017) 34:3388–96. doi: 10.1089/neu.2017.5063
109. Zhang Y, Chopp M, Liu XS, Katakowski M, Wang X, Tian X, et al. Exosomes derived from mesenchymal stromal cells promote axonal growth of cortical neurons. *Mol Neurobiol.* (2017) 54:2659–73. doi: 10.1007/s12035-016-9851-0
110. Xin H, Katakowski M, Wang F, Qian JY, Liu XS, Ali MM, et al. MicroRNA cluster miR-17-92 cluster in exosomes enhance neuroplasticity and functional recovery after stroke in rats. *Stroke.* (2017) 48:747–53. doi: 10.1161/STROKEAHA.116.015204
111. Huang S, Ge X, Yu J, Han Z, Yin Z, Li Y, et al. Increased miR-124-3p in microglial exosomes following traumatic brain injury inhibits neuronal inflammation and contributes to neurite outgrowth via their transfer into neurons. *FASEB J.* (2018) 32:512–28. doi: 10.1096/fj.201700673R
112. Bang OY, Kim EH. Mesenchymal stem cell-derived extracellular vesicle therapy for stroke: challenges and progress. *Front Neurol.* (2019) 10:211. doi: 10.3389/fneur.2019.00211
113. Phan J, Kumar P, Hao D, Gao K, Farmer D, Wang A. Engineering mesenchymal stem cells to improve their exosome efficacy and yield for cell-free therapy. *J Extracell Vesicles.* (2018) 7:1522236. doi: 10.1080/20013078.2018.1522236
114. Xin H, Li Y, Cui Y, Yang JJ, Zhang ZG, Chopp M. Systemic administration of exosomes released from mesenchymal stromal cells promote functional recovery and neurovascular plasticity after stroke in rats. *J Cereb Blood Flow Metab.* (2013) 33:1711–5. doi: 10.1038/jcbfm.2013.152

Conflict of Interest: The authors declare that the research was conducted in the absence of any commercial or financial relationships that could be construed as a potential conflict of interest.

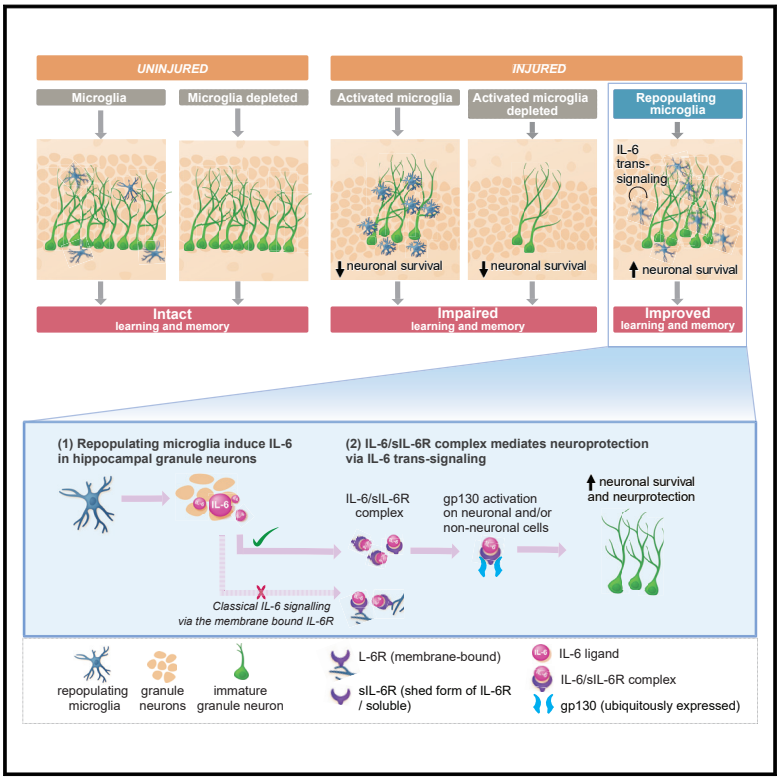
Copyright © 2019 Yates, Anthony, Ruitenberg and Couch. This is an open-access article distributed under the terms of the Creative Commons Attribution License (CC BY). The use, distribution or reproduction in other forums is permitted, provided the original author(s) and the copyright owner(s) are credited and that the original publication in this journal is cited, in accordance with accepted academic practice. No use, distribution or reproduction is permitted which does not comply with these terms.

Article

Cell

Repopulating Microglia Promote Brain Repair in an IL-6-Dependent Manner

Graphical Abstract



Highlights

- Removing microglia from the injured brain does not alleviate cognitive deficits
- Repopulating microglia can attenuate learning deficits and stimulate neurogenesis
- Repopulating microglia positively modulate the microenvironment of the injured brain
- Repopulating microglia induce IL-6 in neurons and mediate neuroprotection

Authors

Emily F. Willis, Kelli P.A. MacDonald, Quan H. Nguyen, ..., Stefan Rose-John, Marc J. Ruitenberg, Jana Vukovic

Correspondence

j.vukovic@uq.edu.au

In Brief

Microglia in the mammalian brain can be manipulated to adopt a neuroprotective and pro-regenerative phenotype that can aid repair and alleviate the cognitive deficits arising from brain injury.

Willis et al., 2020, Cell *180*, 833–846
March 5, 2020 © 2020 Elsevier Inc.
https://doi.org/10.1016/j.cell.2020.02.013

CellPress

Article

Cell

Repopulating Microglia Promote Brain Repair in an IL-6-Dependent Manner

Emily F. Willis,[1,2] Kelli P.A. MacDonald,[3] Quan H. Nguyen,[4] Adahir Labrador Garrido,[1] Ellen R. Gillespie,[1] Samuel B.R. Harley,[1,2] Perry F. Bartlett,[2] Wayne A. Schroder,[3,7] Abi G. Yates,[5] Daniel C. Anthony,[5] Stefan Rose-John,[6] Marc J. Ruitenberg,[1] and Jana Vukovic[1,2,8,*]

[1]School of Biomedical Sciences, Faculty of Medicine, The University of Queensland, Brisbane, QLD, Australia
[2]Queensland Brain Institute, The University of Queensland, Brisbane, QLD, Australia
[3]Department of Immunology, QIMR Berghofer Medical Research Institute, Brisbane, QLD, Australia
[4]Institute for Molecular Bioscience, The University of Queensland, Brisbane, QLD, Australia
[5]Laboratory of Experimental Neuropathology, Department of Pharmacology, University of Oxford, Oxford OX1 3QT, UK
[6]Biochemisches Institut, Christian Albrechts Universität Kiel, Kiel, Germany
[7]School of Environment and Science, Griffith University, QLD, Brisbane, Australia
[8]Lead Contact
*Correspondence: j.vukovic@uq.edu.au
https://doi.org/10.1016/j.cell.2020.02.013

SUMMARY

Cognitive dysfunction and reactive microglia are hallmarks of traumatic brain injury (TBI), yet whether these cells contribute to cognitive deficits and secondary inflammatory pathology remains poorly understood. Here, we show that removal of microglia from the mouse brain has little effect on the outcome of TBI, but inducing the turnover of these cells through either pharmacologic or genetic approaches can yield a neuroprotective microglial phenotype that profoundly aids recovery. The beneficial effects of these repopulating microglia are critically dependent on interleukin-6 (IL-6) *trans*-signaling via the soluble IL-6 receptor (IL-6R) and robustly support adult neurogenesis, specifically by augmenting the survival of newborn neurons that directly support cognitive function. We conclude that microglia in the mammalian brain can be manipulated to adopt a neuroprotective and pro-regenerative phenotype that can aid repair and alleviate the cognitive deficits arising from brain injury.

INTRODUCTION

Microglia, the most abundant type of immune cell in the brain, play important roles in brain development, maintenance, and disease (Kettenmann et al., 2011; Wolf et al., 2017). These distant cousins of peripheral macrophages colonize the brain early in development (Ginhoux et al., 2010; Hoeffel and Ginhoux, 2018) and contribute to the sculpting of neural circuits through the promotion of neural cell genesis, patterning of synaptic connections, and removal of apoptotic cells (Hong et al., 2016; Paolicelli et al., 2011; Schafer et al., 2012). Microglia are believed to play similar physiological roles in the adult brain (Hanisch and Kettenmann, 2007). They also respond vigorously to both chronic disease and acute insults affecting the CNS (Jassam et al., 2017; Hickman et al., 2018). Because microglia share many phenotypic features with monocyte-derived macrophages, elucidating their contribution to CNS injury or disease has proven challenging. The identification of more unique microglia markers has helped distinguishing them from infiltrating monocytes and macrophages and better characterize their biology across a range of settings (Bennett et al., 2016; Butovsky et al., 2014; Buttgereit et al., 2016; Haage et al., 2019; Yona et al., 2013). In addition, the development of CNS-penetrable drugs that inhibit colony-stimulating factor 1 receptor (CSF-1R), on which microglia depend for their survival (Elmore et al., 2014), has enabled further and more direct investigations of microglial function in the healthy and diseased CNS (Bellver-Landete et al., 2019; Dagher et al., 2015; Rice et al., 2017). This, together with genetic approaches to selectively target these cells (Parkhurst et al., 2013), has resulted in more direct evidence for dual and opposing roles of microglia in normal brain function and disease. Specifically, microglia were reported to not only mediate learning-associated synaptic plasticity in the healthy adult brain (Parkhurst et al., 2013), but also to contribute to pathology and cognitive dysfunction during both neuroinflammation (Rice et al., 2017) and normal aging (Elmore et al., 2018). It has been suggested that some of the damaging properties of microglia behavior might be reversible through e.g., short-term CSF-1R inhibitor treatment (Rice et al., 2015, 2017; Weber et al., 2019), but many mechanistic questions remain, and our incomplete understanding of basic microglia biology therefore continues to present a major medical challenge.

Chronic non-resolving inflammation with widespread microglial activation is a defining feature of traumatic brain injury (TBI) (Ertürk et al., 2016; Scott et al., 2018; Simon et al., 2017), and here, we took advantage of this characteristic to directly probe putative roles of microglia in influencing neurodegeneration and cognitive functions. In the acute phase, microglia are known to rapidly respond to damage-associated molecular patterns that are released as a result of brain injury (Bianchi, 2007) and then migrate toward sites damage in an ATP-dependent manner (Davalos et al., 2005). Beneficial aspects of this early microglial activation are thought to include the clearance of cellular

debris, which is a critical part of any successful wound healing process (Giulian et al., 1989; Neumann et al., 2009; Hilla et al., 2017; Bellver-Landete et al., 2019). However, many brain microglia retain an activated phenotype well into the chronic stages of TBI on the basis of inflammatory gene expression and an amoeboid and/or phagocytic appearance. This persistent state of activation is generally viewed as detrimental (Ertürk et al., 2016), although direct evidence for this is scant. Overall, there is still great uncertainty as to what role microglia really have in relation to TBI, i.e., do they indeed worsen the neurological outcome as drivers of secondary inflammatory pathology, do they hamper or support endogenous repair processes, or perhaps are all types of processes in place at different temporal stages of the injury process? Here, we addressed these questions in a well-defined mouse model of TBI.

RESULTS

Eliminating Microglia Does Not Improve Cognitive Performance or Adult Neurogenesis after TBI

We first examined whether microglia absence alters the cognitive outcome from TBI in hippocampus-dependent tasks. For this, we depleted microglia by feeding mice the CSF-1R antagonist PLX5622 (Elmore et al., 2014), which induces death of Iba1^{pos}TMEM119^{pos} microglia, but has minimal effects on circulating monocytes (Bellver-Landete et al., 2019). Controlled cortical impact was used to inflict TBI. Continuous administration of PLX5622, initiated 3 weeks prior to TBI, induced widespread loss of Iba1^{pos}TMEM119^{pos} cells, including in the hippocampus where a 95% depletion efficiency was maintained throughout the experimental time period after TBI (Figures 1A and 1B). These results stood in sharp contrast to mice administered control chow (i.e., vehicle), and in which a 5-fold increase in the number of Iba1^{pos} cells was observed in the hippocampus over the 12-day period after TBI compared with those with sham surgery. Corroborating evidence for these findings was provided through $CX_3CR1cre^{ERT2}$ x tdTomato mice where administration of PLX5622 induced robust depletion of tdTomato-tagged microglia throughout the brain (Figures S1A and S1B). Loss of other CNS-resident macrophage populations was also observed with long-term PLX5622 treatment, specifically in the choroid plexus and meninges (Figures S1C and S1D).

Having confirmed efficient depletion of brain microglia with continuous PLX5622 treatment, we next tested the cognitive abilities of experimental mice in three behavioral paradigms that rely on hippocampal function. Our main test, active place avoidance (APA), is a challenging spatial learning task, in which animals are placed on a rotating turntable and required to continuously change their location on the basis of visual cues to avoid being moved into a stationary shock zone (Vukovic et al., 2013). We employed this task to test spatial learning in both sham and TBI mice over a 5-day APA testing paradigm (Figures 1C–1F). Absence of microglia (and other CNS-resident macrophage populations) in PLX5622-treated mice did not significantly alter the locomotor behavior (distance covered) (Figure 1D). Irrespective of microglia presence or absence, sham-operated control mice quickly learned to avoid the shock zone, as evident from the improved performance (reduction in shock zone entries) over time (Figures 1E and 1F) and also "within session" learning, which is more reflective of short-term working memory (Figure S1E). In sharp contrast, TBI mice were not able to learn this task, making significantly more mistakes (i.e., greater number of entries into the shock zone) than their sham-operated counterparts, and they also failed to show an improvement in performance over time. The absence of microglia (and other CSF-1R-dependent brain macrophages) in the PLX5622-treated group did not affect this impaired APA performance of TBI mice in any way. Pharmacological removal of microglia thus did not interfere with spatial learning outcomes under both sham and TBI conditions. We corroborated these results in the Morris water maze (MWM) and Y-maze task (Figures S1F–S1J).

Our previous work uncovered an important role for microglia in regulating the activity of neural stem/progenitor cells in the adult brain (Vukovic et al., 2012). Therefore, we next determined how the loss of microglia would affect hippocampal neurogenesis after TBI, evaluating both the number of newly generated immature neurons expressing the microtubule-associated protein doublecortin (DCX) (Rao and Shetty, 2004) and the size of the pool of intermediate neuronal progenitor cells expressing the transcription factor Tbr2 (Hodge et al., 2012). In sham-operated controls, continuous PLX5622 treatment had no effect on the different stages of adult neurogenesis (i.e., neuronal precursor proliferation versus newborn neuron generation) (Figures 1G–1J). By contrast, we observed a striking overall reduction in the number of immature hippocampal DCX^{pos} neurons, by more than half, in TBI mice (12 days after injury) (Figure 1G), and the loss of microglia (and other CSF-1R-dependent brain macrophages) in PLX5622-treated TBI mice resulted in a further reduction in the total number of newborn neurons, which was maintained for 19 weeks (Figure S1K). Pulse-chase experiments with bromodeoxyuridine (BrdU) revealed no difference in the number of neurons that were born after injury (i.e., DCX^{pos}BrdU^{pos} cells) and survived up until day 12 (Figure 1H). Consistent with this, both the total and actively proliferating (i.e., EdU^{pos}) number of Tbr2^{pos} neuronal precursor cells did not differ between control and PLX5622-treated TBI mice (12 days after injury) (Figures 1I and 1J). Hippocampal volumes were also unchanged with continuous PLX5622 treatment (Figures S1L and S1M). These findings show that the removal of microglia from brain regions that are not directly impacted but actively undergoing neurodegenerative changes and gliosis (i.e., the hippocampus) might interfere with the survival of DCX^{pos} cells that were born prior to and/or very shortly after TBI. Continuous PLX5622 treatment otherwise had very little bearing on outcomes in the specific behavioral paradigms that directly probe hippocampal function.

Repopulating Microglia Attenuate Spatial Learning Deficits after TBI

We next explored the effect of replenishing the brain with new microglia. We used two independent and complementary approaches to achieve this. First, we used a genetic model ($CX_3CR1cre^{ERT2}$ x iDTR and $CX_3CR1cre^{ERT2}$ x iDTR x tdTomato mice) in which microglia can be selectively ablated through intraperitoneal diphtheria toxin (DT) treatment and then replenished (Figures 2A, 2B, and S2A). Second, we used the established pharmacological approach, but with short-term rather than

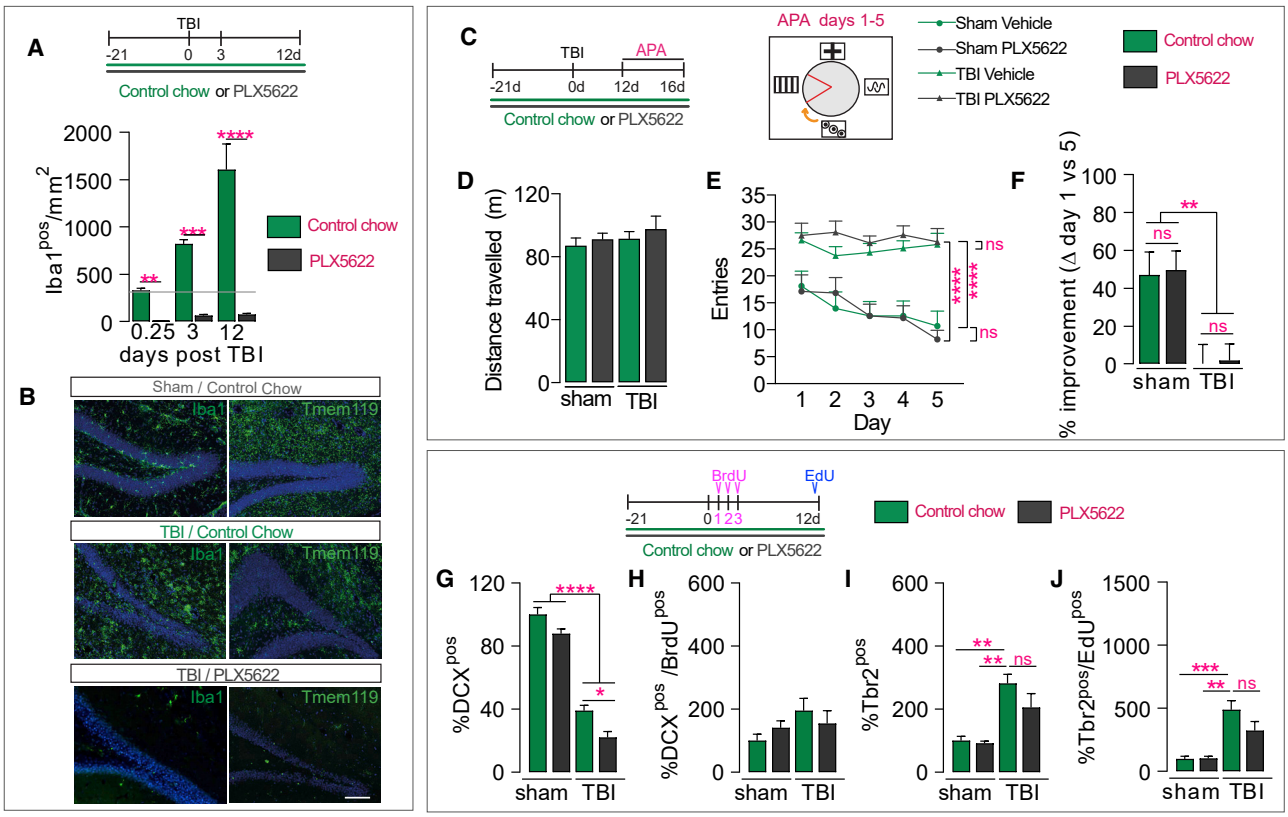


Figure 1. Sustained Depletion of Microglia with Continuous PLX5622 Treatment Does Not Alter Spatial Learning and Memory Abilities

(A) Overview of experimental timeline. PLX5622 treatment was initiated 3 weeks pre-surgery (sham or TBI), and mice were sacrificed 6 h (0.25 days), 3 days, or 12 days later. Quantification of Iba1^{pos} microglia in the ipsilateral dentate gyrus after TBI. The gray line represents sham averages. Note that Iba1^{pos} cell numbers increased over time as a result of TBI in controls (green bars), but were nearly abolished in PLX5622-treated mice (dark gray bars) (day 0.25: $t = 14.41$, $df = 6$; day 3: $t = 20.48$, $df = 5$; day 12: $t = 5.01$, $df = 7$).

(B) Representative confocal images confirming the loss of Iba1^{pos} and TMEM119^{pos} microglia (green) in the hippocampus of PLX5622-treated mice at 12 days after surgery. Cell nuclei are show in blue (DAPI). Scale bar, 50 μm.

(C) Timeline for experiments testing the effect of microglial depletion on acquisition of the active place avoidance (APA) task at 12 days after surgery. Schematic diagram of APA setup, including visual cues, arena rotation (orange arrow), and shock zone location (red triangle).

(D) Distance traveled during habituation of APA testing ($F[1,28] = 0.832$).

(E) Entries into the shock zone across 5 days of APA testing. TBI mice fail to acquire this task ($F[3,28] = 16.17$, $p < 0.0001$), but loss of microglia in either these or sham-operated controls had no (additional) impact on cognitive abilities (testing day 5: "TBI control" versus "TBI PLX5622" and "Sham control" versus "Sham PLX5622," $p > 0.99$).

(F) APA performance plotted as "percentage change" in the number of shock zone entries on testing day 5 versus day 1 for individual mice. Note again the impact of TBI ($F[1,28] = 20.63$, $p < 0.0001$), but no change with PLX5622 treatment ($F[1,28] = 0.045$, $p = 0.83$).

(G–J) Experimental timeline for assessing hippocampal neurogenesis. Mice were fed either control or PLX5622-containing chow for the duration of the experiment. BrdU was injected twice daily on days 1–3 after surgery; a single 5-ethynyl-2′-deoxyuridine (EdU) injection was given 2 h prior to sacrifice at 12 days after surgery. Quantification of the number of immature (i.e., DCX^{pos}) neurons and Tbr2^{pos} intermediate neural progenitor cells in the ipsilateral dentate gyrus at 12 days post-TBI. All data are presented as "percentage change" relative to age-matched sham-operated controls. (G) The total number of DCX^{pos} cells was reduced by TBI ($F[1,28] = 258.2$, $p < 0.0001$) and further decreased with PLX5622 treatment; the number of newly generated neurons born during the (sub-) acute phase and surviving up until 12 days after TBI was not altered by PLX5622 treatment (H). Total (I) and proliferating (i.e., EdU^{pos}) (J) Tbr2^{pos} neural progenitor cells were increased after TBI (Tbr2^{pos}: $F[1,28] = 19.77$, $p = 0.0001$; Tbr2^{pos}EdU^{pos}: $F[1,28] = 22.36$, $p < 0.0001$) but not different between these and PLX5622-treated mice ($F[1,28] = 1.62$, $p = 0.21$).

Data are represented as mean ± SEM. Statistics: unpaired Student's t test (A), two-way ANOVA (D, F, and G–J), repeated-measures two-way ANOVA (E), followed by Bonferroni post hoc comparisons. (A) n = 3–5 per group per time-point; (D–F) n = 8 per group; (G–J) n = 9–10 per group. *$p < 0.05$, **$p < 0.01$, ***$p < 0.001$, ****$p < 0.0001$. ns, non-significant.

continuous PLX5622 treatment to induce microglia turnover (Figure S2B).

Induction of diphtheria toxin receptor (DTR) expression in CX_3CR1-expressing cells was achieved by oral gavage of 3- to 4-week-old mice with tamoxifen, leaving only microglia sensitive to DT-induced cell death after a 6-week rest period during which peripheral monocytes are turned over (Parkhurst et al., 2013); control mice received corn oil only. Administration of DT to tamoxifen-treated $CX_3CR1cre^{ERT2}$ x iDTR x tdTomato mice for three consecutive days prior to surgery indeed led to robust

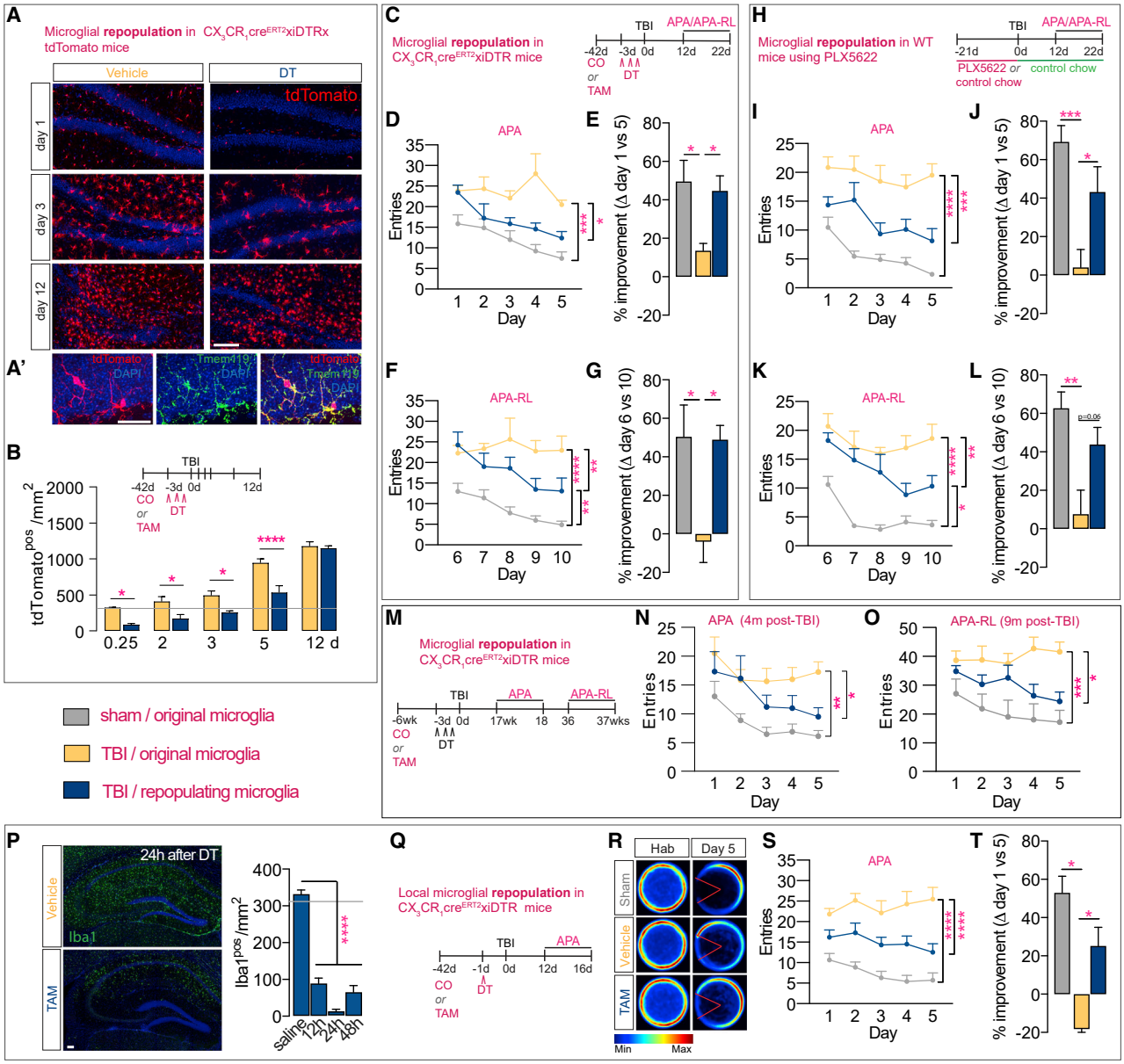


Figure 2. Microglial Depletion and Repopulation Improves Spatial Learning and Memory

(A) Turnover of tdTomato^{pos} microglia in the ipsilateral dentate gyrus of $CX_3CR1^{creERT2}$ x iDTR x tdTomato mice after DT injection and TBI.

(A') Higher-power confocal image confirming that tdTomato^{pos} (red) cells are TMEM119^{pos} (green) microglia.

(B) tdTomato^{pos} microglia numbers in the ipsilateral dentate gyrus of corn oil (vehicle) versus tamoxifen-treated after TBI and DT treatment. The gray line represents the sham average; ($F[1,24] = 44.3$, $p < 0.0001$).

(C) Experimental timeline for microglia depletion and repopulation in $CX_3CR1^{creERT2}$ x iDTR mice and subsequent APA testing.

(D) Entries into the shock zone during APA ($F[2,21] = 17.42$, $p < 0.001$); asterisks indicate post hoc results for testing day 5.

(E) Percentage improvement in APA performance, assessed by the change in entries on testing day 5 versus day 1 for individual mice ($F[2,21] = 5.851$, $p = 0.0096$).

(F) Entries into the shock zone during reversal learning (APA-RL) ($F[2,14] = 14.5$, $p = 0.0004$); asterisks indicate post hoc results for testing day 10.

(G) Percentage improvement in APA-RL performance for individual mice ($F[2,21] = 6.44$, $p = 0.0004$).

(H) Experimental timeline for microglia depletion and repopulation with transient PLX5622 treatment and APA testing.

(I) Shock zone entries for TBI mice with original or repopulating microglia ($F[2,21] = 23.5$, $p < 0.0001$); asterisks indicate post hoc results for APA testing day 5.

(J) Percentage improvement in APA performance for individual mice ($F[2,21] = 9.66$, $p = 0.0011$).

(K) Entries into the shock zone during APA-RL ($F[2,21] = 24.08$, $p < 0.0001$); asterisks indicate post hoc results for testing day 10.

(L) Percentage improvement in APA-RL performance for individual mice ($F[2,21] = 7.57$, $p = 0.0033$).

(M) Experimental timeline for assessing long-term effects of microglial depletion and repopulation in $CX_3CR1^{creERT2}$ x iDTR mice.

(legend continued on next page)

depletion (>70%) of microglia as expected (Figures 2A and 2B). Notably, repopulating microglia (tdTomato^{pos} Iba1^{pos} cells) started to appear in the hippocampus of TBI mice 3 days after the last DT injection (2 days after surgery) and reached sham control levels (corn oil treatment, gray line) by day 3 after injury, after which their numbers gradually became indistinguishable again from those in TBI mice that had not been subjected to microglial depletion (7 days after TBI onward) (Figure S2A); the repopulation dynamics were similar in the pharmacological approach (Figure S2B). Repopulating microglia were morphologically different (i.e., longer and more branched processes) from the brain's original microglia at 3 days after injury (Figures S2C–S2F). Astrogliosis was observed in response to TBI, but the number of astrocytes was not changed by microglia repopulation (Figure S2G).

Strikingly, both the genetic and pharmacological approach for inducing microglia turnover during the acute phase of TBI significantly ameliorated the learning deficits in the APA task at 12 days after injury (Figures 2C–2E and 2H–2J). Improvements in short-term ("within session") working memory were also found (Figure S2H). The behavioral improvements resulting from this microglial depletion and replenishment paradigm were further evident in an expanded re-learning paradigm (measure of cognitive flexibility) in which the shock zone was moved to the opposite location (APA-RL) (Figures 2F, 2G, 2K, and 2L), and also in the MWM (Figure S2J) and Y-maze (Figure S2K) tasks. These benefits were long-lasting and evident for at least 9 months after TBI (Figures 2M–2O). Delaying microglial depletion and repopulation to the more chronic phase of TBI (as well as continuous microglial depletion for >4 months after TBI) had no effect, however, on spatial learning in the APA task (Figure S2L). Last, to rule out any potential confounding effect from the depletion of CNS-resident macrophage populations in the meninges and/or choroid plexus (or elsewhere), we also directly injected DT into the hippocampus of CX$_3$CR1cre^{ERT2} x iDTR mice to selectively target and ablate microglia here (Figures 2P and S2M–S2P). When subjected to TBI and subsequently tested in APA 12 days later, these mice (but not vehicle-injected controls) also learned to successfully avoid the shock zone (Figures 2R–2T) and showed improvements in short-term ("within session") working memory (Figure S2I). Collectively, these findings demonstrate that the emergence of repopulating microglia in the brain significantly improves behavioral outcomes in two independent transient depletion paradigms.

Repopulating Microglia Stimulate Functional Neurogenesis after TBI

We next investigated whether enhanced neurogenesis could be part of the mechanism through which repopulating microglia augment cognitive function. Consistent with earlier observations (Figure 1G), TBI itself led to a >60% reduction in the total number of DCX^{pos} cells within the ipsilateral hippocampus of corn oil-treated CX$_3$CR1cre^{ERT2} x iDTR mice (i.e., those not sensitive to DT-mediated microglia depletion) compared with age-matched sham-operated controls. Strikingly however, the total number of immature DCX^{pos} neurons present in the brain after TBI was increased by ~2-fold in CX$_3$CR1cre^{ERT2} x iDTR mice that were subjected to microglia depletion and replenishment (tamoxifen-treated group) at both 12 days (Figures 3A–3C) and 4 months after TBI (Figure S3A). Pulse-chase experiments with BrdU further revealed a large increase in the number of newly generated neurons that were born after injury (i.e., DCX^{pos}BrdU^{pos} cells) and survived up until day 12 in TBI mice with repopulating microglia (Figure 3D). Increased presence (Figure 3E) and activity (Figure 3F) of hippocampal Tbr2^{pos} neuronal precursors was also observed at this time point. Similar increases in DCX^{pos} cell numbers were obtained when a pharmacological approach was used to induce microglial turnover during the acute phase of TBI (Figures 3G–3I). Greater presence and activity of Tbr2^{pos} neuronal precursor cells was also observed under these conditions (Figures 3J and 3K). To fully rule out peripheral and/or off-target effects, we directly injected DT into the hippocampus of sensitized CX$_3$CR1cre^{ERT2} x iDTR mice to only induce microglia turnover locally (Figure 3L). Once again, we observed significant benefits of microglial depletion and replenishment on after TBI neurogenesis (Figures 3M–3P).

Corroborative evidence for the putative neuroprotective effects of repopulating microglia was provided by experiments employing DCX^{creETR2} x tdTomato mice in which adult-born granule cells can be conspicuously labeled (Figures S3B and S3C). Tamoxifen treatment induced tdTomato expression in ~40% of immature neurons, which express DCX up to 3–4 weeks after their birth (Cheng et al., 2011) (Figure S3B). We observed increased survival of these immature tdTomato^{pos}DCX^{pos} neurons, and also of mature (tdTomato^{pos}DCX^{neg}) granule cells that were born/labeled >6 weeks prior to TBI (Figures S3C and S3D). We further observed greater complexity of tdTomato^{pos} dendrites in the presence of repopulating microglia (Figure S3E), and we were able to visualize tdTomato^{pos} projections and puncta within the

(N and O) Shock zone entries during APA at 4.5 months (N) and 9 months (O) post-TBI. (4.5 months: $F[2,18] = 6.72$, $p = 0.0066$; 9 months: $F[2,18] = 7.31$, $p = 0.0047$); asterisks indicate post hoc results for APA testing day 5.

(P) Local microglia depletion and repopulation through direct injection of DT into the hippocampus of sensitized (i.e., tamoxifen-treated) CX$_3$CR1^{creERT2} x iDTR mice. ($F[3,9] = 103.4$, $p < 0.0001$).

(Q) Experimental timeline for assessing the effect of local DT-induced microglia depletion and repopulation in CX$_3$CR1^{creERT2} x iDTR mice in subsequent APA testing.

(R) Merged heatmaps showing the proportion of time spent in a particular location during APA testing.

(S) Entries into the shock zone during APA testing for sham and TBI mice with original versus repopulating microglia ($F[2,32] = 19.39$, $p < 0.0001$); asterisks indicate post hoc results for APA testing day 5.

(T) Percentage improvement in APA performance for individual mice ($F[2,32] = 11.26$, $p = 0.0002$).

Data are represented as mean ± SEM. Statistics: two-way ANOVA (B), repeated-measures two-way ANOVA (D, F, I, K, N, O, and S), one-way ANOVA (E, G, J, L, P, and T), followed by Bonferroni post hoc comparison; n = 3–4 per group per time point (B and P), n = 8 per group (D–G and I–L), n = 7–8 per group (M–O), n = 10–15 per group (Q–T). *$p < 0.05$, **$p < 0.01$, ***$p < 0.001$, ****$p < 0.0001$. Scale bar, 50 μm (A), 100 μm (P). Abbreviations are as follows: CO, corn oil; TAM, tamoxifen; DT, diphtheria toxin; APA-RL, APA reversal learning.

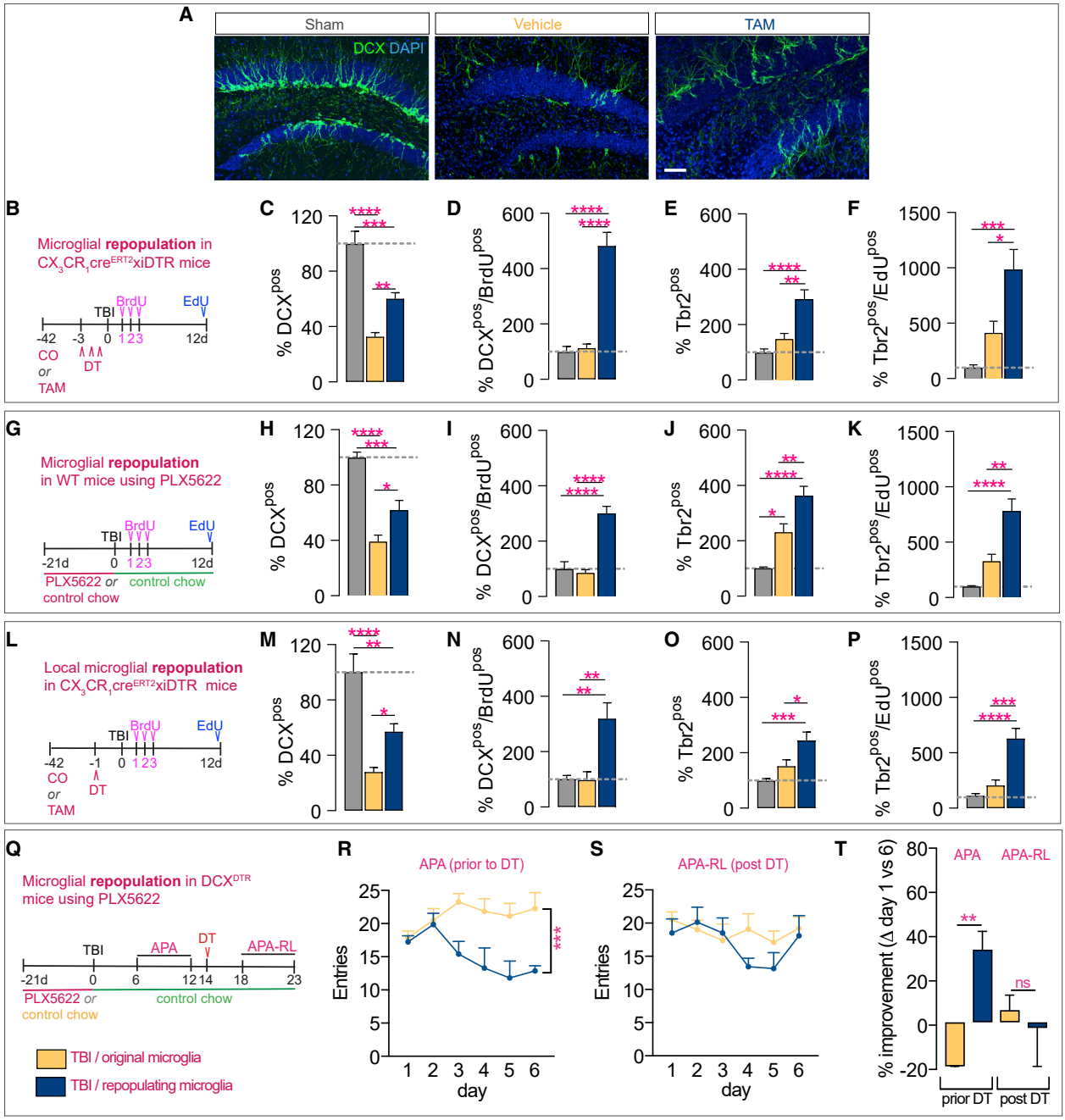


Figure 3. Microglial Depletion and Repopulation Promotes Functional Hippocampal Neurogenesis after TBI

(A) Confocal images of immature DCX^{pos} neurons in the hippocampus of sham and TBI mice with original (vehicle) versus repopulating (TAM) microglia (12 days post-surgery).

(B) Experimental timeline for intraperitoneal (i.p.) injections of DT, BrdU, and EdU in control (CO) and sensitized (TAM) $CX_3CR1^{creERT2}$ x iDTR mice.

(C) Quantification of total immature neurons at 12 days after injury ($F[2,25] = 34.36$, $p < 0.001$).

(D) Quantification of immature neurons born after TBI at 12 days after injury (i.e., DCX^{pos}BrdU^{pos}) ($F[2,25] = 42.87$, $p < 0.0001$).

(E) Quantification of intermediate Tbr2^{pos} neuronal progenitors at 12 days after injury ($F[2,25] = 15.41$, $p < 0.0001$)].

(F) Quantification of proliferating intermediate neuronal progenitors (Tbr2^{pos}EdU^{pos}) at 12 days after injury ($F[2,25] = 11.4$, $p = 0.0003$).

(G) Experimental timeline for microglial depletion and repopulation experiments using PLX5622.

(H) Total immature neurons at 12 days after injury ($F[2,22] = 26.05$, $p < 0.0001$).

(I) Immature neurons generated after TBI ($F[2,22] = 32.17$, $p < 0.0001$).

(legend continued on next page)

CA3 target region, suggesting integration (Figure S3F). Hippocampal tissue volumes were also found to be greater in the brains of mice that had undergone microglial depletion and repopulation (Figures S3G–S3I); for reassurance, these key findings were replicated in an independent laboratory (Figure S3J).

Notably, the neurogenic benefits of microglial depletion and replenishment were restricted to a narrow window during the first 3 days after injury, as microglial turnover after this time did not support the enhanced survival and production of newborn neurons (Figures S3K and S3L). Induction of microglial turnover 1 week prior to TBI also had no effect on the production or survival of newborn neurons at 12 days after TBI (Figure S3M), indicating that there is no benefit associated with replenished microglia per se.

Next, we assessed whether the increased number of DCX^{pos} cells in the brains of TBI mice with repopulating microglia contributed to improved behavioral outcomes. DCX^{DTR} mice were used to selectively ablate DCX^{pos} cells through unilateral intra-hippocampal injection of DT (Figure S3N) in sham and TBI mice, with and without repopulating microglia (Figure S3O). When we examined the spatial learning abilities of these mice (Figures 3Q–3T), the established improvements in APA learning of DCX^{DTR} mice with TBI and repopulating microglia (Figures 3R and 3T) were lost when newly born DCX^{pos} neurons were selectively ablated and the mice were subsequently challenged with a new learning paradigm in which the location of the shock zone was changed (APA-RL) (Figures 3S and 3T). These findings provide direct evidence that post-TBI neurogenesis in the mouse hippocampus is functional given that the microglia-dependent improvements in learning, under conditions where these cells are being actively turned over, disappear when DCX^{pos} cells are removed.

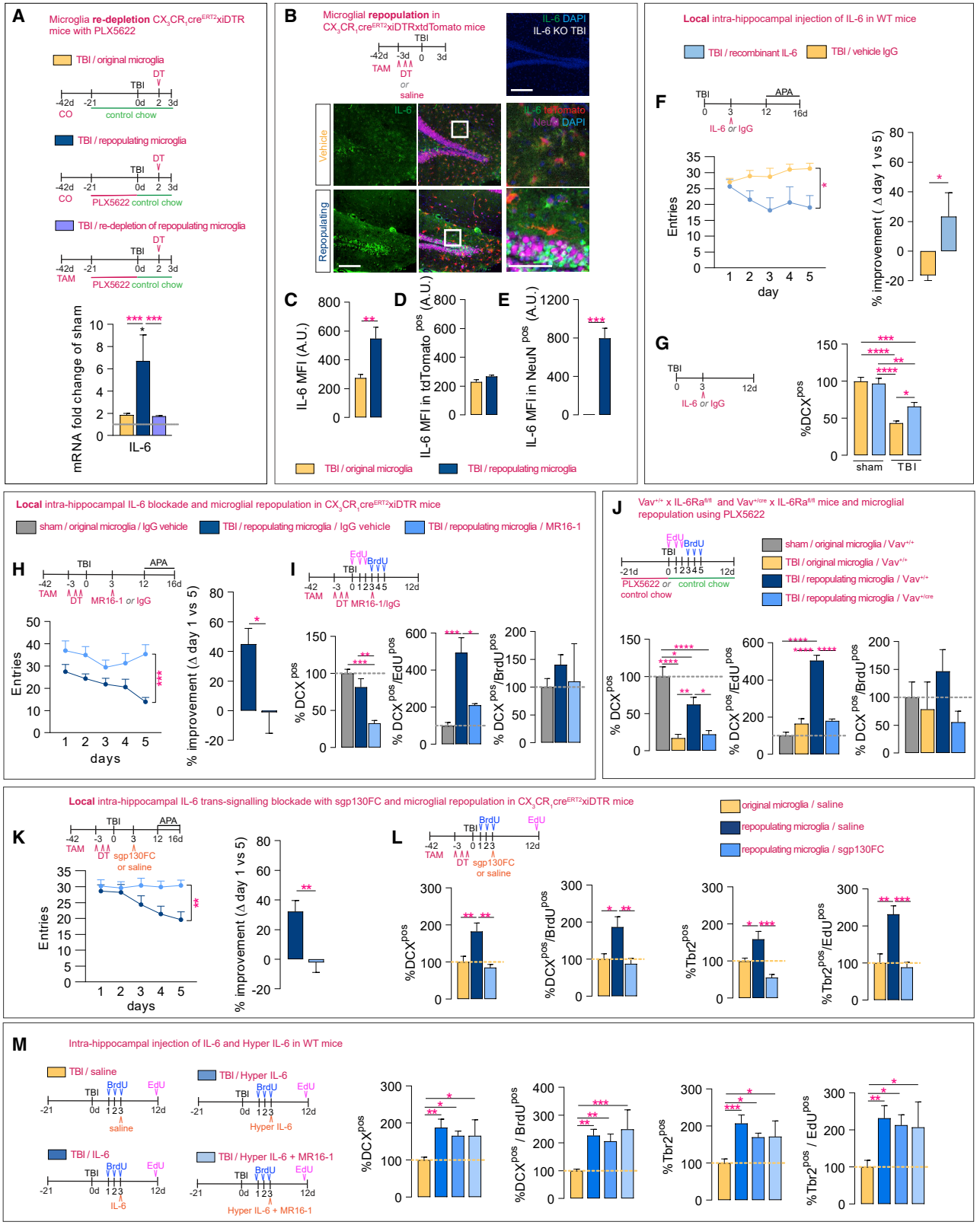
The Neuroprotective Effects of Repopulating Microglia Are Mediated via IL-6 *trans*-Signaling

Having established that active microglial turnover during the acute phase of TBI stimulates functional neurogenesis, we next explored the putative signaling pathway(s) that mediate these effects (Figure S4A). Of the various genes examined through qRT-PCR, we found that only interleukin-6 (IL-6) expression was significantly increased (>2.7-fold; $p < 0.001$) in the hippocampus of sensitized $CX_3CR1^{creERT2}$ x iDTR mice during the repopulation phase (3 days after TBI; i.e., when presence of replenishing microglia is required in order for these cells to be able to exert their neuroprotective and/or pro-regenerative effects). However, it is of note that TBI-induced increases in IL-1β and CXCL1 expression were almost abolished in the presence of repopulating microglia. Further exploration of genes associated with IL-6 signaling in whole hippocampal tissue homogenates showed that expression amounts of IL6Ra, IL-6 signal transducer (IL6st, also known as gp130 [IL6st/gp130]), and signal transducer and activator of transcription 3 (STAT3) were all increased with repopulating microglia (Figure S4B).

Given these findings, we next explored whether elevated IL-6 signaling could underpin the observed improvements in TBI outcomes. We first confirmed that repopulating microglia are indeed critically required for increased IL-6 expression by inducing the turnover of these cells with PLX5622 treatment in sensitized $CX_3CR1^{creERT2}$ x iDTR mice, followed by their local re-depletion with DT (Figure 4A). We then identified hippocampal granule cells as the main source of IL-6 after TBI under conditions where repopulating microglia are present (Figures 4B–4E). We also injected IL-6 itself directly into the hippocampus of wild-type (WT) TBI mice, theorizing that this would mimic a key change associated with the emergence of repopulating microglia. We indeed found that the IL-6 injection alone was sufficient to significantly improve both APA performance (Figure 4F) and neurogenesis (Figure 4G).

To further investigate the importance of increased IL-6 expression, we injected IL-6 receptor (IL-6Ra) blocking antibody MR16-1 (Tawara et al., 2011) ipsilaterally into the hippocampus on day 3 after TBI (i.e., when repopulating microglia are present) (Figure S4C). Blockade of IL-6 signaling locally in the hippocampus with MR16-1 indeed abolished both the behavioral (Figure 4H) and neurogenic benefits (Figure 4I) that were otherwise associated with microglial turnover in sensitized $CX_3CR1cre^{ERT2}$ x iDTR mice. MR16-1 treatment also slightly reduced microglia proliferation, but this did not alter the total number of these cells in the hippocampus compared with cells in that of controls (Figure S4D). To further address the role of IL-6, we next used Vav-Cre x $IL\text{-}6Ra^{flox/flox}$ mice to remove IL-6Ra from Vav-expressing cells, which include microglia (*vav* being one of the top 5% genes expressed by microglia) and hematopoietic cells (Ogilvy et al., 1999). Strikingly, the

(J and K) Total ($F[2,22] = 20.21$, $p < 0.0001$) (J) and proliferating intermediate neuronal progenitors ($F[2,22] = 17.18$, $p < 0.0001$) (K) at 12 days after injury.
(L) Experimental timeline for local microglial depletion and repopulation through intra-hippocampal DT injection into sensitized $CX_3CR1^{creERT2}$ x iDTR mice.
(M and N) Quantification of (M) total immature neurons ($F[2,23] = 19.29$, $p < 0.0001$) at 12 days post-injury, and (N) those born after TBI ($F[2,23] = 10.64$, $p = 0.0005$).
(O and P) Total ($F[2,23] = 10.1$, $p = 0.0007$) (O) and proliferating neuronal progenitor cells ($F[2,23] = 16.78$, $p < 0.0001$) (P) at 12 days after injury.
(Q) Experimental timeline for microglia depletion and repopulation in DCX^{DTR} mice with PLX5622, subsequent APA testing, DCX^{pos} cell depletion, and APA re-learning; all mice received DT injections.
(R) Entries into the shock zone during APA acquisition (i.e., prior DT administration) ($F[2,13] = 19.87$, $p = 0.0006$); asterisk indicates post hoc result for Testing Day 6.
(S) Shock zone entries for DCX^{DTR} mice during APA-RL, i.e., in the absence of newly generated neurons ($F[1,78] = 2.10$, $p = 0.15$; post hoc for testing day 6: $p > 0.99$).
(T) Percentage improvement for individual DCX^{DTR} mice in APA and APA-RL, i.e., before and after DT treatment ($F[1,13] = 9.78$, $p = 0.008$); asterisks indicate post hoc results.
Data are presented as the percentage change (mean ± SEM) from average of age-matched sham-operated control group (C–F, H–K, and M–P). Statistics: one-way ANOVA (C–F, H–K, and M–P), repeated-measures two-way ANOVA (R, S), two-way ANOVA (T), followed by Bonferroni post hoc comparison. (B–P) n = 8–10 per group; (Q–T) n = 7–8 per group. ns, non-significant. *$p < 0.05$, **$p < 0.01$, ***$p < 0.001$, ****$p < 0.0001$. (A) Scale bar, 100 μm. Abbreviations are as follows: DT, diphtheria toxin; APA-RL, APA reversal learning task.



(legend on next page)

increase in hippocampal neurogenesis after microglia turnover was completely lost in these conditional IL-6Ra gene knockout animals with TBI (Figure 4J). Neurogenesis levels in the contralateral (i.e., non-TBI) side were not significantly different between genotypes (Figures S4E–S4G). Collectively, these findings provide direct evidence that IL-6 signaling is critically required for the neuroprotective and/or pro-regenerative phenotype that is associated with repopulating microglia, and microglia-dependent improvements in TBI outcomes are lost under conditions where these cells are still present but where IL-6 signaling is blocked.

Biological effects of IL-6 are highly complex as they can be mediated via multiple pathways. Classic IL-6 signaling takes place mainly in immune cells via membrane-bound IL-6R, which engages the common signal transducing subunit gp130 to initiate downstream events. Importantly, however, IL-6 signaling can also occur in cells that do not express IL-6R through a process referred to as *trans*-signaling (for review, see Garbers and Rose-John, 2018). Here, soluble IL-6R (sIL-6R), generated through the proteolytic shedding of membrane-bound form, can bind IL-6 in the extracellular space and then induce signaling in virtually any cell type as gp130 is ubiquitously expressed.

To determine whether the positive effects of IL-6 signaling were mediated via the classic or *trans*-signaling pathway, we first injected soluble gp130-Fc, a protein that only blocks IL-6 *trans*-signaling (Jostock et al., 2001). We found that injection of sgp130-Fc into the hippocampus of TBI mice completely annulled the behavioral and neurogenic benefits that would otherwise be associated with the presence of repopulating microglia (Figures 4K and 4L). Key involvement of the IL-6 *trans*-signaling pathway was further and independently confirmed through the injection of hyper-IL-6, a fusion protein of sIL-6R and IL-6 that selectively and efficiently stimulates *trans*-signaling in gp130-expressing cells (Fischer et al., 1997) (Figure 4M). Corroborative evidence for this also came from the combined application of MR16-1 and hyper-IL-6, and for which no loss of an IL-6 effect on hippocampal neurogenesis was observed. Because MR16-1 blocks the IL-6 binding site on endogenous IL-6R, but cannot do so for hyper-IL-6, this leaves only *trans*-signaling pathway as the mechanism via which the established

Figure 4. Neuroprotective Effects of Repopulating Microglia Are Reliant on IL-6 *trans*-Signaling

(A) Experimental groups and qPCR data showing IL-6 expression in the ipsilateral hippocampus of $CX_3CR1^{CreERT2}$ x iDTR mice treated with either control chow or PLX5622 to induce microglia turnover, followed by re-depletion of repopulating microglia with DT in sensitized animals 3 days after TBI. Normalized IL-6 amounts are presented as the "fold change" from sham-operated controls (gray line) ($F[2,8] = 4.49$, $p = 0.049$).

(B–E) Experimental design and immunofluorescent images showing the source of cellular IL-6 in $CX_3CR1^{CreERT2}$ x iDTR mice with TBI and undergoing microglial repopulation (B). Quantification of (C) total IL-6 MFI ($t = 3.29$, $df = 6$), (D) IL-6 MFI within $tdTomato^{pos}$ microglia ($t = 2.10$, $df = 6$), and (E) IL-6 MFI within $NeuN^{pos}$ granule cells within the ipsilateral dentate gyrus ($t = 7.50$, $df = 6$) 3 days after TBI.

(F) Timeline and APA results for behavioral studies with wild-type (WT) TBI mice receiving intra-hippocampal injections of IL-6 or-IgG as a protein control. Improved APA acquisition was evident in IL-6-treated mice from both a reduced number of entries into the shock zone over time (left: $F[1,14] = 7.30$, $p = 0.017$; asterisk indicates post hoc result for testing day 5) and the temporal improvement in APA performance for individual mice (right: $t = 2.33$, $df = 14$, $p = 0.035$).

(G) Total immature (DCX^{pos}) neuron numbers in the ipsilateral granule cell layer of IL-6-treated WT TBI mice at 12 days after surgery ($F[1,28] = 3.06$, $p = 0.09$). Asterisks denote post hoc results.

(H) Experimental timeline and APA results for behavioral studies in sensitized $CX_3CR1^{CreERT2}$ x iDTR mice, treated with DT to induce microglia turnover, and then control IgG or MR16-1 to locally block IL-6 signaling. Graphs show shock zone entries (left: $F[1,13] = 11.25$, $p = 0.0052$; asterisks indicate post hoc results for testing day 5) and improvement in APA performance for individual mice (right: $t = 2.64$, $df = 13$).

(I) Timeline and quantitative results for experiments investigating the effect of IL-6 receptor (IL-6Ra) blockade on neurogenesis in $CX_3CR1^{CreERT2}$ x iDTR mice with TBI and repopulating microglia. Graphs show total immature (DCX^{pos}) neurons (left: $F[2,9] = 16.53$, $p = 0.0010$), immature neurons generated in the absence of microglia (i.e., $DCX^{pos}EdU^{pos}$ cells) and surviving to 12 days after injury (middle: $F[2,9] = 18.16$, $p = 0.0007$), and newly generated and surviving neurons born in the presence of repopulating microglia (i.e., $DCX^{pos}BrdU^{pos}$ cells; right); asterisks indicate post hoc results between indicated conditions.

(J) Experimental timeline and hippocampal neurogenesis data for studies involving $Vav^{+/cre}$ x $IL\text{-}6Ra^{flox/flox}$ TBI mice with and without PLX5622 treatment; sham controls are shown in gray. Quantification of total DCX^{pos} neurons (left: $F[3,17] = 18.63$, $p < 0.0001$), immature neurons generated in either in presence or absence of the brain's original microglia (i.e., $DCX^{pos}EdU^{pos}$ cells) and surviving to 12 days after injury (middle: $F[3,17] = 72.85$, $p < 0.0001$), as well as newly generated and surviving neurons that were born in the presence of repopulating microglia (i.e., $DCX^{pos}BrdU^{pos}$ cells), including for conditions where IL-6Ra was absent in Vav-expressing cells.

(K) Experimental design and APA results for experiments where IL-6 *trans*-signaling was blocked with sgp130FC in tamoxifen-sensitized $CX_3CR1^{CreERT2}$ x iDTR TBI mice undergoing microglial repopulation. Graphs show shock zone entries over the course of APA testing (left: $F[1,14] = 6.37$, $p = 0.024$; asterisks indicate post hoc results for testing day 5), and the percentage improvement in APA performance for individual mice (right: $t = 3.40$, $df = 14$).

(L) Experimental design and hippocampal neurogenesis data from control and sensitized $CX_3CR1^{CreERT2}$ x iDTR TBI mice, with repopulating microglia, and that were treated with sgp130FC or saline. Graphs show total (left: $F[2,19] = 11.48$, $p = 0.0005$) as well as newly generated and surviving (i.e., $BrdU^{pos}$) (right: $F[2,19] = 8.27$, $p = 0.0026$) DCX^{pos} neurons that were born in the presence of repopulating microglia, and where IL-6 *trans*-signaling was present or absent. Also shown are total (left: $F[2,19] = 13.26$, $p = 0.0002$) and proliferating (i.e., EdU^{pos}) (right: $F[2,19] = 10.96$, $p = 0.0007$) $Tbr2^{pos}$ intermediate neuronal progenitor cell numbers; asterisks indicate post hoc results for indicated conditions.

(M) Experimental design and hippocampal neurogenesis data for pharmacologic experiments probing the role of local IL-6 *trans*-signaling in TBI mice. Graphs show total (left: $F[3,28] = 5.77$, $p = 0.0033$) as well as newly generated and surviving (i.e., $BrdU^{pos}$) (right: $F[3,28] = 9.61$, $p = 0.0002$) DCX^{pos} neurons that were born in the presence of repopulating microglia, with and without IL-6 or hyper IL-6 stimulation. Total (left: $F[3,28] = 8.05$, $p = 0.0005$) and proliferating (i.e., EdU^{pos}) (right: $F[3,28] = 5.10$, $p = 0.0061$) $Tbr2^{pos}$ intermediate neuronal progenitor cell numbers are also shown for these conditions.

Data are represented as mean ± SEM (G, I, and J) Data presented as the percentage change (mean ± SEM) from average of age-matched sham-operated control group. (L and M) Data presented as the percentage change (mean ± SEM) from average of age-matched saline vehicle TBI-operated control group. (A–E, I, and J) n = 3–7 per group. (F–H, L, and M) n = 8–10 mice per group. Statistics: unpaired Student's t test (C–E; F, right; K, right), one-way ANOVA with Bonferroni post hoc comparison (A, I, J, L, and M), two-way ANOVA with repeat measures followed by Bonferroni post hoc comparison (F, left; H, left); two-way ANOVA followed by Bonferroni post hoc comparison (G). *$p < 0.05$, **$p < 0.01$, ***$p < 0.001$, ****$p < 0.0001$. Abbreviations are as follows: CO, corn oil; TAM, tamoxifen; DT, diphtheria toxin; MFI, mean fluorescence; a.u., arbitrary units.

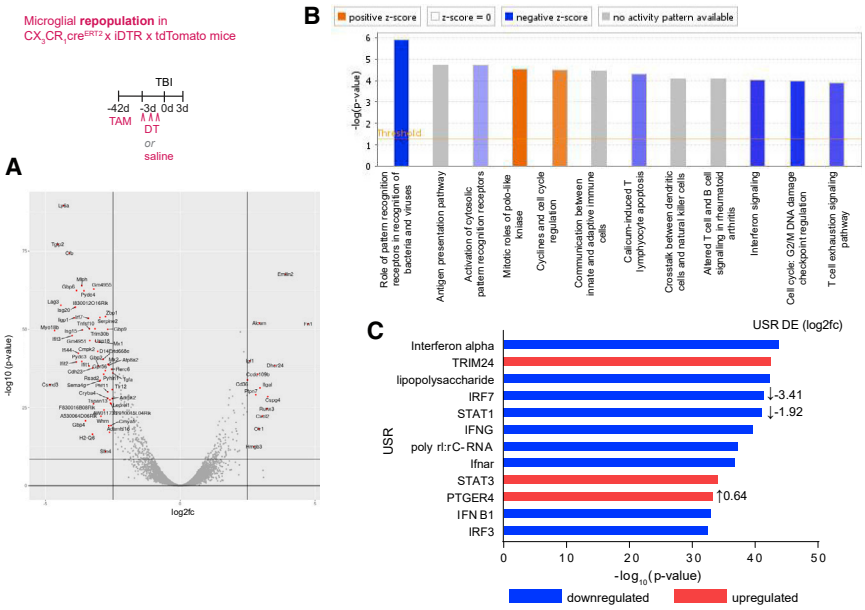


Figure 5. RNA-Sequencing Data of Differentially Expressed Genes and Altered Canonical and Regulatory Pathways in Repopulating Microglia

(A) Experimental design and volcano plot of top DEGs in repopulating tdTomato^{pos} microglia sorted from the ipsilateral hippocampus at 3 days after TBI.

(B) Ingenuity pathway analysis (IPA) for top 12 canonical pathways based on differential gene expression.

(C) Top-12 upstream regulators (USRs) with predicted activity. Differential expression of the upstream regulator (USR DE) is indicated on the right.

IL-6 effects are mediated in the presence of repopulating microglia.

Repopulating Microglia Have a Unique Transcriptional Profile and Modulate the Microenvironment after TBI

Having established that repopulating microglia exert neuroprotection and improve cognitive outcomes after TBI, we last investigated what makes these cells unique at a transcriptional level. For this investigation, we took advantage of $CX_3CR_1^{creERT2}$ x iDTR x tdTomato mice (6 weeks after gavage) in which the brain's microglia can be permanently labeled with the reporter tdTomato and then turned over with DT treatment (Figure 5A). The labeled (i.e., tdTomato^{pos}) original and repopulating microglia were isolated via fluorescence-activated cell sorting (FACS) from the hippocampus of saline and DT-injected mice (3 days after TBI), respectively, and then processed for subsequent downstream bulk RNA sequencing (RNA-seq).

Overall, a large number of differentially expressed genes (DEGs) were found when the transcriptome of the original and repopulating microglia was compared (3,146 DEGs using a false discovery rate [FDR] <0.05) (Figures S5A and S5B). In particular, repopulating microglia exhibited higher expression of genes that encode for proteins with known roles in wound healing and repair (e.g., *Emilin2*, *Fn1*, *Alcam*, and *Cspg4*) (Figure 5A). Ingenuity pathway analysis (IPA) further revealed decreased activity of canonical pathways involving pattern/damage recognition and interferon signaling (Figure 5B), in addition to reflecting the proliferative state of the repopulating microglia. Although the phenotype of the brain's original microglia population after TBI appears to reflect that of disease-associated microglia (DAMs) (Keren-Shaul et al., 2017), a vastly different transcriptional signature was found for repopulating microglia. Top upstream regulator (USR) predictions in repopulating microglia included downregulated activity of multiple type I interferon (IFN) pathway components (IFN-alpha, IRF7, STAT1, IRF3 IFNAR, and IFNB1) and increased activity of the STAT3 pathway (Figure 5C); IL-6 ranked as the 33rd USR. Consistent with the IPA USR predictions, an analysis of DNA-binding motif representation via ISMARA also demonstrated reduced IFN pathway activity in repopulating microglia on the basis of a strong correlation with the expression and activity of IRF7 and Stat2 in the individual samples (Figures S5C and S5D). Thus, the gene expression profile of repopulating microglia in the injured brain is fundamentally distinct to that of the original microglial population, and the major changes were a reduced reactive and enhanced proliferative state of the repopulating cells.

The benefits of repopulating microglia were once again confirmed in experiments involving Scl^{creERT2} x ZsGreen mice (4 weeks after gavage) with regards to neuroprotection (Figures S5E and S5F), and also through an attenuating effect on the recruitment of identified (i.e., ZsGreen^{pos}) infiltrating monocytes/macrophages and neutrophils (Figures S5G and S5I). Spatial transcriptomics further highlighted the influence of repopulating microglia on their local microenvironment. Specifically, there was a suppression of genes linked to the neurotoxic and/or neuroinflammatory (A1) phenotype of astrocytes (Figure S5J), as also confirmed at the protein level by co-staining these cells with the A1 marker C3 (Figure S5K).

DISCUSSION

There has been a long-held view, mostly based on correlative data, that activated microglia in the TBI brain contribute to inflammatory pathology and sequalae secondary to the original insult. In the present study, we took advantage of previously developed genetic (Parkhurst et al., 2013) and pharmacologic (Elmore et al., 2014) tools to selectively remove these cells from the brain and to study their role during various stages of injury. In doing so, we were able to reveal a critical time window during which microglia can be manipulated to adopt a phenotype that drives repair. We also uncovered an important role for IL-6 *trans*-signaling in mediating the beneficial outcomes.

Sustained Microglial Depletion with Continuous PLX5622 Treatment Does Not Alter Spatial Learning and Memory Abilities

Microglia are highly motile cells that rapidly respond to the release of danger signals that follow neuronal damage (Davalos et al., 2005). Their presence has been considered essential for neuroprotection, debris clearance, and repair (Neumann et al., 2009; Szalay et al., 2016; Jin et al., 2017). Normal physiological roles for microglia in synapse formation during motor learning have also been reported (Parkhurst et al., 2013). Somewhat surprisingly, but consistent with previous studies in naive mice (Dagher et al., 2015; Elmore et al., 2018), we show that the absence of microglia in uninjured (sham-operated) animals on continuous PLX5622 treatment had no impact on spatial learning and memory in a range of hippocampus-dependent tasks. Similarly, although TBI mice exhibited severe cognitive deficits, the absence or presence of microglia had no bearing on these. In addition, no change in learning and memory abilities was observed when microglia were removed from the brain during the more chronic phase of injury, providing direct evidence that, contrary to popular belief, the presence of these cells in an activated state does not necessarily interfere with higher cognitive functions.

Repopulating Microglia Support Functional Neurogenesis during a Critical Time Window after TBI

The neurogenic response to TBI might vary based on post-injury time and/or injury severity, but brain insults are mostly known to have disruptive effects on the production of new granule cells in the adult hippocampus (Ngwenya and Danzer, 2019). Our data reveal that this primarily stems from poor survival of newly generated DCX^{pos} neurons in the injured brain, rather than a deficit at the neural precursor level. Survival of newly generated neurons was not improved in the absence of microglia (i.e., with continuous PLX5622 treatment) indicating that, although in an activated state, these cells do not directly contribute to the death of newly generated DCX^{pos} neurons in the injured brain. Significant neuroprotection could be achieved by ceasing PLX5622 treatment, but only if the emergence of repopulating microglia coincided with the acute phase of TBI. We corroborated these pharmacological findings in a genetic model ($CX_3CR1cre^{ERT2}$ x iDTR mice) that similarly allows for rapid and very targeted depletion and repopulation of microglia, thereby allaying any concerns that off-target activity of PLX5622 and/or CSF-1R antagonism itself might have contributed to the outcomes observed. Our experiments in DCX^{DTR} mice further showed that augmented survival of newborn neurons directly contributed to improved spatial learning outcomes that persisted for many months after TBI. Although further studies are required to better understand how adult-born cells improve behavioral outcomes, these findings settle a long-standing debate as to whether neurogenesis in the injured mammalian brain is or can be functional. The timing of the observed effects is also entirely consistent with previous observations that adult-born neurons make synapses in the CA3 region as early as 2 weeks after their birth (Gu et al., 2012). Importantly, replenishing the resident microglial population prior to TBI did not confer any benefit. Thus, once turned over, repopulated brain microglia behave the same as their original counterparts, and there is thus no unique pro-regenerative phenotype associated with these cells per se. Similarly, when repopulating microglia were gated to re-emerge only during the post-acute phase of injury, the benefits in relation to survival of newly generated DCX^{pos} neurons and associated behavioral outcomes were also not present. In other words, we find that the neuroprotective effects of repopulating microglia is highly dependent on proper timing, i.e., it must temporally coincide with the microenvironment of the acute but not post-acute phase of injury. The latter finding is analogous to observations in regenerating organisms like the axolotl and zebrafish where presence of pro-regenerative myeloid cells is also critically required during the acute but not post-acute phases of injury in order for successful organ and/or tissue repair to take place (Godwin et al., 2013; Kyritsis et al., 2012). Collectively, our findings therefore demonstrate that the brain's resident microglial population does not actively inhibit endogenous repair processes, but rather lacks the ability to support these. A pro-neurogenic and/or neuroprotective microglial phenotype that actively supports brain repair can be induced through microglial turnover, as shown, but only if the active repopulation phase is made to coincide with the acute phase of TBI.

Neuroprotective Effects of Repopulating Microglia Require IL-6 *trans*-Signaling

The emergence of repopulating neuroprotective microglia during the acute stage of TBI was hallmarked by several key transcriptional changes. Most strikingly, there was a profound transient upregulation of IL-6, and we identified hippocampal granule cells as being the major source of this. The pleiotropic cytokine IL-6 has been ascribed both detrimental and beneficial roles in a range of neurological conditions (Rothaug et al., 2016), including in the context of CNS injury (Campbell et al., 2014; Codeluppi et al., 2014; Yang et al., 2012). We therefore directly probed the significance of increased IL-6 expression with repopulating microglia through a range of pharmacological studies. This allowed us to show that IL-6 signaling is indeed critically required for both the behavioral improvements and augmented survival of neurons, including newly generated ones, under TBI conditions where repopulating microglia are present. We further provide direct mechanistic evidence that these benefits result from *trans*-signaling by soluble IL-6Rα/IL-6 complexes rather than the classical pathway. Although the repopulating microglia are critical for induction of IL-6 in granule cells, the specific signal remains to be determined, as do questions on whether this IL-6 acts in a para- and/or autocrine manner via gp130. Several lines of evidence already suggest that *trans*-signaling by soluble IL-6/IL-6Rα might directly protect neurons against excitotoxic cell death through restricting the Ca^{2+} response to glutamate (März et al.,1998; Ma et al., 2015; Timper et al., 2017), induction of adenosine A1 receptor, anti-oxidants, and neurotrophic factor expression (Biber et al., 2008). Such a mechanism might not only apply to CNS insult but also more broadly to physiological conditions in which microglia are known to positively modulate adult hippocampal neurogenesis (e.g., voluntary exercise) and where IL-6 is known to be upregulated (Nybo et al., 2002). Other obvious areas for further investigation would be whether IL-6 *trans*-signaling contributes to the unique transcriptional profile

of the repopulating microglia themselves, and also whether it plays a role in astrocyte polarization by suppressing the less favorable A1 phenotype (Liddelow et al., 2017).

We conclude that the presence of activated microglia in brain regions adversely affected by insult does not necessarily have a negative bearing on outcomes and/or cognitive dysfunction. Rather, in the post-insult brain, activated microglia seem to mostly lack the ability to support endogenous repair processes. A pro-regenerative microglia phenotype can be induced, however, in the mammalian brain and, as for regenerating organisms like the axolotl and zebrafish (Godwin et al., 2013), inflammatory signals play a key role in this. We already uncovered a critical role for IL-6 signaling in association with this beneficial phenotype, and future studies can now focus on further defining how the unique phenotypic signature of repopulating microglia can be taken advantage of therapeutically.

STAR★METHODS

Detailed methods are provided in the online version of this paper and include the following:

- KEY RESOURCES TABLE
- LEAD CONTACT AND MATERIALS AVAILABILITY
- EXPERIMENTAL MODEL AND SUBJECT DETAILS
- METHOD DETAILS
  - Microglial depletion and repopulation
  - Controlled cortical impact model of traumatic brain injury
  - Active place avoidance
  - Morris water maze
  - Y-maze
  - Labeling of newborn cells
  - MR Imaging
  - Tissue preparation for histology and immunostaining
  - Immunofluorescence
  - Imaging and cell quantification
  - Replication experiments
  - Intra-hippocampal injections
  - Real time quantitative PCR
  - Hippocampal cell preparations and fluorescence-activated cell sorting
  - RNA sequencing library preparation and NextSeq High Output 1x75bp
  - Analysis of RNA-Seq data
  - Labeling of blood-derived cells
  - Spatial transcriptomics
- QUANTIFICATION AND STATISTICAL ANALYSIS
- DATA AND CODE AVAILABILITY

SUPPLEMENTAL INFORMATION

Supplemental Information can be found online at https://doi.org/10.1016/j.cell.2020.02.013.

ACKNOWLEDGMENTS

We thank J. Yu, K.C. Leong, R. Adams, and N. Kurniawan for experimental assistance; the staff of UQ's Biological Resources Facility for breeding and maintaining the animals in this study; G.R. Hill for vavcre x IL6R mouse line, Alan Ho for statistical assistance; T. Bruxner for RNA-seq assistance; V. Nink for flow cytometry assistance; R. Tweedale for editorial assistance; N. Valmas for graphic design; and S. Millard, S. Thor, J. Goetz, and B. Key for critical reading and comments on the manuscript. Imaging was performed at the School of Biomedical Sciences and the Queensland Brain Institute (QBI)'s Advanced Microscopy Facilities. Behavioral tests were performed at the QBI's Behavior and Surgical Facility. FACS was performed at the QBI's Flow Cytometry Facility. RNA-seq library preparation and sequencing was performed at the Institute for Molecular Bioscience Sequencing Facility (UQ). We acknowledge QIMR Berghofer scientific services, the Genome Informatics Group and Medical Genomics Groups for their support in the RNA-seq analysis, and A. Lam and D. Pham for assisting with generating and analyzing the spatial transcriptomics data. J.V. is the recipient of an Australian Research Council Discovery Early Career Research Award (DE150101578) and National Health and Medical Research Council (NHMRC) project grant (1124503). E.F.W. is supported by the Herdsman Fellowship in Medical Science (UQ). M.J.R. is supported by SpinalCure Australia, the Wings for Life Spinal Cord Research Foundation, and the NHMRC (1060538 and 1163835). A.L.G. was supported by UQ-StemCARE funding.

AUTHOR CONTRIBUTIONS

Conceptualization, J.V.; Methodology, E.F.W., J.V., and K.P.A.M.; Investigation, E.F.W., A.L.G., K.P.A.M., E.R.G., Q.H.N., D.C.A., A.G.Y., W.S., and S.B.R.H.; Writing – Original Draft, E.F.W., J.V., and M.J.R; Writing – Review & Editing, J.V. and M.J.R.; Funding Acquisition, J.V.; Resources, J.V., K.P.A.M., M.J.R., P.F.B., and S.R.-J.; Supervision, J.V.; Funding, J.V.

DECLARATION OF INTERESTS

The authors declare no competing interests.

Received: May 2, 2019
Revised: November 21, 2019
Accepted: February 5, 2020
Published: March 5, 2020

REFERENCES

Bellver-Landete, V., Bretheau, F., Mailhot, B., Vallières, N., Lessard, M., Janelle, M.E., Vernoux, N., Tremblay, M.E., Fuehrmann, T., Shoichet, M.S., and Lacroix, S. (2019). Microglia are an essential component of the neuroprotective scar that forms after spinal cord injury. Nat. Commun. *10*, 518.

Bennett, M.L., Bennett, F.C., Liddelow, S.A., Ajami, B., Zamanian, J.L., Fernhoff, N.B., Mulinyawe, S.B., Bohlen, C.J., Adil, A., Tucker, A., et al. (2016). New tools for studying microglia in the mouse and human CNS. Proc. Natl. Acad. Sci. USA *113*, E1738–E1746.

Bianchi, M.E. (2007). DAMPs, PAMPs and alarmins: all we need to know about danger. J. Leukoc. Biol. *81*, 1–5.

Biber, K., Pinto-Duarte, A., Wittendorp, M.C., Dolga, A.M., Fernandes, C.C., Von Frijtag Drabbe Künzel, J., Keijser, J.N., de Vries, R., Ijzerman, A.P., Ribeiro, J.A., et al. (2008). Interleukin-6 upregulates neuronal adenosine A1 receptors: implications for neuromodulation and neuroprotection. Neuropsychopharmacology *33*, 2237–2250.

Bradley, C.K., Takano, E.A., Göthert, J.R., Göttgens, B., Green, A.R., Begley, C.G., and van Eekelen, J.A. (2007). Temporal regulation of Cre-recombinase activity in Scl-positive neurons of the central nervous system. Genesis *45*, 145–151.

Butovsky, O., Jedrychowski, M.P., Moore, C.S., Cialic, R., Lanser, A.J., Gabriely, G., Koeglsperger, T., Dake, B., Wu, P.M., Doykan, C.E., et al. (2014). Identification of a unique TGF-β-dependent molecular and functional signature in microglia. Nat. Neurosci. *17*, 131–143.

Buttgereit, A., Lelios, I., Yu, X., Vrohlings, M., Krakoski, N.R., Gautier, E.L., Nishinakamura, R., Becher, B., and Greter, M. (2016). Sall1 is a transcriptional

regulator defining microglia identity and function. Nat. Immunol. *17*, 1397–1406.

Campbell, I.L., Erta, M., Lim, S.L., Frausto, R., May, U., Rose-John, S., Scheller, J., and Hidalgo, J. (2014). Trans-signaling is a dominant mechanism for the pathogenic actions of interleukin-6 in the brain. J. Neurosci. *34*, 2503–2513.

Cheng, X., Li, Y., Huang, Y., Feng, X., Feng, G., and Xiong, Z.Q. (2011). Pulse labeling and long-term tracing of newborn neurons in the adult subgranular zone. Cell Res. *21*, 338–349.

Codeluppi, S., Fernandez-Zafra, T., Sandor, K., Kjell, J., Liu, Q., Abrams, M., Olson, L., Gray, N.S., Svensson, C.I., and Uhlén, P. (2014). Interleukin-6 secretion by astrocytes is dynamically regulated by PI3K-mTOR-calcium signaling. PLoS ONE *9*, e92649.

Dagher, N.N., Najafi, A.R., Kayala, K.M., Elmore, M.R., White, T.E., Medeiros, R., West, B.L., and Green, K.N. (2015). Colony-stimulating factor 1 receptor inhibition prevents microglial plaque association and improves cognition in 3xTg-AD mice. J. Neuroinflammation *12*, 139.

Davalos, D., Grutzendler, J., Yang, G., Kim, J.V., Zuo, Y., Jung, S., Littman, D.R., Dustin, M.L., and Gan, W.B. (2005). ATP mediates rapid microglial response to local brain injury in vivo. Nat. Neurosci. *8*, 752–758.

Elmore, M.R., Najafi, A.R., Koike, M.A., Dagher, N.N., Spangenberg, E.E., Rice, R.A., Kitazawa, M., Matusow, B., Nguyen, H., West, B.L., and Green, K.N. (2014). Colony-stimulating factor 1 receptor signaling is necessary for microglia viability, unmasking a microglia progenitor cell in the adult brain. Neuron *82*, 380–397.

DeLuca, D.S., Levin, J.Z., Sivachenko, A., Fennell, T., Nazaire, M.D., Williams, C., Reich, M., Winckler, W., and Getz, G. (2012). RNA-SeQC: RNA-seq metrics for quality control and process optimization. Bioinformatics *28*, 1530–1532.

Dobin, A., Davis, C.A., Schlesinger, F., Drenkow, J., Zaleski, C., Jha, S., Batut, P., Chaisson, M., and Gingeras, T.R. (2013). STAR: ultrafast universal RNA-seq aligner. Bioinformatics. https://doi.org/10.1093/bioinformatics/bts635.

Elmore, M.R.P., Hohsfield, L.A., Kramár, E.A., Soreq, L., Lee, R.J., Pham, S.T., Najafi, A.R., Spangenberg, E.E., Wood, M.A., West, B.L., and Green, K.N. (2018). Replacement of microglia in the aged brain reverses cognitive, synaptic, and neuronal deficits in mice. Aging Cell *17*, e12832.

Ertürk, A., Mentz, S., Stout, E.E., Hedehus, M., Dominguez, S.L., Neumaier, L., Krammer, F., Llovera, G., Srinivasan, K., Hansen, D.V., et al. (2016). Interfering with the chronic immune response rescues chronic degeneration after traumatic brain injury. J. Neurosci. *36*, 9962–9975.

Fischer, M., Goldschmitt, J., Peschel, C., Brakenhoff, J.P., Kallen, K.J., Wollmer, A., Grötzinger, J., and Rose-John, S. (1997). I. A bioactive designer cytokine for human hematopoietic progenitor cell expansion. Nat. Biotechnol. *15*, 142–145.

Garbers, C., and Rose-John, S. (2018). Dissecting interleukin-6 classic- and trans-signaling in inflammation and cancer. Methods Mol. Biol. *1725*, 127–140.

Ginhoux, F., Greter, M., Leboeuf, M., Nandi, S., See, P., Gokhan, S., Mehler, M.F., Conway, S.J., Ng, L.G., Stanley, E.R., et al. (2010). Fate mapping analysis reveals that adult microglia derive from primitive macrophages. Science *330*, 841–845.

Giulian, D., Chen, J., Ingeman, J.E., George, J.K., and Noponen, M. (1989). The role of mononuclear phagocytes in wound healing after traumatic injury to adult mammalian brain. J. Neurosci. *9*, 4416–4429.

Godwin, J.W., Pinto, A.R., and Rosenthal, N.A. (2013). Macrophages are required for adult salamander limb regeneration. Proc. Natl. Acad. Sci. USA *110*, 9415–9420.

Göthert, J.R., Gustin, S.E., Hall, M.A., Green, A.R., Göttgens, B., Izon, D.J., and Begley, C.G. (2005). In vivo fate-tracing studies using the Scl stem cell enhancer: embryonic hematopoietic stem cells significantly contribute to adult hematopoiesis. Blood *105*, 2724–2732.

Gu, Y., Arruda-Carvalho, M., Wang, J., Janoschka, S.R., Josselyn, S.A., Frankland, P.W., and Ge, S. (2012). Optical controlling reveals time-dependent roles for adult-born dentate granule cells. Nature Neuroscience *15*, 1700–1706.

Haage, V., Semtner, M., Vidal, R.O., Hernandez, D.P., Pong, W.W., Chen, Z., Hambardzumyan, D., Magrini, V., Ly, A., Walker, J., et al. (2019). Comprehensive gene expression meta-analysis identifies signature genes that distinguish microglia from peripheral monocytes/macrophages in health and glioma. Acta Neuropathol. Commun. *7*, 20.

Hanisch, U.K., and Kettenmann, H. (2007). Microglia: active sensor and versatile effector cells in the normal and pathologic brain. Nat. Neurosci. *10*, 1387–1394.

Hickman, S., Izzy, S., Sen, P., Morsett, L., and El Khoury, J. (2018). Microglia in neurodegeneration. Nat. Neurosci. *21*, 1359–1369.

Hilla, A.M., Diekmann, H., and Fischer, D. (2017). Microglia are irrelevant for neuronal degeneration and axon regeneration after acute injury. J. Neurosci. *37*, 6113–6124.

Hodge, R.D., Nelson, B.R., Kahoud, R.J., Yang, R., Mussar, K.E., Reiner, S.L., and Hevner, R.F. (2012). Tbr2 is essential for hippocampal lineage progression from neural stem cells to intermediate progenitors and neurons. Journal of Neuroscience *32*, 6275–6287.

Hoeffel, G., and Ginhoux, F. (2018). Fetal monocytes and the origins of tissue-resident macrophages. Cell. Immunol. *330*, 5–15.

Hong, H., Kim, B.S., and Im, H.I. (2016). Pathophysiological role of neuroinflammation in neurodegenerative diseases and psychiatric disorders. Int. Neurourol. J. *20* (*Suppl 1*), S2–S7.

Jassam, Y.N., Izzy, S., Whalen, M., McGavern, D.B., and El Khoury, J. (2017). Neuroimmunology of traumatic brain injury: time for a paradigm shift. Neuron *95*, 1246–1265.

Jin, W.N., Shi, S.X., Li, Z., Li, M., Wood, K., Gonzales, R.J., and Liu, Q. (2017). Depletion of microglia exacerbates postischemic inflammation and brain injury. J. Cereb. Blood Flow Metab. *37*, 2224–2236.

Jostock, T., Müllberg, J., Ozbek, S., Atreya, R., Blinn, G., Voltz, N., Fischer, M., Neurath, M.F., and Rose-John, S. (2001). Soluble gp130 is the natural inhibitor of soluble interleukin-6 receptor transsignaling responses. Eur. J. Biochem. *268*, 160–167.

Keren-Shaul, H., Spinrad, A., Weiner, A., Matcovitch-Natan, O., Dvir-Szternfeld, R., Ulland, T.K., David, E., Baruch, K., Lara-Astaiso, D., Toth, B., et al. (2017). A unique microglia type associated with restricting development of Alzheimer's disease. Cell *169*, 1276–1290.e17.

Kettenmann, H., Hanisch, U.K., Noda, M., and Verkhratsky, A. (2011). Physiology of microglia. Physiol. Rev. *91*, 461–553.

Kyritsis, N., Kizil, C., Zocher, S., Kroehne, V., Kaslin, J., Freudenreich, D., Iltzsche, A., and Brand, M. (2012). Acute inflammation initiates the regenerative response in the adult zebrafish brain. Science *338*, 1353–1356.

Li, B., and Dewey, C.N. (2011). LRSEM: accurate transcript quantification from RNA-Seq data with or without a reference genome. BMC Bioinformatics *12*. https://doi.org/10.1186/1471-2105-12-323.

Liddelow, S.A., Guttenplan, K.A., Clarke, L.E., Bennett, F.C., Bohlen, C.J., Schirmer, L., Bennett, M.L., Münch, A.E., Chung, W.S., Peterson, T.C., et al. (2017). Neurotoxic reactive astrocytes are induced by activated microglia. Nature *541*, 481–487.

Ma, S.H., Zhuang, Q.X., Shen, W.X., Peng, Y.P., and Qiu, Y.H. (2015). Interleukin-6 reduces NMDAR-mediated cytosolic Ca^{2+} overload and neuronal death via JAK/CaN signaling. Cell Calcium *58*, 286–295.

Martin, M. (2011). Cutadapt removes adapter sequences from high-throughput sequencing reads. EMBnet. journal *17*. http://journal.embnet.org/index.php/embnetjournal/article/view/200/479.

März, P., Cheng, J.G., Gadient, R.A., Patterson, P.H., Stoyan, T., Otten, U., and Rose-John, S. (1998). Sympathetic neurons can produce and respond to interleukin 6. Proc. Natl. Acad. Sci. USA *95*, 3251–3256.

Neumann, H., Kotter, M.R., and Franklin, R.J. (2009). Debris clearance by microglia: an essential link between degeneration and regeneration. Brain *132*, 288–295.

Ngwenya, L.B., and Danzer, S.C. (2019). Impact of traumatic brain injury on neurogenesis. Front. Neurosci. *12*, 1014.

Nybo, L., Nielsen, B., Pedersen, B.K., Møller, K., and Secher, N.H. (2002). Interleukin-6 release from the human brain during prolonged exercise. J. Physiol. *542*, 991–995.

Ogilvy, S., Metcalf, D., Gibson, L., Bath, M.L., Harris, A.W., and Adams, J.M. (1999). Promoter elements of vav drive transgene expression in vivo throughout the hematopoietic compartment. Blood *94*, 1855–1863.

Paolicelli, R.C., Bolasco, G., Pagani, F., Maggi, L., Scianni, M., Panzanelli, P., Giustetto, M., Ferreira, T.A., Guiducci, E., Dumas, L., et al. (2011). Synaptic pruning by microglia is necessary for normal brain development. Science *333*, 1456–1458.

Parkhurst, C.N., Yang, G., Ninan, I., Savas, J.N., Yates, J.R., 3rd, Lafaille, J.J., Hempstead, B.L., Littman, D.R., and Gan, W.B. (2013). Microglia promote learning-dependent synapse formation through brain-derived neurotrophic factor. Cell *155*, 1596–1609.

Rao, M.S., and Shetty, A.K. (2004). Efficacy of doublecortin as a marker to analyse the absolute number and dendritic growth of newly generated neurons in the adult dentate gyrus. Eur. J. Neurosci. *19*, 234–246.

Rice, R.A., Spangenberg, E.E., Yamate-Morgan, H., Lee, R.J., Arora, R.P., Hernandez, M.X., Tenner, A.J., West, B.L., and Green, K.N. (2015). Elimination of microglia improves functional outcomes following extensive neuronal loss in the hippocampus. J. Neurosci. *35*, 9977–9989.

Rice, R.A., Pham, J., Lee, R.J., Najafi, A.R., West, B.L., and Green, K.N. (2017). Microglial repopulation resolves inflammation and promotes brain recovery after injury. Glia *65*, 931–944.

Robinson, M.D., McCarthy, D.J., and Smyth, G.K. (2010). edgeR: a Bioconductor package for differential expression analysis of digital gene expression data. Bioinformatics. *26*, 139–140.

Rothaug, M., Becker-Pauly, C., and Rose-John, S. (2016). The role of interleukin-6 signaling in nervous tissue. Biochim. Biophys. Acta *1863* (6 Pt A), 1218–1227.

Schafer, D.P., Lehrman, E.K., Kautzman, A.G., Koyama, R., Mardinly, A.R., Yamasaki, R., Ransohoff, R.M., Greenberg, M.E., Barres, B.A., and Stevens, B. (2012). Microglia sculpt postnatal neural circuits in an activity and complement-dependent manner. Neuron *74*, 691–705.

Scott, G., Zetterberg, H., Jolly, A., Cole, J.H., De Simoni, S., Jenkins, P.O., Feeney, C., Owen, D.R., Lingford-Hughes, A., Howes, O., et al. (2018). Minocycline reduces chronic microglial activation after brain trauma but increases neurodegeneration. Brain *141*, 459–471.

Simon, D.W., McGeachy, M.J., Bayır, H., Clark, R.S., Loane, D.J., and Kochanek, P.M. (2017). The far-reaching scope of neuroinflammation after traumatic brain injury. Nat. Rev. Neurol. *13*, 171–191.

Szalay, G., Martinecz, B., Lénárt, N., Környei, Z., Orsolits, B., Judák, L., Császár, E., Fekete, R., West, B.L., Katona, G., et al. (2016). Microglia protect against brain injury and their selective elimination dysregulates neuronal network activity after stroke. Nat. Commun. *7*, 11499.

Tawara, K., Oxford, J.T., and Jorcyk, C.L. (2011). Clinical significance of interleukin (IL)-6 in cancer metastasis to bone: potential of anti-IL-6 therapies. Cancer Manag. Res. *3*, 177–189.

Timper, K., Denson, J.L., Steculorum, S.M., Heilinger, C., Engström-Ruud, L., Wunderlich, C.M., Rose-John, S., Wunderlich, F.T., and Brüning, J.C. (2017). IL-6 improves energy and glucose homeostasis in obesity via enhanced central IL-6 trans-signaling. Cell Rep. *19*, 267–280.

Vukovic, J., Colditz, M.J., Blackmore, D.G., Ruitenberg, M.J., and Bartlett, P.F. (2012). Microglia modulate hippocampal neural precursor activity in response to exercise and aging. J. Neurosci. *32*, 6435–6443.

Vukovic, J., Borlikova, G.G., Ruitenberg, M.J., Robinson, G.J., Sullivan, R.K., Walker, T.L., and Bartlett, P.F. (2013). Immature doublecortin-positive hippocampal neurons are important for learning but not for remembering. J. Neurosci. *33*, 6603–6613.

Wang, X., Gao, X., Michalski, S., Zhao, S., and Chen, J. (2016). Traumatic brain injury severity affects neurogenesis in adult mouse hippocampus. J. Neurotrauma *33*, 721–733.

Weber, M.D., McKim, D.B., Niraula, A., Witcher, K.G., Yin, W., Sobol, C.G., Wang, Y., Sawicki, C.M., Sheridan, J.F., and Godbout, J.P. (2019). The influence of microglial elimination and repopulation on stress sensitization induced by repeated social defeat. Biol. Psychiatry *85*, 667–678.

Willis, E.F., Bartlett, P.F., and Vukovic, J. (2017). Protocol for short- and longer-term spatial learning and memory in mice. Front. Behav. Neurosci. *11*, 197.

Wolf, S.A., Boddeke, H.W., and Kettenmann, H. (2017). Microglia in physiology and disease. Annu. Rev. Physiol. *79*, 619–643.

Yang, P., Wen, H., Ou, S., Cui, J., and Fan, D. (2012). IL-6 promotes regeneration and functional recovery after cortical spinal tract injury by reactivating intrinsic growth program of neurons and enhancing synapse formation. Exp. Neurol. *236*, 19–27.

Yona, S., Kim, K.W., Wolf, Y., Mildner, A., Varol, D., Breker, M., Strauss-Ayali, D., Viukov, S., Guilliams, M., Misharin, A., et al. (2013). Fate mapping reveals origins and dynamics of monocytes and tissue macrophages under homeostasis. Immunity *38*, 79–91.

STAR★METHODS

KEY RESOURCES TABLE

REAGENT or RESOURCE	SOURCE	IDENTIFIER
Antibodies		
Guineapig anti-doublecortin (polyclonal)	Merck/Millipore	Cat#AB2253; RRID: AB_1586992
Rabbit anti-Iba1 (polyclonal)	Wako	Cat#019-19741; RRID: AB_839504
Rat anti-BrdU (monoclonal; clone BU1/75)	Abcam	Cat#ab6326; RRID: AB_305426
Mouse anti-GFAP (monoclonal; clone GA5)	Merck/Millipore	Cat#MAB360; RRID: AB_11212597
Rabbit anti-Tbr2 (monoclonal)	Abcam	Cat#ab183991; RRID: AB_2721040
Rabbit anti-TMEM119 (monoclonal)	Abcam	Cat#ab209064; RRID: AB_ 2800343
Mouse anti-IL-6 (monoclonal)	Abcam	Cat#ab9324; RRID: AB_307175
Rat anti-C3 11H9 clone (monoclonal)	Hycult Biotech	Cat#HM1045; RRID: AB_10129042
Alexa Fluor® 488 AffiniPure Fab Fragment Donkey Anti-Rat IgG (H+L)	Jackson ImmunoResearch	Cat#712-547-003; RRID: AB_2340687
Goat anti-Rat IgG (H+L) Cross-Adsorbed Secondary Antibody, Alexa Fluor® 647	ThermoFisher	Cat#A-21247; RRID: AB_141778
Goat anti-Rabbit IgG (H+L) Cross-Adsorbed Secondary Antibody, Alexa Fluor 568	ThermoFisher	Cat#A-11011; RRID: AB_143157
Goat anti-Guinea Pig IgG (H+L) Highly Cross-Adsorbed Secondary Antibody, Alexa Fluor 488	ThermoFisher	Cat#A-11073; RRID: AB_142018
Goat anti-Rat IgG (H+L) Cross-Adsorbed Secondary Antibody, Alexa Fluor 647	ThermoFisher	Cat#A-21247; RRID: AB_141778
Goat anti-Rabbit IgG (H+L) Cross-Adsorbed Secondary Antibody, Alexa Fluor 647	ThermoFisher	Cat#A-21244; RRID: AB_141663
Chemicals, Peptides, and Recombinant Proteins		
Tamoxifen	Sigma	Cat#T5648
Diphtheria toxin	Sigma	Cat#D0564-1MG
5-Bromo-2′ -deoxyuridine	Sigma	Cat#B5002-5G
5-ethynyl-2′ deoxyuridine	Santa Cruz	Cat#61135-33-9
Corn oil	Sigma	Cat#C8267-500ML
Formalin, neutral buffered, 10%	Sigma	Cat#HT501128-4L
MicroAmp EnduraPlate Optical 384-well clear reaction plates	Life Technologies	Cat#4483285
TRI Reagent	Sigma	Cat#T9424-200ML
Papain	Worthington Biochemical Corporation	Cat#LS003120
Goat Serum, New Zealand origin	Life Technologies	Cat#16210064
DNase I	Roche	Cat#10104159001
Penicillin Streptomycin	Life Technologies	Cat#15140122
HBSS (10X)	Life Technologies	Cat#14185052
Vectashield Antifade Mounting Media	Vector Laboratories	Cat#H-1000
DMEM/F-12, HEPES	Life Technologies	Cat#11330032
Critical Commercial Assays		
High-Capacity cDNA Reverse Transcription Kit	Life Technologies	Cat#4368814
Quick-RNA extraction Miniprep kit	Zymo Research Corp	Cat#R1054
Click-iT EdU Alexa Fluor 488 Imaging kit	Life Technologies	Cat#C10337
SYBR Green PCR Master Mix	Life Technologies	Cat#4309155
SuperScript II Reverse Transcriptase	Life Technologies	Cat#18064014

(*Continued on next page*)

Continued		
REAGENT or RESOURCE	SOURCE	IDENTIFIER
DNA High Sensitivity Reagent Kit	PerkinElmer	Cat#CLS760672
TruSeq Stranded Total RNA Library Prep Gold	Illumina	Cat#20020598
KAPA Library Quantification Kit Illumina	Kapa Biosystems	Cat#4824
NextSeq 500 kit	Illuminia	Cat#20024906
Deposited Data		
Bulk RNA-seq dataset	This paper	Accession # E-MTAB-8765
Spatial RNA-seq dataset	This paper	Accession # E-MTAB-8768
Experimental Models: Organisms/Strains		
Mouse: C57BL6/J	Animal Resource Centre, Perth, Australia	JAX: 000664; RRID: IMSR_JAX:000664
Mouse: DCX^{DTR}	Vukovic et al., 2013	N/A
Mouse: $DCX^{creERT2}$ x tdTomato	Cheng et al., 2011	N/A
Mouse: $CX_3CR_1^{creERT2}$ x iDTR:	Parkhurst et al., 2013	$CX_3CR_1^{creERT2}$:
$CX_3CR_1^{creERT2}$: B6.129P2(C)-Cx3cr1$^{tm2.1(cre/ERT2)Jung}$	Parkhurst et al., 2013	JAX: 020940; RRID: IMSR_JAX:020940
iDTR: ROSAiDTR	Parkhurst et al., 2013	iDTR: JAX: 007900
Mouse: $CX_3CR_1^{creERT2}$ x iDTR x tdTomato	This paper	N/A
Mouse: Vav-Cre: B6.Cg-Commd10$^{Tg(Vav1-icre)A2Kio/}$J	The Jackson Laboratory	Vav-Cre: B6.Cg-Commd10$^{Tg(Vav1-icre)A2Kio/}$J: JAX: 008610
Mouse: IL-6Ra$^{flox/flox}$: B6;SJL-Il6ra$^{tm1.1Drew/}$J		IL-6Ra$^{flox/flox}$: JAX: 012944; RRID: ISMR_JAX_012944
Mouse: Scl-Cre^{ERT2} x ZsGreen$^{flox/flox}$	This paper	N/A
Oligonucleotides		
See Table S1 for a list of oligonucleotide sequences	N/A	N/A
Software and Algorithms		
FlowJo, version 10.4.2	TreeStar	https://www.flowjo.com
Prism 7	GraphPad Software	https://www.graphpad.com/scientific-software/prism/
ImageJ, version 1.52r	National Institutes of Health	https://imagej.nih.gov/ij/
R	R: The R Project for Statistical Computing	https://www.r-project.org/
Ingenuity Pathway Analysis (IPA)	QIAGEN	https://digitalinsights.qiagen.com/products-overview/discovery-insights-portfolio/content-exploration-and-databases/qiagen-ipa/
Ethovision XT, version 11.5.1022	Noldus	https://www.noldus.com/ethovision-xt
Paravision, version 6.0.1	Bruker	https://www.bruker.com/products/mr/preclinical-mri/paravision-7.html
ITK-SNAP	ITK-SNAP	http://www.itksnap.org/pmwiki/pmwiki.php
Imaris, version 9.2	Imaris, Oxford Instruments	https://imaris.oxinst.com/
Stereo Investigator, version2017.01.1	MicroBrightfield Bioscience	https://www.mbfbioscience.com/stereo-investigator
Analysis pipeline for spatial RNA-seq data	This paper	https://github.com/BiomedicalMachineLearning/TBI

LEAD CONTACT AND MATERIALS AVAILABILITY

Further information and requests for resources and reagents should be directed to and will be fulfilled by the Lead Contact, Dr. Jana Vukovic (j.vukovic@uq.edu.au). This study did not generate new unique reagents.

EXPERIMENTAL MODEL AND SUBJECT DETAILS

Three-month-old female C57BL/6J mice, $CX_3CR1^{CreERT2}$ x iDTR, $CX_3CR1^{CreERT2}$ x iDTR x tdTomato, DCX^{DTR}, $DCX^{creERT2}$ x tdTomato, Vav-Cre x IL-$6Ra^{flox/flox}$ and Scl-Cre^{ERT2} x $ZsGreen^{flox/flox}$ mice were used in this study. Mouse colonies were bred and maintained in a University of Queensland Biological Resources' specific pathogen-free 'behind barrier' facility. Mice were housed socially (3-5 mice per cage) on a 12-h light/dark cycle in individually ventilated cages, and with *ad libitum* access to food and water. The experimental holding room had temperature (21.5°C set point) and humidity control (40% set point), and was supplied with HEPA-filtered air. Littermates of the same gender were otherwise randomly assigned to experimental groups. All experiments were conducted in accordance with the Australian Code for the Care and Use of Animals for Scientific Purposes, with approval from The University of Queensland Animal Ethics Committee.

METHOD DETAILS

Microglial depletion and repopulation

$CX_3CR1^{CreERT2}$ x iDTR and $CX_3CR1^{CreERT2}$ x iDTR x tdTomato mice were 3–4 weeks of age when orally gavaged with tamoxifen (12.5 mg/g body weight (BW)) or corn oil once daily for 5 days. For $CX_3CR1^{CreERT2}$ x iDTR mice and $CX_3CR1^{CreERT2}$ x iDTR x tdTomato mice, exposure to tamoxifen induces CX_3CR1-positive (CX_3CR1^{pos}) cells to express diphtheria toxin receptor (DTR). Because microglia are self-renewing and have a slow turnover rate compared with that of CX_3CR1^{pos} monocytes, only microglia continue to express DTR after several weeks (Parkhurst et al., 2013). After the fifth and final treatment with tamoxifen or corn oil, mice were left to rest for at least 6 weeks. After this rest period, microglia were selectively depleted by administration of diphtheria toxin (DT; 30 ng/g BW; Sigma) via intraperitoneal (i.p.) injection or intra-hippocampal injection (detailed below). For microglial depletion, DT was injected once daily for 3 days prior to injury; for subacute delayed microglial repopulation, DT was injected once daily at 4, 5, and 6 days after injury; for microglial turnover prior to TBI, DT was injected daily at minus 9, 8, and 7 days before surgery, with injury as detailed below.

For PLX5622 microglial depletion and repopulation, mice were placed on a chow diet with PLX5622 incorporated at 1200 ppm (provided by Plexxikon via Research Diets). Control chow mice received standard mouse chow (Research Diets). PLX5622 was used under the permissions of a material transfer agreement from Plexxikon, USA.

Controlled cortical impact model of traumatic brain injury

Mice were subjected to either moderate controlled cortical impact (CCI) or sham surgery, as previously described (Wang et al., 2016). Briefly, mice were anesthetized with 0.01 mg/g BW tiletamine/zolazepam (Zoletil) and 0.01 mg/g BW xylazine, administered via i.p. injection, and placed into a stereotaxic frame. Using sterile procedures, a midline incision was made, the skin retracted, and a 4-mm craniotomy performed at a point midway between the lambda and bregma sutures, and laterally midway between the central suture and temporalis muscle. The skull cap was carefully removed, taking care to not damage the underlying leptomeninges. The tip of the 3-mm impactor piston was angled and kept perpendicular to the exposed cortical surface. The parameters for the CCI were: impact speed, 3.5 m/s; deformation depth, 1.0 mm; duration, 400 ms. After CCI, the incision was sutured, and the mice allowed to recover on a heat pad to maintain core body temperature at 36–37°C. Shortly after injury, mice were subcutaneously injected with Hartmann's solution containing buprenorphine (Temgesic, 0.05%). Sham mice underwent the same surgical operation but without CCI.

Active place avoidance

To assess hippocampal-dependent spatial learning and memory, mice were tested in the active place avoidance (APA) task, as previously described (Willis et al., 2017). Briefly, the APA testing first involved daily handling of the mice after surgery prior to behavioral testing, followed by habituation of the mice to the rotating (clockwise, 1rpm) APA testing arena for 20min, during which time the mice could freely explore with the shock zone turned off. The APA testing arena consisted of an elevated arena with a grid metal floor, fenced by a 32cm-high clear Perspex circular boundary, with black and white A3 size visual cues placed on the 4 surrounding walls. One day after habituation, mice were tested in the APA task, during which they were tasked to avoid a 60° shock zone, the position of which did not move in relation to the room coordinates. Mice were tracked by an overhead camera linked to Tracker software (Bio-Signal Group), with entry of the mice into the shock zone leading to the delivery of a brief foot shock (0.5mA, 500ms, 60 Hz, 1.5 s intervals). The mouse's starting position was always opposite the shock zone location. Each test trial was 20min, with 24h between each test. Reversal learning was conducted using the same spatial cues, but with the location of the shock zone moved to the opposite side of the arena. In-session acquisition of spatial learning was assessed by the number of entries into the shock zone during each 5 min interval of the 20min trial. Longer-term spatial learning and memory was assessed by the total number of entries or shock during each day, across 5 days of testing. The number of entries into the shock zone, the number of shocks received, and the distance traveled during the trial were analyzed using Track Analysis software (Bio-Signal Group).

Morris water maze

Mice underwent testing in the Morris water maze starting at 12 days post-injury. The apparatus consisted of a circular swimming pool (100 cm in diameter, 20 cm high) filled with water (21–25°C), which was opaque due to the addition of non-toxic white paint. Mice were required to locate a submerged platform using the spatial cues located around the arena. For the first 5 days of testing, the

platform was located within the north-east quadrant of the testing arena, hidden beneath 1.5 cm of opaque water. Each day, over four trials, mice were allowed 60 s to locate the hidden platform, with an inter-trial interval of 15 min. At the start of each trial the mouse was released from one of four starting positions (south, west, north or east), chosen in a pseudo-random order. If the mouse was unable to locate the platform within 60 s it was guided there, and allowed to remain on the platform for 10 s. The average latency to locating the platform over the four trials for each test day was recorded using Ethovision software (Noldus Information Technology, version 11.5.1022). On days 7 and 8, a reversal learning procedure was performed, with the platform being re-introduced into the testing arena in the south-west quadrant. During reversal learning, mice were again trained to find the platform over four 60 s trials, with 15-min inter-trial intervals.

Y-maze

As a further test of spatial learning and memory following traumatic brain injury (TBI), mice were also tested in the Y-maze task 30 days post-injury. The Y-maze apparatus was composed of two arms connected to a runway (home arm), each 45 × 15 × 15 cm. The arms contained different visual cues, consisting of black and white symbols/shapes on laminated A4 size paper. The maze was positioned 1 m above the ground, and the mice were tracked by an overhead camera. During training, the animals were placed in the home arm with access to only one arm for 3 min. This training arm was alternated for each mouse. Following a 20-min intermission, mice were placed back into the Y-maze for 3 min with access to the training and novel arms. The time spent in the novel and the training arms, as well as the distance traveled, were analyzed using Ethovision software (Noldus Information Technology, version 11.5.1022).

Labeling of newborn cells

To label newborn or proliferating cells, mice were injected i.p. with either EdU (16.4 mg/kg, molecular weight: 252.22 g/mol, Santa Cruz) and/or BrdU (20 mg/kg, molecular weight: 307.1 g/mol, Sigma).

To genetically fate label newborn cells, we utilized DCXcre^{ERT2} x tdTomato mice, where tamoxifen exposure induces DCX^{pos} cells to express the tdTomato fluorescent reporter. To label a cohort of DCX-positive (DCX^{pos}) immature neurons, DCXcre^{ERT2} x tdTomato mice were orally gavaged with tamoxifen (0.125mg/kg body weight) once daily for 2 days prior to surgery. To label a cohort of mature neurons, DCXcre^{ERT2} x tdTomato mice were orally gavaged with tamoxifen (0.125 mg/kg BW) once daily for 5 days, 6-weeks prior to surgery.

MR Imaging

For *ex vivo* MRI scans, perfusion-fixed brains were kept inside the skull, but with the ventral side opened up to allow for optimal access of contrast agent (0.2% Magnevist [gadopentetate dimeglumine]; Bayer Healthcare) After 4 days of incubation at 4°C, samples were immersed in Fombulin (perfluoropolyether solution, Solvay Solexis, NJ) for high-resolution imaging using a Bruker 16.4T small animal MR imaging system with a vertical wide bore, equipped with a Micro2.5 gradient set and a 15mm linear saw coil (M2M imaging). High resolution T1/T2 imaging was performed using Paravision software (version 6.0.1) and a gradient echo fast low angle shot (FLASH) MRI sequence, with TR/TE = 40/10ms and a 30 degree flip angle. Images were acquired using a 20x12.7x9 mm field-of-view with 400x256x180 matrix to produce 180 slices with 50 μm slice resolution.

T1/T2 FLASH scans were masked using ITK-SNAP software to remove skull fragments, and brains mapped to the Australian Mouse Brain Mapping Consortium (AMBMC) template using FMRIB's linear and nonlinear image registration tools: FLIRT and FNIRT. ITK-SNAP software was then used to manually check and correct regions of interest (i.e., cortex and hippocampus) to ensure ROI specificity following surgery, following which ROI volume measurements were determined.

Tissue preparation for histology and immunostaining

Mice were euthanized using an i.p. injection of sodium pentobarbitone (1.6 mg/g BW), before being transcardially perfused with phosphate buffered saline (PBS) and 4% formalin. Brains were dissected, placed in formalin for 24 h, followed by PBS with 0.01% sodium azide. Tissue was cryoprotected in 30% sucrose with 0.05% sodium azide for 2 days. Free-floating serial brain sections (40 μm) were collected using a sliding microtome (Leica).

Immunofluorescence

Brain sections were blocked in 5% normal goat serum (NGS) with 0.3% Triton X-100, before being incubated overnight at 4°C with primary antibodies diluted in 3% NGS with 0.1% Triton X-100 in PBS: rabbit anti-Iba1 (1:1000; Wako), guinea pig anti-DCX (1:1000; Merck), rat anti-BrdU (1:500; Abcam), rabbit anti-Tbr2 (1:400; Millipore), rabbit anti-TMEM119 (1:500; Abcam), mouse anti-GFAP (1:1000; Millipore), mouse anti-IL-6 (1:500, Abcam), rat anti-complement 3 (1:500; Clone 11H9, Hycult Biotech). Sections were washed in PBS before being incubated with secondary antibodies: Alexa Fluor anti-rabbit 568 (1:2000), Alexa Fluor anti-guinea pig 488 (1:1000), AlexaFluor goat anti-rabbit 647 (1:1000), AlexaFluor goat anti-rat 647 (1:1000), AlexaFluor goat anti-rabbit 488 (1:1000), AlexaFluor AffiniPure Fab Fragment Donkey Anti-Rat 488 (1:1000) diluted in 3% NGS with 0.1% Triton X-100 in PBS. Sections were washed in PBS, then mounted with Vectashield H-100 medium containing DAPI (1:1000). EdU staining was performed

using Click-iT Alexa Fluor 488 Imaging kit, according to manufacturer's instructions (Life Technologies). For BrdU staining, a prior antigen retrieval step was performed, involving incubation in 1M HCl for 35 minutes at 45°C and 10min incubation in 0.1M boric acid at room temperature.

Imaging and cell quantification

Four consecutive sections of the dentate gyrus, located at Bregma −1.50mm, −1.70 mm, −1.94 mm, −2.18mm, were counted per mouse. Cell counts were performed live using StereoInvestigator software (MicroBrightfield Bioscience) using an AxioImager Z2 microscope (Zeiss) and an ORCA-R2 digital charge-coupled device camera (Hamamatsu). DCX^{pos} immature neurons were defined based on their large round cellular body with an apical projection within the granule cell layer of the dentate gyrus. Cell numbers in the granule cell layer were divided by the analyzed length of the granule cell layer as visualized by DAPI. Cell numbers for the whole dentate gyrus were normalized to the area of the dentate gyrus, defined by the border of the hippocampal fissure and a line drawn touching the end of the blades of the dentate gyrus. The average from four consecutive serial sections was recorded.

Cresyl violet imaging was conducted using the Metafer Vslide Scanner (MetaSystems) with a Zeiss Axio Imager Z2. Hippocampal volume changes were calculated by measuring the area in four sections at −1.50mm, −1.70 mm, −1.94 mm, and −2.18 mm relative to Bregma. The area was multiplied by the thickness of the sections (40 μm) to obtain a volume measurement. These volumes were added together to represent 16% of the total dorsal hippocampus.

Confocal images were acquired using an inverted Diskovery spinning disk confocal microscope (Spectral Applied Research) with a Zyla sCMOS camera at either 20x magnification using a CFI Plan Aprochromat VC 20x / N.A. 0.75 / W.D. 1.0mm objective, or at 60x magnification using a CFI Apo Lamda 60x Oil / N.A. 1.4 / W.D. 0.13mm objective.

Analysis of the mean fluorescence intensity (MFI) for confocal images was conducted using Imaris software, with MFI values calculated from the average of four consecutive sections of the dentate gyrus, located at Bregma −1.50mm, −1.70 mm, −1.94 mm, −2.18mm per mouse. All tissue sections were stained within the one batch, with the same imaging threshold and exposure time to ensure maintained consistency for image analysis.

Replication experiments

The pro-neurogenic and neuroprotective effects of repopulating microglia were independently validated in D.C.A.'s laboratory at the University of Oxford. All experimental procedures conducted here were approved by the relevant local ethics committees (LERP, ACER) and performed in accordance with the UK Animals (Scientific Procedures) Act, 1986. In brief, 8-week-old female C57BL/6J mice were purchased from Charles River Laboratories (UK) and allowed to acclimatize for 1 week upon arrival. Next, experimental mice were fed either control or PLX5622-containing chow for 3 weeks and then switched back to a normal diet (see Figure S3J). For TBI, mice were anaesthetised with Zoletil/Xylazine as detailed earlier and placed in a stereotaxic frame. Following excision of the scalp, a craniotomy was performed over the posterior parietal region of the brain. For TBI mice, cortical contusion was induced with the PCI3000 precision cortical impactor device (Hatteras Instruments), using a 3mm flat impactor tip to a speed of 3.5 m/s, a dwell time of 400 ms, and a deformation depth of 1.0mm; sham-operated controls underwent craniotomy surgery only. All mice were euthanized on day 12 post-surgery and transcardially perfused with heparinised saline followed by 4% formalin. Fixed brains were processed for histological staining followed by blinded quantitative assessment of hippocampal tissue volumes (cresyl violet) and DCX^{pos} cell numbers as detailed earlier.

Intra-hippocampal injections

For all experiments listed below, and unless specified otherwise, intra-hippocampal injections were performed under stereotaxic guidance at the following co-ordinates: −2.0mm anterior-posterior, −1.5mm medial-lateral, −2.0mm dorso-ventral.

To deplete sensitized CX_3CR1^{pos} microglia within the hippocampus of tamoxifen-gavaged $CX_3CR1^{CreERT2}$ x iDTR mice, a single unilateral injection of DT (Sigma; 0.1ng, 0.5ul injected over 5 minutes) was given as detailed above and in the experimental timelines (see figures).

To ablate DCX^{pos} cells in DCX^{DTR} mice, a single unilateral injection of 0.1 ng DT (0.5ul injected over 5 minutes) was delivered into the left hippocampus (i.e., ipsilateral to the site of CCI). For TBI mice, the injection was placed at a depth −1.7mm in the dorso-ventral plane.

To block IL-6R signaling within hippocampus after injury with microglial repopulation, tamoxifen-sensitized $CX_3CR1^{CreERT2}$ x iDTR mice received a single unilateral 1 μl injection (infused over 10 minutes) of MR16-1 (10 mg/mL) or control rat IgG (10 mg/mL; Sigma) on day 3 after CCI. MR16-1 was used as permitted under a material transfer agreement from Chugai Pharmaceutical Co. (Japan).

To block IL-6 *trans*-signaling within the hippocampus after injury with microglial repopulation, tamoxifen-sensitized $CX_3CR1^{CreERT2}$ x iDTR mice received a single unilateral injection of sgp130FC (2ug, 1ul over 10 minutes), or saline (1ul) as the vehicle control, on day 3 after CCI.

To stimulate IL-6 or IL-6 *trans*-signaling, wild-type C57BL6J mice with TBI received a single unilateral injection (infused over 10 minutes) of either recombinant mouse IL-6 (500ng, 1ul), or Hyper-IL-6 (200ng, 1ul) (Fischer et al., 1997), on day 3 after CCI; vehicle controls received saline (1ul) injections.

Real time quantitative PCR

Mice were deeply anesthetized with sodium pentobarbital before being euthanized using a transcardial perfusion of 0.1 M PBS (pH 7.4). The ipsilateral hippocampi were snap-frozen using isopentane (Sigma) on dry ice. Total RNA was extracted from hippocampal tissue by Trizol reagent according to the manufacturer's instructions (ThermFisher Scientific), with RNA quality assessed by the NanoDrop spectrophotometer. Total RNA was converted to cDNA using the High Capacity cDNA Reverse Transcription kit according to the manufacturer's instructions (Applied Biosystems). Real-time qPCRs were conducted using Applied Biosystems 7500 Real-Time PCR systems. Relative target gene expression to geometric mean of the reference gene hypoxanthine-guanine phosphoribosyl transferase (*Hprt*) was determined by the formula: $2^{-\Delta CT}$, where $\Delta CT = CT_{(target\ gene)} - CT_{(Hprt)}$. Changes in gene expression are presented as fold changes compared to gene expression in sham controls. Probe sets were tested over a serial cDNA concentration for amplification efficiency. The SYBR-Green primers used are listed in Table S1.

Hippocampal cell preparations and fluorescence-activated cell sorting

Microglia were isolated from the hippocampus of $CX_3CR_1^{creERT2}$ x iDTR x tdTomato mice 3 days after CCI as previously described (Vukovic et al., 2012). Briefly, mice were deeply anesthetized with sodium pentobarbital before being euthanized using a transcardial perfusion of 0.1 M PBS (pH 7.4), their brains immediately removed and the ipsilateral hippocampus dissected out. Tissue was digested in 0.1% papain (Worthington Biochemical Corporation) and 0.1% DNaseI (Roche Australia) in HBSS (Thermo Scientific) for 16 min at 37°C, triturating half-way through the incubation period. Next, cells were centrifuged at 1100 prm for 10 minutes, then filtered into single cell suspension through a 40um cell sieve (Falcon, BD Biosciences), and resuspended in 2mL of DMEM F12 (GIBCO, Life Technologies), 2% BSA (Invitrogen) and 1% Penicillin Streptomycin (Thermo Fischer).

Hippocampal dissociated single cells were sorted using a Cytopeia Influx Cell Sorter (BD Bioscience), with on average 67,000 (resident) and 25,000 (repopulating) $tdTomato^{pos}$ microglia per sample (n = 3 per group). Each sample was directly sorted into 300ul of cell lysis buffer (Zymo Research) and total RNA was immediately isolated using the Quick-RNA MiniPrep kit according to manufacturer's instructions (Zymo Research); RNA quality was analyzed using the Agilent 2100 Bioanalyzer.

RNA sequencing library preparation and NextSeq High Output 1x75bp

RNA-Seq libraries were prepared using the illumina TruSeq Stranded Total RNA Library Prep Gold kit (illumina, 20020598) and TruSeq RNA Single Indexes (illumina, 20020492/20020493), according to the standard manufacturer's protocol (illumina, document # 1000000040499 v00, Oct 2017) described briefly as follows. To enrich for mRNA, 27-100 ng of total RNA was depleted of rRNA using Ribo-Zero Gold. The enriched mRNA was then subjected to a heat fragmentation step aimed at producing fragments between 120-210 bp (average 155 bp). cDNA was synthesized from the fragmented RNA using SuperScript II Reverse Transcriptase (Invitrogen, 18064014) and random primers. The resulting cDNA was converted into dsDNA in the presence of dUTP to prevent subsequent amplification of the second strand and thus maintaining the 'strandedness' of the library. Following 3′ adenylation and adaptor ligation, libraries were subjected to 15 cycles of PCR to produce libraries ready for sequencing. The libraries were quantified on the Perkin Elmer LabChip GX Touch with the DNA High Sensitivity Reagent kit (Perkin Elmer, CLS760672). Libraries were pooled in equimolar ratios, and the pool was quantified by qPCR using the KAPA Library Quantification Kit - illumina/Universal (KAPA Biosystems, KK4824) in combination with the Life Technologies Viia 7 real time PCR instrument.

Sequencing was performed using the Illumina NextSeq500 (NextSeq control software v2.2.0 / Real Time Analysis v2.4.11). The library pool was diluted and denatured according to the standard NextSeq protocol (Document # 15048776 v05) and sequenced to generate single-end 76 bp reads using a 75 cycle NextSeq500/550 High Output reagent Kit v2.5 (illumina, 20024906). After sequencing, fastq files were generated using bcl2fastq2 (v2.18.0). There were three replicates per experimental condition.

Analysis of RNA-Seq data

All sequence reads were trimmed for adaptor sequences using Cutadapt (version 1.11) (Martin, 2011) and aligned using STAR (version 2.5.2a) (Dobin et al., 2013) to the *Mus musculus* GRCm38 assembly with the gene, transcript, and exon features of the Ensembl (release 70) gene model. Quality control metrics were computed using RNA-SeQC (version 1.1.8) (DeLuca et al., 2012) and expression was estimated using RSEM (version 1.2.30) (Li and Dewey, 2011).

Differential expression (DE) analysis was performed using the R package edgeR (Robinson et al., 2010). Note that the inputs for DE analysis are the filtered but not normalized read counts, since edgeR performs normalization (library size and RNA composition) internally. The glmFit() function was used to fit a negative binomial generalized log-linear model to the read counts for each gene. Using the glmLRT() function, we conducted gene-wise likelihood ratio tests for a given contrast. Pathway analysis for differentially expressed genes (DEGs) was performed using Ingenuity software.

Labeling of blood-derived cells

To label and fate-track peripheral immune cells derived from the bone marrow, we utilized $Scl\text{-}Cre^{ERT2}$ x $ZsGreen^{flox/flox}$ mice to permanently induce reporter gene expression in hematopoietic stem and progenitor cells (HSPCs) and their progeny (Göthert et al., 2005). Mice were gavaged with tamoxifen (0.125 mg/kg BW) once daily for 5 days, 4-weeks prior to surgery.

Spatial transcriptomics

Brain samples (n = 3 per condition) were snap-frozen using the isopentane and dry ice procedure, before being embedded into Optimal Cutting Temperature (OCT) blocks. Samples were cut using Leica Cryostat and 10μm thick sections were collected onto library preparation (LP) glass slides, that were then fixed with 4% formaldehyde solution for 10 min at room temperature. Sections were stained with Mayer's hematoxylin for 10 min, followed by 1-minute incubation in Bluing Buffer and counterstaining with Eosin for 3 min at room temperature. H&E images were captured using Zeiss Axio Imager at 20x Magnification. ST sequencing libraries were prepared as per manufacturer's instructions, with pre-permeabalisation and permeabalisation performed with 20 and 7 min incubations in collagenase and trypsin, respectively. On-slide cDNA synthesis, tissue removal, probe cleavage, and library preparation were performed as per the manual. High-quality sequencing libraries were obtained from 107-698 ng and with the average length at 660-780 bp.

ST libraries were sequenced on the Illumina Nextseq500, using a 150 cycles kit with read configuration as read 1 (26 bp) and read 2 (124 bp). Raw sequencing data in BCL format were converted to FASTQ reads using bcl2fastq/2.17. Reads were mapped to the mouse reference genome GRCm38 using STAR-2.7.1a and gene annotation GRCm38.96.gtf. We obtained 46-72 million high-quality, uniquely mapped reads for the six libraries. On average, each ST spot had 528-3345 genes detected, with maximum genes per spot ranging from 3482-9526 genes. Gene-count matrices were generated using an ST pipeline; ST spot coordinates were adjusted using st_spot_detector with inputs from the H&E images and Cy3 images. The dentate gyrus and hippocampus regions were identified on H&E images. Gene expression per spot in the selected regions was plotted on tissue images using Python scripts available in our stlearn github repository.

QUANTIFICATION AND STATISTICAL ANALYSIS

Investigator blinding to experimental conditions was applied and all statistical analyses were conducted using GraphPad Prism software (version 7.02). Statistical differences were determined using either an unpaired two-tailed Student's t test, one-way ANOVA, two-way ANOVA or repeated-measures two-way ANOVA, as appropriate. For all ANOVAs, a Greenhouse-Geisser correction and Bonferroni post hoc comparison were used. The value of n reported within figure legends represents number of animals, with appropriateness of sample sizes for key results confirmed by power analysis, where power = 0.8 and $p < 0.05$. There is no missing data nor were any animals removed post hoc. Values are represented as mean ± SEM, with differences considered significant when $p < 0.05$. Asterisks denote corresponding statistical significance: *$p < 0.05$; **$p < 0.01$; ***$p < 0.001$; ****$p < 0.0001$.

DATA AND CODE AVAILABILITY

All sequencing data from this study have been submitted to ArrayExpress repository (https://www.ebi.ac.uk/arrayexpress/). The bulk RNA-seq dataset is available under accession number E-MTAB-8765. The spatial RNA-seq dataset, accession number E-MTAB-8768 will be publicly available from 15th December 2020. Analysis pipeline for spatial RNA-seq data implemented the code at Spatial Transcriptomics (https://github.com/SpatialTranscriptomicsResearch), including: st_pipeline, st_viewer, st_spot_detector, st_tissue_recognition, and st_analysis. Custom Python 3.6 code is available at the authors github website (https://github.com/BiomedicalMachineLearning/stLearn/TBI).

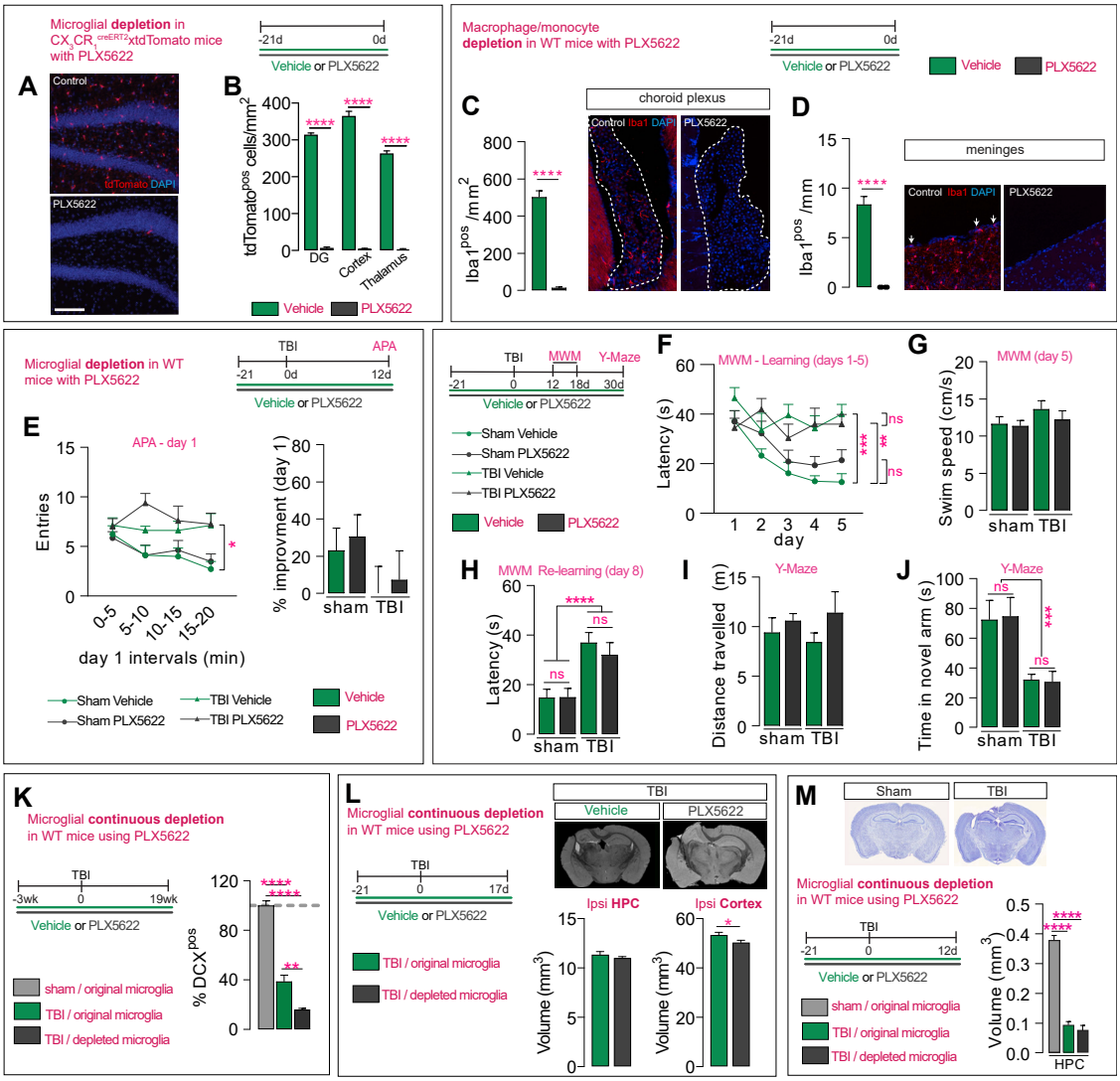


Figure S1. Effect of Sustained Microglia Depletion on Brain Macrophages, Hippocampus-Dependent Learning, Neurogenesis, and Cortical and Hippocampal Tissue Volumes, Post-TBI, Related to Figure 1

(A) PLX5622 treatment was initiated 3 weeks pre-surgery and then continued for the duration of the experiment. Representative confocal images confirm the loss of tdTomato^{pos} microglia in the hippocampus of PLX5622-treated mice. Scale bar, 50 μm.

(B) Quantification of tdTomato^{pos} microglia loss in the dentate gyrus (DG), cortex, and thalamus of tamoxifen-sensitized $CX_3CR1^{CreERT2}$ x tdTomato$^{flox/flox}$ mice treated with PLX5622 [$F(2, 12) = 32.18$, $p < 0.0001$].

(C and D) Quantification of Iba1^{pos} brain macrophages in the choroid plexus (C); [$t = 14.53$, $df = 6$) and meninges (D); [$t = 10.25$, $df = 6$]) of WT mice administered control or PLX5622-containing chow. Dotted white line on the confocal images in (C) outlines the choroid plexus, and arrows in (D) indicate Iba1^{pos} meningeal macrophages.

(E) 'Within session' APA performance (*left*) of sham and TBI mice with and without continuous PLX5622 treatment on Day 1 of testing [$F(3,28) = 6.36$, $p = 0.0020$]; Asterisk indicates post hoc result for the 15-20min interval between Sham and TBI mice. Percentage improvement (*right*) for individual mice, as assessed by the change in shock zone entries between the first and the last 10 min of the session.

(F–J) Morris water maze (MWM) and Y-maze performance following TBI or sham surgery, and in the presence or absence of brain microglia; experimental timeline is shown on the top *left*. In MWM (F-H), mice are required to learn the location of a submerged platform in a pool of white colored water. The Y-maze (I and J) assesses the natural preference of mice to explore novel environments (i.e., a previously closed arm).

(F) MWM mean escape latency. TBI negatively impacts task acquisition [$F(3,28) = 11.76$, $p < 0.0001$], but the absence of microglia does not otherwise influence performance (Testing Day 5: 'TBI control' versus 'TBI PLX5622′ and 'Sham control' versus 'Sham PLX5622′, $p > 0.98$).

(G) MWM swim speeds were not affected by TBI and/or PLX5622 treatment [$F(1,28) = 1.98$, $p = 0.17$)].

(H) Mean escape latency during MWM reversal learning (re-learning) in which the hidden platform was shifted to a new location. Note the impact of TBI [$F(1,28) = 24$, $p < 0.0001$], but lack of a PLX5622 effect [$F(1,28) = 0.37$, $p = 0.55$].

(I and J) Distance traveled (I) and time spent in novel arm (J) during Y-maze. TBI mice spent significantly less time in the novel arm when opened [$F(1,28) = 18.14$, $p = 0.0002$]. PLX5622 treatment did not change Y-maze performance for either TBI or sham-operated mice [$F(1,28) = 0.0003$, $p = 0.96$].

(legend continued on next page)

(K) Long-term effects of continuous PLX5622 treatment in WT mice. Graph shows total DCX^{pos} immature neurons at 19 weeks post-surgery [$F(2,19) = 113.1$, $p < 0.0001$]; asterisks indicate post hoc results.

(L) T1/T2 ex-vivo MRI measurements of total ipsilateral hippocampal (*left*) and cortical (*right*) volumes at 17 days post-TBI. Ipsilateral cortex volumes were somewhat reduced with continuous PLX5622 treatment [ipsilateral cortex: $t = 2.36$ $df = 14$], supporting a role for microglia in the neuroprotective aspects of scar formation at primary impact sites (Bellver-Landete et al., 2019). Ipsilateral hippocampal volumes were unchanged [$t = 1.48$, $df = 14$, $p = 0.30$].

(M) Dorsal hippocampal volumes at 12 days post-TBI using cresyl violet staining. Data were derived from four anatomically defined brain regions (i.e., set distances relative to bregma) for each animal [$F(2,11) = 127.7$, $p < 0.0001$]; asterisks indicate post hoc results for the relevant comparisons.

Data are represented as mean ± SEM (K) Data presented as the percentage change (mean ± SEM) from average of age-matched sham-operated control group. Statistics: two-way ANOVA with Bonferroni post hoc comparisons (B, E – left, G, H-J), unpaired Student's t test (C, D, L), one-way ANOVA (K, M) followed by Bonferroni post hoc comparison, two-way ANOVA with repeated-measures and Bonferroni post hoc comparisons (E – left, F). (B) n = 3/group, (C, D) n = 4-5/group, (E-L) n = 7-8/group. *$p < 0.05$, **$p < 0.01$, ***$p < 0.001$, ****$p < 0.0001$, ns = non-significant, GCL = granule cell layer, DG = dentate gyrus, ipsi = ipsilateral, HPC = hippocampus, MWM = Morris water maze, APA = active place avoidance.

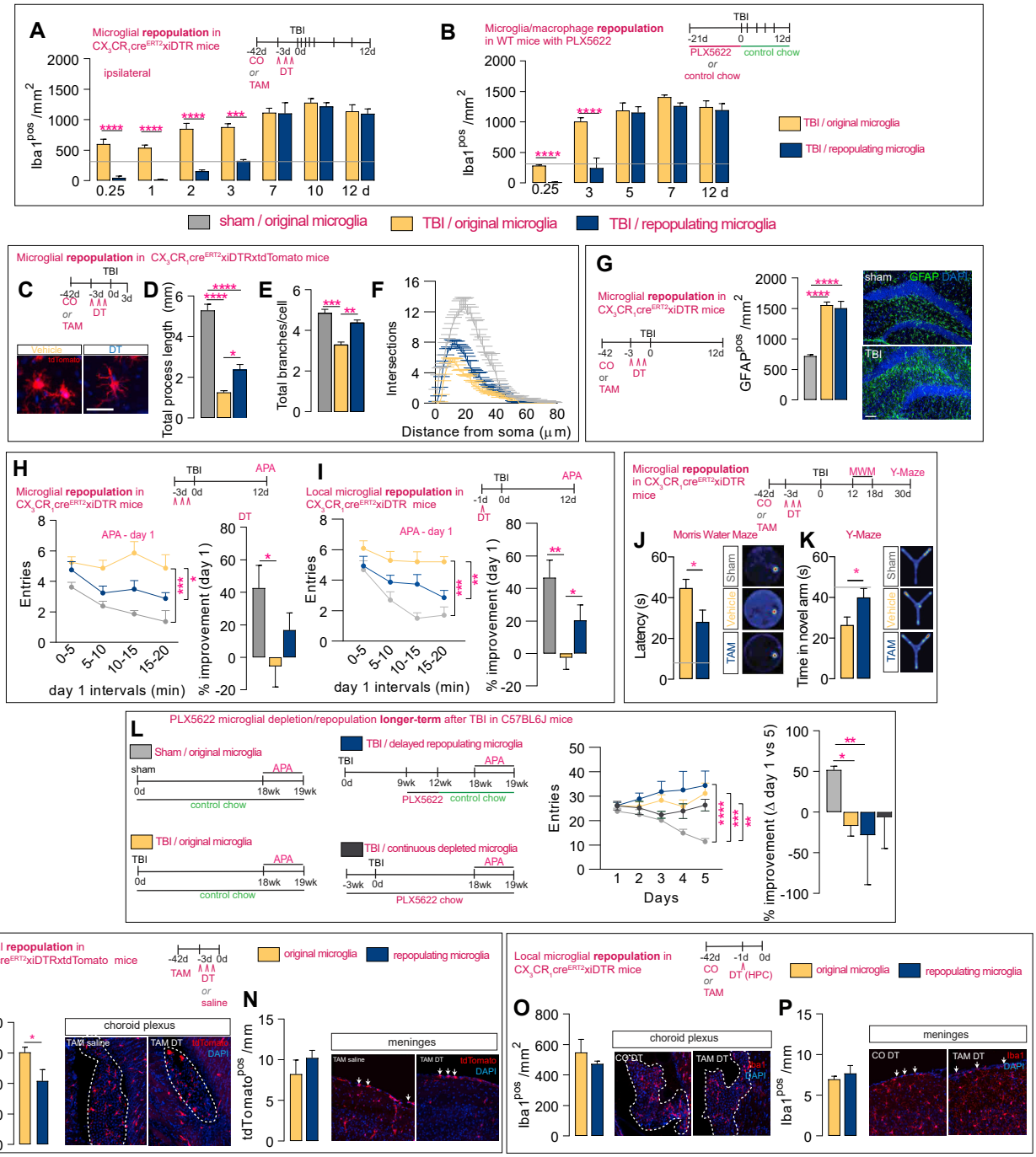


Figure S2. Characterization of Microglial Depletion and Repopulation in the Acute and Chronic Phase of Injury, Related to Figure 2

(A–P) Microglia turnover experiments using both genetic and pharmacologic approaches. For studies involving PLX5622 (B, L), treatment was initiated either 3 weeks prior and then stopped at the time of TBI or sham surgery, or at 9 weeks post-TBI for experiments involving microglia turnover during the more chronic phase. For experiments in $CX_3CR1^{creERT2}$ x iDTR mice (A, G, H–K, O, P), or $CX_3CR1^{creERT2}$ x iDTR x tdTomato mice (C–F, M and N), DT was injected just prior to TBI as shown. Mice were sacrificed at the relevant time point specified in each experimental time line.

(A) Repopulation kinetics of $Iba1^{pos}$ cells in the ipsilateral dentate gyrus of $CX_3CR1^{creERT2}$ x iDTR TBI mice, treated with either corn oil (CO; vehicle) or tamoxifen (TAM), and then DT as shown. The gray line represents the sham average [$F(1,50) = 68.75$, $p < 0.0001$]; asterisks indicate post hoc results.

(B) Replenishment of $Iba1^{pos}$ cells in the ipsilateral dentate gyrus of sham and TBI mice with short-term PLX5622 treatment [$F(1,14) = 108.5$, $p < 0.0001$]; asterisks indicate post hoc results.

(C) Confocal images of 'original microglia' (Vehicle) versus 'repopulating microglia' (DT) in the ipsilateral dentate gyrus of sensitized $CX_3CR1^{creERT2}$ x iDTR x tdTomato mice, 3 days post-TBI. Scale bar, 50μm.

(legend continued on next page)

(D) Total process length of tdTomato^{pos} microglia [F(2,8) = 67.38, p < 0.0001]; asterisks indicate post hoc results.
(E) Total branch number per tdTomato^{pos} microglial cell [F(2,8) = 22.3, p = 0.0005]; asterisks indicate post hoc results.
(F) Sholl analysis of TdTomato^{pos} microglia [F(2,632) = 809.6, p < 0.0001; Sham 'original microglia' versus TBI 'original microglia', p < 0.0001; TBI 'original microglia' versus TBI 'repopulating microglia', p < 0.0001].
(G) Number of GFAP^{pos} astrocytes in the ipsilateral dentate gyrus of $CX_3CR1^{creERT2}$ x iDTR mice with original versus repopulating microglia, 12 days after surgery. [F(2,7) = 130.9, p < 0.0001; TBI 'original microglia' versus TBI 'repopulating microglia', p > 0.99]; asterisks indicate significant post hoc results. Representative images of GFAP^{pos} astrocytes in the ipsilateral dentate gyrus at 12 days after surgery are shown on the right.
(H) 'Within session' learning and individual improvement in APA performance following systemic DT injection. (*Left*) Number of shock zone entries per 5-minute intervals during a 20 min APA session on Day 1 of testing [F(2,21) = 17.16, p < 0.0001]; asterisks indicate post hoc results for the last (15-20min) interval between groups as indicated. (*Right*) Percentage improvement in APA performance for individual mice based on the change in shock entries between the first and last 10 min of testing [F(2,21) = 3.75, p = 0.041]; asterisk indicates post hoc result.
(I) 'Within session' learning and individual improvement in APA performance for mice with intra-hippocampal DT injection. (*Left*) Number of entries into the shock zone during Day 1 of APA testing [F(2,32) = 9.45, p = 0.0006]; asterisks indicate post hoc results for the last (15-20min) interval between groups as indicated. (*Right*) Percentage improvement in APA performance for individual mice [F(2,32) = 11.26, p = 0.0.002]; asterisks indicate post hoc results.
(J and K) Morris Water Maze (MWM) and Y-maze performance with microglia repopulation. (J) Escape latency and representative heatmaps for reversal testing in the Morris water maze task of $CX_3CR1^{creERT2}$ x iDTR mice with original (n = 11) versus repopulating (n = 8) microglia (19 days post-surgery; reversal learning MWM Testing Day 8); the gray line represents the sham average [t = 2.44, df = 17]. (K) Time spent in the novel Y-maze arm and representative heatmaps for $CX_3CR1^{creERT2}$ x iDTR mice treated with corn oil (CO) and tamoxifen (TAM) at 30 days post-surgery; gray line represents the sham average [t = 2.306, df = 16].
(L) APA performance (*left*) of sham and TBI cohorts with continuous long-term depletion or delayed turnover of microglia [F(3,27) = 4.33, p = 0.013]; asterisks indicate significant post hoc results for Testing Day 5 (the number of entries between continuous depletion and delayed repopulation was not significant, p = 0.458). Percentage improvement (*right*) in APA performance for individual mice [F(3,27) = 2.32]; asterisks indicate post hoc results.
(M and N) Quantification of tdTomato^{pos} brain macrophages within the choroid plexus (M) and meninges (N) in tamoxifen-sensitized $CX_3CR1^{creERT2}$ x iDTR x tdTomato mice following systemic DT injections [choroid plexus: t = 2.60, df = 8]. Representative images of tdTomato^{pos} brain macrophages within the choroid plexus (outlined by the dashed line) and meninges (arrows) are shown to the right.
(O and P) Quantification of Iba1pos brain macrophages within the choroid plexus (O) and meninges (P) of corn oil and tamoxifen-sensitized $CX_3CR1^{creERT2}$ x iDTR mice following intra-hippocampal DT injection. Representative images of Iba1^{pos} brain macrophages within the choroid plexus (outlined by the *dashed line*) and meninges (*arrows*) are shown to the right.
Data are represented as mean ± SEM. Statistics: unpaired Student's t test (J, K, M-P), one-way ANOVA (D, E, G, H – right, (I) – right, (L) - right), two-way ANOVA (A, B, F) followed by Bonferroni post hoc comparison, two-way ANOVA with repeated-measures followed by Bonferroni post hoc comparison (H) – left, (I) – left, (L) – left). (A-B), n = 3-6/group/time point; (C-G, M-P), n = 3-6/group; (H-L), n = 7-11/group. For (D-F), means are derived from 6 cells per sham mice and 16 cells per TBI mice. *p < 0.05, **p < 0.01, ***p < 0.001, ****p < 0.0001. CO = corn oil, TAM = tamoxifen, DT = diphtheria toxin.

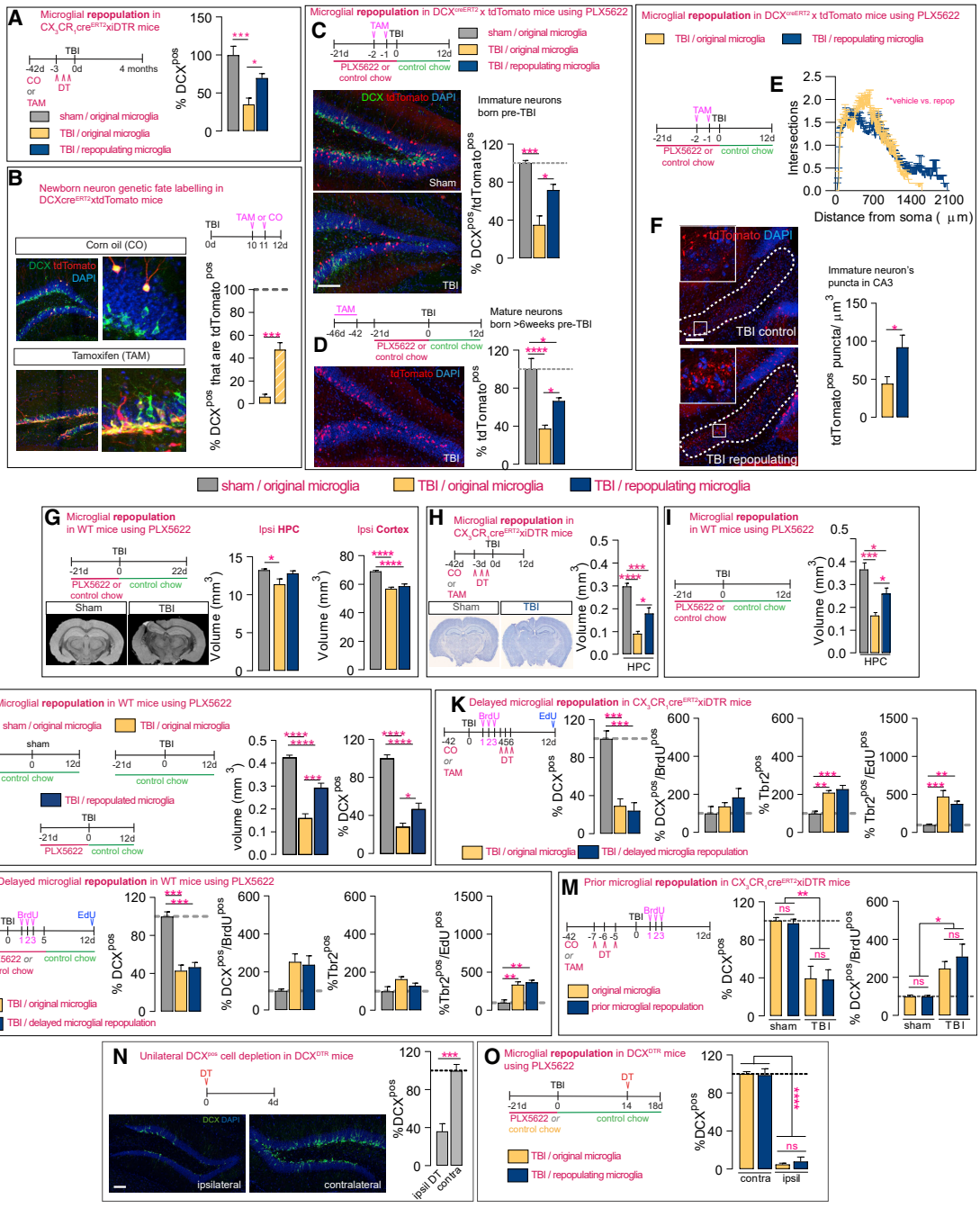


Figure S3. Time-Dependent Effects of Microglial Depletion/Repopulation on Neuronal Survival, Tissue Preservation, and/or Hippocampal Neurogenesis after TBI, Related to Figure 3

(A) Quantification of immature DCX^{pos} neurons in CX$_3$CR1^{creERT2} x iDTR mice, 4 months after surgery [F(2, 15) = 13.03, p = 0.0005]; asterisks indicate post hoc results.

(B) Specificity and recombination efficiency of reporter induction in DCX^{creERT2} x tdTomato TBI mice that were orally gavaged either corn oil (CO) as a control, or tamoxifen to mark adult-born neurons as per the timeline. Graph shows the proportion of DCX^{pos} immature neurons labeled with tdTomato reporter [t = 6.21, df = 6].

(C and D) Assessment of neuronal survival in DCX^{creERT2} x tdTomato mice subjected to PLX5622-mediated microglial depletion and repopulation. Mice were orally gavaged with tamoxifen to mark immature neurons born just before TBI or sham surgery (C), or ≥6 weeks prior (D). Graphs show ipsilateral numbers of immature DCX^{pos}tdTomato^{pos} neurons (C); [F(2,10) = 16.00, p = 0.0008] and mature, > 6-week-old tdTomato^{pos} granule cells (D); [F(2,20) = 18.13, p < 0.0001]) at 12 days post-surgery; asterisks indicate post hoc results for the relevant comparisons.

(legend continued on next page)

(E) Experimental design, timeline and sholl analysis of the dendritic morphology of adult-born (tdTomato^{pos}) neurons in the upper blade of the granule cell layer, 12 days after TBI, with and without repopulated microglia; averaged from 6-10 cells per DCX^{creERT2} x tdTomato mouse [t = 2.80, df = 365].

(F) Representative confocal images (*left*) and quantification (*right*) of tdTomato^{pos} puncta from adult-born neurons in the CA3 target region of DCX^{creERT2} x tdTomato mice [t = 2.80, df = 365].

(G) T1/T2 ex-vivo MRI measurements of total volumes for ipsilateral hippocampus (*left*; [F(2, 20) = 4.06, p = 0.033]) and cortex (*right*; F(2, 20) = 31.11, p < 0.0001]) for sham and TBI mice, with and without PLX5622-induced microglial turnover; asterisks indicate post hoc results.

(H) Quantification of dorsal hippocampal volumes in sham or TBI $CX_3CR1^{creERT2}$ x iDTR mice, with and without repopulated microglia, using cresyl violet staining at 12 days post-TBI [F(2,13) = 52.54, p < 0.0001]; asterisks indicate post hoc results.

(I) Dorsal hippocampal volumes, obtained from cresyl violet-stained sections of control and PLX5622-treated WT mice at 12 days post-surgery [F(2,11) = 21.15, p = 0.0002]; asterisks indicate post hoc results.

(J) Experimental design, timeline and results from independent replication experiments confirming the neuroprotective effects of repopulating microglia (conducted by A.G.Y. and D.C.A). Graphs show quantification of dorsal hippocampal volumes using cresyl violet staining (*left*) [F(2,24) = 51.58, p < 0.0001] and total immature neurons (i.e., DCX^{pos} cells; *right*) [F(2,24) = 53.33, p < 0.0001] in sham (n = 10) and WT TBI mice, with (n = 10) and without (n = 7) repopulated microglia, at 12 days post-TBI; asterisks indicate post hoc results for this replication study.

(K and L) Experimental timeline for delayed microglia depletion and repopulation during the sub-acute phase of TBI in both CX_3CR1creERT2 x iDTR (I) and PLX5622-treated (J) WT mice. TBI-associated changes in adult hippocampal neurogenesis were observed, but no benefit of microglia turnover with either approach.

(M) Experimental timeline and hippocampal neurogenesis data from sensitized (tamoxifen-treated) $CX_3CR1^{creERT2}$ x iDTR mice with induction of microglial turnover 1 week prior to TBI.

(N) Representative confocal images and quantification of immature DCX^{pos} neurons in the ipsilateral (left) and contralateral (right) granule cell layer of DCX^{DTR} mice, 4 days after unilateral DT injection [t = 7.03, df = 8, p = 0.0001].

(O) Confirmation of immature neuron depletion in the ipsilateral granule cell layer of injured DCX^{DTR} mice with and without repopulating microglia, 18 days post-TBI and 4 days after unilateral intra-hippocampal DT injection [F(1,24) = 689.4, p < 0.0001].

Data are represented as mean ± SEM (A-M). Data are presented as the percentage change (mean ± SEM) from average of the contralateral (contra) hemisphere (N,O). Statistics: one-way ANOVA with Bonferroni post hoc comparison (A, C, D, G-L), unpaired Student's t test (B, F, N), unpaired nonparametric Kolmogorov-Smirov t test (E), two-way ANOVA with Bonferroni post hoc comparison (M, O). n = 6-8/group (A, D, G), n = 4-8/group (B, C, E, F-I, K, L), n = 7-10/group (J), n = 5-9/group (N), n = 7-8/group (O). *p < 0.05, **p < 0.01, ***p < 0.001, ****p < 0.0001. (N) Scale bar: 100μm. ns = not significant. TAM = tamoxifen, CO = corn oil, DT = diphtheria toxin.

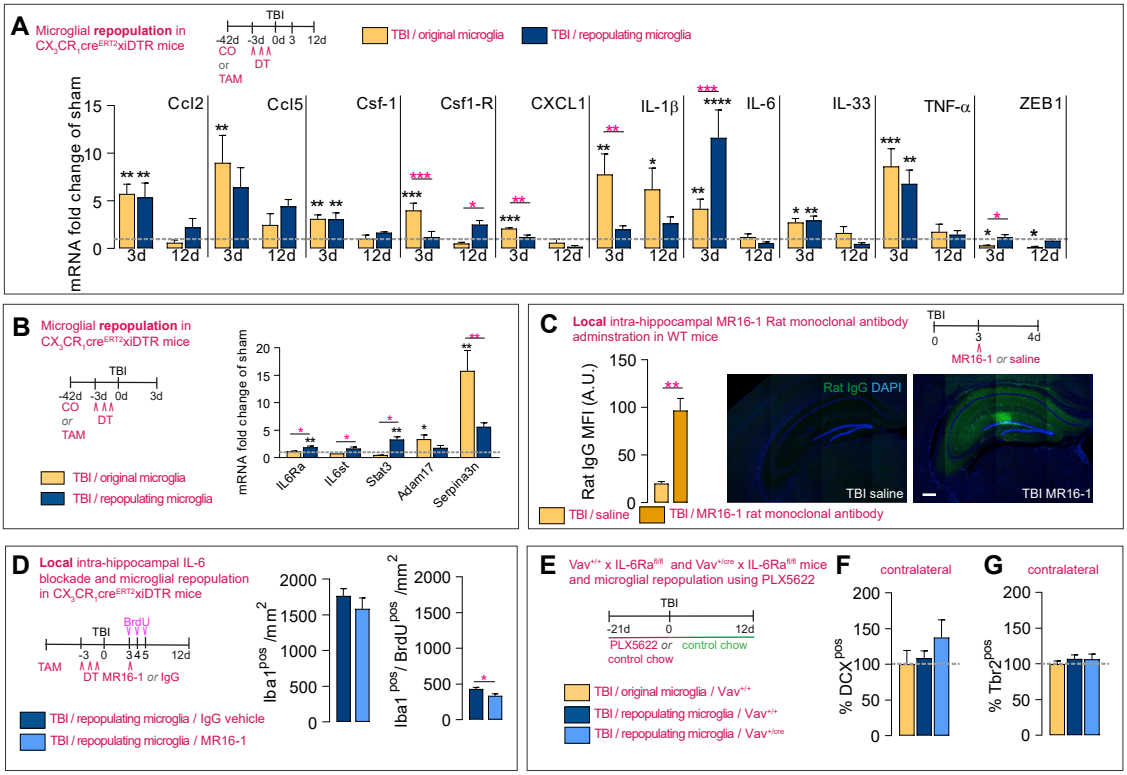


Figure S4. Effects of Microglial Depletion and Repopulation on Immune-related Gene Expression, and that of IL-6 Signaling Blockade on Hippocampal Neurogenesis and Microglia Proliferation, Related to Figure 4

(A and B) qPCR data for select genes associated with TBI-related immune processes (A) and IL-6 signaling (B) in the ipsilateral hippocampus of $CX_3CR1^{CreERT2}$ x iDTR mice with original (yellow bars) versus repopulating (blue bars) microglia at 3 days after TBI. Expression is relative to the Hprt gene and presented as the 'fold change' from sham-operated controls (dotted gray line). Black and magenta asterisks are Sham 'original microglia' versus TBI 'original microglia' and TBI 'original microglia' versus TBI 'repopulating microglia', respectively.

(C) Experimental timeline and assessment of MR16-1 spread. Graph shows mean fluorescence intensity (MFI) of anti-rat immunoglobulin (IgG) immunostaining, 24 h after injection of either MR16-1 or saline into the hippocampus of WT TBI mice [t = 5.91, df = 6, p = 0.0010]. Representative confocal images of anti-rat IgG (F(ab)2-specific) immunostaining are shown on the *right*.

(D) Timeline (left) and quantitative data (right) on $Iba1^{pos}$ cell numbers in $CX_3CR1^{CreERT2}$ x iDTR TBI mice with repopulating microglia and IL-6 receptor (IL-6Ra) blockade with MR16-1. MR16-1 or isotype control IgG was injected directly into the hippocampus at 3 days after injury. Graphs show quantification of total (left) and proliferated (right) $Iba1^{pos}$ microglia in the ipsilateral dentate gyrus. A small (~20%) decrease was observed in the number of microglia generated post-TBI with MR16-1 treatment [t = 2.49, df = 6, p = 0.047].

(E,F) Experimental timeline and contralateral neurogenesis data for microglia depletion/repopulation studies in $Vav^{+/+}$ x $IL\text{-}6Ra^{flox/flox}$ and $Vav^{+/cre}$ x $IL\text{-}6Ra^{flox/flox}$ mice with TBI. Adult hippocampal neurogenesis was unaltered here in $Vav^{+/cre}$ x $IL\text{-}6Ra^{flox/flox}$ mice.

Data are represented as mean ± SEM n = 4-8/group (A-G). Statistics: one-way ANOVA (A,B, F, G) with Bonferroni post hoc for all, and unpaired Student's t test (C, D). *p < 0.05, **p < 0.01, ***p < 0.001, ****p < 0.0001, ns = not significant. DT = diphtheria toxin. CO = corn oil. TAM = tamoxifen. MFI = mean fluorescence intensity, A.U. = arbitrary units.

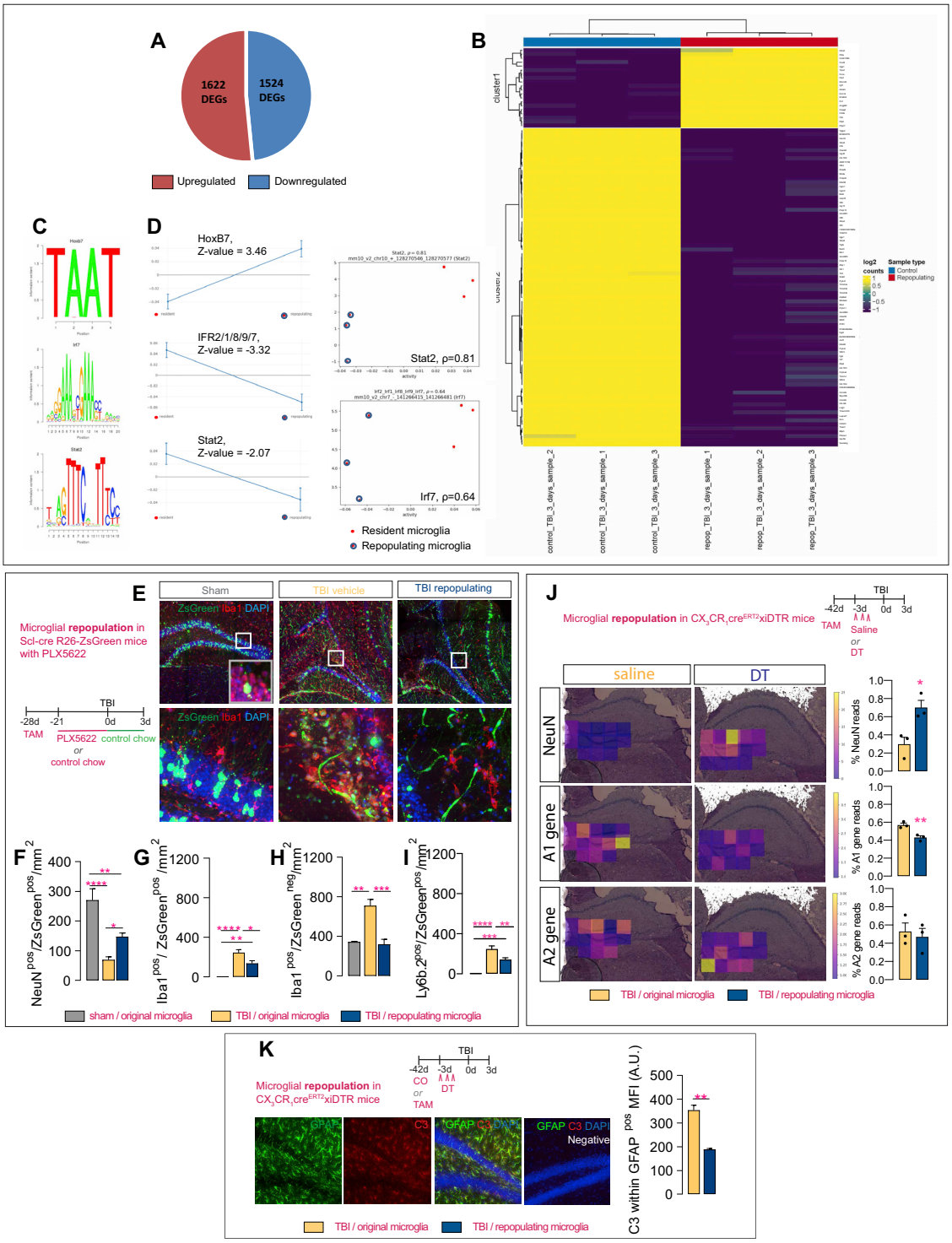


Figure S5. Repopulating Microglia Have a Unique Transcriptional Profile and Their Depletion and Repopulation Modulates Leukocyte Recruitment and Astrocyte Reactivity 3 Days after TBI, Related to Figure 5

(A) Pie chart indicating the number of up- and downregulated genes between original and repopulating microglia using an FDR cut-off of < 0.05.

(B) Heatmap for top 100 DEGs, based on p value, between original microglia ("control TBI") and repopulating ones ("repop TBI"), with 3 biological replicates per group (log gene expression).

(C) Top-3 predicted differentially expressed DNA-binding motifs, as determined by ISMARA analysis.

(D) Activity/expression correlation for STAT2 and IRF7, as determined by ISMARA analysis.

(legend continued on next page)

(E) Timeline and representative confocal photomicrographs from experiments in Scl-cre^{ERT2} x ZsGreen mice, showing infiltrating bone marrow-derived (i.e., ZsGreen^{pos}, arrows) leukocytes in the ipsilateral hippocampus 3 days post-TBI. A small proportion of neurons also expresses ZsGreen (see inset in sham), but not Iba^{pos} microglia; ZsGreen expression was also observed in vascular structures under TBI conditions.

(F-I) Quantification of ZsGreen^{pos}NeuN^{pos} neurons (F), [F(2, 12) = 20.78, p = 0.0001]), peripherally-derived Iba1^{pos}ZsGreen^{pos} monocytes/macrophages (G), [F(2, 12) = 21.54, p = 0.0001]), Iba1^{pos}ZsGreen^{neg} brain microglia (H, [F(2,12) = 17.36, p = 0.0003]), as well as Ly6b.2^{pos}ZsGreen^{pos} neutrophils (I, [F(2,12) = 35.46, p < 0.0001]) in the ipsilateral dentate gyrus at 3 days post-TBI; asterisks indicate post hoc results. Note that, under naive (sham surgery) conditions, intraparenchymal ZsGreen is 100% localized to a subset of Scl-expressing NeuN^{pos} neurons in the adult hippocampus (Bradley et al., 2007). Under injury conditions, intraparenchymal ZsGreen-expressing cells are ~12%–29% NeuN^{pos} neurons, ~33%–36% Iba1^{pos} monocytes/macrophages, and ~31%–48% Ly6B.2^{pos} neutrophils.

(J) Experimental time line and representative images (n = 3 per condition) of spatial transcriptomics data, with the spatial distribution and expression level of NeuN (RBFOX3; top), signature A1 (middle) and A2 (bottom) genes superimposed onto the dentate gyrus. Graphs show the average amount of NeuN [t = 3.65, df = 4], A1 [t = 4.76, df = 4], and A2 genes within this region of interested (percentage of total reads). A1 genes (*H2-T23*, *Serping1*, *H2-D1*, *Ggta1*, *Iigp1*, *Gbp2*, *Fbln5*, *Ugt1a1*, *Fkbp5*, *Psmb8*, *Srgn*, and *Amigo2*); A2 genes (*Clcf1*, *Tgm1*, *Ptx3*, *S100a10*, *Sphk1, Cd109*, *Ptgs2*, *Emp1*, *Slc10a6*, *Tm4sf1, B3gnt5*, and *Cd14*)

(K) Mean fluorescence intensity (MFI) of C3 staining (A1 marker) on GFAP^{pos} astrocytes in the ipsilateral dentate gyrus of CX$_3$CR1^{creERT2} x iDTR mice with original versus repopulating microglia (3 days post-TBI; [t = 6.77, df = 5]).

(F-K) Data are is presented as mean ± SEM (A, B, J) n = 3 biological replicates per group. (E-H) n = 4-6/group, (K) n = 3-4/group.Statistics: one-way ANOVA with Bonferroni post hoc comparison (F-I), unpaired Student's t test (J, K). *p < 0.05, **p < 0.01, ***p < 0.001; ****p < 0.0001.

Yates et al. Journal of Neuroinflammation (2021) 18:15
https://doi.org/10.1186/s12974-020-02050-6

Journal of Neuroinflammation

RESEARCH Open Access

Acute IL-1RA treatment suppresses the peripheral and central inflammatory response to spinal cord injury

Abi G. Yates[1,2], Trisha Jogia[2], Ellen R. Gillespie[2], Yvonne Couch[3], Marc J. Ruitenberg[2] and Daniel C. Anthony[1,4*]

Abstract

Background: The acute phase response (APR) to CNS insults contributes to the overall magnitude and nature of the systemic inflammatory response. Aspects of this response are thought to drive secondary inflammatory pathology at the lesion site, and suppression of the APR can therefore afford some neuroprotection. In this study, we examined the APR in a mouse model of traumatic spinal cord injury (SCI), along with its relationship to neutrophil recruitment during the immediate aftermath of the insult. We specifically investigated the effect of IL-1 receptor antagonist (IL-1RA) administration on the APR and leukocyte recruitment to the injured spinal cord.

Methods: Adult female C57BL/6 mice underwent either a 70kD contusive SCI, or sham surgery, and tissue was collected at 2, 6, 12, and 24 hours post-operation. For IL-1RA experiments, SCI mice received two intraperitoneal injections of human IL-1RA (100mg/kg), or saline as control, immediately following, and 5 hours after impact, and animals were sacrificed 6 hours later. Blood, spleen, liver and spinal cord were collected to study markers of central and peripheral inflammation by flow cytometry, immunohistochemistry and qPCR. Results were analysed by two-way ANOVA or student's t-test, as appropriate.

Results: SCI induced a robust APR, hallmarked by elevated hepatic expression of pro-inflammatory marker genes and a significantly increased neutrophil presence in the blood, liver and spleen of these animals, as early as 2 hours after injury. This peripheral response preceded significant neutrophil infiltration of the spinal cord, which peaked 24 hours post-SCI. Although expression of IL-1RA was also induced in the liver following SCI, its response was delayed compared to IL-1β. Exogenous administration of IL-1RA during this putative therapeutic window was able to suppress the hepatic APR, as evidenced by a reduction in CXCL1 and SAA-2 expression as well as a significant decrease in neutrophil infiltration in both the liver and the injured spinal cord itself.

Conclusions: Our data indicate that peripheral administration of IL-1RA can attenuate the APR which in turn reduces immune cell infiltration at the spinal cord lesion site. We propose IL-1RA treatment as a viable therapeutic strategy to minimise the harmful effects of SCI-induced inflammation.

Keywords: Neurotrauma, Systemic inflammatory response syndrome, Acute phase response, IL-1 receptor antagonist, Neutrophils, Macrophage

* Correspondence: daniel.anthony@pharm.ox.ac.uk
[1]Department of Pharmacology, The University of Oxford, Mansfield Road, Oxford, UK
[4]Sechenov First Moscow State Medical University, Moscow, Russia
Full list of author information is available at the end of the article

© The Author(s). 2021 **Open Access** This article is licensed under a Creative Commons Attribution 4.0 International License, which permits use, sharing, adaptation, distribution and reproduction in any medium or format, as long as you give appropriate credit to the original author(s) and the source, provide a link to the Creative Commons licence, and indicate if changes were made. The images or other third party material in this article are included in the article's Creative Commons licence, unless indicated otherwise in a credit line to the material. If material is not included in the article's Creative Commons licence and your intended use is not permitted by statutory regulation or exceeds the permitted use, you will need to obtain permission directly from the copyright holder. To view a copy of this licence, visit http://creativecommons.org/licenses/by/4.0/. The Creative Commons Public Domain Dedication waiver (http://creativecommons.org/publicdomain/zero/1.0/) applies to the data made available in this article, unless otherwise stated in a credit line to the data.

Introduction

Systemic inflammatory response syndrome (SIRS) is a major and frequent complication in trauma patients with a spinal cord injury (SCI). Development of SIRS not only has the potential to cause multi-organ damage and/or dysfunction [1, 2], it is also thought to influence inflammatory pathology and lesion site development in the injured central nervous system (CNS) itself, including following brain or spinal cord insult. Previous studies from our lab have demonstrated that the latter is heavily influenced by the magnitude of early systemic inflammatory changes, a process referred to as the acute phase response (APR), which predominantly occurs in the liver [3–7]. Here, pro-inflammatory cytokines and chemokines as well as acute phase proteins (APPs) are upregulated as early as 2 hours post-injury [5, 7–10]. These mediators contribute to the mobilisation and priming of leukocytes, facilitating their translocation to sites of CNS injury.

Neutrophils are the first peripheral immune cells to be recruited to CNS lesion sites, including in SCI [11], and they are known to release proteases and generate oxidative species [12, 13]. In peripheral trauma, this enables degradation of debris which is beneficial to the host. However, in the CNS, this causes further membrane damage, lipid peroxidation, DNA fragmentation and cellular injury [14]. Activated neutrophils also release pro-inflammatory mediators, which can contribute to the development of a chronic immune response [15, 16] and exacerbate the neurological deficit [17].

Interleukin-1β (IL-1β) is a key early component of the APR and cytokine cascade initiated after SCI. Undetectable in the uninjured cord [18, 19], this pro-inflammatory cytokine is significantly upregulated within 1 hour of injury [20–23], and thought to play a pivotal role in the recruitment of various leukocyte subsets [24–26]. Early inhibition of IL-1β signalling could therefore be of significant benefit. IL-1 receptor antagonist (IL-1RA) is an endogenous competitive antagonist that inhibits IL-1 signalling and subsequent downstream pro-inflammatory events [18]. IL1-RA expression in the injured CNS is initially downregulated compared to IL-1β [27], but its exogenous administration can lead to improvements in cognitive deficits [28, 29], tissue loss [29] and leukocyte recruitment [30, 31] in models of traumatic brain injury (TBI) and stroke. IL-1RA has also been used in models of SCI [32–34] but the focus, as with studies in the brain, has tended to be on its suppressive effects in the CNS only. With recent papers demonstrating important interactions between migrating neutrophils and components of the CNS immune system [35], a better understanding of the peripheral effects of IL-1RA treatment is highly significant as it potentially negates the need to circumvent the precarious blood-CNS barrier.

In this paper we investigated the peripheral immune response to a lower thoracic SCI and determined how treatment with the endogenous antagonist IL-1RA impacted on the APR and neutrophil recruitment to the injured spinal cord.

Methods

Animals

Female C57BL/6J mice, 8-12 weeks old, were used in this study, as described previously [36, 37], due to reduced risk of post-operative complications. Animals were obtained from the Animal Resource Centre (Canningvale, Western Australia) and housed in individually ventilated cages in a specific pathogen-free facility, under standard diurnal lighting conditions (12 hours) with *ad libitum* access to food and water. The experimental holding room had temperature (21.5 °C set point) and humidity control (40% set point), and was supplied with HEPA-filtered air. Animals were allowed to acclimatise for 4 weeks prior to experiments. All experiments were approved by The University of Queensland's Animal Ethics Committee (Anatomical Biosciences) and were conducted in accordance with the Australian Code for the Care and Use of Animals for Scientific Purposes.

Spinal cord injury model

Mice were anaesthetised by intraperitoneal injection using a combination of tiletamine/zolezepam (50mg/kg; Virbac) and xylazine (10mg/kg; Troy Laboratories). Following incision of the skin over the lower thoracic region of the back, the paravertebral muscles were separated and anatomical landmarks utilised to identify T9 [38]. A dorsal laminectomy was then performed to expose the spinal cord [39–41], after which the vertebral column was clamped for stabilisation and a moderate contusive 70kDyne (kD) SCI inflicted using the Infinite Horizon Impactor (Precision Systems and Instrumentation). Muscle and skin were then closed with 6-90 polygalactin dissolvable sutures (Ethicon) and Michel wound clips (Kent Scientific), respectively. Age- and weight-matched sham-operated controls were subjected to laminectomy only. All mice received a single dose of buprenorphine in Hartmann's sodium lactate (1mg/kg; sub cutaneous; Sigma Aldrich) post-surgery. Naïve control mice, which were included for baseline results, did receive anaesthesia but no surgical intervention.

IL-1RA treatment

Animals received two intraperitoneal injections of human IL-1RA (100mg/kg), the first immediately following impact whilst still under general anaesthesia, and the second 5 hours post-injury. This treatment regime was based on previous papers reporting neuroprotective effects of IL-1RA in models of CNS injury [30, 42].

Sample collection and processing

For time-course analysis, animals were allowed to survive for 2, 6, 12 and 24 hours post-surgery. For IL-1RA experiments, animals were culled 6 hours post-surgery.

All mice were anaesthetised with 4% isoflurane and blood was collected by cardiac puncture into a heparinised tube (BD Microtainer). Mice were then transcardially perfused with 20mL of heparinised saline (0.9% NaCl, 10IU/mL heparin (Pfizer), 2% $NaNO_3$) and fresh liver and spleen samples collected for qPCR. Liver was snap-frozen in liquid nitrogen and stored at -80°C, whilst spleen was processed immediately for flow cytometry (see below). Mouse cadavers were then transcardially perfused with 30mL of Zamboni's fixative (2% picric acid, 2% paraformaldehyde, pH 7.2-7.4), and fixed liver and spinal column samples removed and stored in fixative overnight at 4°C. Spinal cords were extracted from the columns the following day and post-fixed at 4°C for an additional 24 hours. Tissues were cryoprotected (overnight incubations in 10% and 30% sucrose solution), embedded in optimal cutting temperature compound (OCT, ProSciTech), then snap-frozen in dry ice-cooled 2-methyl-butane and stored at -80°C until further use. Fixed liver (10μm) and spinal cord (transverse, 20μm) were sectioned using a Leica Cryostat (CM1850).

Flow cytometry

Fresh spleen samples were mechanically dissociated through a 70μm cell strainer (Life Technologies) and splenocytes pelleted through low-speed centrifugation (300*g* for 10 minutes). Cells were then resuspended in 5mL of red blood cell (RBC) lysis buffer, incubated for 5 minutes at room temperature (RT), before being centrifuged again and resuspended in Dulbecco's PBS (DPBS); 5 million splenocytes per sample were used for analysis. Blood samples were diluted 1:5 in RBC lysis buffer for 5 minutes at RT, after which they were centrifuged and resuspended in 100μl of DPBS for analysis.

To exclude dead cells, splenocyte and blood samples were incubated with Zombie Green or Zombie Near Infrared (1:100 in DPBS), respectively, for 20 minutes at RT in the dark. CD16/32 F_C block (BD Biosciences), diluted 1:200 in blocking buffer (0.5% Bovine serum albumin [BSA], 2mM EDTA in DPBS), was used to prevent non-specific antibody binding. Samples were immunolabelled for 20 minutes in the dark with Alexa Fluor® 647 rat α-mouse Ly6G (1A8; 1:100; BioLegend), V450 rat α-mouse Ly6C (AL-21; 1:100; BD Horizon), PE rat α-mouse F4/80 (1:50; BD Biosciences) and BV 785™ rat α-mouse/human CD11b (M1/70; 1:100; BioLegend) for spleen, or PE rat α-mouse/human CD11b (M1/70; 1:200; BioLegend) for blood. Next, 1mL of blocking buffer was added and the cells isolated by low-speed centrifugation at 4°C. Cell pellets were resuspended in blocking buffer and then analysed using the LSR II flow cytometer (BD Biosciences) with BD FACS Diva software.

Clumped cells, debris and dead cells were removed during the gating process; neutrophils and monocytes were defined as the $CD11b^+SSC^{hi}Ly6G^+$ and $CD11b^+SSC^{lo}F4/80^{lo}Ly6G^-$ populations, respectively. Propidium iodide-fluorescing counting beads (10μl; Beckman Coulter) were added to each sample to enable the absolute quantification of cell numbers.

Immunostaining and quantification

For Immunofluorescent staining, fixed spinal cord sections were blocked for non-specific binding with 10% BSA in PBS with 0.3% Triton X-100 for 1 hour at RT. Sections were then incubated overnight at 4°C with primary antibody (rat α-Ly6B.2, 1:200, Bio-Rad). The following day, sections were washed in PBS and incubated in secondary antibody (donkey α-rat 594, 1:400, Jackson Immunoresearch) and Hoechst 33342 nuclear dye (1:1000, Sigma) for 1 hour at RT. Sections were then washed again, mounted with DAKO fluorescent mounting medium (Sigma) and coverslip.

For immunohistochemical staining with the chromogenic reporter 3,3'-Diaminobenzidine (DAB), fixed liver and spinal cord sections were first blocked for endogenous peroxidase activity (1% H_2O_2 in methanol) and biotin (1:20 in PBS, Vector Labs), followed by incubation with 10% goat serum in PBS for 1 hour at RT to reduce non-specific protein binding. Sections were then incubated overnight at 4°C with primary antibody (rabbit α-MBS neutrophils, 1:10,000, made in house; rabbit α-IBA-1, 1:2000, Abcam), diluted in 1% goat serum in PBS. Next, sections were incubated in goat α-rabbit biotinylated secondary antibody (1:200; Vector Labs) for 2 hours at RT, followed by ABC (1:100; ThermoFisher) for 1 hour at room temperature. After several rounds of washing, sections were incubated in DAB until a satisfactory level of staining was achieved; 1% Harris Haemotoxylin or cresyl violet was used as a counterstain for liver and spinal cord, respectively. Stained sections were dehydrated through graded alcohols (80%, 90%, 2x100%, 5 minutes each), cleared with xylene (2x5 minutes), mounted with non-aqueous mounting medium and coverslipped.

For quantification, stained cells in liver sections were counted directly using a light microscope (Leitz Dialux 20) with an eyepiece grid at x40 magnification, across three sections, in three representative fields per section. For the spinal cord, immunopositive neutrophils were counted at the lesion epicentre and for ±1.0mm in rostral and caudal direction using the either Nikon Eclipse upright automated stereology and slide

scanning microscope with Stereo Investigator software (immunofluorescent staining), or the Leitz Dialux 20 light microscope (immunohistochemical staining). All cell counting was performed blinded.

RNA extraction and qPCR

RNA was extracted from approximately 30mg of snap-frozen fresh liver (Qiagen© RNEasy Mini Kit). RNA concentration was measured using a NanoDrop (ThermoFisher) and 1000ng of sample was converted to cDNA using the Applied Biosystems High Capacity cDNA conversion kit. Real-time qPCR was performed with duplicates for each sample (10-25ng/well) using SYBR green qPCR master mix (Applied Biosystems or PrimerDesign) and the Applied Biosystems QuantStudio Flex 7 or Roche LightCycler 480. The following primers were purchased from PrimerDesign: GAPDH (F: AACGACCCCT TCATTGAC, R: TCCACGACATACTCAGCAC), RPL13a (F: GAGGTCGGGTGGAAGTACCA, R: TGCATCTTGG CCTTTTCCTT), IL-1β (F: CAACCAACAAGTGATATT CTCCAT, R: GGGTGTGCCGTCTTTCATTA), CXCL1 (F: GCTGGGATTCACCTCAAGAAC, R: TGTGGCTAT GACTTCGGTTTG), CXCL10 (F: CATCCCGAGCCAAC CTTCC, R: CACTCAGACCCAGCAGGAT), SAA-2 (F: TGGCTGGAAAGATGGAGACAA, R: AAAGCTC TCTCTTGCATCACTG) and IL-1Rn (F: GACCTTTT ACCTGAGAAACAAC, R: TAGGCACCATGTCTAT CTTTTC). Relative expression was determined by the $2^{-\Delta\Delta Ct}$ method and normalisation to housekeeping genes (GAPDH and RPL13a).

Statistical analysis

All analysis was completed with GraphPad Prism 7 software. Unpaired student's t-test, one- and two-way analysis of variance (ANOVA) were employed, with post-hoc testing as appropriate. Results were considered significant at $p<0.05$ with 95% confidence intervals. All quantitative data are expressed as mean ± standard error of the mean (SEM).

Results

Surgery induces a robust but differential APR in the liver of sham and SCI mice

We first evaluated the temporal profile of the APR in response to a moderate T9 SCI. Previous work from our group has demonstrated that the level of expression of the mRNA for acute phase proteins is a reliable measure of the acute phase response by the liver, and that the levels reflect the subsequent protein expression levels [5, 9]. The relative expression of IL-1β mRNA (Fig. 1a) and CXCL10 mRNA (Fig. 1b) was elevated in both the sham and SCI groups at 2 hours post-injury. By 6 hours, the expression of these mRNA species had returned to naïve baseline levels in the sham controls, but they remained increased in the SCI mice (IL-1β $p<0.01$, CXCL10 $p<0.05$; student's t-test). Expression of CXCL1 was increased in all operated mice (Fig. 1c), yet it was significantly decreased in the SCI mice compared to the sham controls at both 6 ($p<0.05$) and 24 hours ($p<0.01$) post-injury. Expression of SAA-2 (Fig. 1d) was also significantly increased over naïve baseline levels in both sham and SCI mice, although there was a trending decrease in the SCI animals at 6 hours post-injury; direct comparison at this time point indeed revealed a significant difference ($p<0.01$), which was lost when correcting for multiple comparisons ($p=0.182$). Lastly, hepatic expression of IL-1RA, the endogenous antagonist to IL-1, was also significantly increased in response to SCI (6 hours post-injury, $p<0.05$; Fig. 1e), however, peak expression was delayed compared to that of IL-1β expression. Thus, there was a selective increase in the injury-induced expression of specific APR elements (i.e. IL-1β and CXCL10) following SCI while others (CXCL1 and SAA-2) appeared to be suppressed compared to the sham-operated controls. Taken together with the IL-1RA results, these findings highlight the pro- and anti-inflammatory aspects of the SIRS response.

The APR of SCI mice is associated with an increased presence of myeloid cells in the liver that precedes the timing of their recruitment to the spinal cord

We next employed both flow cytometry and immunohistochemistry to investigate downstream myeloid cell responses in the blood, spleen and liver. Circulating $CD11b^{+}SSC^{hi}Ly6G^{+}$ granulocytes, representing predominantly neutrophils and a small proportion of basophils and eosinophils, were significantly elevated over naïve baseline in both sham and SCI mice at 2, 6, and 12 hours post-surgery (Fig. 2a). $CD11b^{+}SSC^{hi}Ly6G^{+}$ granulocytes were also increased acutely (2-12 hours) in the spleens of all operated mice (Fig. 2b), with trending increases in SCI mice at both 2 ($p=0.104$) and 6 ($p=0.072$) hours post-surgery. $CD11b^{+}Ly6G^{-}$ monocytes in the blood were increased in all animals above naïve at 2 hours post-surgery (Fig. 2c). At 6 hours, circulating monocytes in sham animals returned to baseline, but they remained elevated in SCI animals, although this was not statistically significant. In the spleen, the number of $CD11b^{+}SSC^{lo}F4/80^{lo}Ly6C^{lo}$ monocytes showed a non-significant increase at 2 hours, and they then decreased at 6-24 hours in all animals compared to naïve controls (Fig. 2d). Acute increases in (MBS^{+}) neutrophil numbers were also observed in the livers of both sham and SCI mice, although a greater cell density was observed in animals with neurological injury ($p<0.05$ at 2 and 6 hours, and $p=0.055$ at 12 hours; Fig. 2e), before returning to baseline control levels by 24 hours post-surgery. The number of Iba-1^{+} monocytes/macrophages

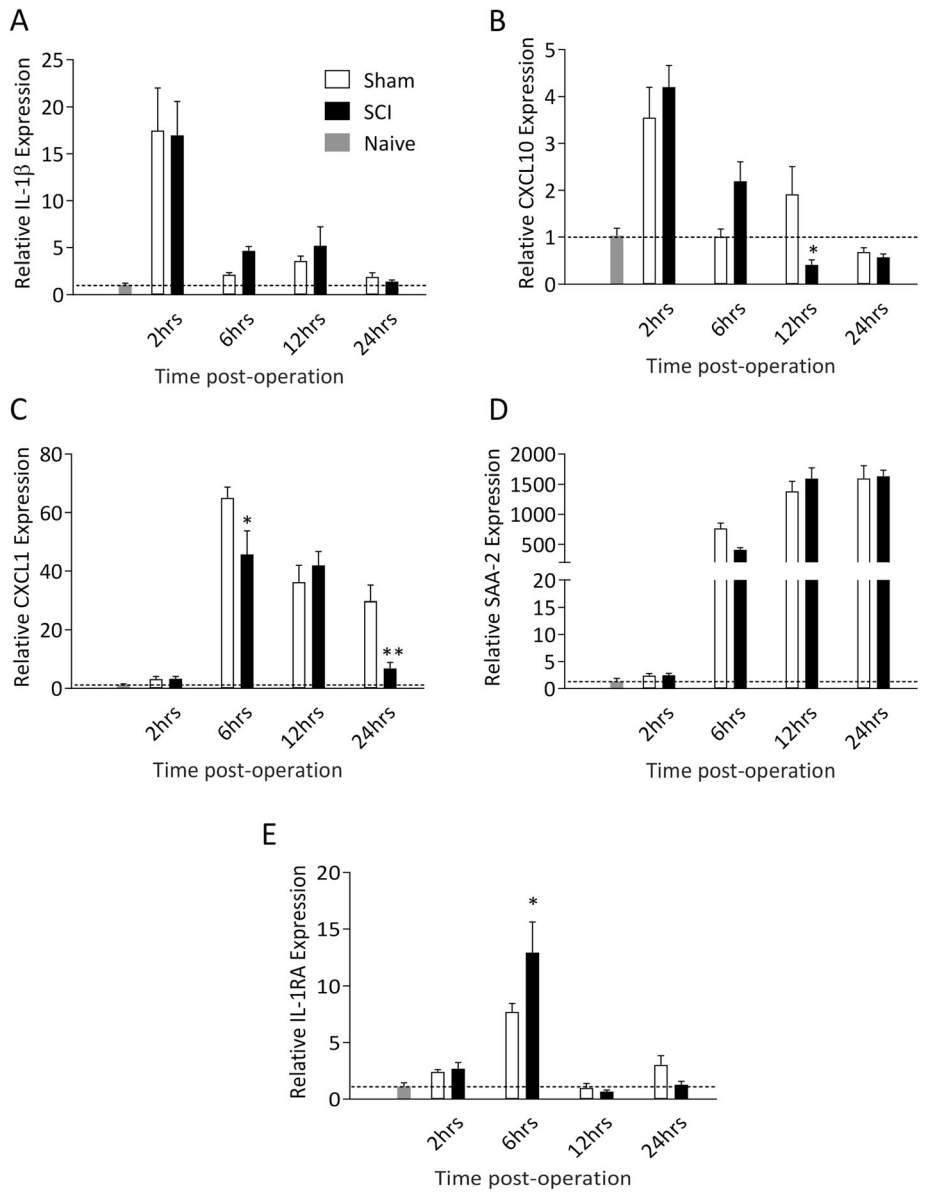


Fig 1. Spinal cord injury induces expression of inflammatory genes in the liver. Female C57BL/6 mice underwent either a 70kD SCI (black bars, *N*=4-5/time point) or sham surgery (white bars, *n*=5/time point). Tissue was collected at 2, 6, 12 and 24 hours post-operation and compared to naïve baseline (grey bar and dotted line, *n*=5). Relative hepatic expression levels of inflammatory genes IL-1β (**a**), CXCL10 (**b**), CXCL1 (**c**) and SAA-2 (**d**), and the IL-1 receptor antagonist IL-1RA (E) were determined by qPCR. Data are presented as mean ±SEM and were analysed by two-way ANOVA. **p*<0.05, ***p*<0.01 with post-hoc test

was also elevated in the livers of SCI, but not of sham mice, and they progressively increased over the first 24 hours post-surgery ($p<0.05$ at 12 hours, $p<0.01$ at 24 hours; Fig. 2f). Finally, while the liver neutrophil response to SCI (or sham surgery) did mostly subside by 24 hours post-surgery, recruitment/presence of these cells at the spinal cord lesion site continued to increase dramatically over the same time period ($p<0.0001$; Fig. 3).

Acute treatment with exogenous IL-1RA attenuates the liver APR and reduces neutrophil recruitment to the injured spinal cord

Given the time delay between IL-1β and the reciprocal IL-1RA expression, we investigated the effect of supplementing IL-1RA on inhibiting the IL-1β-mediated peripheral inflammatory response. For this, human IL-1RA (100mg/kg) was administered intraperitoneally immediately after contusive SCI and then again 5 hours later.

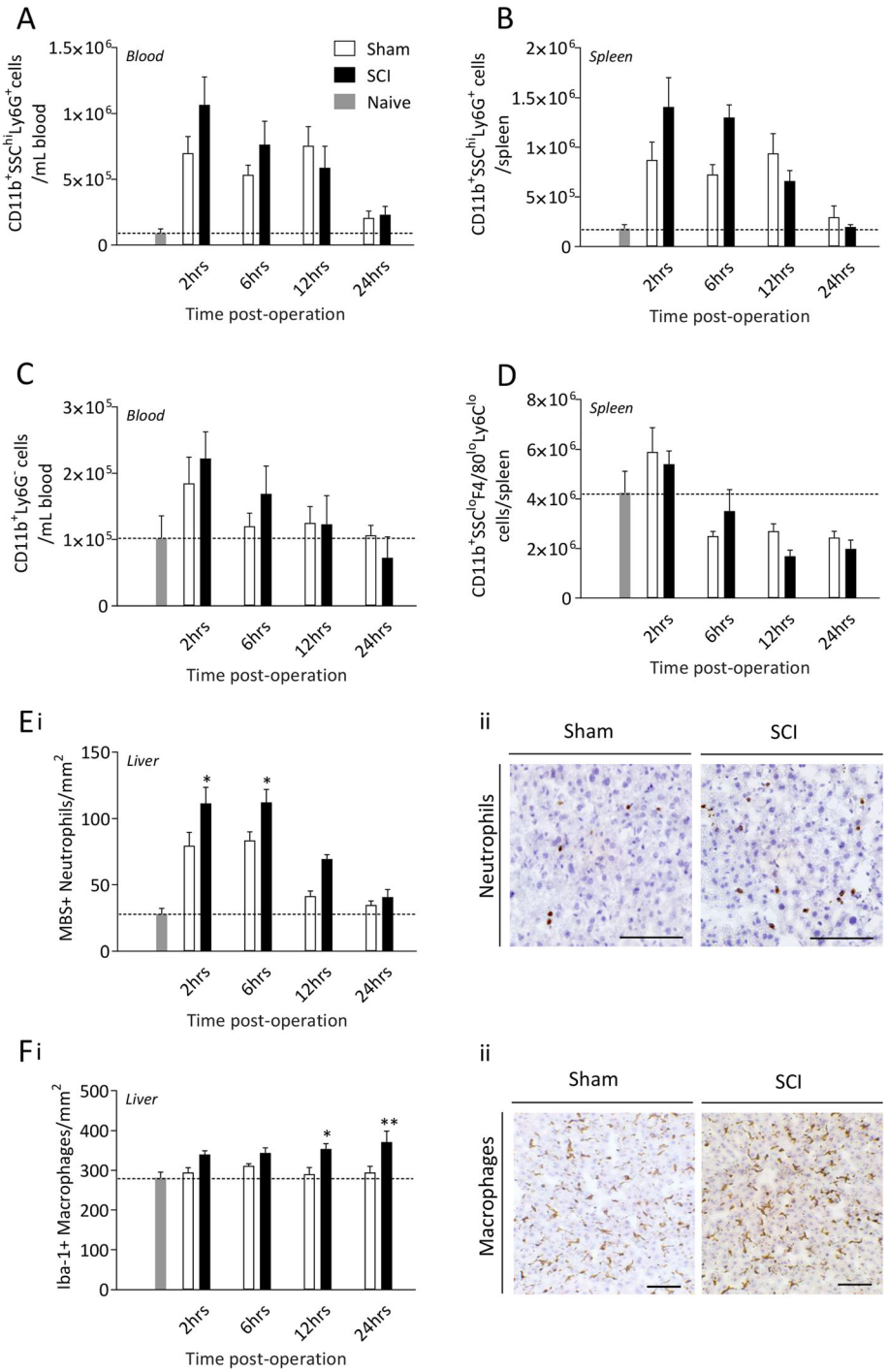


Fig 2. Spinal cord injury induces leukocyte mobilisation in the periphery. Female C57BL/6 mice underwent either a 70kD SCI (black bars, *n*=4-5/time point) or sham surgery (white bars, *n*=5/time point). Tissue was collected at 2, 6, 12 and 24 hours post-operation and was compared to naïve baseline (grey bar and dotted line, *n*=5). Neutrophil mobilisation in the blood (**a**) and spleen (**b**), and monocyte mobilisation in the blood (**c**) and spleen (**d**) was determined by flow cytometry. Neutrophil (**e**) and macrophage (**f**) density in the liver was measured by immunohistochemistry. Representative images of neutrophil and macrophage density in each injury group at peak immune cell density; neutrophil and macrophage density were greatest at 2 and 24 hours post-SCI respectively. Scale bar represents 50μm. Data are presented as mean ±SEM and were analysed by two-way ANOVA, *$p<0.05$, **$p<0.01$ with post-hoc test

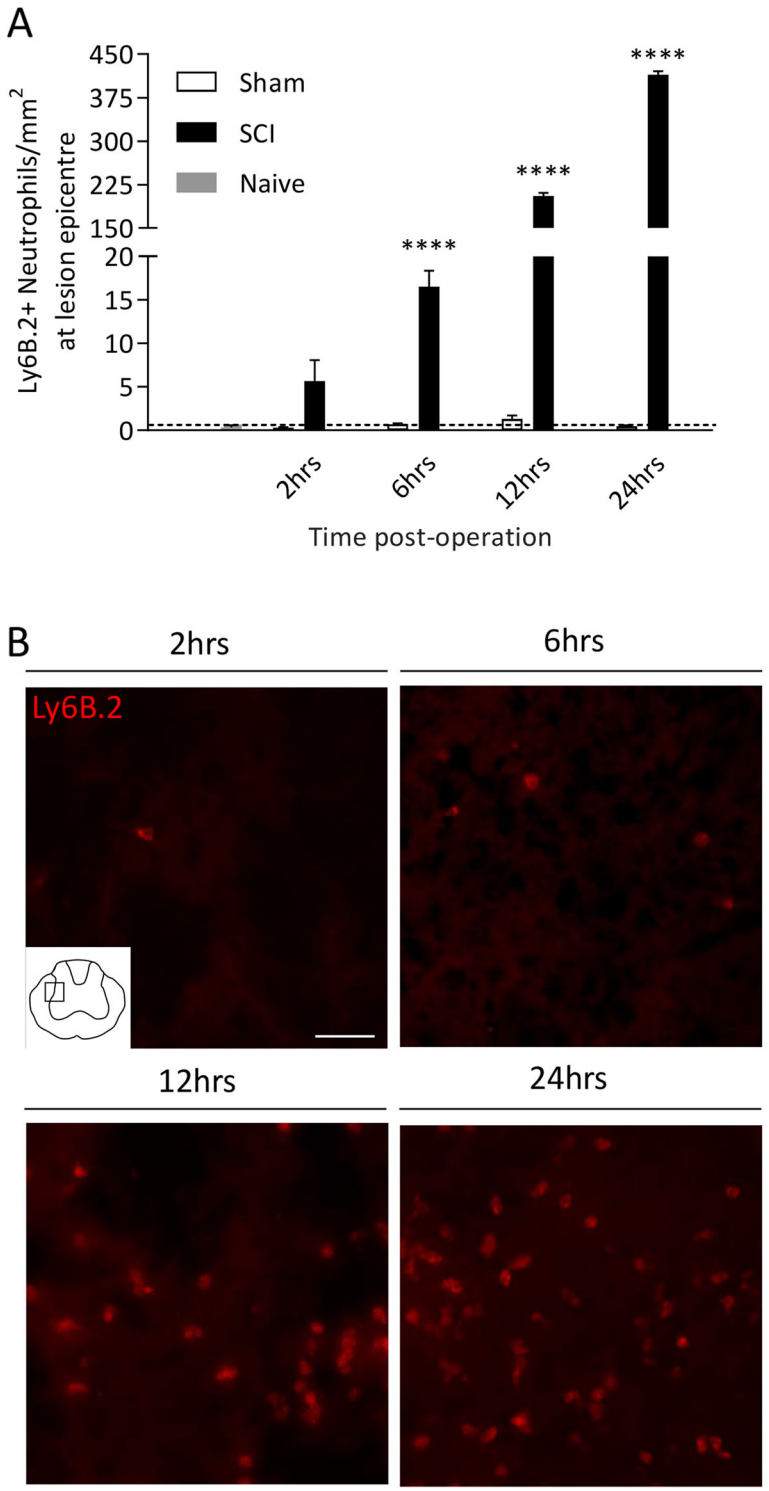


Fig 3. Neutrophil infiltration of the spinal cord lesion peaks 24 hours post-injury. Female C57BL/6 mice underwent either a 70kD SCI (black bars, *n*=4-5/time point) or sham surgery (white bars, *n*=5/time point). Tissue was collected at 2, 6, 12 and 24 hours post-operation and was compared to naïve baseline (grey bar and dotted line, *n*=5). Neutrophil cell density was calculated at the lesion epicentre (**a**). Representative images of neutrophil density in the epicentre of spinal cord lesions at each time point (**b**). Scale bar represents 50μm. Data are presented as mean ±SEM. Two-way ANOVA, ****$p<0.0001$ with post hoc test

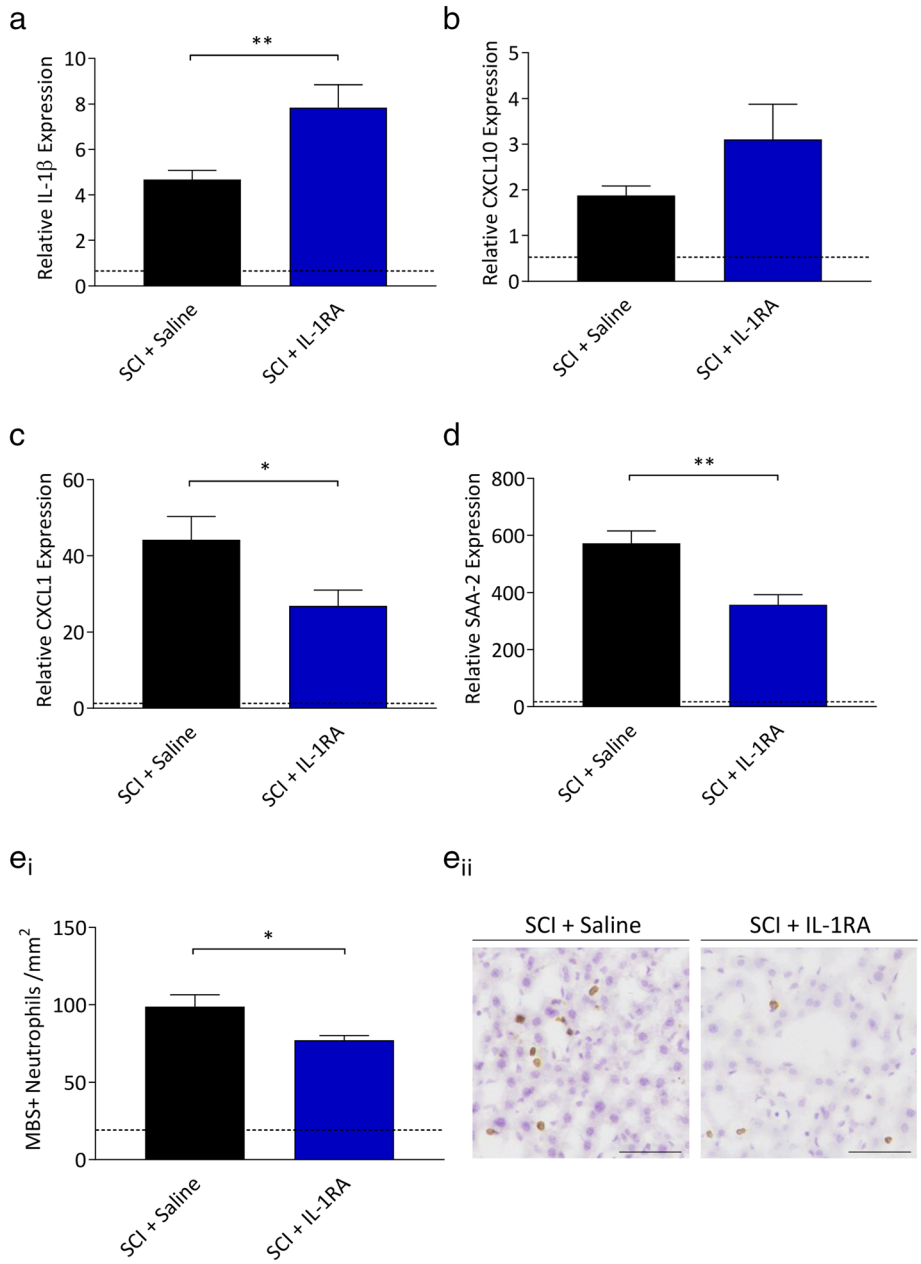


Fig 4. IL-1RA treatment significantly attenuates peripheral inflammation 6 hours post-injury. Female C57BL/6 mice underwent a 70kD SCI and were treated with human IL-1RA (i.p. 100mg/kg, *n*=8) immediately following, and 5 hours after impact, or saline as control (*n*=9). Tissue was collected 6 hours post-injury and compared to naïve baseline (dotted line, *n*=5). Relative expression of IL-1β (**a**), CXCL10 (**b**), CXCL1 (**c**) and SAA-2 (**d**) in the liver, were measured by qPCR. Neutrophil infiltration of the liver was determined by immunohistochemistry ($\mathbf{e}_i$). Representative images of neutrophils staining in the liver ($\mathbf{e}_{ii}$). Scale bar represents 50μm. Data are presented as mean ±SEM and were analysed by student's unpaired t-test, *p<0.05, **p<0.01

IL-1RA treatment induced an increase in hepatic IL-1β expression (p<0.01; Fig. 4a) while CXCL10 expression was unchanged (p=0.126; Fig. 4b). However, significant decreases in the expression of CXCL1 (p<0.05; Fig. 4c) and SAA-2 (p<0.01; Fig. 4d) were observed. Consistent with this attenuated APR, the infiltration of neutrophils into the liver was also significantly decreased in IL-1RA-treated SCI mice (p<0.05; Fig. 4e). We lastly evaluated the effect of IL-1RA treatment on central inflammation, i.e. at the spinal cord lesion site itself (Fig. 5). Strikingly, the SCI-induced recruitment of neutrophils here was significantly attenuated by IL-1RA treatment (p<0.001; Fig. 5a). Intraparenchymal IgG staining was not different between groups (Fig. 5b), demonstrating that injury severity

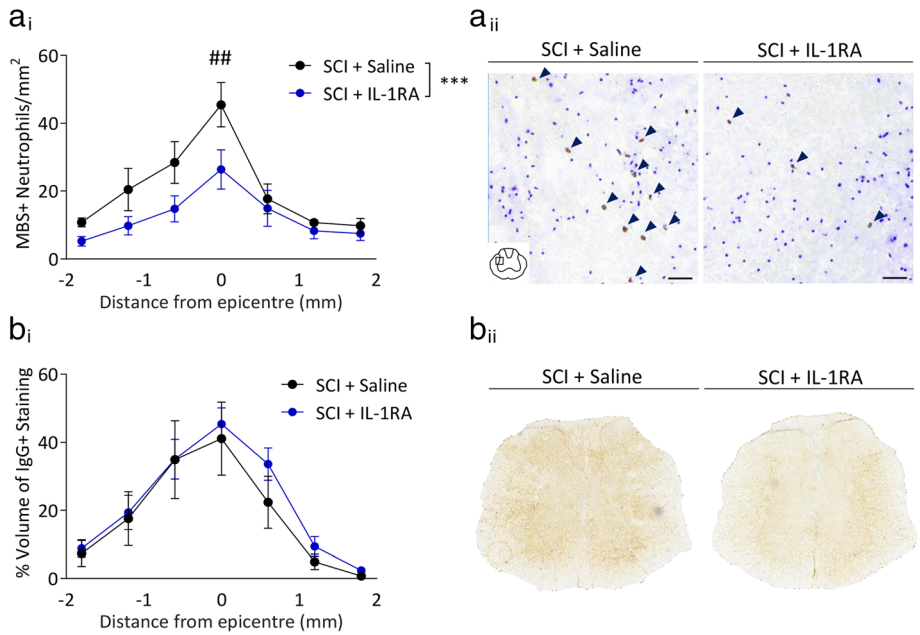


Fig 5. IL-1RA treatment reduces neutrophil recruitment to the injured spinal cord, but not IgG infiltration, 6 hours post-injury. Female C57BL/6 mice underwent a 70kD SCI and were treated with human IL-1RA (i.p. 100mg/kg, n=8) immediately following, and 5 hours after impact, or saline as control (*n*=4). Tissue was collected 6 hours post-injury and fixed spinal cord was stained for infiltrating neutrophils and IgG. Neutrophil cell density was calculated at the epicentre and 3 sections either side, corresponding to ±1.0mm (**a**$_i$). Representative images of neutrophil density in the epicentre of spinal cord lesions with, and without IL-1RA treatment, scale bar represents 50μm (**a**$_{ii}$). Volume of infiltrating IgG was measured as a percent of volume of spinal cord (**b**$_i$). Representative images of IgG staining 0.6mm from the lesion epicentre (**b**$_{ii}$). Data are presented as mean ±SEM. ***p<0.0001 in two-way ANOVA, ##p<0.01 with post-hoc test

was comparable between groups and also that neutrophil recruitment to the lesion site is an active process.

Discussion

We have consistently demonstrated that insults to the CNS induce a systemic response, known as the APR, that both precedes and amplifies local inflammation at the lesion site [5, 9]. In this study, we investigated the initiation and progression of the APR during the acute phase of SCI (≤24 hours), and whether this could be therapeutically targeted with peripherally administered IL-1RA. We show, to our knowledge for the first time, that systemic IL-1RA treatment indeed suppresses peripheral inflammation in response to SCI, and that this is in turn associated with reduced neutrophil recruitment to the lesion site.

Our previous work showed that CNS insults lead to the rapid induction of pro-inflammatory cytokines, chemokines and acute phase proteins in the liver as early as 2 hours post-injury [5, 7–10]. These immune mediators are thought to trigger and/or augment the mobilisation and priming of leukocytes in reservoirs such as the bone marrow [1, 36], after which they translocate to both peripheral organs and the site of CNS injury [43]. The present study demonstrates that a robust APR also occurs in mice with a lower thoracic (T9) contusive SCI, with acute increases in hepatic expression of a range of pro-inflammatory genes and an increase in the circulating leukocyte count, particularly neutrophils.

Temporal profiling of the APR demonstrated a significant disconnect between the hepatic expression of IL-1β and IL-1RA in response to SCI, with IL-1β peaking at 2 hours, but IL-1RA not until 6 hours post-injury. Liu et al. [27] observed a similar dissociation between IL-1β and IL-1RA expression in the injured spinal cord itself, with IL-1β being elevated at 6 hours post-SCI, whilst IL-1RA protein was decreased; a significant increase in IL-1RA protein was observed at 24 hours post-SCI. This delay in IL-1RA expression suggests the existence of putative therapeutic window during which suppression of excessive IL-1β signalling in both the liver and/or spinal cord might be beneficial. Indeed, IL-1β is known to plays a detrimental role in the progression of CNS injury [18], and IL-1 knock out (KO) mice show improved locomotor activity, reduced lesion volumes and cell survival after SCI [20, 44]. Further data by Boato and colleagues [45] demonstrated that direct application of IL-1β to the spinal cord lesion site worsened neurological outcome. Moreover, injection of IL-1β into the spinal cord induced neutrophil recruitment [6]. Acute targeting of IL-1 signalling is thus likely to be a viable strategy to reduce secondary damage after SCI [22, 26].

IL-1RA treatment to dampen IL-1 signalling has previously proven neuroprotective in animal models of both stroke [31, 42, 46, 47] and TBI [28–30], leading to its progression into human clinical trials for these acquired CNS injuries [48–50]. In comparison to brain injuries, treatment of SCI with IL-1RA has been significantly under investigated. Several studies have applied IL-1RA locally to the lesion site itself and reported histological and motor function improvements [27, 32, 51, 52], however, none investigated the influence of this intervention on the APR. Similarly, despite administrating IL-1RA systemically, the studies by Li et al. [33] and Hasturk et al. [34] both focused on neurological endpoint markers such as spinal cord lesion size, cell death and/or apoptosis. Our study is therefore the first to explore the role of IL-1 signalling in the hepatic APR and how peripheral administration of IL-1RA affects both the systemic and central inflammatory response to SCI. Perhaps somewhat counterintuitively at first sight, IL-1β expression in the liver was increased after IL-1RA of SCI mice, but this is likely a compensatory response to its blockade. In another acute CNS injury study, it has been shown that the peripheral neutralisation of TNF after stroke gives rise to an increase in hepatic TNF expression, yet the number of granulocytes in the infarct was reduced [53]. Although the underlying mechanisms driving the increase in IL-1β expression following IL-1RA administration are unknown, the critical aspect is that the downstream IL-1-mediated signalling itself is suppressed. Hepatic CXCL1 and SAA-2 expression, which are induced by IL-1β [5], were indeed decreased, as was neutrophil infiltration into the livers of SCI mice with IL-1RA treatment, which has also been shown to be IL-1β-dependent [54]. Inhibition of IL-1β with IL-1RA during the hyperacute phase after injury thus significantly abrogates the overall hepatic APR.

Exogenous IL-1RA also significantly reduced early neutrophil infiltration to the injured spinal cord. Given the known links between the magnitude of the APR, associated leukocyte mobilisation, and outcome from CNS insults [3, 9, 55], it is tempting to speculate that this reduction in neutrophil recruitment with systemic IL-1RA treatment is due, at least in part, to the observed suppression of the APR. Targeting peripheral inflammation has indeed been demonstrated to be a promising strategy in other CNS injuries, where depletion of liver Kupffer cells [56] and the targeting of acute phase proteins [10] reduced both neutrophil infiltration and lesion size. Conversely, systemic IL-1β administration was shown to worsen neutrophilia and increase infiltration of these cells into the brain in a rodent model of stroke [54]. Interestingly, systemic IL-1β administration no longer had a detrimental effect on lesion pathology if neutrophils were depleted [54]. This demonstrates that IL-1β-mediated neutrophil activation and recruitment is the driving factor for excessive CNS damage after injury, and supports the notion that peripheral effects of IL-1RA convey neuroprotection via suppression of this recruitment. These findings have translational significance as the magnitude of neutrophilia is predictive of outcomes in both mice and human patients [36], and attenuating neutrophil recruitment to the injured spinal cord leads to improved recovery [57]. Targeting the APR thus provides an appealing strategy to reduce the systemic inflammatory response to SCI and, in doing so, ameliorate the spread of secondary injury into spared neural tissue around the impact site. Whilst only female mice have been used in this study, owing to the reduced risk of post-surgery complications, the population of those living with SCI is very heterogeneous. Further studies are therefore warranted to include animals of both sexes and of different ages, to determine whether these factors might affect the response to the IL-1RA treatment.

It must be acknowledged that exogenous IL-1RA may have had some direct effect on the spinal cord itself. Previous studies investigating the pharmacokinetics of IL-1RA report its ability to cross the blood-CNS barrier [58, 59], although uptake of IL-1RA by the CNS is normally extremely poor at around only 1-2% of the plasma concentration [59]. That said, breakdown of the blood-spinal cord barrier after SCI may allow for its passive accumulation here. Pradillo et al. [31] showed that delayed IL-1RA treatment after stroke reduced infarct volume and also neutrophil infiltration, which was attributed to IL-1RA inhibiting cytokine expression in microglia. The reduction in neutrophil accumulation in the injured spinal cord, as observed in this study, could therefore also be due to direct local suppression of IL-1β signalling at the lesion site. However, the temporal kinetics of the APR and neutrophil mobilisation response to SCI, which precedes the recruitment of these cells to the lesion site and also the peak of IL-1β expression here [22], strongly suggest that a significant aspect of the therapeutic efficacy of IL-1RA treatment that we observed here was mediated through targeting the peripheral inflammatory response.

Conclusion

In summary, we show that peripheral administration of IL-1RA following SCI attenuates the APR and reduces neutrophil recruitment to the lesion site. Whether this effect is exerted directly or indirectly by suppression of the APR remains the focus of our ongoing research. Considering that IL-1RA treatment is already in clinical trials for other types of acquired CNS injury, our results warrant longer term studies to further explore its use as a viable and translatable treatment for traumatic SCI patients.

Abbreviations
ANOVA: Analysis of variance; APR: Acute phase response; APPs: Acute phase proteins; BSA: Bovine serum albumin; CNS: Central nervous system; DAB: 3,3'-Diaminobenzidine; IL-1β: Interleukin-1β; IL-1RA: IL-1 receptor antagonist; kdyne: Kilodyne; KO: Knock out; OCT: Optimal cutting temperature compound; RBC: Red blood cell; RT: Room temperature; (D)PBS: (Dulbecco's) phosphate buffered saline; SCI: Spinal cord injury; SEM: Standard error of the mean; SIRS: Systemic inflammatory response syndrome; TBI: Traumatic brain injury

Acknowledgements
Not applicable.

Availability of data and material
All data generated during and/or analysed during the current study are included in this published article.

Authors' contributions
AY, YC, MJR and DCA designed the study. MJR completed SCI surgeries for time course analysis. AY completed SCI surgeries for IL-1RA experiments. Flow cytometry experiments were performed and analysed by TJ and ERG. AY performed the histological examination of the livers and spinal cords, and the liver qPCR analysis for all experiments. The manuscript was written by AY and edited by YC, MJR and DA. All authors read and approved the final manuscript.

Funding
This work was made possible by a Nathalie Rose Barr Award from the International Spinal Research Trust to AY and the support of SpinalCure Australia to MJR's laboratory. TJ and ERG are supported by a Research Training Program Scholarship (Australian Government). DA is supported by the UK MRC under grant MC-PC-15029.

Ethics approval and consent to participate
All experiments were approved by The University of Queensland's Animal Ethics Committee (Anatomical Biosciences) and were conducted in accordance with the Australian Code for the Care and Use of Animals for Scientific Purposes.

Consent for publication
Not Applicable.

Competing interests
The authors declare that they have no competing interests.

Author details
[1]Department of Pharmacology, The University of Oxford, Mansfield Road, Oxford, UK. [2]School of Biomedical Sciences, Faculty of Medicine, The University of Queensland, St Lucia, Queensland, Australia. [3]Acute Stroke Programme, RDM-Investigative Medicine, The University of Oxford, Oxford, UK. [4]Sechenov First Moscow State Medical University, Moscow, Russia.

Received: 30 July 2020 Accepted: 9 December 2020
Published online: 06 January 2021

References

1. Bao F, Bailey CS, Gurr KR, Bailey SI, Rosas-Arellano MP, Dekaban GA, et al. Increased oxidative activity in human blood neutrophils and monocytes after spinal cord injury. Exp Neurol. 2009;215:308–16.
2. Kesani AK, Urquhart JC, Bedard N, Leelapattana P, Siddiqi F, Gurr KR, et al. Systemic inflammatory response syndrome in patients with spinal cord injury: does its presence at admission affect patient outcomes? Clinical article. J Neurosurg Spine. 2014;21:296–302.
3. Campbell SJ, Anthony DC, Oakley F, Carlsen H, Elsharkawy AM, Blomhoff R, et al. Hepatic nuclear factor kappa B regulates neutrophil recruitment to the injured brain. J Neuropathol Exp Neurol. 2008;67:223–30.
4. Campbell SJ, Deacon RM, Jiang Y, Ferrari C, Pitossi FJ, Anthony DC. Overexpression of IL-1beta by adenoviral-mediated gene transfer in the rat brain causes a prolonged hepatic chemokine response, axonal injury and the suppression of spontaneous behaviour. Neurobiol Dis. 2007;27:151–63.
5. Campbell SJ, Perry VH, Pitossi FJ, Butchart AG, Chertoff M, Waters S, et al. Central nervous system injury triggers hepatic CC and CXC chemokine expression that is associated with leukocyte mobilization and recruitment to both the central nervous system and the liver. Am J Pathol. 2005;166:1487–97.
6. Campbell SJ, Wilcockson DC, Butchart AG, Perry VH, Anthony DC. Altered chemokine expression in the spinal cord and brain contributes to differential interleukin-1beta-induced neutrophil recruitment. J Neurochem. 2002;83:432–41.
7. Wilcockson DC, Campbell SJ, Anthony DC, Perry VH. The systemic and local acute phase response following acute brain injury. J Cereb Blood Flow Metab. 2002;22:318–26.
8. Blond D, Campbell SJ, Butchart AG, Perry VH, Anthony DC. Differential induction of interleukin-1beta and tumour necrosis factor-alpha may account for specific patterns of leukocyte recruitment in the brain. Brain Res. 2002;958:89–99.
9. Campbell SJ, Hughes PM, Iredale JP, Wilcockson DC, Waters S, Docagne F, et al. CINC-1 is an acute-phase protein induced by focal brain injury causing leukocyte mobilization and liver injury. FASEB J. 2003;17:1168–70.
10. Campbell SJ, Jiang Y, Davis AE, Farrands R, Holbrook J, Leppert D, et al. Immunomodulatory effects of etanercept in a model of brain injury act through attenuation of the acute-phase response. J Neurochem. 2007;103:2245–55.
11. Fleming JC, Norenberg MD, Ramsay DA, Dekaban GA, Marcillo AE, Saenz AD, et al. The cellular inflammatory response in human spinal cords after injury. Brain. 2006;129:3249–69.
12. Anwar MA, Al Shehabi TS, Eid AH. Inflammogenesis of secondary spinal cord injury. Front Cell Neurosci. 2016;10:98.
13. Neirinckx V, Coste C, Franzen R, Gothot A, Rogister B, Wislet S. Neutrophil contribution to spinal cord injury and repair. J Neuroinflammation. 2014;11:150.
14. Donnelly DJ, Popovich PG. Inflammation and its role in neuroprotection, axonal regeneration and functional recovery after spinal cord injury. Exp Neurol. 2008;209:378–88.
15. Yang L, Jones NR, Blumbergs PC, Van Den Heuvel C, Moore EJ, Manavis J, et al. Severity-dependent expression of pro-inflammatory cytokines in traumatic spinal cord injury in the rat. J Clin Neurosci. 2005;12:276–84.
16. Zhu L, Liu X, Nemeth DP, DiSabato DJ, Witcher KG, McKim DB, et al. Interleukin-1 causes CNS inflammatory cytokine expression via endothelia-microglia bi-cellular signaling. Brain Behav Immun. 2019;81:292–304.
17. Morganti-Kossmann C, Raghupathi R, Maas AIR. Traumatic brain and spinal cord injury : challenges and developments. Cambridge: Cambridge University Press; 2012.
18. Allan SM, Tyrrell PJ, Rothwell NJ. Interleukin-1 and neuronal injury. Nat Rev Immunol. 2005;5:629–40.
19. Vitkovic L, Bockaert J, Jacque C. "inflammatory" cytokines: neuromodulators in normal brain? J Neurochem. 2000;74:457–71.
20. Sato A, Ohtaki H, Tsumuraya T, Song D, Ohara K, Asano M, et al. Interleukin-1 participates in the classical and alternative activation of microglia/macrophages after spinal cord injury. J Neuroinflammation. 2012;9:65.
21. de Rivero Vaccari JP, Lotocki G, Marcillo AE, Dietrich WD, Keane RW. A molecular platform in neurons regulates inflammation after spinal cord injury. J Neurosci. 2008;28:3404–14.
22. Pineau I, Lacroix S. Proinflammatory cytokine synthesis in the injured mouse spinal cord: multiphasic expression pattern and identification of the cell types involved. J Comp Neurol. 2007;500:267–85.
23. Wang CX, Olschowka JA, Wrathall JR. Increase of interleukin-1beta mRNA and protein in the spinal cord following experimental traumatic injury in the rat. Brain Res. 1997;759:190–6.
24. Ching S, He L, Lai W, Quan N. IL-1 type I receptor plays a key role in mediating the recruitment of leukocytes into the central nervous system. Brain Behav Immun. 2005;19:127–37.
25. Schnell L, Fearn S, Schwab ME, Perry VH, Anthony DC. Cytokine-induced acute inflammation in the brain and spinal cord. J Neuropathol Exp Neurol. 1999;58:245–54.
26. Pineau I, Sun L, Bastien D, Lacroix S. Astrocytes initiate inflammation in the injured mouse spinal cord by promoting the entry of neutrophils and inflammatory monocytes in an IL-1 receptor/MyD88-dependent fashion. Brain Behav Immun. 2010;24:540–53.
27. Liu S, Xu GY, Johnson KM, Echetebu C, Ye ZS, Hulsebosch CE, et al. Regulation of interleukin-1beta by the interleukin-1 receptor antagonist in the glutamate-injured spinal cord: endogenous neuroprotection. Brain Res. 2008;1231:63–74.

28. Newell EA, Todd BP, Mahoney J, Pieper AA, Ferguson PJ, Bassuk AG. Combined blockade of interleukin-1alpha and -1beta signaling protects mice from cognitive dysfunction after traumatic brain injury. eNeuro. 2018;5.
29. Clausen F, Hanell A, Israelsson C, Hedin J, Ebendal T, Mir AK, et al. Neutralization of interleukin-1beta reduces cerebral edema and tissue loss and improves late cognitive outcome following traumatic brain injury in mice. Eur J Neurosci. 2011;34:110–23.
30. Sun M, Brady RD, Wright DK, Kim HA, Zhang SR, Sobey CG, et al. Treatment with an interleukin-1 receptor antagonist mitigates neuroinflammation and brain damage after polytrauma. Brain Behav Immun. 2017;66:359–71.
31. Pradillo JM, Denes A, Greenhalgh AD, Boutin H, Drake C, McColl BW, et al. Delayed administration of interleukin-1 receptor antagonist reduces ischemic brain damage and inflammation in comorbid rats. J Cereb Blood Flow Metab. 2012;32:1810–9.
32. Akuzawa S, Kazui T, Shi E, Yamashita K, Bashar AH, Terada H. Interleukin-1 receptor antagonist attenuates the severity of spinal cord ischemic injury in rabbits. J Vasc Surg. 2008;48:694–700.
33. Li T, Li YT, Song DY. The expression of IL-1beta can deteriorate the prognosis of nervous system after spinal cord injury. Int J Neurosci. 2018; 128:778–82.
34. Hasturk AE, Yilmaz ER, Turkoglu E, Arikan M, Togral G, Hayirli N, et al. Potential neuroprotective effect of Anakinra in spinal cord injury in an in vivo experimental animal model. Neurosciences (Riyadh). 2015;20:124–30.
35. Otxoa-de-Amezaga A, Miro-Mur F, Pedragosa J, Gallizioli M, Justicia C, Gaja-Capdevila N, et al. Microglial cell loss after ischemic stroke favors brain neutrophil accumulation. Acta Neuropathol. 2019;137:321–41.
36. Brennan FH, Jogia T, Gillespie ER, Blomster LV, Li XX, Nowlan B, et al. Complement receptor C3aR1 controls neutrophil mobilization following spinal cord injury through physiological antagonism of CXCR2. JCI Insight. 2019;4.
37. Brennan FH, Kurniawan ND, Vukovic J, Bartlett PF, Kasermann F, Arumugam TV, et al. IVIg attenuates complement and improves spinal cord injury outcomes in mice. Ann Clin Transl Neurol. 2016;3:495–511.
38. Harrison M, O'Brien A, Adams L, Cowin G, Ruitenberg MJ, Sengul G, et al. Vertebral landmarks for the identification of spinal cord segments in the mouse. Neuroimage. 2013;68:22–9.
39. Blomster LV, Brennan FH, Lao HW, Harle DW, Harvey AR, Ruitenberg MJ. Mobilisation of the splenic monocyte reservoir and peripheral CX(3)CR1 deficiency adversely affects recovery from spinal cord injury. Exp Neurol. 2013;247:226–40.
40. Blomster LV, Cowin GJ, Kurniawan ND, Ruitenberg MJ. Detection of endogenous iron deposits in the injured mouse spinal cord through high-resolution ex vivo and in vivo MRI. NMR Biomed. 2013;26:141–50.
41. Scheff SW, Rabchevsky AG, Fugaccia I, Main JA, Lumpp JE Jr. Experimental modeling of spinal cord injury: characterization of a force-defined injury device. J Neurotrauma. 2003;20:179–93.
42. Pradillo JM, Murray KN, Coutts GA, Moraga A, Oroz-Gonjar F, Boutin H, et al. Reparative effects of interleukin-1 receptor antagonist in young and aged/co-morbid rodents after cerebral ischemia. Brain Behav Immun. 2017;61: 117–26.
43. Gris D, Hamilton EF, Weaver LC. The systemic inflammatory response after spinal cord injury damages lungs and kidneys. Exp Neurol. 2008;211:259–70.
44. Bastien D, Bellver Landete V, Lessard M, Vallieres N, Champagne M, Takashima A, et al. IL-1alpha gene deletion protects oligodendrocytes after spinal cord injury through upregulation of the survival factor Tox3. J Neurosci. 2015;35:10715–30.
45. Boato F, Rosenberger K, Nelissen S, Geboes L, Peters EM, Nitsch R, et al. Absence of IL-1beta positively affects neurological outcome, lesion development and axonal plasticity after spinal cord injury. J Neuroinflammation. 2013;10:6.
46. Maysami S, Wong R, Pradillo JM, Denes A, Dhungana H, Malm T, et al. A cross-laboratory preclinical study on the effectiveness of interleukin-1 receptor antagonist in stroke. J Cereb Blood Flow Metab. 2016;36:596–605.
47. Zhang DD, Jin C, Zhang YT, Gan XD, Zou MJ, Wang YY, et al. A novel IL-1RA-PEP fusion protein alleviates blood-brain barrier disruption after ischemia-reperfusion in male rats. J Neuroinflammation. 2018;15:16.
48. Emsley HC, Smith CJ, Georgiou RF, Vail A, Hopkins SJ, Rothwell NJ, et al. A randomised phase II study of interleukin-1 receptor antagonist in acute stroke patients. J Neurol Neurosurg Psychiatry. 2005;76:1366–72.
49. Helmy A, Guilfoyle MR, Carpenter KL, Pickard JD, Menon DK, Hutchinson PJ. Recombinant human interleukin-1 receptor antagonist in severe traumatic brain injury: a phase II randomized control trial. J Cereb Blood Flow Metab. 2014;34:845–51.
50. Helmy A, Guilfoyle MR, Carpenter KLH, Pickard JD, Menon DK, Hutchinson PJ. Recombinant human interleukin-1 receptor antagonist promotes M1 microglia biased cytokines and chemokines following human traumatic brain injury. J Cereb Blood Flow Metab. 2016;36:1434–48.
51. Nesic O, Xu GY, McAdoo D, High KW, Hulsebosch C, Perez-Pol R. IL-1 receptor antagonist prevents apoptosis and caspase-3 activation after spinal cord injury. J Neurotrauma. 2001;18:947–56.
52. Zong S, Zeng G, Wei B, Xiong C, Zhao Y. Beneficial effect of interleukin-1 receptor antagonist protein on spinal cord injury recovery in the rat. Inflammation. 2012;35:520–6.
53. Clausen BH, Degn M, Martin NA, Couch Y, Karimi L, Ormhoj M, Mortensen ML, Gredal HB, Gardiner C, Sargent Il, et al. Systemically administered anti-TNF therapy ameliorates functional outcomes after focal cerebral ischemia. J Neuroinflammation. 2014;11:203.
54. McColl BW, Rothwell NJ, Allan SM. Systemic inflammatory stimulus potentiates the acute phase and CXC chemokine responses to experimental stroke and exacerbates brain damage via interleukin-1- and neutrophil-dependent mechanisms. J Neurosci. 2007;27:4403–12.
55. Fleming JC, Bailey CS, Hundt H, Gurr KR, Bailey SI, Cepinskas G, Lawendy AR, Badhwar A: Remote inflammatory response in liver is dependent on the segmental level of spinal cord injury. J Trauma Acute Care Surg 2012, **72:** 1194-1201;discussion 1202.
56. Campbell SJ, Zahid I, Losey P, Law S, Jiang Y, Bilgen M, et al. Liver Kupffer cells control the magnitude of the inflammatory response in the injured brain and spinal cord. Neuropharmacology. 2008;55:780–7.
57. Lee SM, Rosen S, Weinstein P, van Rooijen N, Noble-Haeusslein LJ. Prevention of both neutrophil and monocyte recruitment promotes recovery after spinal cord injury. J Neurotrauma. 2011;28:1893–907.
58. Galea J, Ogungbenro K, Hulme S, Greenhalgh A, Aarons L, Scarth S, et al. Intravenous anakinra can achieve experimentally effective concentrations in the central nervous system within a therapeutic time window: results of a dose-ranging study. J Cereb Blood Flow Metab. 2011;31:439–47.
59. Greenhalgh AD, Galea J, Denes A, Tyrrell PJ, Rothwell NJ. Rapid brain penetration of interleukin-1 receptor antagonist in rat cerebral ischaemia: pharmacokinetics, distribution, protection. Br J Pharmacol. 2010;160:153–9.

Publisher's Note

Springer Nature remains neutral with regard to jurisdictional claims in published maps and institutional affiliations.

Ready to submit your research? Choose BMC and benefit from:

- fast, convenient online submission
- thorough peer review by experienced researchers in your field
- rapid publication on acceptance
- support for research data, including large and complex data types
- gold Open Access which fosters wider collaboration and increased citations
- maximum visibility for your research: over 100M website views per year

At BMC, research is always in progress.

Learn more biomedcentral.com/submissions

